13th EFRC CONFERENCE

September 19th – 21st 2023

Zagreb, Croatia



EFRC

EUROPEAN FORUM for RECIPROCATING COMPRESSORS

WWW.RECIP.ORG

13th EFRC CONFERENCE

PREMIUM CONFERENCE SPONSORS

ARIEL

BORSIG
BORSIG ZM Compression GmbH

Burckhardt Compression

COOK COMPRESSION
a DOVER company

COZZANI

HOERBIGER

PROGNOST
INTELLIGENCE ON DUTY
Part of the Burckhardt Compression Group

TNO innovation for life

MEDIA PARTNERS

GAS COMPRESSION magazine

COMPRESSOR TECH2
DEDICATED TO GAS COMPRESSION PRODUCTS AND APPLICATIONS

COOPERATION

CITY
UNIVERSITY OF LONDON
EST 1894

13th EFRC CONFERENCE
September 19th – 21st 2023, Zagreb



WWW.RECIP.ORG

13th EFRC CONFERENCE
September 19th – 21st 2023, Zagreb

DESIGN

Investigation of excessive crank gear vibration and bearing loading by means of a multibody finite element analysis for a vertical reciprocating compressor and proposed mitigation measures
by: Roger Keller – BURCKHARDT COMPRESSION 15

Compressor and valve challenges in energy transition: the experience on LNG and Hydrogen applications
by: Massimo Schiavone, Andrea Raggi, Giovanni Ballerini – COZZANI 25

Reversible operation of a reciprocating compressor as an expansion machine
by: Christian Stöckel, Konrad Klotsche, Christiane Thomas – TECHNISCHE UNIVERSITÄT DRESDEN 36

Reciprocating Steam Compression Applications in Energy Decarbonization
by: Matt Janssen – VAPOR LOCOMOTIVE 43

DIGITALIZATION & AL

Design Automation and Machine Learning in API 618 Reciprocating Compressors
by: Niccolò Batini – BAKER HUGHES; Niccolò Becattini, Gaetano Cascini – POLITECNICO DI MILANO 57

Real-World Compressor Fault Detection for Digital Twin Environments
by: Gautham Ramchandran, Evangelia Konstantopoulou, Panagiotis Koutsivitis, Nils-Henning Framke – GAMMA TECHNOLOGIES 65

Using Transfer Learning to Construct Accurate Data-driven Compressor Models on Limited datasets of Field Measurements
by: Jonah Poort, Rens Bazuin – TNO 74

CONTENTS

13th EFRC CONFERENCE
September 19th – 21st 2023, Zagreb

EFRC PAPER

Constrained layer damping for small-bore side branches
by: Irma Meijer. Can Tümer, Jan de Vreugd – TNO 87

Diaphragm compressors for hydrogen service: inventory of operational challenges and feasibility of diaphragm optimization
by: Cyril Wentzel – WENTZEL DYNAMICS; Leonard van Lier – TNO 95

HYDROGEN COMPRESSION

Reciprocating Compressors and the Hydrogen Economy
by: Ben Williams – ARIEL 109

Wear Mechanisms of High-Pressure Hydrogen Sealing Materials
by: Michael Schöbel – LEOBERSDORFER MASCHINENFABRIK; Marc Langela – STASSKOL 117

Experimental and numerical investigation on the sealing capability of a high pressure, dry running, hydrogen reciprocating compressor
by: Giorgio Taurian – SIAD; Paul Modern – COOK COMPRESSION; Giovanna Barigozzi, Nicoletta Franchina, Elisa Ghirardi, Otman Kouaissah – UNI BERGAMO 123

Efficient H_2 compression with Pistons & Diaphragms – Recips as a keystone of the energy transition
by: Jens Wulff – NEUMAN & ESSER 132

MONITORING & RELIABILITY

Identifying capacity control related problems using condition monitoring
by: Thorsten Bickmann, Fayyaz Qureshi – BENTLY NEVADA 141

Upgradation of Compressor Lubrication System from Pump-to-Point "to" Divider Block in Worthington and BPCL Compressors of Oil India Limited & benefits obtained
by: Amarish Kamalapuri, Prateek Baruah – OIL INDIA 151

Impact versus Impact – Comparison of different filter modes for vibration measurement
by: Jan Löken – PROGNOST 165

CONTENTS

13th EFRC CONFERENCE
September 19th – 21st 2023, Zagreb

PULSATION & VIBRATION

Effect on Pulsation and Vibration Mitigation Measures when Adjusting a Natural Gas System to Hydrogen Mixtures
by: André Eijk – INDEPENDENT CONSULTANT 173

On solving torsional vibration problems of reciprocating compressor systems
by: David Richter-Trummer, Andreas Thalhammer, Thomas Bozezki – GEISLINGER 185

Optimizing the torsional vibration behavior of reciprocating compressors using a flywheel-integrated damper concept
by: Sebastian Willeke, Stephan Bohmeyer, Norbert Reinsperger and Michael Steidl – HASSE & WREDE 195

Green hydrogen can also pulsate – Successful use of a Helmholtz resonator
by: Johann Lenz; Franz-Josef Düttmann – KÖTTER CONSULTING 206

Pulsation control for a multi-purpose underground storage reciprocating compressor system (natural gas, hydrogen and mixed gas)
by: Leonard van Lier – TNO; Olivier Bore – STORENGY 214

Improved plant reliability due to acoustical and vibrational optimisation
by: Patrick Tetenborg, Christian Jansen – JANSEN + TETENBORG 225

SEALING & EMISSIONS

A non-lube sealing system in a high-pressure fuel gas compressor – field experience
by: Felix Ragg – BURCKHARDT COMPRESSION 237

Improved plant reliability due to acoustical and vibrational optimisation
by: Bernhard Fritz, Georg Meyer, John Ladd – HOERBIGER 245

A simplified approach to the design of nitrogen purge systems to improve safety and reduce emissions
by: Guido Pratelli, Christian Prinz – HOERBIGER 253

Overcoming reliability challenges of sealing highpressure hydrogen diaphragm compression stages
by: Marije Oosterlaak, Rens Hulstijn, Yann Ardouin – HOWDEN 262

CONTENTS

13th EFRC CONFERENCE
September 19th – 21st 2023, Zagreb

ARIEL

Reciprocating Compressors and the Hydrogen Economy
by: Ben Williams – ARIEL 109

BAKER HUGHES

Design Automation and Machine Learning in API 618 Reciprocating Compressors
by: Niccolò Batini – BAKER HUGHES; Niccolò Becattini, Gaetano Cascini – POLITECNICO DI MILANO 57

BENTLY NEVADA, A BAKER HUGHES BUSINESS

Identifying capacity control related problems using condition monitoring
by: Thorsten Bickmann, Fayyaz Qureshi – BENTLY NEVADA 141

BURCKHARDT COMPRESSION

Investigation of excessive crank gear vibration and bearing loading by means of a multibody finite element analysis for a vertical reciprocating compressor and proposed mitigation measures
by: Roger Keller – BURCKHARDT COMPRESSION 15

A non-lube sealing system in a high-pressure fuel gas compressor – field experience
by: Felix Ragg – BURCKHARDT COMPRESSION 237

COOK COMPRESSION

Experimental and numerical investigation on the sealing capability of a high pressure, dry running, hydrogen reciprocating compressor
by: Giorgio Taurian – SIAD; Paul Modern – COOK COMPRESSION; Giovanna Barigozzi, Nicoletta Franchina, Elisa Ghirardi, Otman Kouaissah – UNI BERGAMO 123

CONTENTS BY CONTRIBUTOR

13th EFRC CONFERENCE
September 19th – 21st 2023, Zagreb

COZZANI

Compressor and valve challenges in energy transition: the experience on LNG and Hydrogen applications
by: Massimo Schiavone, Andrea Raggi, Giovanni Ballerini – COZZANI 25

GAMMA TECHNOLOGIES

Real-World Compressor Fault Detection for Digital Twin Environments
by: Gautham Ramchandran, Evangelia Konstantopoulou, Panagiotis Koutsivitis, Nils-Henning Framke – GAMMA TECHNOLOGIES **65**

GEISLINGER

On solving torsional vibration problems of reciprocating compressor systems
by: David Richter-Trummer, Andreas Thalhammer, Thomas Bozezki – GEISLINGER 185

HASSE & WREDE

Optimizing the torsional vibration behavior of reciprocating compressors using a flywheel-integrated damper concept
by: Sebastian Willeke, Stephan Bohmeyer, Norbert Reinsperger and Michael Steidl – HASSE & WREDE 195

HOERBIGER

Improved plant reliability due to acoustical and vibrational optimisation
by: Bernhard Fritz, Georg Meyer, John Ladd – HOERBIGER 245

A simplified approach to the design of nitrogen purge systems to improve safety and reduce emissions
by: Guido Pratelli, Christian Prinz – HOERBIGER 253

CONTENTS BY CONTRIBUTOR

13th EFRC CONFERENCE
September 19th – 21st 2023, Zagreb

HOWDEN

■ **Overcoming reliability challenges of sealing highpressure hydrogen diaphragm compression stages**
by: Marije Oosterlaak, Rens Hulstijn, Yann Ardouin – HOWDEN 262

INDEPENDENT CONSULTANT

■ **Effect on Pulsation and Vibration Mitigation Measures when Adjusting a Natural Gas System to Hydrogen Mixtures**
by: André Eijk – INDEPENDENT CONSULTANT 173

JANSEN + TETENBORG

■ **Improved plant reliability due to acoustical and vibrational optimisation**
by: Patrick Tetenborg, Christian Jansen – JANSEN + TETENBORG 225

KÖTTER CONSULTING

■ **Green hydrogen can also pulsate – Successful use of a Helmholtz resonator**
by: Johann Lenz; Franz-Josef Düttmann – KÖTTER CONSULTING 206

LEOBERSDORFER MASCHINENFABRIK

■ **Wear Mechanisms of High-Pressure Hydrogen Sealing Materials**
by: Michael Schöbel – LEOBERSDORFER MASCHINENFABRIK; Marc Langela – STASSKOL 117

NEUMAN & ESSER

■ **Efficient H_2 compression with Pistons & Diaphragms – Recips as a keystone of the energy transition**
by: Jens Wulff – NEUMAN & ESSER 132

CONTENTS BY CONTRIBUTOR

13th EFRC CONFERENCE
September 19th – 21st 2023, Zagreb

OIL INDIA

■ **Upgradation of Compressor Lubrication System from Pump-to-Point "to" Divider Block in Worthington and BPCL Compressors of Oil India Limited & benefits obtained**
by: Amarish Kamalapuri, Prateek Baruah – OIL INDIA 151

POLITECNICO DI MILANO

■ **Design Automation and Machine Learning in API 618 Reciprocating Compressors**
by: Niccolò Batini – BAKER HUGHES; Niccolò Becattini, Gaetano Cascini – POLITECNICO DI MILANO 57

PROGNOST

■ **Impact versus Impact – Comparison of different filter modes for vibration measurement**
by: Jan Löken – PROGNOST 165

SIAD

■ **Experimental and numerical investigation on the sealing capability of a high pressure, dry running, hydrogen reciprocating compressor**
by: Giorgio Taurian – SIAD; Paul Modern – COOK COMPRESSION; Giovanna Barigozzi, Nicoletta Franchina, Elisa Ghirardi, Otman Kouaissah – UNI BERGAMO 123

STASSKOL

■ **Wear Mechanisms of High-Pressure Hydrogen Sealing Materials**
by: Michael Schöbel – LEOBERSDORFER MASCHINENFABRIK; Marc Langela – STASSKOL 117

CONTENTS BY CONTRIBUTOR

13th EFRC CONFERENCE
September 19th – 21st 2023, Zagreb

STORENGY

- **Pulsation control for a multi-purpose underground storage reciprocating compressor system (natural gas, hydrogen and mixed gas)**
  by: Leonard van Lier – TNO; Olivier Bore – STORENGY 214

TECHNISCHE UNIVERSITÄT DRESDEN

- **Reversible operation of a reciprocating compressor as an expansion machine**
  by: Christian Stöckel, Konrad Klotsche, Christiane Thomas – TECHNISCHE UNIVERSITÄT DRESDEN 36

TNO

- **Using Transfer Learning to Construct Accurate Data-driven Compressor Models on Limited datasets of Field Measurements**
  by: Jonah Poort, Rens Bazuin – TNO 74
- **Constrained layer damping for small-bore side branches**
  by: Irma Meijer. Can Tümer, Jan de Vreugd – TNO 87
- **Diaphragm compressors for hydrogen service: inventory of operational challenges and feasibility of diaphragm optimization**
  by: Cyril Wentzel – WENTZEL DYNAMICS; Leonard van Lier – TNO 95
- **Pulsation control for a multi-purpose underground storage reciprocating compressor system (natural gas, hydrogen and mixed gas)**
  by: Leonard van Lier – TNO; Olivier Bore – STORENGY 214

13th EFRC CONFERENCE
September 19th – 21st 2023, Zagreb

UNIVERSITY OF BERGAMO

■ **Experimental and numerical investigation on the sealing capability of a high pressure, dry running, hydrogen reciprocating compressor**
by: Giorgio Taurian – SIAD; Paul Modern – COOK COMPRESSION; Giovanna Barigozzi, Nicoletta Franchina, Elisa Ghirardi, Otman Kouaissah – UNI BERGAMO 123

VAPOR LOCOMOTIVE

■ **Reciprocating Steam Compression Applications in Energy Decarbonization**
by: Matt Janssen – VAPOR LOCOMOTIVE 43

WENTZEL DYNAMICS

■ **Diaphragm compressors for hydrogen service: inventory of operational challenges and feasibility of diaphragm optimization**
by: Cyril Wentzel – WENTZEL DYNAMICS; Leonard van Lier – TNO 95

CONTENTS BY CONTRIBUTOR

DESIGN

Investigation of excessive crank gear vibration and bearing loading by means of a multibody finite element analysis for a vertical reciprocating compressor and proposed mitigation measures
by: Roger Keller – BURCKHARDT COMPRESSION *15*

Compressor and valve challenges in energy transition: the experience on LNG and Hydrogen applications
by: Massimo Schiavone, Andrea Raggi, Giovanni Ballerini – COZZANI *25*

Reversible operation of a reciprocating compressor as an expansion machine
by: Christian Stöckel, Konrad Klotsche, Christiane Thomas – TECHNISCHE UNIVERSITÄT DRESDEN *36*

Reciprocating Steam Compression Applications in Energy Decarbonization
by: Matt Janssen – VAPOR LOCOMOTIVE *43*

EFRC
EUROPEAN FORUM for RECIPROCATING COMPRESSORS

HIGHEST GAS PURITY AND LOW ENERGY CONSUMPTION

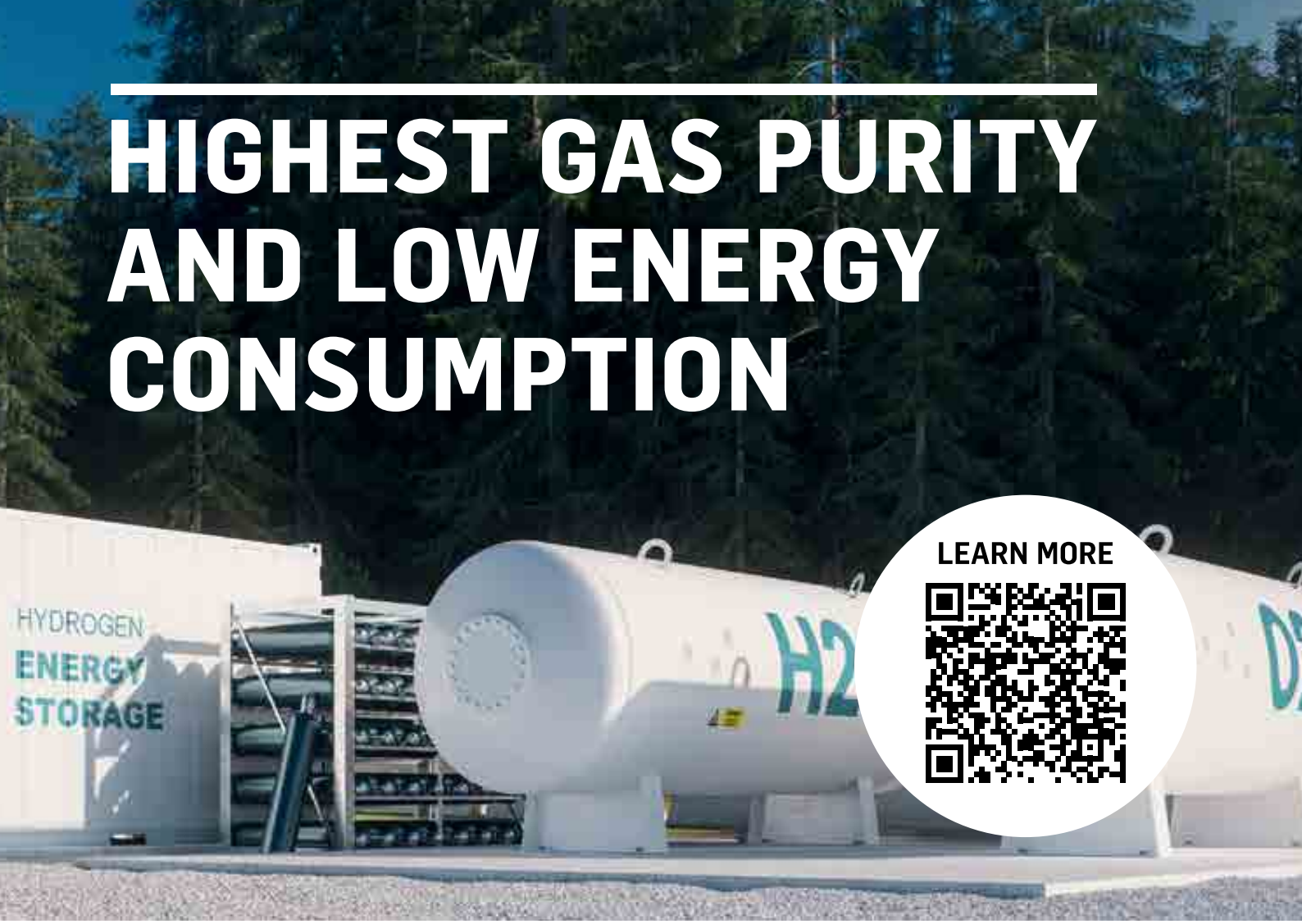

LEARN MORE

Burckhardt Compression offers a complete portfolio of compressor solutions for hydrogen fuel stations and power-to-x applications. Our oil-free diaphragm (900 bar) and piston compressors (550 bar) stand for the highest gas purity at high pressures with low energy consumption and reduced maintenance costs. In addition, Burckhardt Compression has a global network of local service centers that enables us to offer local support with a quick response rate.

burckhardtcompression.com/hydrogen

Diaphragm Compressor



Process Gas Compressor



Compressors for a Lifetime™

Burckhardt Compression

Burckhardt Compression

Investigation of excessive crank gear vibration and bearing loading by means of a multibody finite element analysis for a vertical reciprocating compressor and proposed mitigation measures

by:

Roger Keller
Research & Development
Burckhardt Compression AG
Winterthur, Switzerland
roger.keller@burckhardtcompression.com

13th EFRC CONFERENCE
September 19th – 21st 2023, Zagreb

Abstract:
Vibrations of moving and rotating parts in the crank gear of a labyrinth-seal-type compressor can cause a variety of problems such as bearing failure or increased wear in cylinders and pistons. Investigation of the dynamics of rotating parts often exceeds the possibilities of standard vibrational analysis tools like modal or harmonic response analyses, since large deformations and geometrical non-linearities are not considered. A full transient numerical analysis can handle all these non-linearities at the cost of high computational power requirements which conflicts with time and cost limits. To overcome these constraints, modelling the crank gear with beam-elements is a viable route. A typical simulation model of a compressor can thus be created with less than 5000 degrees of freedom, so that the several thousand timesteps required to capture all significant effects in a complete transient analysis can be performed in a reasonable amount of time. This paper presents the analysis of a 6-Crank vertical machine where bearing damages and excessive piston wear has occurred. A simplified model of the oil film between journal and bearing shell is used to capture its effect on the crankshaft deformation. The simulated minimum oil film thicknesses inside the main bearings are in good accordance with findings from the field, where excessive delamination of white metal in the edge zone has been observed. The analysis of the model reveals that the root cause of this is in the combination of a low crankshaft bending stiffness and a much higher stiffness of bearing supports and the main frame, leading to high reaction moments on the main bearings. A new bearing support design reduces the reaction moments and resulting edge loadings on the bearings significantly. Another important aspect are piston vibrations, which are a specific problem for labyrinth-seal-type compressors where there is no structural connection between piston and cylinder. The simulation highlights the effect of an increased piston rod diameter for reducing the piston vibrations and therefore the wear on the cylinder and piston.

by: Roger Keller – BURCKHARDT COMPRESSION

1. Introduction

Multibody simulation (MBS) is a widely used tool especially in the automotive industry for analyzing suspension systems or even engine parts like pistons and crankshafts.[1] It offers insight into non-linear effects like hydrodynamic bearings or friction between bodies that the traditional tools like modal and forced response analysis are not capable of handling. This comes at the cost of very high hardware requirements, increased computation times and a more complex and time-consuming modelling process. With the increased availability of high-performance hardware, it has become a more viable option for other industries in the recent years.

This paper intends to demonstrate the use of a multibody analysis approach to find the root cause of crank gear related problems in a labyrinth-seal-type piston compressor. While there are several software packages available specifically for MBS, its use is demonstrated with state-of-the-art FEA-Software.

Since hardware capabilities are still the limiting factor, simplifications are part of the modelling process. The main simplification used is the assumption that all parts of the crank gear are relatively slender. Hence, beam elements based on the Timoshenko Beam Theory, can be used to model all the rotating parts of the compressor [2,3].

In the first part of this paper the modelling of the individual parts, the assembly of the compressor model and the boundary conditions are described. In the second part two distinct cases that have occurred in the field are analyzed to showcase the capabilities of the model: Excessive edge loading of main bearings (white metal delamination) and piston vibrations that cause wear on cylinder and piston.

2. Model Description

Although hardware capabilities have grown by several margins in the past years, a full transient analysis of the crank gear of a reciprocating compressor is still driven by hardware and hence time limitations. Simplifications are therefore essential to get a solution in a reasonable amount of time.

2.1. Part models

All the rotating and moving parts like crankshaft, connecting rods and piston rods are slender and therefore the use of beam elements offers a great reduction in model complexity and degrees of freedom to solve. The BEAM188 [2] Elements in the FEA-Software are based on the Timoshenko beam theory [3] and model axial, bending, torsional and shear deformation. With these four deformation modes all the essential dynamic effects within a crank gear can be reproduced. While for the crankshaft mostly torsional and bending deformation is relevant, piston- and connecting rods are mainly subject to axial and bending deformations. The FEA-Model consists of the following parts:

- Motor: Rotor and Bearings
- Coupling
- Flywheel
- Crankshaft
- Connecting Rods
- Crosshead
- Piston Rod
- Piston
- Cylinders
- Frame
- Main-, connecting rod- and pin-bearings

2.1.1 Motor

Only the rotating part of the electric motor is part of the model. The rotor is a single beam with its diameter and mass adjusted to the mass moment of inertia of the real rotor. A single node that rotates at the synchronous speed is mathematically coupled to the rotor, it represents the rotating magnetic field and its mechanical interaction with the rotor. This coupling depends on the motor type and is typically a combination of torsional spring and damper elements. The spring and damper coefficients are derived from the slip and torque characteristics of the motor.

2.1.2 Coupling

A single torsional spring-damper element is modeled for the coupling between motor and flywheel/crankshaft. The mass of the coupling is modelled by a single rotating beam on each side of the coupling.

2.1.3 Flywheel

The flywheel consists of a single rotating beam element with its diameter adjusted so that its total mass and total mass moment of inertia is correct.

by: Roger Keller – BURCKHARDT COMPRESSION

2.1.4 Crankshaft

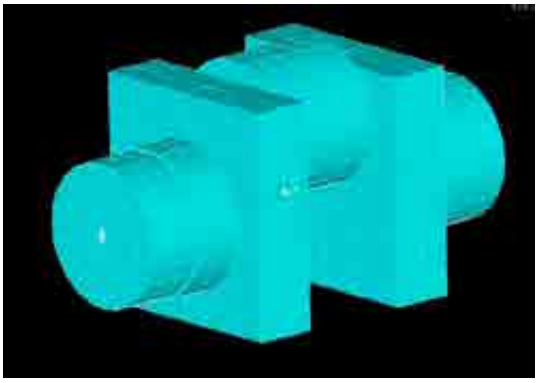

Figure 1: Beam model of crank with beam shapes

The crankshaft is the central part of the model. This behavior is essential to investigate the loads on the main bearings that are of particular interest here. Therefore, the following parameters of the crankshaft beam model need to be in good correlation with the real crankshaft:

- Total mass
- Total mass moment of inertia
- Torsional stiffness
- Bending stiffness
- Center of mass of the individual crank

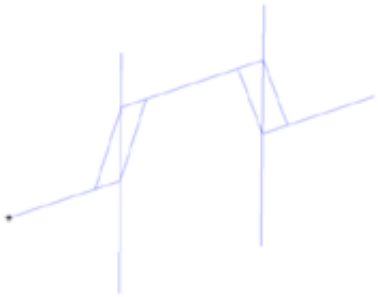

Figure 2: Beam structure of crank

Bringing these parameters into correlation is done by a 3D-solid model. From the 3D-solid model, all mentioned parameters are determined, and the construction of the beam model is adapted accordingly. To get the total mass and the stiffnesses of the crank in correlation, mass-less beam elements are used.

In Figure 1 and Figure 2 an example of a crankshaft part is depicted. All the important mechanical parameters of the beam model are within 2% of that of a more detailed solid-element model (see Table 1), therefore the beam model is suitable to investigate the crankshaft dynamics. At the same time, the number of degrees of freedom in the beam model is reduced by a factor of 1000, so that the computational time required is reduced to a feasible level.

	Solid Model	Beam Model	Deviation [%]
Total Mass [kg]	415.9	415.94	0.01
Center of mass offset [mm]	25.20	25.15	-0.20
Rot. mass [kgm^2]	7.195	7.214	0.26
Bending stiffness Kz [kNm^2]	32172	31815	-1.11
Bending stiffness Kx [kNm^2]	27378	27468	0.33
Torsional stiffness GI [kNm^2]	28093	28300	0.74
DOF	918777	465	-99.95

Table 1: Inertia and stiffness parameters of crank

2.1.5 Connecting Rod

A similar procedure as for the crankshaft is used to create the beam model of the connecting rod. However, only the total mass, the bending stiffnesses and the center of mass needs to be in accordance.

2.1.6 Crosshead

The crosshead is modelled as a single beam that is sliding inside a hollow beam that represents the crosshead guide bearing. The total mass of the beam is adjusted so that it fits the mass of the crosshead.

2.1.6 Piston and Cylinder

The Piston itself is a single beam that moves inside a hollow beam that represents the cylinder.

2.1.7 Compressor frame

The frame supports all the bearings, the crosshead, and cylinders. To assess the deformation of the crankshaft under load, its stiffness and damping properties are important. Since the frame is too complex to model with beam elements it is implemented as a substructure. For this, a solid element model of the frame is created. Certain nodes at the main bearing supports, cylinder and crosshead connections are defined as master nodes. Figure 3 shows the solid model with the specified master nodes [4] at frame anchors, main bearings, crosshead bearings, trust bearings and cylinders. During sub-structuring, the FEA-Software condenses the mass-, damping-, and stiffness matrix of this finite element model down to only the specified master nodes. To reduce computation time of the full transient analysis of the crank gear, only this substructure element is used.

by: Roger Keller – BURCKHARDT COMPRESSION

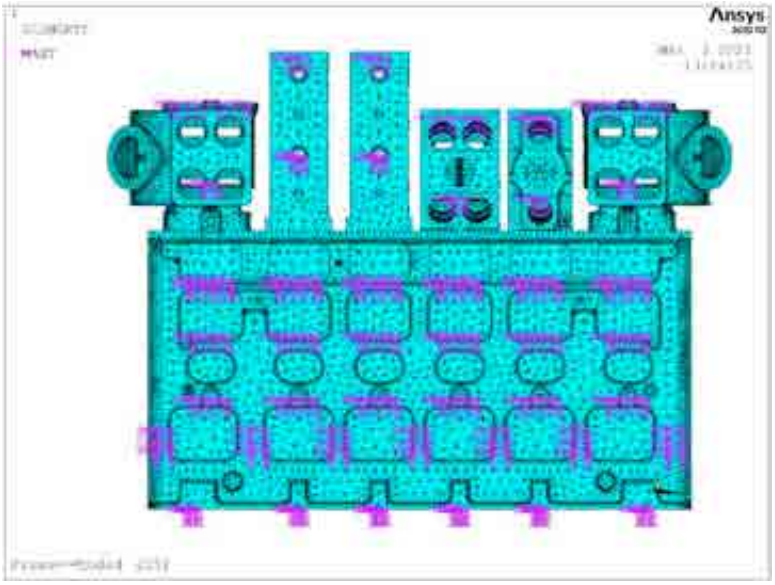

Figure 3: Solid model with master nodes

2.1.8 Bearings

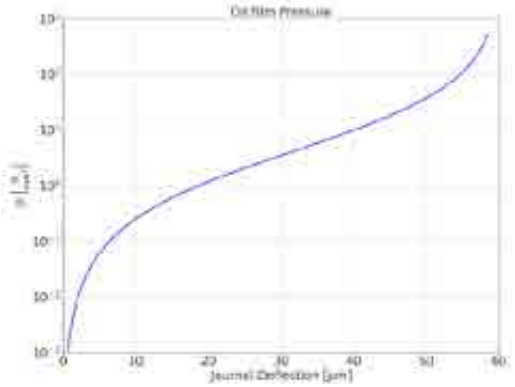

Figure 4 Gap dependent hydrodynamic oil film pressure in main bearing

The used FEA-Software also offers elements for modelling contacts between line bodies. A specialty of these elements is the ability to model beams sliding inside a hollow beam [2]. This functionality is used for the main bearing and large end bearings. The beam that represents the crankshaft slides inside a hollow beam which represents the bearing. For the hydrodynamics of the oil film between journal and bearing shell, a gap dependent contact pressure is defined. This contact pressure relation is derived from a separate model where the Reynold's equation for hydrodynamic lubrication [5] is solved for the specified bearing and oil parameters, as well as different deflections of the journal. Figure 4 shows an example of this oil film pressure for a bearing with journal diameter of 150 mm and radial clearance of 60 µm. The same procedure is used for the large end bearings, pin bearings and crosshead bearings.

2.1.9 Gas Forces

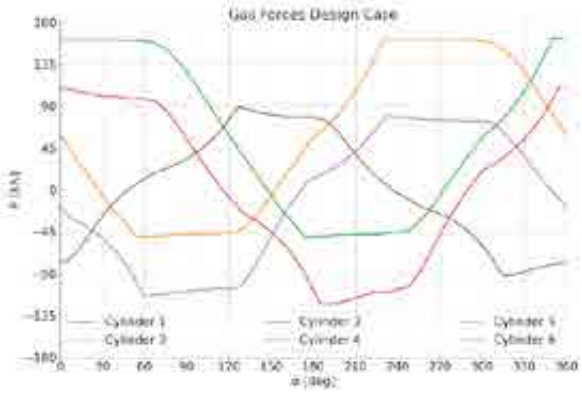

Figure 5: Gas forces on piston 1-6 for design case

While mass forces are generated automatically in a fully transient analysis, the gas forces need to be applied separately. Since the motor is modelled with a slip, the exact position of the crankshaft during the simulation is unknown. Therefore, the gas forces on the pistons are applied dynamically dependent on the crankshaft position of the individual crank. By this, also startup cases can be simulated where the speed of the crankshaft varies over time. Gas forces are extracted from an internal compressor sizing program. Figure 5 shows an example of these forces for standard operating conditions.

by: Roger Keller – BURCKHARDT COMPRESSION

2.2. Model procedure and startup

In a first load step, the synchronous speed is applied to the motor node within 1ms. This will accelerate the model to its nominal speed within 1 revolution. After that, another 5 revolutions are simulated to settle the transient oscillations caused by the sudden acceleration (see Figure 7). This procedure reduces the total time that needs to be simulated to bring the model to speed.

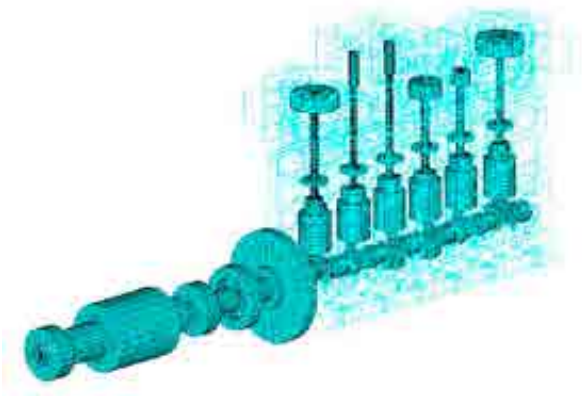

Figure 6: Model assembly

To handle the nonlinear behavior of the bearings (see Figure 4) small timesteps are required. Typically, the timestep size is chosen so that the crankshaft revolves by 0.1° per timestep. This also provides the necessary resolution to cover all the important modes of the model.

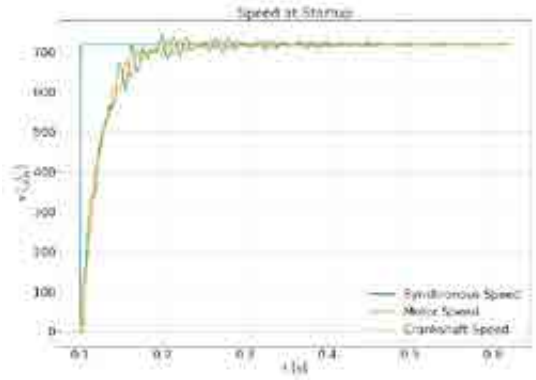

Figure 7: Startup of the compressor model

Damping is introduced to the model in the compressor frame (material damping of grey cast iron) and by separate damping elements in all bearings. For the main bearings and large end bearings, these elements are torsional damping elements, for the crosshead translation dampers. These elements model the damping of the oil film. Experience shows that this damping is sufficient (aside from numerical damping which is low for the chosen time integration schemes)[6] for the model to run stable and produce reasonable results. The damping for the main bearings is determined from the formula for the frictional power of the journal bearing[7]:

$$P_r = 2\pi \frac{\mu W \left(\frac{D}{2}-\delta\right)^3 \omega^2}{\sqrt{1-\varepsilon^2}\,\delta} \qquad [1]$$

Pr	Frictional Power [W]
μ	Dynamic Oil Viscosity [Pas]
W	Bearing Width [m]
D	Bearing Diameter [m]
δ	Radial bearing clearance [m]
ω	Angular frequency [rad/s]
ε	Eccentricity ratio [-]

The damping coefficient is then calculated from:

$$c_{bearing} = \frac{Pr}{\omega^2} \qquad [2]$$

The same procedure applies for the crosshead, the frictional power is determined by[7]:

$$Pr = \frac{2\pi D L \mu v^2}{\delta} \qquad [3]$$

This was validated by measuring the power consumption of the compressor in the idle mode. The motor power consumption was within 10% of the calculation.

by: Roger Keller – BURCKHARDT COMPRESSION

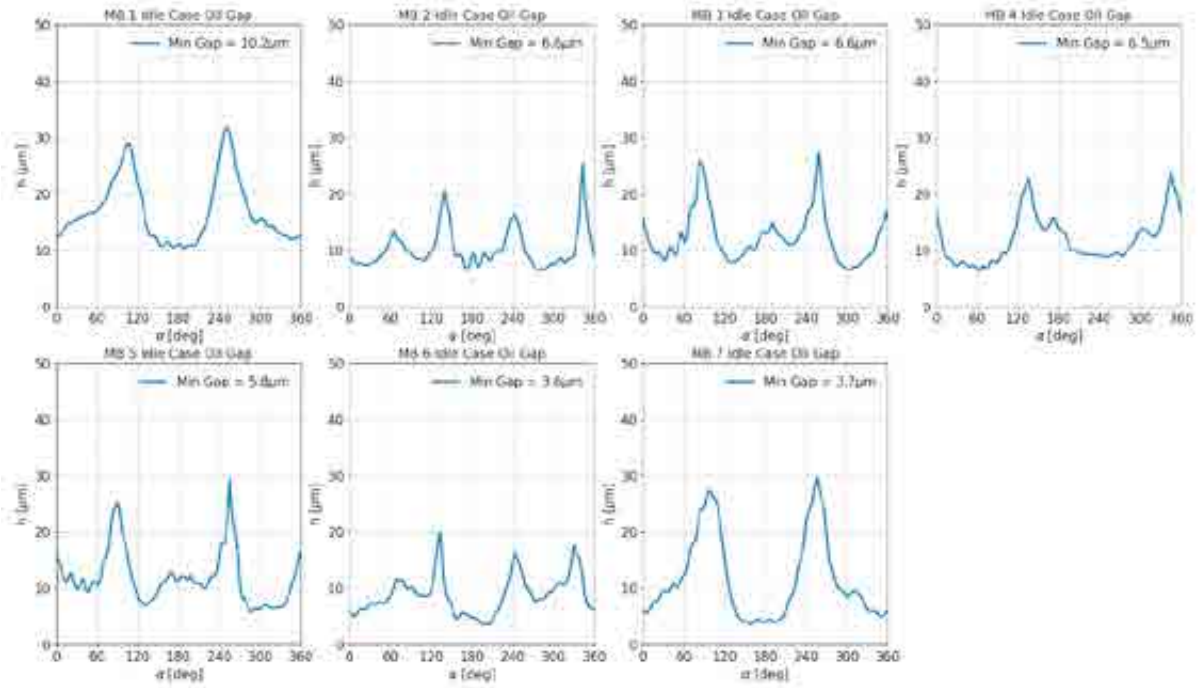

Figure 8: Crank angle dependent minimum oil film thickness for main bearing 1-7 in idle running

3.1. Analysis of Main Bearings



Figure 9: Damaged lower bearing shell of bearing 7

With this extensive mechanical model of the compressor, the dynamics of a large variety of parts can be investigated. However, in the following we want to focus on a 6-crank vertical machine where excessive main bearing damage and piston/cylinder wear has occurred. Especially during the run-in procedure in the workshop, main bearings number six and seven (bearing one on the flywheel side and bearing seven on the non-drive end side) repeatedly suffered from high edge loading and subsequent damage of the white metal surface coating (Figure 9). Extensive measures to increase the oil flow and oil retention time have been taken, with little to no effect on the described damage pattern. For this simulation, no gas forces were applied on the pistons since we are simulating the run-in phase. From the displacements and deformations of the main bearing journals calculated by the simulation model, the minimum gap between journal and bearing for each position of the crankshaft has been determined. Figure 8 shows the results for each of the seven main bearings.

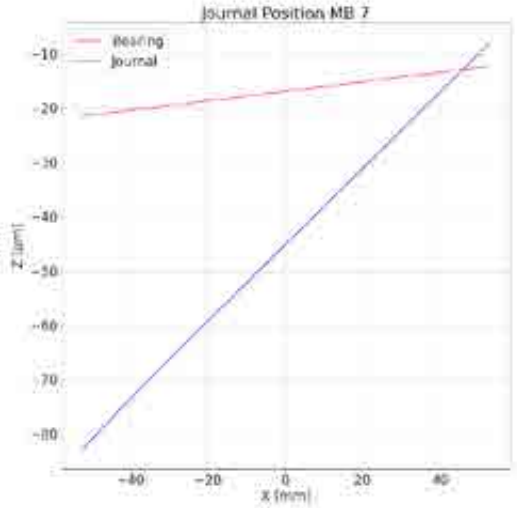

Figure 10: Journal and bearing position main bearing 7

Bearings six and seven have the overall lowest oil film thickness of less than 4 µm at a crank angle position of roughly 180°. The area of minimum oil film thickness is located at the outer edge of the bearing. Figure 10 shows the position of the axes of the bearing and the crankshaft journal at crankshaft position 180°. The x-axis in the diagram corresponds to the middle axis of the crankshaft and the y-axis is along the vertical direction (global z). The deflection in global y-direction (vertical and horizontal to

by: Roger Keller – BURCKHARDT COMPRESSION

crankshaft) at the displayed crankshaft position in this graph is almost zero, therefore a 2-D projection is used to display the axes position. Since just the axes of journal and bearing shell are plotted in this graph, the minimum oil film thickness is at the largest distance between these two lines. This is the case at the outer edge x=-52.5mm at the bottom of the bearing. The results correlate with the observed bearing damages from Figure 9. The simulation model also shows that the oil film thickness is low during a longer period from crank angle 130° to 200°, which explains the large zone of white metal delamination.

With a minimum oil film thickness of 3.7 µm one would not expect this form of damage. However, the model assumes an equally distributed oil film pressure up and until the edge zone. In the simulation model, there is a significant force generated by the oil film in the edge zone. However, the oil film pressure drops to ambient pressure conditions and generates a significantly reduced lifting force. One can therefore assume that the model overestimates the oil film thicknesses especially in the edge zone. Hence it can be derived, that the film thickness in the real bearing will be even less than the 3.7 µm. The damage indicates that it was not caused by direct metallic contact but from fatigue that originates from hammering of the crankshaft on the oil film.

This hammering causes extremely high hydrodynamic pressures that ultimately cause fatigue cracks in the white metal surface coating (Figure 9). From the analysis we follow that the root cause of the observed bearing damages is not an insufficient oil supply but rather comes from the design of the machine. Figure 10 not only shows an inclined position of the crankshaft journal but also that the bearing shell remains stable in its position. This indicates that the bending stiffness of the crankshaft is too low compared to the stiffness of the bearing support within the frame. A lower rotational stiffness of the bearing within the frame would cause the bearing to adapt to crankshaft deformations which ultimately would reduce edge loading.

The reason for this damage to occur on the bearings six and seven can be found in the increased bearing distance to accommodate for larger sized pistons. This results in a higher bending moment acting on the crankshaft.

Figure 11 shows an adapted bearing support design that increases the rotational flexibility of the bearing to reduce the problem of the edge loading. This design is implemented into the substructure of the compressor frame. In Figure 12 the minimum oil film thickness with the old and new bearing support design is plotted. It shows that by reducing the rotational stiffness of the bearing support, edge loading is reduced significantly. The minimum oil film thickness simulated increases by 80% while the curve shape remains similar.

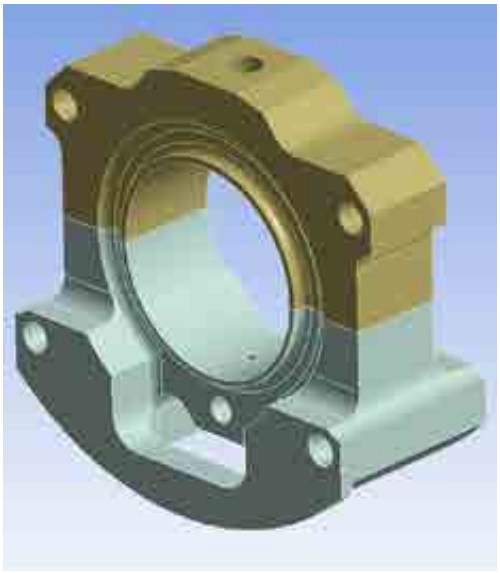

Figure 11: Modified bearing support

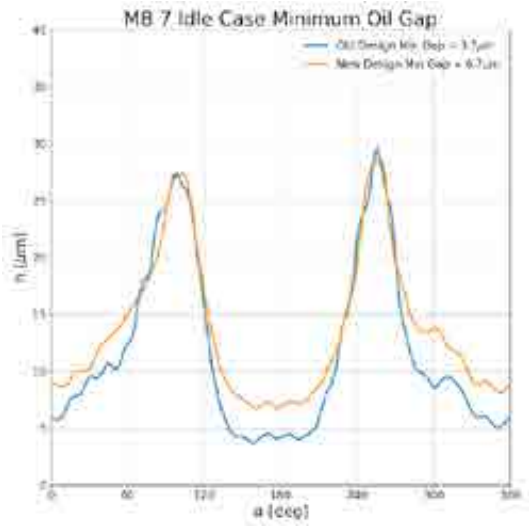

Figure 12: MOFT with modified bearing support

3.2. Excessive Piston Vibrations

For labyrinth-seal-type compressors there is a very small gap between piston and cylinder and therefore no structural connection between these two parts. It is crucial to limit piston vibrations to avoid direct contact and subsequent surface damage of outer piston and cylinder surface. For this the eigenmodes of the piston should not be close to the first, second and third harmonic order of the compressor. In general, having the first eigenmode of the piston above the 3rd order of the compressor (20% margin) is preferable.

by: Roger Keller – BURCKHARDT COMPRESSION

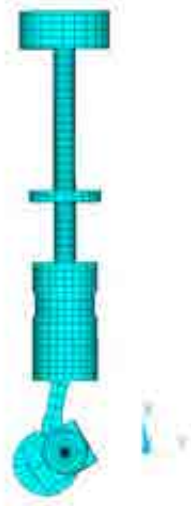

Figure 13: Crank drivetrain of stage 3



Figure 14: Scratch marks on inside of cylinder

Determination of these eigenmodes for the system of crosshead, piston rod and piston (Figure 13) is not straight forward since the free length from the guide bearing to the tip of the piston varies with the position of the crosshead. The lowest eigenmode occurs when the piston is in the top dead center, the highest in the bottom dead center. In addition, the non-linear stiffnesses of the support points of this system, which is the guide bearing (contact conditions) and the cross head (exponential stiffness of oil film), is also affecting the eigenmodes. Therefore, a standard linear modal analysis will not yield reliable results.

Observations in the field showed visible scratch marks on the inside of the 3rd stage cylinder (Figure 14). This is a clear indication of direct contact between piston and cylinder. With the FEA-Model of the compressor, piston vibration in lateral direction during operation can be investigated. For in-line six-cylinder piston machines, the lateral vibration horizontal to the crankshaft is the most critical size (y-Direction in Figure 13).

The frame has the least stiffness in this direction, while at the same time the highest excitation force coming from the crosshead acting lateral to the frame and crankshaft. Therefore, for the analysis of the lateral piston vibration it is important to also include the movement of the frame and cylinder.

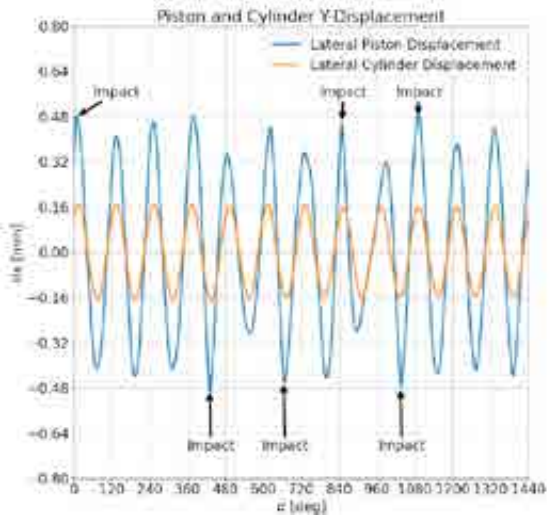

Figure 15: Lateral displacements for stage 3

In Figure 15 the y-displacements from the middle axis for the piston and cylinder are plotted for four revolutions of the crankshaft. It shows that the cylinder is oscillating at a constant frequency of the 3rd order (3 cycles per revolution). The piston itself adopts the same frequency with a higher amplitude. The excitation for the 3rd order comes from the lateral forces of the crosshead. A crankshaft with 120° angle between individual cranks will generate lateral forces on the frame 3 times per revolution. The frame reacts with a harmonic oscillation to this excitation (eigenmode). This movement is transferred to the piston rod through the crosshead guide and guide bearing. The piston and piston rod has an eigenmode that is also close to the 3rd order. Therefore, it adopts this lateral oscillation with an amplitude that increases slowly until the piston hits the cylinder (when the difference between the blue and the orange line exceeds the clearance of 0.32mm). During the first revolution in Figure 15 the buildup of the pistons amplitude over three cycles can be observed until it hits the cylinder wall at 430°. Since this oscillation takes place on the 3rd order of the compressor base speed, the change of length between guide bearing and piston, which determines the eigenfrequency of the piston, takes place on the 1st order and is therefore not fast enough to break the cycle.

by: Roger Keller – BURCKHARDT COMPRESSION

To avoid this problem, either the eigenfrequency of the frame or the piston needs to be increased. Since adapting the frame is not possible in this case, it was decided to increase the diameter of the piston rod from 75 mm to 90 mm.

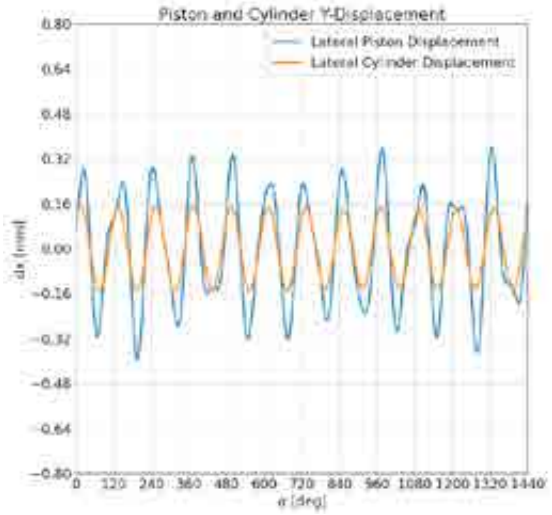

Figure 16: Increased piston rod diameter

In Figure 16 the piston and cylinder displacement is plotted for the increased piston rod diameter. It clearly shows how the eigenfrequency of the piston was moved away from frame excitation so that amplitude of the piston vibration is reduced by more than 30% and contact of the piston with the cylinder is averted.

4. Conclusion

The multibody simulation approach grants insights into dynamic interactions between compressor parts that would not be possible with standard analysis techniques. Based on the gained understanding of these phenomena, the compressor design can be optimized for a higher reliability and mean time between overhauls.

The presented edge zone white metal delamination of the main bearings can be avoided by bringing the rotational stiffness of the bearing support in line with the crankshaft. This may be achieved by a more flexible bearing support or a higher bending stiffness of the crankshaft.

The multibody simulation revealed that the excessive cylinder wear on stage three has its root cause in similar eigenmodes of the crankcase and the system of piston rod and crosshead near the 3rd order of the compressor. By increasing the frequency of the eigenmode of the piston rod the natural frequencies of the two parts are not matching anymore and therefore the excessive piston vibrations are reduced significantly.

References

[1] Blundell, Mike, Harty, Damian (2004) The Multibody Systems Approach to Vehicle Dynamics, Oxford, MA: Elsevier Butterworth-Heinemann, ISBN 0750651121

[2] ANSYS Mechanical Element Reference, Release 2022 R2, Ansys Inc, Canonsburg PA

[3] Goodno, Barry J, Geere, James M. (2013), Mechanics of Materials, Cengage Learning

[4] ANSYS Mechanical Substructuring Analysis Guide, Release 2022 R2, Ansys Inc, Canonsburg PA

[5] Becker, Ernst (1986), Technische Strömungslehre, Teubner Studienbücher, Stuttgart, Page 91 ff.

[6] ANSYS Mechanical Theory Reference, Release 2022 R2, Ansys Inc, Canonsburg PA, Page 784 ff.

[7] Siemens Flomaster Component Simulation Manual, Journal Bearings Heat Transfer Calculations, Flomaster Release 2020.1

















COMPRESSOR VALVES

HIGH PRESSURE • OILFREE • ENERGY SAVING

COMPRESSOR VALVES FOR YOUR GREEN FUTURE

- Hydrogen Mobility Market
- LNG Boil-Off Compression
- Renewable Natural Gas
- Synthetic Fuels
- Solar Panels
- CO_2 Carbon Capture

Hydrogen · Hydrogen FC · Technical Gases · Natural Gas · Boil Off Gas · Gas Storage · Gas Boosting · CNG

EXCELLENCE FOR YOU

COMPRESSOR **VALVES** • SINCE **1946**

COZZANI

www.cozzani.com

Compressor and valve challenges in energy transition: the experience on LNG and Hydrogen applications

by:

Massimo Schiavone, Andrea Raggi, Giovanni Ballerini
Dott. Ing. Mario COZZANI S.r.l.
Arcola (SP), Italy
info@cozzani.com

13th EFRC CONFERENCE
September 19th – 21st 2023, Zagreb

Abstract:
The climate change, as a result of greenhouse gas emissions and their impacts on human health and safety, has forced governments to change their way of thinking and to have more forward-looking views. Moreover, the unpredictable geopolitical scenarios push governments to reduce and diversify energy dependencies.
Energy and its transition towards more sustainable ways of production, transfer and consumption are part of a change process that is developing with several competing technologies.
This scenario led to an increase in LNG plants, investments in Biogas and addresses Hydrogen as the future energy vector. Each of these technologies brings new challenges to the processing systems.
This paper is focused on the specific technological challenges that compressors and its valves face in the applications that are characterizing the current energy transition. In particular, the valves have to face additional critical issues, such as low temperature (cryogenic applications), high pressures (up to 1000 bar), absence of lubrication, risks of Hydrogen embrittlement, and the presence of capacity control systems.
The paper addresses the above challenges for the compressor valves and describes some experiences and solutions achieved starting from the compressor and valve design up to the complete installation on site.

by: Massimo Schiavone, Andrea Raggi, Giovanni Ballerini – COZZANI

1. Introduction

The climate change due to greenhouse gases has an impact on the ecosystems and environment, as well as the air pollution affect the human health. Both phenomena forced Countries and Governments to change the way of thinking and take actions.

The result of this is the deployment of new strategies that break the energy dependence on traditional fossil fuels. However, in the short and medium terms the transition requires to rely on fossil energy sources which are polluting sources. Europe is diversifying the supplies, both importing LNG (Liquefied Natural Gas) and supporting the production of biomethane which is made by compostable wastes.

Green power supplies from photovoltaic and wind power offer a great potential to reduce greenhouse gases, pollution and are widely available worldwide; however, these require a scalable solution to store energy. To overcome this challenge hydrogen is deemed to be the energy vector that will be needed.

Hydrogen has an endless availability since it can be made from water, and it can store energy without the need to rely and to mine fossil materials as Lithium. Hydrogen may become the main energy vector and energy storage together with electric batteries. In addition to that, the growth of hydrogen production and transport technologies allow hydrogen to become more competitive with respect to fossil fuels.

The production of hydrogen from renewable energy sources is to be considered the ideal solution, because in none of the phases of production, transport, and conversion into electric energy or combustion, polluting molecules are created.

This article describes the role of reciprocating compressors and their valves in biogas, LNG and H2 production and supply chain. Diaphragm compressors, piston compressors, and hydraulic compressors play a key role because are the only technological mean to compress Hydrogen high enough to make distribution and usage efficient and practicable.

2. Biogas and Bio-methane

2.1. Gas and process description

Biogas is a gas mixture made by compostable material decomposition (as vegetal biomasses, food wastes, animal wastes, and so on) that occurs thanks to bacterial agents that work in an anaerobic environment. Biogas is composed of 40-60% methane (CH_4), 30-50% carbon dioxide (CO_2), 2-5% hydrogen (H_2), plus traces of other substances such as hydrogen sulphide (H_2S).

Biogas production may occur within an industrial process with specific industrial plants called "anaerobic digestors" in which certain conditions of anaerobic, humidity, pH and temperature are maintained.

Biogas can be used for the production of electricity and heat in special cogenerators. It can also be desulphurized, dehumidified and purified, in order to separate the methane from the other gases that make up the biogas mixture. From the separation of the gaseous elements that make up the biogas derive different solutions for use, such as methane (CH_4) and Carbon Dioxide (CO_2)

Methane (CH_4) – Biomethane can be used and transported in either gaseous or liquified form as it is for natural gas. Biomethane is very similar to fossil methane, so that methane can be replaced by biomethane in most of the final applications: heating systems, cooking gas, cogeneration plants, CNG propelled vehicles and ships, and so on.

Carbon dioxide (CO_2) – Carbon dioxide is used in the food industry as well as for carbonic fertilizers where the increase of CO_2 concentration increases the photosynthesis efficiency.



Figure 1 From Biogas producers to its consumers.

If biomethane is used in gaseous form, then reciprocating compressors can be used to raise the pressure to feed it in pipelines and in the national grids. It can also be compressed to fill cylinders and tanks for vehicles. In case it is liquified (Bio-LNG) reciprocating compressors are also used to carry out the process of storage and transfer, as shown in Figure 1.

2.2. The challenges for valves and solutions

Biogas, due to the way is made, may be a dirty gas, with the probable presence of H_2S and water, which are carried and compressed in the first compression stage. The contaminants may be mixed in the gas phase or can be melt in the water dragged by the gas during compression. These can cause fouling and corrosion, hence causing efficiency loss or even failures. In addition to that, solid particles may also be present and cause failures. In the Figure 2 is shown a suction valve that presents fouling, dirt on both the sealing surfaces and springs.

by: Massimo Schiavone, Andrea Raggi, Giovanni Ballerini – COZZANI



Figure 2 Dirt and fouling on springs and valve sealing surfaces, of a valve used in a biogas plant.

An effective protection of the compression system is a key aspect to ensure a reliable plant operation. In the unlikely event of failure of the compressor, the propagation of contamination has serious consequences.

For these applications, the valves in Figure 3 need to be designed accurately with a series of features. For instance, the use of specific thermoplastic sealing elements makes the sealing element more resilient to the impact of solid particles carried by the gas, and structural integrity is higher with respect to metal sealing elements.



Figure 3 A Typical plate valves (PDL) for low-medium pressures - B Ring valves (CP) for high pressure application - C Metallic particles ingestion by a thermoplastic plate

An additional feature is the use of shaped sealing elements: these elements not only enhance the overall compressor performances by lowering losses (Figure 4), but their internal aerodynamics reduces fouling and deposit of dirt and particles inside the valve.

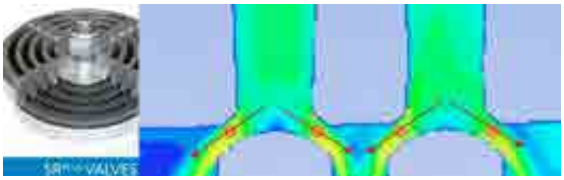

Figure 4 Particles flow easily go through the passages of a high efficiency valve.

The second aspect concerns the gas composition. The valve material in this case must be selected so as to avoid chemical attacks due to the presence of H_2S, which may initiate pitting and stress corrosion cracking phenomena both on the bodies and on the internal parts. The use of materials in accordance with ISO 15156-3 (NACE) for the valve bodies and springs and choosing thermoplastic shutters -where possible- allow the supply of reliable solutions.

3. LNG

3.1. LNG and Small Scale LNG

LNG is an economic and efficient solution, capable of reducing significantly emissions from heavy transport, sea and rail transport -if not electrified- compared to other fossil fuels.

LNG is a natural gas condensate which makes possible to reduce the volume by 600 times and to store it and transport it easily on methane tankers, without the need of gas pipelines. Once at its destination, before being introduced into the national pipeline network, the liquefied natural gas must be re-gasified, i.e. brought back from liquid to gaseous, in special plants.

In road transport, the use of LNG by trucks and coaches allows a significant reduction of local pollutants: it guarantees a reduction of more than 90% of NO_x emissions compared to Euro IV diesel vehicles, and between 40% to 60% when compared to Euro VI diesel vehicles. The ammonia emissions of LNG-powered vehicles are negligible and the levels of polluting particles produced are lower than those of diesel vehicles, even without the use of particulate filters.

Furthermore, by using Bio-LNG, CO_2 emissions can be further reduced and -in some circumstances- can be below zero (the net CO_2 production over the lifecycle is negative). For maritime transport, LNG is considered the most promising alternative fuel in the short and medium term and Bio-LNG can become a long-term solution. To take advantage of these benefits, it is essential to upgrade the infrastructures, with particular attention to the adaptation of regasification terminals, as well as the construction of micro-liquefaction plants and the construction of LNG terminals.

"Small Scale LNG" (or SSLNG) is defined as the method by which natural gas is managed directly in liquid form. When we talk about the liquefied natural gas (LNG) chain, we usually think of the supply of gas in liquid form to then be re-gasified in dedicated terminals to be fed into the methane pipelines.

We can therefore summarize the LNG chain in four main phases:

1. gas extraction and production
2. liquefaction
3. transportation
4. re-gasification

by: Massimo Schiavone, Andrea Raggi, Giovanni Ballerini – COZZANI

When it comes to Small Scale LNG, the supply chain consists of only three phases (without 4. regasification) as the natural gas remains in liquid form and managed by special infrastructures equipped with storage that can supply: tankers or road tankers, ISO-container, LNG Bunkering vessels, shuttles, railway tank cars, and vehicle refuelling stations powered by LNG or CNG (see Figure 5)

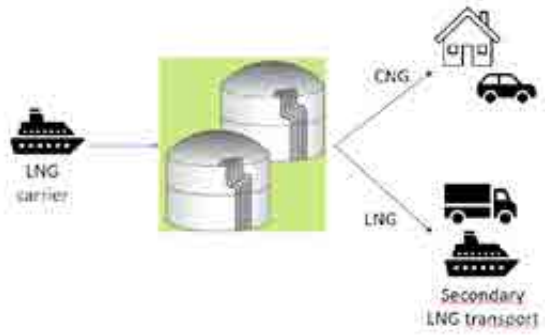

Figure 5 The presence of LNG terminals in the LNG supply chain

Liquefied natural gas can be distributed to fuel refuelling stations for supplying heavy transport vehicles, railway or naval, or to industrial plants or small gas distribution networks not connected to the gas pipeline network.

There are two main services performed by the compressors in this type of plant:

• Boil-off gas (BOG)

• Refrigerant gas

BOG Compressor

The gaseous LNG obtained by evaporation due to the heat coming from the environment around the tank is referred to as boil off gas (BOG). BOG is conventionally pressurized with compressor and then sent as city gas or fuel for power generation, as shown in Figure 6.

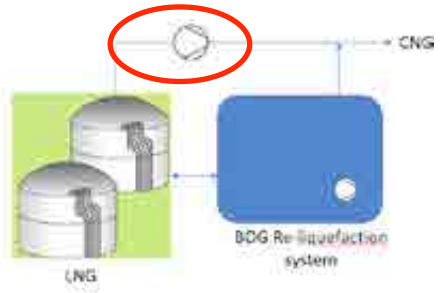

Figure 6 Process scheme with evidence of the BOG compressor

Refrigerant gas

The nitrogen expansion cycle is typically used in SSLNG distribution, as it allows the reduction of flammable gases and of the process and operational complexity. By using nitrogen as the refrigerant gas, the need for recovery lines towards the flare is also eliminated. Given the variability of operating conditions, flow control systems allow the end user to have stable processes.

3.2. The challenges for valves and solutions

In the section of the plant where the BOG is processed there are machines for the compression of methane and of the refrigerant gas required for re-liquefaction (typically nitrogen). The quantity of gas to be compressed is variable and is linked to the environmental and operating conditions of the entire storage site. This characteristic determines the need to dynamically control the flow of gas processed by the compressors dedicated to this purpose. In this context, for a plant in which it was necessary to control the flow rate of nitrogen and BOG to be processed, two stepless flow control systems can be supplied for each service which exploit the principle of the reverse-flow regulation of the flow rate to be installed on compressors also equipped with a bypass valve.

Both the bypasses and the regulation systems make it possible to control the flow rate of the gas to be processed but with different repercussions in terms of power absorbed by the compressor. By transferring part of the compressed gas from the outlet of the final stage of the compressor to the first stage suction vessel with the bypass, the machine will always be kept in operation at full load and the absorbed power will be constant regardless of the flow rate required by the process. With stepless reverse-flow control systems, the amount of processed gas is modified by acting on the closing angle of the suction valves, reducing the flow rate with respect to the full load value. By adopting this methodology, only the gas that must be compressed is processed by the compressor and together with the flow rate, the absorbed power will also be reduced.

The principle of stepless reverse-flow control of the flow rate ensures that a suitable actuation system intervenes on the suction valves, by keeping them open for a portion of each compression cycle. By implementing this methodology, the components of the valve unloading system and the intervention of the latter on the sealing elements of the valves will occur with a frequency coinciding with the number of revolutions of the compressor. The number of actuation cycles is therefore not comparable with that which must be guaranteed by normal pneumatic ON-OFF unloading systems. All components subjected to the stress resulting from actuation have been of an appropriate design both in terms of geometry and in the selection of materials, in order to ensure the functionality and the reliability of the valves (valve with special design shown in Figure 7).

by: Massimo Schiavone, Andrea Raggi, Giovanni Ballerini – COZZANI



Figure 7 Valve for High frequency actuation.

Electromechanical stepless control systems for both Nitrogen and BOG control have actually been delivered to carry out the service described. Since commissioning the behaviour of each of the two compressors (Nitrogen and BOG) equipped with the reverse-flow control system was analysed confirming the effectiveness in adapting to the different plant conditions.

Once the machines have been put into production, supervision and any assistance needs have been ensured by a remote assistance system (Figure 8) integrated in the flow control system which allows you to check their status and perform the main diagnostic activities. The system gives the possibility to offer support immediate to the customer in case of need.

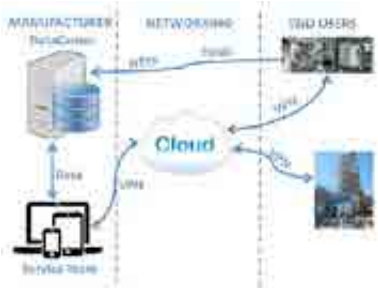

Figure 8 Architecture of the remote control module for Electromechanical stepless capacity control systems

After a significant period of use, the history of the signals that determine the required flow rate with the regulation system for each compressor was analysed. The absorbed power and the energy saved by using the reverse-flow control system could be calculated and also be compared to the bypass-valve option. The calculations can be carried out by processing the historical operating data and using simulation software dedicated to study the behaviour of the compressor as the degree of regulation varies.

Nitrogen compressor



Figure 9 Flow control system actuators installed on N2 compressor

Working gas:	N_2
Motor power:	2100 kW
Compressor capacity	35678 kg/h
Number of stages:	2
Pressure:	8 – 21 – 37 [bara]

Table 1 Main data for N2 compressor

The graphs in Figure 10 show some of the trends of the indicated cycles acquired with the compressor at full load and with two different degrees of regulation. These data acquisitions have been carried out during the system commissioning.

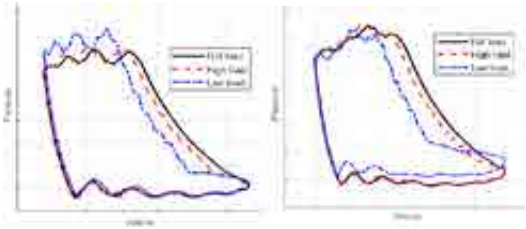

Figure 10 N_2 compressor indicated cycle under different load conditions (first and second stage)

By analysing the operating conditions and the trend of the flow actually processed by the compressor, it was possible to determine that the power of the indicated cycle underwent an average reduction of 12.4% compared to the full load value. Considering that the latter is equivalent to 1744kW and assuming the compressor is running for 8000 hours / year, a power reduction of 217kW and an energy saving of 1736MWh are obtained.

BOG Compressor

Working gas:	CH_4
Motor power:	710 kW
Compressor capacity	3483 kg/h
Number of stages:	3
Pressure:	1 – 4 – 10.5 – 26 [bara]

Table 2 Main data for BOG compressor

by: Massimo Schiavone, Andrea Raggi, Giovanni Ballerini – COZZANI



Figure 11 Flow control system actuators installed on BOG compressor

The graph of Figure 12 shows the trends of the indicated cycles acquired with different degrees of regulation in the system commissioning.

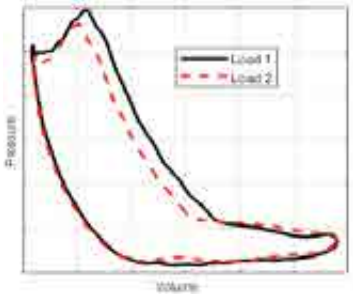

Figure 12 BOG compressor indicated cycle under different load conditions

By analysing the operating conditions and the trend of the flow actually processed by the compressor, it was possible to determine that the power of the indicated cycle underwent an average reduction of 11.7% compared to the full load value. Considering that the latter is equivalent to 554.9kW and assuming the compressor is running for 8000 hours / year, a power reduction of 65.1kW and an energy saving of 521MWh are obtained.

4. Hydrogen

4.1. The hydrogen supply chain

The growing attention towards hydrogen is due to some of its characteristics: it is a light gas with a high energy content per unit mass, it can be produced on an industrial scale, it is easier to store than electricity, and that it can be used to produce clean energy. Hydrogen, in fact, does not produce carbon emissions such as CO and CO_2 when it is burned. If produced from renewable sources, green hydrogen contributes to reduce significantly CO_2 emissions in industry and transport. Therefore, it will play a key role in the success of the global energy transition.

The versatility of this gas also allows an efficient seasonal accumulation of electricity, making it possible to make extensive use of renewable sources. Hydrogen ensures the transfer of the energy produced to other sectors and regions efficiently: for example, transmitting energy over long distances by transporting hydrogen by sea or by pipeline can be more convenient than transmission via high voltage power lines of the electricity grid. The hydrogen supply chain is facing a huge opportunity. Engineering technology and plant engineering are ready to support the transition. The component manufacturers are also moving fast and it can be said that some manufacturers are ready to supply "hydrogen ready" components.

The hydrogen business of "tomorrow" will see the use of this gas for energy generation, through various possible alternatives linked to its philosophy of use. In fact, the gas can be:

i. injected into the network to create a blend to burn instead of the current methane (compression of the blend from atmosphere to a final pressure between 20 and 80 bar is required). This is a typical application for reciprocating piston compressors.

ii. stored for future use or transport on wheels (pressures around 200-350bar). These tanks are filled using both piston and diaphragm compressors, depending on the level of flow and cleanliness of the gas required

iii. used in fuel cells, both for the local production of electricity using reversible power to power (P2P) fuel cells, and in the automotive sector (pressures around 1000bar in both cases). For the last stages of compression that reach these pressures, both diaphragm and hydraulic compressors are used. The former with higher rotational speeds and flow rates, the latter with very long strokes, low rpm and limited flow rates. The hydraulic compressors offer a more convenient cost/scalability ratio.



Figure 13 *Reciprocating compressors within hydrogen supply chain[2]*

4.2. The challenges for valves and solutions

Emerging applications, aimed at compressing hydrogen to use it as an energy source, have led to new challenges regarding the design of automatic valves for reciprocating compressors by combining the already existing supply chain requirements with additional features such as:

by: Massimo Schiavone, Andrea Raggi, Giovanni Ballerini – COZZANI

i. high operating pressures (up to 1000bar);
ii. non-constant (intermittent) services and variable operating conditions;
iii. high levels of cleanliness (non-lubricated applications);
iv. materials compatible with the mixture to be compressed with particular attention to avoid hydrogen embrittlement phenomena.

What makes the hydrogen application unique is the need to simultaneously satisfy all the indicated requirements. In particular, the valves are required to withstand the required pressure level, in variable compression ratio and operating conditions, in non-lubricated services, and to ensure a considerable number of operating hours.

Thanks to more than 75 years of experience in the refining sector, a strong specialization has been developed in company to design and manufacture valves and its components for reciprocating compressors. These parts are used throughout the hydrogen supply chain, and such knowledge comes both from by transferring experiences and technologies from other compression fields, and by overcoming new technological challenges, which have now become standard in hydrogen applications. In fact, the products selected for new applications and compressors under development, have often been in operation for more than a decade.

Significant experiences in this sector are presented below, defining the design challenges to be faced in the field of reciprocating compressor valves.

4.2.1. Oil free applications

The request of clean compressed hydrogen at medium and high pressure can be fulfilled adopting oil free solution.

Membrane compressor has high compression ratio (till 1:20) and the temperatures reached do not permit the use of thermoplastic sealing element, neither thermoplastic guide for metallic rings. In those cases, the valve design is entirely metallic and the sliding friction effects are not negligible. As shown in the Figure 14, the wear can be high, due to the absence of lubrication requested for the process cleanliness.



Figure 14 Worn guide ring

In the Figure 15 a metallic guide ring wear level has been shown, for an H2 oil free application of 120bar and 450rpm.

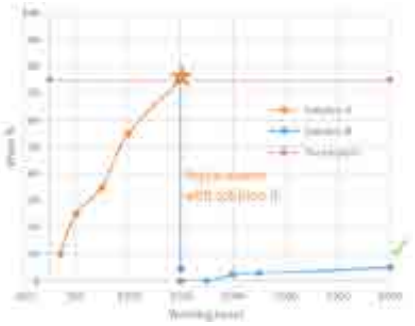

Figure 15 Wear percentage vs working hours.

Solution “A” valve made of treated stainless steel, has been replaced when the wear reached the threshold of 75% of its maximum allowable value. The new solution implementation (Solution “B” in blue colour, in the Figure 15) shown that the use of proper treatment permitted a significant wear reduction, to a negligible level compared to the threshold imposed, allowing the valve to reach properly the MTBM scheduled.

All this has allowed the company to build a broad background necessary for the valve designs required by new applications. Since the early 1980s, the company has also been operating in other sectors for the compression of clean hydrogen at pressures of around 400bar up to 1000bar. They are applications in niche markets, with valves for diaphragm compressors, allowing the accumulation of experience in this sector as well.

4.2.2. Compression from electrolysers – proper material selection

In electrolysers, an electric current is passed to split water molecules into hydrogen and oxygen. The cell is the core of the electrolyser in which this process takes place. The cell is equipped with two electrodes, which are immersed in an electrolyte separated by a membrane. The water splits into oxygen and hydrogen at the electrodes, while the membrane separates these product gases. The membrane keeps the two gases separate during the splitting process by directing the oxygen out. However, gas cross-overs can occur right on the membrane. The hydrogen produced during electrolysis typically contains high levels of moisture and varying amounts of oxygen, which must be removed to produce high purity hydrogen. This is necessary to meet gas quality specifications, for example for compressed hydrogen in downstream applications such as filling stations.

In most electrolyser applications, as shown in Figure 16, the gases produced are saturated with water. Because water vapor neither burns nor carries energy, dehydration is required to effectively transport, store, and use the hydrogen produced during electrolysis.

by: Massimo Schiavone, Andrea Raggi, Giovanni Ballerini – COZZANI

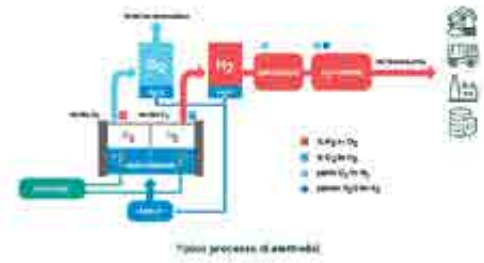

Figure 16 Electrolysis and H2 drainer(source: [5])

The compression of hydrogen at ambient pressure or at relatively low pressures (some types of electrolysers can reach around 30 bar) on the valve side are not in themselves critical, as there are valve types that have been validated over the years in this sector at these pressures.

The novelty of this application lies in the fact that the hydrogen is obtained by electrolysis and suitably drained. The various dryers eliminate the excess moisture from the gas, but it must always be taken into account that the gas may still be saturated with H_2O at the drainer outlet.

As known, the H_2 embrittlement phenomenon is originated by the ease of diffusion of the hydrogen molecule H_2 into the metal microstructure, due to its dimension. The embrittlement is related to the molecular hydrogen accumulation at the dislocation feet, making them stiffer. This stiffening promotes the quick activation of the break-systems and the sudden steel failure. The threshold to move the dislocations can be so high to have a failure without relevant plastic deformation. Condensation and humidity can facilitate the hydrogen accumulation described, in which molecular hydrogen diffuses inside the material structure.

Intermittent service, and therefore the cooling of the gas inside the compressor, can cause the formation of condensate and, if the material of the valve parts stressed is not suitably compatible, damages linked to H_2 embrittlement could be triggered.

The guidelines available within the regulations to date are not yet exhaustive (think, for example, of the EIGA directives or the series of EN 19880 standards). For this reason, a research has been carried out to select the materials that are compatible with the application, and that have acceptable mechanical characteristics for use in conditions of high operating loads.

A second aspect of this service, always related to the formation of condensate inside the machine, is the possibility that in the first instants of switching on the compressor is found to displace not only gas but also a portion of condensate, liquid, incompressible which can cause non-negligible problems with the valves, typically of the intake, damaging the valve major components (such as the bodies, seat or stud), even leading to the complete component failure. For this reason, it is important to always check the moisture content in the process and verify that the drainers are working properly[5].

4.2.3. Fuel cells – High pressure oil free applications

For an efficient use of H_2 inside a fuel cell, whether it is used for automotive purposes (Figure 17) or for the generation of electricity, a very high gas pressure is required, around 900 – 1000 bar. Compressors capable of reaching these pressures, similarly to the CNG service, are characterized by strong intermittence, linked to the demand for fuel, and require a high level of purity and cleanliness of the compressed gas. As previously indicated, compressor operators typically adopt two types of compressors for the last stage of compression that reaches these pressures, diaphragm, or hydraulic compressors.

Cylinder valves for this application face the same challenges previously presented (oil free application with materials suitable for H_2 service) in addition to the very high working pressure.



Figure 17 Typical scheme for car refueling

A diaphragm compressor case

The company has been operating in the valves sector for diaphragm compressors aimed at hydrogen compression since the 1980s. Initially, the typical pressures were around 400 bar with a rotation speed of about 400 rpm and, obviously, in the absence of lubrication. The first applications in the 1000bar hydrogen compression sector date back to 2010, in the Korean market, for which the development of a compression system for car refuelling was entrusted to the leading compressor operator on the local market, KwangShin.

KwangShin designed H2 compressor for fuelling station, as Korean government project since 2009, starting from low pressure hydrogen, through medium pressure tank and trailer storage, to high pressure compressors for various fuelling station up to 1000bar.

For the latter case, the characteristics of the selected compressor (Figure 18) are [4]:
-Type: membrane;
- Oil-free;
- Suction pressure range: from 50 to 110barg;
- Delivery pressure: 870 barg;
- Capacity range: 16 to 40 kg/h;

by: Massimo Schiavone, Andrea Raggi, Giovanni Ballerini – COZZANI



Figure 18 Compressor - courtesy of KwangShin Machine Industry Co., Ltd

On the valve side, based on the specification shown, it was necessary to adopt a solution that satisfied both the structural requirements, the given the pressures, and oil-free operation at the speed indicated. The valve design adopted for this application fell on an all-metal solution (see *Figure 19*), guaranteeing both operating characteristics under operating conditions (see the variability of the first stage inlet pressure and consequent flow rate) and characteristics of the materials used, adopting materials with:

- high mechanical resistance;

- high resistance to wear and impact from parts in relative motion;

- suitability for H_2 service (resistance to H_2 embrittlement phenomena).



Figure 19 Some valves for diaphragm compressors

Thanks to the research on the materials mentioned in the previous chapter supported by FEM analyses (*Figure 20*) for the verification of the fatigue life of the stressed components, excellent results have been obtained both in terms of performance and duration of the valve.

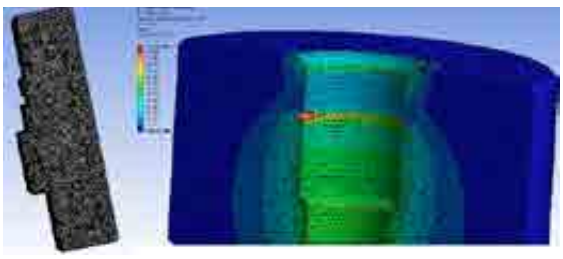

Figure 20 FEM analysis

After the first application, the positive outcome of all the tests allowed the compressor manufacturer to serialize this type of compressor. The Korean market alone, at the end of 2022, had 63 active compressor stations (as *Figure 21*), with supplies only in the last two years of about 750 valves.



Figure 21 Two diaphragm compressors for an H2 filling station courtesy of KwangShin Machine Industry Co., Ltd

Hydraulic compressors

Automatic valves are also used for hydraulic compressors. Also, in this sector the know-how and the experience accumulated on machines typically for the compression of CH_4, N_2 and H_2 up to 400bar has made it possible to extend the applications up to 1000bar.

Hydraulic compressors are characterized by long strokes and very low rotation speeds. In this case, the valves can be housed both inside the compressor head, in a standard housing, and outside, directly on the suction and delivery pipes. The additional dead volume due to this second installation is however negligible compared to the compressor displacement.

From the point of view of the type of valve adopted, the design challenges are very similar to what was seen previously for diaphragm compressors. The low rotation speed plays in favour of the reliability and duration of the products. The experience at higher rotation speeds than the hydraulic compressor, has therefore allowed the extension also to this type of compressor, of the solutions adopted on the diaphragm compressors.

An additional design challenge (see Figure 22) is introduced when the installation of the inlet and outlet valves takes place on the pipes, in this case further verifications are required, especially on the bodies, as these act as a portion of the pipe and therefore require subsequent verifications for compliance with the standards relating to pressure vessels (PED 2014/68/EU).

by: Massimo Schiavone, Andrea Raggi, Giovanni Ballerini – COZZANI



Figure 22 Typical valves for hydraulic compressors: on the left installed inside the cylinder head, on the right if installed in the pipeline

Further applications: hybrid compressors and non-return valves

Today some services require the availability of small plants for the entire production chain from water to high pressure hydrogen, as shown in Figure 23. Due to the need for these small plants, space-contained compressor trains are required. Thus "Hybrid" piston-diaphragm compression systems were born in which the first stages of compression suck in hydrogen at low pressure (typically between 7 and 20bar), raising it to 50 bar, where the previously seen diaphragm compressor intervenes, carrying the gas at final pressure.



Figure 23 Image from UNI 19880-1 small scale plant scheme.

In this case the valves are directly referable to the valves described in the previous paragraphs.

Downstream of the compressors, whether they are hybrid, membrane, hydraulic or piston, the non-return valves are required for the correct functioning of the systems. Also, in this case, the design derives from the experience gained from the applications seen and validated in the previously described sectors. In fact, considering that the suction and discharge valves can be mounted on the pipes of the hydraulic compressors, structural calculations have already been carried out on the bodies relating to the satisfaction of the pressure standards required for non-returns valves. The pulsating gas flow is already managed at the level of automatic cylinder valves, so by combining these designs it has been possible for the Company to introduce robust solutions to the market also for check valves.

5. Conclusion

This paper discussed the specific technological challenges that compressors and its valves face in the applications that are characterizing the current energy transition, such as Biogas, LNG, and Hydrogen. Each application is characterised by issues to be addressed by valves and compressors, such as low temperature, high pressures, absence of lubrication, hydrogen embrittlement, and also the use of stepless capacity control systems.

The biogas, once separated into the main components (CH4 and CO2), is treated as natural methane, compressing it to introduce it into the distribution network or through liquefaction plants it can be transported in liquid form. In both cases the compression systems are characterized by the presence of contaminants and solid particles.

The paper shows how the use of thermoplastic and shaped sealing elements that allow the valves to tolerate impurities by incorporating them and thus ensuring the operational continuity of the compressors. Furthermore, the use of Nace compliant materials ensures the functioning of the valves even in the presence of corrosive elements, such as H_2S.

In LNG plants the presence of compressors is essential to ensure two services: BOG and reliquefaction. These systems require flow control systems to maintain operation condition while saving energy. The use of electromechanical flow control systems requires suction valves dedicated to high-frequency operation, which have been specifically developed to cope with high frequency forcing of opening.

The distribution of hydrogen relies on different types of compressors such as reciprocating, membrane or hydraulic. Hydrogen introduces challenges related to the wear of the valve elements due to the total absence of lubrication (oil-free compressors) which are faced using appropriate validated treatments. The selection of materials deriving from a dedicated research program ensures resistance to hydrogen embrittlement phenomena.

Hydrogen for automotive purposes, requires considerably higher pressures compared to the CNG ones, therefore the design of the valves must be specific, with exclusively metallic sealing elements, materials and assembly solutions dedicated to such heavy use.

In conclusion, the long experience gained in CNG and hydrogen compressors and the transfer of technologies between similar areas has allowed the company to develop know how and a series of products for all areas of the energy transition, both in relation to compressor valves and flow control systems.

Some of these technologies and products have been in operation in plants for more than ten years, a sign that the ecological transition towards hydrogen and also reciprocating compressors for biogas, LNG can rely on valves and systems of high levels of technology readiness.

by: Massimo Schiavone, Andrea Raggi, Giovanni Ballerini – COZZANI

6. Bibliography

[1] Hydrocarbon processing - Choose the best refrigeration technology for small-scale LNG production - Jan 2014
[2] Hydrogen compression – boosting the hydrogen economy,EFRC group, November 2022
[3] Chimica Magazine speciale idrogeno
[4] KwangShin Machine Industry co. Ltd "diaphragm compressor datasheet"
[5] Panametrics products flyer

TECHNISCHE UNIVERSITÄT DRESDEN

Reversible operation of a reciprocating compressor as an expansion machine

by:

Christian Stöckel
Bitzer-Professur für Kälte-, Kryo- und Kompressorentechnik
christian.stoeckel@tu-dresden.de

Konrad Klotsche
Bitzer-Professur für Kälte-, Kryo- und Kompressorentechnik
konrad.klotsche@tu-dresden.de

Christiane Thomas
Bitzer-Professur für Kälte-, Kryo- und Kompressorentechnik
christiane.thomas@tu-dresden.de

Technische Universität Dresden
Dresden, Germany

13th EFRC CONFERENCE
September 19th – 21st 2023, Zagreb

Abstract:
As part of a former EFRC research project carried out at Technische Universität Dresden[1], a new pneumatically force-controlled poppet valve was described enabling the reversible use of a reciprocating compressor as an expansion machine, e.g., for energy recovery from underground gas storage tanks during discharge. The general operation of such a valve was tested experimentally on a compressor in capacity control mode. The present paper deals with the experimental testing of a reciprocating compressor operated as an expansion machine. After a brief introduction regarding the valve system and the experimental compressor, the experimental setup is described. Subsequently, the results are discussed based on measured indicator diagrams. Finally, an outlook on further optimization potential in commercial applications is given.

by: Christian Stöckel, Konrad Klotsche, Christiane Thomas – TECHNISCHE UNIVERSITÄT DRESDEN

1 Introduction

1.1 General

One of the most effective actions for reducing CO_2 emissions to tackle the global warming crisis is saving energy. However, measures to increase energy efficiency are generally limited. Thus, another essential tool is the analysis of processes regarding the utilization of potential exergy sources. Exergy is thereby defined as the maximum proportion of the total energy of a system that can be converted into usable work in relation to the ambient state and is irreversibly converted into anergy during that process.

One energy-intensive but necessary process for securing the energy supply is the underground storage of natural gas (UGS). A constant gas supply over the year typically faces a varying seasonal demand. During summer, when less gas is required than supplied, gas is injected into underground caverns at high pressure using reciprocating compressors. In winter, the demand for gas is higher than the supply, so the gas is unloaded from the UGS and injected into the distribution network. While high amounts of electrical energy are used for pressurizing and storing the gas, only a throttle is used for unloading. The exergy of the pressurized gas dissipates. Thus, a significant optimization of the overall storing process would be utilizing the exergy in the pressurized gas.

Typically, expansion machines are used for recovering mechanical energy from pressurized gases. However, for economic reasons, purchasing an additional expander to increase the efficiency of a UGS is not reasonable. A more cost-effective approach is the utilization of the already existing reciprocating compressor, which is used for the loading process of the storage, as an expansion machine. The valves are a significant design difference between a reciprocating compressor and an expansion machine: In a compressor self-actuated valves are used, which are opened and closed automatically by the pressure levels within the machine. For an expander forced-actuated valves are necessary. An external force is needed to open and close the valves against the pressure differences inside the machine. A well-known concept for an externally controlled valve is an internal combustion engine's camshaft and valve stem system. However, for an existing reciprocating machine in the UGS which should be used both as a compressor and as an expander, a valve system is needed which can be used self- and force-actuated.

Stöckel et al.[1] presented a valve system that meets this task. A pneumatically force-actuated poppet valve was introduced that can be easily adapted to an existing machine without extensive compressor modifications. The compressor and existing pressure levels provide the pneumatic pressure to actuate the valve.

1.2 Summary of previous findings

Various ways to force a movement of a poppet valve without losing the ability to self-actuate have been discussed by Stöckel et al.[1], and a pneumatic force actuation was found to be the most promising concept since it can be quickly adapted to an existing machine. It is suitable for both suction and discharge valves. An electromagnetic slider valve is used for switching the pressure levels acting on the valve. The actuation pressure is supplied by the machine itself using additional piping. A CAD model showing the essential components of a pneumatically force-actuated discharge valve is shown in figure 1. Giving a first assessment of the controllability of the valves, a simple 0D-simulation was presented.

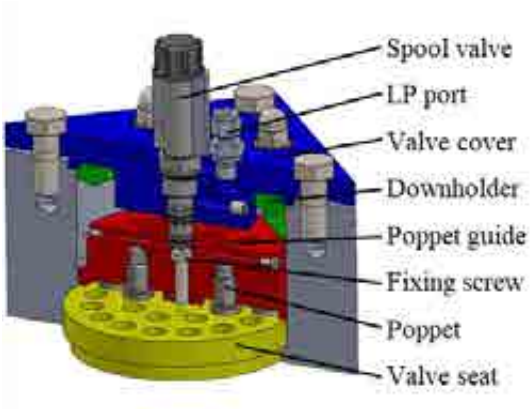

Figure 1: Basic design of pneumatically force-controlled discharge valve

Stöckel et al.[2] discussed the geometrical design parameters for the poppet valve assembly. It was found that when using typical clearance fits for guiding the poppet inside the valve lift limiter, there are only few influences on the poppet reaction speed on changing pressure levels and only minor differences in leakage. The volume where the pressure changes are applied, the poppet control chamber, significantly influences the controllability of each poppet. It should be designed as small as possible.

The evaluation of the flow coefficient of a prototype valve was presented by Stöckel et al.[3]. A flow test rig was used for experimental testing, and the achieved data was used to fit an existing flow coefficient correlation. The simulation model was enhanced with those results. Also, the switching speed of the electromagnetic slider valve for changing the actuation pressure was determined experimentally. Those delays are crucial for the programming of the controller for the reciprocating compressor.

Stöckel et al.[4] show the capacity control range of pneumatically force-actuated discharge valves in a test compressor. Additionally, it was found that the compression ratio and actuation time significantly influence the delay between the control signal input and valve movement. These observations were also gathered with the help of another test rig[5], which was

by: Christian Stöckel, Konrad Klotsche, Christiane Thomas – TECHNISCHE UNIVERSITÄT DRESDEN

set up for detailed studies of the valve behaviour. Finally, Stöckel[6] found that oil adhesion has a significant influence on the valve controllability, and a mathematical model was introduced to account for this effect in the simulation. Valve timing was predicted by simulation for both suction and discharge valves and compared to experimental results. A good agreement was found.

2 Test setup

2.1 General setup

An Atlas Copco AR1KT test compressor (figure 2) was used for the experimental verification of the functionality of the expansion mode of the new valve system. The nominal data are listed in table 1. To reduce the complexity of the system, the second stage and the crank end side working chamber of the first stage were taken out of operation.



Figure 2: Test compressor Atlas Copco AR1KT

The head end working chamber is equipped with two pneumatically forced suction (low pressure: LP) and discharge (high pressure: HP) valves. It must be mentioned that the mass flow inside the compressor is reversed in expander mode. Thus, the suction valve typically designed for a compressor is the outlet of an expander and the discharge valve is the inlet for the expansion machine. The direction of rotation of the crankshaft remains the same, which is also inevitable to drive the oil pump for the lubrication of the machine, which is directly coupled to the crankshaft. The relevant data on the valves are listed in table 2.

Table 1: Machine data of the first stage of the test compressor

Compressor speed	585 rpm
Suction pressure	1.0 bar_a
Discharge pressure	1.0 bar_a
Nominal flow	8.5 $m^3\ min^{-1}$
Piston diameter	285 mm
Stroke	150 mm
Piston rod length	295 mm

Table 2: Valve data

Number of valves	2 LP and 2 HP
Poppets per valve	24
Poppet mass	16.8 g
Poppet seat diameter	14 mm
Max valve lift	2 mm
Valve spring rate	350.0 N m^{-1}
Spring pretension	4 mm
Control chamber size	$49.1 \cdot 10^3$ mm^3

Two limitations of the compressor test field at Technische Universität Dresden had an important influence on the test setup. First, the injection of energy into the electrical grid was prohibited, so the machine was disconnected from the power supply to test the expansion mode. Since there was no energy sink for the power generated by the expansion of the gas, the machine had to be operated at a level where the converted energy was equal to the mechanical losses inside the machine. Thus, the machine could be operated in a stable operating point. A second constraint was the compressed air supply in the test field used to feed the expander. 50 g/s was the maximum mass flow which could be used without overloading the air supply network.

2.2 Valve control

The system for controlling the electromagnetic slider valve to switch the pressure levels for actuating the poppet valves was presented by Stöckel et al.[3]. A sensor detects the top dead centre position of the piston. Based on the assumption of a uniform rotational speed of the crankshaft, the actual crank angle can be predicted for each following time step. Thus, the slider valve positions can be set according to the requirements (figure 3). A personal computer processes the signals from the sensors and the control.

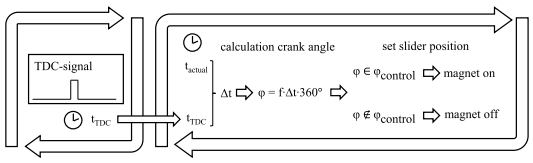

Figure 3: Control scheme for the slider valve actuation

However, due to the above mentioned limiting conditions, this prediction cannot be used to start the expander. On the one hand, only one sensor for the top dead centre is installed. Thus, the correct crank angle is only known when the piston is exactly in that position. On the other hand, the machine could not be started in compressor mode with the original crank angle prediction since the power supply to the electrically driven motor had been removed.

by: Christian Stöckel, Konrad Klotsche, Christiane Thomas – TECHNISCHE UNIVERSITÄT DRESDEN

Thus, an optical cam was used to switch the electromagnetic sliders both for the inlet and the outlet valves. Reflector tape was applied to the axial face of the flywheel in the angular region where power has to be supplied to the high-pressure side slider valve. A photoelectric sensor faced the reflector tape at the top dead center position of the crankshaft. When the reflector tape passes the sensor, an electrical relay is switched, powering the slider of the inlet valve. The power supply of the slider of the outlet valve is simultaneously turned off. When the photoelectric sensor detects no signal, the slider of the outlet valve is powered, and the inlet slider valve is turned off. Essentially, this valve control system directly couples the inlet and outlet valves. A schematic drawing of the modified slider valve control system is shown in figure 4.

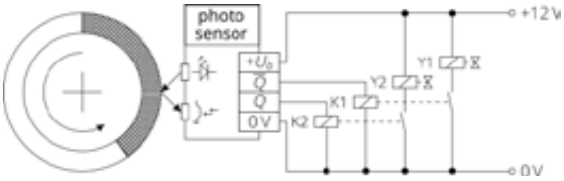

Figure 4: Optical cam for control of the electromagnetic slider valves

2.3 Instrumentation

Static pressure probes were used to measure the mean inlet and outlet pressure. Additionally, fast-reacting piezo-resistive pressure probes have been applied to the inlet and outlet chamber, compression respective expansion chamber and the poppet control chamber of one of the high-pressure valves. Furthermore, one single poppet of the instrumented high-pressure valve was observed using an eddy-current sensor. Thus, in addition to the pressures, the time-dependent valve lift could be measured. A pressure regulator was used to set the inlet pressure.

2.4 Measurement of the rotational speed

Due to the above-described unfavourable boundary conditions of the test field, the flywheel installed on the compressor cannot equalize the non-uniformity of the rotational speed during one crank rotation. Thus, for further evaluation of the measurement results, which are recorded with a fixed sample rate, the crank position and the angular speed needed to be ascertained in dependency of the time.

Since no crank angle sensor was installed, the angular speed was determined by evaluating corresponding marks on the flywheel with a video camera. Afterwards, the flywheel position and, thus, the crankshaft position could be evaluated by the comparison of the time stamp of the video frame and mark in the video frame. The time difference between the two video frames was 33.425 ms, and the mark was applied every 22.5° crank angle with a width of +/-2°.

3 Results and Discussion

3.1 Rotational speed

The progression of the rotational speed over the crank angle is shown in figure 5. 17 subsequent shaft rotations have been used for calculating the mean value and the standard deviation. The crankshaft accelerates from 0° up to 135° crank angle to a maximum rotational speed of 1.04 s^{-1}. During this phase, pressurized air enters the working chamber and is expanded, which leads to the energy transition to the piston. Afterwards, the speed decreases again to 0.73 s^{-1}, caused by the energy consumption due to friction inside the machine and the ejection of expanded gas through the outlet valves. In addition, overexpansion occurs in the working chamber, which can be seen later from the indicator diagram.

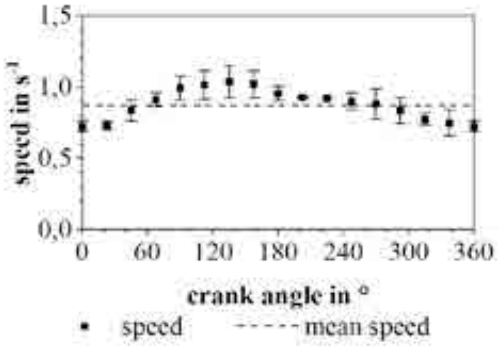

Figure 5: Rotational speed during expansion mode over one crank rotation

Minimum and maximum speeds lead to a mean speed of 0.89 s^{-1} and a degree of non-uniformity of nearly 1/3. Following Küttner[7], for a compressor, the value should be about 1/30 to 1/20, and for a three-phase generator, about 1/300. Different options are available for an enhancement:

- Load on all working chambers
- Independent control of inlet and outlet valve
- Installation of a flywheel with a higher moment of inertia

3.2 Operation with optical cam

Figure 6 shows the pressure curves in the working chamber and the control chamber of the inlet valve (HP), as well as the movement of a single sealing element in the inlet valve as a function of the crank angle. The inlet valve (HP) is actuated until a crank angle of about 60°, as can be recognized by the pressure change within the HP control chamber. The inlet valve closes shortly after reaching the high-pressure level in the HP control chamber. A delay of about 5° caused by oil adhesion can be seen. At about 70° crank angle, the inlet valve is completely closed, and the cylinder pressure decreases until the 105° position. The outlet valve (LP) has opened, and pressure equalization between the outlet chamber and cylinder occurs. At about 330° crank angle, the pressure levels within the control chambers are

by: Christian Stöckel, Konrad Klotsche, Christiane Thomas – TECHNISCHE UNIVERSITÄT DRESDEN

switched again by actuating the electromagnetic slider valves. The pressure level in the HP control chamber is decreasing again, and the cylinder pressure is increasing. At about 345° crank angle, the inlet valve is opening again. At that point, the pressure difference between the HP control chamber and the cylinder is about 0.35 bar.

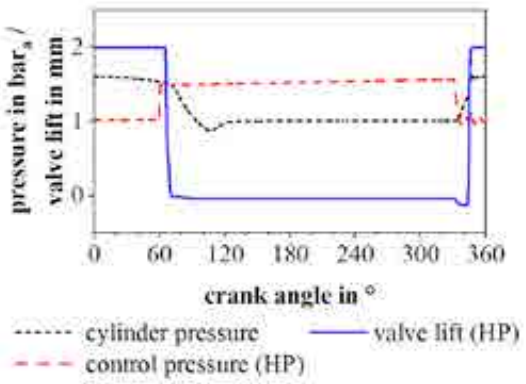

Figure 6: Pressures and valve lift for the test of expansion mode with control by an optical cam

The p-V-diagram of the described test run is shown in figure 7. A large area of under-expansion, means lower than the low pressure level, of the gas within the cylinder begins at about $6.5 \cdot 10^{-3}$ m^3. This "negative loop" decreases the amount of internal work which can be transmitted to the crankshaft and leads to an additional decrease in rotational speed. Another negative loop can be seen at the top dead centre position (lowest displacement). The high pressure level is reached to early. However, in this position, the negative influence is much smaller.

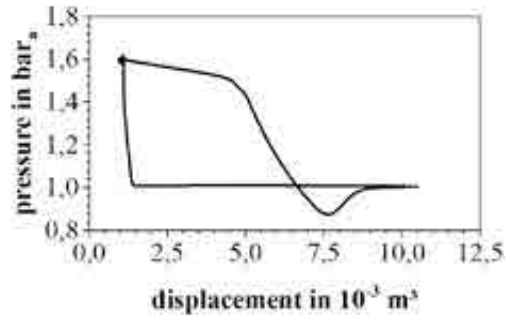

Figure 7: p-V-diagram for the test of the expansion mode with control by an optical cam

The area within the p-V-curve represents the indicated work. It was calculated to 295 J, meaning 263 W of indicated power at a mean rotational speed of 0.89 s^{-1}. Since the machine was operated at a constant operating point and no energy was transferred from the motor to the electrical grid, the internal work corresponds to the mechanical losses of the machine.

3.3 Operation with individual valve control

After the machine was started with the optical cam and running at a constant operation point, the PC control could be used to switch the slider valves individually. Beginning with the known timing from the optical cam, the actuation angles were carefully changed to remove the negative loops from the p-V-diagram. Already small changes in timing significantly influence the stability of the operation point in terms of flow rate, inlet pressure and especially compressor speed. The data of one stable operation point is shown in figure 8 and figure 9.

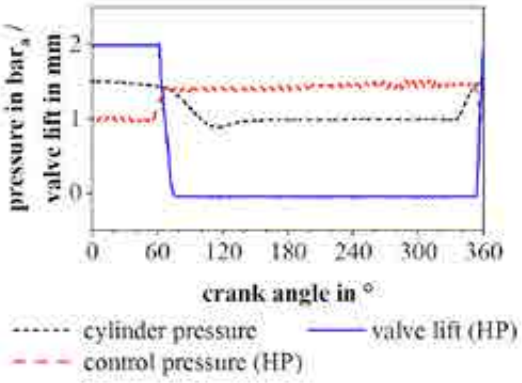

Figure 8: Pressures and valve lift for the test of expansion mode with manual PC control

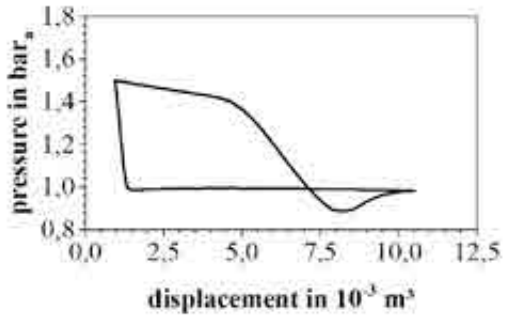

Figure 9: p-V-diagram for the test of the expansion mode with manual PC control

As can be seen, the closing of the outlet valve was moved to a position where the cylinder pressure meets the high-pressure level at the top dead centre (360°). Thus, in the p-V-diagram, the negative loop at the smallest displacement could be removed. However, it was impossible to move the closing position of the inlet valve to a much higher crank angle to remove the big negative loop in the p-V-diagram at the highest displacement (bottom dead centre). Setting a later closing position led to a significant decrease of the pressure on the high-pressure side. Although the compressed air supply from the test stand's supply network was sufficient, the piping to the compressor had too many losses to have an adequate air supply.

by: Christian Stöckel, Konrad Klotsche, Christiane Thomas – TECHNISCHE UNIVERSITÄT DRESDEN

3.4 Comparison to simulation results

The boundary conditions from the experimental tests of the expansion mode with the optical cam were used for a simulation with the model described by Stöckel[6]. A crank angle resolution of 0.01° was chosen to avoid fluctuations in the calculation caused by too small mass flows, and a constant rotational speed of 0.89 s^{-1} was set. Oil adhesion of the poppets was additionally taken into account. A comparative chart between simulation and test results can be found in figure 10.

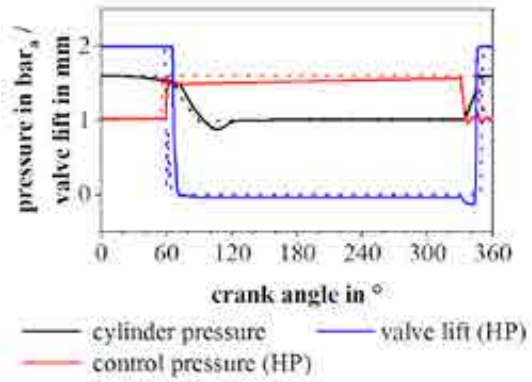

Figure 10: Comparison of experimental (solid lines) and simulation (dotted lines) results for expansion mode with control by an optical cam

In the simulation, the inlet valve closes about 5° crank angle earlier than in the experiment and opens about 5° later. During the expansion phase, when the HP valve is closed, an increase in the pressure inside the HP valve control chambers can be seen in the experiment. This is caused by the already discussed inadequate pressurized air supply to the machine. During this phase, the HP duct is filled with air from the air supply and acts as a buffer, which is, however, too small. Another deviation in the control pressure curve can be found at about 330° crank angle. The pressure level is already decreasing in the experimental test, while in the simulation, it takes another 10°. Since the valve opening has only a deviation of about 5°, the oil adhesion within the model seems to be under-predicted. The operation point itself may cause this. The correlation of oil adhesion was calibrated to a compressor operation at about 100 °C. The test of the expansion mode took place at about 30 °C. This significantly influences the viscosity of the oil and hence the adhesive force. However, overall the curves are in good agreement, showing good reliability of the chosen model for that point of operation.

4 Summary

Within a former research project sponsored by the EFRC R&D working group a pneumatically force-actuated poppet valve was developed, allowing a new operation mode with only minor changes to an existing reciprocating compressor. The present paper shows that it is possible to run a compressor reversible as an expansion machine by applying this new type of valve.

The boundary conditions of the test laboratory significantly influenced the performed experiments. Only limited compressed air supply and a lack of possibility to convert the mechanical energy gained into electrical energy and subsequently feed it into the grid led to untypical operation points at low speed and low pressure level.

An optical cam on the flywheel was used to start the expander, since the previously developed control system could only work correctly if the machine was already running at a stable operating point. Using a crank angle sensor instead of the simple top dead centre sensor solved this problem.

A constant working point for the expansion mode was found, and the pressure and valve lift curves were measured. Due to the non-adequate compressed air supply, only a small filling in the cylinder was achieved, which led to the under-expansion of the gas during the movement of the piston from top to bottom dead centre. In the p-V-diagram, the losses caused by this phenomenon could be detected. However, the indicated work was calculated from the diagram, and due to the experimental setup, the mechanical losses in the machine could be determined.

After starting the machine, the optical cam control was switched to manual control to enhance the operation point and, thus, the p-V-diagram. A significant impact could be performed on the closing position of the outlet valve. However, the test field limited the influence of the closing angle of the inlet valve and, thus, the filling rate of the cylinder.

By observation with a camera, the speed of the crankshaft was evaluated as a function of the crank angle. A high degree of non-uniformity was found. The reason for this was mainly the atypical operation of the machine with only one working chamber in operation and the limited supply of compressed air by the infrastructure of the laboratory. For the test rig under the given boundary conditions, a flywheel with higher moment of inertia would help to improve the non-uniformity.

The tests with control by an optical cam were compared to simulation results, and good agreement was found. Further research potential was found in the calculation of oil adhesion behaviour.

5 Outlook

With the valve system presented, it is possible to operate an existing reciprocating compressor reversibly as an expansion machine. This opens up the possibility of recovering exergy, for example, when unloading UGS. Before the system is used for such an application, further investigations and optimization should be carried out. Some suggestions are summarized below:

by: Christian Stöckel, Konrad Klotsche, Christiane Thomas – TECHNISCHE UNIVERSITÄT DRESDEN

- Improving the valve flow coefficient by an optimized flow geometry. Also, this optimization should be performed for reversible flow through the poppets.
- The prototype valves were made entirely of stainless steel. Typically, poppets should be made out of high-performance polymers to reduce weight and, thus, optimize the poppets' response to pressure changes.
- Oil adhesion significantly influences the opening and closing characteristics of the poppet valves. One possibility for reducing this influence is geometrical changes in the contact area between the poppet and valve seat, respectively, valve lift limiter.
- Additionally, the model of oil adhesion should be enhanced to improve the accuracy of the simulation results.

---

[1] Stöckel, Ch.; Nickl, J.; Thomas, Ch.; Hesse, U. (2016): A novel valve design for combined reciprocating piston expansion and compression machines. 10th Conference of the EFRC, Düsseldorf, Germany

[2] Stöckel, Ch.; Thomas, Ch.; Nickl, J.; Hesse, U. (2017): Investigations on pneumatically forced-actuated compressor valves. IOP Conf. Series: Materials Science and Engineering 232 (2017) 012031, doi:10.1088/1757-899X/232/1/012031

[3] Stöckel, Ch.; Thomas, Ch.; Hesse, U. (2018): Experimental investigations on pneumatically forced-actuated compressor valves. International Compressor Engineering Conference, Purdue, USA

[4] Stöckel, Ch.; Thomas, Ch.; Hesse, U. (2018): Reversible Usage of a Reciprocating Compressor as Expansion Machine by the Application of new Force Actuated Valves. 11th Conference of the EFRC, Madrid, Spain

[5] Stöckel, Ch.; Thomas, Ch.; Nickl, J.; Hesse, U. (2019): Experimental testing of pneumatically forced actuated compressor-expander valves. IOP Conf. Series: Materials Science and Engineering 604 (2019) 012060, doi:10.1088/1757-899X/604/1/012060

[6] Stöckel, Ch. (2022): Zwangssteuerbare Ventile für Hubkolbenmaschinen. Doctoral Thesis, Technische Universität Dresden, Dresden, Germany

[7] Eifler, W.; Schlücker, E.; Spicher, U.; Will, G. (2009): Küttner Kolbenmaschinen, Vieweg + Teubner, Wiesbaden, Germany



Reciprocating Steam Compression Applications in Energy Decarbonization

by:

Matt Janssen
Chief Technical Officer
Vapor Motive Company
Sandpoint, Idaho, USA
mjanssen@vaporlocomotive.com

13th EFRC CONFERENCE
September 19th – 21st 2023, Zagreb

Abstract:
Steam compression with reciprocating compressors is a process that should be considered by the reciprocating compressor industry as a significant opportunity to contribute to carbon neutrality and create a new potential application for reciprocating compressors utilizing automatic valves. Steam compression is the process of upgrading low-pressure steam to a higher temperature and pressure preserving the latent heat of steam vaporization of the low-pressure steam. The energy required to upgrade this steam may have a coefficient of performance exceeding ten versus generating new high-pressure steam. Mechanical vapor recompression of steam involves a two-phase process. First, liquid is removed from a pressurized process by a steam trap then exhausted to a mechanical separator at a lower pressure and flashes to steam. This steam can then be recompressed to a valuable higher pressure and temperature. Challenges for steam compression include controlling the quality and temperature of the steam being compressed and utilizing materials suitable for steam and the shock loads typical of a reciprocating compressor handling a two-phase fluid. Opportunities currently exist for both centralized and decentralized steam compression. For instance, steam may be recovered from various small processes and pass through a low-pressure piping system to a header for a centralized compressor. It also may be viable to develop small compressors that recompress steam at the process vessel trap and discharge it to a local high-pressure header, thereby avoiding expensive large diameter piping and thermal losses. This paper will explore the processes, challenges, and opportunities for compressing steam at multiple scales and configurations including for small-scale and distributed energy systems for which there is little industry precedent. It will also describe Skinner Engine Company labyrinth groove designs for lubricated and oil-free service.

by: Matt Janssen – VAPOR LOCOMOTIVE

1 Introduction

Improving energy efficiency is the only realistic way to achieve energy transition, whether it be motivated by addressing a decrease in fossil energy supply to Europe or reducing the volume of fossil carbon introduced to the atmosphere.

1.1 A Global Perspective

Despite a 300-fold increase in wind turbine and photovoltaic contribution to electricity generation in the last 25 years, the consumption of fossil fuels, largely driven by China's economic expansion, resulted in the rate of global fossil fuel extraction increasing 53% and 57% more CO_2 being released to the atmosphere [1].

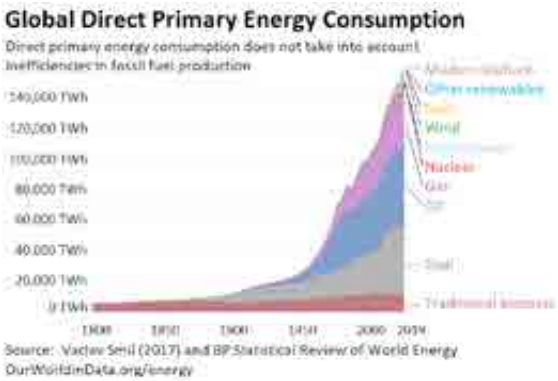

Figure 1: Global Direct Energy Consumption

Energy transition to different energy sources might occur on a national level quickly, however, history shows that global energy transitions have always been gradual, drawn-out affairs. While an increase in renewable electricity generation in some areas has occurred, the world has added 25 times more energy supply in fossil fuels (Figure 1). Much of the renewable energy capacity has been constructed with carbon-intensive materials such as steel, cement, and plastics [2]. Moving the point in the lifecycle of when an energy source emits carbon does not necessarily alter its carbon intensity. The objective of energy transition is not to shift energy sources of a particular country or region, but rather to lower global aggregate emissions of CO_2 as it is quickly distributed in the global atmosphere.

The rising Energy Convenience Standard (W. Petitjean, P.E. personal communications), or degree of ease an energy source is to use, dictates high energy density fuels such as liquified natural gas, compressed hydrogen, and battery-stored electricity be used for consumer and light industrial applications. Additionally, equipment and appliances that run on these energy sources exhibit greater efficiencies, power-to-weight ratios, and quality of combustion (or no combustion.) Replacing fossil-fueled thermal electricity generation with renewables for electric-powered devices is much easier than displacing fossil energy use in production processes for heavy industry (steel, cement, chemicals, plastics) and transportation (cars, airplanes) as these applications require a high grade and/or high energy density fuel to be practical, as well as makes the most use of our fossil-fuel based energy system which represents an embodiment of at least 15 billion tons of crude oil and at least $25 trillion in 1990 dollars [2].

1.2 European Industrial Sector

In 2020, the industrial sector of the EU accounted for 26% of final energy consumption [3]. Steam systems are a part of almost every major industrial process today, the majority of which is created in the EU by burning fossil methane gas. Thirty-seven percent of the fossil fuel burned in US industry is burned to produce steam [4]. Steam is traditionally generated by increasing the temperature of water at a given pressure, for example, to 100 °C at atmospheric pressure. As the pressure increases, so does its boiling point and internal energy. Flash steam occurs when the pressure of water, such as hot condensate, is reduced. Steam released by flashing may be as valuable as steam released from a boiler if the low-pressure and lower-temperature steam is suitable for a process as it contains the energy of the latent heat of vaporization. Most steam applications, however, require steam with higher temperatures and pressures. Mechanical Vapor Compression (MVC) of steam uses the heat of compression to increase the temperature of steam as the pressure is being increased. The use of a reciprocating compressor allows greater flexibility and part load efficiency than other MVC technologies with the opportunity to use renewable sources of energy.

1.3 Increasing Efficiency is an Energy Transition

Efficiency is a lever for energy transition to be able to occur – using less energy and resources for the same outcome. MVC with reciprocating compressors fosters eco-efficiency of industrial steam production across a wide variety of applications and scales and is an essential component of applying industrial ecology.

While representing a significant economic opportunity for industry as well as reciprocating compressor suppliers, steam compression equipment is not widely applied, primarily because of increased system complexity and the knowledge base required crosses multiple engineering disciplines. Unlike many other gases, steam is a two-phase fluid, and the properties of saturated steam in particular are constantly changing significantly if its working environment is dynamic. Opportunities abound in the endeavor of energy transition for those with the knowledge and hardware to manipulate low-grade heat into high-value steam.

2 European Market Analysis

Europe still has a large industrial base and keeping it in place is a matter of security, minimizing energy

by: Matt Janssen – VAPOR LOCOMOTIVE

waste in transportation, and providing safe, meaningful, physical work to its inhabitants.

2.1 Industrial Steam Users

The chemical and petrochemical industry was the biggest energy consumer in the EU in 2020 at 22% or 2121 Petajoules (PJ). The non-metallic minerals industry 1372 PJ or 14%, the paper pulp, and printing industry 1326 PJ or 14%, and the food, beverages, and tobacco industry 1147 PJ or 12% [3]. The total natural gas consumption of the EU was 3094 PJ, and if one were to use the American percentage for total energy used to make steam, it would be about 3500 PJ.

2.2 Flash Steam Recovery

Flash steam recovery represents one of the most tangible opportunities to increase the efficiency of industrial steam systems. If 10% of applications were suitable for MVC with reciprocating compressors and 10% of the condensate was to be recovered and compressed, these 35 PJ represent a value of $663 million per year (If the EU natural gas import price is $20/MMBtu and there is 947,817 MMBtu/PJ.)

2.3 Whole Market Solutions



Figure 2: Example of a distillation facility for mid-latitude with solar thermal and photovoltaic array

The whole industrial steam market of 3500 PJ at $66 billion at $20/MMBtu is, however, available. MVC allows steam from a lower-pressure renewable source to be compressed to a useful pressure. For example, low-pressure steam which is practical to create with rooftop-mounted solar thermal collectors (Figure 2), geothermal sources, and waste heat recovery steam generators can be compressed for a high-pressure process requirement.

2.4 Additional Market Opportunities

A principal challenge that wind turbine and photovoltaic-generated power faces in the EU is that their reliability is insufficient to retire the fossil thermal generation capacity they replace. Despite the installed cost of these technologies going down, the price of electricity in states with high implementation is not. While batteries are a great way to store small amounts of electricity, the only widely adopted, large-scale storage method is pumped storage hydropower. This requires vast amounts of specific terrain and a loss of 25% of the energy to pump the water uphill [1]. The round-trip efficiency, or efficiency through a complete cycle, is however very good. Round-trip efficiency is a valuable measure to compare various methods of energy storage.

Increased renewables for electricity generation on the grid creates a storage issue for storing stranded power. The Zittau/Görlitz University of Applied Sciences is researching storing electrical energy as steam with Thermo-Mechanical Power Storage (TMS-Battery) using a multi-cylinder, multi-stage piston compressor/expander.

The TMS-Battery or Carnot battery using MVC is essentially a pumped storage system that liberates pumped storage from geographical constraints and stores energy for use in thermal processes and electricity generation. Like pumped hydro, MVC allows the concentration of diffuse energy into a higher-grade energy practical to store or use in a process. Also, like pumped hydro, MVC uses water as a working fluid which is a non-toxic, abundant resource. As the scale of the system and level of development the system is operating in is reduced, the likelihood of a working fluid such as glycol, thermal oil, or a refrigerant eventually escaping to the environment becomes an almost certainty. The real-world life-cycle costs of technologies are often much higher than those predicted for ideal circumstances.

2.5 The Embodiment of MVC is Flexible

The low side of an MVC heat pump system can be of such a low temperature that a variety of otherwise unusable sources and stores of thermal energy may be concentrated. As the majority of power generation uses the Rankine cycle, the majority of industrial processes use a high volume of steam, and a large percentage of commercial and residential energy requirements are thermal, using MVC allows a grand scale of energy applications for large and small system capacities. Distributed generation and storage allow for the least transmission losses and least impact an energy technology has on the local environment. MVC with a reciprocating compressor/expander offers one of the highest energy densities possible using hardware with a level of serviceability that facilitates deployment in remote locations and at small scales because people with mechanical aptitude and skills can operate and fix it. At the end of life, MVC components which are primarily cast iron and steel may be easily recycled.

3 Mechanics of Steam Compression

Steam compression is an integral part of steam engines (expanders) to cushion the running gear for admission and rod reversal.

by: Matt Janssen – VAPOR LOCOMOTIVE

3.1 Compression in a Steam Engine

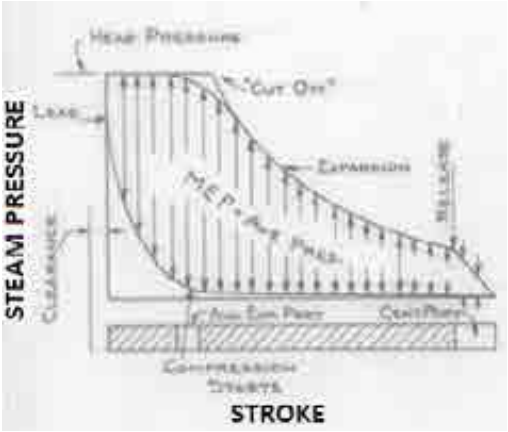

Figure 3: Basic Unaflow Indicator Diagram [5]

In a steam engine, compression occurs as soon as the exhaust ports are closed by a dedicated poppet valve or movement of a slide or spool valve. The valves are not automatic – they are mechanically actuated – the former typically by camshafts and the latter by eccentric rods. The expansion and compression line (Figure 3) may be calculated with sufficient accuracy by determining the pressure relative to the volume at constant entropy Ø = 1.55 from "Ellenwood Steam Charts 1939" [6]. The area formed by the difference between the lines represents the net mechanical work performed by the piston, the average of which is the Mean Effective Pressure (MEP).

3.2 Steam Compression as Net Work

While the objective of a normally operating steam engine is to apply power to the crankshaft from steam pressure, the objective of a steam compressor is to create pressure from the power applied to the crankshaft.

In the case of the steam locomotive, MVC has been applied for more than 150 years to perform valuable work. In 1865, M. L. Le Châtelier conducted a series of experiments to improve steam locomotive compression braking. His experiments, which he characterized as an "inverted steam engine," concluded that using pressurized hot water from the boiler which was allowed to flash to steam at atmospheric pressure prior to admission to the cylinders, prevented the compressed steam from superheating and exceeding cylinder material and lubrication capabilities of the day. This was sufficient to brake trains down grades of 1:260 and stopping for shunting applications, being applied to some 1400 locomotives in France, as well as locomotives in Spain and the U.S. [7]. 'This brake consisted of a globe valve in a pipe line that admitted hot water from the boiler to the exhaust passages of the cylinders. There it immediately formed a heavy vapor which was drawn into the cylinders by suction of the pistons. The reverse lever, which had been set to mid-position, was now gradually moved into back gear until the desired braking power was obtained... cylinder-head relief valves were fitted whenever it was applied' [8, p. 268].

Almost all methods of steam compression generate enough heat to keep water in the vapor (steam) phase with sufficient quality. In fact, as Le Châtelier concluded, very low-quality steam or desuperheating via water mist injection is necessary to control superheat with the high compression ratios his design achieved. For compression with a reciprocating process compressor, much lower compression ratios are typically chosen still with desuperheating or intercooling.

3.3 Steam Compressors

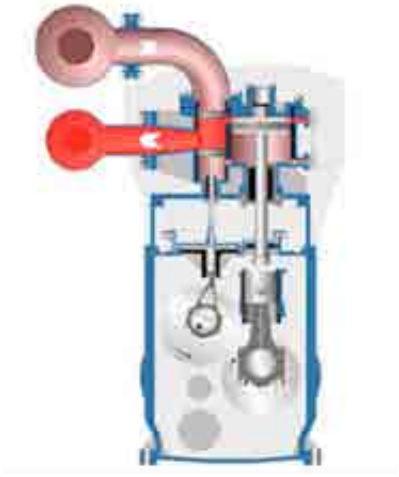

Figure 4: Piston-Valve Counter-flow Steam Compressor [9]

The piston-valve counter-flow steam compressor (Figure 4) uses a mechanical spool valve for control of inlet and exhaust timing that is driven from an eccentric rod which is gear driven from the crankshaft. The eccentric shaft also acts as a countershaft for improved balancing. The valve gear is fixed at a cut-off of approximately 55%.

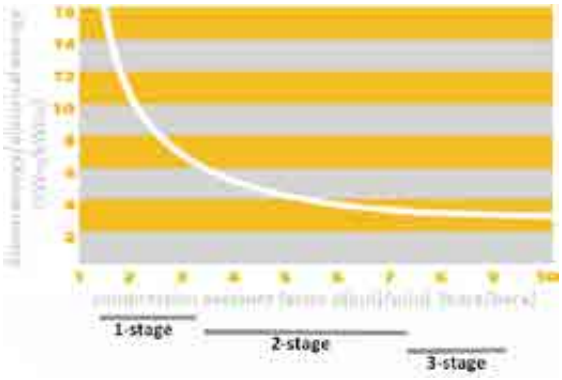

Figure 5: Curve for Estimating Coefficient of Performance for a Steam Compressor [10]

The electrical requirement to drive a motor-driven steam compressor may be estimated from the curve in Figure 5. One first determines the pressure factor with the following equation:

by: Matt Janssen – VAPOR LOCOMOTIVE

$$\frac{p(out)}{p(in)} = CPF, \qquad (1)$$

where *p(in)* is the initial pressure, *p(out)* is the outlet pressure, and *CPF* is the compression pressure factor.

Locating this value on the X-Axis and finding the Y-value along the curve, one finds the approximate kW electrical energy required for each kW thermal, expressed as:

$$\frac{kWth}{kWhel} = COP, \qquad (2)$$

where *kWth* is the thermal energy produced, *kWhel* is the electrical energy requirement, and *COP* the coefficient of performance.

For example, with 8 tons/hour of 3.2 bar_a inlet steam, 16.1 bar_a outlet steam, the CPF given by Formula (1) is 5. The COP given by the graph is 4.

4 Compression of Sub-Atmospheric Pressure Steam

While a conventional counterflow compressor arrangement is suitable for steam pressures above atmospheric pressure, a compounded uniflow arrangement for sub-atmospheric pressure steam should be considered.

In steam engines with high expansion ratios, the exhaust is successfully handled with terminal cylinder ports because the volume of the expanded steam is so great.

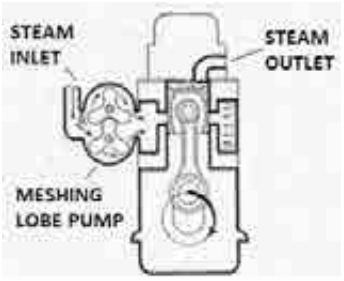

Figure 6: Flow Diagram of a Compounded Uniflow Compressor Concept

A widely applied uniflow compressor which was lobe pump-blown and later turbo-compounded is the two-cycle diesel engine's scavenging and compression stroke. In a diesel engine configuration, terminal ports in the cylinder are supplied air at a pressure of 1.1 to 1.3 bar_a to 2.4 bar_a TIB (turbo-intercooled-bypass) and compressed at a ratio of 16 to 21:1 with sufficient temperature building to allow auto-ignition of spray-injected cold diesel fuel. The cylinder inlet ports give a greater port area than a practical application of valves would for a minor sacrifice of the effective compression stroke. The application of this configuration as a steam compressor (lobe pump-blown, Figure 6) might allow steam to be generated from 60 °C water (A typical waste heat temperature) with a pressure of around 0.2 bar_a and compressed to steam of a useful pressure (say 3 bar_g) for about three times less energy and without the necessary direct use of fossil fuels and CO_2 emissions that generating steam in a gas-fired boiler would have because a higher amount of waste heat can be utilized compared to a direct heating system [11.]

5 Alternatives to MVC

An alternative to MVC is Thermal Vapor Compression (TVC). This is a well-known technology using a jet ejector to compress and thus raise the pressure of the steam to be recycled. The principle advantage of this technology is that it has no moving parts. The principle disadvantages of this technology include that it requires motive steam at a higher pressure than the steam to be recycled, increasing the total mass flow of the system often beyond the need for the process, and the motive steam would most likely have to come from a fossil fuel. Most historic comparisons of MVC to TVC are constrained in scope to MVC technologies using rotary and not reciprocating compressors and therefore limit the applicability of their findings and conclusions for high compression factors and final pressures. For low-pressure, high-volume applications, TVC is an effective tool to decrease fossil carbon introduced to the atmosphere. The objective of this paper is to present an emerging technology and known experience of steam compression to reciprocating compressor users, manufactures, and scientists who may consider MVC with reciprocating compressors worthy of further study to effect energy transition.

6 Storage of Steam

The storage of steam is most practically accomplished with a wet accumulator, where the majority of the vessel is filled with water hot enough to turn to steam if the pressure is reduced, and a small steam space is provided where steam can be readily removed. The water offers a higher energy density than a dry accumulator, but not as immediate a supply as is needed for a high-volume device such as a steam-powered airplane catapult.

6.1 Historical Applications of Storage

Dr. Émile Lamm patented the first fireless locomotive in 1872, and fireless locomotive-propelled streetcars appeared in New Orleans, USA in 1873 [12]. The present sliding pressure steam storage scheme was developed by J. Ruths, who was granted a patent in Germany in 1913. The first

by: Matt Janssen – VAPOR LOCOMOTIVE

steam storage plant with peaking turbine was built in 1920 at Malmö, Sweden, and the largest was built in 1929 at the recently decommissioned Berlin-Charlottenburg power station with a peaking turbine of 50 MW, a storage capacity of 67 MWh, and a storage pressure of 14 bar [13]. These applications involve peak-shaving of steam boiler requirements to allow a smaller boiler to be installed. Professor P. R. Gilli showed that the economic value of storage decreases from 10 bar_g to 30 bar_g, but then increases at higher pressures [14]. He improved high-pressure steam storage up to 120 bar_g by superheating the steam - passing it through superheater units in the steam space of the accumulator after it had been throttled out of the vessel by an automatic reducing valve [15]. The instantaneous reserve plant at the Simmering steam power plant of the Vienna Municipality also used 120 bar_g superheated storage of this design [13].

6.2 Historical Storage Applications with Recompression

John McCallum founded the Heat Conservation Company in 1927. He developed a recompression technique for returning heat to the boiler which showed a fuel saving of 29% at a stationary powerplant with a previously atmospheric exhaust. This was more notably applied to the Holcroft-Anderson Recompression Locomotive of the Southern Railway (UK) in 1930. The principles are explained in US Patent 1,982,060, "Conservation of Heat within a Steam Power System," and described by Holcroft [16].

In 1933, the concept of steam-pumped storage was patented by F. Marguerre and a peak load powerplant of 15 MW with 2 hours full load discharge and steam compressor power of 7.5 MW was designed and apparently built [17].

6.3 Steam Heat Pump Sliding-Pressure Storage

Carnot batteries are an emerging technology for storing stranded electricity. A peak load powerplant of this type does not discharge any pollutants into the environment since it burns no fuel. The Zittau/Görlitz University of Applied Sciences is currently carrying out a project funded by the German Federal Ministry of Economics, which is storing electricity with steam with a Thermo-Mechanical Power Storage (TMS-Battery) with a steam engine serving as a reversible prime mover/compressor.

> The scope of the project is the development, construction, experimental investigation, modeling, and further development of an innovative prototype thermo-mechanical electricity storage system (CARNOT-Battery) for sector coupling of electricity and heat. The project contributes to the creation of scientific and technical prerequisites for the timely provision of an applicable and environmentally friendly electricity storage system for the sector coupling of electricity and heat. The thermo-mechanical electricity storage system works with water as working and storage medium, which is CO_2-neutral, available, non-toxic and economical. The system is characterized by high charging and discharging capacity, high flexibility (fast response times), simple design without complex heat exchangers, very high cycle stability, long lifetime up to 40 years, high overall efficiency and high energy storage density. In terms of security of supply, such an electricity storage system represents a significant system component in the short-, medium- and long-term energy infrastructure and thus contributes to strengthening Germany as an industrial location [18].

In many ways, the Zittau/Görlitz TMS-Battery is a more refined Le Châtelier water brake drawing from a conventional Ruths accumulator and discharging to a high-pressure Gilli -type accumulator.

6.4 MVC to Contribute to Energy Transition

'The efficiency of prime movers (in the case of electricity generation, power plant efficiency) has been improving from about 1% for the first Newcomen engines to about 50% during the last 300 years' [19, p. 20]. With the heating boiler, there is almost no possible further gain in efficiency, whereas heat pump technology with reciprocating compressors acting as an energy concentrator and facilitating practical thermal storage is an emerging opportunity to facilitate energy transition.

It should be evident that the TMS-Battery is ideal for industrial steam processes in addition to electricity storage. The low-pressure heat store need not be an on-site vessel but could be a district steam heat system of a municipal heat and power facility. The practicalities of such "sector coupling" concepts are being explored in practice with this project [20]. Integration of individual energy systems with energy cascading is an industrial ecologically - savvy means of achieving a higher total efficiency of energy production.

Furthermore, lower-pressure steam sources such as heat from parabolic solar thermal micro-troughs and geothermal and waste heat may be upgraded to high-grade thermal energy and stored with a minor addition of energy for compression. The efficiency of these technologies otherwise declines to uneconomic levels if pushed to generate at high temperatures. Using MVC allows high-temperature steam to be provided from these renewable sources at higher levels of efficiency than heating boilers.

Wind and photovoltaic energy, in particular, need a TMS-Battery to effectively provide a substitute for fossil fuels in heat and power generation. This

by: Matt Janssen – VAPOR LOCOMOTIVE

allows the process demand to be aligned with the level of wind or solar insolation available.

Global economic activity has increased by about 3% annually in the last century. Primary energy consumption increased about 2% per year over the same period. While energy intensity has decreased about 1% per year, the primary energy requirements are rising. Theoretical efficiency improvement potentials range from a 10-fold to a 20-fold increase [19]. MVC with reciprocating compressors allows legacy industrial infrastructure with a 10 to 100-year lifespan to be retrofitted with heat recycling technologies, which represent a potential to humanity as much as any energy resource, and it should be evident that without increasing the rate of efficiency improvement significantly or radically reducing demand, energy transition is not possible.

Currently, there is much focus on high-quality forms of energy, such as compressed hydrogen, to provide low-quality service. For example, hydrogen-powered ships are proposed more commonly than sailing ships. However, hydrogen has neither the storage capacity nor energy return on energy invested that a sailing ship has. It is only a more convenient technology for the operator. Such misappropriation of technology makes many renewable energy applications ineffective.

6.5 MVC Can Aid in the Utilization of Geothermal Energy for Carbon Capture

In the United States, about 25 billion barrels of hot water are co-produced every year as a by-product in oil & gas wells [21]. The temperature of this co-produced hot water is around 100 °C. There are also significant low temperature natural geothermal sources available at this temperature, and geothermal wells may be drilled and operated practically at this temperature with 200 °C being the upper limit where present materials prevent the transmission of higher temperatures.

Currently, there is a pilot project operating a direct air capture facility in Iceland using geothermal energy. The CO_2 is captured in air filters with a chemical binder. When the filter is full of CO_2, the collector housing closes and is heated to approximately 100 °C, which causes the filter to release the CO_2 [22]. It is then injected with water around 25 bar_g where mineral carbonation of basalt rock occurs [23]. A geothermal energy startup out of Houston, TX, is using recent oil well drilling technology including gathering subsurface behaviour data in real-time and applying algorithms to optimize flow distribution through the reservoir to maximize heat mining efficiency. These drilling, carbon capture, and sequestering technologies are being combined in a project for a fully integrated geothermal and direct air capture (DAC) facility, with support from the Chan Zuckerberg Initiative (CZI) [24].

When the acceptable temperature is lowered, this decreases capital cost and increases feasibility in broader applications. MVC enables a marginal source for carbon sequestration to be upgraded to a good source with an incremental energy investment.

7 Materials and Design Methods

Traditional materials for steam engine cylinders follow those of traditional process compressors. These include gray cast iron and high lead copper-based alloys. Many contemporary process compressor materials are not compatible with steam engines or compressors. Almost all of the other innovations in the process compressor industry since the decline of the steam engine in the 1950s would serve to improve the steam engine. Though the thermodynamics of the steam engine were well understood by the end, cylinder tribology and frame and running gear designs remained mostly of the Victorian era. A number of smaller and more contemporary designs, often referred to as "steam motors" rather than steam engines, have had only limited success primarily due to the preeminence of the internal combustion engine.

7.1 Piston Design & Materials

Gray iron rings of heavy cross-section are typically used when valves or pistons cross over large cylinder ports. In stationary steam engine practice, the majority of installations used a fitted gray iron or bronzed piston, whereas later locomotive applications used sectional iron or bronze-iron duplex rings which carried the weight of the lightweight piston. For many steam engine applications where the steam passing through the engine may have its own boiler and exhaust system, with perhaps a heat exchanger to a process, the use of cylinder lubricant is desirable with runs of 40,000 to 60,000 hours runtime possible. This is a bright stock with a paraffinic resin viscosity builder and tackifier additives as well as animal fats for emulsivity when permissible.

For some steam engine applications, and almost all steam compression applications, the presence of lubricant in the steam is unacceptable. There are a few notable methods up to this time that have been applied.

7.1.1 Water Seal Grooves

The first technique, developed by a small steam engine manufacturer in New York, uses simple "water seal" grooves on a vertical engine where the piston still provides guidance at a clearance of 0.127 mm per 25.4 mm of diameter. These are square-cut circumferential grooves that interrupt a piston running surface, where a 150 mm piston might have (7) 3.18 mm x 0.79 mm grooves on a 125 mm surface. Cylinder liners are made of nickel chrome iron, approximately 220 Brinell, care being taken that no free abrasive particles are present in the iron. A mixture of 1.36 kg beeswax to 0.45 kg lubricating

by: Matt Janssen – VAPOR LOCOMOTIVE

graphite powder supplied by a steam lubricator was mounted in the main steam line to the engine. This mixture was fed for half a day with the engine just turning over, then over two to three days, the engine was slowly brought up to speed. They recommended that after the engine was installed that it be fed the mixture for two to three weeks at a rate of 0.45 kg per 310,761 square meters of cylinder coverage (based on a 203 mm x 203 mm single cylinder engine, 400 rpm, 200 hours, using 1.81 kg of mixture) [25].

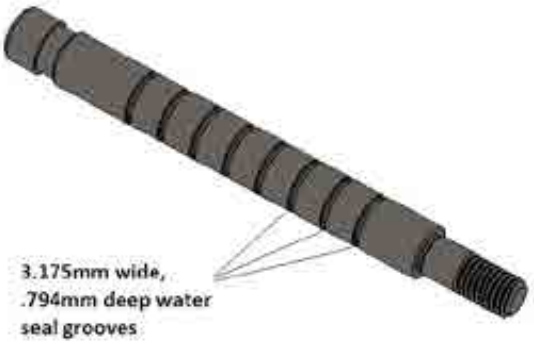

Figure 7: Water Seal-Type Poppet Valve Stem

Many Lentz-type poppet valve steam engine designs also employ similar "water seal" grooved steel Parkerized valve stems (Figure 7) running in lubricated service in gray iron or bronze guides.

7.1.2 Duplex Rings

As part of a study conducted for the U.S. Navy, the small steam engine manufacturer's graphite powder-lube technique was applied to a larger engine with bronze-bronze and bronze-iron sectional duplex piston rings in a two-cylinder 322 mm x 254 mm vertical Unaflow with no success [25].

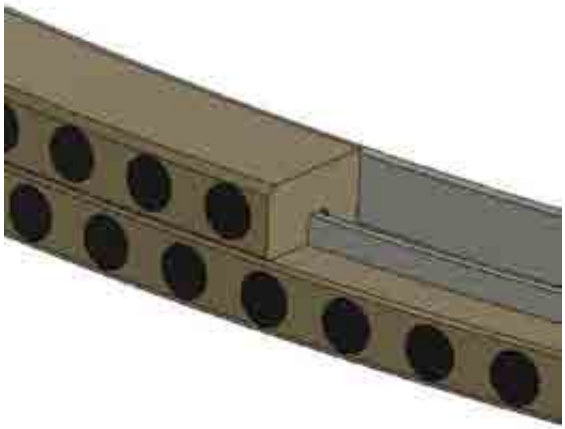

Figure 8: Duplex Bronze Restrained-Type Segmental Piston Ring with the Addition of Graphite Plugs

The addition of graphite plugs in bronze-bronze duplex rings (Figure 8), such as used in dry running bushings, may improve upon the 600 hours of run time the tests for the study achieved.

7.1.3 Carbon-Graphite PTFE Rings

Carbon-graphite PTFE sectional rings with no expanders are currently being used running in Cr15 steel liners. Service lives of 4000 hours on piston spool valve rings running over ports, 8000 hours on piston rings (non-uniflow) are being achieved. [26]

7.1.4 Labyrinth-Grooved Pistons



Figure 9: Labyrinth Groove Piston & Detail

The use of labyrinth grooves with a thread-type profile (Figure 9) has been recently applied in steam applications with promising results. These designs follow published dimensions and clearances [27]. There is very little literature available on condensing flow across a labyrinth seal. Initial operation with steam shows a perceptibly greater level of sealing than with air. This phenomenon may be: 1) Due to the increased density of the steam/water mixture as opposed to air where the throttling point between each chamber acts as a nozzle; 2) Due to the formation of a "water seal" as the pressure across each chamber drops and condensation occurs; and 3) Due to ebullient action of the two-phase fluid within the labyrinth chamber, especially as the velocity of the jet is retarded by the next chamber to almost nothing as the kinetic energy is virtually destroyed. The initial experience gained suggests the thread-type labyrinth profile is an improvement over the throttling characteristics of sharp-edge orifices of the "water-seal" labyrinth [28]. The mechanisms at work deserve more study and optimization.

7.2 Valves

Steam compression can be accomplished with automatic valves with materials compatible with steam. Steam compression and expansion can be achieved with eccentric rod or radial valve gear which is well-suited to driving piston spool valves.

7.2.1 Valves for Compressors

by: Matt Janssen – VAPOR LOCOMOTIVE



Figure 10: Metal Flapper-Type Automatic Valve

Automatic valves allow for very simple industrial compressors, such as those that use reed valves (Figure 10), to accomplish MVC for small-scale and intermittent-duty industrial steam processes such as cooking, microbrewing, and micro distillation. Additionally, in a larger industrial plant, small compressors can be located at individual processes (vessels) such that steam may be recompressed without large and expensive distribution piping with its associated thermal and mechanical losses. Such arrangement may be especially advantageous in intermittent or batch operations.

It should be possible to modify process-type compressor automatic valves for steam service for process-grade MVC applications.

7.2.2 Poppet Valves for Compressors and Expanders



Figure 11: Temperature -Compensating Balanced Poppet Valve

The valve and valve case featured in Figure 11 is a low actuation pressure, double-beat valve which achieves its positive sealing across all operating temperatures with the application of a lower "free-seat."



Figure 12: Stepper-Motor Driven Rotary Cambox for Poppet Valves

The cambox shown in Figure 12 features valve gear originally patented by H. G. Mueller [29]. It has been improved with contemporary cam ramp profiles and stepper motor drives to decrease mechanical complexity and facilitate application to existing compressor frames without modification of the frame for cambox driving means. It is variable lead, direction, and cut-off from 83% of the stroke to zero.

8 Conclusion

The reciprocating steam engine, cast aside long ago in favor of more convenient, larger scale, and higher power-to-weight ratio technologies such as internal combustion engines and gas turbines, is rising from the scrap pile. Unlike its replacements, it does not steal oxygen and dump oxides of nitrogen into the atmosphere to function, nor does it depend on fossil fuels. As demonstrated in this paper, this same prime mover is fully reversible as a pump with no modifications – another feat its replacements cannot perform.

Insufficient resources are being applied to MVC with reciprocating compressors for their potential to enable energy transition. Current participants are very specialized and dedicated, but members of the European Forum for Reciprocating Compressors have the skills, knowledge, and resources to mature the technology to where its reliability and cost enable the rapid implementation needed to preserve Europe's industrial economy and avert global environmental disaster.

9 Acknowledgments

I am especially grateful to the last technician of the former Skinner Engine Company (SECo), Al Mattichak, who taught me real-world cogeneration with Skinner Unaflow steam engines, and last Chief Engineer of SECo, Hal Fuller, P.E., for entrusting me with the SECo engineering files (as well as his own steam engine development files.) Lastly, I wish to thank Bill Petitjean, P.E. of RankOtto, LLC, also formerly of SECo, for sharing his knowledge of the Rankine cycle related to the steam engine, his trials and tribulations, and the inspiration to develop a practical steam engine for the modern world to reduce primary energy consumption– he was only 40 years ahead of his time.

References

[1] V. Smil, *Grand Transitions: How the Modern World was Made*. New York: Oxford University Press, 2021.

[2] V. Smil, "Examining energy transitions: A dozen insights based on performance," *Energy Research & Social Science*, vol. 22, pp. 194–197, Dec. 2016, https://doi.org/10.1016/j.erss.2016.08.017

[3] Eurostat, "EU's industries dependent on electricity and natural gas" https://ec.europa.eu/eurostat/web/products-eurostat-news/w/DDN-20221202-2 (accessed Jan. 12, 2023).

[4] D. Einstein, E. Worrell, and M. Khrushch, "Steam systems in industry: Energy use and energy efficiency improvement potentials," Lawrence Berkeley National Laboratory, Univ. of California, Berkeley. July 22, 2001. Accessed: Mar. 3, 2023. [Online]. Available: https://escholarship.org/uc/item/3m1781f1

[5] R. Whiting. "Calculation of Mean Effective Pressure," unpublished.

[6] R. Whiting. "Steam Rates for Skinner Standard Vertical Unaflow Engines," unpublished.

[7] "The Use of Counter-Pressure Steam in the Locomotive Engine as a Brake," *Scientific American*, vol. 21, no. 18, pp. 277–278, Oct. 1869, https://doi.org/10.1038/scientificamerican10301869-277

[8] A. W. Bruce, *The Steam Locomotive in America*. New York: W.W. Norton, 1952.

[9] M. Wendel. (2018, April). "Spilling Steam Compressors," [Online]. Available: https://mexiko.ahk.de/fileadmin/AHK_Mexiko/user_upload/Spilling.pdf (accessed May 20, 2023).

[10] M. Wendel. (2018, April). "Spilling Steam Compressors," [Online]. Available: https://mexiko.ahk.de/fileadmin/AHK_Mexiko/user_upload/Spilling.pdf (accessed May 20, 2023).

[11] F. Bless, C. Arpagaus, S. S. Bertsch, and J. Schiffmann, "Theoretical analysis of steam generation methods - Energy, CO 2 emission, and cost analysis," *Energy*, vol. 129, pp. 114–121, Jun. 2017, https://doi.org/10.1016/j.energy.2017.04.088

[12] D. Tucker, "Emile Lamm's Self-propelled Tramcars 1870–72 and the Evolution of the Fireless Locomotive," in *History of Technology*, vol. 5, A. R. Hall and N. Smith, Eds. London: Bloomsbury Academic, 1980, pp. 103–118.

[13] G. Beckmann and P. V. Gilli, *Thermal Energy Storage: Basics-Design-Applications to Power Generation and Heat Supply*. Wien: Springer Verlag, 1984.

[14] W. Goldstern, *Steam Storage Installations*, 2nd ed, O. M. Blunn, Transl. Oxford: Pergamon Press, 1970.

[15] A. Giesl-Gieslingen, "The High-pressure Steam Storage Locomotive (Gilli locomotive)," *Locomotive Magazine,* no. 118, Jan/Feb, 1983.

[16] H. Holcroft, "Condensing by compression: A locomotive experiment," *The Engineer,* vol. 182, pp. 202–203, 227–229, 248–249, 1946.

[17] F. Marguerre, "Thermodynamic energy storage method," U.S. Patent 1 979 393, Nov. 6, 1934.

[18] THERESA, "TMS - Thermo-Mechanical Electricity Storage System" https://theresa.hszg.de/en/projects/tms (accessed Mar. 1, 2023).

[19] P.V. Gilli, N. Nakicenovic, and R. Kurz, (1996).*"First- and second-law efficiencies of the global and regional energy systems."* IIASA Research Report (Reprint). IIASA, Laxenburg, Austria: RR-96-002. Reprinted from "More Efficient Use of Energy," In Proc. 16th World Energy Council Congress, Tokyo, Japan, 1995.

[20] C. Haug. (2022, May 27). "Why the steam engine has a future again thanks to the energy transition," *MDR KLIMA-UPDATE* [Online]. Available: https://www.mdr.de/wissen/klima/mdr-klima-update-siebenundzwanzigster-mai-dampf-fuer-energiewende-100.html (accessed Mar. 1, 2023).

[21] V. King. (2016, Oct. 1). "Oil and gas wells prove useful for geothermal energy generation," *The Driller* [Online]. Available: https://www.thedriller.com/articles/90619-oil-and-gas-wells-prove-useful-for-geothermal-energy-generation

[22] Climeworks, "Direct air capture: our technology to capture CO_2" https://climeworks.com/direct-air-capture (accessed Mar. 1, 2023).

[23] J. M. Matter et al., "Permanent carbon dioxide storage into basalt: the CarbFix pilot project, Iceland," *Energy Procedia,* vol. 1, pp. 3641-3646. 2009, https://doi.org/10.1016/j.egypro.2009.02.160

[24] Fervo Energy. (2023, February 23). "Fervo energy to develop combined geothermal and direct air capture facility" [Online]. Available: https://fervoenergy.com/fervo-energy-to-develop-combined-geothermal-and-direct-air-capture-facility/. (accessed Mar. 3, 2023).

[25] G. L Lindsay, "Skinner AV Engine Tests, Lubrication," unpublished.

[26] Voß, Thorsten, Interview. Conducted by Matt Janssen. May 24, 2023.

[27] K. Graunke and J. Ronnert, "Dynamic behavior of labyrinth seals in oilfree labyrinth-piston compressors," In *Proc. International Compressor Engineering Conference*, West Lafayette, IN, USA, July 1984. pp. 7-14. [Online]. Available: https://docs.lib.purdue.edu/icec/425

[28] A. Egli, "The leakage of steam through labyrinth seals," *Trans. ASME*, vol. 57, no. 3, Apr., pp. 115-122, 1935. https://doi.org/10.1115/1.4019911

[29] H. G. Mueller, "Reversing valve gear," U.S. Patent 1 927 525, Sep. 19, 1933.

DIGITALIZATION & AL

Design Automation and Machine Learning in API 618 Reciprocating Compressors
by: Niccolò Batini – BAKER HUGHES; Niccolò Becattini, Gaetano Cascini – POLITECNICO DI MILANO *57*

Real-World Compressor Fault Detection for Digital Twin Environments
by: Gautham Ramchandran, Evangelia Konstantopoulou, Panagiotis Koutsivitis, Nils-Henning Framke – GAMMA TECHNOLOGIES *65*

Using Transfer Learning to Construct Accurate Data-driven Compressor Models on Limited datasets of Field Measurements
by: Jonah Poort, Rens Bazuin – TNO *74*



SUBSCRIBE FOR FREE – visit gascompressionmagazine.com

GAS COMPRESSION magazine

PROVIDING INFORMATION TO KEEP YOUR CRITICAL EQUIPMENT RUNNING



@GasCompressionMagazine
@GasCompressionM
@GasCompressionMagazine
@GasCompressionMagazine

Now available on Apple Podcasts, Spotify, and gascompressionmagazine.com.

GCM ON THE GO

An audioreading podcast of the feature articles from *Gas Compression Magazine*.

Design Automation and Machine Learning in API 618 Reciprocating Compressors

by:

Niccolò Batini
Baker Hughes
Florence, Italy
niccolo.batini@bakerhughes.com

Niccolò Becattini
Politecnico di Milano
Milan, Italy
niccolo.becattini@polimi.it

Gaetano Cascini
Politecnico di Milano
Milan, Italy
gaetano.cascini@polimi.it

13th EFRC CONFERENCE
September 19th – 21st 2023, Zagreb

Abstract:
This paper proposes a process for advanced Design Automation (DA) of Reciprocating Compressors (RCs) cylinder assembly using Artificial Neural Networks (ANNs) to obtain an optimal system configuration. The study found that traditional methodologies for DA limit the system design options to predefined alternatives, while ANNs can overcome this limitation and obtain an optimal configuration of the system quickly, even beyond the constraints of the dataset they were trained on. In this study, the ANNs have been trained using a dataset derived from a database of complete CFD simulations carried out by the COMPANY over the years and integrated into the advanced DA process through a product configurator and an intelligent orchestrator software. The proposed method was applied to a real case study of the COMPANY involving a non-routine design modification of an existing cylinder and compared with the results obtained from the benchmark as-is process of the COMPANY (i.e., CFD simulations). The results showed that the ANN-based method is a reliable tool for optimising the design of RC assemblies, delivering multi-objective optimal solutions of the final non-routine configuration in a short period of time, meeting COMPANY‘s needs. The proposed method is considered a valuable tool for responding quickly to customer requests while improving the efficiency of the design process.

by: Niccolò Batini – BAKER HUGHES; Niccolò Becattini, Gaetano Cascini – POLITECNICO DI MILANO

1 Introduction

The turbomachinery industry is undergoing rapid innovation to meet the demands of new energy transition markets. To keep up with these demands, energy companies are adopting a multi-disciplinary design process that includes parametric CAD modelling, FEA, CFD, and thermodynamics. Many of these companies adopt an Engineering-To-Order (ETO) production approach, which requires a short lead time for key design activities after receiving a customer order. However, the traditional trial-and-error design method can be time-consuming and may not lead to globally optimised designs[1].

Customization in ETO companies is required for several reasons, despite the possibilities of repeating existing designs. While repeating existing designs can be more cost-effective and time-efficient, it may not always align with the unique requirements and demands of customers. Customization enables ETO companies to deliver tailored solutions, differentiate themselves in the market, comply with industry regulations, leverage technological advancements, foster innovation, and enhance customer satisfaction. To improve efficiency and reduce errors and delays in such design processes, ETO engineering companies must look for ways to automate as much of the engineering phase as possible. In this context, this paper explores the significance of customization in ETO companies.

This paper is organised as follows: section 2 embeds the state-of-the-art review, section 3 describes the methodological approach used in the advanced DA process to help Design Engineers (DEs) achieve an optimal design configuration of COMPANY RC cylinders, including details of the various methods and tools integrated within it and section 4 presents an Inquiry-To-Order (ITO) study of a real COMPANY job, evaluating the performance of the integrated approach. Finally, the conclusion section summarises the findings of this research, its scientific contribution, and suggests future research directions related to its limitations.

2 State of the Art

DA solutions have become increasingly important in the ETO sector as companies seek to increase their competitiveness and productivity. To address these challenges, in the literature the use of a system level configurator approach proposed by Kristianto et al.[2] has been applied to achieve a quick solution, while the details related to uncertainties remain unspecified. The work of Willner et al.[3] offers a step-by-step guide for companies on how to use DA to gain a competitive advantage in their sales and delivery processes. High-level 3D CAD configurators[4] and master models[5] can provide a central product model that includes all necessary information for the various engineering disciplines involved in the design but working with large geometric models can also result in a large number of input variables. A 3D configurator is a software tool that allows users to customise and configure a 3D model of a product. A master model is the original 3D model that is used as a basis for creating other variations of the same object. Both technologies are crucial in the design and production of 3D objects, and they complement each other to provide a more efficient and effective production process, but one limitation of their application in DA is the selection of automatically generated alternative solutions, which can pose challenges for flexibility analysis if the model is not constructed or fed correctly. In addition, the design space may be limited to certain morphological transformations, as required in ETO-structured companies.

To address these limitations, methods that find optimal designs using techniques that do not rely on predetermined solutions can be used. Knowledge-Based-Engineering (KBE) offers benefits such as standardisation, error reduction, and shortened lead times, particularly in the early design stage[6], but the exclusion of DA in new product development processes is a limitation that needs to be addressed[7]. ETO companies often face the challenge of finding the best designs without relying on preconceived solutions. Furthermore, the ability to quickly adapt to changes in inputs or constraints requires avoiding the use of gradient or quasi-gradient information during the engineering design process. To address these needs, there are several methods available that either use randomised fluctuations in the design variables or employ learning networks to avoid the direct adjustment of design variables.

One example of the former approach is Genetic Algorithms (GAs), which are optimisation algorithms that use natural selection and genetics principles to identify the optimal solution to a problem. GAs generate a population of potential solutions and select the best ones based on defined criteria, repeating this process over several generations until an optimal solution is found. GAs are particularly useful for problems with a large search space and many possible solutions, as they can explore numerous possibilities in a relatively short time[8].

Another approach is ANNs, which are machine learning algorithms inspired by the structure and function of the human brain. ANNs consist of interconnected layers of "neurons" that can process and transmit information. They can be trained to recognise patterns and make decisions based on input data and are commonly used for image and speech recognition, natural language processing, and predictive modeling[9]. ANNs are a powerful tool in advanced data analytics due to their ability to

by: Niccolò Batini – BAKER HUGHES; Niccolò Becattini, Gaetano Cascini – POLITECNICO DI MILANO

quickly process large amounts of data. This is especially beneficial when it is challenging to identify a suitable a-priori design optimisation model. ANNs have been extensively used in the turbomachinery industry for simulating and predicting the performance of various components, such as gas turbines[10], axial compressors[11], and centrifugal compressors[12,13]. However, most of these applications focus on the performance of a single component and do not consider the impact of variations in internal design parameters on performance. Ghorbanian and Gholamrezaei[14] compared ANNs and other metamodels for predicting the performance of axial compressors. In recent years, ANNs have been utilised for optimising the layout of turbomachinery components[15] and for design optimisation as a surrogate model to reduce computational efforts with respect to more robust optimisation methods such as genetic algorithms, when a large amount of data is available[16]. Applications have been conducted on centrifugal impellers[17], radial turbines[18], and fan blades[19]. ANNs offer an alternative computational approach where the solution to a problem is derived from a set of samples rather than relying on explicit instructions as in traditional calculation methods.

One of the main advantages of using ANNs in advanced DA processes is their ability to quickly process large amounts of data[20]. Moreover, ANNs have the ability to learn and approximate relationships between inputs and outputs independently of the complexity and size of the problem[21].

However, a disadvantage of ANNs is their limited ability to perform well when faced with inputs significantly different from those used during the training phase, or when attempting to extrapolate results to regions where the inputs differ significantly from those used in the training phase[22].

3 Methodology

In this work, the hypothesis that ANNs can overcome the limitations of traditional DA solutions and classical optimisation methods, such as CFD, and meet the requirements of the COMPANY, has been made. This hypothesis has been made due to the fact that ANNs can be trained on the large amount of miscellaneous data already present in the COMPANY database, that contains the results of a total of 365 CFD simulations related to all the families of cylinders that can be offered to customers. By embedding intelligent DA master models in an integrated DA process, this work proposes to leverage ANNs to optimise non-routine design configurations of the COMPANY RCs cylinders that adhere to industry standards, such as API 618[23]. This paper aims to enhance the design process of the COMPANY RC cylinders by ensuring both task repeatability and product customisation while meeting the required lead time for the customer, to create intelligent DA models to serve as a foundation for an integrated design process of the COMPANY RC cylinders, surmounting the limitations identified in the literature and to enhancing it by integrating ANNs. This integration will enable the delivery of optimal design solutions of the COMPANY RC cylinders by exploring design spaces beyond those used during their training phase.

The current process for designing the COMPANY RC cylinders is largely manual and iterative, resulting in longer lead times and potential inefficiencies. This work aims to improve the design process by prioritising customer needs and using a systematic approach that converts input variables, such as flow rate and gas composition, into an optimised cylinder configuration. This section presents the methodology that has been used in this work. The first part presents an overview of the overall DA process implemented for ETO purposes. Then it explains in details which is the rationale behind the integration of the DA master model and the machine learning methodology in the process, specifying which are the criticalities and the choices made during their development, together with a description of the parameters that have been chosen to validate their performance.

3.1 Integrated DA in the ETO process of a RC cylinder design

The proposed method incorporates various models, rules, and constraints, such as parametric 3D models, customer requirements, and thermodynamic laws to guide design choices. To automate the process, tools such as an orchestrator for 3D CAD, CFD software, a product configurator, and ANNs are integrated.

The following is a detailed description of the integrated design development process:

- The preliminary parameters of the RC cylinders, obtained from Calc26 (the COMPANY's thermodynamic and mechanical calculation tool), are fed into a product configurator that houses the DA master model. This helps to create a preliminary solution that can be optimised based on customer requirements. A 3D parametric product configurator was chosen as the software for implementing the DA process as it can interface with the tools already being used by the COMPANY's engineering department, such as its 3D CAD software and PLM software.
- An orchestrator software is used to orchestrate the optimised parameters to obtain the ideal RC design configuration that satisfies the targeted goal parameters. This software was chosen to orchestrate the code developed for the ANNs to deliver the

by: Niccolò Batini – BAKER HUGHES; Niccolò Becattini, Gaetano Cascini – POLITECNICO DI MILANO

optimised parameters of the DA master model.

- The optimised parameters are then implemented in the product configurator to obtain the final configuration of the cylinder, which can be included in the overall thermodynamic and mechanical calculation of the entire compressor to be presented to the customer.

The design of a RC cylinder is a complex process, with pressure losses during gas flow posing a major challenge. One of the most critical areas of concern is the valve pocket section, including the valves and gas ducts, where a significant amount of energy is wasted due to the complex geometry. Evaluating this energy loss is crucial for analysing the cylinder's performance and calculating the $p-V$ cycle characteristic of the compressor. There are two main reasons for this: first, the pressure drop in the valve pocket reflects the valve's effectiveness, which is crucial for compressing the gas. Second, the relationship between the pressure drop and the mass flow rate is essential throughout the cylinder design process.

Clearance volumes, or dead volumes, also play a critical role in a compressor's performance. During the discharge phase, when the piston reaches the top dead centre, some gas volume remains uncompressed, impacting the volumetric efficiency and overall performance of the machine. The negative impact of clearance volumes on suction capacity increases with the size of the clearance volume and compression ratio.

3.2 DA master model

To study each family of RC cylinders, an intelligent master model of the cylinder assembly is developed, taking into account the critical parameters described in section 2.1. The 3D model is created using a 3D CAD software and is fully parametric. It includes all the necessary parameters for optimising the design to achieve the target parameters of the study. The study's focus is on the gas pressure losses in the cylinder valve pocket flow path, and thus a finite number of parameters are considered in the master model. These parameters define the cylinder geometry layout in the valve pocket area, valve properties, and cylinder head topology.

To facilitate communication between the CAD/PLM software and the optimisation tool, a smart 3D master model managed by the product configurator is created. It includes the rules related to the design of an API 618 COMPANY RC cylinder. This ensures consistency and robustness in the design by monitoring and maintaining the constraints of a robust design to overcome limitations related to exploring solutions that are not part of automatically generated design configurations.

3.3 From the COMPANY database to ANNs training

This article builds upon an extensive database created by the COMPANY, which involved conducting CFD analyses of the entire fleet of RC cylinders in the COMPANY. This analysis allowed the COMPANY to determine the global losses of each machine, which were summarised using the global flow coefficient K_s, as well as the clearance volume value ε.

The flow coefficient is defined as the ratio between the real and ideal gas flow rates through the RC valves, expressed as $K_s = \frac{\dot{m}_{real}}{\dot{m}_{id}}$. This coefficient represents the factor necessary to reduce the ideal mass flow rate of an ideal gas through a given valve to obtain the real mass flow rate through the same valve once the pressure drop has been established.

The clearance volume is defined as the ratio between the volume remaining between the piston, the cylinder head, and the valves of an RC cylinder when the piston reaches the top dead centre, expressed as a percentage of the cylinder capacity, i.e., $\varepsilon = \frac{V_{TDC}}{V_C}$.

These two parameters are critical in assessing the performance of the RC cylinder, and are the main inputs for the mathematical calculation of the absorbed power declared to the customer. Indeed, the absorbed power P_{ABS} is a function of both K_s and ε.

$$P_{ABS} = f(K_s, \varepsilon) \quad (1)$$

Therefore, monitoring and optimising these parameters is essential for improving the performance and efficiency of RC cylinders. Simulating the flow through reciprocating compressors to obtain parameters such as the flow coefficient and clearance volume requires significant computational and financial resources. In the past, studies focused mainly on analysing the pressure losses of valves, but with the increasing importance of energy consumption, losses from all machine components have become critical. While CFD simulations have great potential for studying the entire compressor, their high computational costs make them unsuitable for the COMPANY's ETO process schedule. Therefore, innovative methods are needed to quickly find design solutions that meet customer requests.

The COMPANY database used in this work has been obtained through CFD simulations and contains essential data for every cylinder, including a unique code, cylinder bore, number and size of valves, and six geometric parameters that affect the cylinder's performance in terms of flow coefficient and clearance volume. Additionally, K_s and ε values are available for both suction and discharge phases at the head and crank-end sides of the cylinder.

To simplify the analysis, only the suction phase of the head-end side of the cylinder was considered,

by: Niccolò Batini – BAKER HUGHES; Niccolò Becattini, Gaetano Cascini – POLITECNICO DI MILANO

and the medium value of ε between the head and crank-end sides was used. With this simplification, the system will be consistently leaner, but it will contain all the information necessary to assess the performance of the cylinder, as the flow path through from the gas duct to the compression chamber has been studied. Therefore, the database used for this study has eight independent parameters, and for each of the 365 cylinders in the original database, two dependent variables (K_s and ε).

One of the goals of this study is to explore whether ANNs can provide an efficient solution for optimising the design of a RCs cylinder, even beyond the boundaries of the training dataset, as an alternative to computationally expensive optimisation methods. To achieve this, the aforementioned dataset containing data on 365 different cylinders has been prepared and imported into an environment for numerical calculation used within the COMPANY, which has been chosen in collaboration with its IT department as the most appropriate tool for this analysis. To optimise the performance of the ANNs, a sensitivity analysis has been conducted on the number of ANNs and the size of the hidden layer. The time required for training and executing one calculation has been evaluated for various configurations of ANNs with different hidden layer sizes, ranging from 10 to 100 ANNs. The results show that the output values do not vary significantly with more than 30 ANNs with a hidden layer size of 20, while the time consumption increases continuously (see Figure 1).

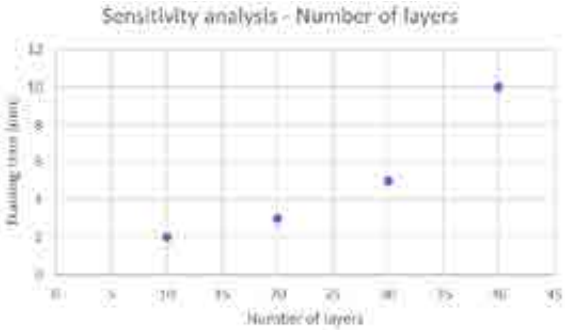

Figure 1. Sensitivity analysis on training time consumption.

Therefore, 30 feedforward ANNs, each with a single hidden layer of size 20 (as shown in Figure 2), have been created and trained to avoid bias and minimize error. The output values are the mean values computed by the 30 ANNs.

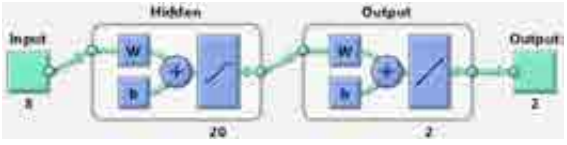

Figure 2: ANN scheme.

This environment employs a combination of training, validation, and test datasets to assess the performance of an ANN. During the training phase, the model is fitted to the training dataset to enable it to learn the correlations between inputs and outputs. The validation dataset is kept separate from the training data and used to estimate the model's performance while adjusting its hyperparameters (such as the number of hidden units) to improve its accuracy. Finally, the test dataset is also kept separate from the training data and used to provide an unbiased evaluation of the final, optimised model's performance when comparing or selecting between models. One method used to evaluate the quality of an ANN is the error histogram (refer to Figure 3). This histogram displays the distribution of errors between predicted and target values obtained from training a feedforward neural network. These errors can be either positive or negative and are separated into 20 smaller bins that are represented by vertical bars on the graph. The Y-axis indicates the number of samples from the dataset that fall into each bin, while the X-axis represents the error values. The zero-error line corresponds to the zero-error value on the error axis.

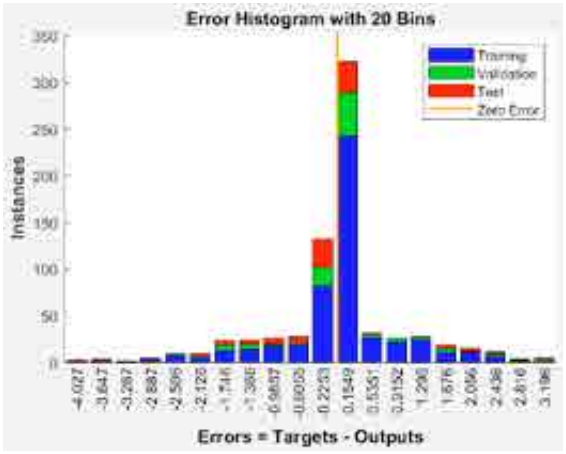

Figure 3: ANN error histogram.

To ensure the RC machine's performance meets customer expectations, the impact of error in terms of absorbed power must be evaluated, as K_s and ε values play a significant role in the machine's operation.

The ANNs' performance quality has been verified by comparing their outputs with a sample from the dataset. The Mean Absolute Percentage Error (MAPE) is a measure of prediction accuracy and has been computed for both K_s and ε variables.

$$\mathrm{MAPE}_{K_s} = \left(\frac{1}{n}\sum_{i=1}^{n}\left|\frac{K_{s,DTR}-K_{s,NN}}{K_{s,DTR}}\right|\right) = 0.1\ \% \qquad (2)$$

is the average absolute difference between the actual value of K_s in the database ($K_{s,DTR}$) and the value of K_s calculated with the ANNs ($K_{s,NN}$), divided by the actual value of K_s in the database.

$$\mathrm{MAPE}_{\varepsilon} = \left(\frac{1}{n}\sum_{i=1}^{n}\left|\frac{\varepsilon_{DTR}-\varepsilon_{NN}}{\varepsilon_{DTR}}\right|\right) = 1.43\ \% \qquad (3)$$

is the average absolute difference between the actual value of ε in the database (ε_{DTR}) and the value of ε calculated with the ANNs (ε_{NN}), divided by the actual value of ε in the database. The number of

by: Niccolò Batini – BAKER HUGHES; Niccolò Becattini, Gaetano Cascini – POLITECNICO DI MILANO

samples present in the database is denoted by n. A MAPE of 0.1% on K_s and 1.43% on ε leads to an error of 0.1% on the declared absorbed power. This error is considered acceptable since the customer has allowed for a tolerance of 3% on the declared absorbed power value, according to the API 618 standard.

3.4 Integration of ANNs in DA process

The ANNs that have been trained and validated are now integrated into a DA tool, which is capable of delivering the optimal solution once the computational goals have been set.

To organize and manage the ANNs, an orchestrator that combines multiple models and multidisciplinary applications into a simulation process flow has been chosen, automating execution across distributed computing resources, exploring the resulting design space, and identifying optimal design parameters that meet the required constraints.

In the orchestrator, the loop named "Task1" automates the updating of cylinder layouts according to customer requirements using ANNs. The routine code embeds the ANNs and allows for the manual input of values by DEs. The output is the values of K_s and ε obtained through the metamodel (i.e., ANNs) of the related cylinder layout. The "Target Solver" component in the orchestrator can be used instead to improve this process by changing the baseline value of variables within a specified range until the target values of the model are reached. The Target Solver is particularly useful for solving a system of equations made up of target parameters, like in the case of this work. The output of this run is the set of parameters for the optimised RC cylinder assembly, which must be exported into the product configurator that embeds the master model to deliver the optimal configuration. This efficient process greatly improves the speed and accuracy of the design optimisation, enabling the creation of high-quality solutions that meet customer requirements.

3.5 Key Performance Indicators (KPIs)

Functional performance and total lead time are two important metrics for ETO projects because they help measure the project's overall success and identify areas for improvement, together with ensuring that the final product or system meets the customer's requirements.

For example, if functional performance is not meeting expectations, engineers may need to revise the design or production processes to improve the product's functionality. Similarly, if lead times are too long, engineers may need to streamline their processes or identify bottlenecks to reduce the time required to complete the project.

More in detail, the KPIs used to evaluate the quality of the method described above are herein specified:

- Functional performance: measures the accuracy of the output relative to the benchmark (CFD analyses) by analysing K_s and ε values.
- Total lead time: the number of hours required to complete the entire process and deliver the optimised solution to the customer.

4 ITO application of the integrated method

In order to evaluate the practical validity of the presented integrated process, a real ITO case study of a job of the COMPANY has been developed with this methodology.

4.1 RC cylinder description

In the case study, depicted in Figure 4, the cylinder design deviates from the standard geometry of the DA master model. The modifications are applied to the geometrical parameters of the gas flow path between the valves and the compression chamber in a single-valve, forged steel cylinder. These changes are necessary to meet the customer's demand for a specific value of absorbed power, which is determined by the values of K_s and ε.

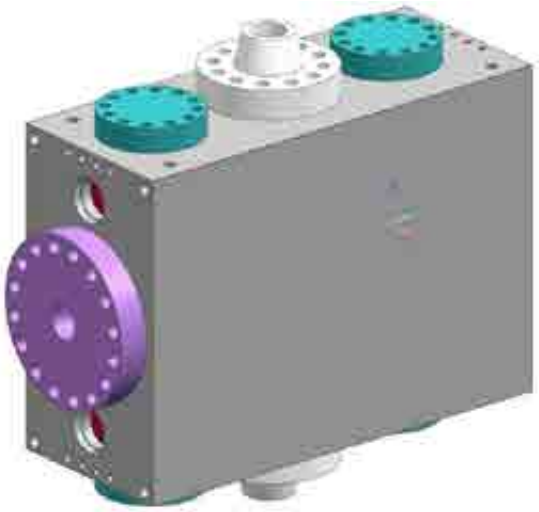

Figure 4: Forged steel cylinder used as a case study for ITO job.

4.2 Pipeline execution

The computational pipeline used for the presented case study can be summarised as follows: first, the product specifications required by the customer are collected as inputs. Calc26 then uses these inputs to outline a preliminary configuration of the cylinder, which is then configured by the product configurator using a smart master model that was previously developed based on the main properties of the cylinder assembly. The parameters of the preliminary configuration are exported to the orchestrator, where they are set according to the corresponding master model. The target parameters

by: Niccolò Batini – BAKER HUGHES; Niccolò Becattini, Gaetano Cascini – POLITECNICO DI MILANO

of K_s and ε for this case study are set in the Targets tab of the Target Solver Editor in the orchestrator, while the other 8 parameters are modified by the orchestrator in order to achieve the final configuration that meets the requirements. The final parameters are implemented in the 3D configuration of the cylinder, and a complete CFD analysis is carried out, as a benchmark to evaluate the predictive capability of ANNs. The results of this analysis are then compared with those obtained through the integrated DA model in order to verify the KPIs of the study and guarantee that the customer needs are met, as described in 2.5.

5 Results and conclusions

In the first part of this section the results are summarised and discussed. In the second part the conclusions and the future perspectives are presented.

5.1 Results and discussion

Table 1 summarises the results of our study. The error between the $K_{s,ANN}$ value obtained from the metamodel and the $K_{s,CFD}$ value obtained from the CFD model is only 0.1%, while the error between the ε_{ANN} value obtained from the metamodel and the ε_{CFD} value obtained from the CFD model is 1%. As a result, the estimated absorbed power has an error of only 0.3%. Using the integrated method, we were able to deliver the optimal configuration in just 10 minutes. In comparison, setting up the CFD model alone takes approximately 8 hours, running it takes approximately 25 hours with an 8-processor HPC, and exporting the results takes another 5 hours. The total lead time is thus around 38 hours. This study focused on modifying some geometrical parameters of an existing standard cylinder. The results show that the metamodel's and the CFD model's performance in terms of absorbed power are almost identical, with negligible errors. Additionally, using the integrated method significantly reduced the time needed to deliver the final solution from 38 hours to just 10 minutes.

K_s error	ε error	Absorbed power error	Operating time	Lead time
0.1%	1%	0.3%	8 min vs 13 hrs	10 min vs 38 hrs

Table 1: Results summary.

5.2 Conclusions and future perspectives

This paper presents an advanced integrated DA process for configuring optimal designs of RC cylinders systems. The final configuration of the target system, which in this case is an RC cylinder assembly, is developed to achieve goal values of a multi-objective function related to the machine's performance. We apply this metamodel to a case study that represents a real job of the COMPANY to explore the potential and the suitability of ANNs as an effective method for predicting cylinder performance (and therefore the entire machine's performance) compared to more time-consuming CFD models.

Our results show that the presented advanced integrated DA method is a reliable tool for the COMPANY DEs requiring modifications to existing RC cylinders design in a short period of time. ANNs allow us to reach the final configuration within a few minutes without running complete CFD models, making them particularly suitable for customer-driven engineering activities within companies following an ETO approach. Furthermore, the metamodel is capable of delivering the optimal solution within the boundaries it has been trained on, but it can provide also a target configuration layout outside these boundaries with sufficient predictive quality.

However, there are limitations to the presented methodology. Training ANNs on mean values of clearance volumes may lead to significant errors in predicting ε when the cylinder's layout is qualitatively different from the ones in the training dataset. Additionally, the lack of self-learning of ANNs after each computational path with CFD validations is a limitation. Furthermore, the integrated DA method only focuses on the gas path between the valve and the compression chamber, neglecting the pressure losses that occur in the cylinders between the gas flanges and the valves. The DA model has been developed through a finite number of parameters that do not allow design exploration outside the design space of the same type of geometry ruled by the master model itself.

To improve the integrated method's predictive capacity, we suggest developing a metamodel that represents a complete RC cylinder without approximations needed on clearance volume values, which appear to be the main contributors to errors in absorbed power calculation. Another possibility is developing advanced DA models that can meet design requirements and customer needs with a disruptive approach by exploring design solutions outside the constraints of pre-defined types of geometry. Finally, implementing self-learning metamodels that can capture CFD results of new cylinder geometries may enhance the predictive capacity of machine learning techniques compared to the one presented in this work. In any case, on-the-job applications will be carried out on future COMPANY's job opportunities to refine the methodology in a continuous enhancement of the design process routine.

by: Niccolò Batini – BAKER HUGHES; Niccolò Becattini, Gaetano Cascini – POLITECNICO DI MILANO

References

[1] Li, Z. & Zheng, X. (2017). Review of design optimisation methods for turbomachinery aerodynamics. Progress in Aerospace Sciences, 93, 1-23.

[2] Kristianto, Y. & Helo, P. & Jianxin Jiao, R. (2015). A system level product configurator for engineer-to-order supply chains. Computers in Industry. Volume 72. Pages 82-91. ISSN 0166-3615. https://doi.org/10.1016/j.compind.2015.04.004.

[3] Willner, O. & Gosling, J. & Schönsleben, P. (2016). Establishing a maturity model for design automation in sales-delivery processes of ETO products. Computers in Industry. Volume 82. Pages 57-68. ISSN 0166-3615, https://doi.org/10.1016/j.compind.2016.05.00.

[4] Raffaeli, R. & Mengoni, M. & Germani, M. (2013). Improving the link between computer- assisted design and configuration tools for the design of mechanical products, Artif. Intell. Eng. Des. Anal. Manuf. 27. 51–64. doi:http://dx.doi.org/10.1017/S0890060412000388.

[5] Frank, G. & Entner, D. & Prante, T. & Khachatouri, V. & Schwarz, M. (2014). Towards a Generic Framework of Engineering Design Automation for Creating Complex CAD Models. International Journal of Advances in Systems and Measurements. 7. 179-192.

[6] Ascheri, A.E. & Furini, F. & Colombo, G. & Atzeni, E. & Ippolito, M. (2016). A knowledge-based framework for automated layout design in an industrial environment. Journal of Computer Applications in Technology, 54, 171-183.

[7] Amadori, K. & Tarkian, M. & Ölvander, J. & Krus, P. (2012). Flexible and robust CAD models for design automation. Advanced Engineering Informatics, 26(2), 180-195.

[8] Sobieszczanski-Sobieski, J. & Morris, A. & Van Tooren, M. (2015). Multidisciplinary Design Optimization Supported by Knowledge Based Engineering.

[9] Meireles, M. & Almeida, P. & Simoes, M. (2003). A comprehensive review for industrial applicability of artificial neural networks. Industrial Electronics, IEEE Transactions on. 50. 585 - 601. 10.1109/TIE.2003.812470.

[10] Lazzaretto, A. & Andrea, T. (2001). Analytical and Neural Network Models for Gas Turbine Design and Off-Design Simulation. International Journal of Thermodynamics. 4. 10.5541/ijot.78.

[11] Yu, Y. & Sun, F. & Wu, C. (2007). Neural-network based analysis and prediction of a compressor's characteristic performance map. Applied Energy. 84. 48-55. 10.1016/j.apenergy.2006.04.005.

[12] Jiang, H. & Dong, S. & Zheng, L. & He, Y. & Ai, F. (2019). Performance Prediction of the Centrifugal Compressor Based on a Limited Number of Sample Data. Mathematical Problems in Engineering. 2019. 1-13. 10.1155/2019/5954128.

[13] Ghorbanian, K., & Gholamrezaei, M. (2009). An artificial neural network approach to compressor performance prediction. Applied Energy, 86, 1210-1221.

[14] Ghorbanian, K. & Gholamrezaei, M. (2007). Axial Compressor Performance Map Prediction Using Artificial Neural Network. 10.1115/GT2007-27165.

[15] Du, Q. & Yunzhu L. & Like, Y. & Tianyuan, L. & Di, Z. & Yonghui, X. (2022). Performance prediction and design optimisation of turbine blade profile with deep learning method, Energy, Volume 254, Part A.

[16] Woldemariam, E. T. & Lemu, H. G. (2019). A Machine Learning Based Framework for Model Approximation Followed by Design Optimisation for Expensive Numerical Simulation-Based Optimisation Problems. Paper presented at the The 29th International Ocean and Polar Engineering Conference, Honolulu, Hawaii, USA, June 2019.

[17] Ji, C. & Wang, Z. & Tang, Y. & Xi, G. (2021). A Flow Information Based Prediction Model Applied to the Non-axisymmetric Hub Optimization of a Centrifugal Impeller. Journal of Mechanical Design. 143. 1-17. 10.1115/1.4050655.

[18] Luczynski, P. & Hohenberg, K. & Freytag, C. & Martinez-Botas, R. & Wirsum, M. (2021). Integrated design optimisation and engine matching of a turbocharger radial turbine. 10.1201/9781003132172.

[19] Lopez, D. & Ghisu, T. & Shahpar, S. (2021). Global Optimisation of a Transonic Fan Blade Through AI-Enabled Active Subspaces. Journal of Turbomachinery. 144. 1-33. 10.1115/1.4052136.

[20] Rojas, R. (1996). Neural Networks: a Systematic Introduction. Berlin: Springer-Verlag.

[21] Haykin, S. (2004). Neural Networks. A comprehensive foundation. Neural networks, 2(2004), 41.

[22] Bishop, C. M. (1994). Neural networks and their applications. Review of Scientific Instruments / Volume 65 / Issue 6.

[23] Reciprocating Compressors for Petroleum, Chemical, and Gas Industry Services. API Standard 618, Fifth edition, December 2007.



Real-World Compressor Fault Detection for Digital Twin Environments

by:

Ramchandran Gautham, Konstantopoulou Evangelia, Koutsivitis Panagiotis, Framke Nils-Henning
Gamma Technologies LLC
Westmont, Illinois, United States of America
g.ramchandran@gtisoft.com

13th EFRC CONFERENCE
September 19th – 21st 2023, Zagreb

Abstract:
With the increasing amount of data being monitored and available in this era of Industry 4.0, fault detection and predictive maintenance of complex physical systems has become a very real and viable possibility today. Multi-physics simulation models of reciprocating compressors as part of Digital Twin Environments have advanced significantly, thus allowing for the quick, easy generation of synthetic training datasets and specific labelled anomalous datasets simulating real-world faults. In this study, a well-known commercial multi-physics simulation software is used to model an industrial reciprocating compressor system with various domains including bearings, valves, compressor shaft mechanics, NVH, lubrication, and gas flow dynamics. The model is exercised with variability of typical physical parameters to simulate real-world operation of well running, non-faulty reciprocating compressor systems and generate "no-fault" virtual input datasets. Faults are then intentionally introduced within the digital twin system to simulate real-world anomalies manifested via behavioural changes in signals of typical sensor data (eg: compressed gas pressure) present in actual compressor systems. Supervised learning techniques are applied to train and optimize machine learning models for fault detection. The trained models can be deployed in real-world scenarios with online real-time monitoring to detect potential failures and identify fault causes. This can help with predictive maintenance of compressor systems, reduce unscheduled downtime, and thereby decrease the economic impact from loss of production. The promise of such a technology is demonstrated as the ability to reproduce and prevent faults without actually creating them on a real machine which would risk severely damaging these large and expensive machines.

by: Gautham Ramchandran, Evangelia Konstantopoulou, Panagiotis Koutsivitis, Nils-Henning Framke – GAMMA TECHNOLOGIES

1 Introduction

Condition monitoring and fault detection technologies for reciprocating compressors have been around for a significant period of time (since the 1950's). With advancements in technology, there is renewed interest and need to ensure that these compressors, especially for large-scale industrial operations, must be effectively maintained to ensure longevity and optimal performance[1]. Being very large machines, it is often difficult to quickly find the sources of problems. Since they often service critical operations at industrial scales such as refineries, oil production facilities, chemical plants, etc., it is not ideal to shut down operations for extended periods of time in order to diagnose operational faults. While it is technically feasible to implement sophisticated instrumentation to measure say the acceleration of the pistons, the valve temperature, or the in cylinder pressure, the complexity of both monitoring and assessing non-optimal function increases along with the capital expenditure to retrofit machines with these devices. As these are large machines with many expensive components, it is also not practical to perform physical tests to study various fault patterns that would end up destroying the components or at the very least, reduce their operational integrity. This limitation curtails efforts to generate large sets of data, especially data consisting of fault patterns during actual operation over a wide operating range.

Given these constraints, there is a strong motivation to leverage advancements related to digital twins in the era of Industry 4.0. This approach consists of first training relevant machine learning models with data transmitted from a compressor under normal operation. This data can either be gathered through on-board diagnostics or using a digital twin of the actual compressor to generate acceptable data that is representative of normal operation. Depending on the technique being utilized, there is a need to train the models with what represents a faulty signal. For instance, unsupervised learning algorithms can only predict whether or not a fault exists, often with reduced accuracy, rather than pinpoint the exact cause of the fault. Also, generating faults on an operational compressor can be costly and so, the digital twin can be utilized to simulate actual faults that may occur during operation. Finally, the trained models can be deployed for condition monitoring and effectively aid in the advanced detection and prevention of faults by alerting operations and maintenance to a developing problem based on the live data being gathered and transmitted from an operational compressor.

The first pre-requisite to adopting such an approach involves having a highly reliable, predictive, accurate, and fast-running virtual representation of the actual machine in operation, i.e., a digital twin. A few different simulation options exist today for modelling different fault relevant systems at various levels of fidelity. However, those options mostly cover only one physical domain. It is important to consider a practical approach that combines predictive, physics-based modelling methods of the various compressor subsystems with being able to generate reliable data quickly that represents true compressor operation, including various faults that may occur over the lifetime of the compressor. To this end, a state-of-the-art multi-physics system simulation software is used to model not only the compressor gas thermodynamics, but also incorporate elements such as valve dynamics, shaft dynamics, lubrication, cooling, bearing performance, noise, vibration and harshness (NVH) calculations, etc. to facilitate the representation of a true digital twin[6,7,9].

The second pre-requisite to leveraging digital twins for predictive maintenance is the ability to analyze the data generated by these models or via sensors on compressors in operation, and accurately predict the cause of a particular fault. This can help reduce compressor downtime, most of which would be spent in identifying the cause of the issue following which an appropriate fix may be put in place.

In this study, various machine learning and deep learning techniques based on literature[2,3,4,5,10,11] have been implemented and studied to analyse whether simulated faults can be detected accurately. It will be shown that even though unsupervised learning algorithms perform well, supervised methods consistently provide better predictive capability.

2 Digital Compressor System Representation

This work focuses on the ability of the algorithms studied to analyse a specific fault and identify its cause. As a proof of concept, the faults being analysed here are valve stiction and valve leakages during the operation of an industrial reciprocating air compressor. As a result, the primary elements of the model that are discussed will encompass the compressor thermodynamics and valve dynamics.

However, the same model shown in Figure 1 can be utilized to study various other aspects of reciprocating compressor physics including:

- Mechanics and NVH to study crankcase vibration due to malfunctions such as an imbalanced crankshaft, grout deterioration or the loosening of foundational bolts, piston nuts, or crosshead attachments.
- Lubrication and cooling to study failures due to low temperatures and associated oil viscosity changes resulting in lack of oil supply to the crosshead during startup.

by: Gautham Ramchandran, Evangelia Konstantopoulou, Panagiotis Koutsivitis, Nils-Henning Framke – GAMMA TECHNOLOGIES

- Main and connecting rod bearing performance to analyze temperature related failures that may result in insufficient load bearing capacity and metal-to-metal contact.
- Piston ring leakages which will result in recompression of gas that will raise cylinder discharge temperatures.

While these are by no means an exhaustive list of faults that could occur during actual operation, a validated digital twin in combination with robust machine learning techniques can be utilized effectively to identify potential faults and their causes very quickly before an extended period of compressor downtime becomes necessary or catastrophic issues manifest.

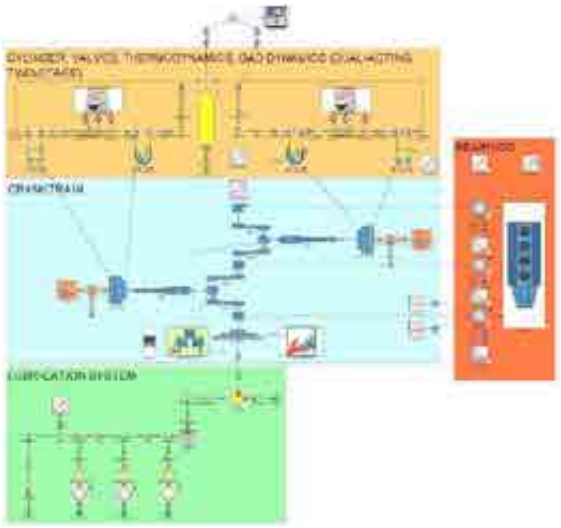

Figure 1: Digital twin representation of an industrial double-acting two-stage reciprocating air compressor

2.1 Multi-Physics Compressor Model

This section describes the reciprocating compressor model and the included physics corresponding to the gas compression and valve dynamics.

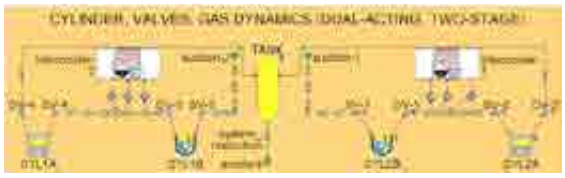

Figure 2: Reciprocating Compressor Gas Dynamics Model with Dynamic Valve Characteristics

Figure 2 highlights these specific aspects of the larger, all-encompassing detailed compressor model.

The specific machine studied is a two-cylinder, two-stage, dual-acting, opposed piston type reciprocating air compressor which is a common design for industrial applications. Each piston is dual-acting since it compresses air in both directions. The compression in each piston is two-stage: the air compressed by the downward stroke in the crankcase is then passed as suction gas to the main cylinder and is compressed again during the upward stroke.

The compression of the two cylinder and crankcase volumes are governed by the reciprocating motion of the opposed pistons within the crankshaft assembly shown in Figure 1. The rotation of the crankshaft leads to the translation of the pistons, thereby compressing the crankcase (CYL1B and CYL2B) and main cylinder (CYL1A and CYL2A) volumes indicated in Figure 2.

The suction and discharge valves of each crankcase and main cylinder volume are modelled as check valves with fluid-structure interaction. The valve flow characteristics are provided via a table of flow area (defined by reference area and discharge coefficients) as a function of pressure drop. The valve dynamics are determined based on valve mass, spring characteristics, and the flow forces on the valve. Reverse flow through the valves may occur while they are in the process of closing since the inertia of the valve mass prevents the valve from instantly closing when the pressure reverses.

On each cylinder bank, the model includes intercooling between the two stages. This is represented by a control system that actuates the intercooler outlet gas temperature based on effectiveness data and sensed upstream conditions.

The suction pressure and temperatures are imposed based on anticipated test conditions. The compressor discharge pressure and temperature are predicted based on the size of the orifice representing the plant restriction downstream of the machine.

The compressible 1D Navier-Stokes equations are solved within various volumes of the compressor flow path. Mass, momentum, energy, and species are conserved throughout. The flow system is discretized based on a staggered grid approach where the scalar variables such as pressures, temperatures, etc. are solved at the centre of each sub-volume while vector quantities such as mass flow rates and velocities are solved at the boundaries between sub-volumes. Flow between adjacent subvolumes is modelled through orifices which are defined via diameters or areas and discharge coefficients as inputs. A variable timestep size Explicit Euler integration scheme is used to march forward in time. Additional details regarding the simulation software's flow solution are available in literature[8].

The model is assumed to be at steady state when the cycle-to-cycle average mass flow rate tolerance for all flow connections is within 0.2%. A pressure convergence criterion is not directly used. However, if the maximum pressure change for all flow components is greater than or equal to 1%, then the mass flow criteria is made four-times stricter.

The model contains 98 flow volumes. The compressor speed is fixed at 1200 RPM. A Design of Experiments Latin Hypercube approach is used to

by: Gautham Ramchandran, Evangelia Konstantopoulou, Panagiotis Koutsivitis, Nils-Henning Framke – GAMMA TECHNOLOGIES

generate a dataset containing 1000 samples of a full working cycle for nominal compressor performance by varying parameters including valve discharge coefficients, spring stiffnesses, intercooler effectiveness, compressor suction pressure and temperature, and the orifice system restriction within the variance of the compressor operating environment and expected manufacturing tolerances. Most cases take an average timestep size of 3.6e-5 seconds (about 0.25 degrees). The overall runtime varies between 10-50 seconds and take 5-15 cycles to reach steady state on a modern PC.

2.2 Introduction of Faults to the Simulation Model

The compressor that is modelled for nominal machine characteristics and performance can be easily extended to include faults that should be detected by machine learning algorithms. In this study, the fault being analysed is with regard to one of the high pressure discharge valves (DV2 or DV4 from Figure 2) which are either stuck or leaking even when closed. These conditions are easily introduced into the model by actuating the valve upstream pressure area to a lower than expected value when closed (valve lift = 0) to simulate a "stuck" state; or by setting the valve discharge coefficient to a non-zero value when the valve is seated (valve lift = 0) to simulate a "leaking" state. The goal is to correctly detect when a fault is present and identify the faulty valve so that it may be replaced. The only signal used to train the algorithms described in the following section is the instantaneous pressure from the tank (TANK in Figure 2) downstream of the compressor discharge port which can be easily measured on an operational compressor using a pressure transducer. For each fault point and type, 1000 full transient working cycle signals with varying operational boundary conditions are calculated, resulting in a dataset of a total 5000 samples.

It is important to note that this simplified representation of the faults was chosen to prove the concept of using supervised learning algorithms on a reduced set of measured quantities. More refined defect modelling approaches can be implemented within the simulation tool which may consider detailed models for the structure and valve dynamics that also account for friction (dry and viscous), compliance (which can vary with deformation), and the temperature of the valve structure.

3 Proposed Algorithms

To explore the capabilities of machine learning methods in the context of fault detection, two main studies will be performed. The first study is a comparison between unsupervised and supervised learning approaches while the second is a comparison between supervised methods in a variety of realistic scenarios. In these studies, different unsupervised and supervised learning techniques were investigated over their performance and robustness for fault detection based on the data from a virtual compressor. Hyperparameter optimization was performed on the models using a grid search algorithm guided by accuracy for binary classification and F1-score for multi-class as evaluation metrics on the validation set. The models' hyperparameters after the optimization can be seen in Tables 1 and 2.

3.1 K-Means

K-Means is an unsupervised clustering algorithm that partitions data into clusters such that each data point belongs to the cluster with the nearest centroid. To apply this for fault detection, the K-Means model is fit on a training set containing only normal points and their clusters are calculated. Then, each of the data in the validation set is assigned to one of the previously created clusters and a threshold in relation to the cluster's distribution standard deviation is defined. In case a data point's distance from its cluster's centroid is larger than the threshold, it is classified as a fault.

More formally, let $x_i \in \mathbb{R}^n$ be the i-th data point and c_k be the centroid of the k-th cluster where x_i belongs. Then:

$$d(x_i, c_k) = \sqrt{\sum_{j=1}^{n} (x_{ij} - c_{kj})^2} \quad (1)$$

$$t = \tau \cdot \sigma_k \quad (2)$$

where $\tau \in \mathbb{R}^+$ and σ_k is the standard deviation of the data belonging to k-th cluster. If $d(x_i, c_k) > t$ then x_i is a classified as fault.

For this implementation, the data was partitioned into 9 distinct clusters and the threshold for each cluster k was set to $\mathrm{t} = 2\sigma_k$ to follow the two-sigma rule.

3.2 Autoencoder

Autoencoder is a type of Deep Neural Network that can be used for unsupervised learning. It is composed of an encoder and a decoder. The encoder maps the input data to a lower dimensional representation, while the decoder tries to reconstruct the original data using this representation. In the case of fault detection, the goal of the model is to minimize the reconstruction error of the normal data points. To do so, a threshold is defined and any data point with a reconstruction error larger than this is classified as a fault. Here, the threshold was defined as the maximum reconstruction error among the training patterns. Formally, if $x_i \in \mathbb{R}^n$ is the i-th data point and $\hat{x}_i$ is the point constructed by the decoder, the reconstruction error is computed as:

$$r(x_i, \hat{x}_i) = \frac{1}{n} \sum_{j=1}^{n} |x_{ij} - \hat{x}_{ij}| \quad (3)$$

and the threshold is defined as:

$$t = max\{r(x_1, \hat{x}_1), r(x_2, \hat{x}_2), \ldots, r(x_N, \hat{x}_N)\} \quad (4)$$

by: Gautham Ramchandran, Evangelia Konstantopoulou, Panagiotis Koutsivitis, Nils-Henning Framke – GAMMA TECHNOLOGIES

$\forall x_i \in Train\ Set$ such that if $r(x_i, \hat{x}_i) > t$ then x_i is a classified as fault. The autoencoder created for the purposes of this paper consists of a 3-layered encoder and decoder and more than 113000 trainable parameters.

Table 1: Optimal hyperparameters found using grid search for unsupervised models.

Model	Hyperparameters	Value
K-Means	Clusters	9
Autoencoder	Encoder Layers	2
	Decoder Layers	2
	Encoder Nodes	128, 64
	Decoder Nodes	32, 64
	Latent space size	8
	Activation function	ReLU[1]
	Loss function	CCE[2]
	Optimizer	Adam
	Learning rate	0.001
	Epochs	500

3.3 KNN

K Nearest Neighbors (KNN) is a non-parametric, supervised learning algorithm mainly used for classification tasks. KNN predicts the class of a new data point by performing a majority vote between the k nearest neighbors' classes and assigning the resulting class to the new point. The Euclidean distance metric was selected to train a KNN classifier, and the number of neighbors was set to $k = 3$.

3.4 SVM

Support Vector Machines (SVM) is a supervised learning algorithm, capable of creating both linear and non-linear decision boundaries, which classifies data by finding a hyperplane on the feature space that best separates them into the different classes. To apply SVM for the multi-fault detection problem, a one-vs-one approach is used which breaks down the multi-fault problem into multiple binary tasks by creating $\frac{m(m-1)}{2}$ distinct classifiers, where m is the number of classes between the results of the different classifiers. The SVM model created has a third-degree polynomial kernel and the regularization parameter used to penalize wrong predictions was set to 1.

3.5 MLP

Apart from the machine learning models mentioned above, two deep neural networks were implemented for the multi-fault detection. First a Multi-Layer Perceptron (MLP) was created, which is a fully connected, feedforward Artificial Neural Network (ANN). It has 3 dense hidden layers with more than 56000 trainable parameters and employs a non-linear activation function to be able to learn non-linear relationships in the data.

3.6 CNN

Finally, a Convolutional Neural Network (CNN) was implemented, which is a type of ANN that uses convolutions to learn and extract underlying features from the data. For the purposes of fault detection, a CNN with a total of 30000 trainable parameters, 2 convolutional layers and a dense layer was created. Two one-dimensional filters of size 3 and 2 respectively for each hidden layer, were slid over each signal in the dataset, extracting 16 channels each. The CNN architecture is visualized in Figure 3 below.

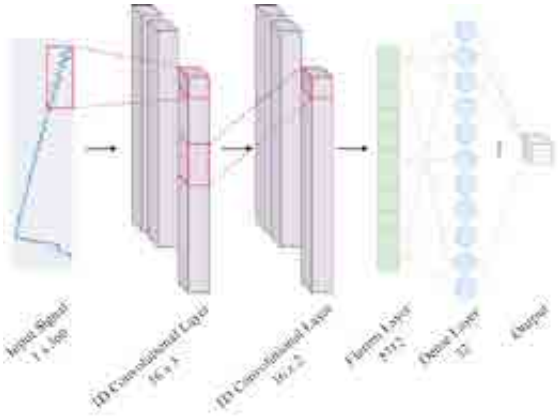

Figure 3: CNN model architecture

Table 2: Optimal hyperparameters found using grid search for supervised models.

Model	Hyperparameters	Value
KNN	Neighbors	3
SVM	C	1
	Kernel	Polynomial
	Degree	3
MLP	Hidden layers	3
	Nodes	128, 64, 32
	Activation function	ReLU
	Loss function	CCE
	Optimizer	Adam
	Stepping size	0.001
	Epochs	500
CNN	Hidden layers	3
	Nodes	16, 16, 32
	Convolution filters size	3, 2
	Convolution filters stride	1, 1

[1] ReLU: Rectified Linear Unit

[2] CCE: Categorical Cross-Entropy

by: Gautham Ramchandran, Evangelia Konstantopoulou, Panagiotis Koutsivitis, Nils-Henning Framke – GAMMA TECHNOLOGIES

	Activation function	ReLU
	Loss function	CCE
	Optimizer	Adam
	Stepping size	0.001
	Epochs	500

4 Methodology and Problem Formulation

In this section, the datasets generated using the simulation model will be described and the pre-processing steps done prior to testing the algorithms are highlighted. Additionally, the various scenarios considered with respect to the training datasets are also explained.

4.1 Dataset Description

The simulation model was used to generate a training dataset for "No Fault" and various "Fault" conditions. As mentioned previously, the instantaneous tank pressure at the compressor discharge was used for fault detection since this is easily measured on an actual operational compressor with the help of a pressure transducer.

Table 3: Fault Codes and their Descriptions to Compare Supervised Learning Algorithms

Fault Code	Description
00	No Fault
1X	Fault on cylinder bank 1 (left)
2X	Fault on cylinder bank 2 (right)
11	Discharge valve DV4 stuck
12	Discharge valve DV4 leaking
21	Discharge valve DV2 stuck
22	Discharge valve DV2 leaking

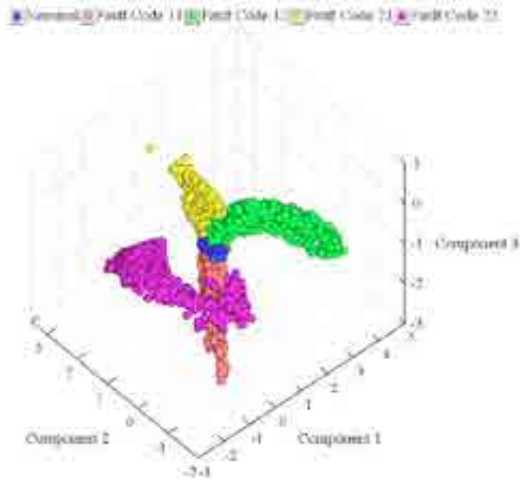

Figure 6: Class distributions projected in 3 principal components space.

Table 3 describes the various fault codes representing the different fault states (no fault, valve stuck, valve leaking, and on which cylinder bank the fault occurs) and their causes, while Figure 6 shows the data distribution for each fault projected in 3D space. These faults were used to compare the various supervised learning algorithms.

Table 4: Fault Codes and their Descriptions for Comparing Supervised vs Unsupervised Learning Algorithms (Binary Classification)

Fault Code	Description
0	No Fault
1	Fault Present

Table 4 shows the fault codes used to directly compare the supervised and unsupervised learning approaches. In the context of this study, unsupervised learning techniques cannot distinguish the different fault classes mentioned in Table 3. Therefore, a binary classification task of "normal vs faulty" operation was studied, with the dataset's faults all being grouped under a single class. This approach allows these algorithms to predict whether an anomaly is present or not without being able to detect the precise location/cause.

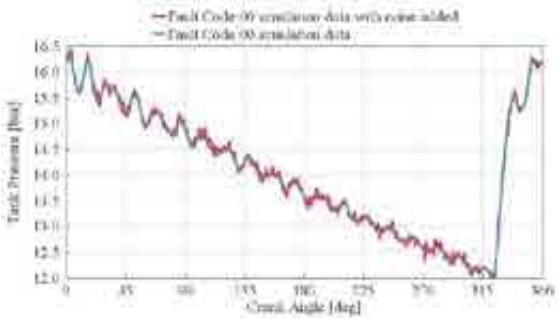

Figure 4: Sample instantaneous tank pressure trace near compressor discharge

Figure 4 shows the typical raw data for the instantaneous tank pressure plotted against crank angle that is generated by exercising the model.

4.2 Data Pre-Processing

Once the dataset has been generated using the multi-physics compressor simulation model, some pre-processing must be done before they can be fed into the machine learning models. First, the dataset was structured such that each row represents a single revolution (referred to as a "pattern") and the instantaneous tank pressure value at each step is considered to be a different feature. The patterns were resampled down to 1 degree per revolution (for 360 degrees of crank angle rotation), reducing the dimensionality of the feature space. This was done to prevent problems caused by the "curse of dimensionality" and to resemble the frequency of data captured by a pressure sensor. Next, to ensure numerical stability of the algorithms, min-max

by: Gautham Ramchandran, Evangelia Konstantopoulou, Panagiotis Koutsivitis, Nils-Henning Framke – GAMMA TECHNOLOGIES

normalization was applied to the data. These actions were performed for both studies and scenarios described.

For the unsupervised learning approach, the dataset was randomly split into a training set containing only non-faulty patterns, a validation set containing 50% fault patterns and a test set of the same size and number of fault patterns. The dataset for the supervised models was randomly split into a training, validation, and test sets containing approximately 2/3, 1/6 and 1/6 of the patterns respectively. The training sets were used to train the models, the validation sets were used to guide the hyperparameter tuning, and the test set was used for the final evaluation of each model.

4.3 Scenarios Considered

To analyse and evaluate the robustness of the various supervised learning methods, multiple scenarios were considered which are briefly described in Table 5. Since unsupervised machine learning methods are not capable of performing multi-class classification in our context, the labels in the dataset are changed as indicated in Table 4 and the problem is redefined as a binary classification task in order to compare them to the supervised methods.

Table 5: Scenario Considered and its Description for Comparing Supervised Learning Algorithms

Scenario	Description
No Changes	No changes were made to the original dataset other than the pre-processing steps.
Added Noise	Gaussian noise of up to 5% of the sampled data's standard deviation was introduced to test for robustness in case physical hardware sensor values are samples with additional parasitic noise from the acquisition system or other sources).
Down Sampled Signal	Instead of 360 samples per cycle, the signal was further condensed to 36 samples per cycle (one pressure measurement for every 10 degrees of crank angle rotation)
Class Imbalance	The dataset was modified to contain a 1:5 ratio of fault vs no fault was applied to every fault type. For instance, for every 1000 normal patterns, 200 randomly selected patterns for each fault (11, 12, 21, and 22) were used.

5 Results and Discussion

The results from the two studies are highlighted in this section.

5.1 Unsupervised vs Supervised Learning

This first study compares the accuracy of various supervised and unsupervised learning algorithms based on the binary classification task of "normal vs faulty" operation.

The unsupervised learning classifiers are fitted on the training data containing only normal operation patterns so that they can learn what is considered to be normal operation. In contrast, supervised learning classifiers were fitted on a training dataset containing both normal and anomalous patterns and as a result can directly learn both normal and faulty operational behaviour.

As seen from Table 6, most of the supervised learning methods outperform the unsupervised learning algorithms for this binary classification task. This important result highlights the benefit of adopting a supervised learning approach that requires both normal and faulty patterns for training purposes, thereby indicating that an accurate simulation model of the compressor system can significantly improve the fault prediction accuracy. As such, it is an important part of enabling real-world predictive maintenance and fault detection in digital twin environments. Additionally, the advantage of utilizing supervised learning techniques is that the precise location or cause of the fault can be reported from a bulk measurement to support maintenance, unlike unsupervised learning techniques which can only detect whether an anomaly is present.

Table 6: Comparison of Unsupervised and Supervised Learning Algorithms

Model	Accuracy	Type
K-means	0.715	Unsupervised
Autoencoder	0.97	Unsupervised
KNN	0.95	Supervised
SVM	0.99	Supervised
MLP	0.995	Supervised
CNN	0.996	Supervised

5.2 Comparing Supervised Learning Methods

In this second study, the various supervised learning methods were compared according to the scenarios described in Table 5.

From Tables 7-10, it can be observed that the CNN algorithm appears to perform the best overall across all the scenarios modelled here. It consistently has the highest performance while at the same time

by: Gautham Ramchandran, Evangelia Konstantopoulou, Panagiotis Koutsivitis, Nils-Henning Framke – GAMMA TECHNOLOGIES

maintaining both low (or zero) false positive and false negative rates. This is a strong indication that using a CNN model to monitor the condition of a compressor will neither cause too many false alarms nor miss too many faults. Figure 7 shows the distribution of Correct & False predictions of the best CNN architecture projected in a 3D space calculated by Principal Component Analysis (PCA).

In general, all the models appear to be fairly robust to moderate noise, perform well even when fewer fault patterns are available, and maintain high accuracy on data with small sampling rates which may be observed in the field. They also manage to achieve a good balance between false positive and negative rates.

Table 7: Scenario 1 Results: No Changes

Model	Accuracy	F1 Score	False Positive Rate	False Negative Rate
KNN	0.956	0.957	0.03	0.04
SVM	0.972	0.972	0.01	0.03
MLP	0.994	0.994	0.01	0.004
CNN	0.996	0.996	0.01	0

Table 8: Scenario 2 Results: Added Noise

Model	Accuracy	F1 Score	False Positive Rate	False Negative Rate
KNN	0.956	0.957	0.03	0.04
SVM	0.972	0.97	0.01	0.03
MLP	0.983	0.983	0.08	0.01
CNN	0.984	0.984	0.06	0.01

Table 9: Scenario 3 Results: Down Sampled Signal

Model	Accuracy	F1 Score	False Positive Rate	False Negative Rate
KNN	0.945	0.947	0.04	0.05
SVM	0.962	0.963	0	0.05
MLP	0.975	0.975	0.03	0.02
CNN	0.993	0.993	0.006	0.007

Table 10: Scenario 4 Results: Class Imbalance

Model	Accuracy	F1 Score	False Positive Rate	False Negative Rate
KNN	0.933	0.906	0	0.17
SVM	0.97	0.96	0	0.07
MLP	0.987	0.982	0	0.03
CNN	0.99	0.987	0	0.02

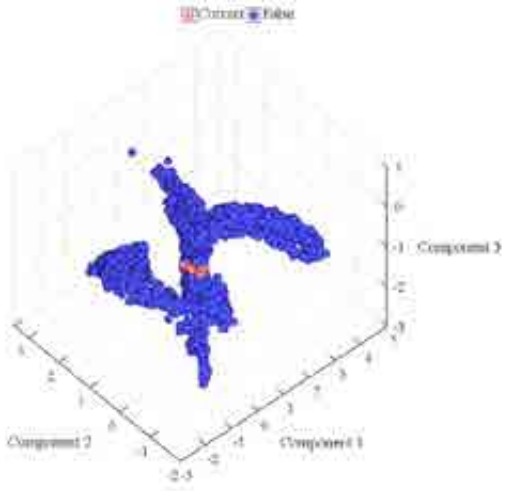

Figure 7: CNN model's prediction distributions projected in 3 principal components space.

An additional study was performed as a variation on Scenario 2 (Added Noise). In order to test the models' robustness to various levels of noise that may exist in real-world sensor acquired data, Gaussian noise of up to 15% of the standard deviation was added to the test set signals. It is worth noting that noise was not introduced to the training or the validation dataset in order to investigate how a model trained on synthetic data created by a simulation software can predict faults coming from real sensors.

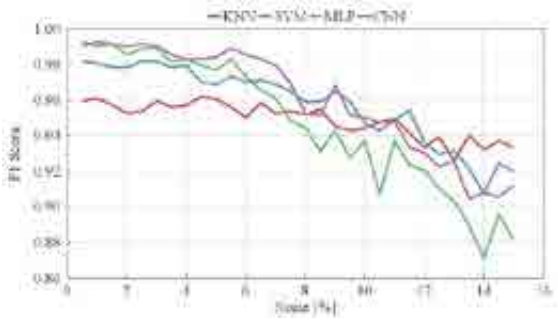

Figure 5: Supervised Learning Algorithms' F1 Score vs Noise %

Figure 5 indicates that a gradual "inversion" occurs with regard to the best performing model when noise above 6% is introduced.

While the neural networks appear to outperform the machine learning models at low noise levels, beyond a certain percentage of noise, the machine learning models exhibit better noise robustness. A more detailed analysis revealed that when noise was increased, the false positive rates increased as well. Since the deep learning models were only trained on

by: Gautham Ramchandran, Evangelia Konstantopoulou, Panagiotis Koutsivitis, Nils-Henning Framke – GAMMA TECHNOLOGIES

simulated data without noise, they classify patterns with too much noise as faults. This can be attributed to a general inclination of the deep learning methods to better generalize when more data are available. This is especially the case when the training data has a significant variance, as it can be a way to limit overfitting.

6 Final Remarks and Conclusion

This work highlights the advantages of using supervised learning models to identify and flag real-world faults such as valve stiction or leaks that may be present during reciprocating compressor operation. In order to train these models to be able to recognize various fault patterns, it is imperative that an accurate digital representation of the actual compressor in form of a multi-physics simulation model is used to generate fault data. This approach avoids damage that may be induced to an operational compressor and can help with preventative maintenance.

As possible next steps to this study, various other faults described in Section 2 could be simulated using the available multi-physics simulation model to identify the ideal supervised learning approach to deploy for real-world predictive maintenance and fault detection. From an algorithmic analysis perspective, the performance of these techniques applied to signals from other sensible measurement locations as well as lower fidelity, cycle, or time averaged signals and their combinations can be studied. It would be interesting to analyze whether a discharge valve leak or stiction fault occurring at the first stage of the compressor (DV1 or DV3) can be detected accurately by the various techniques explored here. Adding noise to the training data as a data augmentation technique might offer valuable insight into how the deep learning models can be made more robust to noise. Finally, the authors are eager to explore the application of the proposed methodology using data available from case studies of various real fault scenarios in existing compressors.

7 References

[1] Schultheis S. M., Lickteig C. A., and Parchewsky R. (2007): Reciprocating Compressor Condition Monitoring, 36th Turbomachinery Symposium, 107-114.

[2] Castellani A., Schmitt S., and Squartini S. (2021): Real-World Anomaly Detection by Using Digital Twin Systems and Weakly Supervised Learning, IEEE Trans. Industr. Inform., Vol. 17, No. 7, 4733-4742.

[3] Britzger M., Beckmann N., and Seehausen F. (2022): Machine Learning Driven Local Assignment of Compressed Air Consumption Anomalies, Proc. of the 13th Int. Fluid Power Conference, Aachen, 1100-1106.

[4] Pang G., Shen C., Cao L., and Van Den Hengel, A. (2021): Deep Learning for Anomaly Detection: A Review, ACM Comput. Surv., Vol. 54, Issue 2, Article No. 38, 1-38.

[5] Charoenchitt C., and Tangamchit, P. (2021): Anomaly Detection of a Reciprocating Compressor using Autoencoders, Second Int. Symp. Instrumentation, Control, Artificial Intelligence, and Robotics, 1-4.

[6] Ramchandran G., Bhatia K., and Aihara, R. (2018): Simulation of 1D Flow Coupled with 3D Multi-Body Dynamics Model of a Double-Acting Swashplate Compressor, 24th Int. Compressor Eng. Conference at Purdue, West Lafayette, USA, paper ID 2623.

[7] Bianchi G., Marchionni M., Kennedy S., Miller J., and Tassou, S. (2019): One-Dimensional Modelling of a Trilateral Flash Cycle System with Two-Phase Twin-Screw Expanders for Industrial Low-Grade Heat to Power Conversion, Designs, Vol. 3, No. 41, 1-16.

[8] Gamma Technologies (2023): GT-SUITE Flow Theory Manual, Westmont, Illinois.

[9] Ramchandran G., and Harrison J. (2021): A Thermodynamic Chamber Modelling Approach for Oil Free and Oil Injected Twin Screw Compressors, IOP Conf. Ser.: Mater. Sci. Eng., Vol. 1180 012002.

[10] Braei, M., and Wagner, S. (2020). Anomaly detection in univariate time-series: A survey on the state-of-the-art. arXiv preprint arXiv:2004.00433.

[11] Lv, Q., Yu, X., Ma, H., Ye, J., Wu, W., and Wang, X. (2021). Applications of machine learning to reciprocating compressor fault diagnosis: A review. Processes, Vol. 9, No. 6, 909.

TNO innovation for life

Using Transfer Learning to Construct Accurate Data-driven Compressor Models on Limited datasets of Field Measurements

by:

Jonah Poort
Heat Transfer & Fluid Dynamics
jonah.poort@tno.nl

Rens Bazuin
Heat Transfer & Fluid Dynamics
rens.bazuin@tno.nl

TNO
Delft, Netherlands

13th EFRC CONFERENCE
September 19th – 21st 2023, Zagreb

Abstract:
Accurate computational models are key in enabling optimal operation of compressor systems. While physics-based numerical models can provide accurate results, they can be complex to set up and can miss some of the finer details of a specific compressor system's operation. Data-driven models (e.g. artificial neural networks), on the other hand, can use field measurements to provide models tailored to the exact (real-world) behavior of a system, and are relatively easy to set up. However, such data-driven models typically require a large number of data points to provide accurate predictions, while in reality the number of field measurements may be limited. The introduction of data-driven models capable of accurate predictions, even when trained on datasets of limited size could be beneficial for (for instance) predicting the internal cylinder pressure.
In this study, a machine learning technique called transfer learning was used to combine numerical simulation results with field data in order to create accurate data-driven models. In this process, an initial neural network model is trained on a large dataset of numerical model predictions to learn general relations, and subsequently fine-tuned to the compressor's specific behavior using a much smaller dataset of field measurements.
In this paper, transfer learning was applied to a compressor system of a Dutch gas production facility using 1400 numerical data points in the compressor's range of operation and 5-40 field measurement data points. Models were trained to predict the internal cylinder pressure, with pressure fluctuations up to the 32nd harmonic, based on compressor speed, suction pressure, and discharge pressure. Results show that the majority of transfer learning models trained clearly surpassed models trained on numerical or field measurements alone. In the future, this could allow for more tailored data-driven modelling solutions for systems with limited field measurements.

by: Jonah Poort, Rens Bazuin – TNO

1 Introduction

In general, (older) compressor fleets do not have elaborate condition monitoring systems installed. Standard sensors (as stipulated by API 618/670) will be available, but for example real-time monitoring of the cylinder pressure is not available, whereas this can provide valuable insight in the performance of the compressor and the condition of its valves[1]. The aim of this work to get more insight in the compressor performance, without taking the measurements that are normally required for this purpose. Standard sensor outputs in combination with physical models will be used to predict the cylinder pressure during a compression cycle. In principle, physical models deliver a high degree of accuracy, however they are computationally expensive and more suited for off-line rather than real time computations. Machine learning techniques are inherently positioned to overcome these challenges, and will therefore be a key part of the prediction routines.

In previous work[2], machine learning was used to model the dynamic cylinder pressure in a compressor system for the purpose of speeding up pulsation calculations for damper design. However, in this work only synthetic numerical data was used to train the model. As such, it is unlikely to perform well on real-world systems and cannot be used for proper condition monitoring application, as there is always a discrepancy between simulation and real-world. In this work, the aim is to use measurement data to bridge this gap between simulated and real-world data. However, in most cases, the amount of data available from field measurements is limited, as they are time consuming and expensive to perform, and thus deriving a data-driven model from this data is challenging. For this reason, the so-called transfer learning principle is investigated. In transfer learning[3,4], the parameters of one model trained on a large dataset of a related problem are transferred to a second model and further finetuned on the actual problem to be solved. In this work, we aim to demonstrate this process by first training a model to predict dynamic cylinder pressures using a large numerically generated dataset, then finetune it using the limited measurement data to improve overall model performance.

In Section 2, a high-level overview on machine learning, and the type of machine learning model and transfer learning method used are given. Then, Section 3 provides an overview of the case study to which the transfer learning process was applied along with the measured and simulation datasets. Section 4 discusses the machine learning test cases that were run, their results and a discussion of the outcomes. Finally, Section 5 provides conclusions and future outlook on the work.

2 Methodology

In this section a brief overview is given of the machine learning methods and transfer learning approach used within this work.

2.1 Machine learning

Machine learning is a broad collection of mathematical methods that aim to "learn from" (take advantage of) data in order to solve a given problem[5]. They do so by adapting their inner model parameters to reflect the relationship between given examples of input-output combinations or patterns within datasets in order to generalize to new, yet unseen, instances[5,6].

Machine learning is typically used in favour of classical analytical or numerical modelling approaches when the problem at hand is difficult or slow to solve with such methods, no conventional models exist, or the problem is not well understood, but there does exist data describing the problem. For instance, it is nearly impossible to create a conventional model that maps an image to the object it depicts (e.g. "is this image a dog?"), but using machine learning and a large number of example images, this is a fairly trivial task.

In addition, once "trained" (see next section), a machine learning model is typically much faster to execute than numerical methods, making them powerful alternatives in design optimization problems[2] or real-time applications.

2.2 Artificial Neural Networks

In this work, the type of machine learning model used is the artificial neural network (ANN), a type of predictive model that maps a given input to its corresponding output. In essence, an ANN consists of a collection of non-linear functions called neurons that are arranged in a network of mutually exclusive layers[5] (see Figure 1). Each neuron receives information from all neurons in the previous layer through the connections between them, combines this information based on the weight of each connection, runs the combined information through its non-linear function, and passes the corresponding outcome on to all neurons in the next layer (ending at the final layer where the outputs are read out).

By changing the values of the weight of the connections between layers, the output of the ANN changes accordingly. By providing a comprehensive dataset of known input-output combinations, an optimization algorithm can be used to find a set of weights such that for each input, the ANN provides the correct corresponding output[5,6]. This process is called training, and is (aside from the technical implementations) generic to all types of machine learning models. Once completed it provides a "trained" machine learning model that can be used to make prediction on new input data.

by: Jonah Poort, Rens Bazuin – TNO

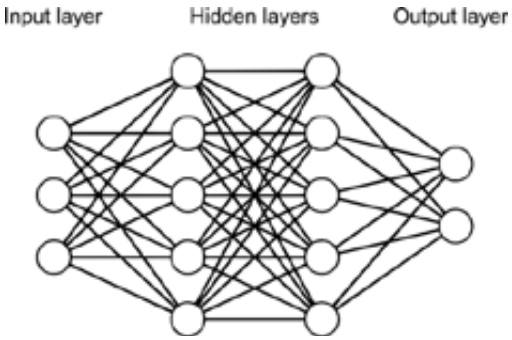

Figure 1: Schematic of a two-layer artificial neural network with three inputs, two outputs and five neurons in the hidden layers.

2.3 Transfer learning approach

One of the main hurdles in machine learning applications is the presence of proper datasets that can be used for training. In many practical cases where machine learning could provide great benefits, there is only very limited data available. As a result, it can be difficult to create machine learning models that learn the correct relations from the data, as the number of known input-output combinations is small and might not cover the full range of possibilities.

In such cases, transfer learning can potentially help solve the problem. Transfer learning is a process in which knowledge or information gained from one problem is transferred to a different but similar problem[3,4]. In machine learning, this is often done by transferring the learned model parameters (e.g. ANN weights) from an existing model trained on one problem (the source) to a new model, and then finetuning this new model to a second problem (the target).

When dealing with limited data for a given target problem, transfer learning can help by first training a source model on a similar problem for which sufficient data is available, transferring the learned parameters to a new model, and using the limited target data to adjust the minor details of the model specific to the target problem[3]. This idea is illustrated in Figure 2. If only the target data is used, the resulting model is typically too simplistic (a). If only the source data is used, the general trends are captured better, but not the details (b). However, by starting off with the general trends from the source model as a baseline, it can be subtly tweaked using the target data (c) to better align with its details without creating a model that is too simplistic, resulting in a model that is better than models trained on either dataset alone (d).

In this work, the target problem is the creation of a predictive model of amplitudes for the harmonics of the cylinder pressure signals of a compressor system based on a limited set of measured data, while a larger set of data generated using a numerical model is used as the source. Just as described above, the source problem has abundant data to train on, but still lacks in accuracy with respect to the details of the real-world system, while the measured dataset better reflects the real-world, but is too limited to create an accurate model with.

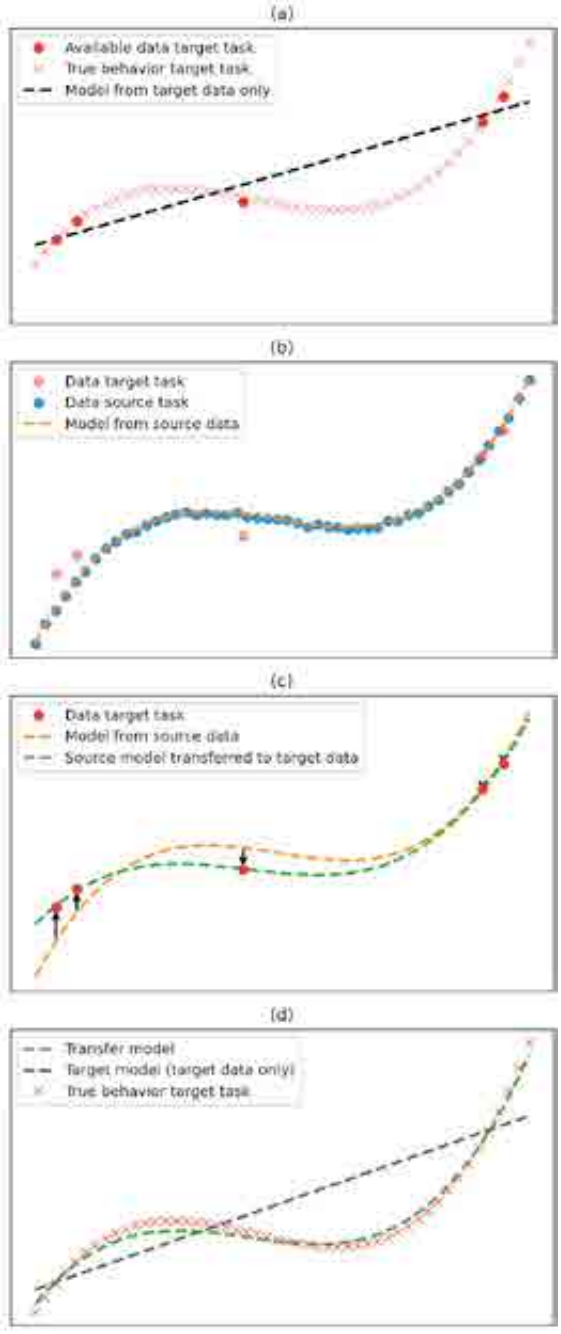

Figure 2: Visualization of the transfer learning principle.

To apply the transfer learning process to ANN models, the following steps were taken:

- A source neural network model is trained on the simulated data to predict the first 32 harmonics of the cylinder pressure based on the RPM, suction pressure and discharge pressure.
- The weights of the source ANN are copied and used as the initial weights of the target model.
- The measurement dataset is divided into one dataset for training, and one dataset that is kept

by: Jonah Poort, Rens Bazuin – TNO

aside for testing and evaluating the trained model.
- The training process is repeated, now with the measured data.
- The final transfer model is evaluated on measured test dataset and compared against a model trained only on the simulation data, and a model trained only on the measured data.
- If successful, the transfer model should outperform both other models.

The specific case the methods were applied to and the data used are described in the next section.

3 Case study

3.1 System description

The compression system considered in this project contains one horizontal 4-throw reciprocating compressor that is operated in two stage mode (stage 1: cylinders 1-3, stage 2: cylinder 4). The compressor speed is variable. The system is used to compress natural gas, with a molar weight of 18 g/mol. Only the 2nd stage cylinder was taken into account during this research (as the primary purpose of the measurements was to study the reliability of the 2nd stage compressor valves).

3.2 Measurement data

Field measurements were conducted for varying operating conditions, on the compressor system shown in Figure 3. The cylinder pressure was measured at the crank-end and head-end side of the 2nd stage cylinder. HBM P3TCP pressure transducers were mounted in the cylinder tap connections, in direct contact with the process gas.



Figure 3: Pressure measurement locations on the 2nd stage cylinder, at the head-end (HE) and crank-end side (CE).

Pressure measurements were conducted for 45 different cases of operating conditions. The compressor speed was regulated by changing the set point of the 1st stage suction pressure, this also resulted in variations in the 2nd stage suction pressure. Figure 4 gives an overview of the 2nd stage suction pressure, discharge pressure and compressor speed of each operating case. The conditions varied in the following ranges:

- Suction pressure: 45 barg to 63 barg.
- Discharge pressure: 87 barg to 91 barg.
- Compressor speed: 170 RPM to 375 RPM.

The suction temperature was around 23 ºC during the measurements.

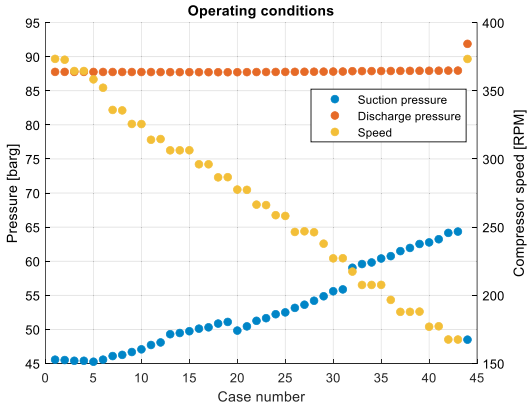

Figure 4: Overview of the operating conditions during the different field measurement cases.

3.3 Numerical model and data

A pulsation simulation tool was used to construct a numerical model of the 2nd stage cylinder. The numerical calculations are used to determine the dynamic cylinder pressure during a compression cycle. For this purpose it is sufficient to only model the cylinder and the pulsation dampers, the field piping is not taken into account. Figure 5 gives an illustration of the simulation model.

Simulations were run for the same range of operating conditions as encountered during the field measurements, 1400 simulation steps were used in total to generate a larger dataset to make training more accurate. The simulations were run with 3 different settings of compressor valve losses, (hereafter referred to as a low, intermediate and high value).

by: Jonah Poort, Rens Bazuin – TNO

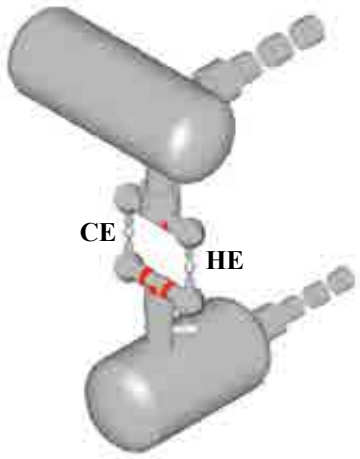

Figure 5: Overview of the simulation model, with the head-end (HE) and crank-end (CE) side of the 2nd stage cylinder.

Figure 7 gives an illustration of the cylinder pressure signal during a compression cycle, for simulations with different settings of valve losses and for the corresponding field measurement case. Figure 7 shows that with increased valve losses, the pressure overshoot will be larger when the discharge valve opens. The models with different settings of valve losses are useful to study the performance of the transfer learning algorithms with respect to the accuracy of the simulation input data. While there are many different parameters that can affect model accuracy, valve losses were used to emulate different accuracy levels as it was an easy to change single parameter, and did not require changes to the numerical model design itself.

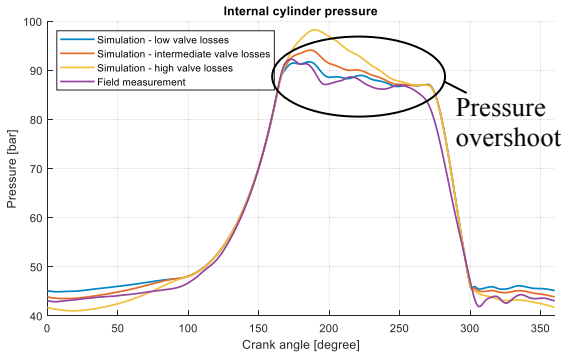

Figure 7: Comparison of the internal cylinder pressure of simulations and a field measurement. The operating conditions match with case number 10 of the field measurements.

The dynamic pressure harmonics, i.e. the distribution of the frequencies in the dynamic pressure spectrum, are relavant to study the dynamic interaction with the compressor valve structural behavior. In order to train the data-driven models, the first 32 harmonics of the dynamic pressure were extracted from both the measured and simulated pressure profiles. Figure 6 shows the minimum, maximum, and mean values of each harmonic for both the simulated and measured datasets. As can be seen for the first few harmonics, both line up quite well, however, as the harmonic number increases, the discrepancy between measured and simulated values increases. As such, it is expected that for these higher harmonics transfer learning will give higher benefits, as it is aimed at bridging the gap between simulated and measured data.

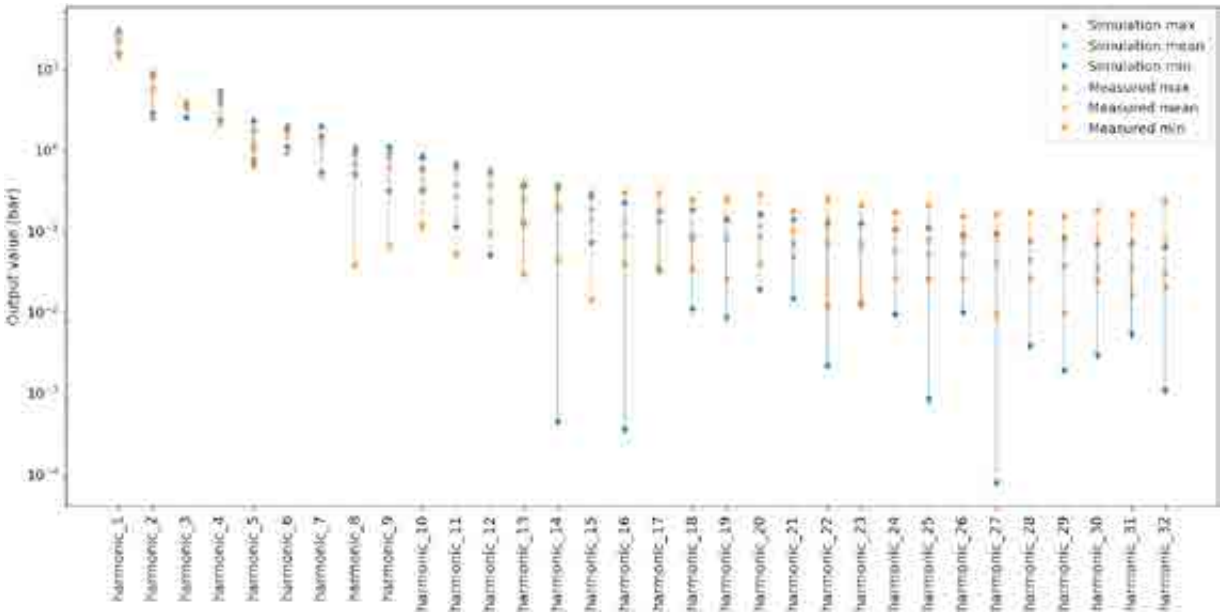

Figure 6: Minimum, maximum, and average values per harmonics of respectively the simulation (blue) and measured (orange) data.

by: Jonah Poort, Rens Bazuin – TNO

4 Transfer learning results

In this section, the different transfer learning tests that were run are first briefly described, after which their results are given and discussed.

4.1 Test descriptions

In order to investigate the potential of transfer learning under different circumstances, a number of different tests were performed. The following three aspects were investigated:

- The effect of the size of the measurement dataset. In this experiment, the number of measurement datapoints was varied in order to evaluate how this affects the accuracy of the resulting models and the potential benefits of the transfer learning process.
- The fidelity of the numerical model used to generate the simulation data. By this experiment it is investigated to what extent the initial accuracy of the numerical model impacts the final performance of the transfer model.
- The number of harmonics included in the analysis. Here the transfer learning process is repeated for a model predicting the first 16 and 32 harmonics respectively in order to gauge where the process performs best.

4.2 Results

In the following subsections the results of each of the tests described in the previous section will be given. All tests provide results for three different machine learning models, these are:

- The **simulation model**. A model that was trained only on the simulation data generated with the numerical model.
- The **measurement model**. A model trained only on measurement data.
- The **transfer model**. The model trained through the transfer learning process; first trained only on simulation data, and then finetuned by training on the measurement data.

For all models, experiments and datasets, the sizes of the neural networks and training settings were kept exactly the same. All models were scored on the same subset of the measurement data to evaluate their performance, and the mean absolute error between the predicted harmonics and true measured harmonics is reported, which is expressed as follows:

$$MAE = \frac{\sum_{i=1}^{n} |y_i - x_i|}{n} \qquad (1)$$

Where n is the number of data samples (predictions), y_i is the predicted value, and x_i is the true value of each predicted sample.

4.2.1 Measurement dataset size

Figure 8 shows the ANN model accuracies as evaluated on the test set of the measurement dataset for 5, 10, 20, and 40 datapoints used to train the measurement model and finetune the transfer model. In all cases the number of simulation model datapoints was not changed. All models were trained on the first 32 pressure harmonics, and the process was repeated three times for each dataset size with randomly selected data points. As can be seen from the figure, as expected, the modelling accuracy in general goes down with a decrease in the number of training points, with the model trained on the largest set of measurement data model clearly outperforming the simulation data only model when using 40 data points, while being roughly equal to or worse than it as the number of points drops to 10 and 5. When looking at the transfer model performance, it can be seen that in most cases except for the 5 datapoints it improves over or performs equally to both the measurement and simulation models, with the clearest improvement being seen for the 10 datapoint case where it shows improvement of around 67%.

In addition, it can also be seen that in general for less points the variance in possible outcomes is much higher, which is to be expected, as there is a much greater chance that the randomly selected points do not provide a good representation of the problem, resulting in a bad model (for instance if all five points are for similar operating conditions, the model will do poorly for other operating conditions).

Finally, there are a few instances in which the transfer model get marginally or significantly worse. This is something that can always occur as the training process is stochastic, and in some cases fails to find the optimal set of weights. This does show that the transfer learning process should not be trusted blindly.

by: Jonah Poort, Rens Bazuin – TNO

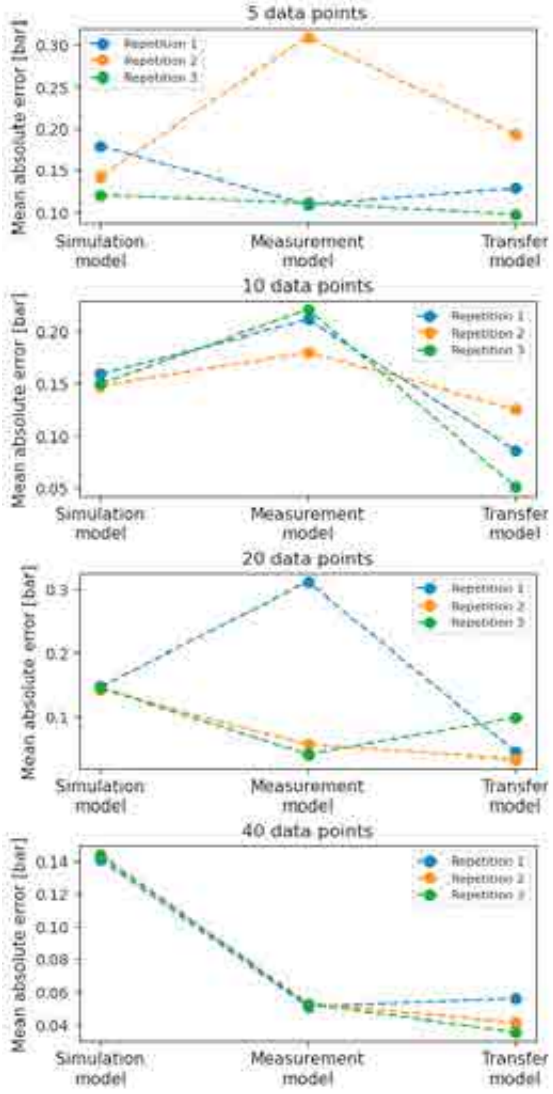

Figure 8: ANN model accuracies based on the number of measurement datapoints used for training. All models were trained to predict the first 32 pressure harmonics using the intermediate valve losses level model simulation data.

4.2.2 Numerical model accuracy

Figure 9 shows the accuracies evaluated on the test set of measurement data for three source models trained on simulation datasets generated using numerical models of different accuracies (see Figure 7). In this, the high, intermediate, and low valve losses levels corresponded to low (model 1), medium (model 2), and highest (model 3) accuracy respectively. For all comparisons, the measurement model was kept the same, and was trained on a measurement dataset size of 10 datapoints (for which the biggest transfer learning benefits were seen previously). As can be seen from the figure, the biggest effect of the numerical model fidelity can be seen in the accuracy of the simulation source model itself, where it is clear that lowest fidelity model (model 1) also results in the worst performance on the measurement data, while in this case the other two simulations models perform much better, even outperforming the measurement model.

Looking at the transfer learning accuracies, we again see that they all outperform both the simulation and measurement model, with the transfer model based on the worst performing simulation model showing the overall highest accuracy after the transfer process. This seems to indicate that the absolute accuracy of the final transfer model is largely independent of the fidelity of the original source model.

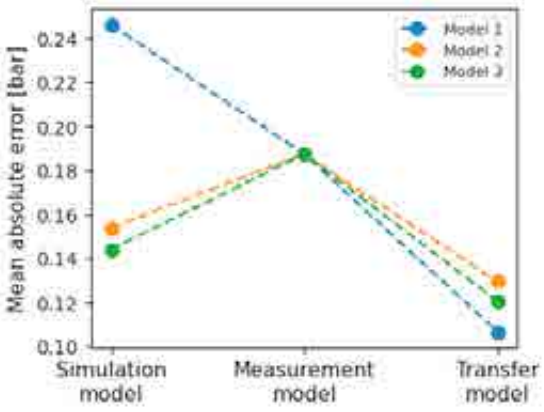

Figure 9: ANN model accuracies based on the fidelity of the simulation model used to generate the simulation training data (low fidelity model 1, intermediate fidelity model 2, and best fidelity model 3). In this case the measurement model was left unchanged and trained on 10 datapoints, for which the best improvement was previously found.

4.2.3 Number of harmonics modelled

Figure 10 shows a comparison between ANN models trained to predict the first 16 and 32 pressure harmonics respectively. Simulation data used came from the intermediate fidelity model, and again 10 measurement datapoints were used for training. As the figure shows, whereas the improvement for the 32 harmonics case is clear, it provides no significant benefits for only 16 harmonics. This is as was expected, as Figure 6 showed that the biggest discrepancy between simulated and measured data occurs primarily for the higher harmonics, and as such, these will benefit the most from the potential improvements that can be achieved with the transfer process.

by: Jonah Poort, Rens Bazuin – TNO

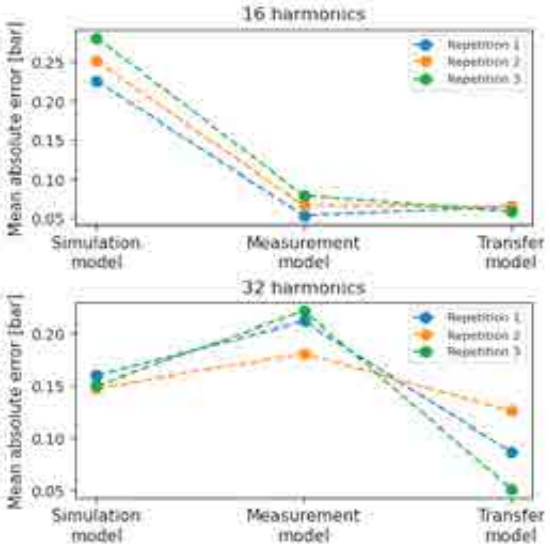

Figure 10: ANN model accuracies based on the number of harmonics predicted by the models. Both measurement and transfer target models used 10 measurement datapoints. Simulation and source models used the intermediate valve losses level model simulation data.

4.2.3 Computational speed

As one of the main benefits of a machine learning model lies in its speed of computation, a speed comparison was performed between the numerical and ANN model. In total, it took roughly 90 minutes to perform all 1400 numerical model simulations, while the same number of calculations done using the ANN model took only an average of around 0.2 seconds, which comes down to a speed up of 5 orders of magnitude.

5 Conclusions and outlook

In this work, machine learning and transfer learning were used to leverage a combination of numerical simulation data and measurement data to train models that could predict the dynamic cylinder pressure of a compressor based on its RPM, suction pressure and discharge pressure. In the transfer learning process, an initial source model was trained solely on the simulation data, before being finetuned on (a subset of) the measurement data. By doing so, the model first learns the overall behaviour of the compressor system, before attuning to its finer real-world details. Models trained using this method generally outperformed models trained on either type of data alone.

In general, no matter the amount of measurement data available, the transfer learning process was found to be able to increase performance, although its robustness decreases as the size of the dataset decreases. Thus, even with very few well-chosen measurement points (10) an accurate transfer model can be created. In addition, it was found that the final transfer model accuracy was largely independent of the fidelity of the original numerical model, meaning that the workflow can be used even with relatively inaccurate simulation data (as long as it covers the general behaviour of the problem). Finally, as expected, the machine learning models were considerably quicker than the numerical model by 5 order of magnitude, allowing them to be used in a real-time condition monitoring system.

It should be noted that in all cases in this work, for demonstration purposes the measurement data was seen as the ground truth, and assumed to be a correct representation of the real-world system. However, when applied in practice, it is important to first validate that this holds true, and that one is not using inconsistent, inaccurate, or too noisy measurement data for training of the transfer model.

In future work, an interesting idea would be to try to use the developed workflow together with a human expert to identify an optimal set of measurement conditions that would maximize the transfer model performance such that a guideline for future field measurements can be set up. Additionally, it would be interesting to apply the transfer learning techniques to the dynamic pressure in the cylinder nozzles rather than to the cylinder pressure, as this may provide additional insights in the compressor valve reliability.

In addition, additional potential avenues of exploration of uses of machine learning in compressor systems could be in condition monitoring, such as anomaly detection (for early warning systems), remaining useful lifetime estimation, and sentiment analysis of reports for identifying potential issues in advance.

6 Acknowledgements

The authors wish to thank NAM (EFRC member and active partner in R&D group) for the field data for the purpose of the investigation and the approval for this publication.

References

[1] Goebel, D. (2014): Reciprocating Compressor Suction And Discharge-Valve Monitoring, CompressorTech2, June 2014.

[2] Poort, J.; Tümer, C.; Shoeibi Omrani, P. (2021): Pulsation Damper Optimization with AI. 12th EFRC Conference Proceedings, 117-127.

by: Jonah Poort, Rens Bazuin – TNO

[3] Pan, S.J.; Yang, Q. (2009): A Survey on Transfer Learning. IEEE Transactions on Knowledge and Data Engineering, Vol 22 (10), 1345-1359.

[4] Weiss, K.; Khoshgoftaar, T.M., Wang, D. (2016): A Survey of Transfer Learning. Journal of Big Data, Vol 3 (9).

[5] Mitchel, T.M. (1997): Machine Learning. McGraw-Hill Science/Engineering/Math.

[6] Bishop, C.M. (2006): Pattern Recognition and Machine Learning. Springer Science+Business Media, New York.

EFRC PAPER

Constrained layer damping for small-bore side branches
by: Irma Meijer. Can Tümer, Jan de Vreugd – TNO *87*

Diaphragm compressors for hydrogen service: inventory of operational challenges and feasibility of diaphragm optimization
by: Cyril Wentzel – WENTZEL DYNAMICS; Leonard van Lier – TNO *95*



PULSIMSUITE

PULSATION & VIBRATION SOFTWARE

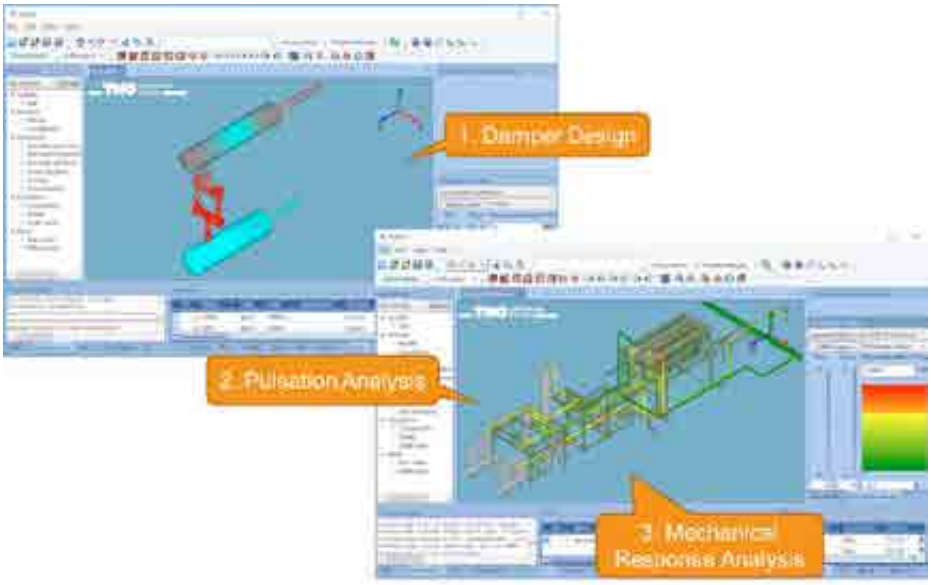

- Comply with standards API 618, 619, and 674
- Seamless Design Approach 3 workflow: check pulsations, vibrations, and cyclic stresses
- Avoid pulsation and vibration problems by design, for current and future operating conditions

Hydrogen case study:

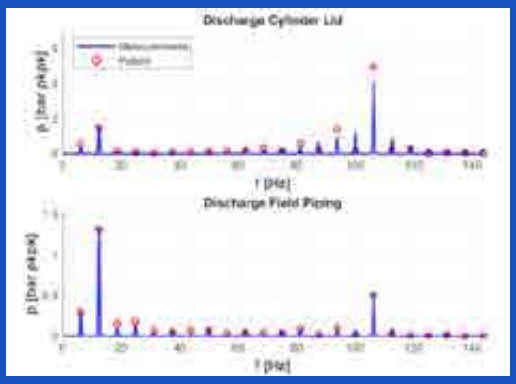

Measured and simulated frequency spectrum of the discharge side of a hydrogen compressor system, on the cylinder lid (top) and in the field piping (bottom)

PulsimSuite captures the main, low frequency pulsations at the 2nd harmonic that propagate into the piping system.

Also well-captured is a strong local (Helmholtz) resonance between cylinder and damper, at the 17th harmonic. This resonance is strong enough to also propagate significantly into the piping system, causing high-frequency vibration issues.

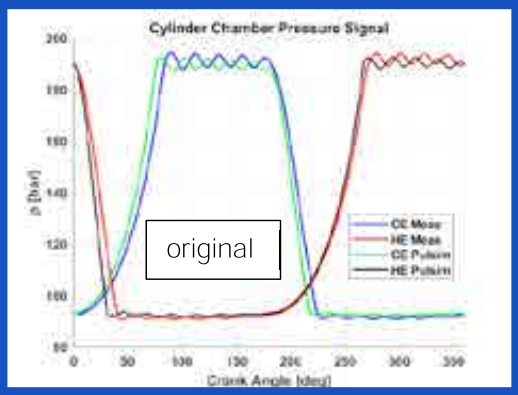

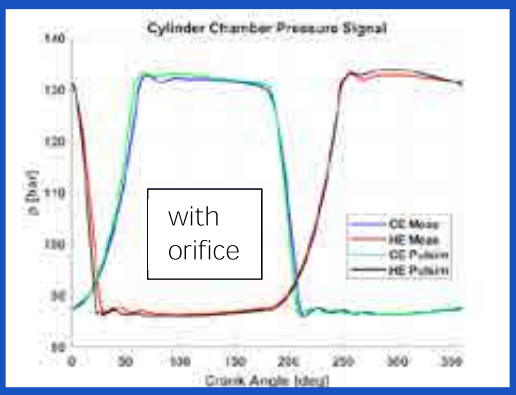

The measured pressure signals in the cylinder are simulated with good accuracy, and show the high-frequency pulsations caused by the Helmholtz resonance (left). With PulsimSuite, we were able to identify this root cause for the high-frequency pulsations, and to recommend the appropriate orifice plate in the cylinder connection nozzle to mitigate this pulsation (right).

TNO innovation for life

Constrained layer damping for small-bore side branches

by:

Irma Meijer, Can Tümer, Jan de Vreugd
Energy Technology – HTFD
TNO, Unit Energy Transition
Delft, The Netherlands
Irma.meijer@tno.nl

13th EFRC CONFERENCE
September 19th – 21st 2023, Zagreb

Abstract:
Small-bore branch connections (SBCs) are known as a prominent failure mode in reciprocating compressor systems[1]. SBCs are for example used for drains, vents, level gauges and pressure sensors. In general, SBCs exhibit low stiffness and mechanical damping while containing heavy components (valves, flanges, or instruments), resulting in low mechanical natural frequencies which are well within the excitation range of a reciprocating compressor. To prevent SBC failures, two conventional approaches exist. Reducing the branch length and overhung weight or stiffening the branch with braces or welded gussets. These approaches tend to have some disadvantages (expensive due to the required downtime, re-qualification in case of welding on existing structure, limited stiffness of braces).
Constrained Layer Damping (CLD), a non-conventional vibration mitigation technique, offers both an effective and an easy-to-use solution to control SBC vibrations. CLD is a combination of three different layers that are held together; a base layer (the side branch), a viscoelastic damping layer and a constraining layer. The shear that is generated due to pipe vibrations and transferred to the viscoelastic layer creates additional damping due to the characteristics of the viscoelastic damping layer. CLD applications have already been successfully field tested for main lines of reciprocating compressor systems[2].
The EFRC R&D working group sponsored an investigation into the application of CLD on small branch connections. Laboratory tests were performed on several SBC layouts. Several CLD layouts were tested (thickness, material, clamping and location). A Finite Element Model analysis was done, allowing to calibrate the non-linear properties of the viscoelastic material, resulting in a good correspondence with test results. As future work, using the FEM analysis, a large variety of SBC and CLD configurations will be evaluated, resulting in practical guidelines to design and evaluate the effect of CLD during design.

by: Irma Meijer. Can Tümer, Jan de Vreugd – TNO

1 Introduction

A recent EFRC investigation on the reliability of reciprocating compressors shows that small bore side branch connections are the primary failure configurations for both low- and high-speed reciprocating compressors, see Figure 1.

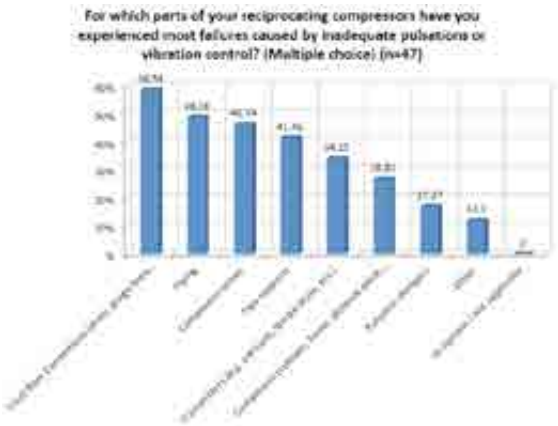

Figure 1: Results of the EFRC reliability study

With a good design strategy, many of the failures on SBCs can be prevented. Recommend design steps are to reduce the length of the side branch, limit the connected weight (e.g. flanges or valves) and increase stiffness of the side branch itself. However, during the design phase the small bore side branch connections are often overlooked. Not only in reciprocating compressor systems, but also in other situations. For example flow induced vibrations, which could lead to excitation of side branches anywhere in the system.

A suboptimal design results in a low mechanical natural frequency which can be triggered during operation. Due to the low damping observed in side branch connections, such a resonance can result in high vibration levels, eventually leading to failures. The recommended mitigation actions are often not feasible during operation. A well-designed clamp bracing the SBC to the main line could reduce the observed vibrations but implementation is sometimes difficult due to space considerations.

Application of Constrained Layer Damping is a self-contained solution, which does not require down time of the system. It is effective for a wide range of frequencies and is easy to install. CLD consists of three different layers, see Figure 2. During the experiments, the adhesive is omitted. The side branch piping is the base layer of the CLD. The viscoelastic layer is a dedicated material with nonlinear properties. The steel constraining layer is clamped around the pipe and viscoelastic material.

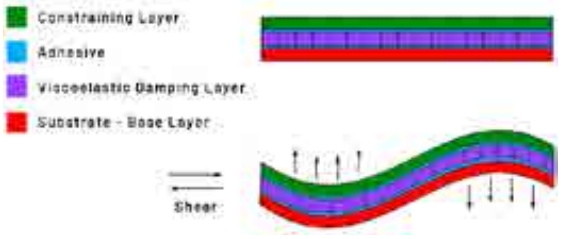

Figure 2: General layout of Constrained Layer Damping

CLD was successfully applied in several field cases with high vibrations[1],[2]. However, creating a CLD design and testing it requires considerable time and modelling effort. For SBCs the need for quick action is often more acute. Ideally, straightforward design guidelines are available, to enable quick improvements on the vibrations experienced in the field. The work discussed in this paper is a first step toward such a design guideline.

The work was carried out as a project assigned by the EFRC R&D group. The scope consisted of an introductory literature survey, tests with CLD in a controlled laboratory environment on various configurations. Finally, a numerical implementation was made of a SBC with and without CLD (parametrized FEM model). The numerical method and results were validated with the test results. An outlook for a path toward a design guideline was made as a final step.

2 Test setup

Tests were performed in the laboratory facilities of TNO. The test configuration consisted of a 10” main line (suspended, to avoid interference of boundary conditions on the results) with various side branch configurations. As a first step, the mechanical natural frequencies were determined using an impact hammer test procedure. The end flange of the branch was hit with an impact hammer (mounted with a force transducer), and the resulting movement was monitored using multiple accelerometers. Combining these measurement signals, a transfer function of the side branch response can be determined, which is used for further analysis and comparison with numerical results.

2.1 Tested geometries

In the tests, two different side branch geometries were studied. The first consists of a straight 2” side branch connection, see Figure 3. The total length of this side branch measured from the outer diameter of the main pipe is 364 mm. The branch is connected to the main branch via a weldolet and includes one blind flange at the end. Such simple straight side

by: Irma Meijer. Can Tümer, Jan de Vreugd – TNO

branch configuration in often used in pipe systems, for example to connect pressure sensors or a drain.



Figure 3: Test layout straight side branch

The second SBC layout has an elbow (see Figure 6). This layout will have a lower mechanical natural frequency than the straight branch, due to the increased length and the flexibility of the elbow. To shift the response frequency down, 5 additional flanges were connected at the top flange. The SB length from main line to elbow is 530 mm, from elbow to the bottom flange the total length is 270 mm.



Figure 4: Detail of hose clamp

To study the effect of CLD, several configurations were tested. All (visco)elastic material samples consist of two half cylinders of 200 mm long, clamped with the constraining layer to the pipe at 68 mm from the weldolet. The ideal location would be directly at the tee, or as close as possible to the weldolet. In practice, it is preferrable to move the CLD slightly further out, so an assessment of the weld can be done. The constraining layer is clamped to the pipe using a hose clamp, see Figure 4. The bolt is tightened at either 5 or 15 Nm using a torque wrench. The thicknesses of both the viscoelastic layer and constraining layer were varied. The viscoelastic layer has a thickness of 1.7 or 6 mm. The constraining layer has a thickness of 3 or 6mm, resulting in 4 different CLD configurations. The pipes, flanges and constraining layer are made of stainless steel. The used viscoelastic material was available from a previous project. For application of CLD in a field case, the conditions should be taken into account when selecting a viscoelastic material. Both temperature and expected vibration frequencies might influence this selection. As an alternative for the viscoelastic layer, also a simple rubber type material with purely elastic properties was tested. In this way, the added mass effect of the attached CLD geometry can be separated from the damping effect created by the viscoelastic properties. Both materials look very similar, see Figure 5.



Figure 5: Viscoelastic layer (left) and rubber material (right).

2.4 Sensor layout & impact directions

To determine the mechanical response of the branch connection, the end flange was excited with a small impact hammer. This measurement hammer was connected to the acquisition module to record the applied force. Four accelerometers were used to measure the response to the hammer impact, see Figure 6. All sensors measure the acceleration in three directions. Sensor 1 is located on the main line, sensor 2 and 3 on the first flange, and sensor 4 on the flange of the elbow piece. When the straight branch configuration is used, the elbow piece is removed and sensor 4 is not used.

by: Irma Meijer. Can Tümer, Jan de Vreugd – TNO



Figure 6: Accelerometer locations

The whole assembly is suspended by means of an overhead crane with a rotating hook. The test setup can thus move freely in all directions but vertically. For each configuration, the branch connection was excited with the hammer on the flange in out-plane direction, see Figure 7. For the elbow geometry, the excitation location was on the end flange.



Figure 7: *Impact hammer tests on the SBC configuration.*

2.5 Post processing

The test setup without CLD exhibited extremely low damping which increased the importance of signal filtering. Filters were required to supress noise in the sensors that only showed a short response time. For example, the input signal from the hammer contained a sharp pulse which last only a couple of samples. The remaining measurement time the signal only exhibits noise. A signal filter was applied such that most of the noise was suppressed to zero. A similar strategy was used for data points with short response time, such as sensor 1 on the main line.
The filtered data was averaged over 10 iterative impact event, limiting the effect of a not perfectly aligned hammer impact. Using the input data from the impact hammer and the resulting accelerations, a frequency response function is determined. Subsequently a commercially available software tool is used to derive the exact peak frequencies and the damping ratio corresponding to each peak. The damping ratio (ζ) can also be written as a Q factor ($Q = 1/2\zeta$) for ease of reference. The factor Q is a direct measure for the amplification in mechanical resonance conditions, or the inverse of damping.

3 Test results

The tests were executed for a wide range of parameters, For clarity, the focus in this paper will be on the out of plane direction (for hit direction see Figure 7). The sensor data used in these results is the out of plane direction, sensor 2 for the straight side branch and sensor 4 for the elbow configuration.

3.1 Straight side branch

The straight branch connection is the simplest design tested. In Figure 8 the frequency response function (FRF) is shown for an undamped (without CLD) and a damped (with CLD) configuration. Both the viscoelastic and the constraining layer are 6 mm thick. The undamped geometry exhibits a sharp peak at a frequency of 102 Hz. This corresponds to the first mode shape (cantilever) of the side branch in horizontal out-of-plane direction. The second mode shape, where the side branch moves in vertical direction is also observed at a different (but very close) frequency of 103 Hz. Both peaks occur at the same time as the excitation is never ideal in one direction, even with averaging over multiple hits. The FRF for the damped system shows a much smoother peak with a maximum at 105 Hz.

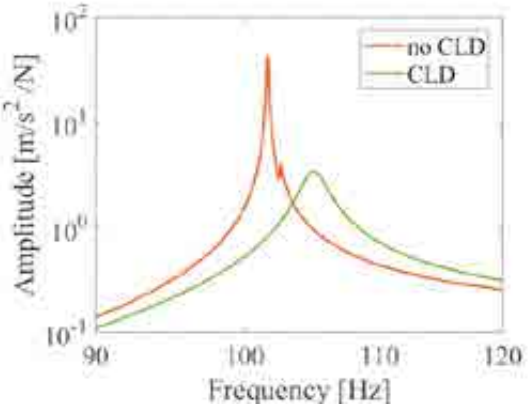

Figure 8: Test results of straight side branch, comparing the non-CLD and CLD configuration

The effect of damping is judged via the Q factor. The first peak of the undamped configuration has a Q factor of 999. With CLD applied this is reduced to 56, a reduction of almost 18 times.

3.2 Side branch with elbow

The elbow configuration was used to study the effect of CLD for a lower resonance frequency. In Figure 9 the FRFs of both the undamped and damped configuration are shown. Two resonance frequencies are found. The undamped system has a first peak at 43 Hz which corresponds to a mode shape in which only the elbow piece is moving. The second peak at 101 Hz is similar in shape and frequency as the straight side branch. In this mode shape, the complete side branch, straight part, and elbow piece are moving out-of-plane.

by: Irma Meijer. Can Tümer, Jan de Vreugd – TNO

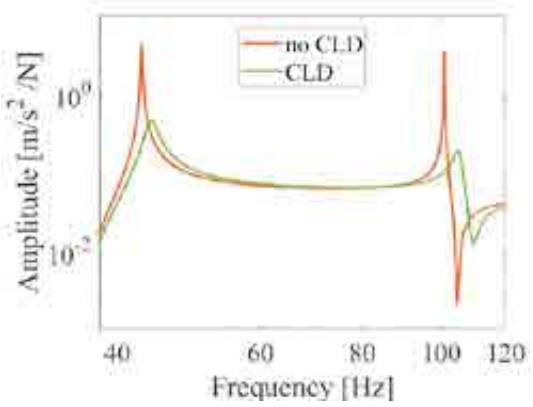

Figure 9: Test results of side branch with elbow, comparing the non-CLD and CLD configuration

The first resonance peak has a Q factor of 138 for the undamped configuration and 33 with CLD applied. The reduction in damping is thus a factor 4. This is significantly less than the reduction obtained in the straight configuration.

At the 2nd resonance frequency peak, the undamped configuration has a Q factor of 343, and 28.5 for the damped configuration. This is a reduction of 12 times, more in line with the value from the straight side branch. An overview of these Q factors is shown in Table 1.

Before concluding that CLD is less effective on lower frequencies, several items should be considered. The length of CLD is equal for both the straight and the elbow configuration. Relatively, much more CLD is added over a larger area for the to the straight side branch compared to the elbow configuration. In addition, in the first mode shape (at 44 Hz) the highest vibration is found in the elbow piece while the straight section experiences mainly torsion. In Figure 10, the relevant mode shapes are shown. Less vibration on the CLD location reduces the shear on the viscoelastic layer and thus a less effective damping.

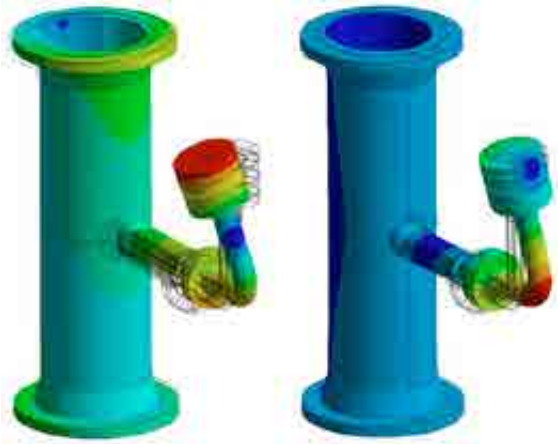

Figure 10: Mode shapes of elbow configuration, for the 1st peak (left) and 2nd peak (right)

3.3 CLD variables

For each side branch, 4 different CLD geometries are tested, different combinations of viscoelastic layer thickness and constraining layer thickness. In Table 1 an overview of the resulting Q factors and reduction compared to the undamped straight side branch is shown. With exception of the configuration with the thinnest layers, the different geometries show a similar reduction.

Table 1: Different combinations of viscoelastic layer thickness and constraining layer thickness, straight SB.

Thickness VE layer	Thickness steel layer	Q factor	Reduction
1.7 mm	3 mm	117	8.5
1.7 mm	6 mm	59	17
6 mm	3 mm	63	16
6 mm	6 mm	56	18

Applying CLD to a side branch geometry influences the frequency and damping. To separate the effects of additional mass and stiffness from the effect of damping introduced by the viscoelastic properties of the constrained layer, testing was done with a simple (purely elastic) type of rubber. Figure 11 shows the data from the straight side branch as discussed in section 3.1, now with the additional data from the CLD with rubber instead of viscoelastic material.

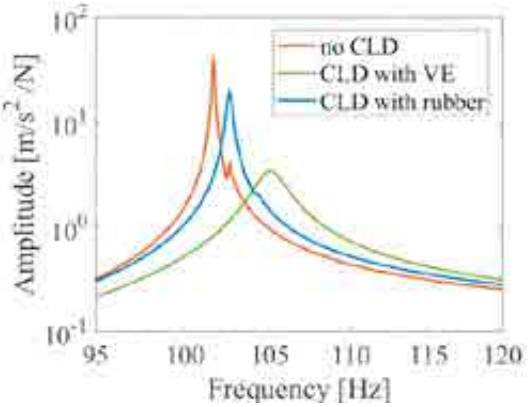

Figure 11: Test results of straight side branch, showing the influence of material selection.

The peak frequency of the CLD with rubber configuration is 121 Hz, and a Q factor of 341 is obtained, only a factor 3 reduction. The effect of added mass and stiffness is still significant, but the contribution of the damping by the viscoelastic layer is larger.

4 Finite Element Analysis

To generalize the results of the test setup to other geometries or CLD designs, an accurate modelling

by: Irma Meijer. Can Tümer, Jan de Vreugd – TNO

strategy is required. The main challenge in this modelling approach is to include the non-linear behaviour of the viscoelastic material. First an overview is given of the general FE model, subsequently the theory behind the viscoelastic properties is discussed.

4.1 Modelling approach

For the modelling, the commercially available finite element simulation tool is used. The FE model is a detailed representation of the test setup, see Figure 12. As an illustration, the CLD configuration with a 6 mm viscoelastic layer (coloured in blue), and a 6 mm steel constraining layer was incorporated. The mass distribution mimics the number of flanges used in the tests. The clamps and bolts were not included in detail, but a point mass was applied to the outermost flange. This point mass was subsequently used to calibrate the model to the correct resonance frequency. The overall damping factor which is used as input of the simulation is 0.005, used for both the bare branch and the CLD configuration.



Figure 12: Finite Element model with branch configuration of elbow and CLD.

The non-linear damping effect of the viscoelastic layer can be modelled with the help of a Prony-series. Prony-series describe the time-dependent relaxation of a material with help of relaxation (α) and time (τ) constants.

To obtain these constants, the viscoelastic material was subjected to a dynamic mechanical analysis (DMA). In this test, the storage and loss moduli of the material were measured for a frequency range up to 100 Hz. A generalized maxwell model was used to fit the relaxation and time constants to the obtained result.

4.3 Results

As a first step, the comparison of the numerical result with the measurements is shown, for the branch configurations without CLD. Figure 13 shows the comparison for the straight side branch. The test data and the numerical result match very well, the resonance frequency matches within 2%. The damping is slightly overestimated; in an updated simulation the general damping factor could be tweaked. The result of the elbow configuration is shown in Figure 14. The numerical results do not perfectly align to both resonance peaks, both have a similar deviation in frequency (< 4%). The damping predicted by the simulation is significantly lower than the value obtained via experiments, which may be considered a conservative result.

The presented results are accurate enough to continue our study on the additional damping created by CLD. If a better match would be desirable, the general damping and mass distribution can be adjusted. In the current modelling approach, the general damping does not change with frequency. While the base model would depict a larger damping at higher frequencies. The mass distribution is simplified with a single point mass. This is not accurate, especially for the elbow configuration. The point mass is added on the top flange, while the additional weight from the CLD clamps and the bolts connecting the elbow piece are located on the straight section, influencing the mode shapes. A higher level of detail in the model would improve the frequency match for both peaks. However, when applying CLD in a specific (field) case, only one peak is most relevant. The model can then be tuned to obtain the best match around that frequency.

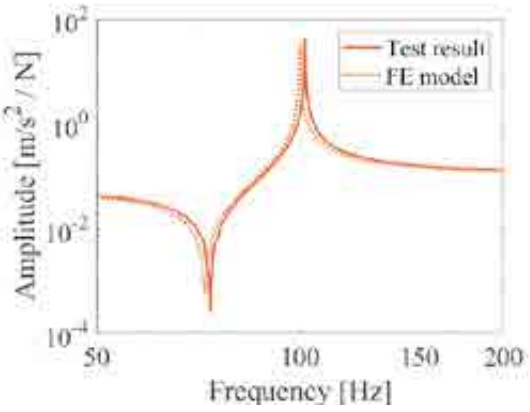

Figure 13: Comparison of test results and numerical simulation of straight side branch without CLD

by: Irma Meijer. Can Tümer, Jan de Vreugd – TNO

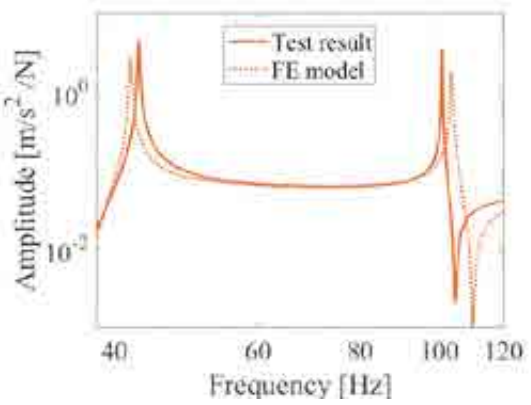

Figure 14: Comparison of test results and numerical simulation of elbow configuration without CLD

The FE models with CLD included have the same general damping value and point masses as the FE models without CLD. In Figure 15, both the experimental data and the results of the FE simulation are shown, for the straight configuration with CLD. The resonance frequencies align very well. The damping induced by the viscoelastic layer corresponds very well to the experimental data. Not only the amplitude is matched correctly, also the general shape of the resonance peak is similar, resulting in accurate Q factors.

For the elbow configuration, the same approach was followed. The frequency response functions of the experimental data and finite element model are shown in Figure 16. The frequency of the first mode aligns very well. Both the frequency and the amplitude match within 2%. For the second mode, out-of-plane motion of the complete side branch (see Figure 10), an offset between the measured and predicted frequency is present (+4%). Nonetheless, the satisfactory match on the first mode and the comparable shape for the second mode confirm that the modelling of the viscoelastic material is sufficiently accurate to predict the effect of CLD.

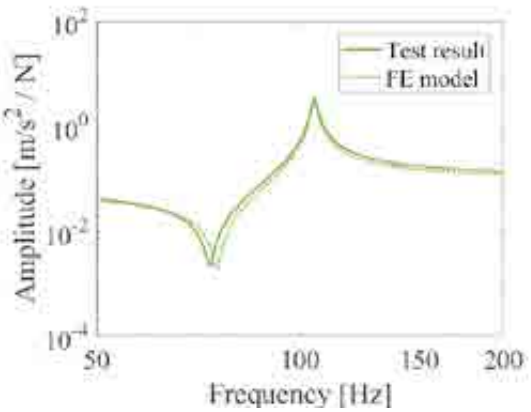

Figure 15: Comparison of test results and numerical simulation of straight side branch with CLD

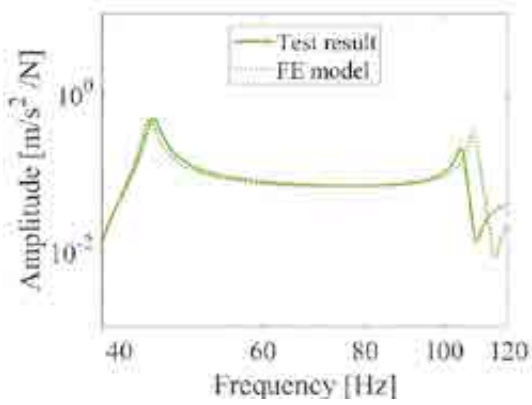

Figure 16: Comparison of test results and numerical simulation of elbow configuration with CLD

5 Conclusions and outlook

The main conclusion from the work is that Constrained Layer Damping techniques is proven (by means of testing) to be potentially very beneficial on small branch connections in vibrating service, for example in reciprocating compressor systems. The CLD appears more favourable than a simple (elastic) rubber material clamped around a SBC. The beneficial effect of a CLD depends on the specific branch geometry and the initial damping in the original branch layout. Numerical Finite Element Analysis can be used to reproduce the results in undamped and damped conditions with acceptable accuracy. If the base-line configuration (without CLD) can be evaluated by means of impact tests, the accuracy of the prediction of the CLD is very good. A parametrized FEA model was setup, to allow for systematic analysis of a larger matrix of layouts.

Now that the current modelling of the viscoelastic material with Prony series is validated, it can be used to optimize CLD designs for specific field cases. Future work could relate to the implementation of CLD in existing systems, testing the obtained damping factors with a more complex excitation source. The tests discussed in this paper were executed at room temperature, while field cases might have higher pipe temperatures, for example on the discharge side of a compressor (>100 °C). The viscoelastic material is temperature sensitive. Therefore, additional tests at a higher temperature would quantify how much the damping is affected. Such test could also be used to study the durability of the material and its properties under long-term high-temperature operation. Another way to access the effectivity of the viscoelastic layer is to execute a new dynamic mechanical analysis, now at a higher temperature. When using this data in the model, a more accurate prediction of the CLD effectiveness at higher temperatures is obtained. A database could be created with several viscoelastic materials, tested at different temperatures.

Future work which is already under investigation in the EFRC R&D group is the extension of the

by: Irma Meijer. Can Tümer, Jan de Vreugd – TNO

simulations on a large matrix of SBC geometries and CLD designs. A parametrized approach allows for a systematic analysis of a large design parameter space and derivation of generic relations, see for example Figure 17.

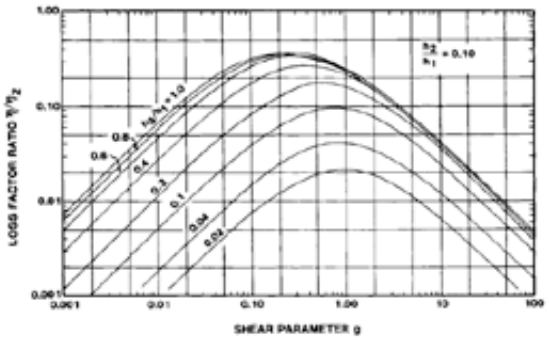

Figure 17: Typical relations for CLD loss factor as function of generic design parameters.

Ultimately, this information will allow for a design guideline, including a practical introduction to operational principles of mechanical damping. With such guideline, end users may engineer and implement CLD solutions for specific field cases with greater confidence, less analysis cost and reduced engineering times.

6 Acknowledgements

The authors would like to thank the EFRC R&D group for their valuable contributions, and their permission to share (a part of) this interesting project in this paper.

[1] A. Eijk, "EFRC reliability survey", report R11238, August 2020.

[2] A. Eijk *et al*, "Non-traditional vibration mitigation methods for reciprocating compressor systems", 3rd International Rotating Equipment Conference, 2016.

[3] A. Eijk *et al*, "Application of a Constrained Layer Damping to reduce pipe vibrations of a reciprocating compressor system", 11th EFRC conference, 2018

[4] J. de Vreugd *et al*, "Damping in Space Constructions", 13th European Conference on Spacecraft Structures, 2014.

[5] Piersol, Allan G., and Thomas L. Paez. *Harris' shock and vibration handbook*. McGraw-Hill Education, 2010.

Diaphragm compressors for hydrogen service: inventory of operational challenges and feasibility of diaphragm optimization

by:

Cyril Wentzel
Wentzel Dynamics
The Hague, The Netherlands
cyril@wentzeldynamics.com

Leonard van Lier
TNO, Unit Energy Transition
Delft, The Netherlands
leonard.vanlier@tno.nl

13th EFRC CONFERENCE
September 19th – 21st 2023, Zagreb

Abstract:
Application of hydrogen as a fuel for the mobility sector, requires reliable compression techniques that are able to provide very pure hydrogen at high pressure. In addition, for the typical operation of Hydrogen Refuelling Stations (HRSs), the compressors must be able to handle intermittent conditions. The diaphragm compressor is a mature technology that has been successfully applied for decades, in various parts of the process industry. Moreover, the diaphragm compressor offers favourable performance indicators, such as high end-pressure, operational flexibility, high efficiency and high purity. Moreover, compared to other traditional (e.g. hydraulic) or innovative techniques (e.g. electro-chemical), the capacity of a diaphragm compressor is relatively large. However, in intermittent hydrogen service, issues were identified amongst operators with the reliability of the diaphragms. The EFRC R&D working group initiated a project focusing on solving the reliability challenges ("HyMem").
A comprehensive overview was made of operational issues that may impact on the diaphragm lifetime. This inventory was based on literature survey, conference proceedings and interviews with manufacturers, end users and service providers. These operation aspects include, amongst others: liquid ingestion, dust, foreign particles and failing components, inadequate control of hydraulic oil supply and start/stops during intermittent operation. The most relevant aspects are discussed in more detail in this paper. Also, typical mitigation strategies will be discussed with an outlook to improved techniques.
In a parallel effort, the potential was investigated to increase diaphragm lifetime. This work involved the study of fatigue performance under complex stress states and fretting conditions at the contact surface. Metallic materials as well as other material classes were reconsidered for potential performance increase to both identify and increase the performance gap between nominal lifetime and observed lifetime of conventional diaphragms.
A major outcome of the study is the need to generate a fundamental understanding of the requirements for stiffness in diaphragm behaviour and design. Moreover, a need was identified for a dedicated test method to evaluate the fatigue performance of sheet metal alloys as well as other materials. Finally, it appeared that with the introduction of non-metallic materials, a substantial increase can be achieved in chamber volume, opening the path to higher capacity machines.

by: Cyril Wentzel – WENTZEL DYNAMICS; Leonard van Lier – TNO

1 Introduction

Diaphragm compressors are considered mature technology, in traditional service. In a multitude of industrial installations, these compressors are applied with a high degree of reliability. However, in recent industry developments around hydrogen compression, new challenges are faced and in some cases concerns are raised about limited reliability of the diaphragms. The issues of reliability may be due to the new circumstances, that put extra challenges on the operation of the compressor and/or extra challenges on the reliability of compressor components, such as the membranes (we will use the word diaphragm to denote the assembly of individual membranes). Moreover, future trends in the hydrogen industry may increase these challenges. In particular, the scope-of-interest focusses on Hydrogen Refuelling Stations (HRSs). In the EFRC R&D new working group Future Energy & Compression (FEC), an idea for a pre-competitive investigation was launched to investigate the reliability of diaphragm compressor. This was done with 2 separate projects (labelled HyMem).

The first project, described in the first part of this paper, was carried out by TNO [1], focusing on the operational aspects. This includes influences on the overall reliability, due to operation, start-up procedure, maintenance strategy etcetera. As input for the investigation, interviews with experts from industry (operators) and compressor manufacturers were used. In addition, a literature survey was performed to obtain additional information on experiences in industry and on state-of-the-art of the research.

The second project focused on the membrane design. Here, the mechanical behaviour of the membrane under simplified loading was investigated by a numerical simulation model. Also various innovative membrane designs were evaluated, for example with alternative (lower) membrane stiffness, alternative clamping properties and design with (fibre) composite materials. This project was executed by Wentzel Dynamics [2] and will be described in the second part of the paper.

A typical, simple example of a diaphragm compressor skid is shown in Figure 1: a skid-mounted vertical compressor (single, horizontal diaphragm), including E-motor and auxiliaries such as hydraulic oil pump. Also horizontal and more complex layouts (multi-cylinder or even multiple heads on a single throw) are found in industry.

Diaphragm compressors are typically applied for hazardous, toxic or corrosive process gases, or when high purity of the process gas is to be guaranteed. In such cases, the diaphragm compressor is considered a powerful alternative to the reciprocating compressor. Due to the hermetic design, there is virtually no leakage toward the crank case and vice versa. This is a powerful feature in the control of emissions of hazardous or other emission-sensitive gases. No purge or buffer gas in the compressor frame is required. Also the contact between the process gas and delicate (wearing) parts is reduced to an absolute minimum, achieving low degradation of these mechanical parts. The separation also has its benefits for the lubricated parts (no degradation of lubricants due to process gas). Finally, the separation of the process gas from wearing parts, (rings, packings) ensures a very clean process gas, free of dust and debris generated by wear.



Figure 1: Example of a vertical diaphragm compressor.

Diaphragm compressors also have beneficial cooling properties. The hydraulic oil provides a considerable cooling capacity, also due to the small ratio between the stroke and the surface area of the head, limiting the outlet temperature of the process under compression. This enables efficient compression and allows for higher pressure ratios per stage, than for example in a reciprocating compressor.

Due to the absence of leakage along the mechanical drive (such as a piston in case of classical reciprocating compressors), very high outlet pressures (>1000 bar) are demonstrated in industry.

A schematic drawing of the internals of a compressor head is shown in Figure 2.

by: Cyril Wentzel – WENTZEL DYNAMICS; Leonard van Lier – TNO

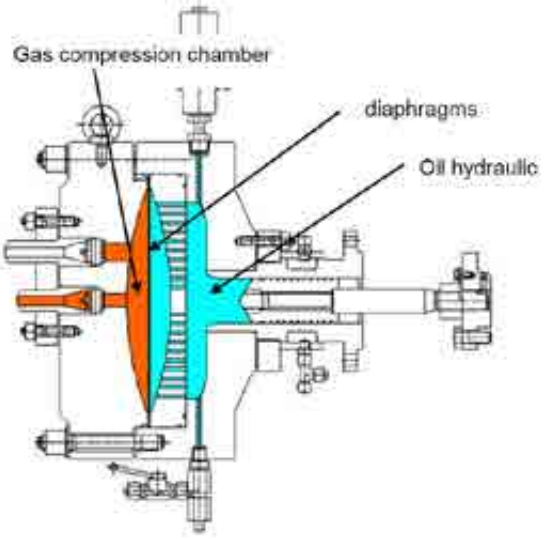

Figure 2: Schematic of a diaphragm head.

The diaphragm compressor is a member of the family of positive displacement machinery. Like with a piston compressor, mechanical energy is directly converted in compression by reducing a controlled volume. The intake and outflow of process gas is achieved by compressor valves. The diaphragm separates the gas side from the hydraulic side. On the hydraulic side, a piston is forced into reciprocating motion by a mechanical drive mechanism, driving the hydraulic fluid. In turn, the fluid drives the diaphragm. The compression cycle is comparable to the typical pressure-volume (PV) chart in reciprocating compressors. This compression and expansion cycle occurs periodically and provides an unsteady (pulsating) flow at both the inlet and outlet.

The above description of the design is very simplified. Several aspects shall be considered or better understood, to improve the reliability of the compressor:

- Diaphragm design. The membrane assembly is generally composed a multi-layered set of sheets. The materials at the gas and oil side may be steel but can also be of different material. The inner membrane can be made of brass. The friction (fretting) in between the membranes and the between the outer membrane's interface to the gas plate is often ignored in dynamic analysis.
- The diaphragms are typically clamped between the flanges of the cylinder head; sealing is done with elastomeric O-rings or even metallic rings.
- The structural dynamics of the membrane are relatively complex. The deformation of the membrane is not free. At the gas plate, the membrane should ideally 'stretch-roll' from outside to inside, following the contour of the gas plate. To promote the smooth 'rolling' from outside to inside, the gas plate has radial grooves, to avoid gas entrapment.
- Design of the gas plate is a very specific aspect of the compressor design. The shape is called the *generatrix*. In general, the diaphragm displacement at the centre is small (<2% of the diaphragm diameter). Thus, the clearances in the working chamber are very tight.
- The layout of the perforated (oil) plate is also specific for the compressor design. It can consist of a pattern of holes, or a specific configuration with grooves. It is designed such, to ensure optimal pressure distribution on the diaphragm to promote a smooth rolling on the gas plate. In normal operation, the diaphragm does not touch the perforated oil plate in Bottom-Dead-Centre position (BDC).
- In Top-Dean-Centre position (TDC), the diaphragm touches the gas plate over the maximum surface area.
- The leak detection system is connected to the central cavity bounded by the outer membranes. A rupture of either membrane will be detected on the pressure signal in the cavity, tripping the machine.
- A hydraulic oil compensating system is required due to leakages over the plunger packing, thermal expansion effects and oil compressibility.
- The oil pressure limiting valve ensures the removal of excess oil once the diaphragm is completely touching the gas plate, while the piston is not yet fully in TDC position.
- The orientation of the diaphragm/cylinder is different from a reciprocating compressor: it has not the natural, favourable location of the outlet at the bottom (providing a leeway for accumulated liquid out of the compression chamber). Thus, the diaphragm compressor is liable to issues with liquid ingestion.

2 Use case: hydrogen refuelling stations

Many historic examples for diaphragm compressor systems are found in industry. In general, in case of high gas purity requirement or operation with very corrosive or toxic gas at moderate capacity, the diaphragm compressor is a suitable candidate.

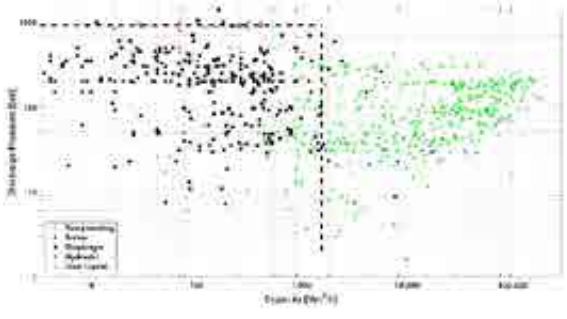

Figure 3: Industrial compressor systems for pure hydrogen (Horizontal: capacity. Vertical: discharge pressure); diaphragm compressors are the black dots [3].

by: Cyril Wentzel – WENTZEL DYNAMICS; Leonard van Lier – TNO

Figure 3 illustrates a diagram with industrial compressors for pure hydrogen. It is obvious that many examples for the diaphragm compressors are found (black dots), with the emphasis on high discharge pressure and low capacity.

In this paper, the focus is on the use case of the Hydrogen Refuelling Station (HRS).



Figure 4: First hydrogen refuelling station in The Netherlands, commissioned in 2020.

A HRS can have multiple methods of hydrogen intake (tube trailer supply, hydrogen transport pipeline, local electrolysis). This leads to a broad range in inlet pressure the compressor has to accommodate. Typical filling pressures are 350 bar (trucks) to 700 bar (cars). An excess pressure is required for the compressor, to accommodate for losses in the supply train toward the vehicle (which includes a cooler, in some cases a separator).

Availability of refuelling stations is of vital importance, for traditional petrol stations but even more so for hydrogen stations which are still less numerous, by typically a factor 100 in Western Europe. Evidence is reported that in case of unscheduled shutdown, the compressor is in most cases the cause of the disruption [12]. In particular, the diaphragm is judged as the most delicate component: once failed this leads to an immediate compressor shutdown. Replacement of diaphragms is a relatively cumbersome and time-consuming procedure, which adds to the unscheduled downtime. Note that in the few reported *incidents* (Norway and USA), the compressor appeared not the main cause [1].

As standard refuelling stations are unmanned, an increased level of reliability is required, compared to dedicated systems on industrial plants. Relevant standards and guidelines can be found in industry branch consortia [4],[5]. The ISO standard 19880-4 is being developed, but the section dedicated to compression is not released yet.

The compressor availability must be ensured, even in intermittent conditions. In HRSs, multiple starts and stops of the compressor are found often in combination with large pressure swings due to switching of buffer volumes, which is a distinctive difference with continuous operation in petrochemical processes. This introduces a considerable challenge for some of the compressor systems, including the diaphragm compressor. Trends that were observed, that may impact on the reliability challenges are: increasing capacity (diaphragm diameters and/or compressor speed), increasing end pressure, increasing temperature (larger pressure ratio per stage) and increasing flexibility/intermittency.

3 Operational challenges and typical remedies

In addition to a literature survey, interviews were conducted within the EFRC network and outside: 20 domain experts were consulted, from the end users, OEMs, service providers and consultants.

The inventory highlighted, amongst others, the following relevant experiences:

- In the domain of HRSs, an overlap is found with the traditional end-users/OEMs (also active in the petrochemical industry), but also many 'new players'. In addition to diaphragm compressors, also other products and developments are found: e.g. non-lube reciprocating compressors, hydraulic compressors, ionic liquid and non-mechanical compressors, all with end pressures in excess of 500 bar. With respect to the compressors, the predominance of a single, leading, design standard (such as API 618, for 'classical' reciprocating compressors) is absent.
- In case of problems, too often an ad-hoc approach is applied to remedy the cause. Communication between operator and OEM, systematic root cause analysis and formalization of lesson-learned are often neglected.
- Ingestion of liquid into the working chamber is identified as a frequent cause of failure [6], although for high purity hydrogen (HRS application) this will not be an issue. Due to the tight clearances, liquid pockets will lead to rapid pressure rises (to which the overflow valve is not designed) and local overloading of the diaphragm. Also, the dynamic rolling of the diaphragm along the gas plate may be disturbed and as a secondary effect the control of hydraulic fluid. The effects may range from broken valves, bolts, piston rods and even oil plates. Adequate control of liquids is essential (separation, draining, avoiding pockets at inlet etcetera, see [7]).
- Dust and foreign (steel) objects damaging the diaphragm (figure 4). Due to the delicate nature of the diaphragm and the tight clearances, any solid object entering the working chamber will result in rapid failure. Reported examples include dust and metallic particles, for example broken valve plates, springs, and non-return valve on the hydraulic side. Installation of

by: Cyril Wentzel – WENTZEL DYNAMICS; Leonard van Lier – TNO

additional filters (typically 5-10 microns, with a recommended inspection period of 300 hours) and selection of more robust design auxiliary components are typical remedies.

- Inadequate hydraulic oil control is detrimental to the correct operation of the compressor. Any anomalies may lead to overloading of the diaphragm. The balance of oil shall be kept by a perfect compensation of leakages along the piston, using the compensation pump and the overflow valve. Even in design conditions, the pressure differential over the diaphragm may be substantial. Wrong sizing of, or obstructions in the overflow conduit will rapidly increase the differential pressure over the diaphragm. Design aspects include the layout of the oil chamber (perforated plate, grooves, cavities) to ensure a uniform pressure loading on the diaphragm. Finally, also due to the compressibility of the oil, especially with dissolved gas, the oil volume may be subject to variable hysteresis effects upon non steady compression and expansion, disturbing the oil compensation.
- Intermittent operation provides an additional challenge, in particular to the oil control. Multiple compressor starts and stops in unmanned, automated operation increase the risk of poor oil control. Upon start-up, the oil side shall be adequately primed and vented (which, in manned operation is usually checked by visual observation). If trapped air is still in the hydraulic circuit, this may be noticed as a noisy and under-performing condition. After the priming, a short duration in unloaded conditions is run before the process pressure is applied. Re-starts in cold conditions may be even more challenging, due to increased viscosity of the oil. An example of the oil pressure in steady conditions and during a start-up is shown in Figure 5 and 6, respectively. During steady condition, the pressure overshoot is substantial (of the order of the operating pressure) with some high-frequency pulsation effects. Upon start-up, the pressure overshoot is strongly increased. Remedies to these start-up issues are adequate procedures and hardware for priming and venting. In addition, basic condition monitoring may be used to detect if the compressor is running in sub-optimal condition (static pressure and flow). More advanced condition monitoring may include dynamic pressure and vibrations.



Figure 4: Examples of failures: pitted and ruptured membranes.



Figure 4: Examples of failures: damaged oil plate.

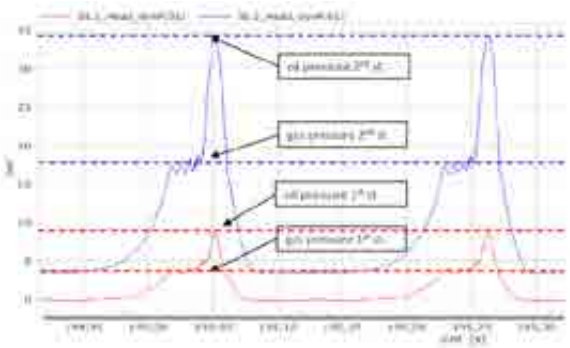

Figure 5: Dynamic pressure signals on oil side; normal operation condition: pressure overshoot and high-frequency pulsation effects.

by: Cyril Wentzel – WENTZEL DYNAMICS; Leonard van Lier – TNO

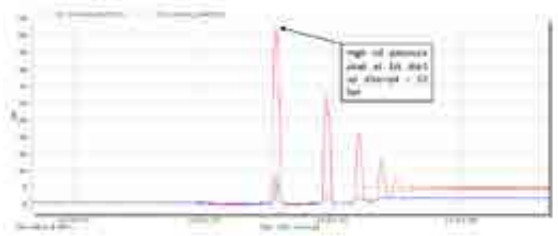

Figure 6: Dynamic pressure signals on oil side; start-up condition with increased loading.

4 Membrane as potential bottleneck of diaphragm compressor reliability

Diaphragms consist of a stack of multiple thin sheets (membranes), 2 or 3, in exceptional cases more.

These membranes are exclusively made of metal. This is in contrast with pump membranes which are in some cases also elastomeric. Material selection depends on the type of gas, but stainless steel is a common choice, whereas also nickel-based alloys are seen. For hydrogen environment, hydrogen permeation and resulting embrittlement are a concern of as yet unknown magnitude especially for high pressures. In spite of the high diaphragm stiffness modulus, pressure differential for full depth deformation is in the order of 1 bar, so much less than the typical discharge pressure. It can be assumed that there is a lower bound design stiffness for the diaphragm.

All metals are prone to fatigue failure. In principle, the stress level can be lowered to be less than the practical fatigue limit, i.e., corresponding fatigue life in the order of $10 \cdot 10^6$ cycles [8]. This choice obviously puts a limit on the membrane strain levels and corresponding cavity volume. Some fatigue limit strain levels are indicated in Table 1.

Table 1 Typical metal fatigue strain limits

Type	Young's modulus [GPa]	Tensile strength* [MPa]	Fatigue Limit strain [‰]
Ni-Cu	160	540	1.3
Fe-Cr (AISI 316L)	193	560	1.2
Ni xxx (Inconel 718)	208	1375	2.6
Ti-Al-V (grade 5)	110	1030	4.2

(* tensile strength excludes strain hardening effect in cold rolled sheet)

We see a limit strain value in the order of 1 to 3 ‰ with the highest nominal score for the titanium grade, which is not currently applied but which is a potential direction for improvement for general application. For hydrogen application, titanium suitability depends on alloy type (α, β, α/β phase) but this is beyond the present scope.

In principle, the application of a fatigue limit is a *safe life* approach in design.

Although this is common practice, there are at least two complications. The first is the challenging influence of fretting and the second is overloading, meaning stress levels or conditions beyond the nominal stress.

Fretting.

Fretting occurs where there is cyclic frictional sliding contact and as a rule fatigue life is diminished depending on amplitude, contact force and other parameters. The topic is a complex one and highly empirical. Use is made of fretting maps for a semi-quantitative understanding.

In the context of diaphragm outer surfaces, there are two configurations that give rise to fretting. The first is the edge clamping configuration under radial stress: in a proprietary inventory of failures, no cracks at this position were seen, therefore this seems to play only a minor role. The second is the radial slip that occurs simultaneously with contact; this is a complicated topic involving frictional physics. An upper limit of slip can however be calculated assuming no friction, as illustrated in the next paragraph.

In this upper bound analysis, it appears that magnitudes of slip were seen of 0.1‰ of diameter, with a peak near the 40% to the 60% radius position and zero at the centre and the edges.

For a 200 to 500 mm diameter range therefore we estimate a corresponding 20 to 50 µm upper limit of slip, which falls in the range of where typical fretting diagrams reveal a 'bucket' shaped fatigue life [9], where mixed stick and slip occur and where decrease of fatigue life depends on the actual magnitude of contact stress. Note that this contact stress is not at all equal to the bulk oil pressure, since the gas pressure on the opposing side may still be assumed to act on the gas side where venting is promoted by radial evacuation grooves in the gas plate. At this stage of the investigation, quantification of fretting contact pressure remains out of the project scope, despite its potentially overriding importance: the data in [9] show that going from no slip to 5 µm slip and from 5 µm slip to 20 µm decreases the fatigue limit by a factor of 2 for every step.

Overloading

At least part of the explanation of less-than-nominal fatigue life should be sought in overloading. The nominal shapes, strains and hence stresses correspond to membranes being in complete contact with the gas plate and semi-free form at the opposite position (Figure 7). When there is a cause (section 3) for higher than nominal oil volumes and peak pressures, the membrane can only be stressed beyond these nominal stress distribution in areas where there are gas cavities. This is near valve openings and evacuation grooves in the gas plate and

by: Cyril Wentzel – WENTZEL DYNAMICS; Leonard van Lier – TNO

near oil channels at the opposite end when there is too little oil. In general, some margin will have been included in the design load.

Beyond such conditions, we can speak of overloading, which will be elastic for moderate levels and by itself can cause reduced fatigue life. When the resulting deformation involves plasticity, there will be embossed features and fatigue performance will be even more difficult to predict.

Robustness

A novel material concept that allows such overloading conditions without detrimental effects on fatigue life would enable a more robust design. A second benefit then goes beyond robustness and reliability: it would create a design space for a deeper cavity and thus higher flow volume for the same diameter.

One important question of the quantitative study (next paragraph) was to establish a relationship between typical design stress levels and textbook fatigue limits under nominal conditions. From the literature [10] it was seen that stresses of 200 to 250 MPa were encountered for steels. This range was confirmed by the current analysis in the HyMem project when assuming less than 2% cavity depth (h/2) and clamped edges.

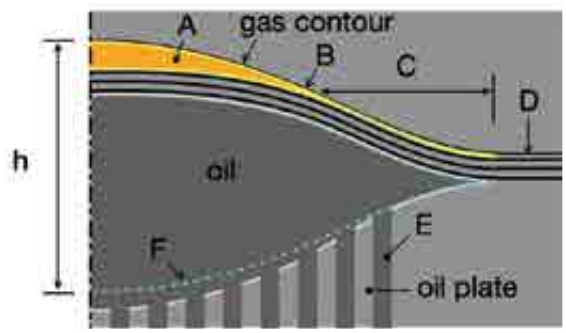

Figure 7 Deformed diaphragm during upward stroke. A compressed gas, B contact line, C contact zone, D clamping and sealing area, E oil channels, F nominal BDC membrane shape, h double cavity depth (< 2% of diameter). No valve and evacuation grooves drawn.

5 Analysis of membrane loads and stresses

For the purpose of re-engineering the membrane, a proper understanding must be gained of the operational and design parameters on stress and possibly also dynamic behaviour. This latter aspect is beyond the scope for the first HyMem project phase, so that the focus is on quasi-static deformation and in particular an estimation of the corresponding stress levels. For this purpose, a generic model was made for non-linear analysis of a single membrane including contact under quasi-static deformation upon uniform oil pressure loading. In addition to stress levels, an idea is obtained of slip.

In general, membrane surface stress consists of 'membrane stress' (deformation) and bending induced stress. Stress reversal from gas side generatrix to oil side shape looks different depending on radial position. Both depend on the cavity gas plate contour and critical conditions may arise near the centre, halfway or near the outside.

Generatrix shape is likely to be a proprietary parameter. In the literature, a common family of shapes is described by this formula, where x is the dimensionless radius and $Z = 8.8$ as an arbitrary design choice:

$$f(x) = 1/(Z-1)*(2*x^{Z+1} - (Z+1)*x^2 + (Z-1))$$

The following results are given as an example for illustration for a diameter of 200 mm and a 0.3 mm thin membrane sheet against a chosen generatrix (in this case resembling closely the scaled analytical linear computational solution for deformation of a transversely loaded disk). Depth of the semi cavity is below 2% of the diameter.

First, some results are shown for the 'membrane stress', i.e. midplane stress components, excluding the effect of bending. Figure 8 shows two principal stress components for two conditions corresponding to one single nominal displaced volume, for TDC (gas plate contact) and BDC (free form) respectively.

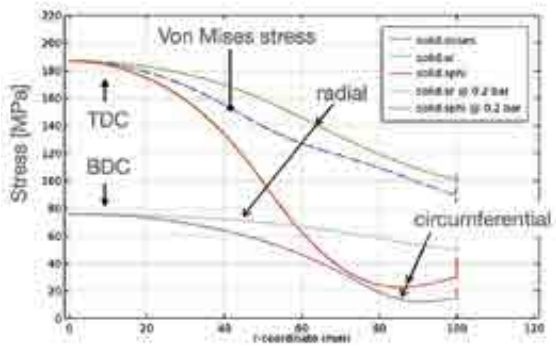

Figure 8 Principal stress components for two opposing membrane conditions (excluding bending).

It is seen that the necessity to apply a flared S-shaped generatrix for the reasons mentioned before, comes at a cost of an increase in radial stress: in the centre there is a biaxial stress condition of nearly 190 MPa whereas the opposite position this lowers to below 80 MPa. Near the clamped edge the difference in radial stress is between 100 and 50 MPa.

For fatigue, we should look at principal stresses occurring at the surface, so bending should be included. On the gas side near r=R, bending stress elevates the stress level to beyond 200 MPa as seen in Figure 9. This undesirable localised bending can be prevented by applying some edge 'support', flaring the contour while leaving clearing space near the centre where the oil grooves are.

by: Cyril Wentzel – WENTZEL DYNAMICS; Leonard van Lier – TNO

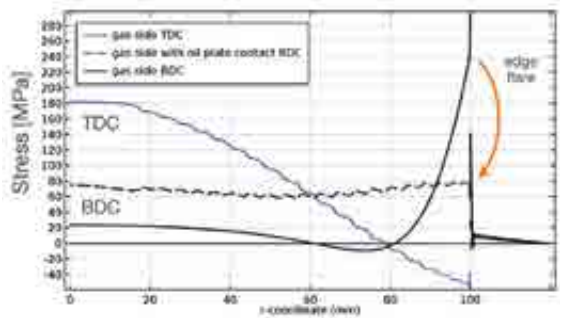

Figure 9 High gas side stress at BDC due to bending; effect of maximum support effect ('edge flare') shown. Radial stress at BDC and TDC.

A further illustration of the computational result is given by considering the lateral displacement. This is an upper limit for fretting amplitude. Figure 10 shows an example result.

The stress levels from the previous results indicate a maximum stress (amplitude) of approximately 200 MPa for materials with steel-like stiffness. This is in a similar range as literature values.

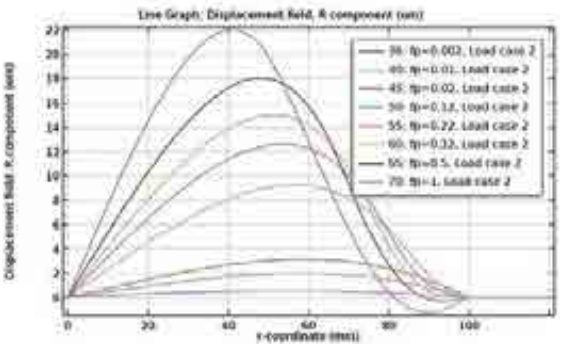

Figure 10 Upper limit fretting amplitude estimation from non-linear contact model.

With the estimate of typical limiting stress in place, we can now look at the margin relative to nominal fatigue limits. Comparison to 250 or 300 MPa indicates that such a margin, though positive, is not large – which is logical.

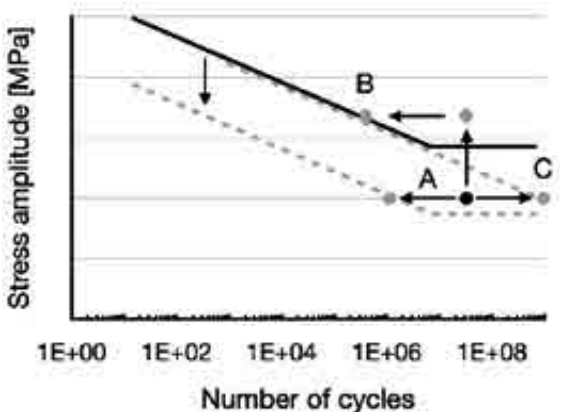

Figure 11 Schematic impression of design point fatigue in fatigue diagram and three directions for error and premature failure. A, B, C are discussed in text. Dashed lines indicate material degradation.

The situation is graphed in Figure 11. We distinguish three possible directions for reduced fatigue life:

A: Reduced life due to material degradation (lower curve, e.g. due to fretting).

B: Overloading related higher than design stresses.

C: Material degradation and higher number of cycles due to fretting and environmental conditions.

The main possibility for overloading seems to be related to intermittent operation, as discussed in section 3.

7 Feasibility of novel membrane materials

We have seen that, by definition, fatigue life is a design driver. Given these lifetime limitations in general and due to intermittent operation in particular, improvement of performance can be sought in a direction involving other materials or *material concepts*. Whereas the first option is straightforward, the latter involves a different diaphragm architecture and separation of functionality, for example the application of polymer layers to reduce fretting.

In reconsidering the material selection, all functional requirements should be firmly defined. The main requirement to constrain material selection other than metals is (a lower bound on) stiffness. This topic is under investigation in a next phase of the HyMem project.

Some promising metallic materials could be selected and investigated, such as the titanium alloy Ti-4Al-4V (Grade 5 titanium) mentioned in Table 1. Assessment involves an empirical investigation under representative fatigue conditions, especially fretting under multi-axial fatigue stress. In such an assessment, it would be beneficial to uncouple the investigation from the machine itself. A dedicated fatigue set-up is also under investigation for a next HyMem phase.

A final consideration is presented to illustrate the potential for eliminating fatigue as a design driver. As noted before, the required fatigue limit is properly understood as a deformation-driven parameter, i.e. fatigue strain limit rather than a stress limit. Figure 12 illustrates this point by plotting membrane (midplane) strain for a generic generatrix (shape) as a function of cavity semi depth z. The radial fibre strain is evaluated for general generatrix shapes to be somewhat higher than the simple straight line length increase following from Pythagoras' law by approximately 30%. Obviously,

by: Cyril Wentzel – WENTZEL DYNAMICS; Leonard van Lier – TNO

this excludes bending effects which are proportional to membrane thickness.

This simple graph illustrates the potential for deeper cavities when materials exhibit significantly higher fatigue limit strains. This is the case for several engineering polymers and a class of polymer-based fibrous composites, which have strain limits in the range of 0,3% to 0,8% [11], corresponding to the right part of the diagram. This potential provides a strong motivation to quantify required diaphragm stiffness, both in extension and bending.

Also indicated is the dashed curve for a typical light weight metal alloy in terms of equivalent reference stress.

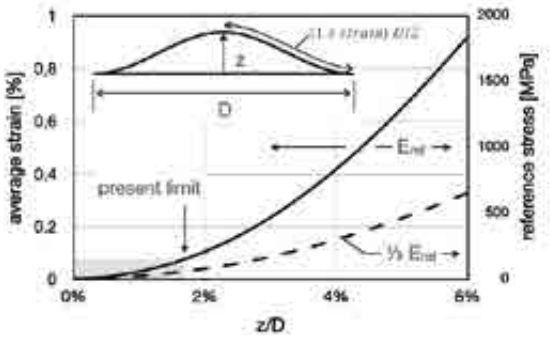

Figure 12 Variation of radial strain as a function of cavity depth, and corresponding stress indication (reference stress = strain × E) for two values of Young's modulus.

When the class of polymer materials is considered for application, there are at least two requirements which become relevant constraints and demand a design solution, i.e. membrane permeability and temperature cycling on the gas side. The latter is important because of the low thermal conductivity, creating high thermal gradients near the surface, whereas gas temperatures could cycle between approximately 40° and 200°C. The thermal stress can no longer be ignored.

If the departure from the original metallic membrane material is large, also the clamping and sealing configuration will be subject to change. This should be an integral part of any novel concept development.

8 Conclusions

- Hydrogen compression is an active and growing business. Hydrogen Refuelling Stations for transportation are a relevant part of the future hydrogen chain. In HRSs, specific requirements apply to the compression. The most important are the high outlet pressure, the purity of the hydrogen and the intermittent operation. In addition, a future trend is observed to increased capacity, increased pressure ratio and efficiency.
- The HRSs are not subject to the traditional design codes (API 618). No special control pulsation and vibration techniques are included in the designs (pulsation dampers, restriction orifices)
- The integrity of the diaphragms is experienced as an issue, for the overall reliability of diaphragm compressors. In many real compressor systems, the operational circumstances are not optimal and shall be improved. Often, these circumstances are the primary effects that trigger diaphragm failures, as a consequential damage. Examples of such operational circumstances are liquid ingestion, dust and foreign particles, inadequate setting of the oil control system and intermittent service.
- Controlling the negative operational circumstances by creating awareness, sharing experiences and ensuring compliance with guidelines and procedures is a first step to improve the overall reliability.
- As a next potential for improvement, the intrinsic design of the membrane shall be studied, in order to create more robust diaphragm designs.
- The figure of merit for fatigue is fatigue limit strain, which is more favourable for several types of non-metallic materials. Before investigating such alternative concepts, it should be quantified what the role of stiffness is in diaphragm and oil and gas flow behaviour.
- If less fatigue sensitive materials can be applied, there is a promise of increased flow to be achieved for the same head diameter, while retaining a more robust and hence more reliable design.

9 Outlook

As a future EFRC R&D activity, numerical and experimental techniques to simulate, measure and validate the detailed loading and response of membranes will be developed.

Also, as novel types of membranes (alternative materials, treatments and clamping) are developed by suppliers or OEMs, these can be evaluated by representative testing for endurance on a dedicated test rig which may even develop into an industry standard. This work is in progress during 2023.

If and when successful, reliability of the diaphragm compressor for the very challenging use case for unmanned hydrogen refuelling stations will be significantly enhanced.

by: Cyril Wentzel – WENTZEL DYNAMICS; Leonard van Lier – TNO

10 Acknowledgment

The authors express their gratitude to the EFRC R&D group, and in particular the steering group members, for their kind support during the execution of the work and for the permission to publish the results in this paper.

References

[1] C. Tümer, L. van Lier, EFRC Report TNO-2022-R12304, "Inventory of operational aspects, influencing the reliability of membranes in diaphragm compressors", November 2022.

[2] C. Wentzel, EFRC Report 2022-002, "Diaphragm Compressor Membrane Material Concepts", October 2022.

[3] EFRC Whitepaper, "Hydrogen compression – boosting the hydrogen economy", November 2022.

[4] The Green Hydrogen Organization, "The Green Hydrogen Standard", May 2022.

[5] www.cleanenergypartnership.de.

[6] H. Habel, „Condensate in diaphragm compressors", IREC Conference Düsseldorf, 2016.

[7] EFRC guidelines on how to avoid liquid problems in reciprocating compressor systems, revision 3, 2018.

[8] Fatigue of structures and materials, J. Schijve, Springer, 2009.

[9] Test methods to investigate the influences of fretting corrosion on the endurance, Materialprüfung 11, 1969.

[10] A new cavity profile for a diaphragm compressor used in hydrogen fuelling stations, Yuanlin Hu et al., 2017.

[11] Composite materials in aircraft structures, Middleton, Longman Scientific & Technical, 1990.

[12] M. Dolman *et al*,EU union JIVE 2 report 779563, "Operators' guide to fuelcell bus deployment", October 2019.

HYDROGEN COMPRESSION

Reciprocating Compressors and the Hydrogen Economy
by: Ben Williams – ARIEL *109*

Wear Mechanisms of High-Pressure Hydrogen Sealing Materials
by: Michael Schöbel – LEOBERSDORFER MASCHINENFABRIK; Marc Langela – STASSKOL *117*

Experimental and numerical investigation on the sealing capability of a high pressure, dry running, hydrogen reciprocating compressor
by: Giorgio Taurian – SIAD; Paul Modern – COOK COMPRESSION; Giovanna Barigozzi, Nicoletta Franchina, Elisa Ghirardi, Otman Kouaissah – UNI BERGAMO *123*

Efficient H_2 compression with Pistons & Diaphragms – Recips as a keystone of the energy transition
by: Jens Wulff – NEUMAN & ESSER *132*

EFRC
EUROPEAN FORUM for RECIPROCATING COMPRESSORS



COMPRESSION YOU CAN COUNT ON



For our customers, compression is critical – always. So when they need us, we spring into action. Ariel works to build and maintain a trusting relationship that grows stronger with time. We look at everything from our customers' perspective, so we can truly understand the best ways to make their operations more successful.

Compression you can count on, now and always.



Reciprocating Compressors and the Hydrogen Economy

by:

Ben Williams
Specialist – Process Sales and Market Development
Ariel Corporation
Mount Vernon, Ohio, USA
bwilliams@arielcorp.com

13th EFRC CONFERENCE
September 19th – 21st 2023, Zagreb

Abstract:
The global push for decarbonization and decreased greenhouse gas (GHG) emissions will require a significant amount of hydrogen. Green hydrogen (hydrogen produced by the electrolysis of water using only renewable energy sources, such as wind and solar), is perceived by some as the best source of hydrogen needed to meet current decarbonization goals. While this may or may not be true, increased hydrogen production will require additional hydrogen compressors. While multiple compressor types are used for hydrogen, this paper will focus on reciprocating piston-type compressors.
Reciprocating compressors have been used in hydrogen service for years, primarily in the refinery and petrochemical industries. Recently, companies have been trying to determine what is required for the energy transition and how they can participate. Companies have come up with several „new“ hydrogen applications. These new applications, such as hydrogen storage, hydrogen mobility, and hydrogen blending (with natural gas) will have different requirements for hydrogen compression than have been typical for refinery and petrochemical applications.
This paper will describe the „new“ applications, including summarizing the operating conditions and the compressor requirements, along with some of the projects being considered. These can be complex applications and because of that, some users are willing to operate outside of the typical hydrogen operational limits that have been used for years in the refinery and petrochemical industries.
Gas cleanliness is crucial for these hydrogen applications so the majority of them are non-lubricated. Nonlubricated compressors do not use oil for cylinder lubrication, these compressors typically use „selflubricating“ materials. The decision to use lubricated or non-lubricated cylinders, along with the source of the hydrogen, whether from an alkaline electrolyzer or a PEM electrolyzer, will determine the design of the compressor.
If it proceeds as expected, the Hydrogen Economy will be an opportunity for reciprocating compressors to shine and we should all look forward to seeing where things go from here.

by: Ben Williams – ARIEL

1 Introduction

Reciprocating compressors, both with lubricated and non-lubricated cylinders (if within OEM discharge pressure limits), have been used in hydrogen service for decades, primarily in the refining, petrochemical, and industrial gas industries. Among the many hydrogen applications typical to these industries are hydrogen production, syngas, desulphurization (H2 Makeup and Recycle), and tail gas compression. Other non-traditional hydrogen applications include hydrogen transmission via pipeline and hydrogen storage.

As governments around the world establish mandates regarding the goal of reducing carbon emissions to a "net zero" value. Hydrogen is considered key to this, "energy transition" and the term "Hydrogen Economy" is once again routinely being used. (The term hydrogen-based economy was first used during the 1970s by John Bockris.[1]) To meet the decarbonization goals, significant amounts of hydrogen and hydrogen compression will be required

Green hydrogen is the focal point of the energy transition. Producing hydrogen using electrolysis, powered by renewable energy sources, such as wind and solar is considered by many to be the only way to meet the Net-Zero carbon goal. That remains to be seen.

Renewable hydrogen applications will include those applications mentioned above, as well as hydrogen fueling. The compressors used for these applications will depend on the source of renewable hydrogen, whether it be an alkaline or PEM electrolyzer or a tube trailer.

The design of the compressors will also be determined by whether or not the End User applies the traditional operating limits of API 618 and ISO 13707 or is willing to "stretch" these limits to reduce the initial compressor cost or the overall Total Cost of Ownership (TCO).

The goal of this paper is to discuss design considerations for reciprocating hydrogen compressors both in the "traditional" and renewable applications, typical operating conditions for both, and how expectations and operating limits may differ between the two.

2 Hydrogen Applications

This section will discuss the typical hydrogen applications, as well as some "new" applications that are being considered as part of the energy transition.

Note, although almost half of the hydrogen produced today is used for the production of ammonia (NH_3), the compression of ammonia is very specialized and will not be addressed herein, except to say liquid ammonia is one of the numerous means of transporting hydrogen under consideration at this time.

2.1 Hydrogen Production

Hydrogen is the most abundant element in the universe, but due to its level of reactivity and chemical properties, hydrogen is primarily found as part of a compound. The primary compounds containing hydrogen are water and hydrocarbons. There are several processes used to separate the hydrogen from these compounds, including steam methane reforming and electrolysis.

2.1.1 Steam Methane Reforming

Approximately 95% of the hydrogen produced today comes from the reforming of natural gas by the steam methane reforming (SMR) process. Reacting natural gas with steam at high temperatures (approximately 600-1000 degrees C) produces hydrogen and carbon monoxide (CO). After undergoing a shift conversion process, the carbon monoxide and water produce hydrogen and carbon dioxide (CO_2).

The SMR hydrogen is sent to a pressure swing adsorber (PSA) system which cleans the hydrogen. Typical PSA hydrogen has a purity of 99.9999% pure. The pure hydrogen out of a PSA is sent to the hydrogen product compressor with discharge pressures ranging from approximately 34 to 100 Bar, depending on the plant design.

Because CO_2 is formed in the steam methane reforming process, this is sometimes referred to as "gray hydrogen" If CO_2 capture is included in the process, this is considered by some as "blue hydrogen".

A steam methane reformer unit located near Chicago, IL, USA is shown in Figure 1.



Figure 1: Steam methane reformer in Illinois, USA[2]

by: Ben Williams – ARIEL

The steam methane reforming process involves multiple gas streams, each of which may require compression. These include natural gas feed, fuel gas, hydrogen product (from the outlet of the PSA), and tail gas.

2.1.2 Electrolysis

Electrolysis is the process of separating water into hydrogen and oxygen using electricity. If the electricity used by the electrolyzer comes from a renewable source, such as wind or solar power, the hydrogen produced is considered "green hydrogen".

There are multiple types of electrolyzers, including Alkaline, Proton Exchange Membrane (PEM), or Solid Oxide. The most commonly discussed and the types covered herein are the Alkaline and PEM electrolyzers. The electrolyzer process has a significant impact on the hydrogen compressor selection.

The alkaline electrolysis process was discovered over 200 years ago. The basic process involves an anode and a cathode with hydroxide (OH-) ions passing from the cathode to the anode through an electrolytic solution, such as potassium hydroxide. Hydrogen is produced on the cathode side and oxygen on the anode side. Figure 2 shows the basic principle of an alkaline electrolyzer.

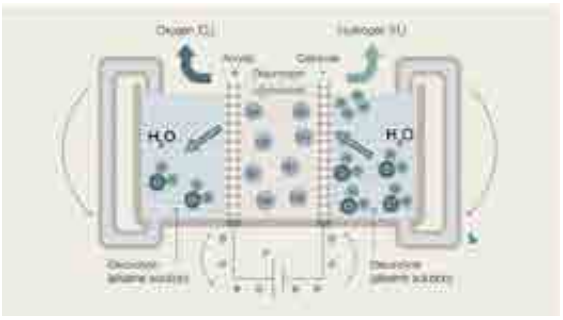

Figure 2: Alkaline Electrolyzer Schematic[3]

The typical alkaline electrolyzer produces hydrogen at or slightly above atmospheric pressure (1.01 BarA). Conversely, a Proton Exchange Membrane (PEM) electrolyzer can discharge between 8 and 30 BarA.

PEM electrolysis uses an anode, a cathode, and a membrane as the electrolyte. Water is "split" on the anode side and the hydrogen ions pass through the membrane to the cathode side. Figure 3 shows a schematic of the PEM electrolysis process.

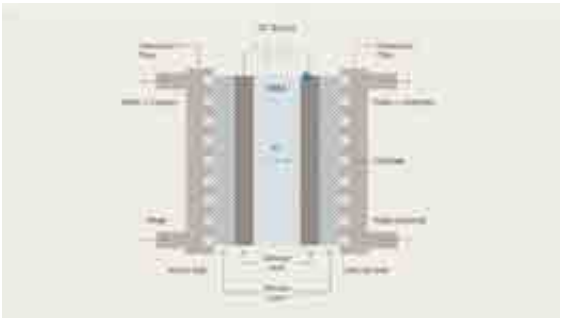

Figure 3:Proton Exchange Membrane (PEM) Electrolyzer Schematic[4]

The discharge pressure produced by the electrolyzer determines the suction pressure for the compression system. For a given application, hydrogen produced from a PEM electrolyzer will have a significantly reduced number of stages than that of alkaline electrolyzer hydrogen.

The following example shows how the electrolyzer process impacts the compressor design for a hydrogen application requiring a discharge pressure of 200 BarA and delivering 50 kg/hr.

Using OEM reciprocating compressor software to select a compressor based on the above parameters and to prevent exceeding the API 618 discharge temperature limit of 135° C (275° F), the following compressor designs were selected. These are based on one reciprocating compressor manufacturer's product line-up.

- **Alkaline Electrolyzer – 1.01 BarA electrolyzer outlet pressure.**

  A six-throw compressor with eight stages of compression is required. 129 kW is needed. (See Figure 4)



Figure 4: Six throw, eight-stage compressor selection[5]

- **PEM Electrolyzer – 25 BarA electrolyzer outlet pressure.**

  A two-throw compressor with three stages of compression is required. 54 kW needed. (See Figure 5.)

by: Ben Williams – ARIEL



Figure 5: Two throw, three-stage compressor selection[6]

The low discharge pressure from an alkaline electrolyzer will often require larger cylinders to meet the capacity requirements of the application. Depending on the application, it may require a series of compressors to reach the required discharge pressure. This depends on the cylinder size, compressor stroke and rod load limits, and the number of compressor crankshaft throws available. The number of throws depends on the manufacturer and varies from one to ten.

As you can see, the type of electrolyzer used has a significant impact on the compressor selection.

2.2 Hydrogen Desulfurization

The most common use of hydrogen in a refinery is in the desulfurization of fuels. Figure 6 shows a schematic of the desulfurization process.

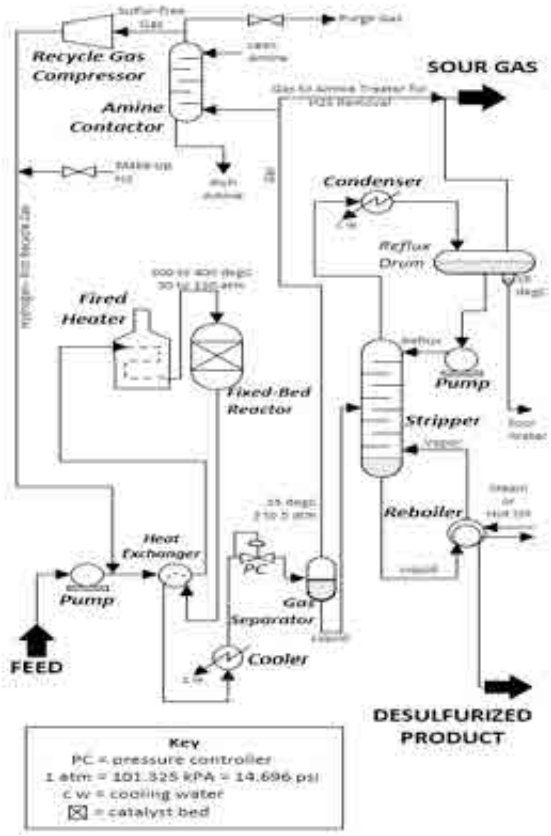

Figure 6: Desulfurization Process of Liquid Fuels[7]

Sulfur is removed from the liquid fuel(s) by reacting it with hydrogen in catalytic vessels at high temperatures and pressures. The process produces low or ultra-low sulfur fuels. The sulfur-rich gas is sent to an amine contactor which removes most of the sulfur. The "cleaned" recycle stream is compressed and makeup hydrogen is added to the system and the desulfurization process continues. The two hydrogen services (streams) involved in this process, hydrogen makeup and recycle may be handed with individual compressors or as a multi-service compressor with each stream independent of the other.

Typically, the discharge pressures for the hydrogen makeup and recycle services are similar, however, actual conditions depend on the process license used and the size of the refinery.

Several renewable hydrogen fuel facilities are under consideration and although they may be smaller in scale, these facilities will require similar desulfurization processes and therefore hydrogen compression.

2.3 Hydrogen Storage

Hydrogen gas is typically stored in tanks, vessels, or underground salt caverns. Currently, there are four operational underground hydrogen storage (UHS) facilities in the world; three in the United States and one in the United Kingdom. The US facilities are used to supplement the hydrogen supply to a petrochemical plant and industrial gas hydrogen pipelines. The U.K. facility stores hydrogen for turbine generator use during peak electricity demand periods. Figure 7 shows a reciprocating compressor at a UHS facility in Texas, USA.



Figure 7: Reciprocating compressor package at an underground hydrogen storage facility in Texas, USA[8].

by: Ben Williams – ARIEL

There are a number of pilot projects involving underground hydrogen storage under consideration.

Current underground hydrogen storage facilities operate at pressures between 45 and 200 BarA. Inquiries for renewable underground hydrogen storage pressures of up to 350 BarA have been received. The majority of compressors used in hydrogen storage at these pressures use lubricated cylinders. Typically. non-lubricated compressors will have lower discharge pressure ratings.

Hydrogen is also stored and transported in tube trailers. This has been relatively commonplace for years; however, the use of tube trailers will likely increase to transport renewable hydrogen from its production location to where it is needed. This application is also known as a "virtual pipeline"

The hydrogen storage pressure in tube trailers depends on the type of storage tubes used. Figure 8 shows a typical hydrogen tube trailer arrangement.



Figure 8: Hydrogen tube trailer[9]

Hydrogen tube trailers are classified based on the materials of construction and the storage pressure.[10]

Type I (Type 1) Older steel tube trailers are a simple design and are limited to less than 200 BarA but newer Type IV (Type 4) hydrogen tubes are constructed from composite materials and wrapped in carbon fiber. These lighter tubes are expected to be used for hydrogen mobility applications and the tube trailers will be rated for greater than 500 BarA.

Compressors are needed to fill the tube trailers and compress the tube trailer's discharge to the required hydrogen fueling pressure.

2.4 Hydrogen Pipeline Applications

Currently, there are over 5,000 km of operational hydrogen pipelines worldwide; approximately 2600 km are in the United States and 2000 km in Europe.[9] Hydrogen pipelines operate at pressures ranging from 45 to 100 BarA.

The European Hydrogen Backbone (www.EHB.eu) project continues plans to add additional renewable hydrogen infrastructure, including pipelines and storage facilities, for decarbonization. This will include the construction of new hydrogen pipelines and when possible, converting existing natural gas pipelines to hydrogen.

Another pipeline application that has drawn quite a bit of attention, primarily in North America, is the blending of hydrogen with natural gas in existing pipelines. The primary reason for doing this is to reduce greenhouse gas (GHG) emissions.

The amount of hydrogen that can be added to an operating natural gas pipeline is still being determined. Although some inquiries may mention blending hydrogen concentrations of 50% or more to the existing natural gas stream, most projects moving forward with less than 20% added hydrogen.

Regarding the reciprocating compressors used for hydrogen blending applications, any new compressor will be designed specifically for hydrogen service. However, existing natural gas pipeline compressors used in hydrogen blending applications must now be suitable for lower mole-weight gas.

The following is an example of the impact on an existing lubricated, natural gas pipeline compressor (Figure 9) when 30% hydrogen is mixed into the gas stream (Figure 10). For simplicity, have assumed a direct swap of hydrogen and methane from the original gas composition.

- **Existing Compressor**



Figure 9: Example of existing natural gas pipeline compressor performance[11]

by: Ben Williams – ARIEL

- 30% Hydrogen blended into the gas stream (30% methane removed)



Figure 10: Example of compressor performance with 30% hydrogen blended into the existing natural gas stream[12]

As expected the gas is now lighter and mass flow is reduced. Additionally, the ratio of specific heat ("n-value') has increased, therefore the discharge temperature has also increased.

For this example, the compressor valves should be reviewed to determine whether they are still suitable for the lighter gas. As for the compressor itself, no material changes would be required, however, the compressor system (package) should be evaluated to determine whether the system components are suitable for the lighter gas. The lighter gas may also impact gas pulsations and a new pulsation study should be performed to ensure no changes to piping or vessels are needed.

2.5 Hydrogen Fueling

According to the International Energy Agency (IEA), in there are currently 56,000 hydrogen fuel cell electric vehicles (FCEV) on the road today. These vehicles require fueling with hydrogen. Figure 11 shows a chart from 2021 comparing the distribution of hydrogen fuel cell electric vehicles to the number of available hydrogen fueling stations.

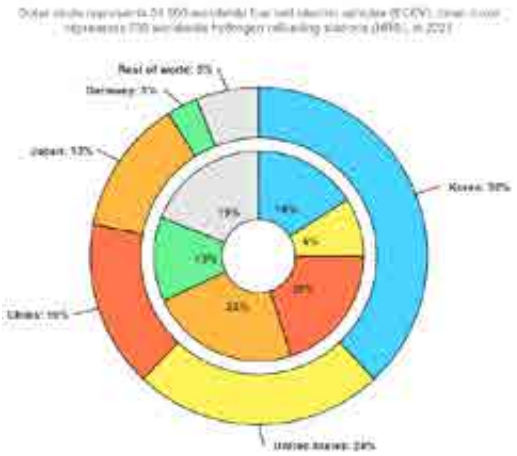

Figure 11: International Energy Agency chart showing the current location for hydrogen fuel cell electric vehicles and the available hydrogen fueling stations[13]

A search of the internet shows a number of reports that have been written about the future of hydrogen FCEV and the majority of them predict a sharp increase in the number of vehicles. One such study by Precedence Research (https://www.precedenceresearch.com/hydrogen-fuel-cells-market) predicts the hydrogen FCEV market to be over $130 billion USD by the year 2030. This will require a significant number of hydrogen fueling stations.

Hydrogen fueling pressures will vary depending on the manufacturer or the application, whether it be cars, light-duty trucks, buses, or long-haul over-the-road trucks. Typical pressures vary from 350 to 1000 Bar.

Although there are fueling stations that use lubricated compressors with coalescing or oil removal systems downstream of the compressor; hydrogen fueling compressors are normally non-lube. Non-lube means that oil is only supplied to the running gear. Lubricating oil is not supplied for the cylinder or packing. This is to prevent fouling of the vehicle's fuel cells. According to ISO 14687 (Hydrogen Fuel Quality – Product Specification), The typical hydrogen purity requirement of an H2 fueling dispenser is 99.97%.

Depending on the volume of hydrogen needed and the discharge pressure required, it is not uncommon to use a non-lubricated reciprocating piston compressor feeding into a diaphragm compressor or hydraulic intensifier. There are reciprocating compressor systems being developed that will reach higher pressures with non-lubricated compressor cylinders.

Design standards for hydrogen fueling compressors, as well as other renewable hydrogen compressors, are detailed in the following section.

by: Ben Williams – ARIEL

3 Traditional vs. Renewable Hydrogen Compressors

API 618 and ISO 13707 are the most commonly referenced standards for hydrogen compressors used in the refinery, petrochemical, and industrial gas sectors. These standards are guidelines for compressors and system components to achieve three years of uninterrupted service and a service life of 20 years.

Due to the similarity of the applications, expectations would be that API 618 or ISO 13707 would be required for compressors used in renewable hydrogen service. However, based on inquiries received for renewable hydrogen compressors, that is not always the case. In a large number of cases, we have seen customers who are willing to forgo those standards and do not require the longer runtimes associated with each.

3.1 Achieving longer runtimes

Among the key design features described in API 618 and ISO 13707 that contribute to longer compressor runtimes are:

- **Piston speed –** Piston speed affects the non-metallic wear parts that rub, such as piston rings, wear bands, and packing. Lower piston speeds promote longer non-metallic wear part life.
- **Discharge temperature –** The maximum discharge temperature for hydrogen-rich applications is 135 degrees C (275 degrees F). Typical TFE-based wear parts are suitable for operating up to 175 degrees C (350 degrees F). The lower the discharge temperature, the better it is for non-metallic wear part life. Oil viscosities are higher with lower discharge temperatures; as temperature increases, the oil viscosity decreases.
- **Wear band loading –** Wear band loading is the force (bearing load) due to the piston weight and half of the piston rod weight divided by the projected area of a 120-degree arc of the wear bands. API 618 and ISO 13707 limit this to 0.035 N/mm2 (5 PSI) for non-lubricated units and 0.070 N/mm2 (10 PSI) for lubricated cylinders. Reduced wear band loading leads to longer wear part life.
- **Cylinder lubrication –** It is crucial to select the proper type and amount of lubricating oil, based on the gas composition and compressor operating conditions. It is also important to remember that more oil is not always better. Divider blocks, pump-to-point, or a combination of both are commonly used in cylinder lubrication systems.

  NOTE – Non-lubricated cylinders are also used in these “traditional” hydrogen applications, where suitable.

3.2 A Different Viewpoint

As previously mentioned, based on inquiries received for renewable hydrogen applications, API 618 or ISO 13707 are not always required. In many cases, the end user is not the typical process compressor customer and is open to taking a new approach to these applications.

With this new approach to renewable hydrogen compressors, the design may include:

- **Non-lubricated cylinders** - Many of the renewable hydrogen compressors are non-lube and therefore 3 years is not expected. Hydrogen fueling compressors are normally non-lubricated. When discussing current hydrogen fueling compressors, whether reciprocating, diaphragm, hydraulic, or a combination, with several End Users, expectations of wear part life is less than a year.
- **Higher Discharge Temperatures** - These customers are often willing to accept discharge temperatures greater than the 135° C (275° F) limit in API 618. The API 618 limit was established years ago with the goal of achieving three years between shutdowns. It is interesting to note that in a lubricated hydrogen compressor, the non-metallic wear parts (piston rings, packing, and wear bands) used are often the same materials used for other lubricated compressors in different applications, to which the 135° C (275° F) limit does not apply. The majority of these non-metallic materials are suitable for temperatures up to 175° C (350° F).

  To illustrate the point about discharge temperature, using the alkaline electrolyzer conditions shown earlier in this document, if the discharge temperature was allowed to exceed the API 618 limit but stay under 150° C (300° F) only seven stages would be required, rather than 8. This reduces the capital cost (CAPEX) of the compressor system. This combined with the cost of operation (OPEX), determines the Total Cost of Ownership (TCO) which is often the determining factor in the compressor selection.
- **Higher rotating speeds –** A higher rotating speed results in smaller cylinders which decrease the size of the compressor package or system. Attention must be paid to the compressor valve design with the higher rotating speeds. Rotating speed and valve lift affect the impact velocity of the valve sealing elements.

It is important to note that in those cases where API 618 or ISO 13707 are not required, safety is not compromised. Safety is always paramount regardless of the reciprocating compressor

application. An example of this is hydrogen fueling compressor systems.

Currently, the primary standard used for hydrogen fueling compressor systems is the National Fire Protection Standard (NFPA) 2 Hydrogen Technologies Code. This standard is designed to provide safety rules for hydrogen generation, installation, storage, piping, and handling of gaseous and liquid hydrogen.[8] At least one organization, ISO, is in the process of writing a standard for hydrogen fueling, including a section on hydrogen fueling compressors.

4 Conclusion

Although global decarbonization is universally accepted, there are questions about the timeline and the availability of resources to see it through. The hydrogen economy has been predicted before and went nowhere. What is different this time is that governments have issued hydrogen strategies and mandates to meet Net Zero Carbon initiatives by 2050 or earlier in some cases. A lot of money is being spent on new and existing infrastructure to enable transporting of hydrogen from the renewable source to the point of use. With this will come a need for hydrogen compression.

The compressors needed for renewable hydrogen may not be the typical refinery or petrochemical hydrogen compressors used in the past. End users will decide whether they can accept less conservative design features such as higher temperatures and speeds to reduce overall TCO. Whatever their decision, we can expect increased demand for hydrogen and hydrogen compressors as we move forward with the goal of global decarbonization.

5 Acknowledgements

Special thanks to Ms. Kaley R. Coss (Ariel Corporation – Application Engineer) for her assistance with the review and editing of this document.

References

1 U. Bardi, “A concise history of the concept of “Hydrogen Economy.’” Resilience, 21 May 2021. https://www.resilience.org/stories/2021-05-21/a-concise-history-of-the-concept-of-hydrogen-economy/ (accessed 13 March 2023).

2 Steam methane reforming unit in a facility near Chicago, IL USA. Ariel Corporation. [Photo].

3 N. Ironside, “Electrolysis: The Backbone of the Green Transition.” COWI, 28 April 2022. https://www.cowi.com/insights/electrolysis-the-backbone-of-the-green-transition (accessed 13 March 2023).

4 N. Ironside, “Electrolysis: The Backbone of the Green Transition.” COWI, 28 April 2022. https://www.cowi.com/insights/electrolysis-the-backbone-of-the-green-transition (accessed 13 March 2023).

5 Ariel Performance Software

6 Ariel Performance Software

7 The *Role of Hydrogen in Removing Sulfur from Liquid Fuels.* Praxair (Now Linde), 1 March 2017. [Online] Available: https://www.linde.com/-/media/linde/merger/documents/sustainable-development/the-role-of-hydrogen-in-removing-sulfur-from-liquid-fuels-w-disclaimer-r1.pdf?la=en#:~:text=Hydrogen%20is%20a%20proven%20solution,tons%20per%20year%20of%20SO2. (accessed 13 March 2023).

8 Reciprocating compressor package at an underground hydrogen storage facility in Texas, USA. Ariel Corporation. [Photo].

9 “Hydrogen Tank – FAQ Guide.” Hyfinder, 15 January 2023. https://hyfindr.com/hydrogen-tank/ (accessed 13 March 2023).

10 Hydrogen tube trailer. https://www.energy.gov/eere/fuelcells/hydrogen-tube-trailers

11 Ariel Performance Software

12 Ariel Performance Software

13 https://www.iea.org/data-and-statistics/charts/fuel-cell-electric-vehicle-stock-and-hydrogen-refuelling-stations-by-region-2021

14 J. M. Bermudez, S. Evangelopoulou, F. Pavan. “Hydrogen Supply.” IEA, September 2022. https://www.iea.org/reports/hydrogen-supply (accessed 13 March 2023).

15 *NFPA Hydrogen Technologies Code,* National Fire Protection Association, 2023. [Online] Available: https://www.nfpa.org/codes-and-standards/all-codes-and-standards/list-of-codes-and-standards/detail?code=2 (accessed 13 March 2023).

Wear Mechanisms of High-Pressure Hydrogen Sealing Materials

by:

Michael Schöbel
Leobersdorfer Maschinenfabrik GmbH
Südbahnstraße 28, 2544 Leobersdorf, Austria

Marc Langela
STASSKOL GmbH
Maybachstraße 2, 39418 Stassfurt, Germany

13th EFRC CONFERENCE
September 19th – 21st 2023, Zagreb

Abstract:
Hydrogen compression is one of the critical technologies for the value chain from electrolyzers to fuel cell membranes, needed to achieve the transition from fossil energy sources to renewable energy concepts. The reliability of the hydrogen compression by reciprocating piston compressors relies on the wear resistance of the compressor spare parts. These are predominately piston and rider rings and internal parts of pressure packings out of PTFE-based materials. The downside of PTFE are the poor mechanical properties and the high cold flow; both disqualifying PTFE for high pressure applications within the hydrogen value chain. Thus, the work within this paper concentrates on new material solutions where most of the sealing material is based on a thermoplastic polymer with a higher pressure resistance than PTFE-based solutions. Pressure resistance is only one key aspect – the more important is the wear resistance and the combination of both – wear resistance and superior mechanical properties into one recipe. Therefore, the paper investigates the wear behaviour of polyimide-based material recipes and their mechanical properties in dependence on the ingredients to identify the critical aspects that enable PI-based formulations to work as high-performance sealing materials in demanding hydrogen compressor applications.

by: Michael Schöbel – LEOBERSDORFER MASCHINENFABRIK; Marc Langela – STASSKOL

1 Introduction

The energy sector is responsible for a significant amount of CO2 emissions worldwide. For emission reduction, one promising alternative is to use alternative energy sources (wind power, solar power, and others) and store the energy by using hydrogen [1]. With the 'power-to-gas'-concept, electric energy is converted to hydrogen gas which can be produced by water electrolysis, stored over long periods, and converted back to electricity on demand using fuel cells. To achieve a useful energy density, the volume needs to be decreased significantly, either via low-temperature liquid storage (LH2) or high-pressure gaseous storage (GH2) [2]. High-pressure storage up to 350 bar is state-of-the-art and utilized in many applications, as there are no boil-off losses, and the readily available infrastructure can mostly be used for this purpose. For many applications reciprocating compressors are responsible for elevating the gas pressures for storage as they can realize high discharge pressures and high flow rates. The operating principle bases on a linearly oscillating piston introducing work into a compression chamber, reducing the volume of the gas [3]. The sealing components of such a system are under high thermo-mechanical loads due to the sudden rise of temperature and pressure in the compression chamber. The optimal design of the piston and packing rings prevents unwanted losses – also called 'blow-by' – reducing the efficiency of the compression process significantly [4].

The high shear forces and the need for a minimal gap size demand material pairing with high wear resistance and excellent sliding properties [5, 6]. Additionally, the system needs to run free of oil-based, dry lubricants to guarantee high-quality hydrogen suitable for use in polymer electrolyte membrane (PEM) fuel cells [7]. Recent development aims to reach gas pressures of 500 bar at flow rates over 30 kg/h. The combination of these requirements makes the tribosystem highly challenging for the material pairing in terms of thermo-mechanic, sliding and wear properties. Conventional dry-running piston machines use PTFE (Polytetra-fluorethylene) piston rings, benefitting from their self-lubricating properties when sliding against metallic – usually mild steel or cast iron - surfaces [8]. However, as pressure differentials of over 100 bar will be necessary for use in hydrogen technology, materials with much higher strength are required. PI (polyimide) and PPS (polyphenylene sulphide) composite materials strengthened with CF (carbon fibre) have yield strength above 50 MPa and are promising candidates for piston compressors above 500 bar discharge pressure [9,10,11].

The increased hardness and abrasion resistance of the piston rings needs improved cylinder materials. Therefore, high-strength or hardened steels and surface coatings [12] are developed for the optimal combination of low friction with high wear resistance at this highly stressed tribo-contact. The main goal of this study was to improve the understanding about the life cycle limiting wear mechanism present in the piston compressor to develop advanced concepts for piston rings and cylinder tribo-contacts.

Within the scope of this paper, different material mixtures based on polyimide are characterized and mechanically and tribologically analysed. Furthermore, the microstructures of the different material compositions were analysed by microscopy.

2 Experimental setup

2.1 Materials

The PI matrix composites test specimens are obtained from cylindrical rods with a diameter of 50 mm. The polyimide test materials are made by dry powder blending. Particle sizes of the powder are 20 to 40 microns, except carbon fibres, which had an average diameter of 8 microns. A small lab mixer from Reimelt-Henschel (FML10) is used as a mixing device with special geometry and high rotational speeds for maximum homogenization of the powder ingredients. The powder mixtures were hot compression moulded at high pressure (≈ 350 bar) and high temperature (≈ 360 °C) simultaneously to enable an optimized sintering procedure. The composition (fractions are in weight-%) of the PI test polymers is listed below:

Sample A: PI + PTFE (10%) + Carbon Fibre (10%)

Sample B: PI + PPS (10%) + Carbon Fibre (10 %)

Sample C: PI + Carbon Fibre (20 %)

2.2 Mechanical analysis

The characterization of the mechanical properties is done by standard tensile testing using a Zwick Z005 testing machine. A sample is vertically installed between 2 manual clamps, and the sample is pulled by a linear electric motor at a speed of 1 mm/min for measuring the elastic modulus (between 0.05 % to 0.25 % deformation) and 50 mm/min for the rest of the stress/strain-curve. Contact-type extensometers are used for a high resolution of the strain measurement.

The standard sample geometry is the SPI test bar FD-105 with a thickness of 1.5 mm (see Figure 1).

by: Michael Schöbel – LEOBERSDORFER MASCHINENFABRIK; Marc Langela – STASSKOL

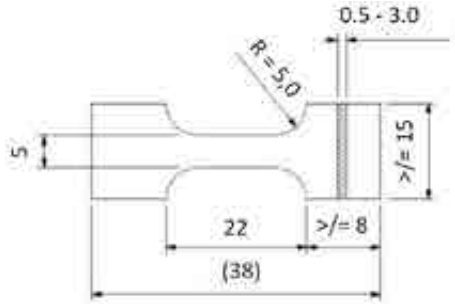

Figure 1: SPI test bar FD-105 (dimensions in mm)

2.3 Tribological analysis

For test conditions close to the application, a special test rig was developed, which allows tribological measurements under the conditions prevailing in the reciprocating compressor (see Figure 2). A reciprocating rod (like a piston rod in a compressor) was equipped with a specimen holder, and the moving specimens are surrounded by a mating surface. While the specimens perform their oscillating motion, the mating surfaces are pressed against the specimens with contact pressure. The average speed of the specimen movement is adjustable, as is the contact pressure and the tempering of the mating surfaces to the test temperature. Sensors continuously measure the distance between the specimen grip and the mating surface to determine the wear rate by the decrease in the distance over time. Furthermore, the temperatures of the mating surfaces and the frictional forces generated by the specimen are recorded. The coefficients of friction of the corresponding material pairings are obtained from the quotient of the frictional forces and the contact forces.

The tribometer has a hood which can be pressurized with a wide variety of test gases such as air, nitrogen, hydrogen, methane, and other bottled gases. In addition, the dew point of the gas can be adjusted by selective humidification or drying. Thus, the surrounding medium can realistically match the process gas in the reciprocating compressor.



Figure 2: Reciprocating tribometer; p ≤ 10 MPa; v ≤ 6 m/s; s = 130 mm

3 Results

3.1 Microstructures

The composite structure is shown in the LOM (light optical microscope) images in Figure 3 in comparison. (a) PI/CF/20f composite shows a heterogeneous distribution of bright C-fibres in a dark grey polymer matrix. Small cavities, as well as graphite flakes, are visible in between the fibres. (b) PI+PTFE/CF/10f shows a lower content of bright fibres. Dark PTFE is homogeneously distributed but seem to prefer to accumulate at the fibre matrix interface. (c) PI+PPS/CF/10f shows dark spherical PPS inclusions, which do not concentrate at the fibre-matrix interfaces but are more homogeneously distributed in the polymer.

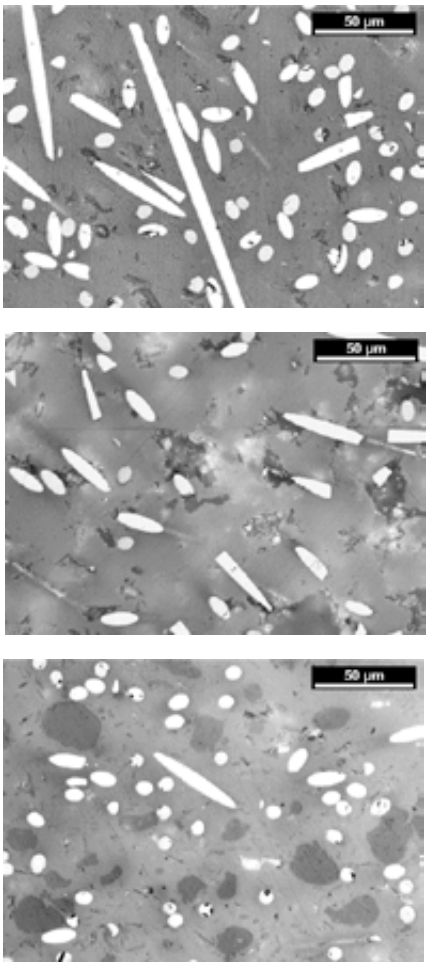

Figure 3: Microscopy of the microstructures of (a) PI/CF/20f, (b) PI+PTFE/CF/10f and (c) PI+PPS/CF/10f

3.2 Mechanical properties

Mechanical properties influenced by the addition of PPS and PTFE are characterized by tensile testing, as shown in Figure 4. PI/CF/20f, without additional lubricants and 20 wt.% CF shows the steepest stress-strain curve, with ultimate strength up to 85 MPa.

by: Michael Schöbel – LEOBERSDORFER MASCHINENFABRIK; Marc Langela – STASSKOL

PI+PTFE/CF/10f with 10 wt.% PTFE and 10 wt.% CF has the flattest stress strain curve and a lower ultimate strength up to 70 MPa. PI+PPS/CF/10f with 10 wt.% PPS and 10 wt.% CF shows a median stress strain curve, but an exceptional low ultimate strength, up to 55 MPa.

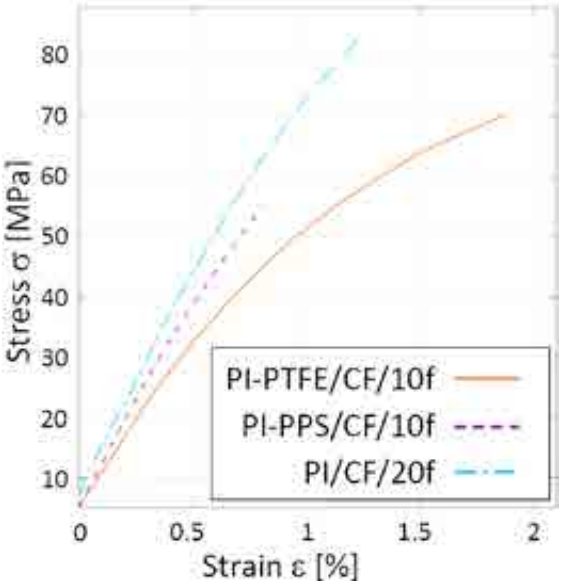

Figure 4: Tensile test at room temperature (mean curves of 5 specimens

3.2 Tribological investigation

For the use within reciprocating compressors, it is valuable to assess the tribological properties of the PI composites characterized in this study. Therefore, the samples were measured at the reciprocating tribometer against tungsten carbide coating (86WC 10Co 4Cr) using the following parameters:

- Average velocity: 2.7 m/sec (Stroke 130 mm)
- Temperature at contact zone: 120 °C
- Pressure load: 20 bar(g)
- Surrounding medium: Pure hydrogen (1.25 bar) from gas bottles (purity 5.0)
- Dew point of the gas: ~ - 76 °C

The in-situ measured wear in micrometre against the test duration shows Figure 5. Every curve is the mean curve of 2 measurements. After a short run-in period of 100 min (beginning of the graph), the PI+PTFE/CF/10f and the PI+PPS/CF/10f samples are developing a linear wear behaviour. The wear of the sample with the PTFE filler shows a lower wear ratio, which means that the wear resistance is superior to the other two material compositions. Significantly, the wear of PI/CF/20f dramatically increases after approx. 500 minutes test duration resulting in a high slope of linear wear behaviour. The test was aborted after 1200 minutes because PI/CF/20f did reach the maximum wear limit of ~ 1000 microns. The trigger for changing from moderate wear after run-in to high wear after 500 minutes could not yet been investigated.

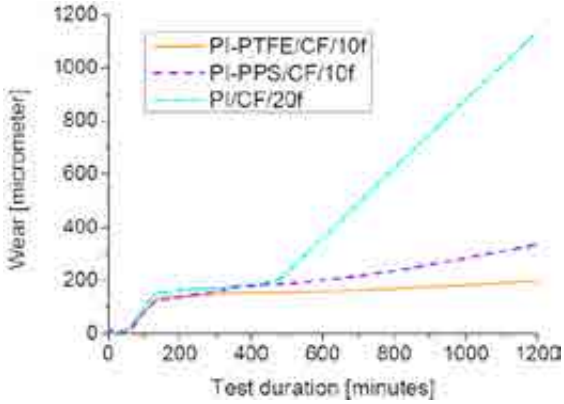

Figure 5: Wear behaviour of the polyimide samples at the reciprocating tribometer.

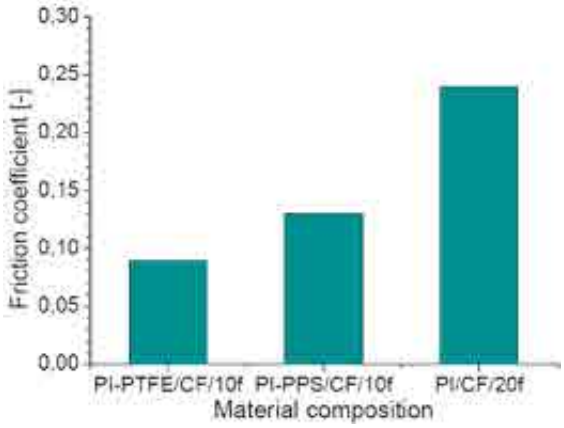

Figure 6: Coefficient of friction (CoF) of the three polyimide samples



Figure 7: Tribofilm (illustrated by the red lines) of PI-PTFE/CF/10f on tungsten carbide coating

Figure 6 shows the coefficient of friction (CoF) as the ratio between sliding force and contacting force (within the regime of linear wear behaviour) of the PI samples against the tungsten carbide-coated countersurface. The high coefficient of friction of the PI/CF/20f is in-line with its high linear wear. The smallest friction coefficient was identified at the PI-PTFE/CF/10f. It shows the importance of the presence of PTFE for high wear resistance, as the PTFE is responsible for a tribo-film generation (Figure 7), which minimizes both, the coefficient of linear wear and the friction coefficient. This is also a valid argument for the need of PTFE for reciprocating compressor sealing elements at the actual discussion about a possible PFAS ban [13].

by: Michael Schöbel – LEOBERSDORFER MASCHINENFABRIK; Marc Langela – STASSKOL

4 Conclusion and Outlook

CF-reinforced PI matrix polymers are promising materials for compressor piston rings and packings, having good thermo-mechanical properties at elevated temperatures up to 200 °C by their thermoplastic nature. The current study investigates mechanical properties related to the microstructure of CF-reinforced PI composites with PTFE and PPS additives. All specimens produced by hot compression moulding show homogeneous phase distribution resulting in quasi-isotropic material properties. Here, the fibres are oriented isotropic within the plane perpendicular to the axial compression stroke. It proves that the production processes in place yields consistent material properties and predictable part performance.

PPS addition to the matrix does not improve mechanical properties, attributed to low PPS stability embedded in PI. PPS addition contributes to a reduction of wear and lower CoF. Both polymers without PTFE show excellent fibre-matrix bonding quality, proven by tensile testing.

Tribological properties can be significantly improved by the addition of PTFE, reducing CoF by deposition of a self-lubricating protective tribo-film at the counterpart surfaces. Nevertheless, decreased mechanical strength of the fibre-reinforced polymers could be observed with PTFE, which conglomerates at the interfaces of the fibre reinforcements, weakening the fibre-matrix interface strength.

In CF-reinforced PI polymer composites, matrix-reinforcing additives like PPS in PI not only contribute their individual properties according to the rule of mixture but are also influenced by production and processing. PPS addition in the thermally more stable PI suffers a decay of its advanced mechanical properties compared to its pristine condition.

The addition of PTFE improves friction and wear behaviour significantly but also degrades mechanical properties by fibre-matrix interface weakening.

Literature

[1] G. Kakoulaki, I. Kougias, N. Taylor, F. Dolci, J. Moya, A. Jäger-Waldau, Green hydrogen in Europe – A regional assessment: Substituting existing production with electrolysis powered by renewables, Energy Conversion and Management, Volume 228, 2021, 113649, ISSN 0196-8904.

[2] J. Zheng, X. Liu, P. Xu, P. Liu, Y. Zhao, J. Yang (2012). Development of high pressure gaseous hydrogen storage technologies, *International Journal of Hydrogen Energy,* Volume 37, Issue 1, 1048-1057.

[3] M.I. Frenkel, Piston Compressors, VEB Verlag Technik, Berlin (1969).

[4] N. Feistel, Influence of piston ring design on the capacity of a dry-running hydrogen compressor; *Burckhardt Compression*, 12 pages (2013)

[5] P.S. Maer, P.J. Mitchell, B.R. Atkins (1973). Multi-phase filled-plastics piston rings for non-lubricated compressors: A comparison of the performance of filled ptfe and epoxy-bonded materials in dry gases, *Tribology*, Volume 6, Issue 41973, Pages 129-134, ISSN 0041-2678

[6] Madhan, K., Padmanaban, R., Venkatesh, G. (2023). Formulation and Numerical Investigation of PTFE-Based Composites for Piston Rings of Oil Free Air Compressors. In: Rajkumar, K., Jayamani, E., Ramkumar, P. (eds) *Recent Advances in Materials Technologies.* Lecture Notes in Mechanical Engineering. Springer, Singapore

[7] Cheng, X., Cheng, X., Shi, Z., Glass, N., Zhang, L., Zhang, J., Song, D., Liu, Z., Wang, H., & Shen, J. (2007). A review of PEM hydrogen fuel cell contamination: Impacts, mechanisms, and mitigation. *Journal of Power Sources*, 165, 739-756

[8] Y. Wang, F. Yan (2006) Tribological properties of transfer films of PTFE-based composites, *Wear*, Volume 261, 1359-1366

[9] Qi, H., Zhang, G., Zheng, Z. et al. Tribological properties of polyimide composites reinforced with fibers rubbing against Al2O3. Friction 9, 301–314 (2021)

[10] U.S. Tewari, J. Bijwe (1991). Comparative studies on sliding wear of polyimide composites, Composites, Volume 22, Issue 3, 204-210, ISSN 0010-4361

[11] V. Saikko, Wear and friction properties of prosthetic joint materials evaluated on a reciprocating pin-on-flat apparatus, Wear, Volume 166, Issue 2, 1993, 169-178, ISSN 0043-1648

[12] V. Totolin, M.R. Ripoll, M. Jech, B. Podgornik (2016) Enhanced tribological performance of tungsten carbide functionalized surfaces via in-situ formation of low-friction tribofilms, *Tribology International*, Volume 94, 269-278

[13] https://echa.europa.eu/de/-/echa-publishes-pfas-restriction-proposal



YOUR PARTNER
FOR THE HYDROGEN TRANSITION

For over 100 years, Cook Compression has partnered with OEMs and end users to design innovative solutions for the gas compression industry. This includes a long history of engineered products with proven success in refining, petrochemical, and industrial hydrogen applications.

Today, we're leveraging this experience and investing in the research and testing capabilities needed to develop the next generation of products for renewable hydrogen applications.

See how we can help you with the coming hydrogen transition at www.cookcompression.com/hydrogen.

COOK COMPRESSION

North America +1 877 266 5226
Europe +44 151 355 5937
China +86 21 24112600

cookcompression.com

Cook Compression is a proud part of Dover Precision Components

DOVER PRECISION COMPONENTS

Experimental and numerical investigation on the sealing capability of a high pressure, dry running, hydrogen reciprocating compressor

by:

Taurian Giorgio
Siad Macchine Impianti
Bergamo, Italy
giorgio_taurian@siad.eu

Modern Paul
Cook compression
UK
pmodern@doverprecision.com

Barigozzi Giovanna, Franchina Nicoletta, Ghirardi Elisa, Kouaissah Otman
University of Bergamo
Bergamo, Italy
nicoletta.franchina@unibg.it

13th EFRC CONFERENCE
September 19th – 21st 2023, Zagreb

Abstract:
Green energy transition and decarbonization commitment require to design innovative machines, to successfully handle multiple fuels and accommodate an ever increasing quota of renewables. In the mid-long term, the hydrogen is expected to play a key role both as a fuel in the long range mobility context, as well as an energy vector within an innovative industry panorama, traditionally hard-toabate. Several technical applications require a high degree of gas purity, thus the development of dryrunning compressors, at high pressure levels, becomes a challenging objective that requires proper investigation and design tools. During compression and expansion strokes, large non-uniformity of the pressure distribution in the sealing system may lead to premature excessive wearing of the piston rings within the reciprocating compressors. Accurate experimental campaign and numerical computations are needed to obtain a reliable digital twin of the capacity of a newly designed high pressure, dry running, hydrogen compressor, during its lifetime. In this work, the sealing effectiveness of specialized piston rings, ad-hoc developed for a newly designed high pressure hydrogen compressor to avoid severe leakage and excessive wearing, is discussed by a proper test model, taking into account numerical predictions and experimental results. The proposed combined theoretical, experimental and CFD approach allowed to deepen the behavior of newly designed rings, showing their superior performance for high pressure, light gases applications, when compared with more conventional designs.

by: Giorgio Taurian – SIAD; Paul Modern – COOK COMPRESSION; Giovanna Barigozzi, Nicoletta Franchina, Elisa Ghirardi, Otman Kouaissah – UNI BERGAMO

1 Introduction

The challenging climate-neutral targets set by the EU for 2050 demand for active and innovative pathways to be explored and this entails that all parts of society and economic sectors must play a role. Ever increasing quota of energy from renewables, reduced pollutants, usage of "green" fuels are a bunch of opportunities that need to be pursued to carry on a global climate action. In this perspective, clean hydrogen shows a great potential in reducing direct emissions of pollutants avoiding greenhouse effect. Hydrogen[1] is expected as breakthrough in achieving a clean, secure and affordable energy future, mainly in strategic sectors such as transport and power generation[2].

Hydrogen is mainly required to be delivered with the highest degree of purity, and clearly handled and stored at very high-pressure levels. Oil-free compressors are needed in several processes when ensuring high-performance operation and high-quality products becomes essential. In this operating framework, dry-running compressors have to cope with very severe operating conditions and need to be suitably devised to ensure safety and reliability. Sealing capability of the piston rings pack becomes cornerstone along with the prediction of its expected lifespan which clearly is a relevant issue to deal with.

In this work a combined numerical modeling and experimental investigation approach is presented to evaluate the sealing capability of specialized piston rings (coded 262 NN) designed to minimize the flow leakages in piston ring packs of reciprocating compressors to be installed in a new HP H_2 compressor. The 1D numerical approach is first described and validated with an ad-hoc experimental campaign led at the Energy Systems and Turbomachinery laboratory of the University of Bergamo (UniBg Est Lab). Further study on the fluid dynamic phenomena occurring in the 262 NN rings is also presented by means of high-resolution CFD computations. The 1D H_2 dry code implemented has been developed to predict the compressor performance in terms of mass leakage, inter-ring pressure, wear quantification during operations. It has been realized as a complementing tool for compressor companies to promote the development of a reliable digital twin of a newly designed compressor, able to predict the sealing capability of the machine operating with hydrogen at high pressure loads. Description of a novel H_2 compressor design is also provided. Few concluding remarks are finally reported.

2 Dry running hydrogen reciprocating compressor: test bench

Reciprocating compressors in their multi-stage configuration can achieve high level of performance in terms of discharge pressure and offer also high degree of flexibility in terms of size and capacity. However, the recent requirement of high-pressurized hydrogen has pushed forth a number of technical challenges, *i.e.*, i) high pressure loads with, ii) H_2 embrittlement material selection robustness, iii) light weight gases, using iv) self-lubricated systems, that must be properly faced in order to ensure good operating conditions. Complex unsteady flow phenomena, relevant mass leakages, increased thermal heat transfer, occurring when the machine is self-lubricated, are expected to play a key role in the definition of the overall performance. Hydrogen compressors manufacturers have to extend their design experience through innovation and research. In the activity's framework required by the development of high-performance hydrogen compressors, a roadmap to define an innovative, digital-oriented, design of the machine has been drawn. In this perspective, the sealing topic is cornerstone and entails to select a high-level partner, developer of specialized solutions in sealing systems for high performance compressors.

Early machine design relying upon the well-established know-how of an experienced compressor company is performed employing ad-hoc devices and materials selected for their enhanced capabilities and properties when applied to hydrogen compression. Figure 1 shows the new compressor, also developed taking advantage from the results of this research. It is four stages, single effect V-type compressor. First and second stages are crank-end (CE) effect while third and fourth stages are head-end (HE) effect. Maximum discharge pressure is about 450 barG. Compressor valves and sealings (piston/packing) are dedicated design. At present, the compressor is successfully running under performance condition at a company workshop. In the upcoming months it will be placed on duty at a hydrogen production plant.

As already indicated, a deeper investigation is necessary to carry on the compressor design and testing phases when self-lubricated systems are considered. Proper tools and procedures must be defined and, owing to the challenging task, a multi-disciplinary approach is envisaged, and herein pursued by a combined experimental and numerical approach as described in the following sections.

by: Giorgio Taurian – SIAD; Paul Modern – COOK COMPRESSION; Giovanna Barigozzi, Nicoletta Franchina, Elisa Ghirardi, Otman Kouaissah – UNI BERGAMO





Figure1:H_2 HP reciprocating compressor.

3 Sealing performance 1D modeling

Any modeling approach adopted to predict the performance of a compressor requires to reliably define the mass leakage amount and the acting pressure on the sealing system.

The description of the fluid dynamic behavior within a sealing pack system requires to define hypothesis both from the geometric and physical point of view. First, we identify possible leakage passages within the cylinder-piston-rings pack, in particular, the gas may flow within gaps located between: i) rings and internal surface of the cylinder; ii) rings and lateral face of the piston ring groove; through iii) cuts of the rings.

From the point of view of physical modeling, several reduced-order discretization approaches have been presented in the open literature which can be roughly divided into two groups: a) labyrinth-like structure with fluid modeled as an isentropic flow through convergent nozzle, see *e.g.* the work by Furuhama and Tada[5] and b) labyrinth passages like orifice for end-gap regions and laminar compressible flow within ring-side clearance. Most of the models are related to internal combustion engine applications and therefore they are typically applied to lubricated sealing systems. The choice between a) and b) is a function of the flow regime assumptions and overall operating conditions. A mixed viscous and inviscid modeling is proposed by Flade[4] where a calculation of sealing performance is also presented to investigate the unsteady flow in reciprocating compressors. It is however suggested that the laminar viscous assumption in small gaps can be applied only when the ring is sitting at either the top or bottom surface of the groove[6]. Yu et.al.[8] presented a method to simulate the unsteady flow behavior within end-gap piston rings in a high-pressure non-lube hydrogen compressor, by means of 1D compressible isentropic flow modeling, considering only gas passing in the end-gap region. Braga et. al.[3] proposed a numerical analysis on the effect of the clearance geometry and piston velocity on leakages of an oil-free reciprocating compressor efficiency. The discretization is based on a simplified form of the Reynolds equation to approximate the pressure field and the mass flow rate is computed as a Couette-Poiseuille flow. More complex modeling approaches have also been presented in the open literature, by combination of the inviscid flow assumption in the end-gap region with a laminar viscous approximation in the ring-side clearance, see, *e.g.*, Kuo et.al. [7]

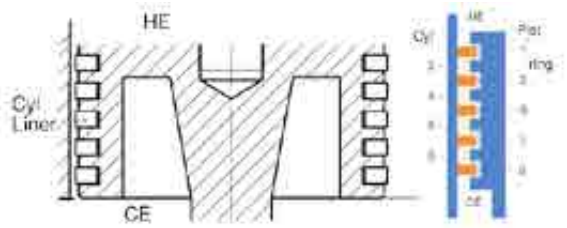

Figure 2: Conceptualization of the sealing system adopted in the 1D mode.

In the 1D sealing modeling code, herein presented, the discretization relies upon inviscid flow assumption through labyrinth-like structure. The flow field is discretized as 1D along the stroke direction and it is subject to the following assumptions: the fluid is in a single gaseous phase, the ideal gas equation of state is applied, the flow is considered as iso-thermal and the temperature of the gas assumed equal to the piston temperature; finally, the flow behaves as an isentropic flux through an orifice. Figure 2 displays the conceptualization of the sealing system through chambers and orifices from head-end (HE) to crank-end (CE).

The governing equation for each chamber reads

$$\frac{dP_i}{d\varphi} = \frac{R_g T_i}{\omega V_i}\left(\dot{m}_{i-1} - \dot{m}_i\right), \qquad (1)$$

where omega defines the speed of rotation, V the volume, P and T the pressure and the temperature values at chamber i.

The governing system describes the unsteady pressure evolution within the operating cycle. At each angular position φ, an implicit system arises, since the mass flow rate is a function itself of the

by: Giorgio Taurian – SIAD; Paul Modern – COOK COMPRESSION; Giovanna Barigozzi, Nicoletta Franchina, Elisa Ghirardi, Otman Kouaissah – UNI BERGAMO

overall pressure distribution $\dot{m}_i = f(P_i)$. Therefore, a proper linearization procedure must be performed before computing the pressure values. Mass flow is computed as a function of the regime: at total fixed upstream condition (pressure and temperature), when the critical (sonic) condition is achieved,

$$\beta > \left(\frac{2}{\gamma+1}\right)^{\gamma/(\gamma-1)} = \beta_{cr}, \quad (2)$$

the flow is choked and the mass flow is constant and computed as

$$\dot{m}_i = K_C A_i \left[\frac{2\gamma}{R_g(\gamma-1)}\right]^{1/2} \frac{P_i}{T_i^{1/2}} \left(\beta_{cr}\right)^{(1/\gamma)} \left[1\right. \quad (3)$$

Otherwise the mass flow rate is obtained as:

$$\dot{m}_i = K_C A_i \left[\frac{2\gamma}{R_g(\gamma-1)}\right]^{1/2} \frac{P_i}{T_i^{1/2}} \left(\frac{P_{i+1}}{P_i}\right)^{(1/\gamma)} \left[\right. \quad (4)$$

A key issue in the mass leakages computation is the discrepancy between the maximum mass flow rate (Eqs. (3) and (4)) and the actual one, which is also influenced by viscous phenomena. In order to account for this effect, the discharge coefficient K_C is typically employed. In the simplest definition it can be assumed equal to a constant value as for example shown by Furuhama and Tada[5] which indicates that K_C can be safely fixed in the range 0.8-0.9. Another, widespread K_C approximation is provided by a quadratic function of the local pressure ratio acting on a selected chamber $\beta_i = \frac{P_i}{P_{i+1}}$, namely $K_C = 0.85 - 0.25\,\beta_i^2$. This coefficient is an important parameter to characterize the sealing capability of piston-rings, that allows to compare different geometries, flow of different gases operating at different temperatures and pressures. This topic will be addressed in the following sections.

The ring dynamics is modeled by assuming that the ring side and groove are flat and axisymmetric, and therefore only the ring axial movements are considered. By using a balance of acting forces, provided by the simple Newton's law of motion, the ring position is established.

The discretization herein proposed allows to account for unsteady phenomena, such as the time-lag occurring in terms of chamber pressurization. In Figure 3 the 1D model is applied to a three-rings test case with imposed HE and CE pressures. The computed inter-ring pressure distribution in chambers labeled as 2 and 4 is reported as a function of the crank angle. Notice a ring has changed its position within its groove when the pressure distribution highlights a curvature discontinuity. Furthermore, a time-lag establishes since, in each chamber, the maximum P value is reached at different positions.

Figure 4 shows the results obtained for a validation test case selected in Furuhama and Tada[5] investigating the mass leakages in a two rooms system toward the crank case. Under imposed HE pressure load, the inter-ring pressure distribution within rooms herein named 2 and 4 (according to the nomenclature of the present discretization) are computed for a shaft revolution. The results highlight good agreement between the 1D predicted profiles and the reference levels, both in terms of functional distribution and maximum pressure occurring.

Further validation of the model capability against experimental data and high-resolution simulations is presented in the next section.

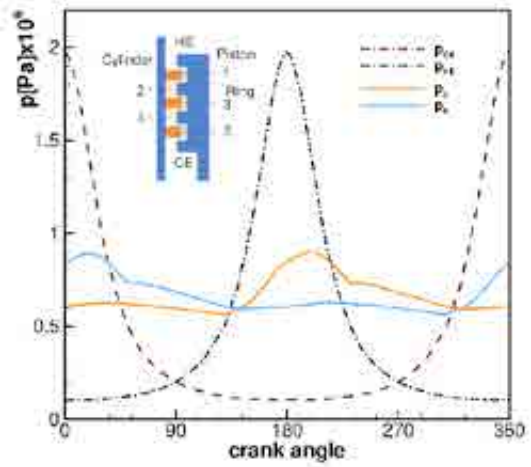

Figure 3: 1D modeling of a three rings system - double effect compression: inter-ring pressure distribution of chamber labelled 2 and 4 (end gap regions) due to imposed HE and CE pressure distributions.

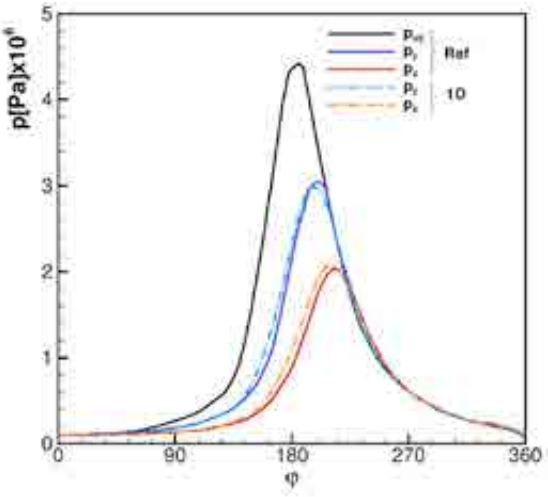

Figure 4: 1D Modeling validation: inter-ring pressure distribution computed in comparison with reference data.

by: Giorgio Taurian – SIAD; Paul Modern – COOK COMPRESSION; Giovanna Barigozzi, Nicoletta Franchina, Elisa Ghirardi, Otman Kouaissah – UNI BERGAMO

4 Modeling validation: test rig measurements over model cylinder and CFD computations

This section is dedicated to the validation and discussion on the 1D code capability in predicting the sealing performance of the selected piston-rings.

4.1 Test rig measurements

A test rig at the UniBG Est Lab consisting of a single piston of characteristic dimension D=125 mm equipped with two rings has been used to characterize the behavior of sealing devices featuring different design, subject to varying operating conditions and different gases. The cylinder test cases were monitored by standard control and measurement devices, two pressure transducers and a mass flow meter as shown in Figure 5(a). The cylinder model may be equipped with up to two 125 mm diameter rings. Detail of the inner core of the model is provided in Figure 5(b).

The mass flow meter can deal with clean gases up to $1000\,Nl/min$ and it is characterized by an accuracy of $\pm 1.5\,\%$ full scale.

a)





b)

Figure 5: Test bench at UniBG EST Lab (a); detail of the sealing apparatus (b).

A thorough measurement campaign has been carried out to evaluate the sealing capability of the piston rings operating at high pressure. The test rig corresponds to a static configuration of the real machine. Tests have been carried out by imposing the total inlet conditions and subsequently modifying the static outlet pressure. Data acquisition has been done for the steady configuration for each pressure ratio considered.

In particular, in this work we considered standard sealing devices, such as the 45deg inclined cut and the step cut, along with the specialized rings specifically developed do deal with HP H_2 compressor, called for the sake of brevity 262 NN, see Figures 6 and 7.



Figure 6: Piston rings tested: 45deg inclined cut, step cut, 262 NN.

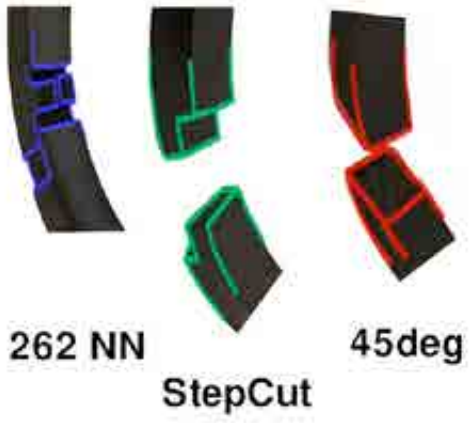

Figure 7: Piston rings tested end gap detail.

The 262 NN ring has been designed to handle light gases compression at very high-pressure levels. They have been conceptualized to enhance the flow blockage within the ring packs by devising complicated flow passages and using high-quality dedicated materials. Effective sealing at low and high pressure loads is ensured by means of a mixed radial and axial design of narrow flow passages using a multi-pieces assembly. The 262 NN piston ring consists of paired two-piece outer rings and a single one-piece inner ring. The two outer rings include an anti-rotation tongue that is milled into the ID of the rings and fits into the clearance gap of the inner ring. This keeps the clearance gaps of the outer rings at opposite orientations to prevent any direct flow path through the assembled piston ring.

This ring was developed for small-bore high pressure applications, where the milled feature provides a more robust anti-rotation method than a dowel pin. Also, the segmented assembly can be installed on a solid piston.

by: Giorgio Taurian – SIAD; Paul Modern – COOK COMPRESSION; Giovanna Barigozzi, Nicoletta Franchina, Elisa Ghirardi, Otman Kouaissah – UNI BERGAMO

The test cases have been performed at fixed inlet total conditions, by varying the static outlet pressure value. At each pressure ratio β, the HE and CE pressure values and the mass flow rate data acquisition has been performed at 1kHz, with measurements run as soon as the steady state condition was achieved in every case. The data have been averaged over one thousand samples and then analyzed to obtain inlet and outlet pressures and corresponding mass flow leakage rates.

Figure 8 displays the non-dimensional mass flow rate for the three different geometries, scaled with respect to the maximum value recorded. Helium was the working gas. Such measurements highlight how the sealing capability scales with varying pressure loads and how it varies with different installed rings. Very good sealing capability is ensured by the 262 NN rings.

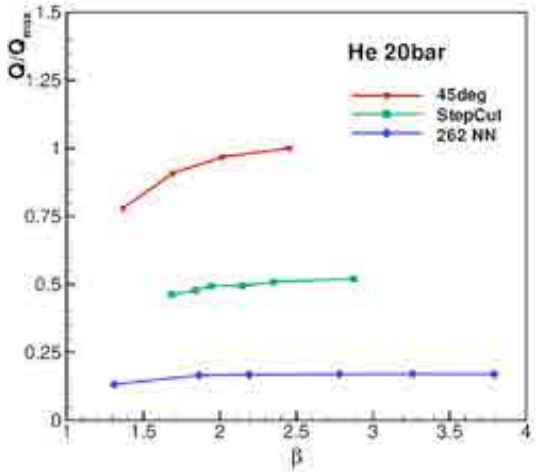

Figure 8: Experiments: non-dimensional mass flow rates measured as a function of the compression ratio, helium at 20 barG inlet total pressure imposed.

The definition of the discharge coefficient is a scaling of the mass flow passing within the rings, a general approach that requires an accurate evaluation of the maximum flow rate admitted by each configuration, *i.e.* accurate definition of the isentropic, adiabatic flow rate as given by Eqs (3) and (4). This target is not straightforward at all, the actual flow is only approximately adiabatic, real fluid effects take place, compressibility also plays a role, furthermore, an accurate measurement of the passage area is also required. This last parameter is not trivial since during operations different flow passages may establish. To draw considerations in terms of a general discharge coefficient we used a "comparative approach" useful both to estimate the passage area A and to validate the 1D prediction against measurements.

The comparison between the 1D mass prediction and experimental data stems into the results highlighted in Figure 9 which displays, as an example, the non-dimensional mass flow rate values obtained for a sealing system equipped with a 262 NN ring operating with helium at 20 barG. The numerical calculations have been performed by prescribing the experimental boundary data, *i.e.*, pressure loads and using as passage area the value derived by targeting the measured choked mass flow. The measured and numerical mass flow rate trends appear in very good agreement with one another.

Using the choke condition as target state, an estimation of the passage area is thus obtained for all tested geometries and then adopted to define the K_c distribution shown in Figure 10. Also, these results indicate the good sealing capability of the 262 NN device.

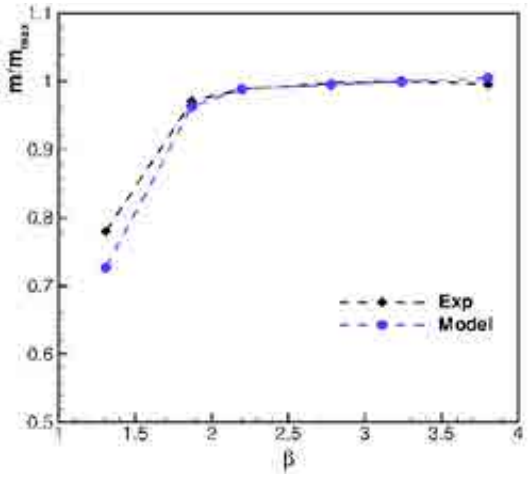

Figure 9: 1D model vs experiments, 262 NN ring operated at 20 barG with helium: non-dimensional mass flow rate as a function of β.

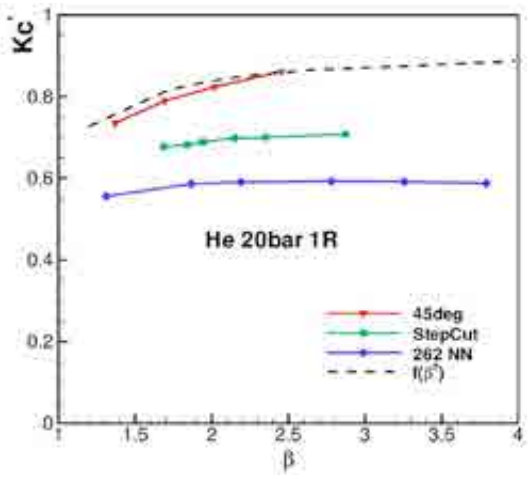

Figure 10: Experiments: K_C values of 45deg, step cut and 262 NN rings operating at high pressure with helium.

Finally, Figure 11 reports the discharge capability of the case with two specialized HP rings in comparison with the most common 45deg rings

by: Giorgio Taurian – SIAD; Paul Modern – COOK COMPRESSION; Giovanna Barigozzi, Nicoletta Franchina, Elisa Ghirardi, Otman Kouaissah – UNI BERGAMO

when operated at HP with such a low molecular weight gas. As it readily appears, better sealing is still highlighted by the 262 NN elements when operated at 20 bar gauge. The measured leakage also suggests that the specialized piston rings can properly cope with increasing pressure loads imposed at head-end. Worth to be noticed, such a peculiar behavior when considering the 262 NN sealing rings, the flow factor in fact decreases whilst the prescribed pressure at HE is increased from 20 to 80 barG. This may even be a matter of the actual passage area, though fair comparison at fixed passage area, suggests the above commented characteristic. Figure 12 displays the sealing behavior measured when using the model cylinder equipped with two 262 NN rings operated at imposed 20 to 80 bar gauge at head-end, using helium or nitrogen. The comparison shows that the predicted K_C value obtained using the helium is equal or higher than using nitrogen. In this case, the lower molecular weight appears to play a major role as the pressure increases.

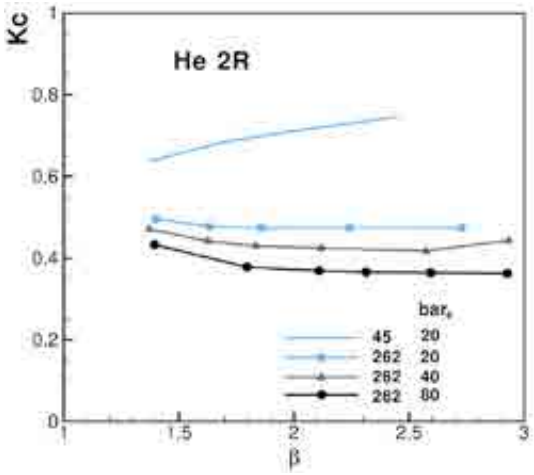

Figure 11: Experiments, 45deg and 262 NN rings operated at 20, 40, 80 bar$_g$ with helium using two rings.

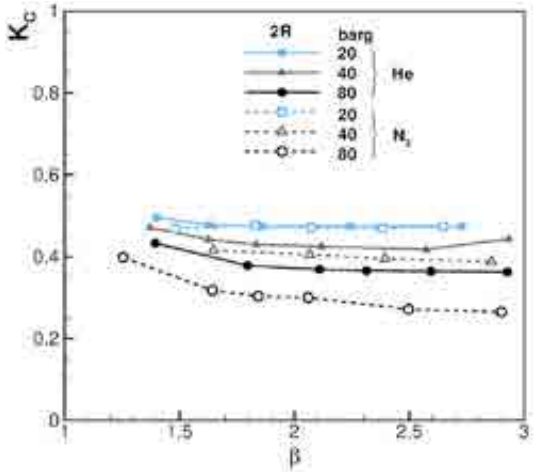

Figure 12: Experiments, 262 NN rings operated at 20, 40, 80 bar$_g$ with helium and nitrogen using two rings.

4.2 3D CFD simulations

Further study on the complex behavior developing within the considered D125 piston equipped by two 262 NN rings is provided by means of high-resolution CFD computations. In particular, 3D steady-state computations, based on a second-order accurate discretization, have been carried out by means of the numerical suite StarCCM+ by Siemens. Proper sensitivity analysis on the mesh coarseness has been performed (not reported here for the sake of brevity) and the final computational grid consists in 21 million polyhedral elements. Convergence of the computations was achieved with scaled residuals lower than 10^{-6}, also evaluated by monitoring the variation of relevant physical values, *e.g.* mass flow rate balance. The computation has been done imposing the inlet total conditions and the static outlet ones according to values prescribed during experiments. Static operational behavior has been investigated by varying the imposed static pressure at the outlet to match the selected pressure ratio.

by: Giorgio Taurian – SIAD; Paul Modern – COOK COMPRESSION; Giovanna Barigozzi, Nicoletta Franchina, Elisa Ghirardi, Otman Kouaissah – UNI BERGAMO

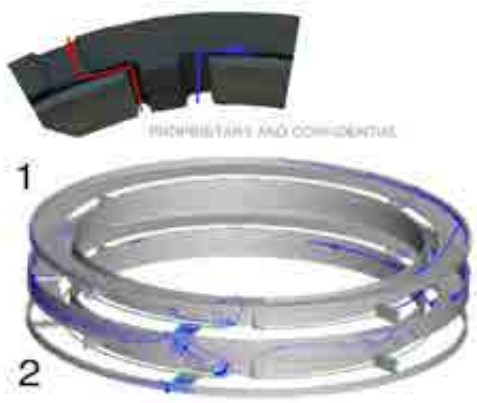

Figure 13: 3D CFD: streamlines path within inter-ring flow passages at $\beta=2.2$.

Figure 13 displays the simulation result at $\beta=2.2$ showing the complex streamlines paths originated at the narrow gaps and chamfers of the ring. The computed non-dimensional inter-ring pressure contours are displayed in Figure 14 showing how the first ring bears most of the pressure load. Notice that these contours may be helpful to evaluate the wear status and to introduce information needed to perform a lifetime prediction of the machine.

4.3 Discussion of results

Finally, comparison in terms of sealing capability is provided by Table 1 reporting the percentage deviation of discharge capability predicted by CFD against measurements assumed as a reference. The passage area adopted in the simulations corresponds to the end gap area (this quantity has been employed to computed the discharge coefficient). As shown, the results highlight a good mutual agreement. Possible reasoning behind small discrepancies may be found in the fact that steady-state simulations only accounting for the CAD "end-gap" region have been led, whilst possible alternative leakages may occur otherwise.

Final remarks are devoted to the comparison of the 1D prediction values against experiments and 3D CFD simulations. The former one (1D vs exp) gives rise to a perfect agreement, with a relative error of order lower than 1%. This is directly related to the ad-hoc tuning procedure used in the code against the available choked reference condition. Instead when comparing 1D vs 3D results, we had a different outcome. We first remind that in this case, the passage area considered is the one adopted in the computational domain, i.e., the CAD area. We observe that larger discrepancies arise, amounting to a relative error on K_C equal to about 10% (see Table 2). This difference is clearly related to the missing viscous contribution underlying to the 1D discretization employed. However, the trend of the discharge coefficient is perfectly captured. Furthermore, good agreement is also obtained in the evaluation of the inter-ring pressure level, for which few points per cent of relative difference have typically been observed (not reported here for the sake of brevity).

β	CFD vs. Exp
1.8	-2.56%
2.0	-2.69%
2.2	-0.61%

Table 1: Two rings 262 NN: Exp and CFD discharge coefficient for different pressure ratios.

β	1D vs. CFD
1.8	+7.26%
2.0	+9.89%
2.2	+8.61%

Table 2: Two rings 262 NN: 1D and CFD discharge coefficient for different pressure ratios.

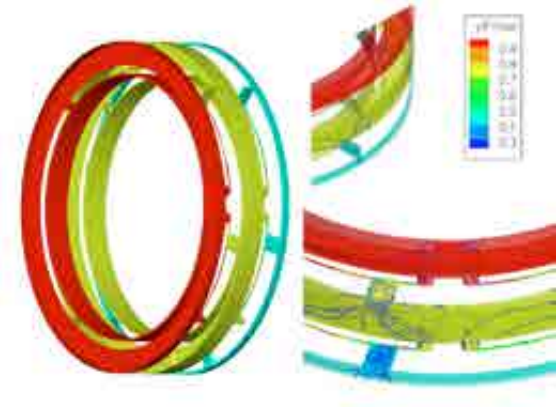

Figure 14: 3D CFD: streamlines path within inter-ring flow passages at $\beta=2.2$.

5 Conclusion

Theoretical, experimental and numerical activities have been adopted in the presented research in a synergistic way to reliably predict gas leakage when operating at very high pressure with light gases. The effect of gas blow-by on the ring's tribological behavior still needs to be investigated, as well as the ring's dynamic motion within its pertaining groove to also predict ring wear. Optimization of geometrical parameters and shapes of labyrinth seals to minimize the leakage is a further research topic for future investigation.

Looking at the H_2 HP dry compressors growing market, sealing rings of enhanced capability, like

by: Giorgio Taurian – SIAD; Paul Modern – COOK COMPRESSION; Giovanna Barigozzi, Nicoletta Franchina, Elisa Ghirardi, Otman Kouaissah – UNI BERGAMO

the 262 NN model, are requested. The efficiency of this kind of rings has been investigated and compared to most common solutions and the results validated by lab experiences and a CFD study.

A 1D numerical model that can perform a sealing capability estimation under imposed pressure load has been developed, herein presented and validated. The 1D model will be useful to predict pressure across each sealing ring, the leakage flow amount and, through data coming from ad-hoc wear tests, the numerical tool is expected to give an estimation of the working lifespan.

Activities are still ongoing to have a better modelling and to fit the model against real cases like the field data coming from the ongoing testing of the new H_2 HP dry compressor delivering hydrogen at 450barG.

References

[1] J. Rissman, C. Bataille, E. Masanet, N. Aden, W. Morrow, N. Zhou, N. Elliott, R. Dell, N. Heeren, B. Huckestein, J. Cresko, S. Miller, Technologies and policies to decarbonize global industry: Review and assessment of mitigation drivers through 2070, Applied Energy (C). doi:10.1016/j.apenergy.2020.1

[2] Energy transitions commission. mission possible: reaching net-zero carbon emissions from harder-to-abate sectors by mid-century, Tech. rep. (2021).

[3] V.M. Braga and C. J. Deschamps. Numerical analysis of gas leakage in the piston-cylinder clearance of reciprocating compressors considering compressibility effects. volume 232, pages 1–9, 2017.

[4] G. Flade. Calculation of transient flow in sealing system. In Proceedings 11th EFRC Conference, pages 24–29, September, 13-14, 2018 - Madrid.

[5] Shoichi Furuhama and Tosio Tada. On the flow of gas through the piston-rings: 1st report, the discharge coefficient and temperature of leakage gas. Jsme International Journal Series B-fluids and Thermal Engineering, 4:684–690, 1961.

[6] Shoichi Furuhama and Tosio Tada. On the flow of gas through the piston-rings: 2nd report, the character of gas leakage. Jsme International Journal Series B-fluids and Thermal Engineering, 4:691–698, 1961.

[7] T.-W. Kuo, M.C. Sellnau, M.A. Theobald, and J.D. Johns. Calculation of flow in the piston-cylinder-ring crevices of a homogeneous-charge engine and comparison with experiment. SAE Transactions, 98:1469–1482, 1989.

[8] W. Yu, X. Dianbo, F. Jianmei, and P. Xueyuan. Research on sealing performance and self-acting valve reliability in high-pressure oil-free hydrogen compressors for hydrogen refueling stations. International Journal of Hydrogen Energy, 35:8063–8070, 2010.

NEUMAN & ESSER

Efficient H_2 compression with Pistons & Diaphragms – Recips as a keystone of the energy transition

by:

Jens Wulff
Managing Director
NEUMAN & ESSER GROUP
Übach-Palenberg, Germany
Jens.wulff@neuman-esser.de

13th EFRC CONFERENCE
September 19th – 21st 2023, Zagreb

Abstract:
The defossilization of our economy to achieve climate neutrality is the biggest challenge mankind is facing today. Hydrogen, especially with a low carbon footprint, will support this transition by serving as an energy vector and an energy storage medium. Furthermore, it can be used as a feedstock or reaction partner for various industrial processes.
All these applications require reliable and well controllable compression technology. Especially due to the low molecular weight positive displacement compressors are best suited. As oil-free compression is often required by e.g., fuel cells, non-lune piston and diaphragm compressors are ideally suited for H_2-compression.

by: Jens Wulff – NEUMAN & ESSER

1 Introduction

Hydrogen is one key components for successfully solving the ongoing climate crisis. To facilitate a globally effective defossilzation process, an integrated approach, taking into account the interdependence of the H_2-value chain components, is necessary. Compressors are a central and essential factor in this process.

The defossilization of our economy to achieve climate neutrality is one of the biggest challenges mankind is facing in the next decades. This goal shall be achieved by transiting to renewable energy generation and by coupling the sectors energy, industry, buildings and mobility mostly via electricity.

Due to the high volatility of renewable energy generation from wind or solar power, reliable and cost-effective storage and transport means for huge energy quantities are a vital prerequisite. Furthermore, the recent events in Eastern Europe have shown that a strategic energy reserve is a cornerstone of geostrategic independence.

Only when they are fulfilled also the goal of carbon neutrality can be achieved. Hydrogen offers exactly these required capabilities and can additionally also be used as an educt or a reaction partner in the process industry.



Figure 1: The H2 Value Chain[1]

Compressors are the linking components in the H_2 value chain (see figure 1), connecting the process steps from H_2 generation to end user. They play a central role for storing and transporting hydrogen.

Even though the gravimetric energy density of H_2 is excellent, its low density, the lowest of all gases, make compression, liquefaction or binding it to other materials or elements necessary for sensible technical usage. For all these processes to increase the volumetric energy density of hydrogen efficient compressors are required.

To achieve a globally optimized solution for each case, a holistic integrated approach of adjusting and selecting the components along the value chain is paramount. To successfully achieve this, it is important to know the possibilities and requirements for the individual process steps in the value chain.

2 Hydrogen Value Chain

2.1 Energy Sources for H_2 Generation and Generation Methods

”Green Hydrogen” can be produced from renewable energy sources like solar, wind, hydro, biomass, geothermal or tidal power plants. When H_2 is produced from nuclear energy it is called “red H_2”. Hydrogen can also be produced from fossil energy carriers like natural gas.

The still most widespread and cost-efficient method for H_2 generation is the steam reforming of methane (SMR) from fossil natural gas to “Gray Hydrogen”. However, per ton of H_2 around 10 tons of CO_2, i.e., 300 g/kWh[2] are produced as well. By separating, storing, or utilizing (CCSU) the generated CO_2 the carbon balance of this process can be significantly improved. H_2 generated from fossil methane by SMR combined with CCSU is called „Blue Hydrogen”.

Pyrolysis is another method for H_2 generation. When fossil methane flows through a molten tin filled bubble column reactor, “Turquoise Hydrogen” and Carbon powder are formed.

“Green hydrogen”, which is the choice for the future, is mostly produced by using renewable electric power for water electrolysis. Currently three methods have achieved market maturity, alkaline electrolysis (AEL), proton exchange membrane electrolysis (PEM), see figure 2, and high temperature electrolysis (HTE) based on solid oxide electrolyzer cells (SOE). A future option on the way to market maturity is the anion exchange membrane (AEM) technology, which basically is a mix of AEL and PEM.

With regards to required compressor technologies, it is worth to mention that none of the stated electrolysis methods comes with an inherent output pressure level. Considerations which compressor technology is the most efficient are depending on the specifics of each use case. An example is given under point 3.3.

On average all the methods require around 50 kWh of electric energy per kilogram of H_2 produced[3]. This underlines the importance of low priced “green electricity” for competitive “green hydrogen”.



Figure 2: 2 MW Class PEM Electrolyzer[4]

by: Jens Wulff – NEUMAN & ESSER

In addition to the (electro-) chemical processes as described above, research is going on in the field of biotechnology for e.g., photolysis or H_2 based on algae.

All these sources have their individual characteristics concerning volatility, investment costs and achievable full load equivalent hours per year. Furthermore, their individual outlet conditions regarding pressure, temperature, humidity and purity have a significant impact to the design of the downstream components in the value chain like compressors, dryers and purifiers.

It must be noted that currently, only 1% of the around 100 million tons of global annual H_2 production are not "Gray Hydrogen". With worldwide annual demand forecasts ranging between 500 and 700 million tons for the year 2050[5] onwards, it is clear that huge investments especially into "Green hydrogen" technology are necessary. Furthermore, a globally accepted certification system setting clear rules and CO_2 footprint thresholds for "Green H_2" must be developed.

2.2 Storage of Hydrogen

Due to its low volumetric energy density, it does not make sense to store H_2 under ambient conditions. In order to achieve an acceptable energy density, the following basic methods can be used:

• Binding to a carrier material like metal hydrid solid storage or organic carrier liquids (LOHC). The latter achieve storage factors of around 50 kg/m^3.[6]

• Liquefaction (LH_2) by cooling below the boiling point (-252°C) with a density of around 70 g/l.

• Pressurized gas storage (GCH). Depending on the pressure level and the required storage mass and load cycles different vessel types from steel vessels up to composite material vessels are used. Also, a combination of cryogenic cooling and compression can be used to achieve higher energy densities that in the liquid state.

• Another alternative to store high energy quantities with high energy densities lies in the production of synthetic fuels by binding hydrogen to other atoms like carbon or nitrogen.

All these methods have their individual characteristics and limits, but they have one thing in common: Hydrogen must be compressed by compressor plants to store it with a sufficient energy density. When it comes to large scale energy storage in the magnitude of several Terrawatt hours only GCH-salt caverns with a pipeline connection and H_2-derivatives like ammonia and methanol offer the necessary capacity.

2.3 Transport and Distribution

To transport the H_2 to the end user or to a storage site several methods can be used. Mobile pressure storage systems like trailers and containers can, depending on the pressure, store several kilograms to around 1.5 tons of H_2. When using a freight train as a „rolling pipeline", around 60 tons of H_2, or speaking in energy terms, 2 GWh can be transported at a time. A truck trailer for LH_2 contains 3-4 tons and a big LH_2 tanker can transport 160.000m^3 of LH_2 which corresponds to 10.000 tons of hydrogen[7].

Pipelines offer the possibility to transfer very high amounts of energy. When compared to natural gas it must be considered that for the same energy content around 3.7 times the volume of H_2 is needed. Due to the 9 times lower molar mass of H_2 vs natural gas it is possible to transport H_2 at much higher speeds than natural gas. Therefore, a 48" pipeline operating at around 80 bar and transporting the hydrogen at a speed of around 35m/s can transfer up to 30 GW of power and additionally also form a significant storage volume, bringing it practically on par with natural gas pipeline systems.



Figure 3: Piston Compressor, 6-Crank[8]

2.4 End Users

The energy stored in Hydrogen can be reconverted for using it in mobility applications, for generating electricity and heat or it can also be used as a reaction partner for industrial processes.

The latter mostly offers the highest CO_2 emission saving potential. Conventional steel carries an "emissions rucksack" of 2 tons of CO_2 per ton of steel[9] caused by the chemical process of splitting off oxygen from the iron ore in the blast furnace. Thus, a ton of "Green Steel" which is produced by electric smelting and employing hydrogen for the direct reduction of the iron allows for an almost 100% elimination of CO_2. Apart from the production of synthetic fuels, hydrogen and carbon dioxide can also be used as feedstocks to produce plastics.

If fuel cells are used for the electrification around 50-60% of the lower heating value of H_2 are converted into electric energy and the remaining energy is emitted as heat. This makes them usable both in mobility and in stationary combined power and heat applications for, e.g. residential quarters. Fuel cells

by: Jens Wulff – NEUMAN & ESSER

require H_2 of highest purities, this requirement can be neglected when using it as a combustible fuel for turbines or engines. The drawback of using it in this form is the lower efficiency of around 30-40%.

3 Choosing the best fitting compression technology

3.1 Compressor Technology Overview

Even this short overview of the components of the H_2 value chain shows that a detailed knowledge of its individual steps is necessary to come to optimized solutions. Additionally, it becomes obvious that compressors are of central importance especially for storing and transporting H_2.

Therefore, choosing the best fitting compression technology for the individual use case which is defined by the components left and right of the compressor in the value chain is paramount.

The low mol-weight of hydrogen makes compressor working by the displacement principle the solution of choice. They achieve isothermal efficiencies of more than 80%. When high purity H_2 without oil contamination is needed, water injected screw compressors and especially non-lube piston or diaphragm compressors are the suitable answer. For these applications, water injected screw compressors can go up to 15 bar, dry running crosshead-type piston compressors achieve more than 300 bar discharge pressure and diaphragm and piston compressors with a hydraulic drive easily surpass 1000 bar. For reasonable flow rates the latter two depend on higher suction pressures. A diaphragm compressor (Figure 4) can compress around 1000 Nm³/h from 30 to 1000 bar in three stages.



Figure 4: 3-stage Diaphragm Compressor for Hydrogen Tube Filling[10]

A high-volume piston compressor on the other hand can compress more than 800,000 Nm³/h from 40 to 80 bar with a drive power of 22 MW[11] while transporting 2.4 GW of power bound in the transported H_2. When purity is not of central importance oil-flooded screw compressors can be used up to 50 bar pressure and piston compressors with cylinder and packing lubrication can be used up to 1000 bar.

3.2 Individual Demands of Use Cases – Case Study

Already the rather simple case of an H_2 trailer filling station shows how many different approaches and solutions exist. The task: In Germany 300 tons of H_2 shall be generated annually from renewable energy to supply a train and bus refueling station. The station is less than 50 km away from the end users. This offers several options.

The production of 300 tons of H_2 via electrolysis requires around 16 GWh of electric energy. With respective annual full load hour equivalents for Germany of 1000 hours for photovoltaics (PV), 2000 hours for wind and around 5000 hours for biomass, this would require either a 16 MW photovoltaic power plant or wind power of around 8 MW from typical onshore wind parks or 3 MW from a biogas fired combined heat and power plant (CHP).

When relying solely on power from photovoltaics, slightly more than 16 MW of electrolyzer capacity are needed. Due to the very volatile production pattern resulting, e.g., from cloud shadowing PEM should be the technology of choice, as it offers the fastest load change capability. Additionally, a battery buffer might be helpful to flatten the load curve and to reduce the needed power. As PV produces electricity with direct current on which the electrolyzers are also running, the rectifier system which is normally needed is not necessarily required.

With the rather constant power supply from a CHP unit around 3 MW of cheaper alkaline electrolysis would be sufficient. The size of the electrolyzer determines the maximum hydrogen flow which in turn determines the peak flow the compressor and the gas treatment unit must be able to handle.

3.3 Different Pressures result in different Systems

Typical trailers used to supply hydrogen refueling stations have maximum filling pressures of around 300 to 500 bar. Depending on the used electrolyzer the suction pressure for the compressors ranges from a few millibar to around 50 bar. In the given case study, a system with atmospheric discharge pressure from the electrolysis shall be compared to a system offering 30 bar on the hydrogen side, for the trailer 500 bar are selected as the filling pressure.

As outlined under point 3.1, choosing the right technology for compression for a well-balanced overall system is depending on the specifics of each application. For the case described above, a diaphragm compressor is the most efficient, as it can handle flow and compress to more than 500 bar in two stages at 30 bar suction pressure.

At atmospheric pressure from the elctrolyzer, the low stroke volume of a diaphragm compressor

by: Jens Wulff – NEUMAN & ESSER

makes precompression a must. A four-stage piston compressor is needed to achieve 30 bar pressure. This precompressor very likely nullifies the investment cost advantage of a cheaper atmospheric electrolysis systems and adds more complexity through four more stages and having to mix two compression methods. The efficiency of the mechanical compression is very much in line with the efficiency of the electrochemical compression in the pressurized electrolyzer.

Furthermore, the choice of the outlet pressure and the method of electrolysis has significant effects on the selection of the gas drying and deoxo units to achieve the necessary purity.

Between the electrolyzer and the compressor a buffer vessel to decouple the systems should be used. This vessel must be bigger for atmospheric systems. This shows the significant impact the choice of power source and the outlet pressure of the electrolyzer have on the selection, design and complexity of the compressor and gas treatment systems.

For the transport of the hydrogen to the refueling stations the type of chosen vessel plays the determining role. Trailers with conventional steel tubes or bottles operating at 300 bar can transport around 500 kg of H_2 and often are limited in the number of full load cycles. A 40-foot gas container (MEGC-type) with 380 bar pressure can transport a useful quantity of around 1000 kg and offers a significantly longer lifetime, but this has to paid with a higher investment price[12]. This little case study emphasizes the importance of knowing the characteristics and the interdependence of the components along the H_2 value chain. Cost advantages which seem to be achievable when using low pressure electrolysis are more than eaten up by the investment and operating costs of a then required much more complex compressor system. Here providers of integrated solutions which also have a good eye on servicing the systems can generate a significantly higher customer benefit and thus achieve a competitive advantage.

4 Summary and Outlook

Compressors are ubiquitous in the current and future hydrogen value chain. While there are still a lot of known and unknown development demands inside this chain, the available reciprocating compressor technology already now offers a high level of maturity and reliability. Whereas e.g., electrolyzers still require industrialization and significant scale-up, the compressors for feeding huge amounts hydrogen into pipelines and salt caverns is already available. The main challenge in these applications lies in the achievement of the required purities depending on the type of end user.

Maintaining the highest purity continuously over the pipeline and cavern transport and storage systems currently seems to be hardly achievable. With the ongoing conversion of mobility especially in the heavy-duty applications like trucks, buses and trains the demand for high purity H_2 will significantly increase. This calls compressor systems for fuel stations and trailer filling being able to compress much higher flows to around 500 bar while maintaining the purity demands of fuel cells. The development push must focus on dry running piston compressors delivering more than 1000 kg/h to this high pressure level.

For providers of integrated solutions, the digital connection of the components for a better communication of the systems with each other and also allowing for condition based predictive maintenance concepts, is another important development area.

The one who masters the compression challenges and understands the process surroundings already early in the design phase can provide significant added value to the clients.

by: Jens Wulff – NEUMAN & ESSER

[1] NEUMAN & ESSER, The H2 Value Chain, own graphic (2021).

[2] Robert Rapier, "Estimating The Carbon Footprint Of Hydrogen Production", forbes.com, (2020).

[3] Chem. Soc. Rev., 2022, 51, 4583, p. 17, p.21

[4] NEUMAN & ESSER, 2 MW Class PEM Electrolyzer, own graphic (2022).

[5] RystadEnergy, "Energy Transition Report – Hydrogen Market Update – The hydrogen economy in 2023", rystadenergy.com, p. 15, (2023).

[6] HYDROGENIOUS LOHC TECHNOLOGIES GmbH, „Stationary LOHC infrastructure", https://hydrogenious.net/what/, (2023).

[7] Kawasaki Heavy Industries, Ltd., "Kawasaki Obtains AIP for Large, 160,000 m³ Liquefied Hydrogen Carrier", https://global.kawasaki.com/en/corp/newsroom/news/detail/?f=20220422_3378, (2022).

[8] NEUMAN & ESSER, Piston Compressor, 6-Crank, own graphic (2021).

[9] Sustainable Ships, "What is the carbon footprint of steel?", https://www.sustainable-ships.org/stories/2022/carbon-footprint-steel, (2022).

[10] NEUMAN & ESSER, 3-stage Diaphragm Compressor for Hydrogen Tube Filling, own graphic (2021).

[11] NEUMAN & ESSER, Own Calculations, NEUMAN & ESSER KO³ Software, (2023).

[12] Vito Milella, Bodo Nachbar et al., "Potenzialbeschreibung Wasserstofftransport über das Schienennetz", LandesEnergieAgentur Hessen GmbH, White Paper, p.15, (2020).

MONITORING & RELIABILITY

Identifying capacity control related problems using condition monitoring
by: Thorsten Bickmann, Fayyaz Qureshi – BENTLY NEVADA *141*

Upgradation of Compressor Lubrication System from Pump-to-Point "to" Divider Block in Worthington and BPCL Compressors of Oil India Limited & benefits obtained
by: Amarish Kamalapuri, Prateek Baruah – OIL INDIA *151*

Impact versus Impact – Comparison of different filter modes for vibration measurement
by: Jan Löken – PROGNOST *165*



PROGNOST
INTELLIGENCE ON DUTY

Part of the Burckhardt Compression Group

Machinery Diagnostics
at your Fingertips

PROGNOST® Cloud Dashboard - Unlimited access to vital **machinery health information**



Read more on prognost.com

Bently Nevada
a Baker Hughes business

Identifying capacity control related problems using condition monitoring

by:

Thorsten Bickmann
Senior Technical Leader for Recips, Germany
thorsten.bickmann@bakerhughes.com

Fayyaz Qureshi
Senior Technical Leader for Recips and Analytics, UAE
fayyaz.qureshi@bakerhughes.com

Bently Nevada, a Baker Hughes business

13th EFRC CONFERENCE
September 19th – 21st 2023, Zagreb

Abstract:
High costs for energy and global focus towards reduction in carbon emissions are demanding to operate reciprocating compressors at their optimum capacity, continuously adjusted to the requirements of the production. Wasting energy by using a recycle valve to expand compressed gases to suction pressure is economically inefficient. Thus, several capacity control devices such as suction valve unloaders, clearance pockets, reverse flow control or variable speed drives for motors are used to operate the reciprocating compressor as per downstream requirement.
Condition Monitoring Systems can support to monitor the health of capacity control systems so that operators can rely on them. Automated rules can be programmed to automatically detect malfunctions of capacity control devices.
This paper will describe the impact of capacity control systems on dynamic pressures, calculated performance and vibration and will show several cases.

by: Thorsten Bickmann, Fayyaz Qureshi – BENTLY NEVADA

1 Introduction

As the cost of electricity and fuel continues to increase, efficient plant operation requires more flexibility in compressor loading and capacity control.

A few of the most commonly used methods of varying compressor load and capacity include the following:

- Unloading of suction valves by suction valve unloaders
- Varying the cylinder end clearance
- Reverse flow control
- By starting and stopping the compressor
- Speed Control
- Recirculation or bypass

Depending on the variations in flow throughput requirements, the correct capacity control techniques are deployed. Some capacity control devices are more expensive than others and hence a trade-off between horsepower losses and cost of relevant capacity control technique is evaluated. Simultaneously the performance of capacity control system is equally critical for optimal production. Advanced online asset health management systems help in performance monitoring of reciprocating compressors and provide insights into the efficacy of capacity control by monitoring their affects on pressure, temperature, and vibration signatures.

2 Methods for controlling the compressor output

2.1 Unloading of suction valves

The suction valve unloaders (shown in Figure 1) can be used to hold suction valves open continuously, or during a selected portion of each compression stroke to control capacity.



Figure 1:: Suction Valve with Gas Actuated Unloading Device

One style of suction valve unloader is the finger unloader, shown in Figure 2. For the cylinder chamber to be in the unloaded condition, the fingers push the plates or concentric rings down against spring force and allow the gas to flow in both directions through the valve.

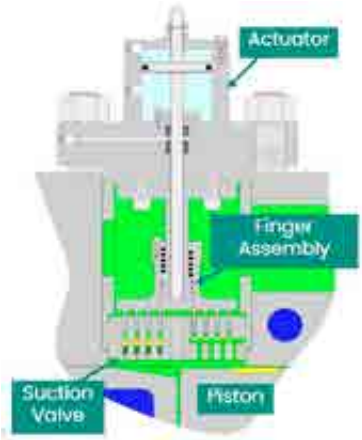

Figure 2: Finger Type Suction Valve Unloader

The dynamic cylinder pressure versus crank angle curves show the effect of the unloader on cylinder operation.

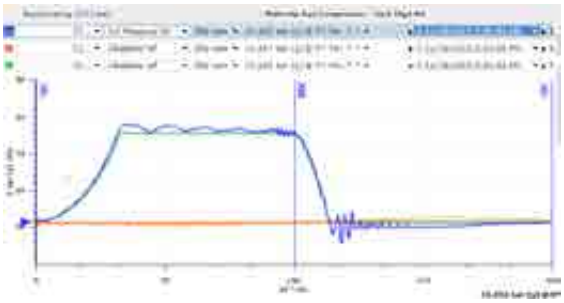

Figure 3: Pressure versus crank angle (CE chamber loaded, HE chamber unloaded), 50% loaded

In the pressure versus crank angle plot in Figure 3, the fingers hold the suction valves of the head end (HE) chamber open during the entire stroke. Since the suction valves never close, there cannot be any compression and the pressure in the chamber is equal to the suction line pressure during the entire stroke.

At the crank end (CE) chamber, the fingers of the unloader do not engage the suction valve components at all to achieve a loaded state. The actuator has moved upwards, allowing the valve plates or rings to operate normally and enables the chamber to compress gas normally.

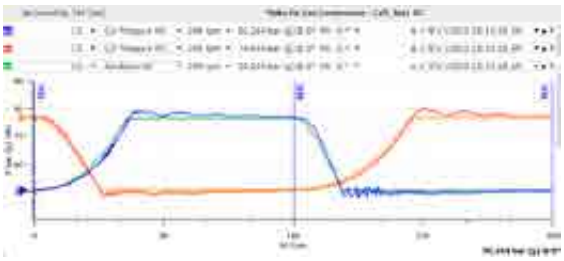

Figure 4: Pressure versus crank angle (100% loaded)

by: Thorsten Bickmann, Fayyaz Qureshi – BENTLY NEVADA

Figure 4 shows both HE and CE chamber in operation. Thus, the capacity of one double acting cylinder can be controlled between 50% and 100% load.

Considering a two-throw single stage reciprocating compressor with four compression chambers and suction valve unloaders, the capacity of the total machine can be controlled to 100%, 75%, 50% and 25%.

When both chambers in a cylinder are unloaded, the gas just shuttles between the chambers. This can lead to an overheating condition. In addition, when the cylinder is unloaded in this fashion, the cylinder lubrication cannot escape through the discharge valves and builds up in the cylinder.

2.2 Clearance Pockets

Clearance pockets allow operators to adjust the capacity by varying the "unswept" volume of the cylinder.

Clearance pockets are commonly used to allow changing the compressor loading during operation. Some clearance pockets can only be valved-in or isolated from the chamber completely. Other clearance pockets can provide a volume that is adjustable based on the position of a moveable plunger.



Figure 5: Clearance Pockets installed on the head end of the cylinders

Figure 5 shows the pneumatic actuators for a set of head-end clearance pockets. The existence of hand wheels at these locations would indicate that the pockets are manually operated.

The design cylinder clearance value for a compressor affects how steep the expansion and compression curves will be on the P-V plot, shown in Figure 6.

Increasing the clearance causes the dynamic cylinder pressure curves to have a shallower slope, which reduces the discharged capacity of the cylinder. Design clearance values are selected based on the anticipated requirements of cylinder loading and the ability to change loading during various phases of compressor operation.

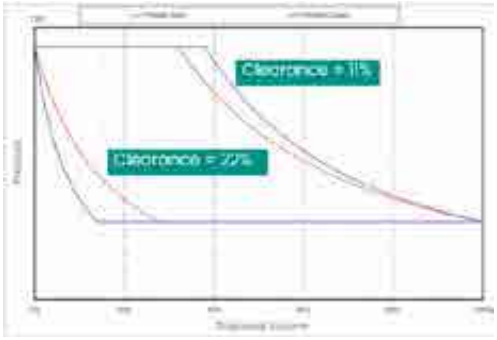

Figure 6: P-V plots with different clearances for the head-enc compression chamber

Combining e.g. suction valve unloaders with clearance pockets allows additional load steps as shown in Figure 7.

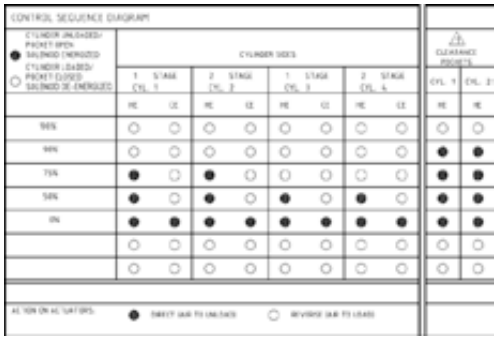

Figure 7: Control sequence diagram with suction valve unloaders and clearance pockets

2.1.2 Fixed-Volume Pocket

Clearance pockets change the discharge capacity of the cylinder by increasing or decreasing the clearance volume inside the cylinder.

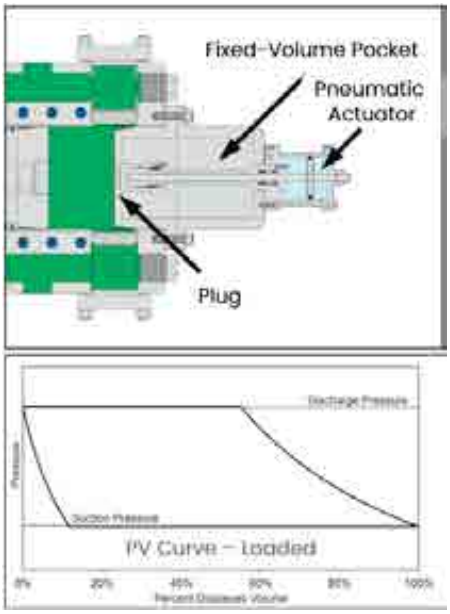

Figure 8: PV curve with HE clearance pocket off

by: Thorsten Bickmann, Fayyaz Qureshi – BENTLY NEVADA

Figure 8 shows a head-end fixed volume clearance pocket, which can be either completely closed or opened.

The cylinder pressure versus volume (P-V) curves show the effect of the clearance pocket unloader on cylinder operation, assuming nothing else in the cylinder changes.

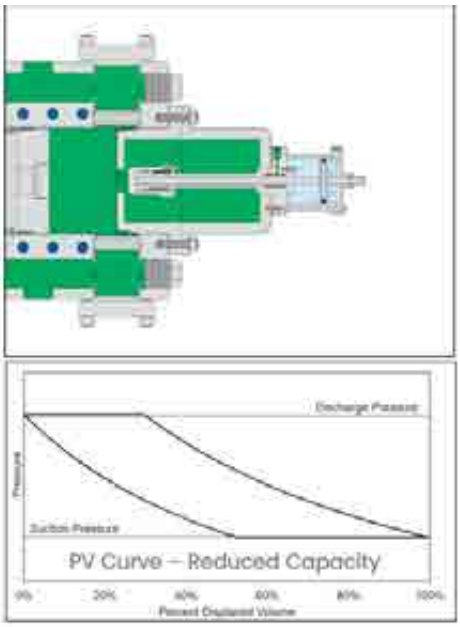

Figure 9: PV curve with HE clearance pocket on

In Figure 8, the actuator closes the plug, which reduces the clearance volume of the chamber. This increases the flow and indicated/consumed horsepower (area inside the P-V curve) for the affected chamber. In Figure 9, the actuator unloads the cylinder by opening the plug increasing the clearance volume in the head-end chamber of the cylinder. In this position, the flow and indicated horsepower (area inside the P-V curve) are lower than when the plug is closed.

2.1.2 Variable-Volume Pocket

Some clearance pockets have a volume that can be adjusted by the position of a piston or plunger that can be moved within the pocket. In older designs, clearance pockets were placed into service and removed by manually operated hand wheels. As shown in Figure 10, hydraulic actuators are now commonly used to provide remote control.

The variable volume unloader influence on the P-V curves is shown in Figure 10. As the control piston moves to the left (inwards), clearance volume decreases and capacity increases. As the control moves to the right (outwards), clearance volume increases and capacity decreases. OEM´s may use HE variable clearance pockets combined with valve unloaders to achieve variable machine loading.

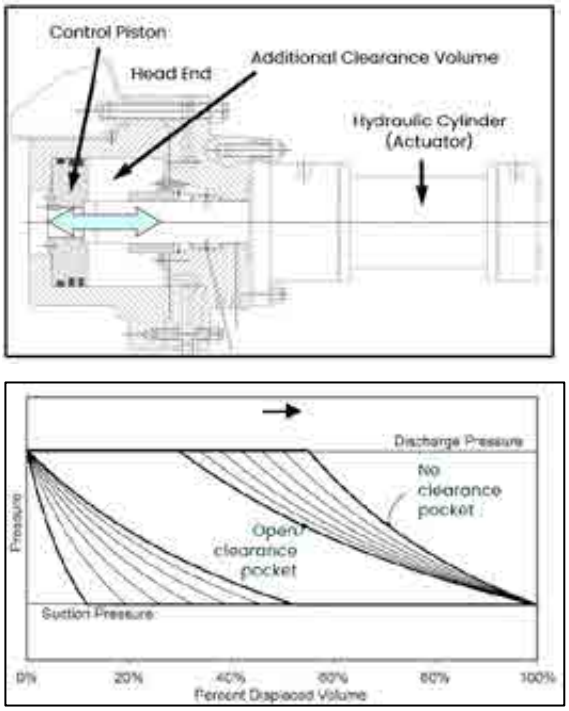

Figure 10: PV curves with variable clearance pocket installed at HE chamber

2.3 Reverse Flow Control

Another type of capacity control is the Reverse Flow Control. Active valve control devices installed on the suction valves can be used to hold suction valves open continuously, or during a selected portion of each compression stroke to control capacity.

The fingers push the plates or concentric rings down against spring force and allow the gas to flow in both directions through the valve. The cylinder pressure versus crank angle curves show the effect of the unloader on cylinder operation in Figure 11. When the suction valve is released, the compression process starts and only the remaining gas in the cylinder is being compressed. The dynamic controller has to operate very fast to ensure desired capacity is being delivered.

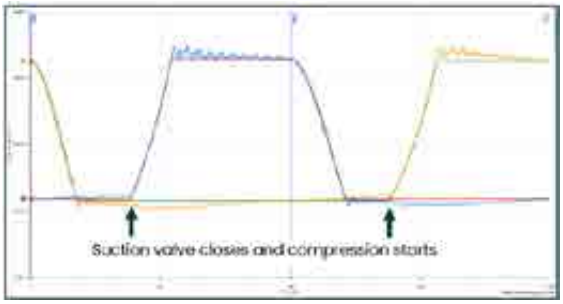

Figure 11: For every revolution, the reverse flow control holds the suction valves open for a certain part and releases it. The compression starts delayed.

Thus, a Reverse Flow control system allows to achieve any desired capacity and is very cost efficient.

by: Thorsten Bickmann, Fayyaz Qureshi – BENTLY NEVADA

2.4 Starting and Stopping of the compressor

Starting and stopping the compressor provides the most basic and coarse form of load control. This way is more common when compressors are smaller and fits to applications like for small air compressors or LPG compressors at filling stations.

2.5 Speed Control

Variable speed drivers can adjust the compressor load and capacity by operating at different speeds. Examples are compressors with turbine drives, combustion engines and electric motor drives consisting of a frequency controller and thyristor motor.

The rotational speed of the compressor determines how long it takes to complete each compression cycle. As the rotational speed decreases, the cycle time lengthens, resulting in less discharged flow per unit of time. An increase in rotational speed results in more flow per unit of time.

The relationship is (approximately) linear, so that if the crankshaft rotational speed falls by 50%, then so does the flow rate. Similarly, if the crankshaft rotational speed were to increase by 50%, the flow rate would increase by approximately 50%.

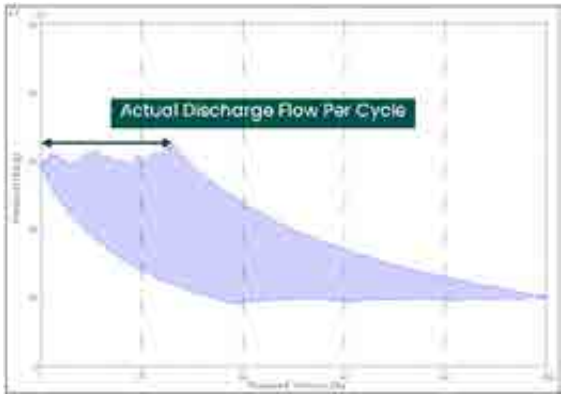

Figure 12: PV curve, increase of speed results in increased discharge flow per unit time:

From the pressure versus volume (PV) curve the actual discharge flow occurs from the opening of the discharge valve to the end of the stroke as shown in Figure 12. The amount of time it takes for this discharge process to occur is determined by the rotational speed of the crankshaft.

2.6 Recirculation or Bypass

A recirculation or bypass line is typically installed around the compressor and /or around the 1st stage. The portion of the gas that has been compressed is circulated back to the suction of the compressor.

When the compressor is in the start up procedure, the bypass lines are typically opened to ensure a smooth start up. When in operation, the bypass lines are closed, and the capacity is controlled by previously described techniques. Continuous operation with recirculation results in no horsepower savings.

3 Capacity Control Case Histories

3.1 Suction Valve Unloader Setup Error

On a 6-throw makeup gas reciprocating compressor, the cylinder chamber pressure versus crank angle plot in Figure 13 showed a deviation between measured (brown) and theoretical (green) pressure curves for CE chamber of cylinder 6 (stage 3). The measured pressure was rising slower than expected which delineates that as pressure was increasing during compression, high pressure gas was leaking to a low-pressure area, hence delaying compression. Leakage to low pressure zone around CE chamber would mean either suction valve leak or leak through pressure packing. The crosshead synchronous (unfiltered) vibration waveform showed broadband of high frequency energy in Figure 13. This high frequency content was appearing in the crosshead vibration versus crank angle plot during the time when CE suction valve is closed. During closed state of valve, the leaking gas was producing a high frequency sound “hiss” which was captured by accelerometer installed on top of crosshead of the same throw.

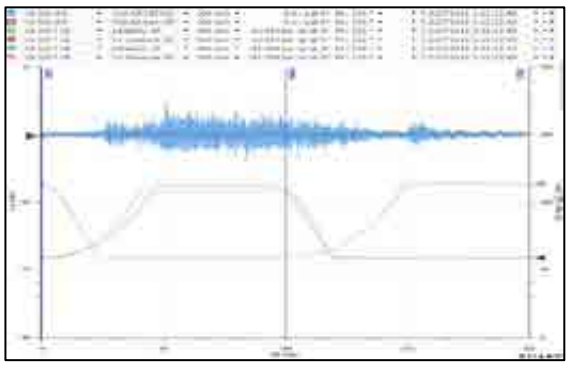

Figure 13: Crosshead vibration overlayed on cylinder chamber pressure vs crank angle plot

Further, the trends for suction valve temperatures were also checked and temperature of CE suction valve was found significantly higher than the HE suction valve as shown in Figure 14.

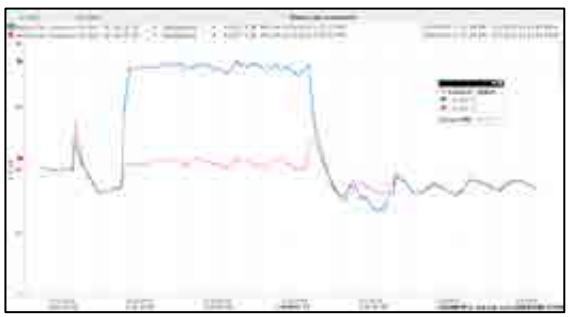

Figure 14: Trend of HE and CE suction valves' temperatures

by: Thorsten Bickmann, Fayyaz Qureshi – BENTLY NEVADA

Hence, maintenance teams were advised to inspect the suction valve on the CE chamber and valve cage was found broken causing severe leakage.

Following the maintenance activity, the machine was restarted. Few minutes after start-up, the piston rod vibration (pk-pk displacement) started increasing significantly in vertical orientation on cylinder 6 (same throw where maintenance was carried out). This customer had a history of piston rod failures wherein piston rod vibration (pk-pk displacement) would show an increasing trend 30 mins before the piston rod breaks. Based on the history and a simultaneous increase in crosshead vibration as shown in Figure 15, it was decided to shut down the machine immediately.

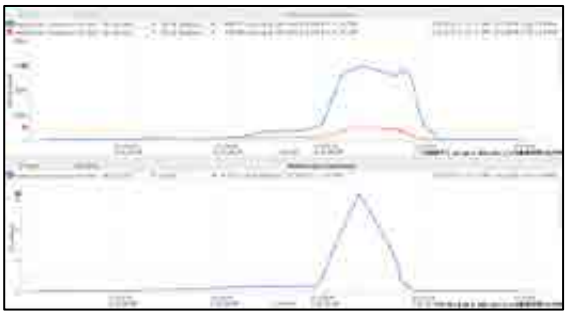

Figure 15: Trend of pk-pk displacement (upper) and crosshead vibration (lower)

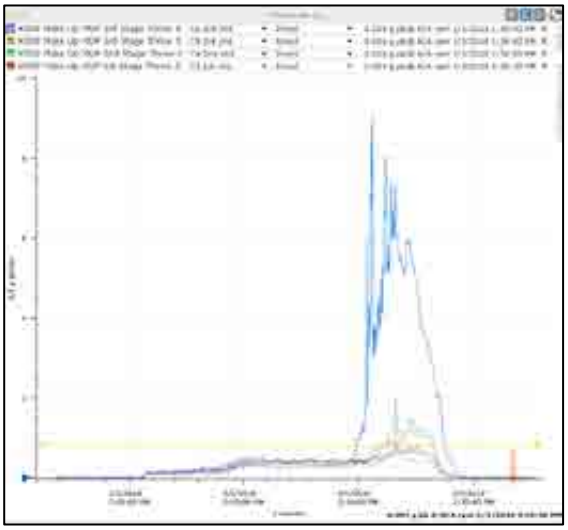

Figure 16: Trend of crosshead vibration (all throws)

In parallel, dynamic data was reviewed to identify potential failure to reduce time for inspection. Filtered crosshead vibration (red waveform) versus crank angle plot (upper plot in Figure 18) showed two high amplitude impacts during the revolution which represents possibility of mechanical looseness in the running gear. At the same crank angle instants of those impacts, piston rod displacement waveform showed considerable change resulting in very high pk-pk displacement in the lower plot in Figure 18.

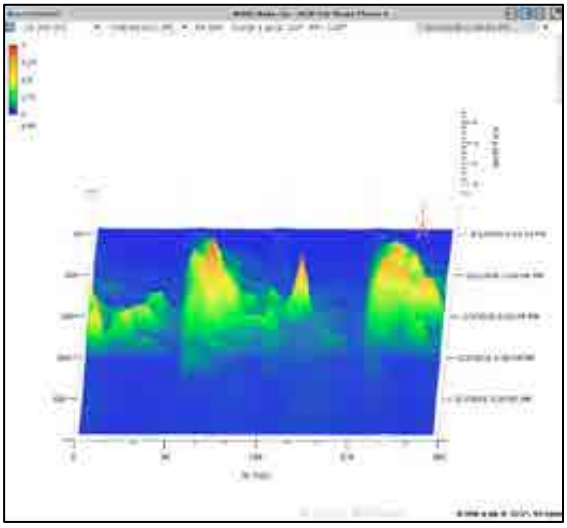

Figure 17: Cyl 6 crosshead filtered vibration band waterfall

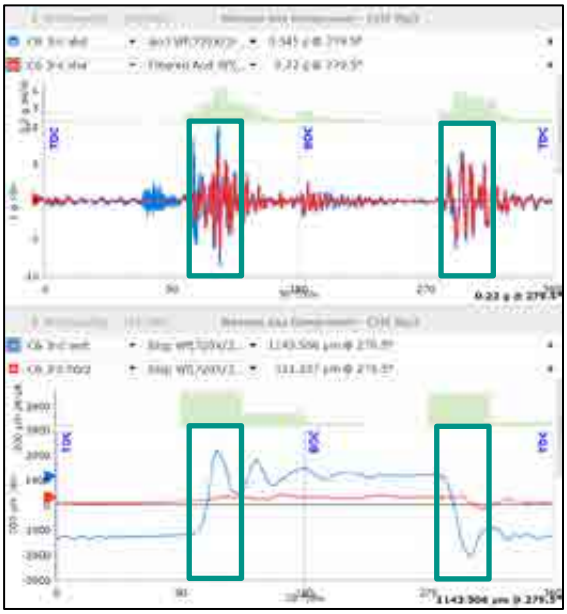

Figure 18: Crosshead vibration (upper) and piston rod displacement (lower) vs crank angle plots

Calculated vertical forces on this down-running crosshead also showed abnormal upward movement in Figure 19 aligned with one of the vibration impacts as piston travelled from top dead center (TDC) towards bottom dead center (BDC) and the maximum force in downward direction was found aligned with the other vibration impact as piston travelled back from BDC to TDC.

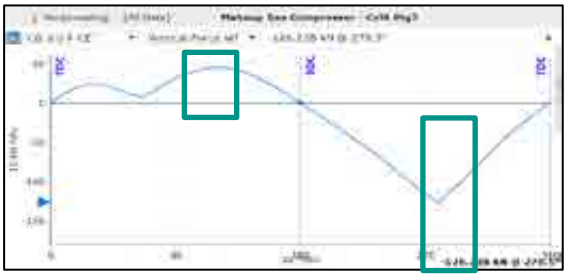

Figure 19: Vertical forces on crosshead vs crank angle plot

by: Thorsten Bickmann, Fayyaz Qureshi – BENTLY NEVADA

One very important observation came from rod load curves in Figure 20 (upper plot) where the degrees of rod load reversal were found to be 0 degrees i.e. combined load forces (green) on crosshead pin were found to be in compression throughout the revolution; hence no force reversal from tension to compression or vice versa. Loss of rod load reversal is a disastrous phenomenon which causes loss of adequate lubrication to crosshead pin or bushing leading to pin or bushing failure. Correlating all these coherent signatures, it was speculated that the crosshead pin or bushing may have failed due to loss of rod load reversal resulting in high crosshead and piston rod vibration attributed to the abnormal crosshead motion.

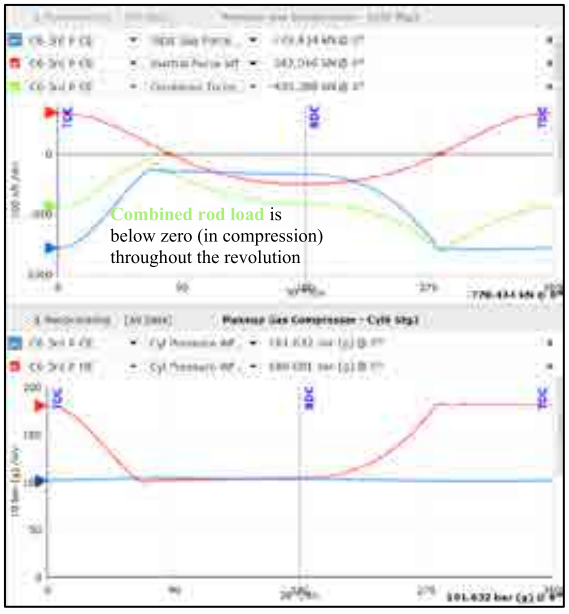

Figure 20: Rod load forces (upper) and pressure (lower) vs crank angle plots

Upon inspection, crosshead pin was found bent and small end bushing was found broken. But why would Operations load the machine in such a sequence where the machine will be in distress due to no rod load reversal? It was not intentional. The unloader sequences for different load conditions were programmed within DCS based on standard operating procedure provided by OEM. However, during maintenance for suction valve replacement, the instrument air tubing for suction valve unloaders' solenoids were removed. During reassembly, the tubing between CE and HE chambers got swapped mistakenly which resulted in unloading CE chamber instead of HE chamber as shown in lower plot of Figure 20 and hence zero degrees of rod load reversal.

Through adequate instrumentation and effective condition monitoring, timely accurate identification of failing component enabled repair in minimal downtime and saved the machine from expensive secondary failures.

3.2 Suction Valve Unloader Malfunction

To increase reliability and availability of their fleet of reciprocating compressors, customer's Reliability team decided to equip their assets initially with basic protection measurements (frame vibration, crosshead vibration and piston rod monitoring in line with API 670 recommendations) to avoid any catastrophic damages resulting in expensive repairs and extended downtime; and then progress towards advanced predictive monitoring (by adding cylinder pressure measurements) further optimizing maintenance costs. The main intent was to save the machines from any major damage and to proactively detect faults at their outset to plan maintenance effectively.

After monitoring system retrofit when the machine was started, unusual high amplitudes were observed in crosshead vibration for stage 3 cylinder as shown in Figure 21. No change/increase was observed in crankcase/frame vibration, rod position magnitude or piston rod vibration for this cylinder as shown in Figures 22, 23 and 24. [1]

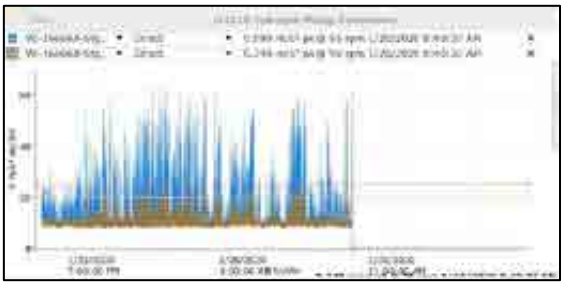

Figure 21: Trend of crosshead vibration for stage 3 cylinder

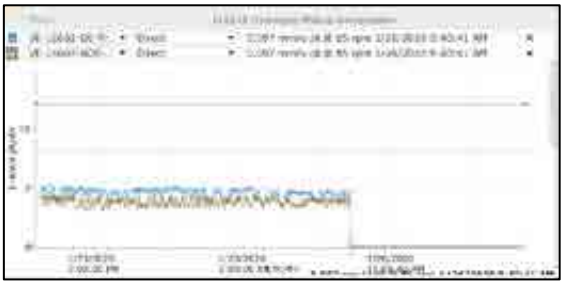

Figure 22: Trend of crankcase (frame) vibration



Figure 23: Trend of average piston position and position magnitude

by: Thorsten Bickmann, Fayyaz Qureshi – BENTLY NEVADA

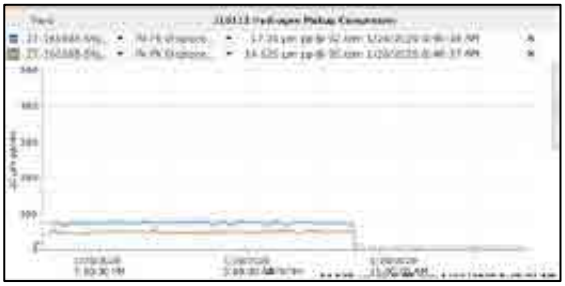

Figure 24: Trend of piston rod vibration (pk-pk displacement)

During the first 10 minutes of machine operation, crosshead filtered vibration magnitude was within limits as shown in Figure 25. No significant mechanical impacts were observed in the filtered waveforms of both redundant accelerometers as shown in Figure 26.

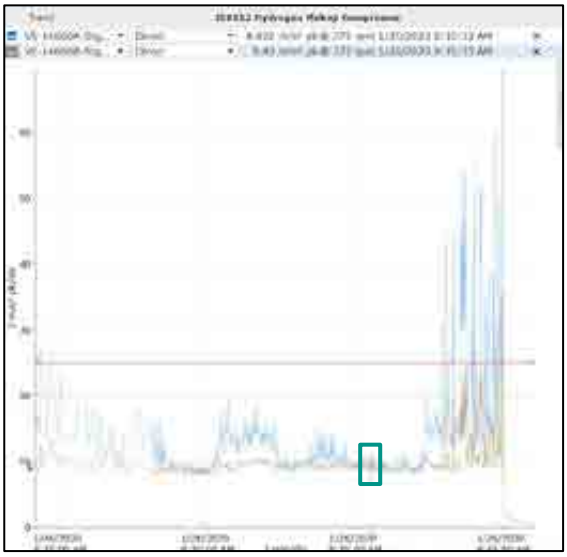

Figure 25: Crosshead vibration trend

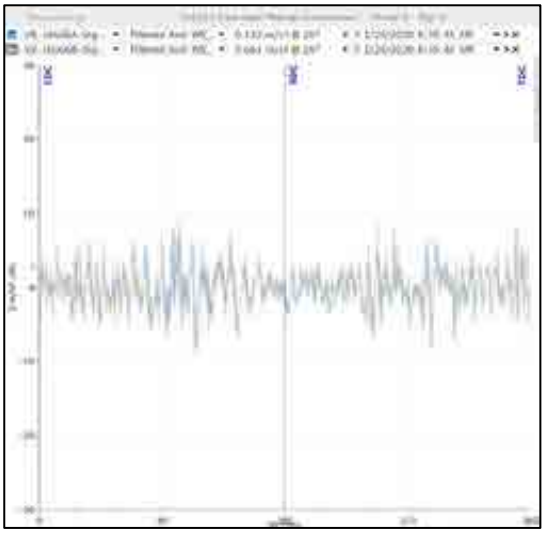

Figure 26: Crosshead acceleration vs crank angle waveform (at the cursor instant from Figure 25)

Once the crosshead vibration exceeded setpoints in Figure 27, the knocks (impacts) were prevalent in filtered crosshead vibration waveform in Figures 28 and 29 near 30 deg crank angle where, typically for a double acting cylinder and for similar suction and discharge pressures of makeup hydrogen gas, the suction valve(s) in head end chamber open(s) as shown in Figure 30.

Customer was advised to inspect suction valve(s) and its unloader at HE chamber. Upon inspection, the stem length of unloader was found a little too long. After adjusting the clearance between valve and stem by 2 mm, the compressor was restarted, and the crosshead vibration reduced back to normal. This showed the effectiveness of monitoring setup which was able to capture faults occurring at cylinder while sensor was installed at crosshead (few meters away).

One would think why the crosshead vibration was not high immediately upon compressor start-up and then started increasing after few minutes of operation?

The speculation is that over time, the valves becomes sticky and need higher differential pressure to open. This higher differential results in more valve lift / displacement which was probably causing an impact with the extended length of unloader stem.

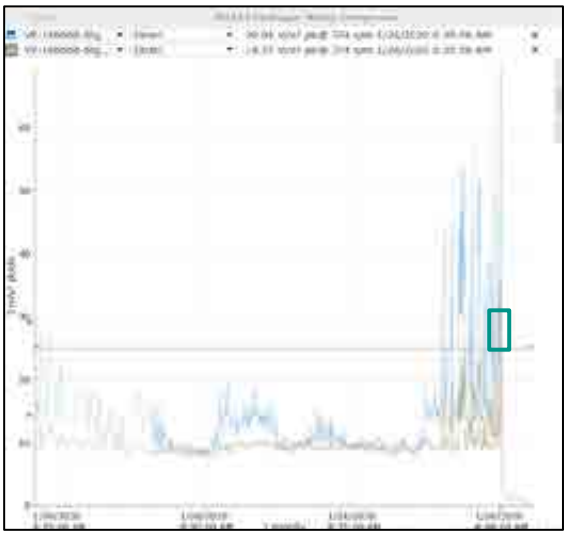

Figure 27: Crosshead Vibration Trend

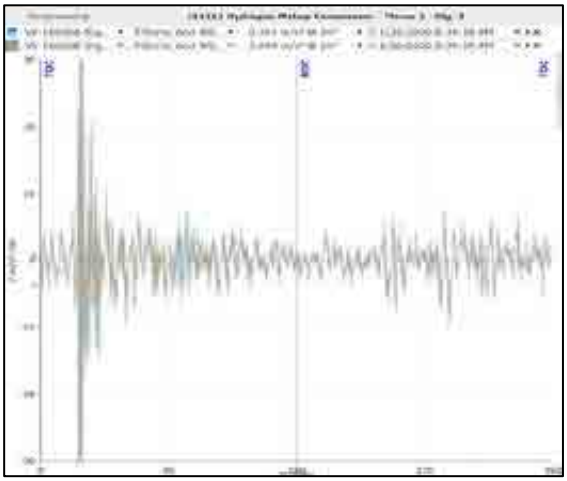

Figure 28: Crosshead acceleration vs crank angle waveform (at the cursor instant from Figure 27)

by: Thorsten Bickmann, Fayyaz Qureshi – BENTLY NEVADA

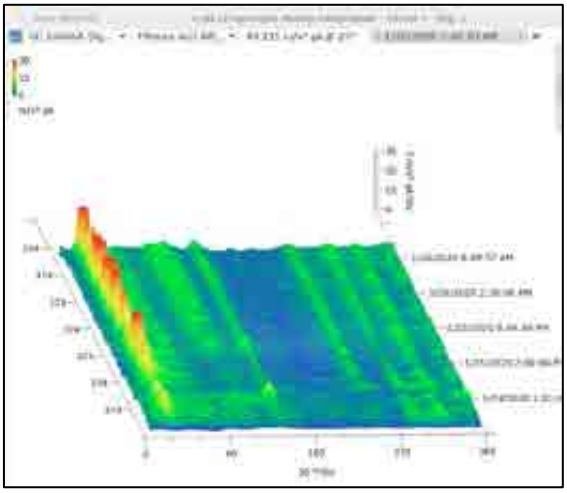

Figure 29: 3D band waterfall plot for crosshead acceleration filtered vibration

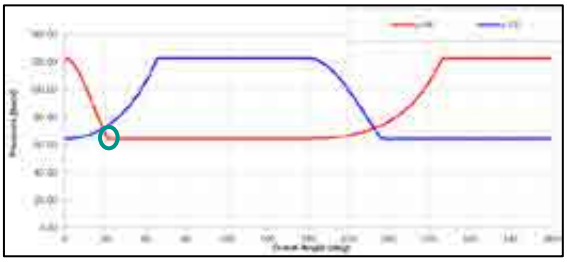

Figure 30: Theoretical Pressure vs Crank Angle plot for Stage 3

3.3 Reverse Flow Control Problems

Following the effective findings similar to case 3.2, customer decided to enhance monitoring on their fleet of reciprocating compressors by adding cylinder chamber pressure measurement to activate PV curves, rod load analysis and performance calculations helping them to take informed decisions for optimizing operation and further reducing maintenance costs. This compressor is equipped with a stepless unloader capacity control system and the diagnostic software has a patented algorithm enabled for such control devices to adapt its theoretical (adiabatic) plots according to changing load conditions by tracking the suction valve closure point hence aiding continuous pattern recognition for fault identification.

After few days of machine start-up following monitoring system upgrade, Operators noticed a considerable reduction in stage 2 discharge pressure. To rule out any instrumentation issues, discharge line pressure was compared with discharge pressures for both HE and CE chambers (available from the newly installed cylinder chamber pressure transducers) and the same reduction was observed.

According to working principle of these stepless unloaders, the load on both chambers of a throw should be similar and hence same capacity signal is provided to both HE and CE unloaders. When the condition monitoring system data was compared with the DCS signal of the reverse flow control system, it was noticed from pressure versus crank angle plot in Figure 31 that the CE capacity followed the pattern as commanded i.e. pressure started increasing in CE chamber almost immediately after top dead center (TDC) for 94% capacity signal. The HE pressure curve showed as if the suction valve unloader was stuck at 37% capacity as the pressure did not start increasing in HE chamber immediately after bottom dead center (BDC). It was hence diagnosed that HE unloader was not functioning as expected and needed to be repaired / replaced.

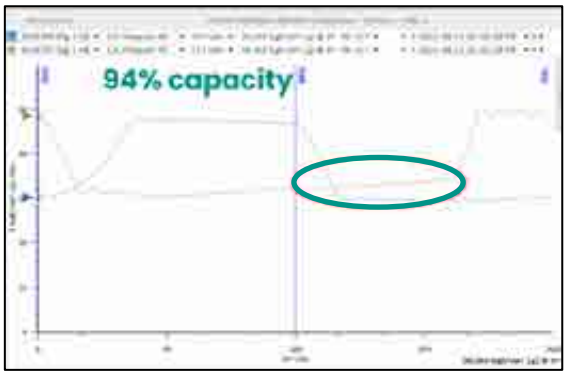

Figure 31: Pressure vs crank angle plot

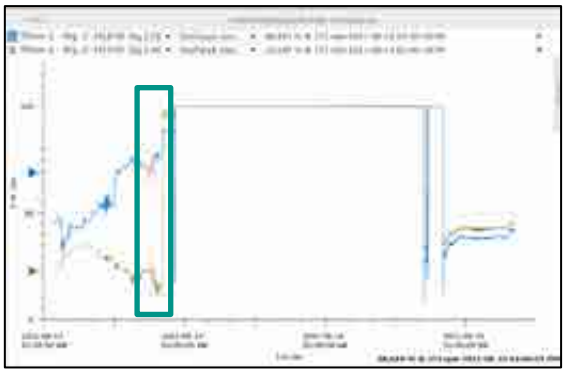

Figure 32: Trend of discharge volumetric efficiency for CE and HE (drifting away during malfunction)

As soon as the machine was started after replacing the HE stepless unloader, the target 60% capacity and pressures were achieved in both chambers as shown in Figure 33. Timely identification of failure root cause helped in achieving optimum machine operation.

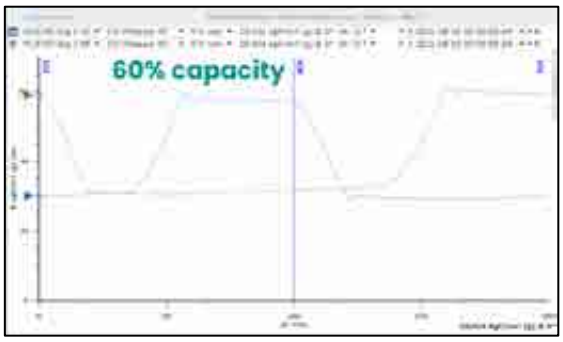

Figure 33: Pressure vs crank angle plot

by: Thorsten Bickmann, Fayyaz Qureshi – BENTLY NEVADA

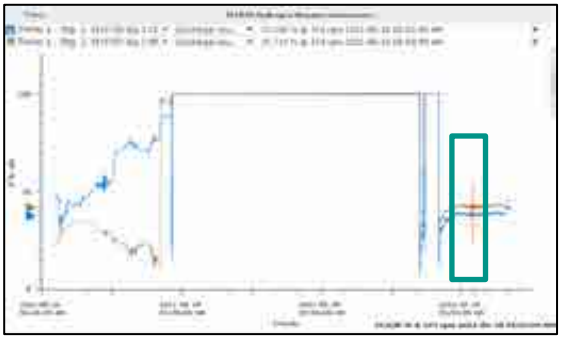

Figure 34: Trend of discharge volumetric efficiency for CE and HE (healthy state after HE stepless unloader exchange)

As can be seen from the example above, the difference between discharge volumetric efficiencies for both CE and HE should be constant as shown in Figure 34. The malfunction in one of the stepless unloaders will be depicted as the CE and HE discharge volumetric efficiencies start to drift apart as presented in Figure 32. This is what is embedded in automated diagnostics (Figure 35), which is an autonomous logic engine continuously ingesting monitoring data from machine, process and auxiliaries, and providing insights about failing components. This analytics delineates that if the absolute difference between the discharge volumetric efficiencies in both chambers of a cylinder increases beyond the pre-defined offset threshold (in this case, it was set as 10%), then the defective stepless unloader rule will trigger notification for action.

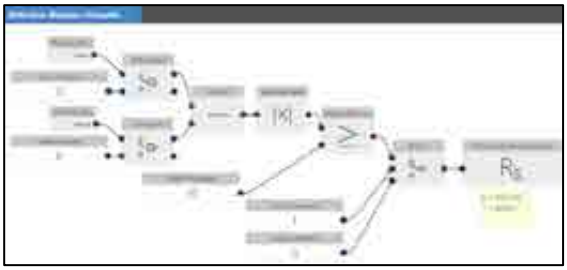

Figure 35: An example of Decision Support Analytics - Defective Stepless Unloader

Another example shows high frequency content overlaid to the dynamic cylinder pressure signal, when the stepless unloader requires maintenance. [2]

4 Conclusion

Capacity control devices are used to operate reciprocating compressors at their optimum capacity to reduce the carbon emissions. Condition Monitoring Systems support to monitor the health of capacity control systems so that operators can rely on them.

Each capacity control technique has distinct effects on the vibration and cylinder pressure waveform, and compressor's performance indicators. Deviations from the baseline readings and signatures can be used to identify developing malfunction of a capacity control device.

Autonomous diagnostic platforms can be leveraged to build logics to automate the capability to detect the changing load conditions; hence enabling continuous automated pattern recognition for fault identification. These notifications can be further sent over SMTP to the action owners with the severity of malfunction coupled with advisory insights.

References

[1] Qureshi,Fayyaz; Ernest Ralidzhivha; Basil Mkize: https://www.bakerhughes.com/bently-nevada/success-stories/natref-reliability-and-maintenance-teams-collaborate-together?utm_source=bhds

[2] Bickmann, Thorsten: 12. EFRC Conference - Warsaw, Poland, EFRC Conference Training Workshop 2020, Trouble-shooting using condition monitoring of online pressure data



ऑयल इंडिया लिमिटेड
(भारत सरकार का उद्यम)
Oil India Limited
(A Government of India Enterprise)

Upgradation of Compressor Lubrication System from Pump-to-Point "to" Divider Block in Worthington and BPCL Compressors of Oil India Limited & benefits obtained

by:

Kamalapuri Amarish
akamalapuri@oilindia.in

Baruah Prateek*
prateek_baruah@oilindia.in

Gas Management Services Department
Oil India Limited
Duliajan, Assam, India

13th EFRC CONFERENCE
September 19th – 21st 2023, Zagreb

Abstract:
We are Oil India Limited (OIL), an upstream Indian National Petroleum Company under the aegis of Govt. of India. The roots of OIL date back to 1889 when its parent company Burmah Oil Company Ltd, UK discovered Asia's first crude oil in Digboi (Assam) in North East India.
OIL has been using Reciprocating Compressors for compression of field gas for flare reduction and delivery of Gas Lift Gas to Artificial Gas Lift Wells since 1970s. We take pride in maintaining more than 130 numbers of Reciprocating Gas compressor packages placed in 19 Nos. of Gas Compressor Stations(GCSs) spread across an area of 1400 Square KMs in the state of Assam.
OIL started its gas business with integral slow speed compressors, subsequently moving on to high speed separable compressors with either Electric Motors or Gas Engines as prime movers. The journey encompasses compressors makes of Nuovo Pignone, Ingersoll Rand, Worthington, Dresser Rand, Energy Industries (Gemini) and Indian BPCL, which is a plethora of different makes on a platter.
Constituting 1/3rd of our entire arsenal, our Worthington and Indian make BPCL compressors had been factory equipped with PUMP TO POINT Lubrication Systems. Owing to serious drawbacks of the system as explained in this paper, we decided to upgrade the compressors to DIVIDER BLOCK system. Our paper is highlighting, in detail, disadvantages encountered while using the earlier PUMP TO POINT system AND the advantages, both technical and financial, we have been harvesting since the induction of DIVIDER BLOCK system in the above mentioned reciprocating gas compressors.

by: Amarish Kamalapuri, Prateek Baruah – OIL INDIA

1. Introduction

Oil India Limited[1] (mentioned as OIL from here onwards) is one of the only two national petroleum E&P companies of Republic of India. OIL produces crude oil, natural gas and Liquefied Petroleum Gas (LPG) and has diversified its business to Alternate and Renewable Energy sectors like Wind, Solar and Green Hydrogen energy in recent times. Having its foot print all over India along with 8 countries around the world, the company's primary operational area is around its FHQ situated in Duliajan City in the state of Assam in the North Eastern region of India.

The natural gas, coming in from petroleum rich fields of upper Assam, is received in our Gas Compressor Stations (GCS) in two pressure ranges viz. 1.5 – 2.2 kg/cm^2 (termed as LP Gas) and 14 – 16 kg/cm^2 (termed as HP Gas). In the GCS, our Low Pressure Booster (LPB) compressors compress the LP Gas to 14 – 16 kg/cm^2 range. The Gas Lift (GL) compressors compress a part of HP Gas to a pressure range of 85 – 90 kg/cm^2. This gas termed as "Gas Lift Gas" is sent to oil wells equipped with Artificial Gas Lift technology. The remaining part of HP Gas is utilised to maintain the natural gas distribution grid pressure in our FHQ region in the range of 14 – 16 kg/cm^2. This distribution grid connects all the 19 nos. of GCSs of the company which helps to maintain the GL compressors' suction pressure to individual GCSs, gas pressure to OIL's in-house LPG production plant at Duliajan City and also to a plethora of downstream industries viz. Power generation, Fertiliser, Petro chemical, Refinery, Tea gardens and Plastic producing Gas cracking industry in Assam.

Gas Management Services (GMS) Department of OIL works relentlessly to keep looking for advanced equipment, procedures and services to minimise downtime of its reciprocating gas compressors for smooth running of the company's business.

The overwhelming majority of compressors in the petroleum industry is either the dynamic (axial/centrifugal) or positive displacement (reciprocating and screw-type) type, consisting of moving components. As such, the lubricating system of any gas compressor package becomes THE most vital component for running reliability of the package, as they require some form of lubricant to either cool, seal or lubricate internal components. Inadequate lubrication often leads to premature wearing/seizure of pressure packings, piston rings and may escalate the damage to costlier internals like pressure packing stuffing boxes, pistons, piston rods, oil scraping separation covers and cylinder liners. On the other hand, over-lubrication leads to avoidable loss of lube oils, affects fouling of piston ring grooves, stuck piston rings and/or pressure packings, valve plate sticking, ultimately leading to loss of gas sealing ability of these components and results in deration of compressor capacity and loss in production.

Currently, The "PUMP TO POINT" (P to P) system and relatively advanced "DIVIDER BLOCK" system occupy the market as the go to systems for obtaining optimum lubrication of the compressor cylinder system.

In our fleet of 130+ reciprocating gas compressors, almost 1/3rd is occupied by Worthington (**WT**) Compressors (all commissioned in **1986**) and Indian make **BPCL** (Bharat Pumps and Compressors) (Commissioned between **1979** and **2013** at different times). These compressors were factory equipped with **Pump To Point** lubrication systems. We upgraded this fleet of compressors (17 nos. Worthington and 23 nos. BPCL) to divider block systems as we were facing several issues with the Pump to Point system.

The arrangement of our earlier pump to point system and the disadvantages faced while using this system are elaborated below:

2. Pump to Point lubrication system

2.1 The arrangement of the system

Ref. Figure 1 and 2, the pump to point system consists of a compressor crankshaft driven lubricator box with pumping units for each and every lube injection point. Each pump may have same/different pressure ratings and sizes. A rocker arm with screw helps adjust the lube oil feed rates. Rate is observed through sight glass, the reliability of which often proves to be a critical point in the system.

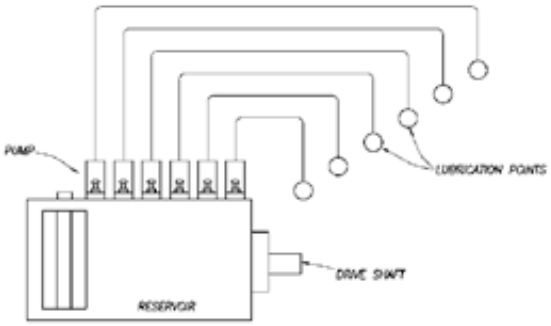

Figure 1: Pump to Point Lube simple schematic



Figure 2: Pump to Point Lubricator Box

by: Amarish Kamalapuri, Prateek Baruah – OIL INDIA

2.2 Disadvantages of Pump to Point lubrication system

2.2.1 More injection points – more pumps

Increased lubrication points result in equal increase in number of lubricating pumps requiring us to maintain a very large lubricator box (Ref. Figure 3). A few of our 4 throw / 2 stage type compressors were earlier having as many as 12 lubrication points being supplied by l2 nos. of individual pumps! This would, thus be a 6/12 fold increase in no. of pumps as compared to a typical divider block system with 2/1 pumps. The associated financial disadvantage is understandable, which, however has been presented later in the paper.



Figure 3: Pump to Point Lubricator Box with many pumps making O&M cumbersome

2.2.2 More injection points – more time consuming feed rate adjustment

In this system, the lube oil injection feed rate has to be adjusted individually and manually which results in a many fold increase in set up and adjustment time. Maintenance of individual oil drip sight glass (Ref. Figure 4), critical for optimum feed rate adjustment, is also a lengthy job due to the increased number of pumps in this type of lubrication system.

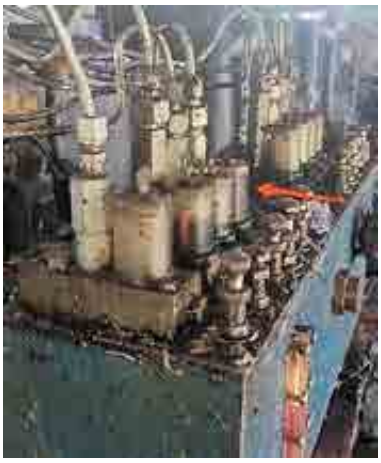

Figure 4: Pump to point lubricator box discovered with several leakage points in a remote installation

2.2.3 More components – more time in servicing and parts maintenance

Number of components to be inspected and maintained also increase as not just the individual pumps and tubings, but also, lubricating box shaft, increased individual cam lobes (Ref. Figure 5 A& B) also need servicing and maintenance for adequate lube oil feed to individual injection points.





Figure 5 (A & B): One of the Pump to Point Lubricator Boxes undergoing servicing with several lobes in camshaft making maintenance a much more challenging job

2.2.4 More lubricating pumps, more probability of failure, more probability of downtime

Extensive Monitoring of the system was required as the compressor would continue to run even after 2/3 pump (Ref. Figure 6) failures in the system which led to avoidable compressor downtime owing to major component failure. This unwanted increase in failure rate probability and vindicated by our experience in such compressors also inspired us to go for divider block system of lubrication.

by: Amarish Kamalapuri, Prateek Baruah – OIL INDIA



Figure 6: One of the many lubricating pumps in Pump to Point System

Table1: Lube Oil Pump Units malfunction comparison in **17 Worthington + 23 BPCL units**:

Lube Oil Pumping Unit in	5 Year Period	No. of Pumping Units replaced due to malfunction
Pump to Point System	2012 – 2016	76 nos.
Divider Block Lubrication System	2018 – 2022	39 nos. (***48.68 % decrease in malfunction count***)

2.2.5 Pump to Point lubrication – frequent filling and more lube oil consumption:

This system operates with vacuum type lubricating pumps wherein the lubricator box itself acts as a reservoir for the lube oil. This arrangement has inherent drawbacks as the box needs frequent refill to maintain adequate lube oil level for optimum suction to the pumps. Any inadvertent error on the part of the operator failing to refill the box may lead to catastrophic failure in the entire system. It was also observed that pump to point lubrication system lube oil consumption was higher than divider block counter-parts.

Considering compressor units selected randomly:

Table2: Lube Oil Consumption Comparison

GCS Jorajan / Unit	Pump to Point Lube Oil Consumption [Compressor + Lubricator (L)] Period June'18 – May'19	Divider Block Compressor Total Lube Oil Consumption Period April'20 – March'21	Percentage Reduction of Lube oil consumption per hour for divider block system equipped compressor
LP B-2	**[474 L + 536 L]** Run for = 4658 Hrs Consumption / hr = **.216 L**	720 L Run for = 3487 Hrs Consump. / hr = **.206 L**	**4.63%**
LP B-3	**[634 L + 776 L]** Run for = 5944 Hrs Consp / hr = **.237 L**	531 L Run for = 3511 Hrs Consp / hr = **.151 L**	**36.29%**
LP B-4	**[659 L + 930 L]** 6430 Hrs Consp / hr = **.247 L**	1126 5614 Hrs Consp / hr = **.200 L**	**19.03%**

2.2.6 Pump to Point lubrication additional draw backs

i) We found it difficult to monitor the output of each lube pump because a Single Point Test Device (SPTD) was required to be fitted at each injection point which was not economically feasible.

ii) Adding pressure gauges at the outlet of each pump was a possibility but unwieldy option as far as O&M is concerned.

iii) Worn piston/cylinder assemblies caused metered oil to leak around the outside of the piston and into the lubricator reservoir instead of along the feed line. As such sight glass drip rates were no longer a perfect measurement of actual pump output and we encountered deficient lube oil supply causing issues in compressor internals.

iv) Our Pump to point system also had no over pressure protection.

v) The installation of any no flow alarm or shutdown required an extra lubricating pump, which was connected to a pressure transmitter. However even if that pump was working, there was no automated way to verify if the other pumps were delivering oil or not.

by: Amarish Kamalapuri, Prateek Baruah – OIL INDIA

vi) The operator has to monitor each individual sight glass to determine the working condition and amount of lube oil injected, which is time consuming and also elevates chances of human error due to lack of focused illumination on the pumps and/or fatigue.

3. Divider Block lubrication systems

3.1 The arrangement of the system

This system receives lube oil from one/two positive displacement pumps and distributes the oil via a divider block mechanism to the injection points to lubricate pressure packings and cylinders. This system is capable to serve additional lube injection points just by addition of extra divider block sections to the system. OEM recommended lube rates coupled with our on-field experience helps to easily set the optimum lubrication rates to avoid unwanted lube oil consumption in this system.

Ref. Figure 7, the system components are depicted below:



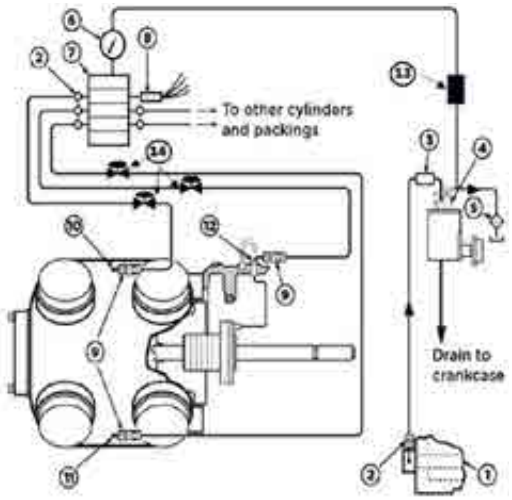

Figure 7: Block System View & Schematic

Sl. No. Ref. in Figure 7:

***1**- Frame Oil Gallery, **2**-Single Ball Check Valve, **3**-Sintered Bronze Filter (optional), **4**-Force Feed Lube Pump, **5**-POPR (Ref. Sec 3.3.2), **6**-Pressure Gauge, **7**-Divider Block, **8**- Cycle Indicator & No-Flow Shutdown Device (in BPCL) / Sentry Valve (in Worthington), **9**-Check Valve with Protector, **10**-Top Cylinder Injection Point, **11**- Bottom Cylinder Injection Point, **12**-Packing Injection Point, **13**- HP inline filter, **14**- Balance Valves*

3.2 Basics of Divider Block lube distribution

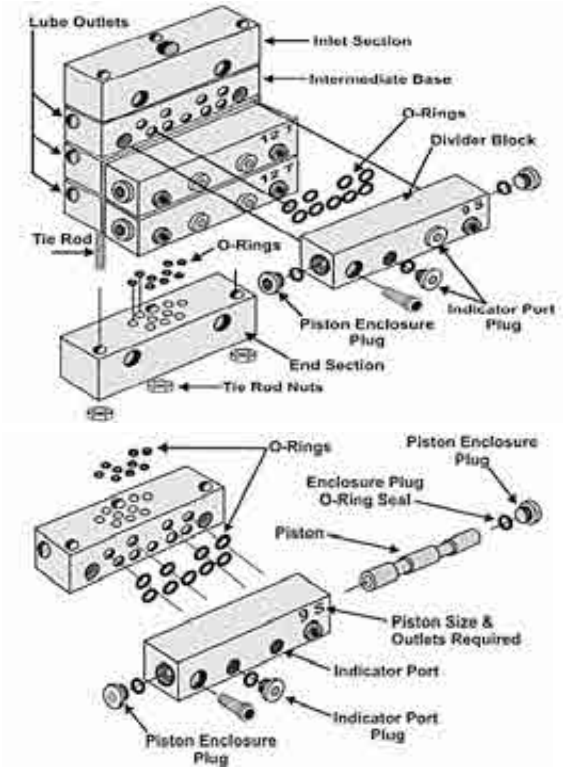

Figure 8: Divider Block : Exploded View

Apart from the self-explanatory components in the exploded view (Ref. Fig. 8) , the heart of our divider block assemblies usually consist of three metering valves mounted to a segmented baseplate. The metering valves have solitary or twin outlets which are either externally singled or cross-ported. Extremely close tolerances between piston and valve body is the precise reason why these valves are able to deliver precise volumes of lubricant at desired pressure. Illustrating the functioning of the divider block lube distribution in 4 simplified steps:

Step 1: Ref. figure 9, the lube inlet passage is connected to all piston chambers at all times with only one piston free to move at a time. With all the pistons positioned extreme right, lube oil via the inlet flows to push against the right end of piston 1 (top)

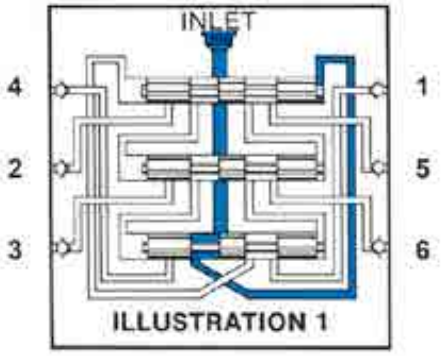

Figure 9: Divider Block functioning: ***Step 1***

by: Amarish Kamalapuri, Prateek Baruah – OIL INDIA

Step 2: Ref. figure 10, presurrised lube oil shifts piston 1 from right to left, dispensing already present lube oil from outlet 1. In the process, piston 1 simultaneously directs the lube oil flow to push against the right side of piston 2 (middle piston).

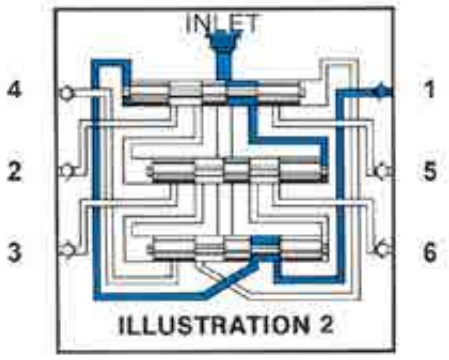

Figure 10: Divider Block functioning: ***Step 2***

Step 3: Ref. figure 11, incoming lube oil pressure shifts piston 2 from right to left, dispensing lube oil via valve ports of piston 1 and eventually through outlet 2. The shifting of piston 2 ensures incoming lube oil to push at the right side of piston 3 (bottom).

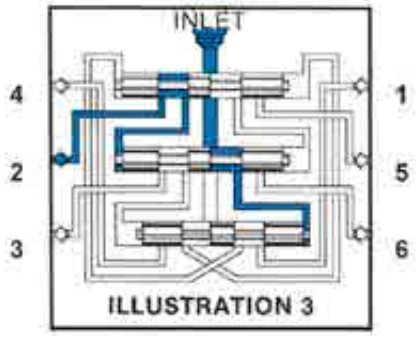

Figure 11: Divider Block functioning: ***Step 3***

Step 4: Ref. figure 12, incoming lube oil this time shifts piston 3 (bottom) from right to left, dispensing lube oil via the valve ports of piston 2 and finally through outlet 3. The shifting of piston 3 directs lubricant through a connecting passage **this time** to the left side of piston 1. Thus, lube oil flow against the left side of piston 1 **begins the second half-cycle**, which shifts pistons from left to right, dispensing lubricant through outlets 4, 5 and 6 of the divider valve.

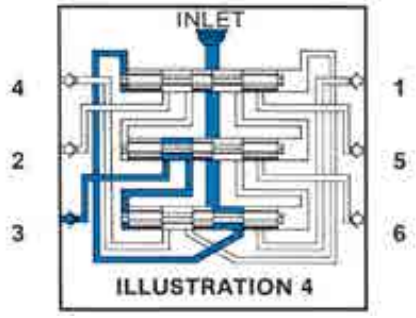

Figure 12: Divider Block functioning: ***Step 4***

In our industry, the Divider Block Lubrication System is also termed as a single line progressive system because it contains only one oil supply line from the pump discharge to divider block. If any one piston (in a divider valve) of the divider block stops moving, the entire system is affected by the blockage and the remaining pistons also stop moving. The blockage can be witnessed by facilities as explained in Section 3.3 below.

3.3 Advantages of Divider Block lubrication system[2]

3.3.1 Advantage of Pin indicator



Figure 13: Indicator Pin Out, showing root cause

The pin indicators in the divider block simplify troubleshooting by signalling to users specific lubrication lines that have an over pressure condition (Ref. Figure 13) .This minimises root cause analysis time to bare minimum fast tracking attention to the specific blocked lube oil injection tubing. This helps reduce Compressor downtime.

3.3.2 Advantage of POPR

Pop Open Pressure Relief or POPR protects the divider block system from any damage due to overpressure situations. Ref. fig. 14, we improvised this safety accessory of the system and connected the POPR return line back to the compressor oil sump via a drilled hole in the crankcase explosion relief system to save the lube oil from spillage and loss.

by: Amarish Kamalapuri, Prateek Baruah – OIL INDIA

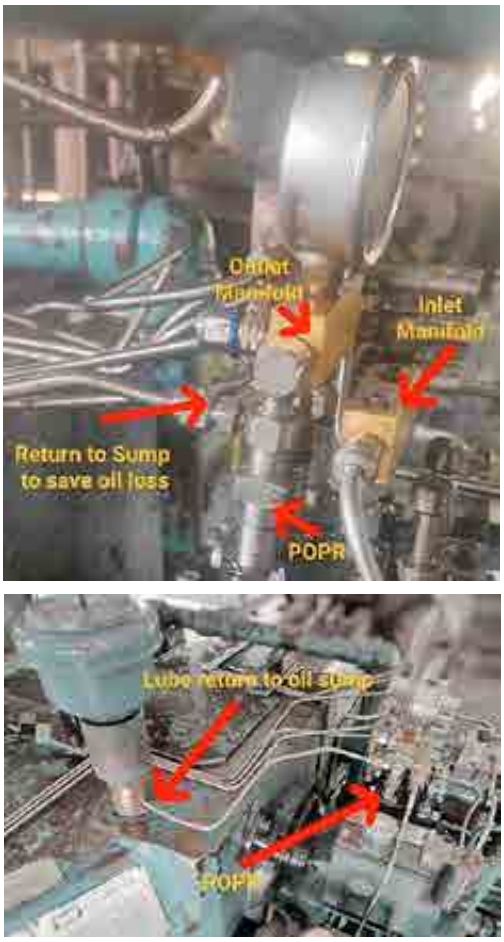

Figure 14(A&B): POPR and return line to compressor oil sump – our improvisation in safety to obtain financial advantage by saving lube oil

3.3.3 Cycle Indicator for accurate lube oil injection

Ref. fig. 15, The distinct reflective orange colour cycle indicator visible from a distance of over 30 feet has a snap-action movement which makes it convenient for the user to observe and determine the precise timing of each divider valve cycle. This helps to monitor and control the lube oil consumption, set proper lube rates and identify malfunctions in the divider block system. It's a boon for us mechanical engineers, for whom documenting the cycle times and determining the system cycle time pattern shall remain the most accurate method of setting the correct lubrication flow rates. The UV stabilized clear polycarbonate material is not affected by exposure to sun and remains clear providing easy indicator visibility.

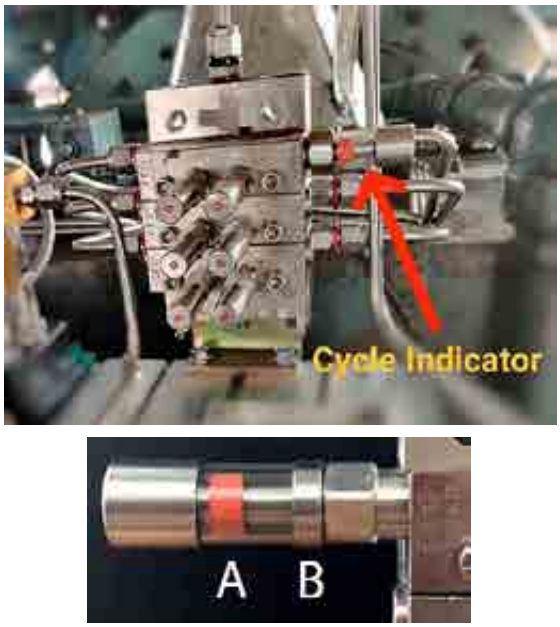

Figure 15 (A&B): Cycle Indicator use to calculate cycle time

3.3.3(A) Cycle time to Oil flow Quantity

Ref. Fig 15(B), timer is to be started when the indicator begins moving from position A towards position B. The indicator reaches position B and then retracts back to position A. Timer is to be stopped the moment indicator starts moving from position A. This is one complete cycle of movement. We usually repeat this process 10 consecutive times and calculate the average to get the accurate cycle time.

After determining the cycle time, the quantity of oil flowing through the lubrication system can be ascertained by the following formula:

Q = 6M / T

Where, **Q** = Flow Rate in Pints Per Day

M= Total Value of the Divider Block Elements

6 = The constant resulting from converting cubic inches to pints and seconds to days

T = Time in seconds for one complete cycle of the Divider Block.

3.3.4 Advantage of Extreme Duty Check Valves with Check Valve Protector

Our divider block systems are state of the art upto the lube oil injection points. Unlike earlier pump to point lubrication's traditional NRVs, the upgraded system has a combination of extreme duty check valve guarded by an immediate downstream placed Check Valve Protector (CVP). Self guiding poppets in the check valve ensure positive sealing and OEM manufactured ORB (O Ring Boss) fitting eliminates

by: Amarish Kamalapuri, Prateek Baruah – OIL INDIA

the need of sealant in its connection to the CVP. This CVP provides an oil barrier to protect the check valve sealing surfaces from hot process gas and impurities in the gas stream. Also, with its minimal reserve capacity, it facilitates immediate delivery of oil to cylinders and packings (Ref. fig. 16).

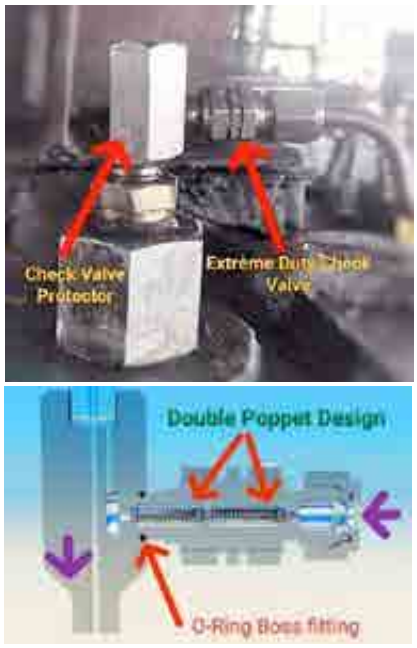

Figure 16 (A&B): Check Valve with Protector

3.3.5 Advantage of in-line filter

Ref. fig. 17, our Divider Block systems are equipped with 25 micron stainless steel filters downstream of the lube pumps. This helps to keep debris from damaging the high pressure system components.

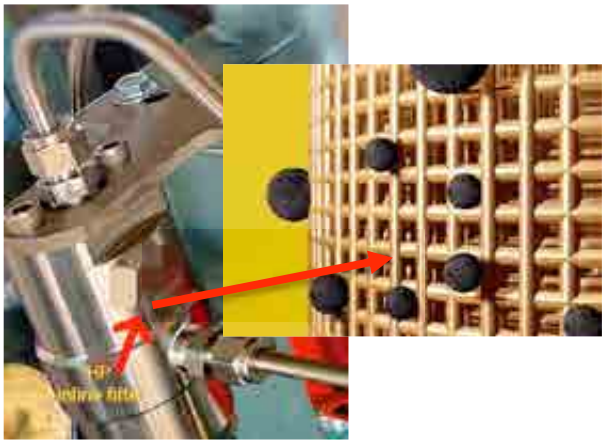

Figure 17: In-line filter downstream of lube pumps

3.3.6 Flow monitoring shutdown protection in BPCL make compressors divider block system

The monitoring device installed on the divider block (ref. fig. 18) provides shutdown protection by monitoring the cycle times of the lube system.

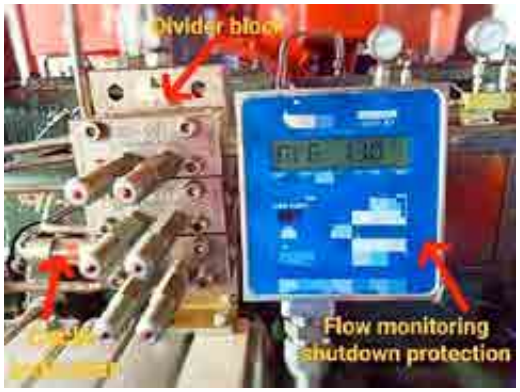

Figure 18: Flow monitoring Shutdown Protection

In the event of pump failure or change in the lube oil delivery rate, the device alerts the opeartor by displaying the changed cycle time on the LCD display. The device initiates compressor shut down via electronic instrument control panel in case lubrication rate drops below set trip limits, thereby preventing damage to the compressor internals. The device also allows data to be retrieved and analyzed using the OEM's USB-IR adaptor and Assist software.

3.3.7 Lube Sentry Valve Shutdown protection in Worthington compressors divider block system

The pneumatic Lube Sentry Valve (ref. fig. 19) which is a simple, compact unit, is installed in the main lube line between the lube pump and the divider block in our worthington compressors because these have penumatic instrument control panels. The valve provides automatic warning and shutdown of compressors via pneumatic control panel when oil is not flowing properly to divider block. It consists of two separate units - an actuator and a 3-way pneumatic valve on the Pneumatic Lube Sentry assembly. Absence of check valves in this piece of accessory helps avoid trapping contamination from inadvertenly included solid particles in the lube oil.

by: Amarish Kamalapuri, Prateek Baruah – OIL INDIA



Figure 19: Pneumatic Lube Sentry Valve

4. Challenges

4.1 The challenge to adapt the workforce to the new technology

Any industry, introducing new equipment or a system in its operation, faces its biggest hurdle while acclimatising its workforce to the new operating scenario. Operation, maintenance and instrumentation crew as well as concerned engineers of the company, were given extensive hands on training at all the upgraded lubrication system compressor locations to acquaint them with the new system, so that efficient operation and prompt trouble shooting can be applied. (Ref. fig. 20)



Figure 20: Onsite hands on training

4.2 Challenges and teething problems during and after the upgrade to the new technology

4.2.1 Physical replacement of old lubricator box with new one

Ref. fig. 21, our team took up the challenge to accurately fabricate lube box supporting plates with in-house welding-cutting infrastructure to perfectly place the new box to match it with the drive-end coupling.



Fig 21: Lubricating Box support plates fabricated

4.2.2 Preventing POPR released lube oil loss

The challenge was overcome innovatively as already explained in section 3.3.2 above.

4.2.3 Teething problem - Compressor Shutdown due to Airlock in new system

The challenge was overcome by procurement of purging gun from OEM and imparting the technical know-how to the workforce to resolve the airlock issues. Ref. fig. 22, the challenge was to make the workmen proficient at this job and ensuring proper procedure, like holding of the purge gun vertcially to prevent inadvertant air flow and ensure lube oil flow.

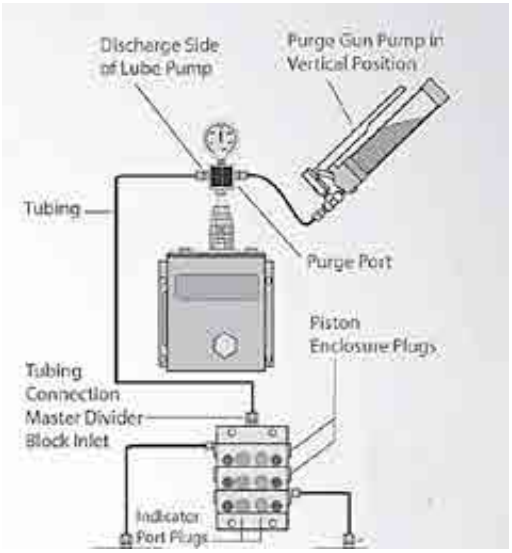

Figure 22: Use of purge gun to resolve lubricating system airlock

4.2.4 Lubrication no flow shutdown due to debris accumulation in Pump and filter

As usually seen with such mechanical upgrades, minute foreign particles and debris accumulation made some of the new pumps faulty and also filters were clogged. The same was easily overcome via thorough cleaning, servicing /replacement of the affected compoenents.

by: Amarish Kamalapuri, Prateek Baruah – OIL INDIA

4.2.5 Adjusting of balance valves

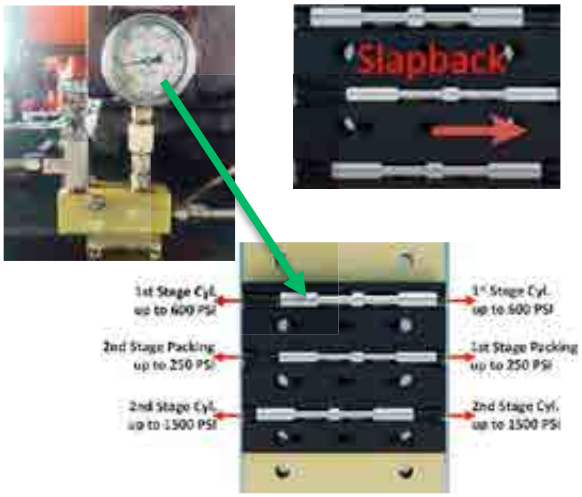

Fig. 23 (A, B & C): balancing valve with pressure gauge preventing divider valve piston slap back

When lube oil is injected into high pressure cylinder, excessive system pressure may cause divider valve piston **slapback** in which the pistons become out of sync preventing lube oil delivery to injection points. Adpating the workforce in proper adjustment of the balance valves installed downstream of the divider block was a challenge as it was required to ensure smooth movement of the pistons reducing wear and tear in the divider valves. (Ref. Fig 23 A,B & C).

The adjustment of any balancing valve, which is essentially a pressure relief valve, is based on the requirement of lube oil pressure at its downstream injection point, which in turn must be higher than the maximum gas pressure to be encountered in the injection point (which is the key parameter to be monitored during the valve adjustment). For example, suppose we require lube oil injection at 1200 psig at one compressor's 2nd stage cylinder. If the lubricating box's main oil pump is developing a pressure of 2000 psig and the pressure gauge installed on the "balancing valve assembly" is showing a pre-set pressure of 800 psig, then we need to rotate the balancing valve stem clock-wise to increase the pressure downstream of it to beyond 2000 psig. The pressure gauge on the "balancing valve assembly" helps by showing the exact pressure at which the balancing valve is allowing the lube oil to flow to the injection point. Counter-clock wise rotation of the valve stem can reduce the downstream lube oil injection pressure as per requirement.

5. Benefits obtained

Since introduction of divider block system which replaced the pump to point regime, we have been benefited in the following ways till the end of 2022 (Ref. Charts 1 - 6) below:

5.1 Benefits in Worthington Compressor

We introduced Divider Block system in a fleet of 17 nos. Worthington Compressors at the start of 2020. We are displaying the direct financial benefit by comparing 3 year "before-after" periods of this upgradation job:

***Chart 1**: Worthington Compressor Breakdown maintenance cost comparison of 2 periods – 3 years since introduction in 2020 and a 3 years period prior to the upgrade*

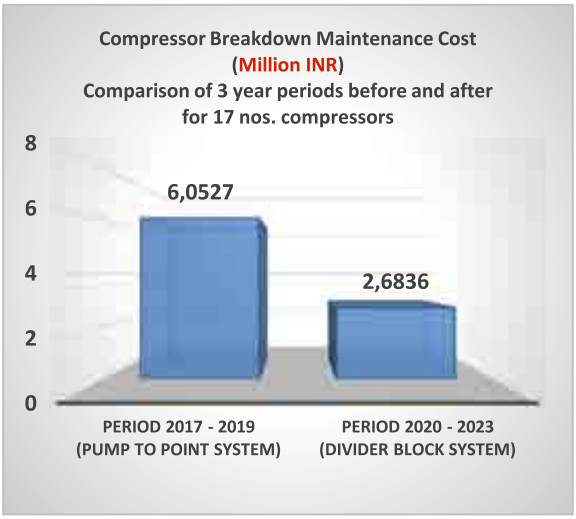

***Chart 1(A):** Worthington Compressor Breakdown maintenance cost comparison (due to lubrication system failures only) of 2 periods – 3 years since introduction in 2020 and a 3 years period prior to the upgrade*

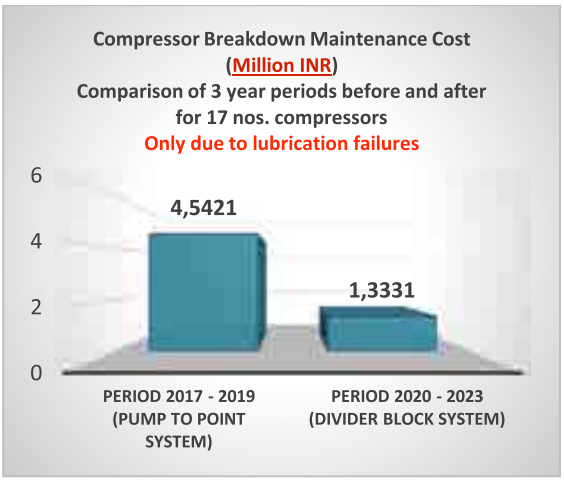

by: Amarish Kamalapuri, Prateek Baruah – OIL INDIA

Chart 2: *Worthington Compressor Breakdown maintenance cost comparison of 2 periods – 3 years since introduction in 2020 and a 3 years period prior to the upgrade job (Period Comparison vis-a-vis* ***average spares cost per Unit***

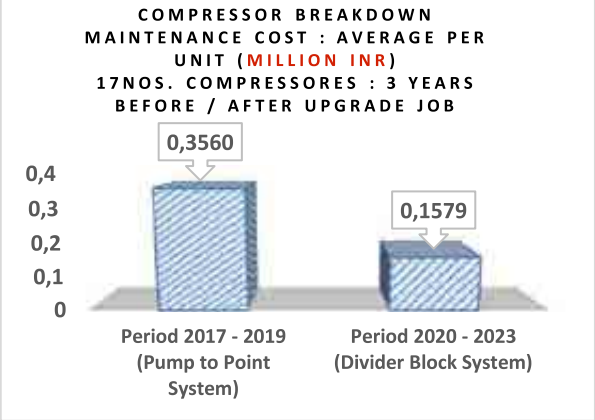

Chart 2(A): *Worthington Compressor Breakdown maintenance cost comparison (due to lubrication system failures only) of 2 periods – 3 years since introduction in 2020 and a 3 years period prior to the upgradation (Period Comparison vis-a-vis* ***average spares cost per Unit***

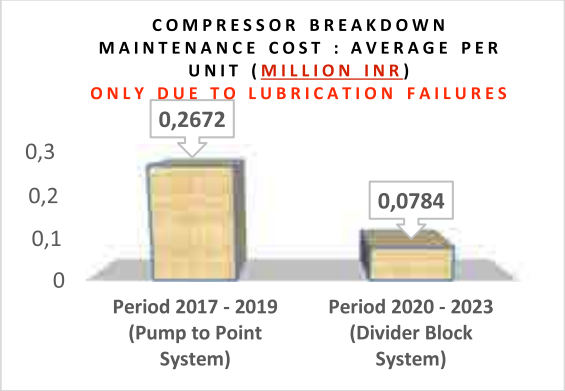

5.2 Benefits in BPCL Compressors

In case of our fleet of Indian make BPCL compressors, we carried out the upgrade job in 3 phases.

During the **first phase**, we upgraded the lubrication system in 3 Gas compressors at the start of 2013. Hence, we are comparing a 6 year "before-after" period of this upgrade to see how we got benefitted by this advanced form of lubrication:

Chart 3*: BPCL Compressor (**1st phase**) Breakdown maintenance cost comparison of 2 periods – a 6 year period since introduction in 2013 and a 6 year period prior to the upgrade*

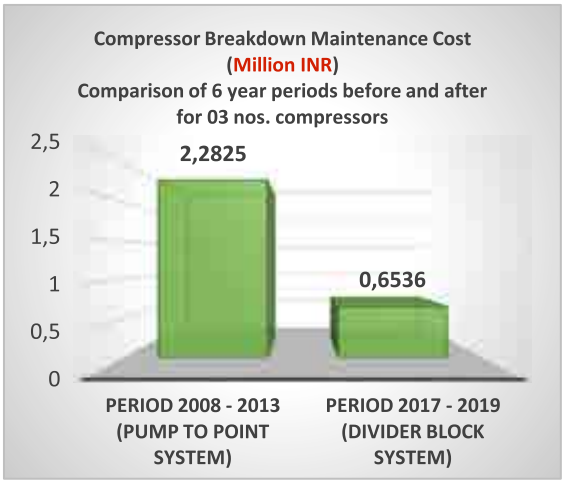

Chart 3(A)*: BPCL Compressor (**1st phase**) Breakdown maintenance cost comparison (due to lubrication system failures only) of 2 periods – a 6 year period since introduction in 2013 and a 6 year period prior to the upgrade*

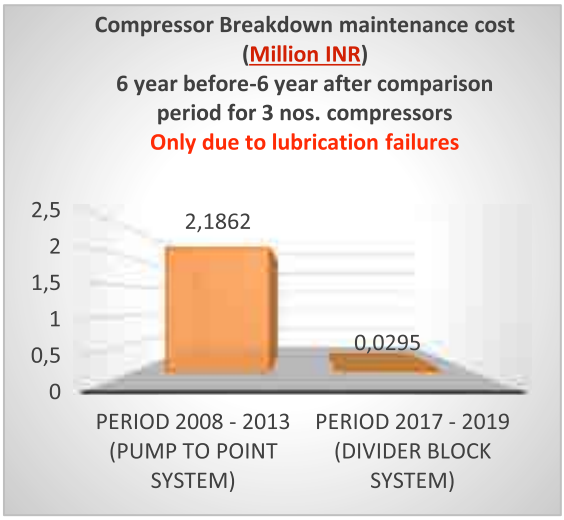

During the **2nd phase**, we upgraded the lubrication system in 5 BPCL Gas compressors during 2016. Hence, we are comparing a 6 year "before-after" period of this upgrade job to see how we got benefitted by this advanced form of lubrication:

by: Amarish Kamalapuri, Prateek Baruah – OIL INDIA

Chart 4: *BPCL Compressor (**2nd phase**) Breakdown maintenance cost comparison of 2 periods – a 6 year period since introduction in 2016 and a 6 year period prior to the upgrade*

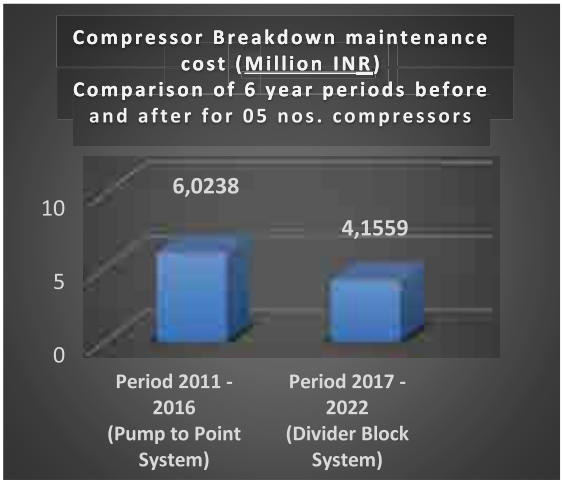

Chart 5: *BPCL Compressor (**3rd phase**) Breakdown maintenance cost comparison of 2 periods – a 4.5 year period since introduction in June 2018 and a 4.5 year period prior to the upgrade*

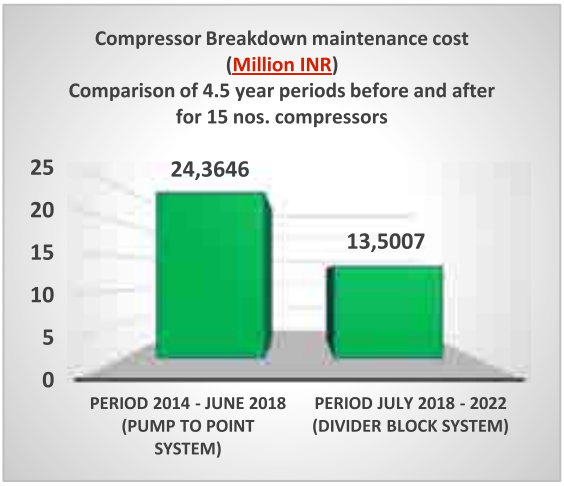

Chart 4(A): *BPCL Compressor (**2nd phase**) Breakdown maintenance cost comparison (due to lubrication system failures only)of 2 periods – a 6 year period since introduction in 2016 and a 6 year period prior to the upgrade*

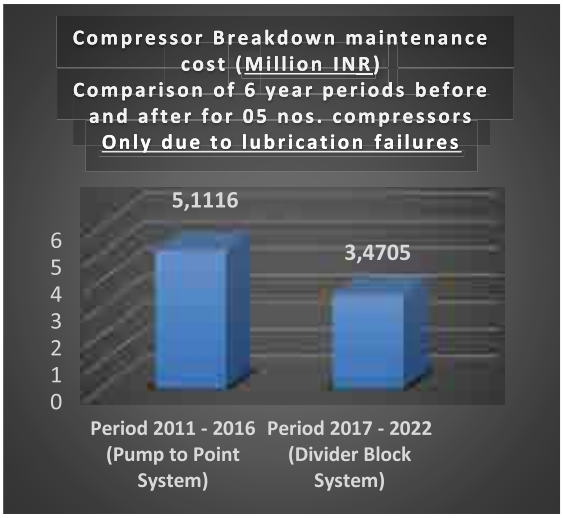

Chart 5(A): *BPCL Compressor (**3rd phase**) Breakdown maintenance cost comparison of 2 periods (due to lubrication system failures only) – a 4.5 year period since introduction in June 2018 and a 4.5 year period prior to the upgrade*

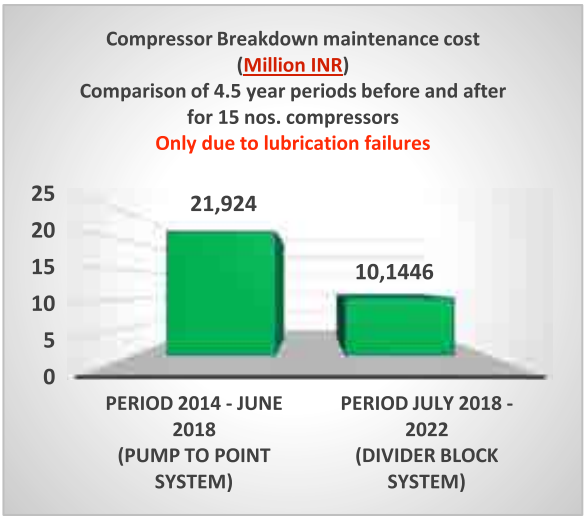

Bolstered by the benefits derived from these 2 phases, we decided to go ahead to carry out the upgrade job in 15 nos. BPCL compressors during the **3rd and final phase** of the upgrade job. We installed the divider block lubrication system in the said 15 nos. Gas compressors during June 2018. Hence, we are comparing two 4.5 year "before-after" periods vis-a-vis this upgrade to see if we could really continue the trend of reaping the benefits from this new system:

by: Amarish Kamalapuri, Prateek Baruah – OIL INDIA

Chart 6: *Compressors which were upgraded to divider block system, showing a significant cumulative drop in number of breakdown reports* ***(which include breakdown due to teething problems of the new system)***

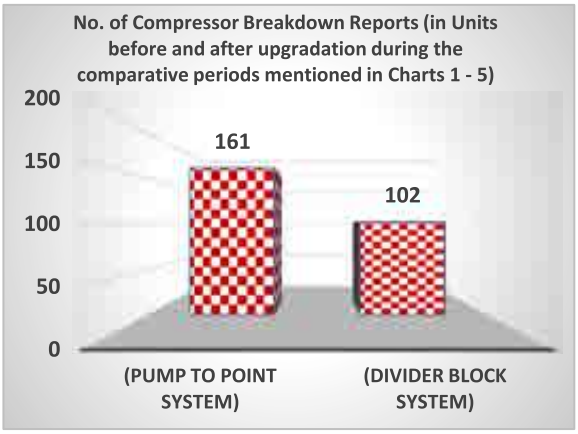

Chart 6(A): *Compressors which were upgraded to divider block system, showing a significant cumulative drop in number of breakdown reports(due to lubrication system failures only)* ***(which include breakdown due to teething problems of the new system)***

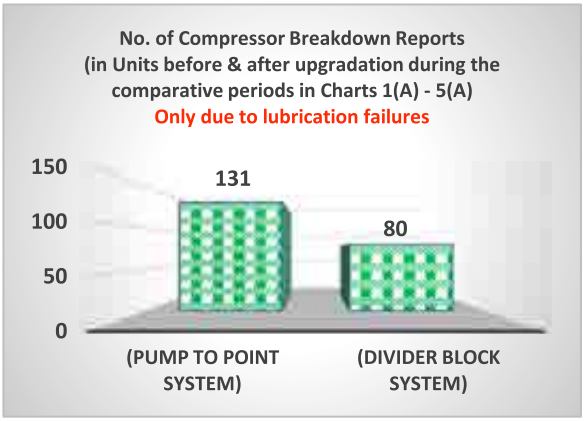

5.3 Benefits in Nominal Working Condition of the Plant

The gas compressor packages installed with divider block lubrication system displayed remarkable enhancement in reliability as illustrated above. We could drastically reduce the requirement of no. of pumps as the new lubrication system requires a smaller lubricator with one or two pumps only. As the output of the divider block is a true measurement of the quantity of oil being delivered to the compressor, we could determine the quantity of oil delivered just by using the right divider valve for the right component/stage/cylinder. Incorporated with a plethora of safety and monitoring devices as detailed in Section 3.3, we could drastically reduce compressor downtime.

Quantifying the reduction of downtime and going down to the level of Units, we have picked up two Worthington Compressors upgraded to Divider Block technology during the middle part of year 2020. Hence, considering Shutdown hours of both the Units in the FY prior and after the upgrade job, we find the following tabulated figures:

Table 3: Compressor Downtime Comparison (LPB)

GCS Jorajan / Unit No. LPB-3 **(WT)**	Running Hours	Stand By Hours	Total Shutdown Hours	Shutdown Hours due to Lubrication related failures
FY'19-20	4208	3888	688	355
FY'21-22	4120.5	4268	371.5	96

Table 4: Compressor Downtime Comparison (GL)

GCS Jorajan / Unit No. GL-2 **(WT)**	Running Hours	Stand By Hours	Total Shutdown Hours	Shutdown due to Lubrication related failures
FY'19-20	7215	1089.5	455.5	240
FY'21-22	6500.5	2023.5	236	72

In our Company, record keeping of shutdown periods as well as lube oil consumption comes under the domain of compressor operation section. However, the same is shared to us (maintenance section) periodically. Reduction of downtime, has been observed in all the divider block upgraded Units as detailed for the randomly selected Units above (Ref. Table 3 and 4).

6. Conclusion

Charts in section 5 above clearly depict the following financial advantages for the divider block system:

i) Breakdown maintenance cost in our Worthington Compressors reduced by **55.66%** when a 3 year period was considered for assessment for 17 compressors. (ref. Chart 1), whereas ref. Chart 1(A), if we consider only lubrication failure related/induced maintenance costs, then we observe a cost reduction of **70.65%**.

ii) Via the first phase of divider block upgrade in our BPCL compressors, we obtained a breakdown maintenance cost reduction of **71.36%** when a 6 year before-after period was considered for evaluation for the 3 compressors (ref. Chart 3), whereas ref. Chart 3(A), if we consider only lubrication failure related/induced maintenance costs, then we observe

by: Amarish Kamalapuri, Prateek Baruah – OIL INDIA

a cost reduction of **98.65%**, which depicts that the failures due to lubrication related issues reduced to bare minimum in these Units.

iii) In case of our second phase of divider block upgrade in BPCL compressors, we got benefitted by a **31.01%** reduction in breakdown cost when a 6 year "before – after" upgrade timeline was considered for estimation for 5 compressors (ref. Chart 4 above), whereas ref. Chart 4(A), if we consider only lubrication failure related/induced maintenance costs, then we observe a cost reduction of **32.11%.**

iv) These upgrade projects already provided us immense benefits, however, our 3rd phase of upgrade in 15 nos. BPCL compressors provided a humongous benefit of approx. 10.86 million INR (ref. Chart 5) in a 3 year comparison period, which is **44.59%** less than the earlier system. Again, ref. Chart 5(A), if we consider only lubrication failure related/induced maintenance costs, then we observe a cost reduction of **53.73%.**

The above mentioned financial advantages vindicate our stance that, not just in terms induction of an advanced technology and upskilling the workforce, we have provided our company with increasing financial benefits as we kept on upgrading to divider block technology. It is highly noteworthy that, not just in terms of spares cost, the reduction of number of reports (ref. Chart 6 and 6-A) in upgraded compressors located in far flung installations have helped to reduce company's vehicle mileage, reduction of man hours, manpower remuneration / overtime expenditure and most importantly aided in sustaining production apart from reduction of avoidable gas flaring in those installations, **a few details of which shall be presented in the presentation due to space constraint in this paper**.

With deep roots in history, OIL has been proactively working on introduction of advanced technology to sustain itself in the future. Introduction of Divider Block Lubrication System in Gas Compressor Packages of Oil India Limited has significantly improved the reliability of the packages and this is always the sole aim of any reciprocating compressor maintenance group.

7. Acknowledgements

The authors sincerely thank Mr. Sumitra Goswami, Chief General Manager and H.O.D – GMS Dept (OIL) and Compressor Maintenance Section (GMS) for their invaluable assistance throughout this endeavour.

8. References

1. https://www.oil-india.com/
2. https://www.cpicompression.com/products/lubrication/divider-blocks
3. Technical Paper titled *New concept lubrication system application on a HP reciprocating compressor* presented in 11th Conference of the EFRC September13th / 14th, 2018, Madrid (by Marco Sacco, Pamela Tani, Massimo Maffeis and Alessio Scialpi) [Cited for acquisition of knowledge only on the relevant topic]

Table of Figures:

Figure 1: *Pump to Point Lube simple schematic,* ***Page 2***
Figure 2: *Pump to Point Lubricator Box,* ***Page 2***
Figure 3: *P to P Lube Box with many pumps,* ***Page 3***
Figure 4: *P to P Lube Box with leakage,* ***Page 3***
Figure 5 (A & B): *P to P Lube Box servicing,* ***Page 3***
Figure 6: *Lubricating pump in P to P System,* ***Page 3***
Figure 7: *Divider Block System View & Schematic,* ***Page 4***
Figure 8: *Divider Block : Exploded View,* ***Page 5***
Figure 9: *Divider Block functioning:* ***Step 1****,* ***Page 5***
Figure 10: *Divider Block functioning:* ***Step 2****,* ***Page 5***
Figure 11: *Divider Block functioning:* ***Step 3****,* ***Page 5***
Figure 12: *Divider Block functioning:* ***Step 4****,* ***Page 5***
Figure 13: *Indicator Pin Out, showing root cause,* ***Page 6***
Figure 14(A&B): *POPR and return line to Sump,* ***Page 6***
Figure 15 (A&B): *Cycle Indicator – Cycle Time,* ***Page 6***
Figure 16 (A&B): *Check Valve with Protector,* ***Page 7***
Figure 17: *In-line filter downstream of lube pumps,* ***Page 7***
Figure 18: *Flow monitoring Shutdown Protection,* ***Page 7***
Figure 19: *Pneumatic Lube Sentry Valve,* ***Page 8***
Figure 20: *Onsite hands on training,* ***Page 8***
Figure 21: *Lubricating Box support plates fabricated,* ***Page 8***
Figure 22: *Use of purge gun to resolve airlock,* ***Page 8***
Figure 23: *(A, B & C): Balancing valve with pr. gauge,* ***Page 8***
Table 1: *Lube Oil Pump Units malfunction comparison,* ***Page3***
Table 2: *Lube Oil Consumption Comparison,* ***Page 4***
Table 3: *Compressor Downtime Comparison (LPB),* ***Page 11***
Table 4: *Compressor Downtime Comparison (GL),* ***Page 11***
Chart 1: *Worthington (**WT**) Cost Comparison (**C/C**),* ***Page 9***
Chart 1A: ***WT*** *(**C/C**), (Only Lube. fail),* ***Page 9***
Chart 2: ***WT*** *(**C/C**), Average Spares Cost,* ***Page9***
Chart 2A: ***WT*** *(**C/C**), Average Spares Cost for Lube fail,* ***Page 9***
Chart 3: *BPCL 1st Phase Cost Comparison (**C/C**),* ***Page 10***
Chart 3A: *BPCL 1st Phase **C/C** (Only Lube. fail),* ***Page 10***
Chart 4: *BPCL 2nd Phase Cost Comparison (**C/C**),* ***Page 10***
Chart 4A: *BPCL 2nd Phase **C/C** (Only Lube. fail),* ***Page 10***
Chart 5: *BPCL 3rd Phase Cost Comparison (**C/C**),* ***Page 11***
Chart 5A: *BPCL 3rd Phase **C/C** (Only Lube. fail),* ***Page 11***
Chart 6: *Breakdown Report Comparison,* ***Page 11***
Chart 6A: *Breakdown Comparison, Only Lube. Fail,* ***Page 11***

PROGNOST
INTELLIGENCE ON DUTY

Part of the Burckhardt Compression Group

Impact versus Impact – Comparison of different filter modes for vibration measurement

by:

Jan Löken
Customer Support
PROGNOST Systems GmbH
Rheine, Germany
jan.loeken@prognost.com

13th EFRC CONFERENCE
September 19th – 21st 2023, Zagreb

Abstract:
Root cause analysis, impact detection and verification for reciprocating machinery such as piston and hyper compressors are always challenging. When talking about condition monitoring of reciprocating machines, vibration signals are an integral element used for monitoring of different components, such as crosshead, valves, frame, etc. Analysing vibration signals is a challenge for each monitoring system, and analysts needs to be aware of the filter configuration to take the right conclusion for proper action. The goal is to minimize nuisance alarms and maximize the capability of early (automatic) failure detection. Filtering a vibration signal helps to avoid noise, but on the other hand it should be set in the right way to indicate problems and not conceal them. For the right procedure, filtering, and protection limit adjustment always must be considered together.
In the paper, signal analysis considerations and their consequences for failure detection will be explained, such as filtering, analysing RMS vs. Zero-to-Peak, Good vs. Bad condition, etc..
The paper introduces the theoretical background proven by real-life case studies as an add on the publication of Dr. Eisenmann and Mr. Franz[3]. It is showing different failures on crossheads, piston/plunger, and valves.

by: Jan Löken – PROGNOST

1 Introduction

History has shown that within the fleet of reciprocating compressors numerous catastrophic failures result in significant losses. Although adequate machinery protection systems are available, they are not always in place or applied correctly to avoid catastrophic failures.

Numerous case studies with several different failure modes identify that appropriate frequency filter setting have major impact on the machinery protection system´s ability to function as needed when critical conditions arise. Additionally, the application of RMS-based analysis instead of peak-analysis is also discussed.

This article discusses the most important aspects to consider when implementing machinery protection systems using crosshead acceleration and frame velocity on reciprocating compressors – specifically:

- Requirements and the Frequency Filter Setting Challenge
- Signal analysis consideration – Filter Setting / RMS / Peak
- Crosshead acceleration – Why - Where applied – Effective analysis approach
- Frame velocity – Why - Where applied – Effective analysis approach
- Conclusion

Knowledge surrounding proper low pass filter settings for acquisition systems performing critical shutdown function is very limited and often misapplied. This paper illustrates why the common practice of setting low pass signal filters at 2 kHz introduces risk that serious failure modes go undetected compromising plant safety, health, and the environment.

Which frequency range should be used for the low pass filter for crosshead guide acceleration to provide the earliest and best representation of the compressor health? Figure 1 is an example of crosshead guide acceleration data from 0-7 kHz during an event showing what data would be missed if only 0 - 2 kHz verse 0 - 7 kHz are used.

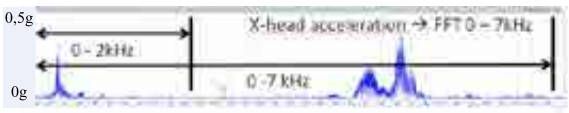

Figure 1: Crosshead guide acceleration data from 0-7 kHz during an event (in "g").

In the case studies investigated, we can conclude that frequency filter setting is vital in detecting failure modes such as wrist pin seizures, developing cracks in pistons and piston rods.

2 Signal Analysis Considerations

2.1 RMS

Modern machinery protection systems apply a fully continuous online RMS analysis of focus signals such as crosshead acceleration and velocity. This is a beneficial approach specifically on reciprocating compressors where an early indication of damaging impacts is of the essence and RMS values are best to describe the energy within a given signal as calculated by the equation in figure 2.

$$x_{\mathrm{rms}} = \sqrt{\frac{1}{n}\left(x_1^2 + x_2^2 + \cdots + x_n^2\right)}$$

Figure 2: RMS value for an evaluation period represented by a number of "n" data samples is the square root of the arithmetic mean of the squares of the "n" values.

While the proper representation of contained energy is a positive factor, there is a risk that individual, high data samples get lost in the average. This is specifically the case if the number of total samples "n" in the evaluation period is high e.g., when the X_{rms} equation above is evaluated over one entire revolution of the rotating machine or one second eventually containing hundreds or thousands individual data samples. Furthermore, the reliable RMS computation and alarming in real time requires modern, redundant CPUs to handle this significant processor workload eventually occurring on multiple sensor channels in parallel.

2.2 Zero-to-Peak analysis

Some systems take a different path by employing Zero-to-Peak (Peak) analysis instead of RMS. This addresses the effect that RMS analyses may undervalue high individual samples when evaluation periods are relatively long (e.g., 1 compressor revolution or 0.2 sec @ 300 rpm) and compares maximum values detected in that period against a set of Alert and Shutdown limits.

Unfiltered peak analysis however leaves users vulnerable for nuisance alarms, e.g., caused by isolated, high frequency events, non-repetitive signal spikes and sensor glitches.

In order to address these nuisance alarms some users apply a low pass filter (e.g., @ 2 kHz) so only the 0-2 kHz frequency content is analysed for its peak vibration content.

While the above strategy reduces nuisance alarms when using peak analyses, it also eliminates capability to detect many critical failure modes containing majority damaging energy in higher frequency ranges as will be discussed next.

by: Jan Löken – PROGNOST

2.3 Crosshead - Acceleration Sensors

Looking at the working principal of reciprocating compressors the crosshead clearly is a focal point. Here, the rotating movement of the crankshaft is transformed into a reciprocating (linear) movement of the piston rod. It is the central component where the major drive forces are transferred from the running gear to the crosshead and ultimately the piston rod assembly. To contain these forces into the right direction, the crosshead travels within the crosshead guide. The crosshead guide is the most direct connection of the running gear to the frame/crosshead guide and therefore is the best position to install vibration sensors. Therefore, API 670[1] – (Annex P.4.3.4.4) recommends that crosshead accelerometers should be mounted in the vertical direction on the top or bottom of the crosshead guide as shown in Figure 3. API 670[1] also stats that a monitoring system should be capable to monitor at least 2 kHz, with the add on "up to 7 kHz", which is useful in many cases (Chapter 3).



Figure 3: Proper placement of crosshead accelerometers – ideally these are installed vertically, external to the loaded crosshead shoe.

2.4 Frame - Velocity Sensors

The reciprocating compressor frame and crosshead guides are the stationary components anchored to the foundation to retain the compressor during operation. The frame/foundation is subjected to the normal unbalanced forces and moments from the reciprocating compressor inertial and gas loads as well as forces experienced during failure events. Transducers placed on the corners of the frame in the horizontal and/or vertical direction are used to detect issues with the support structure/foundation. Transducers mounted in the horizontal direction directly opposing each throw are used to detect impacts and mechanical issues. API 618[2] also identifies high frame vibration as alarm and shutdown parameter but does not fully define what should be provided. API 670[1] clause P4.3.4.2 and P4.3.4.3 identify the recommendations of frame monitoring and running gear monitoring respectively.

In many cases the acceleration sensor on the crosshead detects machine issues earlier like a frame velocity sensor, therefore following chapters focus on acceleration monitoring and filtering. Anyhow the velocity sensor is important as an additional information about low frequency vibrations at the machine and notable in this paper.

3 Practical examples and case study material for acceleration signals

3.1 Seized Wrist Pin

During the commissioning and start-up of a new API 618[2] compressor in H2 service the machine was suddenly tripped by the machinery protection system. A first data review revealed that crosshead acceleration amplitudes reached the default protective limits having saved the asset from consequential damage or loss of containment. During a detailed analysis of the high-resolution data available this first case study is an excellent example illustrating the importance of high frequency (0-7 kHz) data for effective machinery protection with crosshead acceleration sensors.

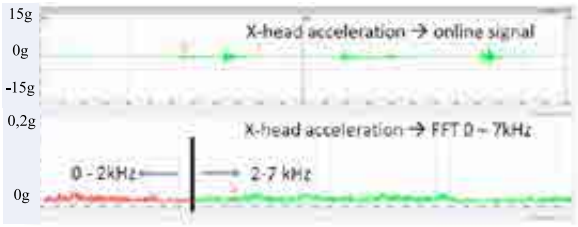

Figure 4: Good condition signal – Top: time-waveform, online signal (0-7kHz) Bottom: Spectrum 0-7kHz

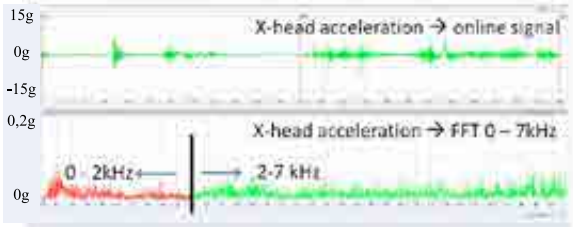

Figure 5: Bad condition signal – Top: time-waveform, online signal (0-7kHz) Bottom: Spectrum 0-7kHz

The wrist pin seizures detected did not involve true mechanical impacts typical of loose components (showing lower frequency content primarily below 2 kHz). Comparison of Figure 4 "Good Condition Signal" to Figure 5 "Bad Condition Signal" shows most of the failure related energy as well as relative signal change has higher frequency content above 2 kHz. To initiate the trip function prior to a catastrophic failure and potential loss of containment the full 0-7 kHz frequency spectrum suggested by API 670[1] must be monitored.

3.2 Failed Piston Rod

A broken piston rod is potentially one of the worst-case failure scenarios for a reciprocating compressor. Detecting this critical failure mode timely and accurately is very important.

by: Jan Löken – PROGNOST



Figure 6: Fragments of the piston rod thread region. Top view of the failed piston rod thread region.

This end user suddenly experienced increased crosshead acceleration impacting which ultimately lead into an automatic shutdown of his protection system. The maintenance team found the piston rod failed within the thread region connecting the piston rod and crosshead as shown in Figure 6. This second case offers additional insights regarding the importance of proper frequency filter settings.

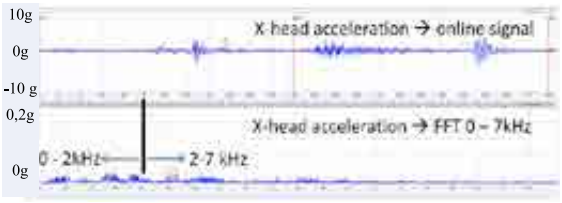

Figure 7: Good condition signal – Top: time-waveform, online signal (0-7kHz) Bottom: Spectrum 0-7kHz

The online vibration and spectral data shown in Figure 7 represents a very characteristic crosshead acceleration signal of a reciprocating compressor with some limited vibration around the rod load reversal points and little to no energy content visible in the higher frequency section within the FFT spectrum.

Please note that those data plots following now titled with "bad condition" represent data from the revolution when the machine was automatically tripped by the machinery protection system. Before that the vibrations increased over time.

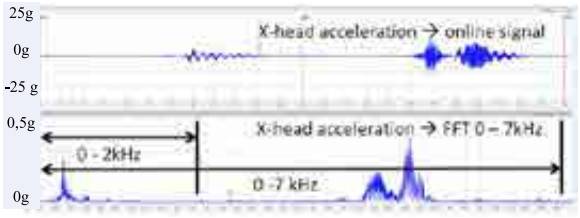

Figure 8: Bad condition signal – Top: time-waveform, online signal (0-7kHz) Bottom: Spectrum 0-7kHz

As shown in Figure 8 a true amount of energy was found between 4 – 5 kHz which made us apply different frequency filters to determine how important the appropriate filter setting really is to detect a case like this effectively.

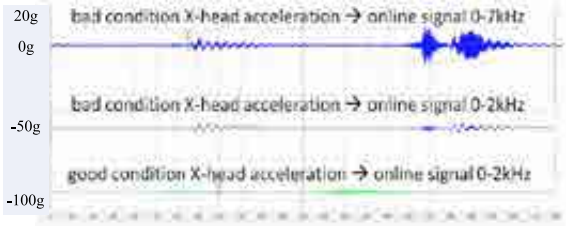

Figure 9: 360°crank angle online signals applying different filters 0-2 kHz and 0-7 kHz under good and bad condition.

When comparing the "good" (Figure 9 bottom) vs "bad" (Figure 9 middle) 0-2 kHz the measured online signals differ not much, and a machinery protection system would have missed this critical failure if the signal does not exceed and alarm or trip level.

The failure however becomes obvious inside the online data set "bad" at 0-7 kHz (Figure 9 top) which shows a significantly different picture and lot of energy around 270° crank angle (CA) and 300°CA not visible in the "bad" 0-2 kHz filtered online data (Figure 9 center).

This failing piston rod was automatically detected using a 36 segmented RMS analysis of the crosshead acceleration signal using the full signal bandwidth (in this case 0-10 kHz).

It subdivides each revolution in smaller segments (e.g., 10-degree crank-angle wide increments) each with a dedicated protection limit. Areas with naturally higher vibration levels within each revolution (e.g., rod load reversal points) get the appropriate focus and at the same time solid ten-degree averages eliminate isolated spikes in each segment.

While we have discussed the basics of RMS vs. Peak analysis in a previous chapter, a 36 segmented RMS

by: Jan Löken – PROGNOST

vibration analysis combines the best of both approaches.

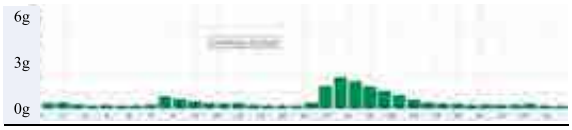

Figure 10: Good Condition 0 – 7 kHz RMS 36 segmented analysis

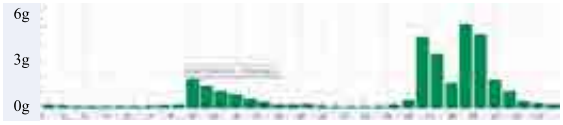

Figure 11: Bad Condition 0 – 7 kHz RMS 36 segmented analysis

Reviewing data plots of Figure 10 and Figure 11 above the effectiveness of this approach becomes apparent. Segments 27-33 (270 – 330°CA) show a massive increase in amplitude for 0-7 kHz – some by more than factor 10.

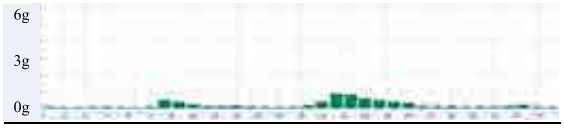

Figure 12: Good Condition 0 – 2 kHz RMS 36 segmented analysis

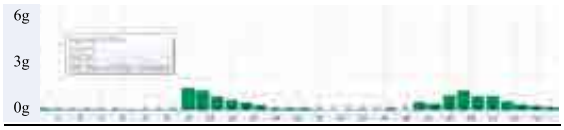

Figure 13: Bad Condition 0 – 2 kHz RMS 36 segmented analysis

However, even when applying a sophisticated analysis like the 36 segmented RMS analysis it should include higher frequency data. Figures 12 and 13 represent data employing a 2 kHz low pass filter. Between good (Figure 12) and bad condition (Figure 13), a much lower relative change in amplitude is found – and while under good condition worst acting segments show around 1g – values only increased to 1.3g as the piston rod cracked due to the fact that the majority of failure related energy is filtered out and not part of the evaluation.

4 Conclusion and Recommendations

The latest additions to API 670[1] provide valuable information for machinery protection on reciprocating compressors. Specifically, the addition of crosshead acceleration is essential, and users should take care employing this powerful protection parameter at its best capacity. As we have demonstrated certain failure modes show majority of energy at higher frequencies (e.g., 4 - 7 kHz). This is why we suggest following API 670[1] and employ full signal bandwidth 0 – 7 kHz ideally combined with a segmented RMS analysis – this way repetitive impacts are not missed at critical stage and RMS based segments represent a solid (e.g., 10°crank angle) weighted average, and single isolated signal spikes do not lead to nuisance alarms, which may occur using unfiltered peak analysis.

Modern machinery protection systems employing crosshead acceleration sensors in the first place and frame velocity as an additional layer of protection per recommendations provided within this paper will help detecting many critical failure modes in an early stage preventing catastrophic failures.

References

[1] API Standard 670, 5th Edition, November 2014 – Machinery Protection Systems

[2] API Standard 618, 5th Edition, December 2007 – Reciprocating Compressors for Petroleum, Chemical and Gas Industry Services

Citations

[3] Paper based on “Why proper low-pass filter settings on crosshead vibration signals are crucial to minimize risk of missed detects”, Turbomachinery and Pumps Symposia 2016, Presentation by Oliver Franz and Bob Eisenmann

PULSATION & VIBRATION

Effect on Pulsation and Vibration Mitigation Measures when Adjusting a Natural Gas System to Hydrogen Mixtures
by: André Eijk – INDEPENDENT CONSULTANT *173*

On solving torsional vibration problems of reciprocating compressor systems
by: David Richter-Trummer, Andreas Thalhammer, Thomas Bozezki – GEISLINGER *185*

Optimizing the torsional vibration behavior of reciprocating compressors using a flywheel-integrated damper concept
by: Sebastian Willeke, Stephan Bohmeyer, Norbert Reinsperger and Michael Steidl – HASSE & WREDE *195*

Green hydrogen can also pulsate – Successful use of a Helmholtz resonator
by: Johann Lenz; Franz-Josef Düttmann – KÖTTER CONSULTING *206*

Pulsation control for a multi-purpose underground storage reciprocating compressor system (natural gas, hydrogen and mixed gas)
by: Leonard van Lier – TNO; Olivier Bore – STORENGY *214*

Improved plant reliability due to acoustical and vibrational optimisation
by: Patrick Tetenborg, Christian Jansen – JANSEN + TETENBORG *225*



BORSIG

Process Gas Compressors.

BORSIG ZM Compression GmbH.





→ API 618 reciprocating compressors

- horizontal and vertical design
- long service life, high wear resistance durability, low life-cycle costs

power ranges:
p= (... 1,000) bar
V= (... 115,000) m³/h
P= (21,000) kW

hydrogen applications

- transport of H_2
- storage of H_2
- refuelling of heavy-duty vehicle fleets

Think. Create. Change.

BORSIG ZM Compression GmbH is one of the leading manufacturers for tailored compressor solutions.

Every compressor is a product of our integrated approach – from planning and assembly to comprehensive services.

- reciprocating compressors
- integrally geared centrifugal compressors
- compressor services

Key technologies for the compression of hydrogen and other process gases have been part of our product portfolio for many years. Based on decades of experience, we offer the machines necessary for the compression of hydrogen and hydrogenous gases in various sizes and designs.

With our tailor-made solutions for reciprocating and turbo compressors we are well prepared to meet our customers´ needs.

To learn more about our products and projects, please visit **www.borsig.de/zm**.

BORSIG ZM Compression GmbH

Effect on Pulsation and Vibration Mitigation Measures when Adjusting a Natural Gas System to Hydrogen Mixtures

by:

André Eijk
Independent Consultant
Delft, The Netherlands
andre.eijk@ziggo.nl

13th EFRC CONFERENCE
September 19th – 21st 2023, Zagreb

Abstract:
Reciprocating compressors have been used for a long time in the field of oil refining, chemical and petrochemical industries, air separation as well as gas transport and storage applications. The reciprocating compressor‘s flexibility to handle wide flow variations, and to generate a high pressure independent of the applied gas, makes it a vital component in today‘s energy markets, and must operate reliably, efficiently, and safely for long-term operation.
Hydrogen will play a key role in the energy transition and will replace natural gas in several sectors of industry. Due to the advantages of reciprocating compressors, they will also be applied in new hydrogen applications such as production, storage, or fuelling stations. Large reciprocating compressors may replace turbo compressors because turbo compressors are less efficient in compressing hydrogen due to the low molecular weight.
Hydrogen has a low caloric value per volume and larger volumes are required compared to natural gas for the same energy, so existing reciprocating compressor systems need to be redesigned and increased in size. The reciprocating compressor generates pulsations and vibrations which can lead to failures, inefficiency, flow meter errors and capacity limitations, and for those reasons the requirements as stipulated in the API 6181 shall be met. Due to the high speed of sound and low molecular weight of hydrogen, changes to pulsation and vibration mitigation measures may be required when an existing natural gas system is adjusted to hydrogen mixtures (mixture is defined as a blend of natural gas and hydrogen). This paper discusses this effect for the damper/filter design, orifice plate, side branch absorber, volumes, and pipe support layout. The effect on the design of the reciprocating compressor itself is not discussed in this paper. Despite the fact that the AVIFF (Avoidance of Vibration Induced Fatigue Failure) guidelines of the Energy Institute (EI) for process pipe work are not widely applied for reciprocating compressor systems, they will be briefly discussed to give some background information in case engineers will use them. More detailed information as discussed in this paper can be found in the book[2] “Machinery and Energy Systems for the Hydrogen Economy”.

by: André Eijk – INDEPENDENT CONSULTANT

1 Introduction

One of the disadvantages of a reciprocating compressor is that it generates pulsations and vibrations, which, without limitation and proper attention during design, manufacturing, installation, and operation, can lead to fatigue failures, inefficiency, capacity limitations and unsafe situations. Detailed procedures to control pulsations and vibrations for reciprocating compressor systems are laid down in the API Standard 618[1] and the API 688[3]. These API standards reflect a clear objective to ensure safe and efficient reciprocating compressor systems that meet capacity and power requirements. These standards are accepted worldwide by the reciprocating compressor community. However, if existing natural gas transportation or storage systems are adjusted to pure hydrogen or hydrogen mixtures, the systems must be checked on negative changes of the pulsations and vibrations. The change in pulsations and vibrations is caused by the substantial change in the speed of sound and density of hydrogen mixtures, which may lead to different pulsation and vibration amplitudes (lower or higher) and a shift in frequencies. This may require major modifications or even a redesign of the pulsation and vibration mitigation measures. However, this strongly depends on the operating conditions, the amount of hydrogen gas in the mixture and the relationship between the excitation forces and the acoustic and structural response of the system.. This must always be checked with a pulsation and mechanical response analysis as stipulated in the API 618.

2. Relation between pulsation forces and structural response

In the frequency domain as shown in figure 1, high vibration levels will occur if the frequency of the source of acoustic excitation (a) coincides with the acoustic natural frequency (b) resulting in high pulsation levels (c). This in turn must coincide with the structural natural frequency (d) to cause high vibration levels (e) at 40 Hz. However, if the structural natural frequency (d) does not coincide with the pulsation (c) at 60 Hz, there will be pulsations but only at a low level of vibration at 60 Hz (e). The amplitude of this forced vibration will be significantly lower than the resonant response of matching acoustic and mechanical natural frequencies. Furthermore, if the acoustic natural frequency (b) does not correlate with the excitation force (a), then there will be little pulsation and therefore also lower vibration levels (e) at 20 Hz. In short, the most serious vibration problems, the worst-case situation, will occur if the frequency of acoustic excitation, acoustic natural frequency, and structural natural frequency coincide. The chance of this occurring is greater for variable speed compressors.
To avoid worst-case situations, the frequency of the excitation source and acoustic and natural frequency shall be separated by a minimum of ±20%. It is noted that high levels of non-resonant vibration can also be experienced if there are significant levels of acoustic excitation present in the system.

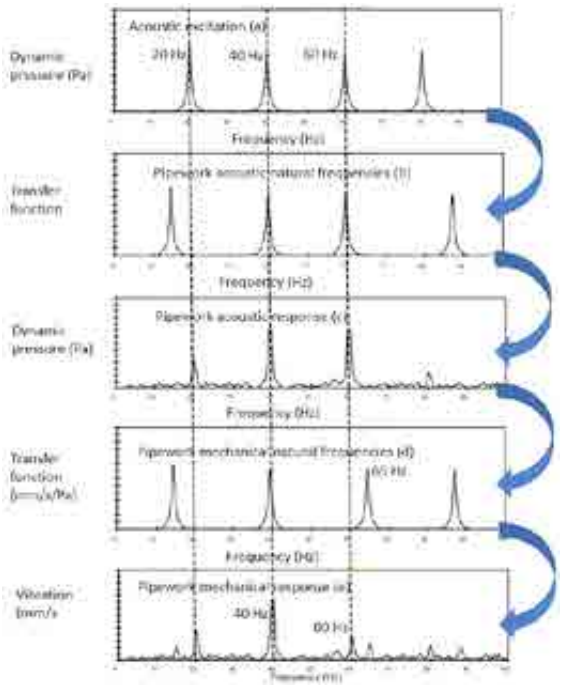

Figure 1 Example of relation between acoustic and mechanical natural frequencies and structural response (source: Energy Institute[4])

In the spatial domain, the location and phase of the dynamic forces relative to the mode shape are important. The mode shape determines the pipework's receptance of dynamic force and this means that if the dynamic force occurs at the structural nodes of vibration e.g., at a pipe support, then there will not be a vibration. On the other hand, if the dynamic force is located elsewhere and if the force and deflection of the mode are in phase, high vibration levels will occur.

In view of the above, if a system is changed to a mixture of hydrogen, the effect on pulsations and vibrations and a possible change or redesign of the mitigation measures must always be investigated with a pulsation and mechanical analysis as stipulated in the API Standard 618[1].

3 Acoustic wave theory

Some basics of acoustic theory will be discussed in this section to understand the most important effects on the pulsation and vibration behaviour when a system is adjusted to a mixture of hydrogen.

3.1 Speed of sound

One of the dominant parameters in acoustics is the speed of sound, of which the equation is given in (1). The equation for density is given in (2).

by: André Eijk – INDEPENDENT CONSULTANT

$$c = \sqrt{\frac{\gamma Z R_0 T}{M}} \quad (1) \qquad \rho = \frac{MP}{R_0 T} \quad (2)$$

where:

c speed of sound [m/s]	T absolute temperature [K]
Z compressibility factor [-]	γ isentropic constant [c_p/c_v]
M molecular weight [kg/kMol]	P static pressure [Pa]
R_o general gas constant [kJ/kMol]	ρ density [kg/m^3]

An example of the speed sound shift of hydrogen compared to natural gas is given in figure 2 for a typical suction and discharge side of a reciprocating compressor system. It can be concluded that a hydrogen mixture has a strong effect on the speed of sound. The maximum increase is approximately a factor three for 100% hydrogen which is mainly caused by the large difference in molecular weight of natural gas and hydrogen, approximately a factor three. In nearly "pure hydrogen" the results strongly depend on the exact mix, and here the system is sensitive to small fluctuations in composition.

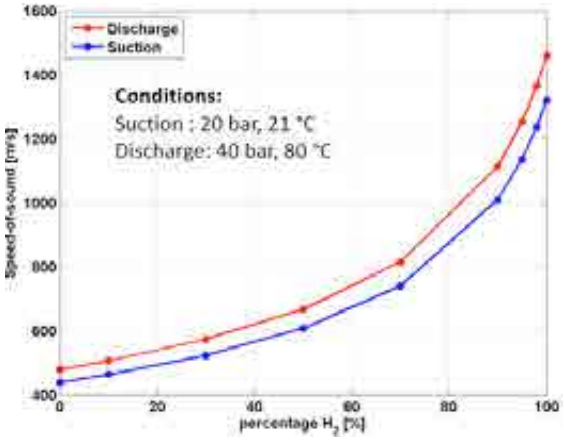

Figure 2 Speed of sound shift of hydrogen mixtures

3.2 Increased flow velocities

Hydrogen has the highest caloric value of fuels per *mass* but it has the lowest caloric value of fuels per *volume*. The ratio of the caloric value per volume of natural gas and Hydrogen is approximate a factor three. That means that to transport the same amount of energy with 100% Hydrogen, the gas velocities need to be increased by a factor three compared to natural gas. These high velocities are not foreseen in the near future due to prognosed demand and it erosion[14] may become a limiting factor.

3.3 Acoustic resonances

Due to its reciprocating action, a reciprocating compressor generates dynamic flow pulses. These flow pulses will propagate into the compressor piping system at the speed of sound. Depending on the geometry of the system and process parameters, these flow pulses may be amplified in (parts of) the system. This amplification is called an acoustic resonance and occurs when the pulsation frequency matches one of the pipe system's acoustic natural frequencies, its resonance frequencies. The acoustic resonances are described by an amplitude and frequency and two resonances can occur: standing wave and Helmholtz resonance. It is also possible that a combination of these resonances occur.

Too high pulsations (flow and velocity) can cause undesired effects such as fatigue failures, inefficiency, capacity limitations and unsafe situations of the compressor system.

3.3.1 Standing waves

A standing wave, also known as a stationary wave, is a wave that oscillates in time but whose peak amplitude profile does not move in space. The peak amplitude of the wave oscillations at any point in space is constant with respect to time and the oscillations at different points throughout the wave are in phase. The locations at which the absolute value of the amplitude is minimum are called nodes, and the locations where the absolute value of the amplitude is maximum are called anti-nodes, see also figure 3. The general equation for the standing wave is given in equation (3).

$$\lambda = \frac{c}{f} \quad (3)$$

where: λ wavelength [m]; c speed of sound [m/s]; f frequency [Hz]

The pressure and velocity (flow) fluctuations and the frequency at which this occurs, depend on the distances between acoustic boundary points (reflection points) of the pipe system e.g. volumes, closed valves, large diameter changes, etc. These typical boundary conditions can be grouped into open-open, closed-closed, and open-closed boundary conditions.

The amplitude of the pressure and velocity pulsations as a function of length for a closed-open end configuration, e.g. from a closed valve to a volume, is shown in figure 3. The first standing wave that can occur is the ¼ lambda (λ) resonance. The next one is a ¾ lambda resonance, and so on.

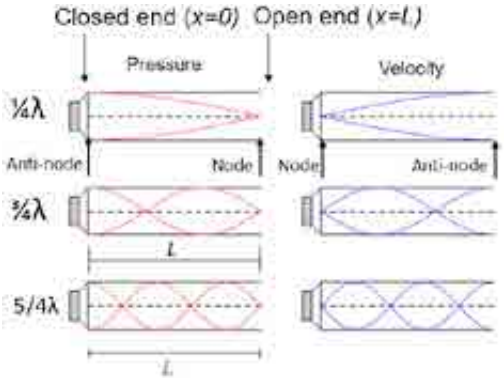

Figure 3 Pressure and velocity pulsation amplitude as a function of length for a ¼λ and ¾λ closed-open end configuration

The effect of a change from natural gas to a mixture of hydrogen for the standing wave type resonance as shown in figure 3 can be explained as follows:

by: André Eijk – INDEPENDENT CONSULTANT

Assume a length of twenty meters between the open and closed end, a compressor speed of 300 rpm and a speed of sound of natural gas of 400 m/s. The ¼λ mode can be excited by 5 Hz which is the first harmonic of the compressor speed. For hydrogen with a speed of sound of 1200 m/s the frequency of excitation for the ¼λ mode will be 15 Hz which is the third harmonic of the compressor speed.

The acoustic energy for higher harmonics is in general lower than for lower harmonics of which an example is shown in figure 4. As explained in section 2, it strongly depends on the acoustic response of the system if higher or lower pulsation levels will occur. Excitation at higher harmonics for a hydrogen mixture can be a realistic scenario because higher harmonics are in general also present in the compressor flow pulses. This is shown in figure 4 where the discharge flow pulse (light grey line) of a compressor is shown. The vertical bars are the frequency components (spectrum) and it is shown that also higher harmonics are present. The left vertical belongs to the discharge flow pulse (kg/s) and the right axis belongs to the components of the frequency spectrum (kg/s).

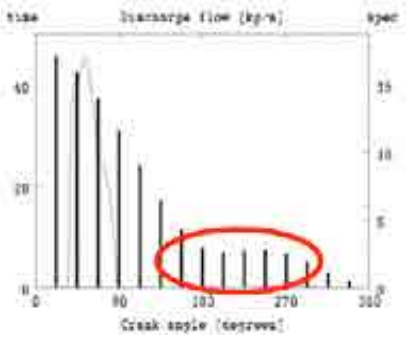

Figure 4 Example of a cylinder pulsation excitation source at the discharge side

3.3.2 Helmholtz resonator

A Helmholtz resonator is a closed, or partially closed, cavity where fluid oscillates at a particular frequency controlled by a few parameters. The result is a resonance effect which is widely used in acoustics, from sound absorbers to musical instruments. In reciprocating compressor systems, it can have a negative effect when this resonance is excited because unacceptable pulsations and vibrations may occur. However, this type of resonator can also be used in the design of acoustic filters. An example of this is the Helmholtz resonator with two volumes as shown in figure 5. The gas moves between the two volumes and behaves like a mass-spring system.

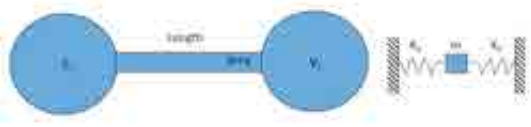

Figure 5 Helmholtz type resonator with two volumes

The frequency of this resonance can be calculated with equation (4) and the Frequency Response Function (FRF) is shown in figure 6. When used in the design of an acoustic filter, the Helmholtz (cut-off) frequency (f_H) shall be at least 20% lower than the excitation frequency (f_c). The effect is that the pulsation amplitude will be lower for frequencies higher than that of the Helmholtz frequency.

If an existing natural gas system is changed to a mixture of hydrogen, the speed of sound will shift to higher values as shown in figure 6 and it might occur that the Helmholtz frequency (f_H) and excitation frequency (f_c) coincide. In this situation, the pulsations will be amplified which can lead to unacceptable vibration levels and fatigue failure of parts of the system.

$$f_H = \frac{c}{2\pi}\sqrt{\frac{A}{L}\left(\frac{1}{V1}+\frac{1}{V2}\right)} \quad (4)$$

where:

f_H Helmholtz frequency [Hz]; c speed of sound [m/s]

L choke length [m]; V volume [m^3]; A pipe area [m^2]

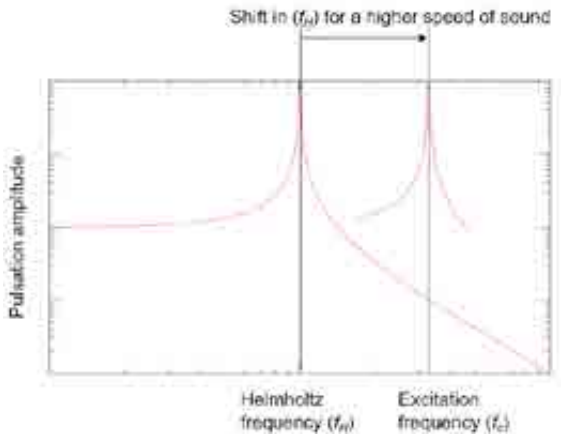

Figure 6 Frequency Response Function (FRF) of a Helmholtz filter

4 Pulsation mitigation measures

4.1 Introduction

Pulsation and vibration control measures for reciprocating compressor systems operating on hydrogen mixtures will need to address the higher speed of sound and the low density. When designed as a new unit, this must not be overly difficult although the dramatic increase in speed of sound will make the pulsation filter bottles and other volumes like separators, volumes used for acoustic separation purposes, larger due to the limited effect of hydrogen's hydraulic capacity ($\div V/c^2$) as explained in section 4. 3, and acoustic impedance differences. When designed in retrofit applications, the pulsation and vibration control measures is more challenging.

The effect of changing an existing natural gas system to a mixture of hydrogen on the pulsation and vibration mitigation measures will be explained in detail in the next sections. It is noted that a change in

by: André Eijk – INDEPENDENT CONSULTANT

temperature and pressure is not considered. This optimum way to investigate this effect is with a pulsation analysis as stipulated in the API 618[1].

4.2 Allowable pulsation levels according to the API 618

The allowable pulsation levels of parts of the system (pulsation damper, cylinder flange, pipe system) are defined in the API Standard 618[1]. The allowable pulsation levels for the pipe system are calculated with equation (5).

$$P_{all.} = \frac{400}{\sqrt{P_L D f}} \sqrt{\frac{c}{350}} \quad [\%pp] \quad (5)$$

where:

$P_{all.}$ all. pulsation level [% of the static pressure]

c speed of sound [m/s]; D inner pipe diameter [mm]

P_L mean static pressure [bar]; f frequency [Hz]

It can be concluded from equation 5 and the example from figure 7, that one of the benefits of hydrogen is that the allowable pulsation levels for the pipe system are higher compared to natural gas. The background of this is that the pulsation induced forces on pipe sections are in general lower for gases with a high speed of sound due to their larger wavelengths.

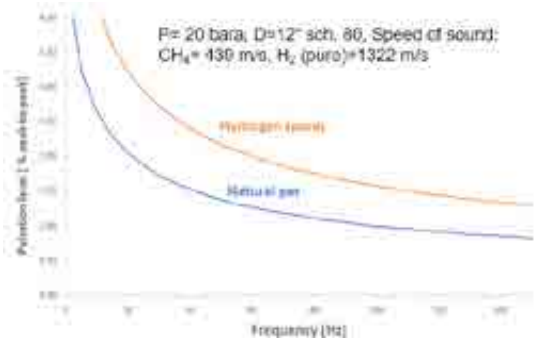

Figure 7 Example of the API 618 allowable pulsation levels for pure hydrogen and natural gas

It is noted that the allowable API 618 pulsation levels for pressures lower than 3.5 bara need to be calculated with a pressure of 3.5 bara. For a 4" pipe with a frequency of 6 Hz, the allowable level is ≈12% peak-to-peak. This level may be much too high for low pressure hydrogen systems with (alkaline) electrolysers. There is a lack of knowledge at the moment as to which level can be allowed; from recent project experiences most electrolyser manufacturers specify a level of 1% peak-to-peak. Further research is needed to arrive at a reliably permissible level.

4.3 Pulsation damper/filter design

One of the most effective pulsation mitigation measures is the installation of a pulsation damper at the inlet and outlet of the compressor cylinders.

There are several configurations, but the most commonly applied dampers are empty bottles, bottles with internals such as baffle plates and baffle choke tubes to create an acoustic filter, and a damper design with a secondary bottle which also can function as an acoustic filter. Several examples of pulsation dampers are shown in figure 8.

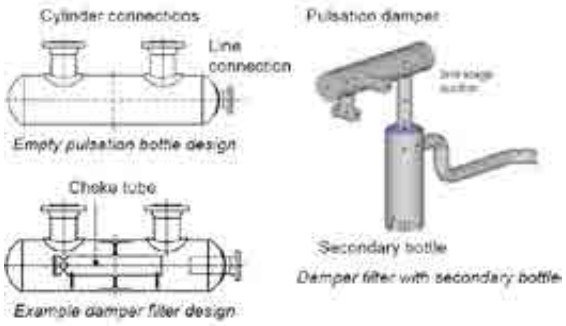

Figure 8 Some examples of pulsation dampers

Pulsation and vibration control systems for reciprocating compressor systems operating on hydrogen mixtures will need to predominantly address the higher speed of sound. When designed as a new unit, this should not be overly difficult although the dramatic increase in speed of sound will make the pulsation filter bottles and other volumes like separators, volumes used for acoustic separation purposes for e.g. multiple running reciprocating compressors larger. This is due to the limited effect of hydrogen's hydraulic capacity and acoustic impedance differences as explained below. When designed in retrofit applications, the pulsation and vibration control system will be more challenging, e.g. to fit the dampers on the same compressor cylinder arrangement.

Important parameters which affect the damper design/effectiveness for hydrogen mixtures are:

1. Acoustic effectiveness volumes

The acoustic effectiveness (hydraulic capacity) of a volume is inversely proportional to the square of speed of sound the ($\div V/c^2$). This is much lower for hydrogen mixtures compared to natural gas due to the higher speed of sound of hydrogen. This means that the pulsations at the outlet of a volume for a hydrogen mixture are much higher compared to natural gas which is illustrated in figure 9. In general, larger volumes are required for hydrogen applications to achieve acceptable pulsation levels. As explained in section 4.2 the benefit of hydrogen is that the allowable pulsation levels in piping systems are higher for hydrogen mixtures according to the API 618. A detailed acoustic analysis according to the API 618 will reveal if a redesign of the damper design is required.

by: André Eijk – INDEPENDENT CONSULTANT



Figure 9 Effect of a volume on the pulsations at the outlet of the volume

2. Shifting frequencies of Helmholtz resonances

Acoustic filters are in general designed with one or more volumes in order to achieve a cut-off (Helmholtz) frequency below the compressor running speed (first harmonic) which is the driving excitation for pulsations. However, the Helmholtz frequency is sometimes chosen between the 1st and 2nd harmonic of the compressor speed.

An example of the acoustic response for a 750-1000 rpm compressor with natural gas is shown in figure 10. It can be concluded from this figure that there are overlapping areas of the excitation frequencies for the higher harmonics, in this case above the fifth harmonic.

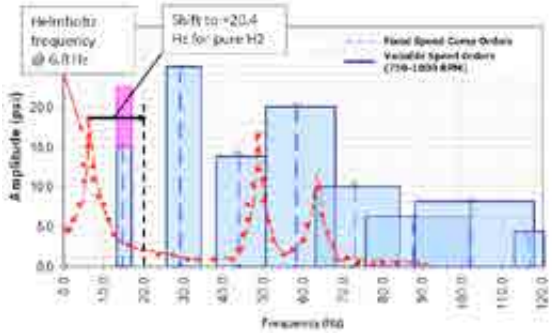

Figure 10 Example of an acoustic response for a 750-1000 rpm compressor with natural gas

The Helmholtz frequency is linearly proportional to the speed of sound, and this will cause all acoustic modes to shift upwards in frequency for hydrogen mixtures compared to natural gas. Assuming pure hydrogen it will mean that the Helmholtz frequency of 6.8 Hz from figure 10 will shift to ≈20.4 Hz which is between the first and second harmonic of the compressor speed. In that case the shift will be beneficial because the first harmonic pulsation cannot excite any resonances anymore. However, for lower hydrogen mixtures it might be possible that the Helmholtz frequency will shift into the range of the first harmonic which means an amplification of the pulsations at that frequency.

Furthermore, the resonance shift can cause problematic overlapping resonances and the chance of this occurring is greater for variable speed compressors and for medium (600-1000 rpm) and high-speed machines (>1000 rpm). The effect is that acoustical resonances in the overlapping areas may be excited by more than one harmonic excitation which makes it more challenging in designing acoustic filters.

Depending on the system, a redesign might be necessary when hydrogen mixtures will be used for an existing system. A detailed acoustic analysis according to the API 618 will reveal if a redesign of the damper design is required.

3. Pulsation-induced forces

An example of the pulsation-induced force over a pulsation damper is shown in figure 10. This pulsation force will generate vibrations of the pulsation damper and compressor manifold. Due to the much larger wavelength of hydrogen mixtures compared to natural gas, the pulsation-induced forces over the damper will in general be lower. This depends on the relationship between the excitation forces, the acoustic and mechanical natural frequencies, and the acoustic and structural response of the system, as discussed in section 2. Although it depends on the system, this is generally one of the benefits of a hydrogen mixture.

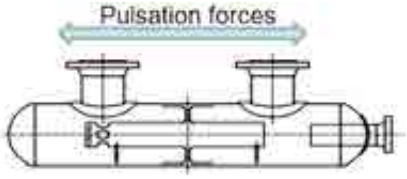

Figure 11 Example of a pulsation force over a damper

4.4 Orifice plates

Orifice plates are typically used to control amplified acoustic resonances and vibrations, where the pulsation filter may not be completely effective, such as compressor cylinder nozzles or the inlet or outlet of a two-volume filter.



Figure 12 Example of a single bore orifice plate

Orifice plates are also highly effective in the pipe system to mitigate pulsations caused by acoustic resonances. Examples are standing waves between (acoustically) closed valves, volumes, large diameter changes, etc. and Helmholtz resonances between e.g., volumes such as pulsation dampers, separators, filter elements, etc.

Orifice plates are most effective when placed at *velocity* (acoustic) maxima (anti-nodes) as shown in figure 3. These are locations where in general the *pressure* pulsations are minimum e.g. at the inlet and outlet of volumes. Besides that, the effectiveness of an orifice plate also strongly depends on the pressure drop over the orifice plate. This is a function of the density and flowrate as given in equation (6).

$$\Delta P = K \frac{1}{2} \rho v^2 \quad (6)$$

where:

by: André Eijk – INDEPENDENT CONSULTANT

ΔP pressure drop [N/m^2]; v flow velocity [m/s]

K friction factor [-]; ρ density [kg/m^3]

To achieve the same energy transport for pure hydrogen compared to natural gas, it means for an existing system that the flow velocity must be increased by a factor of three for the same pipeline pressure. Although this energy transport target may not be achievable at excessively high flow velocities for hydrogen, e.g. due to erosion[14] problems, it is possible that hydrogen systems will realize higher velocities. Although flow velocities may be higher in hydrogen pipelines, the density of pure hydrogen at the same line pressure is a factor nine lower than natural gas. This means that the orifice pressure loss, and thus its effectiveness, will be in the same order for pure hydrogen. However, for gas mixtures with less than 100% hydrogen or for flow velocities smaller than three times that of natural gas, the effectiveness of the orifice plate is much less, and the orifice plate must be redesigned.

It is noted that the same pressure drop for natural gas and hydrogen does not always mean the same acoustic damping. This also depends on the frequency shift of acoustic responses. In general, the acoustical resonances will likely be seen at much higher frequencies for hydrogen and the disadvantage of this is that the effectiveness of a single bore restriction orifice plate will decrease, as shown in figure 13. For those situations, a Multiple Bore Restriction Orifice[5] (MBRO) may be required, which is effective up to higher frequencies.

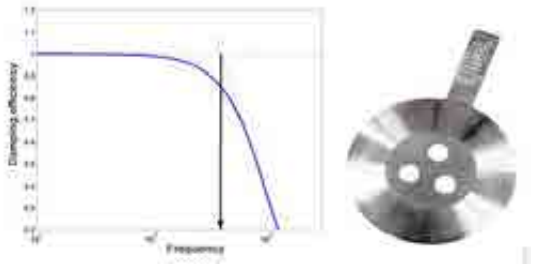

Figure 13 Effectiveness of a single bore restriction orifice plate (source: TNO)

In addition to installing an orifice at the inlet and outlet of volumes, it may happen that one or more orifice plates are installed at other locations in an existing pipe system. This might e.g. be necessary for combined acoustic resonances. When the system is adjusted to hydrogen, it might be necessary to relocate these orifice plates to another location due to the larger wavelength.

The general conclusion is that for all situations as described, the orifice plates of an existing system must be redesigned and/or relocated when hydrogen mixtures are used. This is even more challenging for variable speed compressors and in that case a Dynamic Variable Orifice[6] (DVO) can be effective of which an example is shown in figure 14. The DVO features a variable opening that can be adjusted in place, either actuated manually or automatically, while the compressor is running to account for different compression conditions such as different hydrogen mixtures, speeds, pressures, etc. This DVO provides a much wider effective range of operation and minimizing flow restrictions as much as possible.



Figure 14 Example of a Dynamic Variable Orifice (source: ACI Services)

4.5 Side branch absorbers (SBA)

Another way of an effective mitigation measure at resonance is a side branch absorber. Examples are a closed branch pipe mounted to the main pipe which acts like a standing wave, or a volume which acts like a Helmholtz resonator, see figure 15.

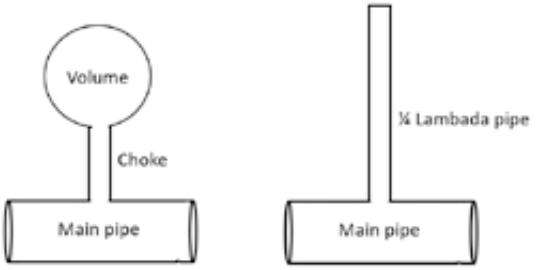

Figure 15 Side branch absorbers (left Helmholtz type resonance, right standing wave type)

A special type of SBA[7] for variable speed compressors, is the Tuneable Side Branch Absorber (TSBA), of which an example is shown in figure 16. The TSBA is essentially a tuneable Helmholtz resonator that produces pressure pulsations which are then used to cancel the compressor generated pressure pulsations without producing flow induced pressure losses in the main piping. The TSBA can be set to track the compressor speed to cancel the offending pressure pulsations without restricting gas flow. This device can be used very effectively for different mixtures of hydrogen, both for fixed and variable speeds.

by: André Eijk – INDEPENDENT CONSULTANT



Figure 16 Tuneable side branch absorber (source: ACI Services)

This can be an advantage, especially to retrofitting existing systems where a design study must be conducted to resize and re-locate, or possibly eliminate, older controls if the acoustic lengths are no longer resonant with the shifted speed of sound.

4.6 Volumes used as acoustic separation.

Volumes, such as e.g. separators, can have a beneficial effect in mitigation pulsations and vibrations. If they are mounted in close vicinity of the compressor, they are sometimes used in the acoustic filter design, as discussed in section 4.3. If acoustically designed well, separators can function as an adequate acoustic separation between the pulsations generated by the compressor and those in the piping upstream or downstream of the separator.

If an existing system is adjusted to a mixture of hydrogen, the acoustic behaviour of the separator will change due a limited acoustic effect of the separator volume as explained in section 4.3. In that case, the acoustic behaviour of the system needs to be checked, and if necessary redesigned.

Multiple large reciprocating compressors running in parallel are required if large volumes of hydrogen mixtures need to be transported to achieve the same energy transport compared to natural gas. In that case, the pulsations at the common suction and discharge pipe system will increase by the share of pulsations of each compressor train. This can cause unacceptable pulsations and vibration levels leading to fatigue failure of (parts of) the piping.

From a pulsation and vibration perspective, the complex acoustic interaction between the various compressor trains, all necessary capacity step combinations, and the large size of the complete system of which an example is shown in figure 17, will pose major challenges, especially for hydrogen applications due to the limited acoustic effect of volumes that aim to separate the systems.

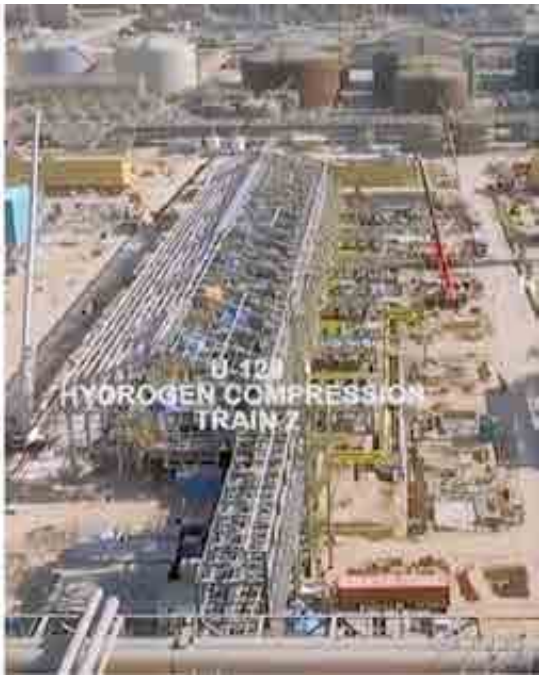

Figure 17 Example of a hydrogen compressor train with multiple running compressors[8]

The API Standard 618, fifth edition does not provide any specific guidance on how to address these challenges. The evaluation process as described in two papers[8,9] can be used to control the acoustic interaction between different compressor trains. The engineering approach as proposed by the authors of both papers facilitate the selection of a realistic amount of analysis cases and appropriate evaluation criteria.

In the first paper[8], large volumes for each individual compressor at the common suction and discharge side together with a large common header obtained adequate acoustic separation between the compressor trains, leading to an efficient pulsation and mechanical response analysis process with acceptable pulsation and vibration levels.

As an alternative to the first paper, the second paper[9] discusses the principle of cancelling out the pulsations of different trains as much as possible by means of tuning the phase relation of the compressors in combination with dynamic variable orifice plates.

With these approaches, it should be possible to run multiple reciprocating compressor units in parallel with no pulsation and vibration issues on hydrogen mixtures.

5 Vibration mitigation measures

The amplitude of the pulsations and pulsation-induced forces may change when an existing natural gas system is adjusted to a mixture of hydrogen. This means in general that also the amplitudes and frequencies of the vibrations and cyclic stress levels of (parts of) the pipe system, the compressor manifold, the pulsation dampers, and pipe supports will change.

by: André Eijk – INDEPENDENT CONSULTANT

Experience has shown that the amplitude of the pulsation-induced forces will be lower due to the larger wavelength of hydrogen, but the frequencies may be higher.

In general, lower pulsation-induced forces are beneficial, but higher frequencies can be a disadvantage because vibrations with higher frequencies are more difficult to mitigate, especially if the pipe system and pipe supports are mounted on flexible supporting structures.

It may be difficult sometimes to avoid overlapping of acoustical and mechanical resonance conditions by a frequency shift which may lead to a worst-case scenario. This also depends on the operating conditions, the amount of hydrogen gas in the mixture and the relationship between the excitation forces, the acoustic and mechanical natural frequencies, and the acoustic and structural response of the system as explained in section 2.

In the worst-case scenario, there is a higher change on fatigue failures of (parts of) the compressors, pipe system and process equipment. The risk of encountering worst-case conditions is especially high for variable speed compressors and for medium and high-speed compressors. One of the practical solutions to avoid the worst-case scenario is to install additional pipe supports or to stiffen supporting structures to increase the mechanical natural frequencies. With this approach the lowest mechanical natural frequency shall be at minimum ±20% away from the dominant excitation frequencies. This will result in shorter distances between pipe supports, but this may lead to a large number of additional pipe supports, especially for high frequency excitation However, avoiding resonances is not always necessary if the vibrations and cyclic stresses at resonance are acceptable.

A more efficient method, leading to fewer additional pipe supports, is to conduct a full mechanical response analysis according to the API Standard 618. In this approach the vibrations and cyclic stresses are calculated for the worst-case situations and are compared against allowable levels. If necessary, the pipe support layout including supporting structures are redesigned.

It is sometimes a challenge to achieve a stiff and robust pipe support structure. If for instance an additional pipe support structure is required in the middle of the vertical pipes as shown in figure 18, a very stiff pipe (rack) supporting structure is required.



Figure 18 Example of a flexible pipe system

The solution for this case might be a Constrained Layer Damping (CLD)[10,11] device. This device will increase the local damping of the structure, resulting in lower vibration levels at resonance conditions. CLD devices can be produced at low costs, are quite easy to install and are highly effective for a broad frequency range. An example of a CLD application is shown in figure 19.



Figure 19 Example of a Constrained Layer Damping

6 AVIFF Guidelines of the Energy Institute[4]

6.1 Introduction

The AVIFF guidelines of the Energy Institute (EI) are developed to help minimize the risk of vibration induced fatigue failures of general process piping, in the design phase, for existing plants and in cases where a problem has occurred during operation.

It is intended for use by engineers with no prerequisite knowledge of pipe vibrations. They offer a proactive approach to pipework vibration issues. The EI guidelines make use of a *qualitative* and *quantitative* assessment instead of detailed numerical techniques as stipulated by the API 618. Despite the fact that the EI are not widely used by engineers in the reciprocating compressor industry because the API 618 is most prescribed for reciprocating compressor systems, a brief introduction is given in this paper for those engineers who will use the AVIFF. A more detailed summary for reciprocating compressor systems is given in the book[2] "Machinery and Energy Systems for the Hydrogen Economy"[2].

The EI guidelines provide a staged approach, which means that initially a *qualitative* assessment of (parts) of the pipe system is made as described in technical module T1 of these guidelines to identify the potential excitation mechanisms that may exist.

6.2 Qualitative and quantitative assessment

The *qualitative* assessment provides a means of rank ordering of several process systems or units to prioritize the subsequent assessment.

A *quantitative* assessment is then undertaken on the higher risk areas to determine the likelihood of a vibration induced failure (LOF) of (parts) of the pipe system, see next section. The parts are summarized in technical modules T2 through T4 of the EI Guidelines for the application of reciprocating

by: André Eijk – INDEPENDENT CONSULTANT

compressors: the mainline, small-bore connections (SBC's) and thermowells.

6.3 Likelihood of failure (LOF)

The LOF is a form of scoring to be used for screening purposes. It is not an absolute probability of failure nor an absolute measure of failure. The calculation of the LOF's is based on simplified models to ensure ease of application and are necessarily conservative. The LOF together with the consequence of failure determines the risk level, which is shown in the criticality matrix of figure 20.



Figure 20 AVIFF's criticality matrix

6.4 Small Bore Connections (SBC's)

SBC's are small diameter side branches e.g. drains, level gauges, P, T connections, etc. of which an example is shown in figure 21. A definition of SBC's is given in the ISO 20816-8[12]. SBC's have in general a low stiffness, heavy mass, and a low mechanical damping. Fatigue failures are common to occur even when the main pipe vibrations are acceptable.



Figure 21 Example of typical SBC's

SBC's often fail due to fatigue failure in reciprocating compressor systems, especially at higher frequencies. An example of a failed SBC is shown in figure 22.



Figure 22 SBC fatigue failure (source: TNO)

One of the quantitative actions is to check the LOF of Small-Bore Connections (SBC's) which is described in section T3 and Appendix C of the AVIFF If the LOF exceeds the acceptable value, the design of the SBC needs to be improved. The AVIFF gives guidelines for the (re)design of SBC's in Module T5 "Visual Inspection Piping". Design guidelines are also given by the Gas Machinery Research Council[13] (GMRC).

One of the missing points of the AVIFF in the LOF assessment of SBC's is that it only considers the geometry, supporting and pipe properties, and not the *frequency* of excitation. As explained before, when adjusting a system to hydrogen, the frequency of excitation *may* increase which means a higher risk on failure, especially for medium and high-speed compressors.

6.5 Thermowells

Fatigue failure of thermowells, caused by flow induced pulsation (vortex shedding) of the gas around the thermowell, is often forgotten in the design of a system. This is the case if the vortex frequency (f_V) coincides with a mechanical resonance frequency (f_M). An example of the fluid vortices is shown in figure 23.

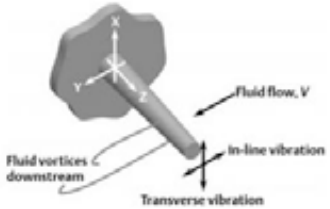

Figure 23 Fluid vortices of a thermowell (EI)

One of the *quantitative* actions of the AVIFF is to check the LOF of thermowells. The LOF will increase if the flow velocity in hydrogen applications increases and might exceed the AVIFF acceptable value. In that case a redesign is required, e.g., a shorter length, larger diameter, or a twisted design, of which an example is shown in figure 24.

by: André Eijk – INDEPENDENT CONSULTANT



Figure 24 Twisted thermowell (source: Emerson)

7 Conclusions

Hydrogen may replace natural gas in the energy transition as an energy carrier. Existing turbo compressor systems for gas transport and storage may be replaced by large reciprocating compressors.

Due to the substantial change in speed of sound and density of hydrogen mixtures compared to natural gas, these systems require a careful and complete investigation of the pulsation and vibration behaviour.

A possible redesign of pulsation dampers, orifice plates, volumes (e.g. separators), small bore connections, thermowells and pipe supporting structures might be required.

Dedicated standards such as API 618, engineering experience, and adequate design tools are readily available and need to be used for those systems and will reveal if a redesign of the pulsation and mechanical mitigations measures are required.

Reciprocating compression will remain a valuable technology for the future hydrogen value chain.

References

[1] API 618, "Reciprocating Compressors for Petroleum, Chemical and Gas Industry Services", 5th edition 2010.

[2] Klaus Brun Elliot Group, Timothy Allison SWRI, "*Machinery and energy systems for the hydrogen economy*", Elsevier, 2022

[3] API Standard 688, *"Pulsation and Vibration Control for Positive Displacement Machinery Systems for Petroleum, Chemical, and Natural Gas Industry Service"*, 1st edition

[4] Energy Institute, *"Guidelines for the Avoidance of Vibration Induced Fatigue Failure in Process Pipe Work"*, 2nd edition 2008

[5] Van Lier L, Korst H, TNO, "*Mitigation of high-frequency pulsations, using Multi Bore Restriction Orifices"*, 5th EFRC Conference March 21-23, 2007 Prague, Czech Republic

[6] Shade N, Clark T, Adair J, *"Evaluation of a dynamic variable orifice for reciprocating compressor pulsation control", GMRC Conference Nashville, 2014*

[7] Harris R, Scrivner C, *"Gas compressor with side branch absorber for pulsation control"*, GMRC Conference, Oklahoma City, October 2006.

[8] Albers Howden Thomassen Compressors NL; Leonard van Lier TNO NL; Maarten van der Biezen FLUOR NL "*Engineering approach for world's largest hydrogen compression system"*, EFRC Conference 2018, Madrid

[9] Passeri, Guerrini, Baker Hughes, Florence Italy; Rossi, Mazzoli SAIPEM SpA, Fano Italy; Melis, Florence University Italy; Ferrari NIDEC ASI Spa, Cinisello Balsamo Italy, *"Pulsation optimization by dynamic variable orifice & Recips starting phase selection"*

[10] Eijk, A, de Lange D, de Vreugd J, Slis E (all TNO) "Non-traditional vibration mitigation methods for reciprocating compressor systems" 10th EFRC Conference – September 14 – 15, 2016 Düsseldorf, Germany.

[11] André Eijk, Hajo Pereboom Heat Transfer & Fluid Dynamics TNO Delft, NL, Jörg Fröbel ESK GmbH, *"Application of a Constrained Layer Damping to reduce Pipe Vibrations of a Reciprocating Compressor System"* EFRC Conference 2018, Madrid.

[12] ISO 20816-8 "*Mechanical vibration — Measurement and evaluation of machine vibration — Part 8: Reciprocating compressor systems"*

[13] *"Design Guideline for Small Diameter Branch Connections"*, Releases 1.0, Gas Machinery Research Council, March 2011.

[14] González Díez, N.; van Lier, L.; Belfroid, S.; Meijer, I. "*Impact of high speed hydrogen flow on system integrity and noise",* HYDelta report D1E.1 –WP1E

COMPRESSOR TECH2

DEDICATED TO GAS COMPRESSION PRODUCTS AND APPLICATIONS

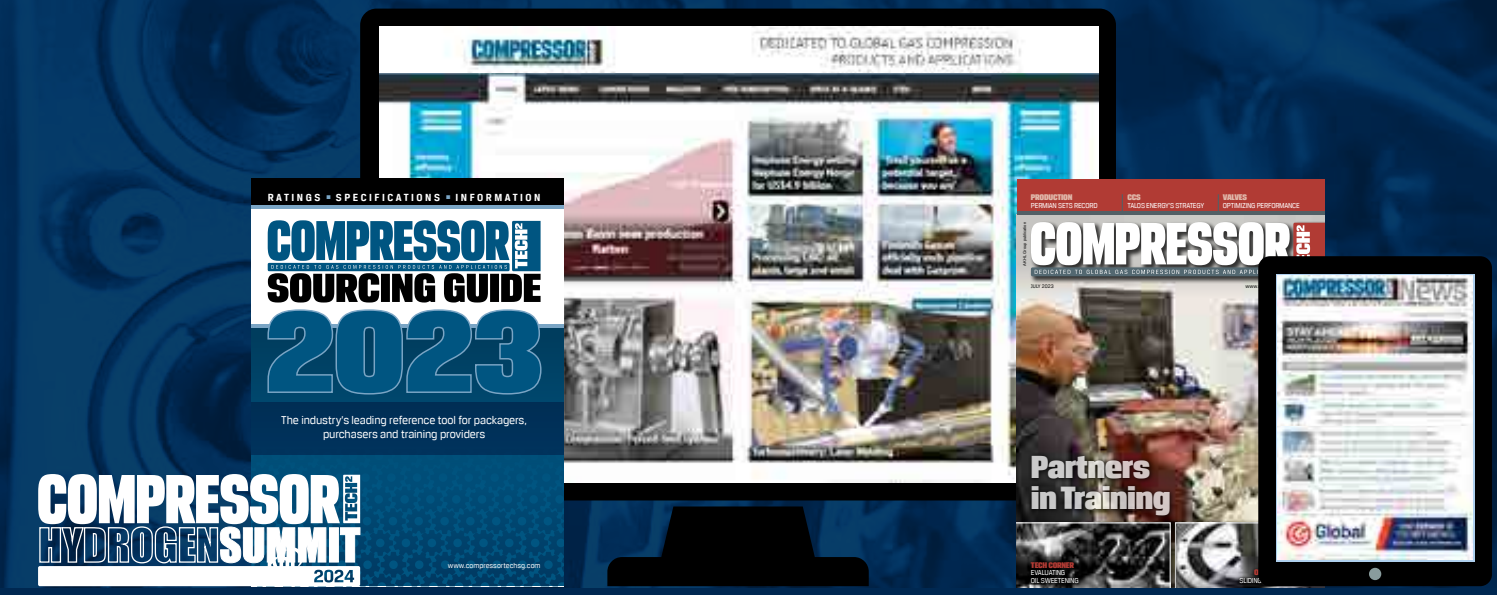

The world leader in gas compression news and information, covering products, systems, services and technologies.

- 10 issues per year of the magazine plus the Compressortech2 Sourcing Guide
- Weekly eNewsletter - keep up-to-date with the latest industry news
- Subscribe for free for your magazine and Newsletter khl.com/free-subscription

SCAN ME TO SUBSCRIBE

www.ct2summit.com www.compressortech2.com www.ctssnet.net

GEISLINGER®
POWERTRAIN SOLUTIONS. BUILT TO LAST.

On solving torsional vibration problems of reciprocating compressor systems

by:

David Richter-Trummer, Andreas Thalhammer and Thomas Bozecski
Torsional Vibration Calculation
Geislinger GmbH
Salzburg, Austria
richter-trummer@geislinger.com

13th EFRC CONFERENCE
September 19th – 21st 2023, Zagreb

Abstract:
Flexibility, safety, endurance, and cost efficiency of compressor applications can significantly benefit from a correct treatment of torsional vibrations. Especially for multi-cylinder applications with large operation speed ranges for flow control as well as for compressors driven by combustion engines, torsional vibration issues often lead to unnecessarily high vibrations and as a consequence to increased wear, noise and failure risks of powertrain components.
To simply avoid critical speed ranges is often not an admissible countermeasure since it increases the operational complexity and does not target the root cause of the problem. However, a sustainable solution has to primarily solve the vibration issue at its origin, for which simulation studies and subsequent dimensioning of appropriate countermeasures, such as tuning masses, flexible couplings or torsional vibration dampers, might be used to minimize the risk of preventable failure and wear of shafts, bearings and other system parts.
It is the scope of this paper to introduce two case studies to demonstrate the possibilities of state-of-the-art technical measures like high-flexible and high-damping couplings and torsional vibration dampers. The focus lies on identifying, assessing and solving torsional vibration problems for various reciprocating compressor applications by specifically reducing potentially harmful resonances without restricting the operation speed ranges.

by: David Richter-Trummer, Andreas Thalhammer, Thomas Bozezki – GEISLINGER

1 Introduction to torsional vibrations

No rotating shaft is torsional completely rigid. There is always a certain level of torsional elastic deformation possible when applying a torque between the front end and the rear end of a shaft. If the shaft becomes longer compared to its diameter, its flexibility or elasticity increases, i.e., by applying the same torque the shaft with the higher flexibility twists with a higher angle compared to stiffer or less flexible shafts. The energy that is used to twist the shaft is stored as potential energy and eventually is released again. The second storage of energy is the (mass) moment of inertia of the rotating parts which is referred to as kinetic energy. The two energy forms, i.e., potential and kinetic energy, can be transformed into each other. Thus, every elastic shaft, that connects two mass inertias, can be seen as a system capable to resonate in different orders and modes. For the 2-mass system from Figure 1, the one-dimensional angular motion can be described by the set of differential equations stated in (1) that combine both inertias J, deflection angles φ, its stiffness c and damping k.

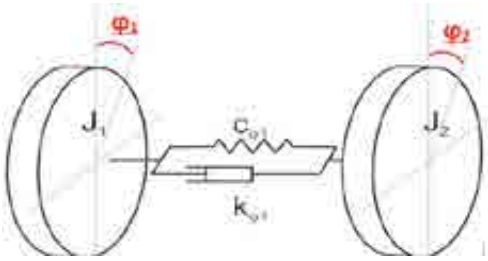

Figure 1: A torsional system consists of inertias coupled by a stiffness- and damping element.

$$\begin{aligned} J_1 \cdot \ddot{\varphi}_1 &= k \cdot (\varphi_2 - \varphi_1) + c \cdot (\dot{\varphi}_2 - \dot{\varphi}_1) \\ J_2 \cdot \ddot{\varphi}_2 &= -k \cdot (\varphi_2 - \varphi_1) - c \cdot (\dot{\varphi}_2 - \dot{\varphi}_1) \\ \ddot{\varphi}_r &= -k \cdot \left(\frac{1}{J_1} + \frac{1}{J_2}\right) \cdot \varphi_r - c \cdot \left(\frac{1}{J_1} + \frac{1}{J_2}\right) \cdot \dot{\varphi}_r \end{aligned} \quad (1)$$

It is the aim of a torsional vibration analysis to translate a physical system into a mathematical torsional system and then to study its vibration behavior under forced excitations.

1.1 Model building

To achieve a complete mathematical model, the entire system from the first to the last connected rotating part needs to be modelled. For this, the dimensions of every part as well as their material specifications need to be known.



Figure 2: Example of a technical sketch of a shaft

To reduce the complexity of the considered mathematical model, a representative, but simplified geometry of every shaft is deduced from complex technical drawings as e.g. presented in the example of Figure 2. Since every shaft has a specific mass moment of inertia and stiffness, a whole torsional system can be set up by representing the most flexible parts of the machine as a shaft and sum up relevant contributions to the inertias in between. Following the shaft from Figure 2, this procedure is visualized in Figure 3, where a one-dimensional model is finally obtained.

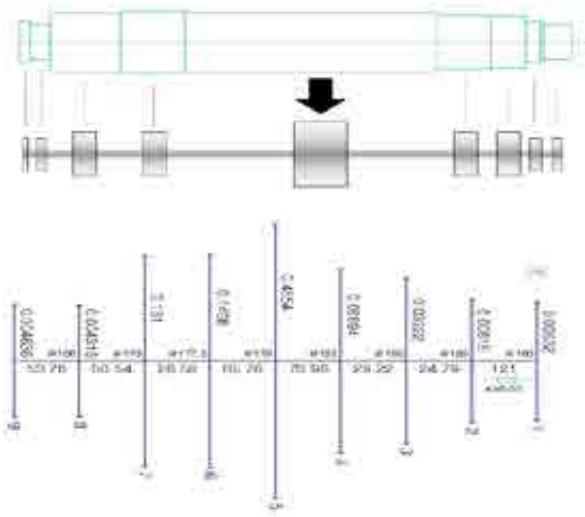

Figure 3: Model building to get a torsional system.

When all connected components have been modeled as a single model, the whole torsional system of the complete drivetrain is merged from the corresponding component models. Furthermore, absolute and relative damping can be applied on and in between the mass inertias. Absolute damping comes from outside the system - like for example friction between cylinder and piston - and acts on a mass inertia as an external torque. Internal damping on the other hand is a result of internal resistance against twisting of a shaft that leads to heating up of the material itself and acts on a shaft. This relative damping is highly dependent on the material properties. When being deformed, rubber for example achieves higher relative damping values compared to steel.

by: David Richter-Trummer, Andreas Thalhammer, Thomas Bozezki – GEISLINGER

1.2 Eigenfrequency and mode shape analysis

A complete torsional system can be analyzed regarding its natural frequencies and mode shapes. Mode shape diagrams (as shown in Figure 4 below) can be used to identify the specific locations in the system where the sign of φ (the angle of deflection) changes. Every point of the system where φ becomes zero is called a node. There are typical two, sometimes three different mode shapes relevant for a system. In the first mode vibration, there is just one node in the system. In the second mode vibration, there are two points on the shaft, where the relative angle φ becomes zero.

The eigenfrequency of vibrations of different modes are different. The second mode vibration has a higher frequency than the first mode, and the eigenfrequency of the third mode is of course even higher.

In Figure 4, an illustrative mode shape diagram of a modified version of the shaft model from Figure 3 is presented. For this, two mass inertias to the above system are added and a gear wheel at the previous position 7 is increased such that its inertia is 450 kgm². Further a second high mass component was added to the right-hand side of the shaft.

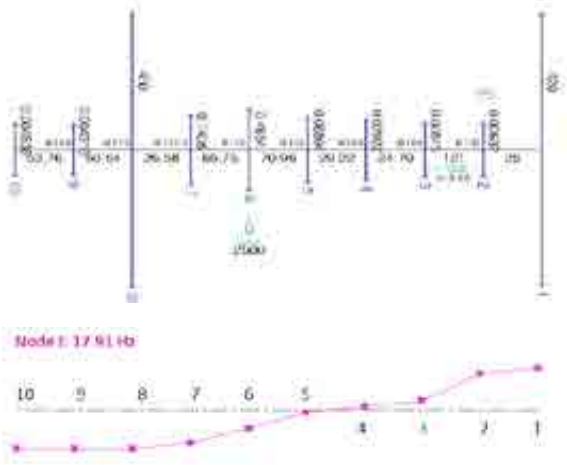

Figure 4: Modified torsional system and corresponding mode shape diagram for first mode.

The first node of this new system just crosses between mass 4 and 5 and vibrates with a frequency of 17.91 Hz. That means in the first mode the entire fore parts 5-10 of the system vibrate against the rear parts 1-4 and in the middle of the shaft there is no angular motion φ at all for first mode.

One can further study the natural frequencies in a Campbell diagram. In this diagram the plants rotation speed [rpm] on the x-axis is compared to the frequencies [Hz] on the y-axis.

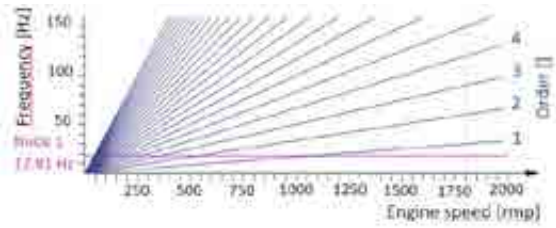

Figure 5: Campbell diagram for frequency analysis

The first node eigenfrequency for the above example has 17.91 [Hz] and is shown as a straight horizontal line. As a set of straight inclined blue lines starting from the zero speed, zero frequency point, the orders of vibration are plotted in the diagram (figure 5) as well.

A first order vibration has a periodicity of one in every revolution. Therefore, this first order frequency reaches the first node eigenfrequency of 17.91 Hz at around 1075 rpm. One can see this crossing point at the Campbell diagram.

A second order vibration has two periods in one revolution, so the frequency of 17.91 Hz is reached at around 537 rpm.

In the speed of every intersection point between orders and nodes in the Campbell diagram the system is prone to build up a resonance if the vibration excitations are favorable.

1.3 Forced excitations

The natural frequencies of the system need to be further related to the vibration excitations to which the application is exposed in operation. Since the working principle of a reciprocating piston machine generates highly fluctuating pressure patterns in its cylinders, the torsional system is typically excited by various frequencies.

To get accurate simulation results of real operation conditions it is necessary to excite the torsional system with realistic excitations at every relevant load case. It is important to study in which harmonic orders and with what amounts of energy it is forced to vibrate. The pressure inside every cylinder is transferred to a tangential force and further to the resulting torque. This generated torque pattern is periodic over a certain number of revolutions and it can be represented as a Fourier series containing sine and cosine vibrations for the different harmonic orders.

by: David Richter-Trummer, Andreas Thalhammer, Thomas Bozezki – GEISLINGER

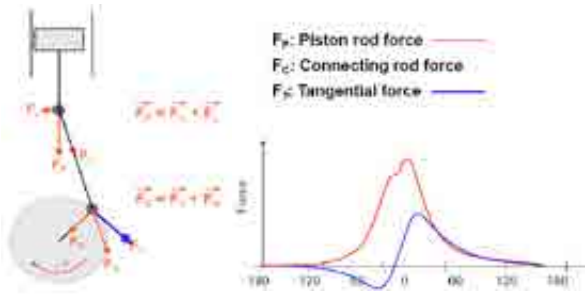

Figure 6: Conversion of pressure forces to tangential forces on the crank of the machine.

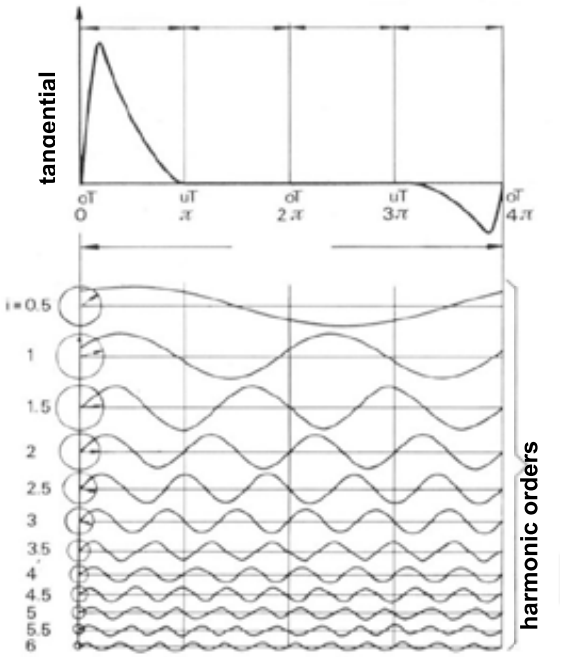

Figure 7: Representation of a torque excitation composed by a Fourier series of multiple orders.

In reciprocating compressors, the mass of oscillating parts adds up to relevant excitation forces, especially at higher speeds. Mass forces rise with squared speed whereas gas pressure forces typically rise proportional with the underlying load. Therefore, excitations are always valid for certain loads at certain speeds. Thus, it is necessary to distinguish between different load cases.

In a typical four-stroke internal combustion engine excitation the gas (dashed curve) and the mass excitation (dotted) are opposite in the first half of working stroke and in the last half of compression stroke. This is done to reduce total peaks in tangential forces.

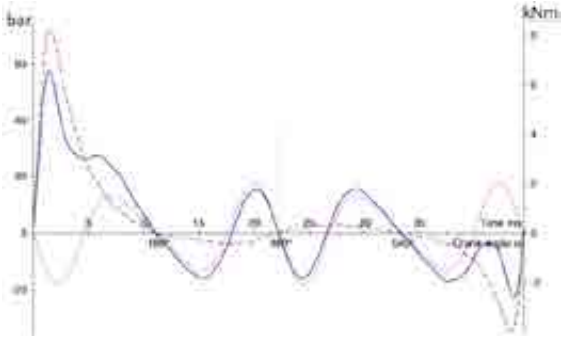

Figure 8: Typical excitation for a four-stroke diesel engine. Mass (dotted and gas dashed excitations).

A typical compressor excitation does not exist, since a lot of different operation modes for pressure and flow control beside single way acting or double acting piston concepts are frequently used. They all have in common that compression and mass excitations respectively follow a two-stroke cycle, so the whole cycle has a periodicity of 360°.

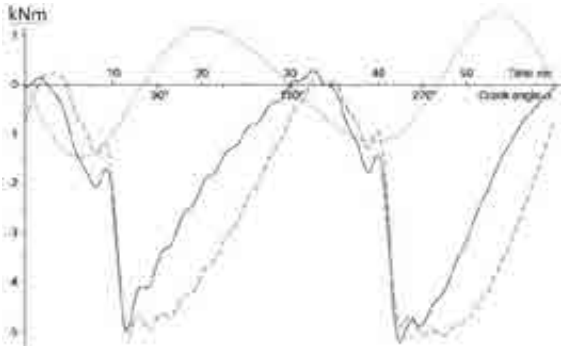

Figure 9: Example for compressor excitations.

In the torsional vibration analysis, the torsional system is excited with all the harmonic orders and amplitudes of the Fourier series of the compressor excitation.

As we discussed in section 1.2 every torsional elastic system has characteristic eigenfrequencies and orders in which it is prone to vibrate. If the external excitation now gives its vibration energy in comparable frequencies to the systems eigenfrequencies the resulting vibrations may increase towards not controllable values. Therefore it is important always to consider the right set of excitation when studying the torsional behavior of a system in the analysis.

The results of this first torsional vibration analysis are further compared regarding permissible values of stress, acceleration, angles of deflection or total torque. If the calculated values exceed the permissible limits adequate counter measures are considered and the simulation needs to be repeated.

by: David Richter-Trummer, Andreas Thalhammer, Thomas Bozezki – GEISLINGER

2 Treatment of torsional vibration issues

Identified torsional vibration problems can be solved by various measures. Flywheels, tilgers, dampers, or couplings are frequently used. Sometimes all these measures cannot solve the problem properly, such that it is necessary to change the general outline of the shaft line, the concept or to restrict the operation to certain speed ranges or load cases.

2.1 Torsional vibration dampers

A powerful way to change the torsional vibration behavior of many machines is the use of dampers. Torsional vibration dampers are additional devices that are bolted to the free end of a crankshaft to change the vibration nature of the whole torsional system.

The two most common constructions of torsional vibration dampers are viscous-type dampers and steel spring dampers. Both have in common that they consist of an inner member that is connected to the free end of the crankshaft and a seismic part that is connected to the inner part by a flexible and damping element. This flexible and damping element is a highly viscous silicon oil in case of a viscous-type damper. However, the effect regarding dissipated vibration energy is quite limited and these types of torsional vibration dampers are highly dependent on the surrounding temperature. By the occurring shear stresses, they show mechanical wear of the silicone oil so that they lose performance with cumulated operation time.

In Figure 10 a steel spring damper is shown. Here the outer seismic part is connected via steel springs and can twist for an assigned angle around its neutral position. The springs define the torsional stiffness of the damper that is typically very low compared to the torsional system.



Figure 10: Principal outline of a spring type damper.

Torsional deflection leads to a bending of the springs and thus changes the volume of oil filled chambers positioned left and right of each spring pair, shown in Figure 11.

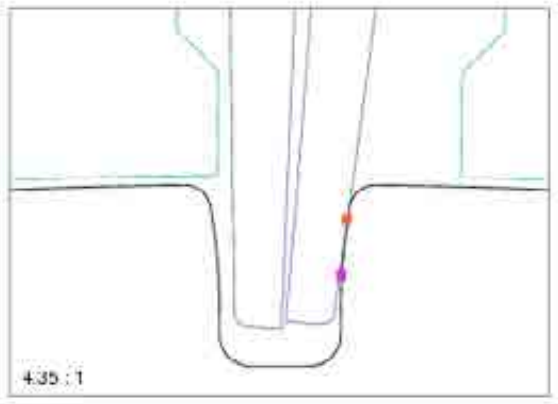

Figure 11: The deflection of the springs changes chamber volume and introduces an oil flow.

This periodic change of volume leads to an oil flow through specifically designed gaps which leads to resistance and therefore hydrodynamic damping. The damping energy is transferred out of the damper by the oil flow itself. Steel spring dampers are capable to dissipate more energy and are the choice if space restrictions, large temperature ranges or simply the necessary amount of damping cannot be achieved with other measures.

The working principle of a steel spring damper is described in Figure 12 below: By adding the seismic inertias in combination with the constant stiffness, it can influence the natural frequencies and torsional vibration behavior of the whole system such that critical vibrations can be reduced, shifted or even split up into other less harmful ones.

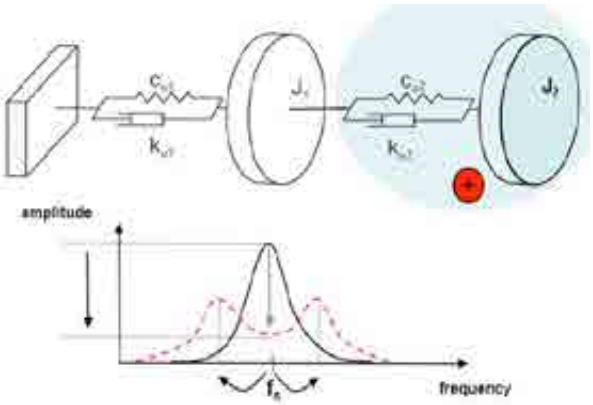

Figure 12: Working principle of a steel spring damper.

by: David Richter-Trummer, Andreas Thalhammer, Thomas Bozezki – GEISLINGER

2.2 Highly flexible, damping couplings

Very long and therefore more flexible shaft lines can resonate in more relevant vibration modes compared to short and rigid ones. This can lead to superposition of many orders of different vibration modes at the same time. To avoid an overload of shafts, it is often necessary to separate torsional systems by torsional elastic and high damping couplings.

By applying a flexible coupling, the resulting sub-systems on both sides of the coupling are separated with respect to torsional vibrations[2]. Each side can further be treated separately and is not affected by the opposite one[1].

The cost of decoupling one torsional system into two sub-systems by a high elastic coupling is, that another low natural frequency is added to the whole system[1]. Typically, the added first node through the coupling generates a startup resonance at a low frequency that needs to be passed quickly to avoid an overload of the coupling.

There are many concepts of flexible couplings available that vary in the used damping and flexibility properties as well as in the used material. Among the different options, this paper focuses on torsional elastic, high damping steel spring couplings. The concept of radially aligned steel springs of the torsional vibration damper can be also extended to a power transmitting coupling. Its stiffness is again defined via the geometry and number of spring packs, whereas the use of pressurized oil that is pumped between the resulting chambers is also providing hydrodynamic damping.

The big advantages of this concept are the constant stiffness and that very high damping values can be achieved without a thermal overload of the couplings. Steel spring couplings show high robustness against oil, dirt and varying ambient temperatures and are only exposed to low wear.

3 Conclusive case studies

In this section, typical approaches how torsional vibration issues are identified and solved are illustrated. For this, two case studies with real existing reciprocating compressor applications are considered.

3.1 Four-cylinder compressor directly driven by an E-Motor

The frist case study deal with a simple system of a directly driven four-cylinder compressor shown in figure 13. Since this compressor is driven by an electric motor the only relevant source of forced excitation is caused by the compressor.

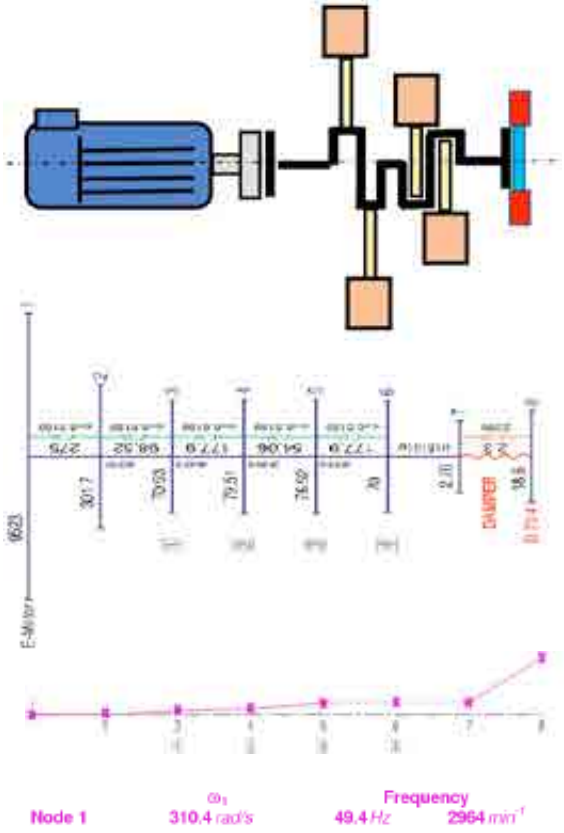

Figure 13: Four-cylinder compressor driven by an electric engine. Sketch, model, and mode shape diagram of first vibration mode.

As can be seen in the mass elastic system (fig. 13) the relatively large electric motor with an inertia of 9523 kgm² is directly connected to the crankshaft. At the free end of the compressor crankshaft a torsional vibration damper D 73/4 is mounted to the crankshaft. This steel spring-type Geislinger damper produces a relative damping of 2300 Nms/rad when pumping oil from one chamber into another.

Further you can see in the torsional system that the connecting shaft is short and rigid which lead to a high first order frequency near 49.4 Hz. The corresponding Campbell diagram shows a lot of higher order frequencies involved in the first and second node in the relevant operation speed range. As one can see in figure 14 some of them are just overlaying like the 8th order 1st node and the 11th order 2nd node at around 370 rpm.

by: David Richter-Trummer, Andreas Thalhammer, Thomas Bozezki – GEISLINGER

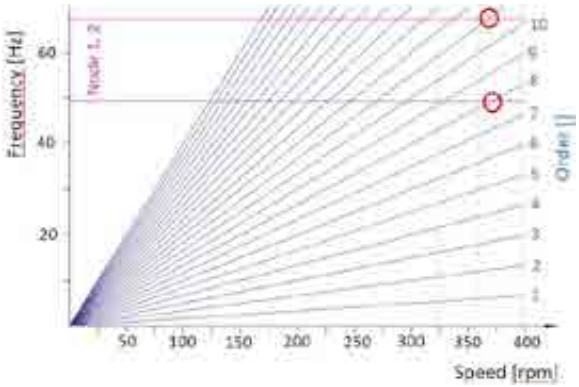

Figure 14: Campbell diagram of compressor system.

In the example of the four-cylinder compressor above, the system vibrations connected to the first eigenfrequency near 50 Hz are dominating and are generating rather high stresses in the crankshaft. Therefore, the damping effect of the damper was predominantly used to reduce the stress on the crankshaft over a widely varying speed range.

The damper was tuned to an eigenfrequency of about 56 Hz to get the optimized reduction of occurring torsional vibration amplitudes. Figure 15 shows the effect of this additional damping in the right frequency on the crankshaft stress of the compressor.

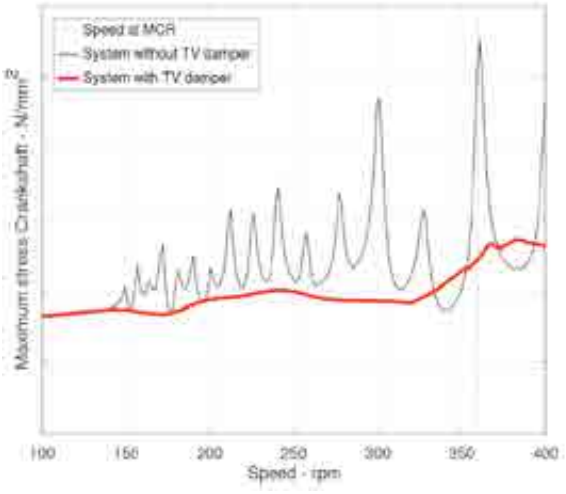

Figure 15: Reduction of crankshaft stress, when the D 73/4 damper is applied on the compressor.

Applying a torsional vibration damper results in lower dynamic torsional loads and thus, in lowering of crankshaft stresses, vibrations, noise and consequently to less wear [1]. The harmful vibration energy is dissipated as thermal load and transported by the oil to the cooling system.

3.2 Multiple cylinder four stroke engine with a 6-cylinder compressor

When compressors are getting bigger and performance increases, the driving machine typically becomes a four-stroke combustion engine. In these cases where a multiple piston four-stroke engine drives a compressor, the whole torsional system as well as the sources of excitations gain in complexity. Furthermore, it is not practicable anymore to combine both excitations into a single Fourier-series, since the four-stroke excitations contain dominant half order members which are completely missed in a "two-stroke"-like compressor excitation. Therefore, the calculation needs to be done twice for both sources of excitation separately and the output needs to be combined by superposition thereafter.

The torsional system of the second example is more complicated but as mentioned above the highly flexible coupling in the middle separates engine crankshaft and compressor crankshaft into two torsional vibration sub-systems. The benefit of this separation is that the compressor is not affected by any disturbing excitation torques from the engine and vice versa. Furthermore, a damper at the free end side of one of these crankshafts does not interfere with the second machine in any unexpected way.

In this application, the V 12 is coupled by a BC 100/20/175H/L Geislinger coupling to the compressor. This setup adds a low speed first node resonance with its node just in the coupling, as it can be seen in the mode shape diagram for the first node in figure 16.

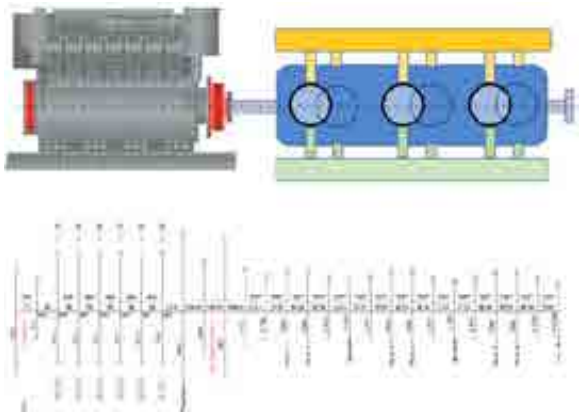

Node 1 6.717 Hz



by: David Richter-Trummer, Andreas Thalhammer, Thomas Bozezki – GEISLINGER

Node 2 36.89 Hz



Node 3 48.35 Hz



Figure 16: Sketch, model and mode shape diagrams of a 6-cylinder compressor driven by a V12 diesel engine.

The first excitation source is related to the combustion of fuel in the cylinders of the driving engine, where gas pressure pushes the piston down the cylinders. The mass of each piston and connection rod is partly compensated by an unbalance at the crankshaft. However, all these masses sum up to a separate mass excitation that is the second source of excitations.

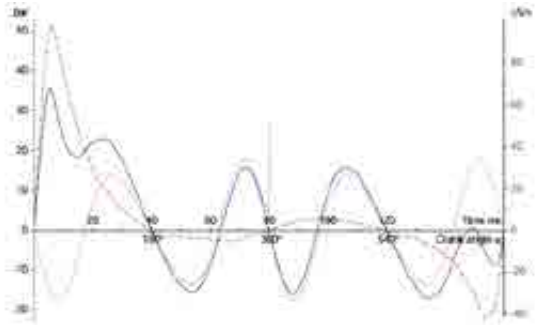

Figure 17: Excitations of the four-stroke diesel engine at full speed and full power. The dashed-brown line indicates the resulting tangential pressure from the combustion and the dotted-pink line shows the mass excitation. The blue line shows the sum of the 2 excitations.

For a detailed analysis, there are not only load cases relevant where every cylinder is running perfectly smooth. In process of outlining, also the worst case of one cylinder compression but not igniting is considered. This operation is referred to as misfiring operation and leads in many cases to the highest torsional vibration loads.

It is important that the speed and engine load has a high influence on the excitations and the dimensioning of couplings and dampers must ensure in all relevant operation condition sufficient safety. Therefore, it is necessary to analyze different load cases when outlining the optimized components.

Since there are two piston machines that can be operated in many ways, the sources of excitations and in particular their interactions must be covered in the torsional vibration analysis.

As mentioned above, the compressor is a significant source of forced torsional vibrations. The excitations can vary in a large range and look completely different to the excitations of a combustion engine, as shown in Figure 18. Since the compressor is a consumer of power the resulting torque of mass (dotted) and gas (dashed) is integrated as negative torque over the whole cycle of 360° crank angle.

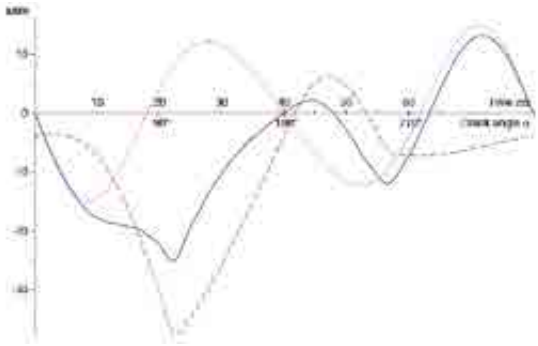

Figure 18: Excitations of the two-stroke compressor

After modelling the torsional system, setting up the relevant load cases and applying the appropriate excitations, it is the scope of torsional vibration engineers to identify and eventually solve occurring torsional vibration problems. Frequently set tasks are to keep the crankshaft stresses below certain limits for torsional vibration stress. For some components like chain drives, generator rotors or oil pumps also the rotational acceleration must be limited.

In this specific case the maximum stress due to torsional vibrations on the engine crankshaft is of main interest. The goal to reduce this stress as much as practicable, which is fulfilled best by using a high effective and compact D 85/6 damper at the engine free end side. It is important to state that a reduction of vibration energy in a frequently used speed range does not only reduce the shaft stress and angular acceleration, since torsional vibrations also can lead to lateral vibrations caused by the instantaneous speed fluctuations [1]. The resulting smoother run of a well dampened system reduces noise and the all-over load on many components and increases the long-term durability of many components of the system [1].

In case of the considered V12 four-stroke engine, the tuning of the damper is rather challenging. On the crankshaft a 6th order 3 node resonance led to a high load on the crankshaft near 450 rpm. These resonances increased the total synthesis dynamic stress to nearly 80 N/mm² at 440 rpm as it can be seen in the below diagram 19 where the occurring loads without any damper applied are shown. One can see that the synthesis of load (blue) is mainly

by: David Richter-Trummer, Andreas Thalhammer, Thomas Bozezki – GEISLINGER

composed of a 6th, the 5.5th and the 6.5th order resonance.

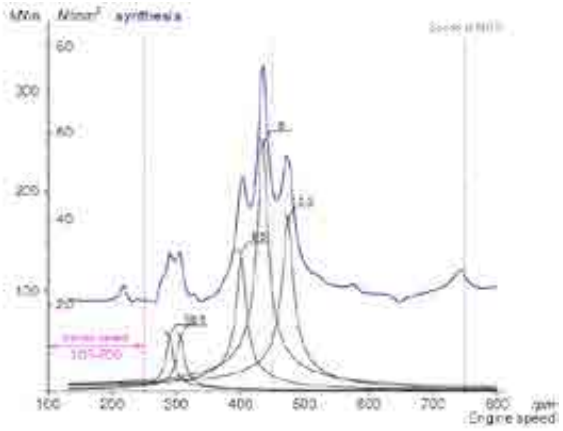

Figure 19: Engine crankshaft stress without damper

A compact D 85/6 damper was outlined to split and dampen mainly the 6th order frequency and could reduce the crankshafts torsional vibration stress from over 75 N/mm² to well below 30 N/mm² as illustrated in the following figure 20.

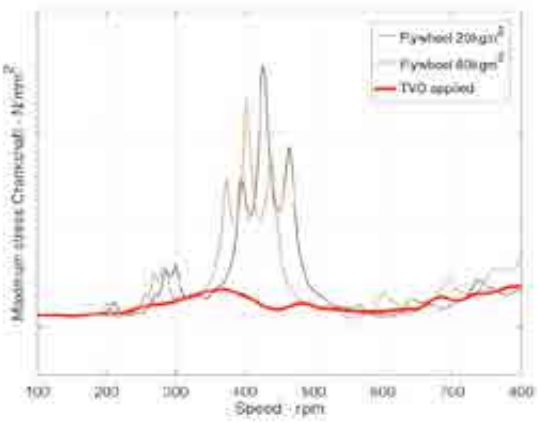

Figure 20: Effect of damper or different flywheels on the stress of the crankshaft

As one can see in figure 20 if we would apply just a flywheel instead of the damper, the shaft stress could by far not be reduced to comparable low values. Increasing the flywheel size only leads to a shift of resonances. This can for instance help to avoid a resonance that is appearing on the lower bound of the operation speed range.

In many applications, a wide operation speed range is needed, for example for the flow control of compressors[3]. In addition, the acceptable torsional vibration stress is limited. In such scenarios there is simply no way around a torsional vibration damper.

For the selection of an admissible flexible coupling, it is important to fulfil the given crankshaft limit that is provided by the engine manufacturer as well as having a closer look on the compressor's crankshaft loads. As explained above a torsional flexible coupling separates a torsional system into mainly independent sub-systems. It is then much easier to handle the problems of the separated systems individually without influencing the opposite system at the same time.

To conclude this case study, it is analyzed what are the results if the engine is connected to the compressor rigidly compared to applying a flexible coupling. For this, the direct comparison of the maximum crankshaft stress for both rigid and flexible coupling is shown in figure 21 below.

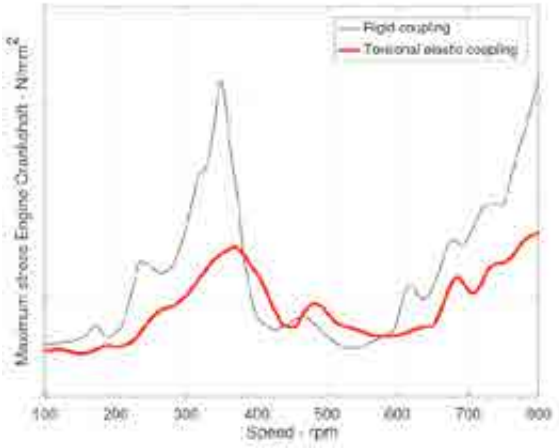

Figure 21: Influence of soft coupling on the crankshaft of the engine.

A stiff connection would result in increased crankshaft loads of the engine, but the influence on the compressor is far bigger in this case. A rigid connection would increase the dynamic load on the compressor crankshaft by a factor 8 as it can be seen in figure 22.

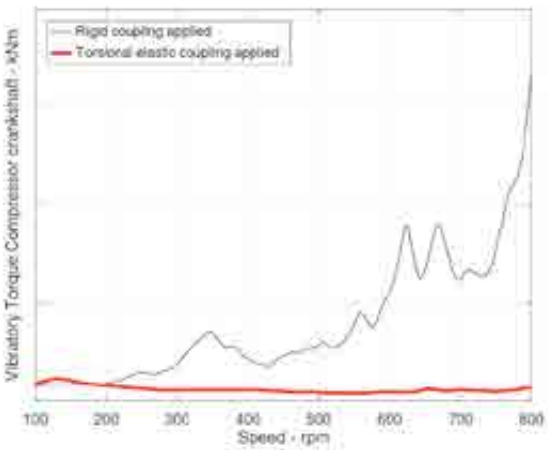

Figure 22: Compressor crankshaft torque for rigid a soft coupling.

by: David Richter-Trummer, Andreas Thalhammer, Thomas Bozezki – GEISLINGER

The high crankshaft stress in the engine could be reduced to less than 50% of its originally value by decoupling the compressor from the engine and apply a torsional vibration damper. The load on the compressor's crankshaft could also be significantly reduced.

4 Conclusion / Sum up

As shown in the two examples above, the starting investment in identifying and eventually solving torsional vibration issues in the outline phase of a new or even present plant pays off in the long run and ensures performance, durability and thus reduces cost and trouble for maintenance.

Flexibility, safety, endurance, and cost efficiency of compressor applications can significantly benefit from a correct treatment of torsional vibrations. Especially for multi-cylinder applications with large operation speed ranges for flow control as well as for compressors driven by combustion engines, torsional vibration issues often lead to unnecessarily high vibrations and as a consequence to increased wear, noise and failure risks of powertrain components.

Identifying, assessing, and eventually solving torsional vibration problems is therefore worth the effort.

References

[1] Newman, F; Stephens, T; Harris, R; (2012): Lateral-Torsional Vibration Coupling in Reciprocating Compressors, GMRC.

[2] Stephens, T; Prenninger, K; Yeister, C; Noon, S; PA (2017): Torsional Damping Benefits for Reciprocating Compressors, GMRC – Pitsburg

[3] Kacani, V; Rockel, C (2018): Management der Torsionsschingungen in Kolbenverdichteranlagen, 22. Workshop Kolbenverdichter KCE-Akademie Rheine

HASSE & WREDE

Optimizing the torsional vibration behavior of reciprocating compressors using a flywheel-integrated damper concept

by:

S. Willeke, S. Bohmeyer, N. Reinsperger and M. Steidl
Technology and Innovation department
Hasse & Wrede GmbH
Georg-Knorr-Stra.e 4, 12681 Berlin, Germany
sebastian.willeke@hassewrede.de

13th EFRC CONFERENCE
September 19th – 21st 2023, Zagreb

Abstract:
Due to the discontinuous working principle of reciprocating compressors, their drivelines are prone to detrimental torsional vibrations. During each working cycle, the cylinders experience a non-uniform gas pressure as a function of the crank angle. Therefore, the corresponding load components tangential to the crankshaft yield periodic fluctuations around the mean value of the static driving torque. Besides these gas loads, the linear translational motion of the reciprocating piston masses represents an additional source of excitation. These varying dynamic loads lead to torsional vibrations which are transmitted through the driveline and detrimentally affect the fatigue lifetime of the crankshaft and any connected components. As a countermeasure, barred speed ranges are defined around critical operating points to avoid large-amplitude resonant vibrations. Consequently, the compressor's operating range is reduced to a limited amount of feasible shaft speeds. In addition, flywheels, torsional vibration dampers, and couplings may be used to reduce torsional driveline vibrations to an acceptable level. Since the additional inertia of these components has to be driven by the powering unit of the driveline, the overall power demand may increase. Furthermore, the components required for torsional vibration mitigation have to be accommodated within the available installation space.
To address this issue, the application of a novel concept of a flywheel-integrated damper and coupling to mitigate torsional vibrations of reciprocating compressor drivelines is presented: the FIDC. Since the FIDC concept combines all components for torsional vibration reduction in a single compact device, it benefits from a reduced installation space comparable to that of an individual flywheel as well as a lower overall inertia when compared to using separated flywheel, damper, and coupling components. Consequently, it allows the realization of more compact driveline assemblies while requiring less driving power. To illustrate the benefits of the FIDC concept over conventional torsional vibration control strategies, an exemplary case study of a generic reciprocating compressor is presented. By simultaneously adapting the flywheel and damper properties of a rigidly coupled FID layout, an optimal tuning with respect to the target compressor application is achieved. Finally, the numerical results of torsional vibration analyses indicate an increase of the compressor's operating range since formerly inaccessible barred speed ranges become available.

by: Sebastian Willeke, Stephan Bohmeyer, Norbert Reinsperger and Michael Steidl – HASSE & WREDE

1 Introduction

1.1 Torsional vibrations in reciprocating compressors

The drivelines of reciprocating machines, like piston compressors for pipelines and internal combustion engines, are prone to torsional vibrations due to their discontinuous working principle. During each working cycle, the cylinders feature a non-uniform gas pressure as a function of the crank angle. Therefore, the corresponding pressure load components tangential to the crankshaft yield periodic fluctuations around the mean value of the static driving torque. Besides these gas loads, the linear translational motion of the reciprocating piston masses represents an additional source of excitation. The combination of both dynamic loads yields torsional vibrations which are transmitted through the driveline and detrimentally affect the fatigue lifetime of any connected components, e.g., the auxiliary oil pump[1]. This may lead to increased bearing wear and stresses which may, eventually, result in a cracking of the driver shaft.

To reduce the risk of a driver shaft fatigue failure, various countermeasures, e.g., blocked speed-ranges are defined around critical operating points which are in the proximity of the driveline's eigenfrequencies. A steady-state operation within these barred speed ranges (BSRs) is prohibited. Although a limited number of transient BSR passages can be accepted, they prevent a continuous operation at certain driveline speeds. Consequently, the compressor's possible operating range is reduced to a limited number of feasible shaft speeds. To shift, relieve or even remove these speed restrictions, various concepts for vibration mitigation can be applied to reduce torsional driveline vibrations to an acceptable level.

1.2 Torsional vibration mitigation

To mitigate the torsional forced response of reciprocating compressor drivelines, various countermeasures are taken to avoid large-amplitude resonant vibrations. One possibility is the tuning of the driveline's mass-elastic properties in order to achieve a specific dynamic behavior (e.g., eigenfrequencies shifted outside of the operating speed range)[2]. A common example for a passive vibration mitigation strategy is the application of an additional flywheel at the rear end of the compressor crankshaft. The flywheel's main purpose is the absorption, storage, and release of kinetic energy in order to compensate for any torque fluctuations. Furthermore, the flywheel increases the overall rotational inertia of the driveline which shifts the eigenfrequencies of critical low-order modes below the operating speed range.

In a similar way, torsional vibration isolation may be achieved by replacing the rigid connection between the compressor and its driving motor with a flexible coupling[3]. Such a decrease of the coupling's torsional stiffness will also yield reduced eigenfrequencies. Due to its reduced torsional stiffness, however, the coupling will suffer from increased static and dynamic deformations (i.e., larger torsional deflection angles). Consequently, the isolation capability of soft couplings is usually limited by the requirement of maintaining an acceptable level of static deflection while transmitting the static driving torque from the driver to the compressor. Besides the above measures which allow a mass-elastic tailoring of the driveline dynamics in terms of its modal properties (i.e., eigenfrequencies and mode shapes), the increase of the overall damping level offers another option to reduce torsional vibrations. To this end, torsional vibration dampers (TVDs) are used to dissipate the vibrational energy into heat by various means. Their main working principle is that of a damped torsional vibration absorber, see Fig. 1. They usually comprise an absorbing inertia component J_{abs} which is elastically coupled by a dissipating medium to the crankshaft J_{cs}. Since the FIDC concept presented in this paper is based on a viscous torsional vibration damper, a detailed description of this damper type is presented in the following Sec. 2. The viscoelastic coupling medium (e.g., rubber or a viscous fluid) provides a torsional stiffness k as well as a torsional damping d.

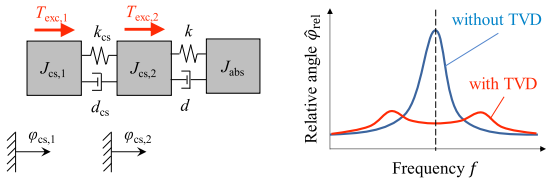

Figure 1: Schematic of a driveline model with torsional vibration damper (left) and forced response (right)

Finally, it has to be noted that the additional components (flywheel, flexible coupling, and damper) required for torsional vibration mitigation will usually increase the driveline's overall inertia which has to be driven by the motor. Consequently, the power demand during start-up of the compressor setup may increase. Furthermore, each component adds to the axial length of the driveline and has to be accommodated within the available installation space.

2 Viscous torsional vibration dampers

The present paper focuses on a novel vibration mitigation concept which is based on a viscous torsional vibration damper. The basic structure of such a viscous damper is shown schematically in Fig. 2. The damper consists of an inertia ring (secondary mass) floating inside a damper housing (primary mass)

by: Sebastian Willeke, Stephan Bohmeyer, Norbert Reinsperger and Michael Steidl – HASSE & WREDE

supported by axial and radial bearings. The clearance between the inertia ring and the damper housing is filled with a viscoelastic medium (e.g., a poly-mer like silicone oil).

In the absence of torsional vibrations, all damper components rotate with the rotational speed of the driveline. In the presence of torque fluctuations, however, a relative motion between the inertia ring and the damper housing occurs. The resulting shear of the viscous silicone oil dissipates vibrational energy into heat and, thus, dampens torsional vibrations. In addition, the elasticity of the polymer provides a torsional stiffness which couples the absorber mass (inertia ring) to the housing. Consequently, the damper acts as a damped torsional vibration absorber, see Fig. 1. To tune the damper's mechanical properties to the critical frequency of a specific compressor application, equivalent torsional stiffness and damping values are predicted based on a viscoelastic model of the silicone oil and the clearance geometry between the inertia ring and the damper housing.

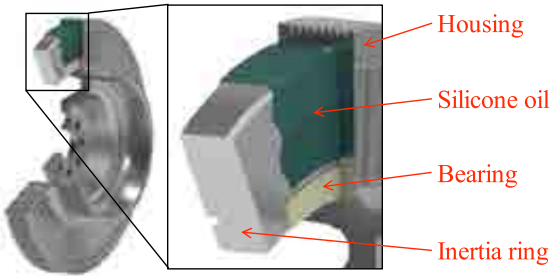

Figure 2: Viscous torsional vibration damper

2.1 Viscoelasticity

Polymers, like silicone fluids, often feature a viscoelastic behavior. While viscosity describes the shear behavior of fluids, elasticity is used to characterize the reversible deformation of solids. The term *viscoelasticity* indicates that the behavior of a fluid or solid combines both *viscous* and *elastic* properties. While the deformation of a purely elastic material is fully reversible, a viscous material is dissipating a certain amount of energy throughout a deformation cycle.

On the one hand, the shear stress τ of a Newtonian fluid depends on its dynamic viscosity η

$$\tau = \eta\dot{\gamma} \tag{1}$$

and the shear rate $\dot{\gamma}$, i.e., the gradient in the perpendicular direction y of the flow velocity component u that is parallel to the shear

$$\dot{\gamma} = \frac{du}{dy}. \tag{2}$$

On the other hand, the shear stress τ of an elastic solid body depends on the real-valued shear modulus G

$$\tau = G\gamma \tag{3}$$

and the shear strain γ, i.e., the gradient of the deformation x in perpendicular direction y

$$\gamma = \frac{dx}{dy}. \tag{4}$$

In other words, the shear modulus G represents the ratio between stress τ and strain γ

$$G = \frac{\tau}{\gamma}. \tag{5}$$

The dynamic response of a purely elastic material is characterized by time-dependent stress and strain variations which are in-phase, i.e., the variations exhibit a relative phase lag of 0°. For a purely viscous material, the strain variation $\gamma(t)$ lags a shear stress fluctuation $\tau(t)$ by a phase difference of 90°. Viscoelastic materials show a certain amount of stress-strain phase lag between 0° and 90°. To model this phase lag between the oscillating stress and strain, a complex dynamic modulus $\underline{G}$ is introduced

$$\underline{G} = G_{\Re} + \mathrm{i}G_{\Im}\,. \tag{6}$$

The real and imaginary parts $G_{\Re}$ and $G_{\Im}$ are called *storage modulus* (i.e., elastic property) and *loss modulus* (i.e., viscous property), respectively.

2.2 Clearance factor

For a given relative angular velocity $\dot{\varphi}$ between the inertia ring (IR) and the damper housing (H) in Fig. 3, the relative flow velocity u at a radius r is

$$u(y) = \dot{\varphi}\frac{r}{s}y\,. \tag{7}$$

Since the corresponding shear rate $\dot{\gamma}$ according to Eq. (2) is

$$\dot{\gamma} = \dot{\varphi}\frac{r}{s}, \tag{8}$$

the resulting shear stress τ in Eq. (1) becomes

$$\tau = \eta\dot{\varphi}\frac{r}{s}, \tag{9}$$

where s denotes the gap size of the oil-filled clearance between the inertia ring and the damper housing in the y-direction. Integrating the local shear stress τ over a surface area A yields the shear force F

by: Sebastian Willeke, Stephan Bohmeyer, Norbert Reinsperger and Michael Steidl – HASSE & WREDE

$$F = \int_A \tau \, d\tilde{A} \,, \tag{10}$$

and eventually the torque T at a radius r

$$T = Fr \,. \tag{11}$$

The tilde operator (~) in Eq. (10) is used in order to ensure a concise separation between the integration limit A and the integration variable $\tilde{A}$. Based on the orientation of the considered gap between the inertia ring and the damper housing in Fig. 4, the torque T will take one of the following forms[4]:

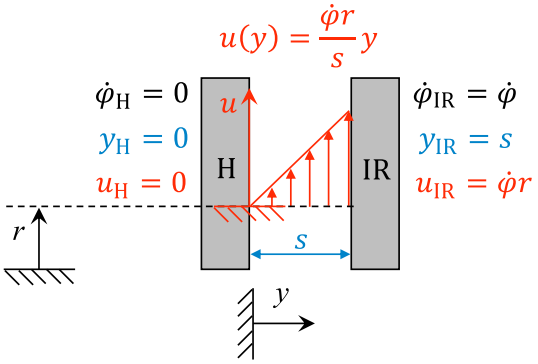

Figure 3: Schematic Couette flow across the axial gap between damper housing and inertia ring

- **Axial gap s_a between parallel circular faces**

The area dA of an incremental surface element of radial and angular dimensions dr and $d\varphi$ at the radius r is

$$dA = r \, d\varphi \, dr \,. \tag{12}$$

Combining Eqs. (11) to (12) yields the torque T_a for a circular sector with inner radius r_i, outer radius r_a and angular width θ

$$T_a = \int_{r_i}^{r_a} \int_0^{\theta} \tau \, r^2 \, d\tilde{\theta} \, d\tilde{r} = \int_{r_i}^{r_a} \tau \, r^2 \, \theta \, d\tilde{r} \,. \tag{13}$$

With the shear stress τ from Eq. (9), it follows

$$T_a = \int_{r_i}^{r_a} \eta \dot{\varphi} \theta \frac{r^3}{s_a} d\tilde{r} \,. \tag{14}$$

By assuming constant values for the dynamic viscosity η and the relative angular velocity $\dot{\varphi}$, the torque T_a for a full circular area (i.e., $\theta = 2\pi$) becomes

$$T_a = 2\pi\eta\dot{\varphi} \int_{r_i}^{r_a} \frac{r^3}{s_a} d\tilde{r} \,. \tag{15}$$

By defining the axial clearance factor $f_{c,a}$ as

$$f_{c,a} = 2\pi \int_{r_i}^{r_a} \frac{r^3}{s_a} d\tilde{r} \,, \tag{16}$$

the torque T_a becomes

$$T_a = \eta \dot{\varphi} f_{c,a} \,. \tag{17}$$

- **Radial gap s_r between coaxial cylindrical faces**

The area dA of an incremental surface element of axial and angular dimensions dx and $d\varphi$ at the radius r is

$$dA = r \, d\varphi \, dx \,. \tag{18}$$

The torque T_r results from a combination of Eqs. (10), (11), and (18) as follows

$$T_r = \int_0^{\ell} \int_0^{\theta} t \, r^2 \, d\tilde{\theta} \, dx = \tau \, r^2 \theta \, \ell \,. \tag{19}$$

With the shear stress τ from Eq. (9), it follows

$$T_r = \eta \dot{\varphi} \theta \frac{r^3}{s_r} \ell \,. \tag{20}$$

For a full annular radial clearance (i.e., $\theta = 2\pi$) of size s_r, the torque T_r is

$$T_r = 2\pi\eta\dot{\varphi} \frac{r^3}{s_r} \ell \,. \tag{21}$$

By defining the radial clearance factor $f_{c,r}$ as

$$f_{c,r} = 2\pi \frac{r^3}{s_r} \ell \,, \tag{22}$$

the torque T_r becomes

$$T_r = \eta \dot{\varphi} f_{c,r} \,. \tag{23}$$

By adding the torques of all axial and radial clearances, the total torque T of the damper becomes

$$T = \sum_i T_{a,i} + \sum_j T_{r,j} = \eta \dot{\varphi} f_c \,, \tag{24}$$

where f_c denotes the total clearance factor

$$f_c = \sum_i f_{c,a,i} + \sum_j f_{c,r,j} \,. \tag{25}$$

Further definitions of clearance factors for various gap shapes are available[4].

by: Sebastian Willeke, Stephan Bohmeyer, Norbert Reinsperger and Michael Steidl – HASSE & WREDE

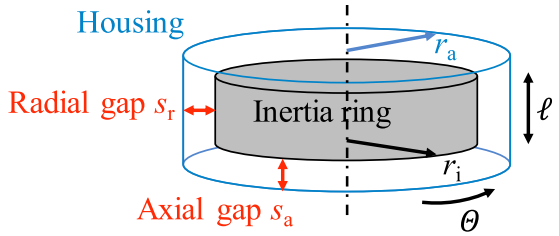

Figure 4: Schematic of the axial and radial gaps

2.3 Torsional damping and stiffness

In the following, the relative angular motion $\varphi(t)$ between the inertia ring and the damper housing is assumed to be a harmonic function of time t with a complex amplitude $\underline{\hat{\varphi}}$ and an angular frequency $\omega = 2\pi f$

$$\varphi(t) = \Re\left(\underline{\varphi}(t)\right) \text{ where } \underline{\varphi}(t) = \underline{\hat{\varphi}}\mathrm{e}^{\mathrm{i}\omega t}\,. \quad (26)$$

Replacing the relative angular velocity $\dot{\varphi}$ in Eq. (24) with the complex angular velocity $\underline{\dot{\varphi}}$

$$\underline{\dot{\varphi}}(t) = \mathrm{i}\omega\underline{\hat{\varphi}}\mathrm{e}^{\mathrm{i}\omega t} \quad (27)$$

yields the complex harmonic torque $\underline{T}$

$$\underline{T}(t) = \mathrm{i}\omega\underline{\eta} f_c\underline{\hat{\varphi}}\mathrm{e}^{\mathrm{i}\omega t}\,, \quad (28)$$

where the complex dynamic viscosity $\underline{\eta}$ is

$$\underline{\eta} = \eta_\Re + \mathrm{i}\eta_\Im\,. \quad (29)$$

According to the definition in Eq. (3), the harmonic variation of the complex shear stress $\underline{\tau}$ follows as

$$\underline{\tau}(t) = \underline{G}\,\underline{\hat{\gamma}}\mathrm{e}^{\mathrm{i}\omega t}\,, \quad (30)$$

where the complex shear modulus $\underline{G}$ is given in Eq. (6). In the same way, the definition of the shear stress in Eq. (1) yields

$$\underline{\tau}(t) = \mathrm{i}\omega\underline{\eta}\,\underline{\hat{\gamma}}\mathrm{e}^{\mathrm{i}\omega t}\,. \quad (31)$$

A comparison of the shear stresses in Eqs. (30) and (31) leads to the following relation between the complex shear modulus $\underline{G}$ and the complex dynamic viscosity $\underline{\eta}$

$$\underline{G} = \mathrm{i}\omega\underline{\eta}\,, \quad (32)$$

where

$$G_\Re = -\omega\eta_\Im \text{ and } G_\Im = \omega\eta_\Re\,, \quad (33)$$

or alternatively

$$\eta_\Re = \frac{G_\Im}{\omega} \text{ and } \eta_\Im = -\frac{G_\Re}{\omega}\,. \quad (34)$$

Substituting this complex dynamic viscosity in Eq. (28) yields the complex torque $\underline{T}$

$$\underline{T}(t) = (G_\Re + \mathrm{i}G_\Im)f_c\underline{\hat{\varphi}}\mathrm{e}^{\mathrm{i}\omega t}\,. \quad (35)$$

Introducing the torsional stiffness k_φ and torsional damping coefficient d_φ leads to

$$\underline{T}(t) = k_\varphi\underline{\varphi}(t) + d_\varphi\underline{\dot{\varphi}}(t)\,. \quad (36)$$

Finally, a comparison between Eqs. (35) and (36) results in the following torsional stiffness k_φ and damping coefficient d_φ of a viscous torsional vibration damper

$$k_{\mathrm{visc}} = G_\Re f_c \text{ and } d_{\mathrm{visc}} = \frac{G_\Im}{\omega}f_c\,. \quad (37)$$

By neglecting its temperature and shear dependence and assuming a constant oil viscosity η, a linearized mechanical model of the viscoelastic damper is obtained.

3 Modeling and analysis

3.1 Torsional driveline modeling

In the present study, the driveline of a reciprocating compressor configuration is represented by a lumped parameter model as shown in Fig. 5.

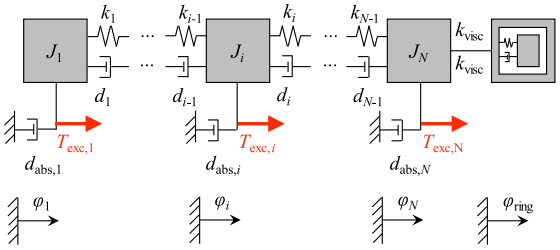

Figure 5: Lumped parameter model of compressors driveline with viscous damper

Each driveline component is represented by a rotational inertia J_i which motion is described by a single degree of freedom φ_i as a function of time t. For simplicity, the modeled torsional components in Fig. 5 are depicted using their corresponding symbols for linear translational motions. The motion of the driveline is governed by the following equation of motion in the time domain

$$\boldsymbol{J}\ddot{\boldsymbol{\varphi}}(t) + \boldsymbol{D}\dot{\boldsymbol{\varphi}}(t) + \boldsymbol{K}\boldsymbol{\varphi}(t) = \boldsymbol{T}_{\mathrm{exc}}(t)\,, \quad (38)$$

by: Sebastian Willeke, Stephan Bohmeyer, Norbert Reinsperger and Michael Steidl – HASSE & WREDE

where $\ddot{\boldsymbol{\varphi}}$, $\dot{\boldsymbol{\varphi}}$, and $\boldsymbol{\varphi}$ denote the angular acceleration, velocity, and displacement as a function of the time t, respectively. The diagonal matrix of the rotational inertia, the torsional damping matrix, and the torsional stiffness matrix are represented by $\boldsymbol{J}$, $\boldsymbol{D}$, and $\boldsymbol{K}$, respectively. The tridiagonal structure of the matrices $\boldsymbol{D}$ and $\boldsymbol{K}$ depends on the analyzed driveline configuration comprising the compressor's crankshaft, the viscous torsional vibration damper as well as additional components (e.g., flywheels and couplings). The vector $\boldsymbol{T}_{\mathrm{exc}}(t)$ on the right-hand side of Eq. (38) denotes the multiharmonic excitation torque of the compressor cylinders.

Assuming a harmonic angular motion and excitation of the i-th degree of freedom according to Eq. (26)

$$\underline{\varphi}_i(t) = \underline{\hat{\varphi}}_i \mathrm{e}^{\mathrm{i}\omega t} \text{ and } \underline{T}_{\mathrm{exc},i} = \underline{\hat{T}}_{\mathrm{exc},i} \mathrm{e}^{\mathrm{i}\omega t} \tag{39}$$

the equation of motion (38) is transferred from the time-domain into the following system of algebraic equations in the frequency-domain

$$(-\omega^2 \boldsymbol{J} + i\omega \boldsymbol{D} + \boldsymbol{K})\underline{\hat{\boldsymbol{\varphi}}} = \underline{\hat{\boldsymbol{T}}}_{\mathrm{exc}}(\omega)\,, \tag{40}$$

where the vectors of the complex displacement and torque amplitudes $\underline{\hat{\boldsymbol{\varphi}}}$ and $\underline{\hat{\boldsymbol{T}}}_{\mathrm{exc}}$ include the corresponding phase angles ξ_i and ζ_i, respectively

$$\underline{\hat{\varphi}}_i = \hat{\varphi}_i \mathrm{e}^{\mathrm{i}\xi_i} \text{ and } \underline{\hat{T}}_{\mathrm{exc},i} = \hat{T}_{\mathrm{exc},i} \mathrm{e}^{\mathrm{i}\zeta_i}\,. \tag{41}$$

Although the algebraic system of equations in Eq. (40) is linear, if the viscosity's dependence on the shear and temperature is neglected, it still comprises various harmonics due to the multiharmonic content of the excitation signal.

3.2 Torsional driveline analysis

The torsional vibration analysis (TVA) of a compressor driveline usually includes the following basic steps:[2]

1. Setup of the mass-elastic driveline model (incl. excitation data for all relevant operating points),
2. Modal analysis and multiharmonic forced response analysis of the driveline,
3. Interpretation of results (e.g., stress limits, electrical current fluctuations, and lifetime prediction).

One of its main purposes is the prediction of the driveline's forced response to the provided excitation signal as this is required in order to evaluate the corresponding stress distribution across the modeled driveline components. If an electric driving motor is used, its effect on the torsional driveline dynamics has to be considered[5,6]. Based on the outcome of the TVA, a suitable vibration mitigation concept (e.g., design of a TVD) is derived in order to fulfill the specified limit values and lifetime requirements for a given load profile. While the forced response is predicted by solving Eq. (39), the modal properties of the driveline are computed based on the following homogeneous equation of motion

$$(-\omega^2 \boldsymbol{J} + \boldsymbol{K})\hat{\boldsymbol{\varphi}} = \boldsymbol{0}\,. \tag{42}$$

Rearranging Eq. (42) yields the eigenvalue problem

$$\lambda_j \boldsymbol{J}\hat{\boldsymbol{\psi}}_j = \boldsymbol{K}\hat{\boldsymbol{\psi}}_j\,, \tag{43}$$

where $\lambda_j = \omega_j^2$ denotes the eigenvalue (i.e., the eigenfrequency $f_j = \frac{\omega_j}{2\pi}$) corresponding to the j-th mode shape $\hat{\boldsymbol{\psi}}_j$ of the driveline.

4 The FIDC concept

If a compressor driveline suffers from increased torsional vibrations, several countermeasures exist in order to reduce the occurring stresses below an acceptable limit value, see Sec. 1.2. An exemplary overview of five alternative driveline setups with different mitigation concepts is presented schematically in Fig. 6.

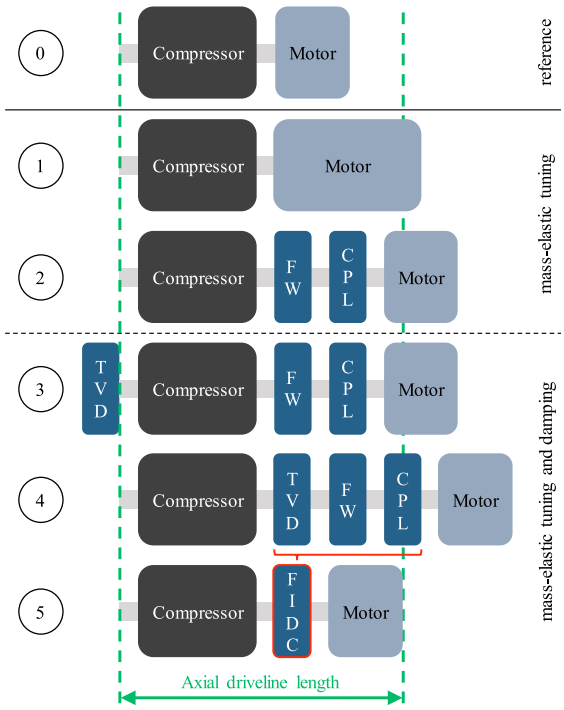

Figure 6: Schematic compressor drivelines with various concepts for torsional vibration mitigation

4.1 Setup 0: Reference driveline

In the reference configuration ⓪, the compressor is rigidly connected to the driving motor. This setup comprises only the most essential components and, thus, benefits from a very compact driveline.

by: Sebastian Willeke, Stephan Bohmeyer, Norbert Reinsperger and Michael Steidl – HASSE & WREDE

The driveline components, however, may experience increased dynamic stresses due to the absence of a vibration mitigation concept.

4.2 Setup 1: Driveline with large motor

In order to avoid resonant torsional vibrations, an intersection of the driveline's eigenfrequencies and the speed lines for various orders of the multiharmonic excitation should be prevented. To this end, the driveline's mass-elastic properties are tuned accordingly in configuration ① and ②. In configuration ①, the inertia of the driving motor has been increased to shift the eigenfrequencies of any critical modes to rotational speeds below the compressor's operating range. Consequently, the motor acts as a flywheel. The size of the installed motor is, however, much larger than it would be required to drive the compressor. Although torsional vibration issues can be solved by this setup, the overall configuration may become rather expensive due to the oversized motor.

4.3 Setup 2: Driveline with flywheel and coupling

To limit the motor in size, additional components have to be installed within the driveline, see configuration ②. For example, a separate flywheel (FW) can be added to the driveline in order to compensate for the missing rotational inertia of the downsized motor. As an alternative or in addition to the flywheel, an elastic coupling element (CPL) can be installed to realize torsional vibration isolation. Although the number of required driveline components increases, this setup may be favored over configuration ① from a financial point of view if the expenses of the additional components remain below the cost of an oversized motor. On the downside, however, the overall axial length and complexity of such a driveline is increased due to the additional installation space required for mounting the flywheel and coupling components.

4.4 Setups 3 & 4: Driveline with damper, flywheel and coupling

If the design space spanned by the mass-elastic driveline properties is not sufficient to realize the required driveline dynamics, an additional damping component may be considered. A torsional vibration damper (TVD) can usually be mounted either at the front end (configuration ③) or at the rear end (configuration ④) of the compressor crankshaft. The optimal damper location as well as its design depends on the specific properties of the driveline, e.g., the mode shapes under consideration or the available installation space. Since low-order torsional modes often feature a modal displacement node in the proximity of the crankshaft's rear end, the TVD is usually installed at its front end. By adding the damper as a separate component in order to fulfill the given vibration limits, the overall driveline length usually increases.

4.5 Setup 5: Driveline with FIDC

In order to decrease the number of separate driveline components and to minimize the driveline's axial length, the last setup ⑤ in Fig. 6 makes use of a novel flywheel-integrated damper and coupling (FIDC) concept, see Fig. 7. Within the scope of the FIDC concept, the functional purpose of the TVD component is twofold: On the one hand, the relative motion between the damper components provides an additional source of energy dissipation by viscous damping. On the other hand, the rotational inertia of its components (especially the damper housing) acts as a flywheel. The same holds true for an optional elastic coupling component which does not only provide a reduced torsional stiffness but also adds to the moment of inertia. While the flywheel functionality is mainly focused on the low speed range (i.e., the primary and secondary inertia act as a single rigid body), the viscous damping properties take effect at higher frequencies. Consequently, the FIDC component provides torsional vibration damping as well as vibration isolation capabilities in a single component by combining the mitigation concepts ② and ④ in Fig. 6. By integrating the functionality of the flywheel, damper, and coupling into a single component, the FIDC-equipped driveline setup ⑤ benefits from a reduced axial length when compared to configuration ④ with separate components. Furthermore, the properties of all three components can be optimally tuned with respect to each other during the FIDC design phase. The FIDC concept can be applied to machines with fixed and variable speed.

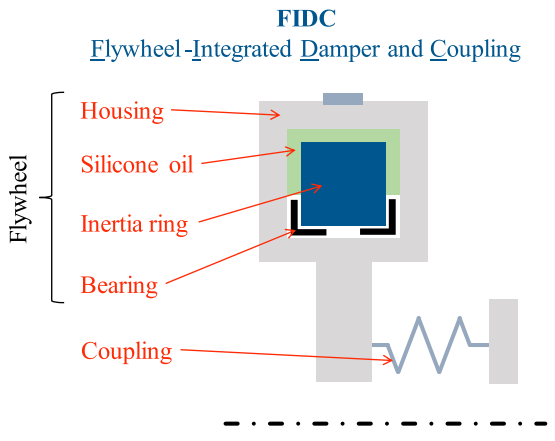

Figure 7: Schematic concept of the FIDC compo-nent

Finally, it has to be noted that the option of adding a flexible coupling to the driveline depends on the specific compressor configuration. Usually, a rigid connection between the compressor and driving motor is used. Flexible couplings may be an option for applications with variable speed in order to shift the

by: Sebastian Willeke, Stephan Bohmeyer, Norbert Reinsperger and Michael Steidl – HASSE & WREDE

driveline's eigenfrequencies and avoid barred speed ranges[3]. Consequently, the FIDC concept may be reduced to an FID approach (without a flexible coupling) for compressor applications with rigidly coupled drivers, see Sec. 5.

5 Application of the FIDC concept

In this section, the FIDC concept presented in Sec. 4 is applied to a generic compressor driveline. A short description of the compressor configuration and its vibration issues is presented in Sec. 5.1. The design of the FID component and the TVA results are discussed in Sec. 5.2 and 5.3. The main findings are summarized in Sec. 5.4. The values are presented in normalized form.

5.1 Compressor configuration

The generic drive train resembles a reciprocating compressor with six cylinders driven by an electric motor. It comprises a flywheel which is located at the rear end of the compressor crankshaft. A rigid coupling between the compressor and driver is used. For the current driveline setup, the stress limits (i.e., the torsional fatigue strength) are not fulfilled in the operating range. As a consequence, the risk of potential driver shaft failures due to increased resonant stresses exists.

As an initial solution, the installation of a conventional viscous TVD at the compressor front end is proposed. This approach, however, proves to be insufficient in terms of stress reduction. To solve this issue, an alternative mitigation concept based on the FIDC approach presented in Sec. 4 is applied. Since replacing the rigid connection between the driver and compressor is not an option for the current configuration, the installation of a flexible coupling is not considered. Therefore, the FIDC concept is condensed to an FID approach by excluding the coupling element.

5.2 Design of FID component

As stated in Sec. 4, the FID component provides both viscous torsional vibration damping as well as increased rotational inertia (i.e., the damper acts as a flywheel). From a design perspective, the contouring of the inner housing geometry is mainly driven by damping considerations. To this end, established design guidelines[4] for conventional torsional vibration dampers can be applied (i.e., the geometry of the fluid-filled clearance between the housing and the inertia ring in Sec. 2). The design of the outer housing geometry, however, is mainly focused on the compensation of the replaced flywheel's rotational inertia. This includes all functions and interfaces of the flywheel which are integrated into the FID housing.

5.3 Torsional vibration analysis

For the TVA, the analyzed compression train is represented by a lumped parameter model comprising 24 degrees of freedom, see Fig. 5. Within this model, the compressor crankshaft is discretized with 12 inertia elements which include the six compressors throws. At each throw station, the corresponding excitation torque $T_{\mathrm{exc},i}$ is applied.

Based on this model, a modal analysis of the compressor train without any TVD is conducted, see Eq. (43). The resulting first torsional mode shape is normalized and shown in Fig. 8. The front end (station 1) and rear end (station 12) of the compressor crankshaft are marked in blue and red, respectively. It can be seen that the normalized modal displacement amplitude $\hat{\psi}_{\mathrm{norm},1}$ at the front end features a maximum value. In contrast to this, the corresponding value at the rear end is $\hat{\psi}_{\mathrm{norm},12} = 0.73$. From this modal perspective, the installation of a viscous damper at the front end in combination with the present flywheel at station 12 appears to be a valid approach to mitigate torsional vibrations.

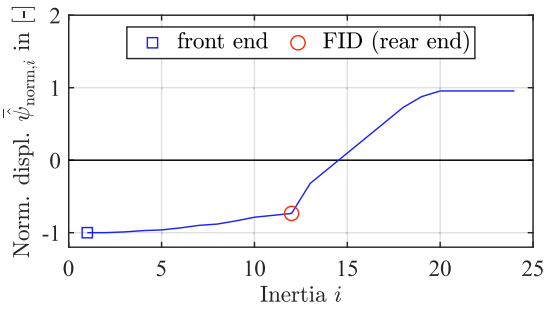

Figure 8: Normalized first torsional mode shape of the compressor driveline

In order to compare different vibration mitigation concepts for the present driveline configuration, the following TVAs are conducted:

- reference driveline without vibration mitigation concept (config. ⓪ in Fig. 6),
- driveline with conventional viscous TVD mounted at compressor front end (config. ③ in Fig. 6),
- driveline with FID component mounted at compressor rear end replacing the flywheel (config. ⑤ in Fig. 6 without flexible coupling).

By connecting the conventional TVD rigidly to the front end (station 1) of the compressor crankshaft, the housing inertia $J_{\mathrm{hous,visc}}$ is added to the crankshaft's rotational inertia J_1. In this configuration, the flywheel inertia J_{fw} is added to the inertia J_{12} at the crankshaft's rear end. If the FID component is added to the driveline, the flywheel inertia J_{fw} is first subtracted from station 12 and then replaced by the FID

by: Sebastian Willeke, Stephan Bohmeyer, Norbert Reinsperger and Michael Steidl – HASSE & WREDE

housing. Since the FID component features about the same rotational inertia as the replaced flywheel, the overall inertia of the driveline remains almost unchanged compared to the reference configuration.

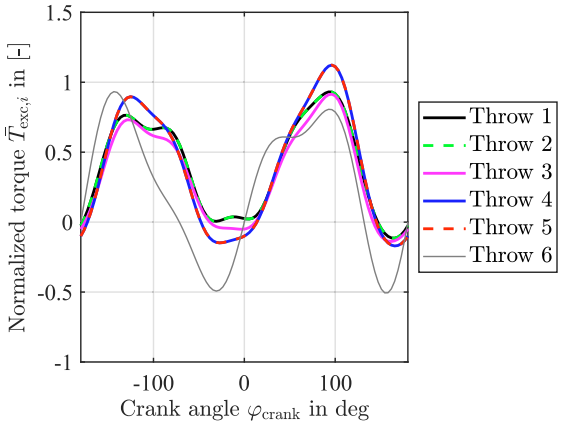

Figure 9: Normalized excitation torque at compressor throws

The time-dependent excitation torque $T_{\mathrm{exc},i}(t)$ which is applied to the six compressor throws is shown as a function of the crank angle φ_{crank} in Fig. 9. It can be seen that each throw features a multiharmonic torque signal. This is due to the periodic variation of the cylinder pressure which is superposed with a different harmonic of the mass forces caused by the moving pistons and their connecting rods.

The results of the forced response analysis are shown in Figs. 10 and 11 in terms of torque and stress peak-to-peak amplitudes. All results are normalized with respect to their corresponding limit values. Geometric features (e.g., holes, notches and fillets at shaft shoulders) which may cause local stress concentrations are not considered in the preliminary stress prediction for a generic compressor setup.

Fig. 10 reveals, however, that the torque at the crankshaft's rear end exceeds the limit value at two speed ranges if no TVD is installed. Although the torque limit at high rotational speeds can be fulfilled by installing a viscous TVD at the front end, its damping capability is not sufficient to mitigate the low frequency resonance. The FID, however, is able to significantly reduce the torque amplitudes at both resonance speeds below the corresponding limit value.

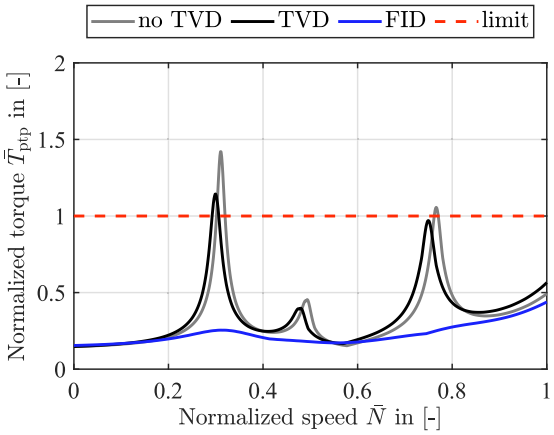

Figure 10: Normalized torque at rear end of compressor crankshaft

The same holds true for the dynamic stress results in Fig. 11: While the conventional TVD is not able to provide sufficient damping to fulfill the stress limit, the driveline configuration equipped with an FID component yields a significant stress reduction.

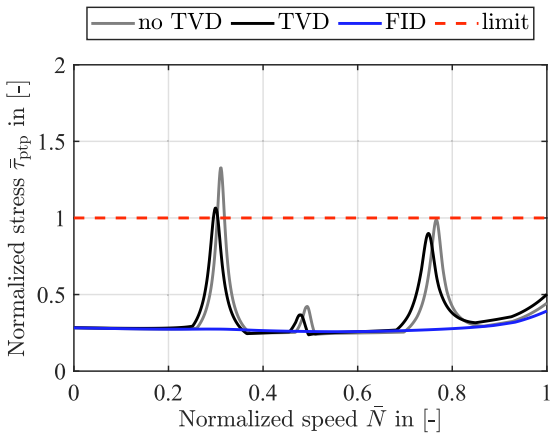

Figure 11: Normalized stress envelope over all components

5.4 Findings

The forced response of the reference driveline without any torsional vibration mitigation concept reveals the presence of two barred speed ranges in which the specified limit values are not fulfilled. By installing a conventional TVD at the front end of the compressor crankshaft, the torque and stress levels at high rotational speeds can be reduced sufficiently. The blocked speed range at low rotational speeds, however, persists. On the contrary, the FID component is able to mitigate the torsional response across the entire analyzed speed range. By resolving both barred speed ranges, the compressor's operating range is maximized.

In summary, it can be noted for the analyzed driveline configuration that the FID component at the compressor's rear end yields a better vibration mitigation performance than a conventional TVD

by: Sebastian Willeke, Stephan Bohmeyer, Norbert Reinsperger and Michael Steidl – HASSE & WREDE

combined with a flywheel. This result may, however, appear surprising at first, when considering that the modal displacement at the compressor's front end exceeds the corresponding deflection at its rear end, see Fig. 8. The main reason for this is the unique functionality of the FID component which acts both as a flywheel as well as a torsional vibration damper, see Sec. 4. In addition, the number of components for the FID-equipped driveline, its axial length, as well as its overall rotational inertia are identical to the reference case without any mitigation concepts applied. Consequently, the FID component showcases a superior performance and a reduced amount of parts when compared to a front end-mounted viscous TVD in combination with a rear end-mounted flywheel.

6 Conclusions

In the present paper, a novel concept for torsional vibration mitigation has been presented. The FIDC approach combines the concept of mass-elastic driveline tuning with viscous torsional vibration damping in a single component which can be used to replace an existing flywheel. An exemplary case study of a generic reciprocating compressor setup suffering from torsional vibration issues reveals that an FID-equipped driveline outperforms a setup with a conventional front end-mounted TVD and rear end-mounted flywheel. In summary, the benefits of replacing an existing flywheel by an FID component are:

1. The overall rotational inertia of the driveline does not change.
2. The number of driveline components remains unchanged (or even reduces when compared to a TVD solution with external flywheel).
3. The axial length of the driveline is not changed (or even reduces when compared to a TVD solution with an external flywheel).
4. The FID concept may outperform alternative TVD-equipped setups in terms of torsional vibration mitigation of reciprocating compressor drivelines.

By resolving the driveline's torsional vibration issues using the FIDC approach, blocked speed ranges are avoided and the overall operating range for the compressor application is maximized.

Nomenclature

A	surface area
abs	absolute, absorber
CPL	coupling
CS	crankshaft
d	torsional damping
exc	excitation
f_c	clearance factor
f_i	eigenfrequency of mode j
F	shear force
FIDC	flywheel-integrated damper and coupling
FW	flywheel
$G, G_\Im, G_\Re$	shear modulus, loss modulus, storage modulus
H, IR	damper housing, inertia ring
i, i	index, imaginary unit
J	rotational inertia
k	torsional stiffness
N	rotational speed
r	radius
s, s_a, s_r	gap size of clearance between inertia ring and damper housing, axial clearance, radial clearance
t	time
T, T_{exc}	torque, excitation torque
TVA	torsional vibration analysis
TVD	torsional vibration damper
u	flow velocity parallel to shear
visc	viscous
y	gap coordinate perpendicular to shear
$\gamma, \dot{\gamma}$	strain, shear rate
ζ, ξ	phase angles of excitation and response
η	dynamic viscosity
θ	circumferential angle
λ_j	eigenvalue of mode j
τ	shear stress
φ, φ_{crank}	angular coordinate, crank angle
ψ	modal displacement angle
ω	angular frequency
$\overline{(\ )}$	normalized quantity
$\tilde{(\ )}$	integration variable
$\hat{(\ )}$	amplitude
$\underline{(\ )}$	complex-valued quantity
$(\ )_{ptp}$	peak-to-peak value

References

[1] Murray, B. D.; Howes, B. C.; Chui, J. and Zacharias, V.: Sensitivity of Torsional Analyses to Uncertainty in System Mass-Elastic Properties. In Proceedings of the First International Pipeline Conference, Calgary, ASME (1996).

[2] Murray, B. D.; Howes, B. C. and Zacharias, V.: A Systems Approach to Torsional Analysis. In Proceedings of the Canadian Machinery Vibration Association National Conference, Halifax (1995).

[3] William, B. F.: Modularized Reciprocating Compressor Systems and the Factors That Influence Their Design. In Proceedings of the 11th EFRC conference, Madrid (2018).

[4] Hafner, K. E. and Maass, H.: Torsionsschwingungen in der Verbrennungskraftmaschine. Springer, Vienna (1985).

[5] Holopainen, T. P.; Jörg, P.; Niiranen, J. and Andreo, D.: Electric Motors and Drives in Torsional Vibration Analysis and Design. In Proceedings of the 42nd Turbomachinery Symposium, Houston (2013).

[6] Brunelli, M.; Fusi, A.; Grasso, F.; Pasteur, F. and Ussi, A.: Torsional Vibration Analysis of Reciprocating Compressor Trains driven by Induction Motors. 9th International Conference on Compressors and their Systems, IOP Conference Series: Materials Science and Engineering, Vol. 90(1), (2015).

Green hydrogen can also pulsate – Successful use of a Helmholtz resonator

by:

Johann Lenz
Technical Director
j.lenz@koetter-consulting.com

Franz-Josef Düttmann
Senior Engineer

KÖTTER Consulting Engineers GmbH & Co. KG
Rheine, Germany

13th EFRC CONFERENCE
September 19th – 21st 2023, Zagreb

Abstract:
For injection of hydrogen into the existing natural gas pipeline system, a 1 MW electrolysis plant was installed in Haurup near Handewitt, directly adjacent to the neighboring wind farm. For this purpose, two diaphragm piston compressors are used, which feed the hydrogen with up to 2 % volume fractions into the natural gas pipeline system. During commissioning of the plant, volume measurements by rotary piston meters showed a significant over-reading, which did not allow regular operation of the plant. Increased pulsations of the compressor could be identified as the cause. To solve the problem, a special Helmholtz resonator was designed and installed. As a result, a pulsation reduction of up to 96 % was achieved. Since then, the plant has been able to inject green hydrogen during regular operation without any pulsation problems.

by: Johann Lenz; Franz-Josef Düttmann – KÖTTER CONSULTING

1. Introduction

In the context of the transition to sustainable energy solutions, the use of hydrogen as an energy carrier is becoming increasingly important[1]. The use of hydrogen offers a high potential for saving greenhouse gas emissions.

Due to the strongly increasing share of renewable energies in the electricity mix, temporary peaks in power generation are occurring more and more frequently. In order to guarantee a stable electricity grid, wind turbines have to be shut down or even switched off in the event of such power surpluses. In order to use these peaks, the wind power can, for example, be electrolytically converted into hydrogen on site ("power-to-gas") and then fed into the natural gas grid.

The following article deals with the specific problems of commissioning such a hydrogen feed-in plant. In order to feed the hydrogen generated from electrolysis into the existing natural gas system, the hydrogen must first be compressed. For this purpose, piston compressors with variable delivery rates (speed control, bypass) were used to feed the hydrogen into the existing natural gas pipeline system at a pressure of up to approx. 84 bar.

2. Technical project description

In the **Windgas Haurup**[2] project near Flensburg, surplus wind power is converted into hydrogen by means of electrolysis and fed into the gas grid, as previously described. The project is part of the ”Norddeutsche Energiewende 4.0“ (NEW 4.0) programme, in which technologies with particular benefits for the energy transition are tested in practice.

2.1 Electrolysis

The conversion of surplus wind power into hydrogen is carried out by an H-TEC SYSTEMS ME450/1400 electrolyser (Figure 1).

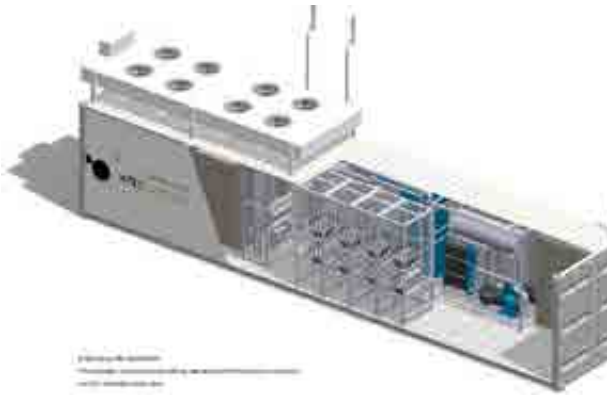

Figure 1: Used Electrolyser H-TEC SYSTEMS ME450/1400 (Windgas-Haurup[3])

The existing gas grid on site is used for the H2 admixture. This means that the existing infrastructure can quickly and easily take over the storage and transport of the hydrogen.

The nominal electrical output is 1 MW and the production rate is 210 Nm³/h. The technical information is listed in Table 1 below.

Type	PEM electrolysis (Protone Exchange Membrane)
Power	1 MW; 210 Nm³/h
Manufacturer	H-TEC SYSTEMS (www.h-tec-systems.com)
Operator	Energie des Nordens
Electricity procurement	Wind energy
Operating modes	Top-shelf power (EinsMan); Electric power supply for regulation
Use of hydrogen	Feeding into the gas grid (heat supply)
Approximate hydrogen production	Approx. 3,000 MWh/year
Possible heat supply	600 apartments*
Potential CO2 avoidance	530 t per year**

*Assuming an average annual consumption for a 50 m² flat of 5,000 kWh of gas.

**at 25 g CO2e emissions per kWh of green hydrogen used compared to 202 g CO2e/kWh of natural gas; corresponds to the annual storage capacity of 53 ha of forest.

Table 1: Performance overview of the PEM electrolysis used in Haurup (Windgas-Haurup[3])

2.2 Hydrogen compression

Two piston diaphragm compressors (Fig. 2) are used in Haurup to compress the hydrogen from approx. 30 bar to 84 bar. Both, piston diaphragm and piston compressors, are characterised by their very wide range of application with varying operating conditions with regard to suction and discharge pressures as well as a good controllability of the delivery rate. In relation to this high flexibility, piston compressors offer excellent efficiencies and are characterised by a particularly robust operating behaviour. A significant advantage in the compression of hydrogen is, among other things, possible discharge pressures of up to 500 bar. A disadvantage of the piston compressor is its periodic operating principle and the associated dynamic

by: Johann Lenz; Franz-Josef Düttmann – KÖTTER CONSULTING

excitation mechanisms with regard to pulsations and vibrations.

Pulsations and vibrations in piping systems close to compressors are often directly related. Pulsations within the system lead to dynamic forces at any changes in cross-section, pipe bends and other installations, which represent a direct excitation for the piping system and often result in vibrations.

In order to prevent possible inadmissible vibrations already in the planning phase, so-called pulsation studies are often carried out in advance. In pulsation studies, the interaction of the compressor with the associated system is checked numerically. If unacceptable pulsations are to be expected in the connected piping system, optimisations of the plant design or basic countermeasures are worked out. A substantial result of such a pulsation study is the design and dimensioning of mostly individually manufactured pulsation dampers. These are installed as close as possible to the cylinder flanges and enable a first significant reduction of the pulsations induced by the compressor operation.



Figure 2: Belt-driven piston diaphragm compressor for hydrogen compression and vertical suction- and discharge-side pulsation dampers visible in the background

The exact calculation designs are specified in API Standard 618 (American Petroleum Institute)[7]. The further acoustic calculations refer to the "gas column vibrations" within the connected piping system. Experience has shown that one-dimensional flow simulations in the time domain are suitable to calculate the expected pulsation level during the operation of reciprocating compressor systems already in the planning phase and to elaborate necessary measures.

In addition to considering the pressure pulsations in the piping system, a pulsation study can also include a structural-mechanical consideration of the system layout. The scope of such a study usually depends on the individual requirements of the system. One criterion for the selection can be the permissible pulsation amplitudes, as for example in the present case.

2.3 Quantity measurement

Compared to calibrated natural gas quantity measurement, the possibilities for measuring the quantity of pure hydrogen have been limited so far. In Haurup, a proven measuring method for hydrogen was used in the form of the rotary piston meter, which represents a good compromise between construction length (virtually no inlet and outlet sections required), measuring range, accuracy and cost-effectiveness for this application.

The rotary piston meter is a volumetric measuring meter based on the positive displacement principle. When there is a pressure difference between the inlet and outlet side, a torque is exerted on the rotary pistons and they start to rotate. The volume of the gas enclosed in each case is known. The two rotating pistons are separated by a very narrow gap of approx. 1/100 mm and do not touch each other as they are synchronised via gear wheels.

The revolutions are transmitted mechanically to a roller counter via a gear and are proportional to the gas volume passed through. Furthermore, electrical pulse generators are often used as a low-frequency signal (LF signal, 1 to 10 pulses/m³) or high-frequency signal (HF signal, 1,000 to 15,000 pulses/m³). A disadvantage of this meter principle is the mode of operation, which can lead to pressure fluctuations and resulting vibrations in the connected piping system. In addition, rotary piston meters are sensitive to pulsations of the piping system with regard to measuring accuracy. In addition to the common two-lobe piston design (see Figure 3), a three-lobe helically twisted piston design was used in the present case. Due to the continuously sloping trailing edge, this can be assumed as almost pulsation-free.

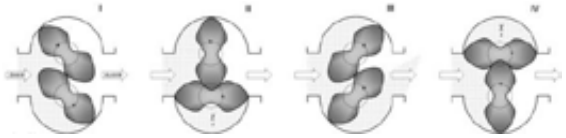

Figure 3: Functional principle of a rotary piston meter (Wikipedia[4])

2.4 Overall hydrogen feed system

The hydrogen feed system downstream of the electrolysis consists of a filter unit, a V = 5 m³ buffer vessel, two rotary piston meters connected in series and the two single-stage, single-cylinder diaphragm piston compressors E-100/200, see Figure 4. The compressors are designed redundantly and are not operated in parallel.

by: Johann Lenz; Franz-Josef Düttmann – KÖTTER CONSULTING

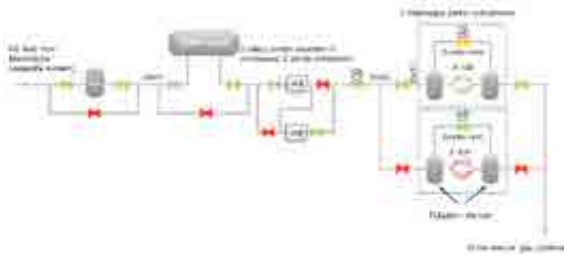

Figure 4: Schematic illustration of the hydrogen compression after electrolysis

The large buffer vessel, see Figure 5 is used to bridge the regeneration operation of the high-pressure PEM electrolyser (process-related pausing of hydrogen production for approx. 20 min. and up to 48 times a day). The volume meters ensure that the maximum amount of hydrogen fed into the natural gas pipeline does not exceed a volume share of 2 %. The delivery rate is primarily adjusted with a compressor bypass between the discharge and suction sides. For higher delivery rates, the speed of the compressor can also be increased.



Figure 5: Buffer vessel (V = 5 m³) for bridging during regeneration operation

3. Problems during commissioning

Already during commissioning the measured volumetric flow rate was found to differ considerably from the quantities fed in (set values from the electrolyzer). In part-load operation, the rotary piston meters always determined a volume that was far too large (estimated error ≥20%). With larger quantities, this error seemed to decrease. Furthermore, there is a technical requirement to interrupt the hydrogen feed into the natural gas grid several times a day without shutting down the compressor. In this case, the compressor should continue to run with the compressor bypass open without delivery. The problem with this mode of operation was that an apparent delivery rate of up to approx. ¼ of the maximum rate was displayed via the rotary piston meters, although definitely no hydrogen was being delivered. Under these conditions, it was not possible to precisely regulate the volume of hydrogen to 2 % in the natural gas pipeline.

All components of the system were then checked again and various tests were run. However, the cause of the mismeasurement remained unclear, leading to consideration of a targeted investigation.

4. Metrological investigation

KÖTTER Consulting Engineers GmbH & Co KG (KCE) was commissioned by the plant manufacturer, Streicher Anlagenbau GmbH & Co KG, to carry out an investigation of the problem in order to analyse the exact cause. For this purpose, an extensive measurement of the pressure pulsations was carried out in the first step. In the present case, the situation was not clear, since pulsations are generated by the piston compressor - but at the same time the operation of a rotary piston meter also leads to forced pressure fluctuations and, in addition, the acoustics of the piping system can amplify the pulsations through acoustic resonances depending on the position. For this reason, the measuring points for pulsations were applied extensively in the system (see Figure 6).

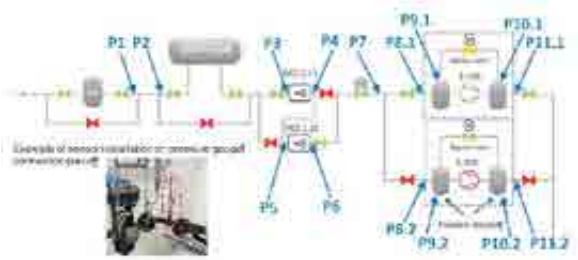

Figure 6: Measuring points for the acquisition of pressure pulsations

In addition, the compressor speed and the HF signals of the two series-connected rotary piston meters were also recorded. All measured variables were recorded time-synchronously and at high frequency via a central data acquisition system for various operating points (see Table 2). The electrolysis plant provided a delivery rate as a target value and the plant was controlled via the compressor bypass to match this delivery rate.

by: Johann Lenz; Franz-Josef Düttmann – KÖTTER CONSULTING

Time (start)	Delivery quantities of Hydrogen production (target value) Nm³/h	Com-pres-sor speed min⁻¹	Suction pressure MP P8_1 bar abs	Gas temp. °C	Bypass position of the Com-pressor %	Displayed Quantity (converter) Nm³/h
2:00 pm	160	285	35,2	-	25 - 29	181 - 166
2:37 pm	210	285	35,1 - 35,3	6,9	0 - 35	140 - 310
3:04 pm	180	285	35,1 - 35,3	7,0	24 - 28	183 - 203
3:35 pm	120	285	35,1 - 35,3	7,2	36 - 39	107 - 124
3:55 pm	100	285	35,1 - 35,3	1)	1)	105 - 120
4:13 pm	80	285	35,1 - 35,3	1)	1)	94 - 108
4:28 pm	60	285	35,1 - 35,3	1)	1)	81 - 97
4:40 pm	30	285	35,1 - 35,3	8,6	48 - 51	76 - 91
5:02 pm	30	253	32,5	9,3	43,5	26
5:17 pm	50	253	28,0	9,9	28 - 32	50
5:30 pm	0	253	31,0	10,8	100	50 - 72

1) Failure of the DCS data storage

Table 2: Extract of the operating points reached during the measurement.

It turned out very early, that in addition to unwanted controller fluctuations of the rotary piston meters, significantly higher delivery quantities were displayed at the converter than were delivered by the electrolysis as a target value. This phenomenon was almost independent of the operating point (see Figure 7, above at VN_DKZ = standard volume flow from the rotary piston meter). The pressure pulsations measured at the same time at the measuring points P7 and P8.1 on the suction side of the piston compressors show a peak-to-peak value of approx. 100 mbar, independently of the operating conditions. These are below the limit value (required by the planer) of 0.5 % peak-to-peak of the absolute pressure in the suction-side piping system.

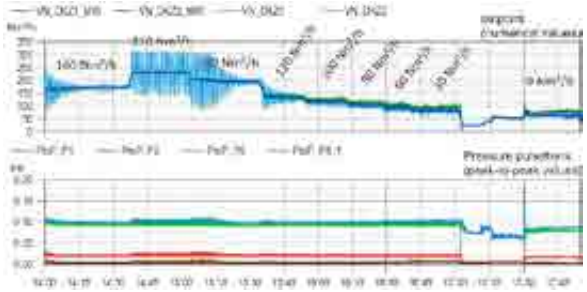

Figure 7: Top: standard volume flow (averaged and unaveraged) of both rotary piston meters; set and measured volume flow are given numerically and graphically respectively; bottom: the pressure pulsations at different measuring points.

Figure 8 shows chronologically consecutive frequency spectra of the pressure pulsations at measuring point P6 and similar frequency spectra of the volume flow fluctuation of the DKZ-1.21 rotary piston meter (determined from the HF-signal). The spectra show another series of measurements in which constant standard volume flows between 210 Nm³/h and 30 Nm³/h were set over several hours. A constant main frequency of 4.7 Hz can be seen for both signals. This corresponds to the speed of the compressor (n = 284 min-1 ≙ 4.73 Hz).

It is known that pressure pulsations and in particular - an associated pulsating differential pressure in rotary piston meters - often lead to an additional reading. The influence is strongly dependent on the characteristics of the rotary piston meter (e.g. mass inertia of the rotary pistons).

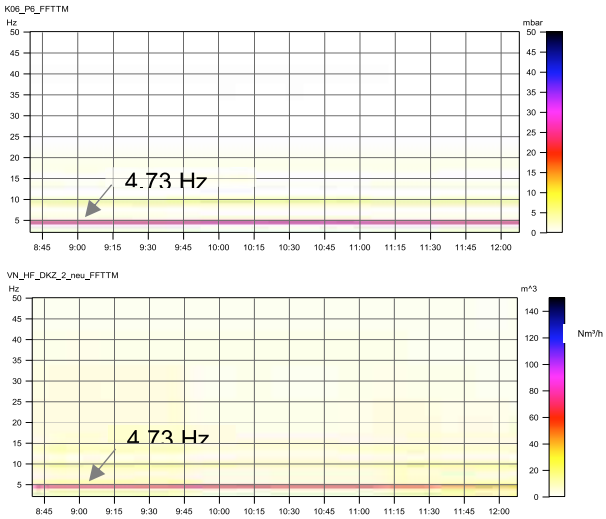

Figure 8: Amplitude spectra of the pressure pulsations at measuring point P6 and the volume flow fluctuations of the DKZ-1.21 rotary piston meter for different operating conditions.

In this application, the differential pressure was determined via the second DKZ-1.21 rotary piston meter and is shown in Figure 9 together with the high-frequency (HF) pulse signal and the calculated operating volume flow. It can be seen that the rotary movement of the meter is caused by increasing differential pressure. Due to the rotational inertia of the pistons, the rotary piston meter starts with a time delay and therefore continues to rotate even after the differential pressure changes sign.

The comparison of the operating volume flows QB of both meters shows that they behave almost the same and cannot be influenced by the enclosed gas volume between the two closely neighbouring flow meters.

by: Johann Lenz; Franz-Josef Düttmann – KÖTTER CONSULTING

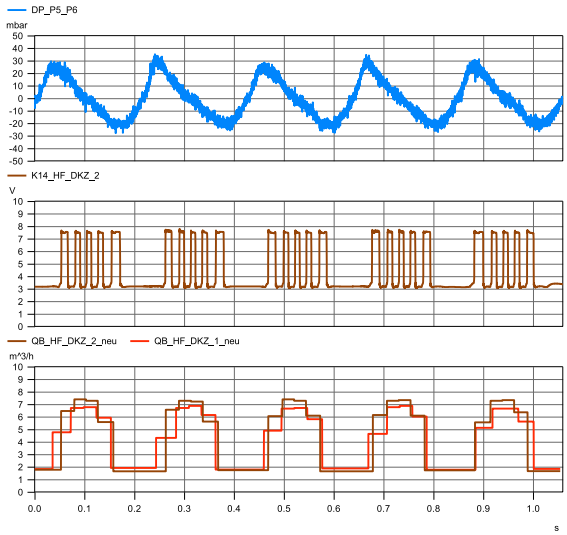

Figure 9: Time curve of the pressure difference, HF signal and the calculated operating volume flow of the rotary piston meters at 140 Nm³/h.

The Figure 10 illustrates the relationship for the entire volume flow range. The standard volume flows averaged and converted from the HF-signals are shown for different delivery rates at constant compressor speed. The compressor speed is constant, the flow rate is set by the compressor bypass position. As the volume flows become smaller, the previously sinusoidal volume flow fluctuations flatten out and influence the measurement result due to inertia.

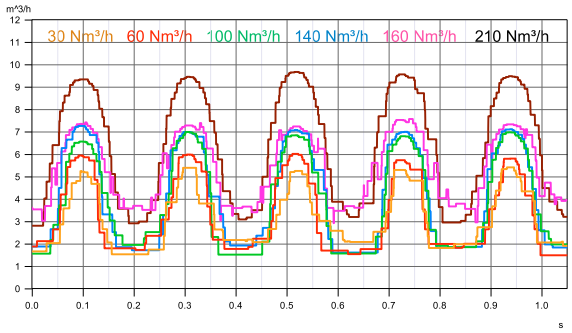

Figure 10: Operating volume flow averaged from the HF-signal of the DKZ-1.21 rotary piston meter for the operating conditions measured.

In order to directly reduce the influence of pulsations on the rotary piston meters, an additional pressure loss was generated for a short time (approx. at 13:20 to 13:33) with the manual valve S1.22 (downstream DKZ-1.21). Figure 11 shows the effects on the behaviour of the rotary piston meters.

It can be seen that by reducing the pressure pulsations to around 1/10 of the initial value (from 13:23), the specified setpoint of the electrolysis of 100 Nm³/h is displayed on DKZ-1.21. However, this requires a pressure loss of around 100 mbar.

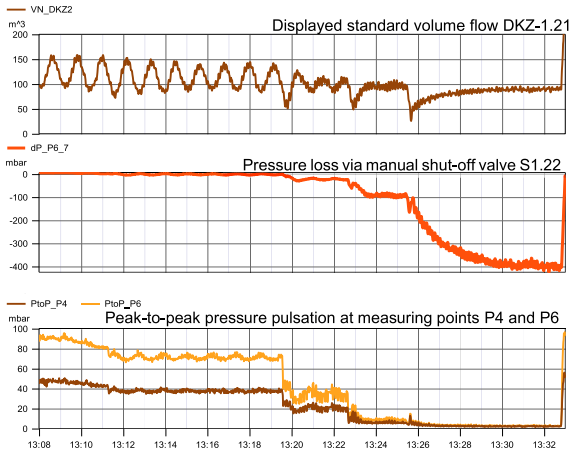

Figure 11: Throttle test: Standard volume flow and pressure loss via the manual shut-off valve S1.22 as well as pressure pulsation at the measuring points P4 and P6 (in each case downstream of the meters), setpoint: 100 Nm³/h.

The most important insights are summarized below. The detected volume flow fluctuations of the rotary lobe meters are generated by the pulsations of the compressor and lead to excessive volume flows being displayed. In order to minimise the effects mentioned above, the level of pressure pulsation and thus the volume flow fluctuations must be significantly reduced. As determined in the additional test, the pressure pulsation should not exceed a target value of around 10 mbar (peak-to-peak value) in the area of the rotary piston meters.

5. Design of measures

In order to develop effective pulsation-reducing measures, an acoustic pulsation study was conducted. First, a validation of the acoustic model (with passive flow meter) was carried out. A comparison between measured and calculated pressure pulsations shows a good agreement with amplitude deviations smaller than 10 %.

Subsequently, various measures to reduce the pulsation level, which were mainly caused by an acoustic resonance between the two compressors, were investigated. For the different operating conditions, pulsation reduction through the use of orifice plates alone is not sufficient. Changing the order of the existing buffer vessel and the rotary piston meters could also not be implemented due to operational reasons.

A practicable solution is the combination of orifices with an additional volume as a non-flow-through Helmholtz resonator[6]. The principle of Helmholtz resonator (see Figure 12) has been well known in acoustics for over 10,000 years. It works like a 1-mass oscillator with the main volume V (inner volume) as the spring and the gas volume in the

by: Johann Lenz; Franz-Josef Düttmann – KÖTTER CONSULTING

throat as the mass, and it can be used for effective pulsation reduction with careful design and planning.

Based on the pulsation study, the following measures were proposed in detail (see Figure 13)

- the implementation of a Helmholtz resonator directly downstream of the control valve near measuring point P7 (see Figure 6)
- the implementation of 4 orifice plates on the piping system close to the compressor

With these measures, the maximum pulsation at the rotary piston meters calculated is below 10 mbar (peak-to-peak value).

After the presentation and discussion of the results, the measure was professionally implemented by the plant constructor (see Figure 14) and put into operation without any problems.

Finally – initiated by the plant operator, Gasunie Deutschland Transport Services GmbH – the success of this measure was checked by KCE within the scope of a metrological investigation.[5]

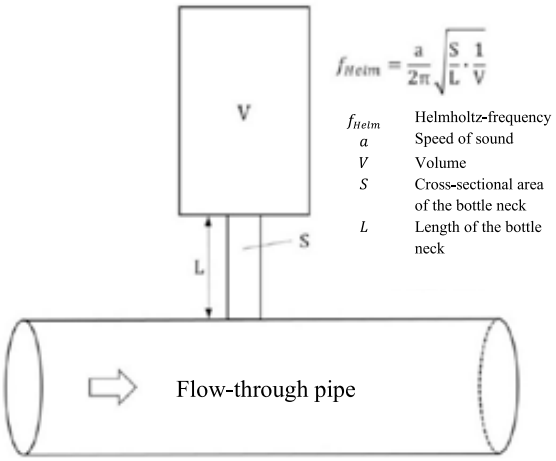

Figure 12: Helmholtz resonator as a simple model on a flow-through pipe.

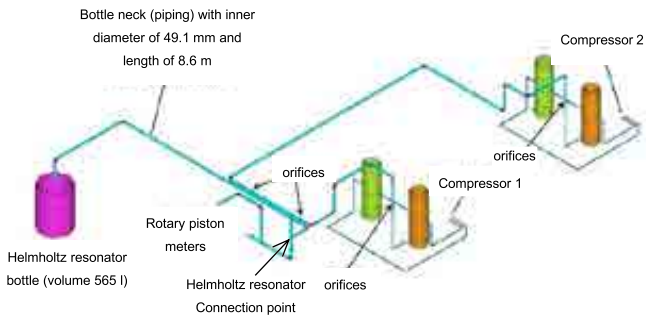

Figure 13: The acoustic model with the Helmholtz resonator connected.

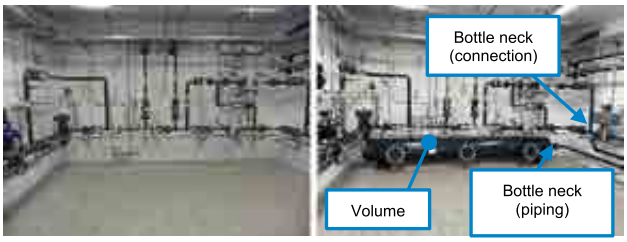

Figure 14: Original situation (left) and after the implementation of the Helmholtz resonator as a mitigation measure (right).

by: Johann Lenz; Franz-Josef Düttmann – KÖTTER CONSULTING

6. Conclusion

Compared to the original situation, the pulsations at the rotary piston meter could be reduced independently from the operating conditions by a factor of 10, see

Figure 15. The volume flow indication of the rotary piston meters matched the volume flow indication of the electrolysis, thus enabling a smoothly controllable feeding of hydrogen through the compressor.

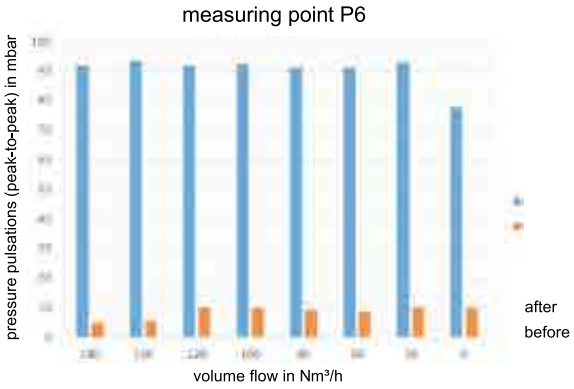

Figure 15: Pressure pulsations in the original state (before) and after application of the reduction measure "Helmholtz resonator with orifices" (after).

7. References:

Web document:

[1] Nationale Wasserstoffstrategie der Bundesregierung zu einer vielfältigeren Anwendung von Wasserstoff (https://www.bmu.de/download/nationale-wasserstoffstrategie/).

[2] Windgas-Haurup (o.D.): https://www.windgas-haurup.de/das-projekt.html.

[3] H-TEC SYSTEMS, https://www.h-tec.com/produkte/detail/h-tec-pem-elektrolyseur-me450-1400/me450-1400/

[4] Wikipedia: Drehkolbenzähler, https://de.wikipedia.org/wiki/Drehkolbenzähler

[5] Lenz, Düttmann, Rücker-Greve, Vulkan-Verlag GmbH, Jahrgang 163, ISSN 2366-9594 | B 5398: Auch grüner Wasserstoff kann pulsieren, 05/22.

[6] Brümmer, 1.KÖTTER-Workshop Gasmengen-messung 2002: Gasmengenmessung in pulsierenden Strömungen,02/2002

Standard:

[7] API STD 618: Reciprocating Compressors for Petroleum, Chemical, and Gas Industry Services, 5th Edition, December 2007.

Pulsation control for a multi-purpose underground storage reciprocating compressor system (natural gas, hydrogen and mixed gas)

by:

Leonard van Lier
TNO, Unit Energy Transition
Delft, The Netherlands
leonard.vanlier@tno.nl

Olivier Bore*
Storengy
Paris, France

13th EFRC CONFERENCE
September 19th – 21st 2023, Zagreb

Abstract:
Storengy operates 14 underground gas storage sites in France. These UGS systems typically have a large operating window. In these highly variable operational conditions, various design aspects must be optimized, often involving compromises. One of the key design aspects is the control of pulsations and vibrations for reciprocating compressors.
For the specific compressor system subject of this paper, the operational window is even larger, due to a multi-purpose requirement for natural gas, blended and pure hydrogen storage. This multi-purpose requirement, combined with variable inlet/outlet pressure, variable compressor load and variable compressor speed, makes the design very challenging.
This paper discusses the specific challenges for the control of pulsations, under these conditions. Some aspects for hydrogen service are judged as favorable (comparison with pulsation limits in the API 618 standard [1], shaking forces). However, other aspects are not necessarily favorable in case of hydrogen, such as efficiency of restriction orifice plates, the effect of damper volumes and the occurrence of flow pulsations.
This paper describes the design of the pulsation dampers and the optimization of restriction orifice plates, for the multiple purposes. In addition to traditional 'fixed' solutions such as restriction orifice plates, also more flexible, variable solutions are presented and discussed. For example exchange of orifice plates in various phases of the compressor's lifetime. Or variable orifice plates that can be dynamically adapted to the actual conditions. Some other design challenges, for example discharge temperature will be discussed. A compromise design was found that satisfies the entire operational envelop.

*see acknowledgements

by: Leonard van Lier – TNO; Olivier Bore – STORENGY

1 Introduction

Storengy has been active in the area of natural gas storage, for many years, with the main basis of operation being in France (Figure 1). Storage of hydrogen will be a future expansion of its commercial portfolio. In a recent association with multiple industrial partners, the possibilities to produce and store hydrogen are explored. There, the subsurface is suited for storage of natural gas and hydrogen [2].

Typically, the compressor design for underground gas storage has to meet a great deal of flexibility. The range of operating pressures is highly variable. In injection mode, the inlet pressure is dictated by the gas grid, which is a moderate variation typically within +/- 15 bar. The outlet pressure is dictated by the cavern pressure, and can have a variation in excess of 100 bar. In principle, the timescale of the pressure swings can be both day/night and seasonal variation. Due to the (economic) nomination for energy storage, a flexible and reliable capacity control is also of adamant importance for the compressor design. In future, with also the renewable power supply for the compression being highly variable (solar, wind), the demands for operational flexibility will be even more important. Finally, the system must also be able to handle fluctuations in gas composition (foreign gas import, LNG, biogas, admixing with hydrogen). The most robust and efficient compression solution for this large matrix of operational demands and considerable pressure ratios, is the reciprocating compressor.

The reciprocating compressor, while being a mature and reliable compression device, delivers an intrinsically unsteady (pulsating) flow. These pulsations shall be mitigated with an adequate design. The pulsation control strategy will be the main topic of this subsequent paper, with special attention to effects that play a role when a design for natural gas is applied for a system operated with hydrogen.

For the storage system under investigation, a new reciprocating compressor has been purchased.



Figure 1. Storage sites operated.

2 Multi-purpose compressor design

The compressor was procured and designed with the performance for natural gas storage as primary focus. As a secondary requirement, the compressor shall be designed for the best possible application in hydrogen service as well. However, this secondary requirement may require a compromise on various design aspects. The operation in natural gas service will be applicable for the immediate situation after commissioning. On the mid-term, an admixed scenario (hydrogen blended with the natural gas, at small fractions) can be foreseen for the compressor in several years. For the long-term, an operation at pure hydrogen can be foreseen as a future application (new, dedicated H_2 cavern excavation required, typically foreseen in 10 years).

The multi-purpose ambition for hydrogen storage has many different aspects. Of primary interest is the environmental impact and economic viability (not part of this paper). In addition, several technical challenges need to be identified and resolved. For example, the geology of the storage cavern, the re-use of equipment, the alternative process conditions, the impact of H_2 on materials, the compliance with design standards and additional safety constraints for flaring/venting. Reciprocating compressors are the most mature technology for compression of (pure) hydrogen. Therefore, a main aspect is the impact of a transition to hydrogen on the reciprocating compressor design. More specific: the impact on the *pulsation control strategy* is the key focus of this paper.

The most fundamental consequence of mixing or replacing the heavier natural gas with the lighter hydrogen is the change in molecular weight (MW), see Figure 2.

by: Leonard van Lier – TNO; Olivier Bore – STORENGY

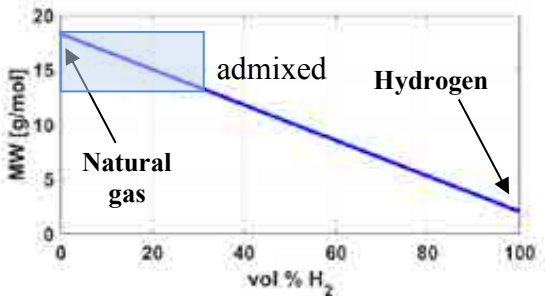

Figure 2. Molecular weight for mixtures of natural gas and hydrogen.

As an example, the impact of the gas composition on basic thermodynamic parameters is discussed below. The thermodynamic properties of natural gas and hydrogen are relevant for the compression process and the rise in outlet temperature. Note that the outlet temperature of each compression stage is bound to specific limits as formulated in the API 618 standard. At typical compressor inlet conditions for underground storage systems, the isentropic expansion coefficient (γ) is larger for hydrogen than for natural gas (Figure 3). As a consequence, for the same compression ratio, a larger temperature rise is predicted for hydrogen. On the other hand, for hydrogen-rich gases, API 618 imposes a stricter limit for the outlet temperature (135 °C instead of 150 °C). The combination of these effects is illustrated in Figure 4. In practice this means that either the number of stages for hydrogen service shall be increased, or (for the same design) that the total pressure ratio over the compressor shall be limited (ultimately bottlenecking the storage pressure).

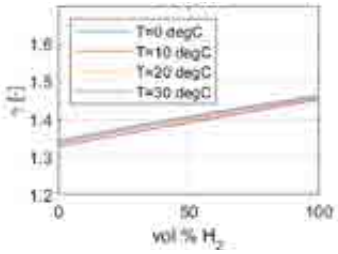

Figure 3. Isentropic expansion coefficient for natural gas – hydrogen mixtures at typical inlet conditions (P_{suc}=50 bar).

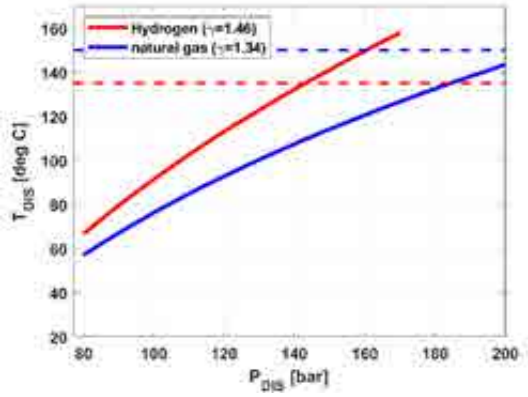

Figure 4. Predicted gas outlet temperatures for natural gas and hydrogen, and API 618 limits for outlet temperature.

Even though this is clearly a relevant aspect for the design and selection of materials and compressor parts, this challenge resides with the OEMs. It shall be mentioned that reciprocating compressors have a vast track record for hydrogen service (both hydrogen-rich process gas as pure hydrogen), which confirms that these aspects are well understood and controlled in industry.

In the remainder of this paper, the focus will be on the impact of introduction of hydrogen on compressor pulsations.

3 Bench-mark description

In many benchmarking studies for re-use of natural gas infrastructure for hydrogen service [3], the basic assumption is that the *same energy content* is transported. In such case, the gas velocities need to be tripled to achieve the same energy flux. This would demand a major re-design of the compressor, which is not the intention of the end user in this case. Therefore, in this paper, another benchmarking philosophy is used. The compressor is simply 're-used' with a different gas composition. The volume flow will remain (approximately) the same, and hence the energy flux will be lower for the re-use case with hydrogen. In reality, for example cylinder diameters may be enlarged, clearance may be modified and valve passage areas may be different. These aspects are not considered in the comparisons in this paper.

4 Case study system description

The compression system under investigation contains one horizontal 4-throw reciprocating compressor that is operated in single stage mode (all cylinders parallel, see Figure 5).

by: Leonard van Lier – TNO; Olivier Bore – STORENGY

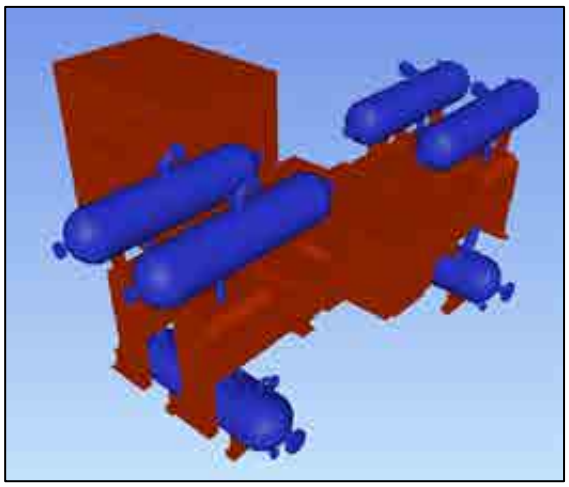

Figure 5. View of reciprocating compressor.

The compressor system under investigation has an extremely broad operating window, even for a storage application. The following operational design parameters had to be considered in the pulsation study:

- Variable suction pressure, depending on the pressure in the gas supply grid. Values range from 45 bar to 80 bar.
- Variable discharge pressure, dictated by the pressure in the underground cavern. Values range from 67 bar to 174 bar.
- Storage capacity. A nominal storage capacity of 130.000 Nm^3/h shall be met for storage pressures up to 137 bar. For higher storage pressures, the capacity shall be limited, with a linearly declining slope down to 30.000 Nm^3/h at the maximum storage pressure.
- The above capacity requirement is realized by a combination of suction valve unloading (stepped control) and variable compressor speed (stepless control). The capacity steps by valve unloading are 12.5%, from 100% down to 25%. The speed range is from 420 RPM down to 297 RPM.

Due to the requirements for capacity, not all load steps and speed combinations are applicable for each pressure condition. Based on the compressor performance curves, a realistic selection of pressure conditions and associated load & speed conditions shall be considered.

To expand the design map even further, also different gas compositions have to be considered, in different phases:

- Phase 1: operation with natural gas. The range in molecular weight is relatively limited (16.9 - 18.5 g/mol).
- Phase 2: operation with natural gas, blended with hydrogen (admixing). Exact admixing scenarios were not available, but based on recent studies, an upper limit of 20-30% of hydrogen has been considered [4]. The estimated shift in molecular weight is down to 14-15 g/mol.
- Phase 3: operation with pure hydrogen. The nominal molecular weight reduces to 2 g/mol. However, even small (volume) fractions of heavier components (CH4, N2, O2) will cause a significant upset in the molecular weight.

The transition from phase 1 to phase 2 will be 'smooth'. By introducing more and more hydrogen into the gas grid, the molecular weight will reduce gradually. As fluctuations of hydrogen content between 0% to 20% are to be expected, the system design shall be optimized to control pulsation issues for any point within this range. On the other hand, the step from phase 2 to phase 3 will be 'abrupt' and irreversible. In other words, an optimization strategy may be considered, dedicated to phase 3, with a clear-cut implementation moment.

5 Pulsation analysis philosophy and scope definition

Any design study for systems with a very large operational window is a challenge. For pulsation and vibration control this is not different. A careful selection of the scope is required. On one hand, the selection shall be all-encompassing, considering the worst-case conditions that may occur, even for short durations. On the other hand, the selection shall be realistic (to keep the analysis effort within manageable proportions and avoid over-conservative designs). A pulsation study for large, reciprocating compressor systems, is generally executed in accordance with the API 618 standard, design approach 3. This contains an acoustic analysis (pulsations and shaking forces) and a structural analysis (vibrations and cyclic stresses). The typical worst-case conditions for either of these perspectives are associated with resonance effects. The highest pulsations and shaking forces are typically found in *acoustic* resonance conditions (e.g. excitation of standing waves in the process gas). The highest vibrations and stresses are typically found in *mechanical* resonance conditions (e.g. excitation of cantilever modes of small branch connections). In case of low damping, the resonances occur at very specific conditions, with a sharp and narrow response. This implies that the search for these critical resonance conditions requires a very fine 'mesh' in the calculations, by sweeping of all possible conditions. This is typically done in small steps <1%, in the compressor speed range or in the speed-of-sound range, requiring a large set of simulation runs. The absolute worst-case is found when the excitation frequencies (the orders of the compressor speed) coincide with acoustic resonance frequencies and coincide with mechanical resonance frequencies. These coincidence effects are

by: Leonard van Lier – TNO; Olivier Bore – STORENGY

schematically illustrated in Figure 6. In this example, an acoustic source at the 4th order of the compressor speed (28Hz) may trigger the 2nd acoustic mode (30 Hz) AND the 2nd mechanical resonance mod (26Hz), within the uncertainty ranges in the acoustic and mechanical modelling. Obviously, the pulsation study shall consider these risks. Depending on the choice of the sensitivity ranges (around nominal conditions) the calculations may be very conservative and extensive.

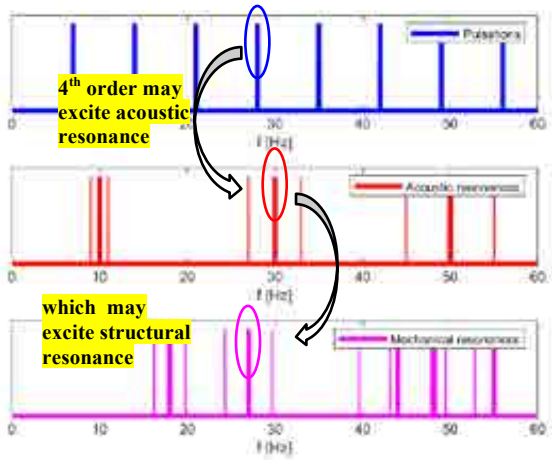

Figure 6. Coincidence of excitation, acoustical and mechanical resonance frequencies for a fixed speed compressor, including sensitivity ranges (small lines).

For a fixed speed compressor, such coincidences may be readily observed. In case of a variable speed compressor, also the excitation frequencies will occur within a bandwidth and the chances on coincidence increase even further.

In addition to the scope of the operation conditions, also the extent of the piping simulation model needs to be determined. Here, engineering practice is to extend the model up to those areas where pulsations effects are still expected to be significant (the significance often expressed as a ratio to the recommended pulsation limits in API 618). Adequate boundary conditions for the pulsation analysis are typically large vessels, large diameter transitions, closed valves (or with large Δp) or very long pipe lines. A specific feature of hydrogen systems is the high speed-of-sound (consequence of the low molecular weight). This implies also large acoustic wavelengths and intrinsically little acoustic damping. Moreover, the 'capacity' effect of volumes (vessels) is also less pronounced than for heavier gases. In other words, in hydrogen systems, pressure pulsations can generally propagate over larger distances from the source. This effect demands for a careful selection of the simulation scope during the design phase, to avoid problems upon start-up at remote locations from the source. Also the interaction between neighbouring compressors may be stronger. This effect also demands a critical consideration of the 'additive pulsation effects' in case of parallel operation of multiple compressors [5].

Considering the above aspects, for multi-purpose reciprocating compressor systems, the following general pulsation analysis approach is deemed adequate:

1. Include all future scenarios during the design of the system, even if some details of future phases are not available. This allows the end user to forecast potential issues, and take appropriate actions in a very early stage. Also agree clearly with the project team, in case design compromises are to be made, which scenario shall be leading for the design. This allows for the most economical and effect system design.
2. Select a representative number of gas conditions, that span the operating window. Preferably datasheet cases are used, not averaged or interpolated values, to avoid confusion in subsequent discussions. Gases with molecular weight separated by more than 20-30% are to be treated separately. For example, one calculation case for the natural gas operation (MW=18.5) one calculation case for the admixed operation (MW=14) and one calculation case for the pure H2 condition (MW=2). Sensitivity range around the nominal gas condition values shall be used, to ensure adequate overlap. Overlap may be in the speed-of-sound (fixed speed compressors) or in the acoustic wavelength (λ=c/f) for variable compressor speed. Note that for pure hydrogen, the sensitivity range may not be equally distributed around the nominal value, but 'eccentric': foreign traces in pure hydrogen (hydrocarbons, nitrogen, etc) will shift the speed-of-sound to lower values, never to higher values.
3. Select an adequate set of pressure conditions. For storage applications, the minimum and maximum inlet pressures shall be considered in conjunction with the minimum and maximum outlet pressures. Possibly, also intermediate pressure conditions may be selected; as a guideline, a maximum of 40% is recommended for subsequent pressure steps.
4. Select all relevant load steps, that may appear in conjunction with the chosen as conditions and pressure duty. Compressor load has a significant effect on the pulsation amplitude and dominant frequencies. For loaded (double-acting) cylinders usually the 2nd order of the compressor speed is dominant. For unloaded cylinders, in general the 1st order of the compressor speed is dominant. In case of manifold dampers with multiple cylinders connected to a single damper, the unloading scheme/sequence is also relevant, even if the number of unloaded cylinders on a damper

by: Leonard van Lier – TNO; Olivier Bore – STORENGY

remains the same. In case of simple volume bottles with a single cylinder mounted on each damper the effect of unloading sequence is usually small.

5. The pulsation damper design shall be judged according to the stipulations in API 618, including as a minimum the verification of PV diagrams, the pulsations at line and cylinder flanges, pulsations near the compressor valves, shaking forces on the dampers and the damper internals, pressure loss over the dampers and orifices. In case of inadequate performance, optimization may include the damper volume, the cylinder nozzle layout, internals (baffles, chokes, half pipes) and cylinder orifice plates. A specific remark for pulsation bottle sizing for hydrogen compressors is the fact that the recent API 618 release (5th edition) is more permissive for light gases than the previous 4th edition. This implies that, for hydrogen compressors, pulsation dampers that are traditionally designed according to the 4th edition are *larger* than dampers sized according to the 5th edition, depending on the exact gas composition. This also implies higher pulsations and shaking forces in the piping, for systems sized according to the 5th edition. A comparative approach, including economical aspects is discussed in a previous EFRC conference paper [6].
6. It is recommended to select a broad matrix of cases for the sizing of the pulsation dampers (pre-study). This is an essential step toward a robust system design, and allows to scan a large window at low computational cost, in an early stage of the project. Later in the analysis, when the pipe system is added to the simulation model, the number of cases may be reduced, based on the observations in the pre-study.
7. When the pulsation simulation model is extended with the field piping, select an adequate, ample scope, bearing in mind that in hydrogen, pulsations may travel over very long distances. The residual pulsation amplitudes at the model boundaries shall be validated and confirmed to be low (recommended value: lower than 20% the pulsation criterion for piping in the API 618 standard).
8. During the optimization of the system by means of fixed orifice plates (which suppress the acoustic resonances in the system) a careful design shall be chosen for the pressure loss over the orifices. The shall consider the various operating phases of the system. Within each phase, due to the variance in loads steps and capacity, a compromise is necessary. Here, the most critical conditions shall be leading for the 'nominal' choice of the orifice bores. To ensure a minimum performance of the orifices at the minimum capacity (smallest load step and/or minimum compressor speed), a pressure loss may be chosen that results in a considerable loss at the maximum capacity. An exceeding of the recommended values in API 618 shall be clearly communicated and agreed with the end user of the system. If the compromise is judged as unsatisfactory (in rare cases) a dedicated solution with dynamic orifice plates may be considered.
9. For transitions between phases, a new dedicated set of restriction orifice plates may be proposed. For the transition from phase 2 (admixed)-3 (pure H_2) this is more straightforward than for the phase 1-2, due to the larger difference in MW. In general, it is recommended to evaluate in the analysis the benefits of orifice re-fitting in various phases. This will enable to plan a swap of orifices well in ahead, and based on solid arguments.

6 Case study: pulsation damper design

The basic design for the pulsation dampers was proposed by the compressor vendor. The design is rather typical for natural gas applications, with a multi-throw single stage compressor. Each cylinder has a single suction damper, with a half pipe, to ensure a central connection to the damper compartment (to minimize damper shaking forces). The discharge dampers are of a manifold type (2 connections to 2 cylinders). The discharge dampers have a centred baffle with a hole. The internals have the primary purpose to limit the shaking forces acting on the dampers. The cylinder nozzles of the discharge damper have a considerable length, which causes a risk on high pulsation levels in the cylinder gas passage [7]. To avoid excessive pulsations, the discharge silencers have orifice plates in the damper cylinder nozzles, located close to the vessel entry point. This is the most effective location to suppress acoustic resonances.

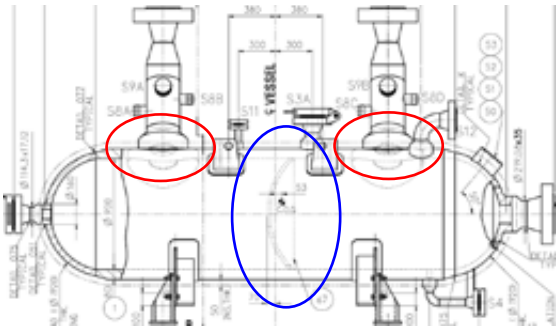

*Figure 7. Discharge damper with **baffle** and **cylinder orifices**.*

To enable a clear benchmarking between the various gas conditions and optimization steps, not the complete calculation matrix is discussed here.

by: Leonard van Lier – TNO; Olivier Bore – STORENGY

Instead, the nominal pressure ratio (certification point, P_{suc}=48 bar and P_{dis}=137 bar) from the datasheets was selected as the reference condition, for the Natural Gas and the admixed case. For the pure hydrogen case, the nominal discharge pressure ratio is limited to 120 bar (to limit the outlet temperatures). For each gas case, all load steps were considered (100% down to 25%). For each case, a sweep over the complete speed range is made.

For the natural gas case, which is the focal point of the design, the pulsation damper performance is judged as adequate:

- The pulsations at the line connections (LC) are smaller than 70% of the API 618 limit, which the requirement for the pre-study.
- The pulsations at the cylinder connections (CC) are within the limits formulated in API 618.
- The shaking forces on dampers are considerable: 8 and 11 kN peak-to-peak at suction and discharge side, respectively. However, considering the robust mechanical layout the forces are judged as acceptable according to the OEM standards.
- The pressure loss over the dampers is within the API 618 limit for the certification point.

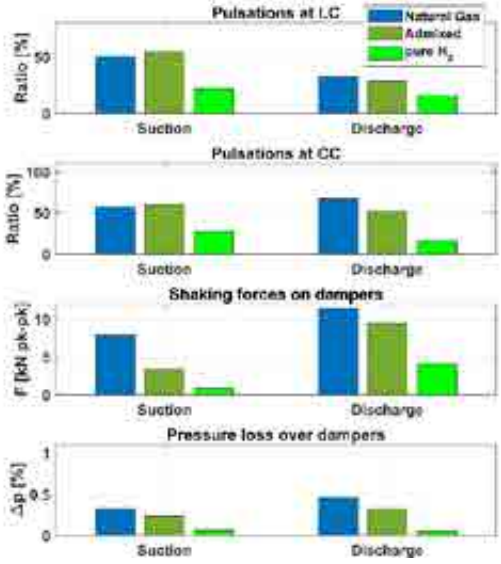

Figure 8. Pulsation damper analysis results.

For the future admixed case and the future hydrogen case, the following trends are observed (see Figure 8):

- In the admixed case, the pulsations at the line connections are relatively comparable. A slight increase at the suction side is caused by a Helmholtz resonance that is not triggered in the heavy MW, but is in case of the lighter admixed gas. This effect will be less prominent, once orifice plates are designed at the line side of the dampers (see next section). For the pure hydrogen case, the pulsation levels are more favourable, if compared to API 618
- The pulsation amplitudes at the cylinder connection are comparable for admixed gas cases. For pure hydrogen, the pulsations are significantly lower.
- Also the shaking force amplitudes are reducing for lighter gases.
- The pressure loss over the dampers is lower for admixed case and much lower for pure hydrogen, due to the reduced gas density.

In general, the pulsation effects for natural gas (high MW) are more severe than for admixed and pure hydrogen (lower MW). The main reason is for low MW, the increased acoustic wavelength shifts the occurrence of critical resonances to higher orders in the pulsation spectrum (which have less energy).

As a general and important observation, it must be noted that the limit value for pulsation amplitude in API 618 depends on the speed-of-sound (symbol *a*). The other parameters are line pressure (P_L), line inner diameter (D_I) and frequency (f).

$$P_L = \sqrt{a/(350)}\left(\frac{400}{(P_L \times D_I \times f)^{0.5}}\right)$$

Thus, API 618 is (much) more permissive for hydrogen. Even though the pulsations may appear more favourable compared to API 618, the *absolute* pulsation amplitudes may be comparable. This shall be kept in mind when comparing pulsations in natural gas service with hydrogen service.

7 Case study: pulsation analysis of the field piping

In the next step of the pulsation analysis, the field piping is added to the simulation model. This is illustrated in Figure 9.

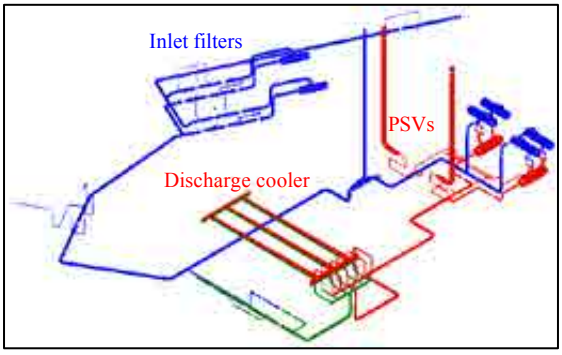

Figure 9. Simulation model including field piping. The colours indicate the sections of the system (suction, discharge and after-cooler).

by: Leonard van Lier – TNO; Olivier Bore – STORENGY

At the upstream side, the model is bounded by the inlet filters. At the downstream side, the discharge cooler is included, truncating the model downstream the bypass line. The long relief lines are mounted directly to the discharge dampers (reasons for this choice will be explained further down). The study focusses on pulsation analysis; results of the mechanical study (vibrations, stresses) are not presented in this paper. Note, that the mechanical behaviour does not depend on the gas composition of the process fluid (or extremely weakly). For the sake of comparison, the amplitude and frequency of the shaking forces are sufficient input for the present discussion.

The full set of simulations was re-run, for the natural gas baseline. Even though the pulsation dampers are compliant with the guidelines in API 618, the pulsation levels in the field piping significantly exceed the limits (up to 3x in main lines and up to 6x in closed side branches), a situation judged as unacceptable. The high pulsations are explained by the occurrence of acoustic resonances in the field piping. To suppress these resonance effects and to limit the pulsations, the beneficial effect of restriction orifice plates at the damper line connections was investigated (the first and foremost optimization step in such systems). A significant effect was obtained, by optimizing the orifice plates for the natural gas duty, at full load and maximum speed. At the higher speeds and the high part loads, the effect of the orifices is optimal. However, at lower speeds and low part loads, the pressure loss over the orifices becomes very low and the beneficial effect is much lower. As an example, the pressure loss over the discharge line connection orifices are shown in Table 1 (in % of static pressure), for the various conditions.

		max speed		min speed	
	MW	full load	part load	full load	part load
Natural gas	18,5	0,63	0,04	0,32	0,02
Admixed	13,9	0,45	0,03	0,23	0,01
Hydrogen	2,0	0,09	0,00	0,04	0,00

Table 1. Pressure loss of discharge orifice plates, for various conditions.

From this table, the challenge of the compromise for the orifice design is obvious. If tuned for the maximum capacity in natural gas service, there will be no effective pressure loss in hydrogen service, in particular at lower capacity.

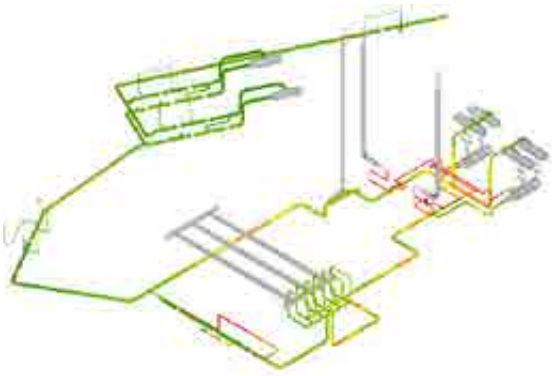

Figure 10. Maximum pulsation levels for natural gas service, with fixed orifice plates (red color indicates a high level, green color a low level). Residual exceeding occurs at lower part loads.

At full load, the pulsation amplitudes are considerably reduced due to the fixed orifices. However, at the lower part loads the performance is 'bottlenecked' for further improvement. For 50% load and lower, the API 618 limits are exceeded. The exceeding in the relief lines is not at all mitigated by orifices at the line connection of the dampers. Here, additional (local) measures are needed for effective control of pulsations and vibrations.

Also the admixed and pure hydrogen services were analysed, with the same fixed orifice plates. The admixed case is relatively comparable to natural gas case: the pulsation levels on the main lines remain within limits, the worst-case conditions occurring at lower part load and a strong, local exceeding in the relief lines. The hydrogen case is significantly better: lower pulsations (compared to API 618) and lower shaking forces. Therefore, even with the sub-optimal orifice plates, the pulsation issues appear to be better under control.

A special aspect is the effect of unsteady flow, associated with the pressure pulsations. These flow pulsations, though not directly related to integrity, may be relevant, for example for flow meters (reduced accuracy) and non-return valves (hammering). Here, the *relative* flow pulsation amplitude (relative to the mean flow) is of importance. Therefore, especially at low-flow conditions (low speeds, low part load) issues may be observed [8]. The main point of interest here is, that in case pure hydrogen, the relative flow pulsations near the flow meter may increase significantly, even if the comparison of pressure pulsations with API 618 is more favourable. At the location of the flow meter (~15 meter upstream of the compressor) the pressure pulsation amplitudes (p') are comparable for the different gas duties. The flow pulsation amplitude (q') is roughly a factor 3-4 lower for hydrogen, proportional to the inverse of the speed-of-sound. However, for hydrogen, the *relative* flow pulsations (q'/Q_0) are a factor 2-3 larger, due to the

by: Leonard van Lier – TNO; Olivier Bore – STORENGY

difference in static mass flow. The largest relative flow pulsation levels are found in part load conditions, in excess of 200% peak-to-peak. As the most severe effects occur at low mean flow, this cannot be conveniently resolved with re-fitting orifices plates (see section 6.2).

8 Dedicated optimization strategies

8.1 Detuning resonances

As a theoretical optimization strategy, the piping layout may be modified, in an attempt to avoid the occurrence of acoustic resonances. This may be done by limiting the length of piping, in order to achieve a 'compact layout' compared to the acoustic wavelength. If this would be achieved, no resonance would occur, and pulsation levels would be minimal. However, a quick glance at the real system confirms that this a vain approach. For natural gas and admixed cases, the acoustic wavelengths (assumed up to 4th order of the compressor speed) are 10-20 meter. The distances between main equipment and connections to the inlet/outlet headers are well above these wavelengths: resonant conditions cannot be avoided. Note also that due to the variable speed, the range of excitation frequency is continuous and broad, which makes a separation of excitation and resonance frequencies virtually impossible. Even in case of pure hydrogen – with much larger wavelengths (50-100meter) – the system dimensions are considered large. Only specific local resonances, such as ¼λ standing wave in pressure relief lines, may be avoided by a sufficiently short length.

8.2 Re-fitted orifices to gas condition

The standard engineering optimization strategy was described above. This included an adequate damper layout, and optimized orifice plates (at cylinder and line connections), tuned for the natural gas service. For this 'standard layout' residual concerns are: 1) increased pulsations at lower part load conditions, 2) increased pulsations that are found in the admixed cases 3) increased flow pulsations for the admixed and hydrogen service. Issue 1) is a fundamental limitation, for a system with 'fixed' orifice plates that shall be run over a large range of capacity: fixed orifice plates cannot be swapped on a hourly or daily basis. For issue 2) it may be considered to swap the orifice plates upon a transition to a new project phase; optimized (re-fit) orifices for the admixing service and later for the hydrogen service. The new orifice plates will have smaller bores, larger pressure losses and will more effectively suppress the pulsations. While a small step for the admixed case, for the transition to pure hydrogen, this re-fit may be a major step, allowing for a much more squeezed orifice bore.

The effect of the re-fitting is overall beneficial, but limited. The limitation is again due to the bottleneck at part load conditions, where the orifices have virtually no pressure loss.

8.3 Dynamic adjustable orifices

A rigorously new concept of optimization is a really 'dynamic' restriction orifice. Such orifice shall be adjustable to the actual conditions in real time, ensuring an optimal pressure loss at the actual conditions. Thus, at part load conditions, the pressure loss can be set to the optimally required values, and pulsations may be better reduced. Commercial products for such a dynamic solution are available, but rarely seen in practice. The end user has previous experience with an alternative approach, where a Pressure Control Valve is used as a dynamic orifice plate. Considering the limited dimensions of the valve, compared to the acoustic wavelength, the control valve should have the same acoustic effect on pulsations, as an orifice. The adaptive PCVs are located relatively close to the compressor, but cannot be fitted at the line connection flange. Instead, they are mounted in the two inlet and outlet lines (Figure 11).

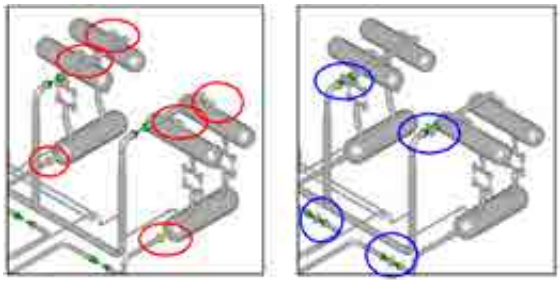

Figure 11. Fixed orifices at LC (left), dynamic orifice plates with PCV (right).

For the pressure loss, the following upper limit was investigated, as suggested by the end user: a maximum 2% static pressure loss for both suction and discharge PCVs (at maximum speed). The beneficial effect of the fixed orifices, the re-fit orifices and the dynamic orifices are shown in Figure 12, for the 3 different gas conditions.

by: Leonard van Lier – TNO; Olivier Bore – STORENGY

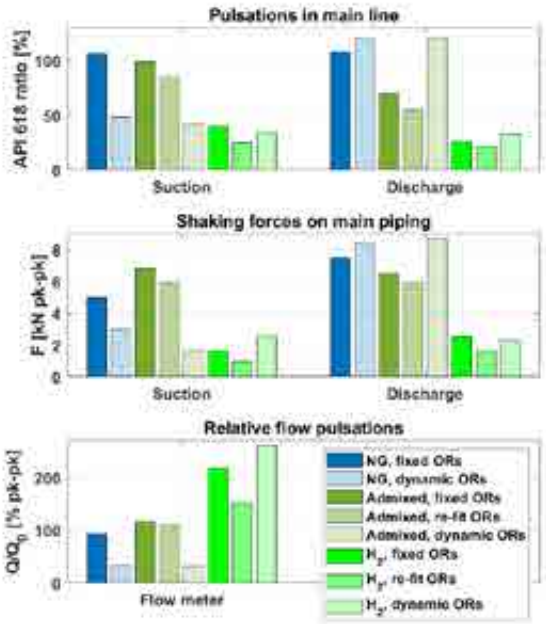

Figure 12. Effects of orifices (fixed, re-fit and dynamic) for the different gas duties.

While the re-fitted orifices are always (moderately) beneficial, this is not the case with the dynamic orifices. The dynamic orifices may perform much better (especially at part loads) but also worse. This is observed for the pulsations, the shaking forces and relative flow pulsations. The observation that, with a higher pressure loss, a lower performance is reached can be understood as follows. Compared to LC orifices, the dynamic orifices (PCV) are located further from the pulsation damper volume (~4-5 meter). This is in principle a less favourable location. Moreover, certain resonance types (e.g. standing waves or Helmholtz resonances between the suction bottles) are not effectively suppressed. The effect of the orifice depends strongly on the acoustic resonance condition (location of pressure nodes/anti-nodes, frequency) and is thus specific for each system. To circumvent this disadvantage, it shall be considered to re-locate the PCVs closer to each line connection flange of the dampers. In addition to these fundamental limitations of the dynamic orifices, also a number of practical points must be considered carefully:

- An additional investment must be made, for the procurement of the PCVs, which are expensive equipment compared to simple orifices.
- The PCVs shall be able to control accurately a relatively small differential pressure, in the order of 1-2% of the mean pressure. This is not a typical operating range of standard control valves. In addition, the PCV shall be able to control in highly dynamic (pulsating) conditions).
- The PCV are relatively heavy components with considerable dimensions (stem), that are typically liable to mechanical excitation from the vibrating pipe work and/or compressor. On the suction side, this introduces a risk on vibration issues and an adequate mechanical layout around the PCV is mandatory.
- A HAZOP scenario includes failure mode of the control valve, which dictates the pressure relief connection upstream of the discharge PCV. This leads to the design of long pressure relief lines mounted directly onto the discharge dampers. Here, high pulsations and observed that are not easily mitigated. The options to use short relief lines, connected to the main line are considerable limited by the introduction of the PCVs.

9 Conclusions

Based on a careful consideration of pulsation effects in reciprocating compressor systems designed for multi-purpose gas conditions, and a case study for an underground gas storage, the following conclusions are proposed:

- When designing a multi-purpose gas system, the various gas conditions shall be investigated as separate cases (e.g., natural gas, admixed, pure hydrogen). Pressure duties, load steps and compressor speed shall be fully considered for each gas case, including an adequate sensitivity range around the nominal conditions, to account for resonance effects
- For hydrogen systems, a careful assessment of the model boundary conditions shall be made. Due to the larger wavelength and the limited effect of volumes, pulsations may propagate over large distances from the source without significant acoustic damping.
- In the case studied for this paper, when comparing pulsations to the limit values in API 618, the admixed gas conditions are comparable to the natural gas conditions, while the hydrogen cases appear much better than natural gas. However, it must be kept in mind that the API 618 criterion is more permissive for hydrogen: absolute pressure pulsations may be comparable.
- Due to the increasing acoustic wave lengths for admixed and hydrogen service, the shaking force amplitudes are generally lower than for natural gas. However, the frequency spectrum for the shaking forces has a tendency to shift from lower orders to higher orders, when migrating from natural gas to hydrogen. The shift in frequency generally scales with the speed-of-sound (typically a factor 3 upward).

by: Leonard van Lier – TNO; Olivier Bore – STORENGY

Control of vibrations at higher frequencies may require special techniques, such as adequate bracing of small branch connections or mechanical damping techniques.

- The relative flow pulsation effects may be more severe for hydrogen than for the natural gas conditions. The critical pulsation effects mainly occur at low capacity, and hence cannot be conveniently controlled with fixed restriction orifice plates. The design of critical equipment, such as flow meters and non-return valves shall be carefully checked before application into the new gas service.
- The concept of a dynamic orifice plate, that is able to set the optimal pressure loss in real time is in principle much more effective at lower part loads. However, the dynamic orifice plates shall be located at the optimal positions (damper line connections), to exploit its full potential. If placed a unfavorable locations, the dynamic orifices may perform even worse than fixed orifice plates at the line connections.
- The application of fixed orifices is considered a well-proven practically effective approach. At lower part loads, fixed orifices are less effective to suppress pulsations. It is recommended to design dedicated sets of orifice plates (specific for new gas condition such as admixed gas and pure hydrogen), to be implemented upon the start of the new gas service.
- Specific requirements due to the new gas services that are related to the equipment, shall be addressed by the OEM. This includes for example the selection of materials of compressor parts. In particular the wearing parts such as compressor valves, piston rings and packings.
- It is advised to gain further experience with dynamic pulsation control techniques and optimize the approach. This should be a combination of simulation techniques and verification in the field with pulsation measurements.

Acknowledgement

The main author kindly thanks the members from Storengy's project team, for the collaboration and for the permission to share the main findings of the investigation in this conference paper.
In addition, please note that Olivier BORE's activities within Storengy have been taken over by Frédéric CIOLFI (frederic.ciolfi@storengy.com)

References

[1] API standard 618, "Reciprocating Compressors for Petroleum, Chemical and Gas Industry Services", 5th edition, 2007.
[2] R. Groenenberg, "Large scale energy storage in salt caverns and depleted fields", public TNO report, October 2020.
[3] HyDelta report "Impact of high speed hydrogen flow on system integrity and noise", January 2022, https://hydelta.nl/.
[4] IAE Bioenergy report "Renewable gases – hydrogen in the grid", IINAS, January 2022.
[5] N. Albers *et al*, "Engineering approach for world's largest hydrogen compression system", 11th EFRC conference, September 2018.
[6] C. Fernández Valdés *et al*, "The impact of an API 618 4th or 5th edition analysis on the design of a very large hydrogen compressor", 7th EFRC conference, October 2010.
[7] L. van Lier *et al*, "Identification and mitigation of Cylinder Gas Passage pulsations", EFRC conference, September 2018.
[8] L. van Lier, *et al*, "Impact of pulsations on flow metering accuracy: identification and remedies", EFRC conference, September 2012.

JANSEN+ TETENBORG
VIBRATION + PULSATION CONSULTING

Compensating uncertainties of mechanical calculations during commissioning

by:

Patrick Tetenborg
Senior Consultant

Christian Jansen
Senior Consultant

Jansen + Tetenborg – Vibration and Pulsation Consulting
Rheine, Germany
ptb@vibration-pulsation-consulting.com

13th EFRC CONFERENCE
September 19th – 21st 2023, Zagreb

Abstract:
Setting up a new compressor plant is a challenging task. Many different physical aspects must be considered when designing the pipework. In addition to the fluid mechanical design, the dynamic loads on the piping and support structure are also an important component. The mechanical load and the pulsation excitation coming from the compressor are considered in an acoustical and a structural study during the design phase. Modern software and accumulated experience of the design engineers have led to a high predictive accuracy in these studies. However, it is not uncommon to face increased vibrations during start-up.
Especially the mechanical study is known to be of limited accuracy regarding the avoidance of resonance conditions with potentially excessive vibration levels. To avoid the problems associated with this uncertainty, a methodology with is presented that allows the engineering firm to accept a residual of uncertainty. This methodology implements a modal analysis of the as-built condition. Based on the findings regarding natural frequencies, conspicuous pipe sections are provided with dynamic pipe supports having a maximum flexibility. The highly damped design of these devices eliminates the critical natural frequencies and enables a safe start-up regarding the dynamic load on the piping system. The unique approach with its new flexible dynamic pipe support reduces the time frame for vibration reduction from weeks/months down to hours.

by: Patrick Tetenborg, Christian Jansen – JANSEN + TETENBORG

1 Introduction

The current market situation and ongoing challenges related to a sustainable environment for all of us are the permanent promoters for new and modified chemical and petrochemical sites around the world.

Several technological, engineering and commercial disciplines are considered for modified as well as new built reciprocating compressor plants.

One discipline that is already considered within the design phase but can only be finally validated during commissioning is the dynamic operating behaviour of the compressor with its connected piping system. Therefore, the pulsation excitation coming from the compressor as well as the mechanical load are considered in an acoustical and a structural study during the design phase. These studies are well guided by the API 618 standard[1]. But experience from several commissioning projects has shown that it is quite difficult to perform these numerical studies with 100 % accuracy. Thus, there is always a residual uncertainty when it comes to the first start-up of a new / modified reciprocating compressor plant.

A new methodology and optimization tool of vibration engineering is described within this paper. This approach shall be used for giving the operator as well as the engineering and construction companies a confidence when starting up new compressor units. The tool allows EPC-companies and their clients to minimize the effort on structural numerical models within the design phase and to speed up commissioning when it comes to unexpected vibration issues in their plants.

2 Design Engineering

This chapter describes the general approach regarding the Design Approach 3 guided by the API 618 standard.

The Design Approach 3 is the common methodology for setting up a well working acoustical and structural design for the interaction of the reciprocating compressor with the process equipment. A model of an interstage of a 4 cylinder two stage reciprocating compressor with variable speed (360 up to 600 RPM) is used to describe the steps within this engineering phase. The design of this piping section is shown by the model in the subsequent figure 1.

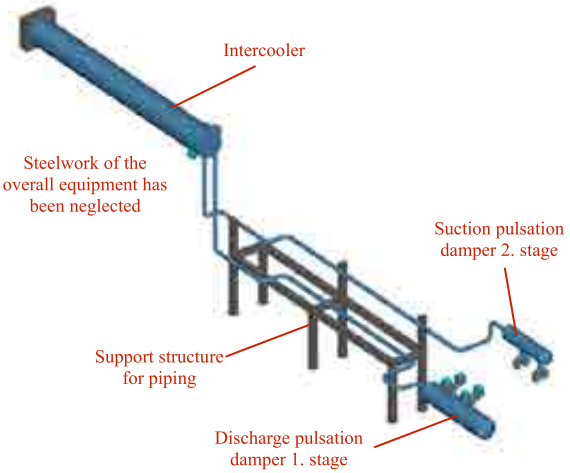

Figure 1: Model of the interstage.

2.1 Pulsation Study

The interaction of the reciprocating compressor with the attached piping system is checked for all stages and all relevant operating conditions within the pulsation study. Therefore, a numerical one-dimensional model is used. It consists of the cylinder and valve design with the local gas passage as well as the whole piping system with all implemented equipment like pulsation dampeners, separators and heat exchangers.

Within a first step an applicable size and design of the pulsation dampener is chosen. This can be single volume or multi chamber setup. After some preliminary checks the interaction of the compressor with its attached pulsation dampeners and the whole piping system will be simulated. Figure 2 shows a standing wave as a typical result for such a simulation.

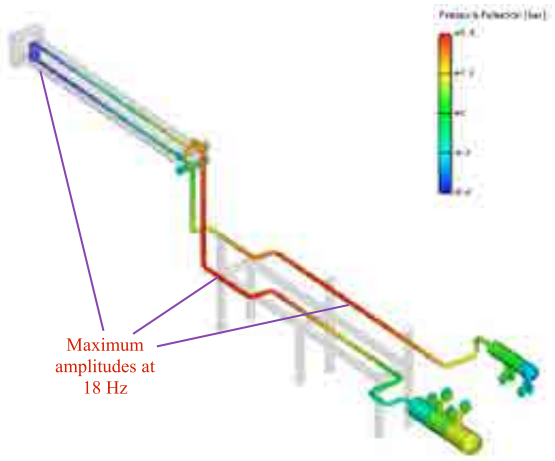

Figure 2: Distribution of pressure pulsations along the whole interstage piping for an acoustical resonance at 18 Hz.

by: Patrick Tetenborg, Christian Jansen – JANSEN + TETENBORG

The local distribution of the pressure amplitudes gives direct insights to possible optimisation measures for acceptable pulsation limits. In this case an acoustical resonance has been identified. As the overall pulsation level is within the allowable pulsation limit no further improvement is necessary, see figure 3.

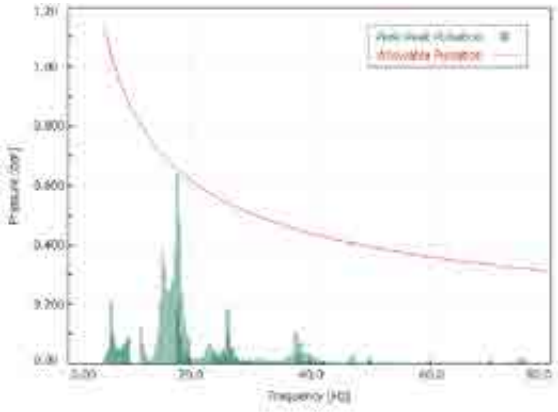

Figure 3: Maximum peak-to-peak pulsation level for all piping sections compared to the pulsation limit of API 618 standard.

The calculated pulsation level for the interstage as well as for the overall compressor system fulfils the requirements of the API 618 standard.

2.2 Mechanical Study

The acoustical design of the interstage is acceptable and now the structural design of the piping and its support structures will be checked within the mechanical study.

The whole support structure of the piping and equipment needs to be implemented in the numerical model (FE-Model) for structural analysis. Therefore, adequate boundary conditions for the supports itself and e.g. the local installation of a heat exchanger in the complex plant steelwork needs to be specified.

Figure 4 shows the considered support structure and local assumptions for boundary conditions related to the compressor and site data.

A mechanical natural frequency analysis of the compressor and piping system will be performed after setting up the FE-model. As a first step within this analysis the following separation margins need to be checked:

- Minimum mechanical natural frequency of any system element shall be designed to be greater than 2.4 times maximum running speed.
- All predicted mechanical natural frequencies shall be designed to be separated from significant excitation frequencies (e.g. harmonics of running speed) by at least 20%.

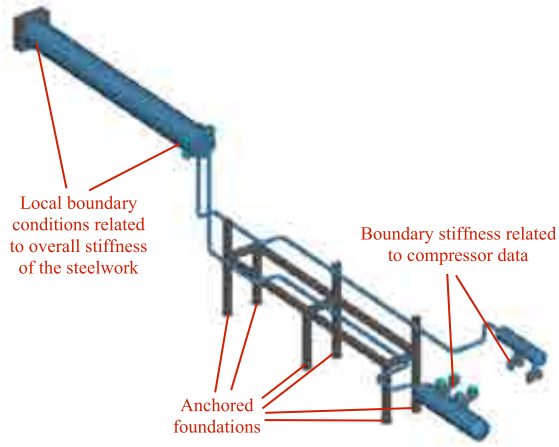

Figure 4: Boundary conditions for the structural numerical model.

The first six calculated natural frequencies are presented in the Campbell-diagram in figure 5 and the corresponding modes are shown in figure 6.

The first natural frequency at 13.2 Hz does not even match the first separation margin and seems far too low for a reciprocating compressor system. Due to the nearby I-Beam-support structure an additional support will be placed. Modified calculations have led to a natural frequency of 27.5 Hz, which is acceptable.

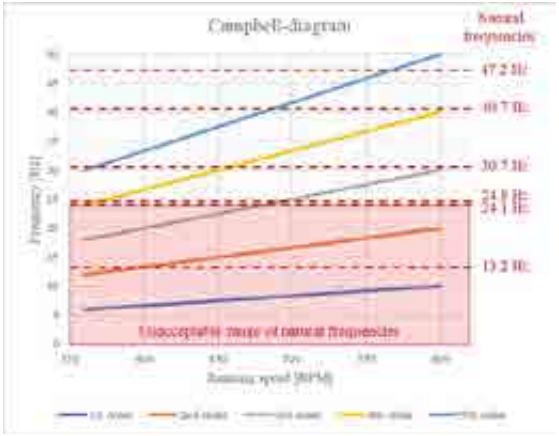

Figure 5: Campbell-diagram with first five harmonics of compressor running speed and calculated natural frequencies by mechanical study.

In this case with a variable speed compressor the second separation margin is difficult to handle. Thus, additional analysis will be necessary by following the Design Approach 3.

Beside the opportunity for checking the shaking forces on the piping system it is also possible to directly perform a forced mechanical response analysis on the piping system. For the presented interstage the vibration level met the API 618 vibration criteria. The cyclic material stress has not been calculated. In general, these calculations are causing an additional effort and all uncertainties of acoustical and mechanical studies will be affecting the overall accuracy of this procedure.

by: Patrick Tetenborg, Christian Jansen – JANSEN + TETENBORG

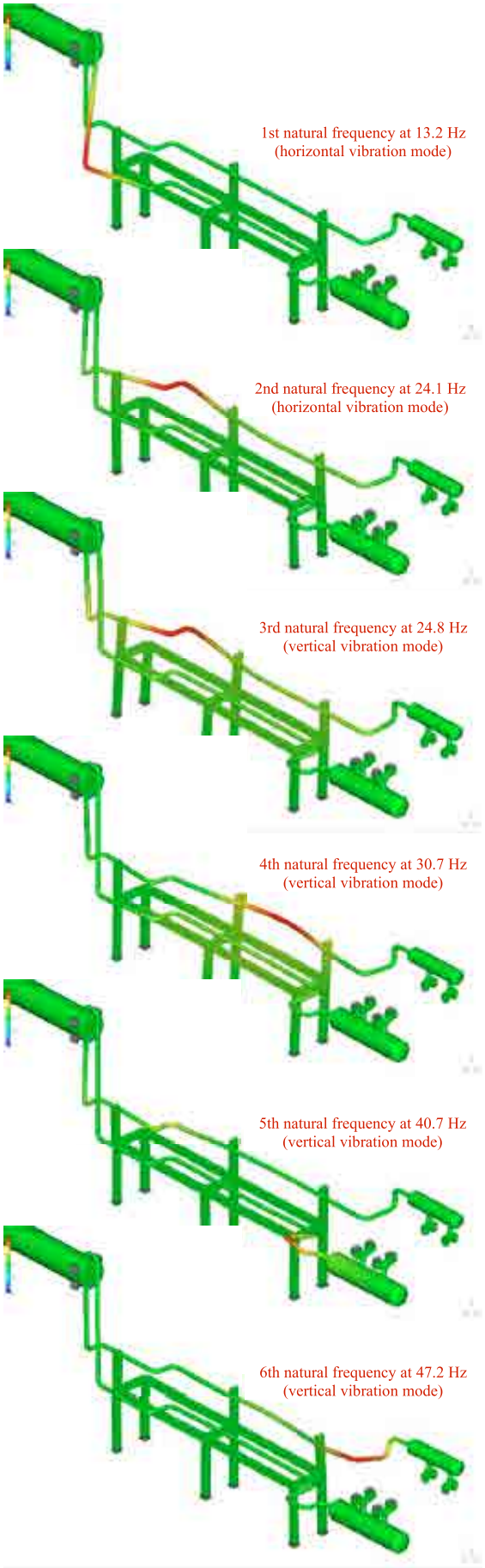

Figure 6: Natural mechanical frequencies and modes of the investigated interstage.

2.3 Simplified Mechanical Study

At this point the new method to compensate numerical uncertainties in mechanical calculations during commissioning will be introduced. The approach is applicable on piping sections that might be facing elevated vibrations due to an excitation of the higher harmonics of the compressor. The approach is an alternative to the complex calculations on shaking forces and expected piping vibrations for these piping sections.

Thus, the already existing separation margin of minimum natural frequencies for every piping section needs to be greater than 2.4 times running speed is still indispensable. In the presented example this is 24 Hz (2.4 times the maximum running speed of 600 RPM / 10 Hz). The general support design of the plant is considered acceptable within this approach when all natural frequencies of several piping sections are above this limit. The 20% separation margin for significant excitation frequencies (especially higher harmonics of running speed) will be neglected.

Nevertheless, vibration issues might occur at the higher natural frequencies during commissioning. Unfortunately, the general prediction of the operating vibration level is affected by several conditions:

- Absolute excitation level based on the accuracy of the pulsation study.
- Exact natural frequencies depend on the estimations for local boundary conditions of supports.
- Coincidence of the mechanical natural frequencies with remaining acoustical resonances.
- Damping coefficient of the natural mode for each individual natural frequency.

Numerical studies will always stay a necessary and important tool for the design of reciprocating compressor systems. But unavoidable assumptions will always lead to a remaining uncertainty on the expected vibration level. If increased vibrations are detected during commissioning, immediate assistance is required. A common approach is to work with additional support structures, which usually takes a lot of time and may require additional numerical calculations.

A universal tool and a straightforward method for its implementation needs to be available to overcome this situation when a new / modified compressor plant is commissioned. One possible approach will now be described based on the idea of a partly simplified mechanical study for piping sections.

by: Patrick Tetenborg, Christian Jansen – JANSEN + TETENBORG

3 Commissioning

The first start up is the most spectacular event at the end of the construction and commissioning phase for a reciprocating compressor plant. Beside all process relevant setups, the dynamic operating behaviour of the compressor and the attached piping is always one of the key aspects during start up.

3.1 Vibration-heat-map

The as-built situation is compared to the design within the first site inspection of the compressor. The first important step within this new approach that allows us to eliminate vibration issues immediately during commissioning is to quantify the vibration level with a **vibration-heat-map**. The heat-map gives a direct overview on local vibration hot-spots for the investigated system. Figure 7 shows an excerpt of relevant locations (Measurement Positions – "MP") that have been spotted within this approach. Usually, the heat map consists of much more measurement locations.

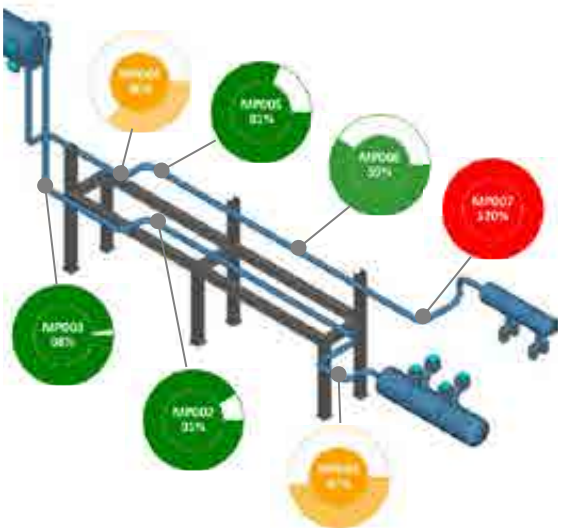

*Figure 7: Excerpt of a **vibration-heat-map** for the interstage.*

The individual colour code and the given quantification in percentage quantifies the vibration level itself. This quantification is based on the assessment regarding international standards. The heat map differentiates three assessment zones:

- "green": acceptable vibration limit
- "orange": vibrations under concern
- "red": problematic vibrations

For the assessment of piping vibrations, the VDI 3842[2] and ISO 20816-8[3] are proven. In this case, the VDI 3842 standard is used because it is considering the dynamic material stress within its evaluation. Thus, it provides frequency dependent guidance values for permissible piping vibrations which are based on measured values and experience in the petrochemical industry over a period of more than 25 years. Figure 8 shows the assessment range regarding the used VDI 3842 guideline for piping vibrations.

The given example shows the spectrum of vibrations at the highest vibration level for measurement location MP007. The maximum peak of vibrations at 49 Hz is 20% above the guideline limit for problematic vibrations. Thus, the heat map indication is in the "red" zone and the relative vibration level is on 120%. A vibration mitigation is mandatory for this location.

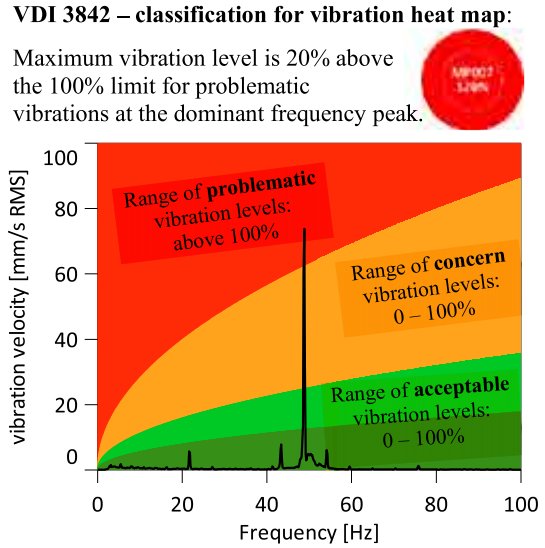

Figure 8: Example of vibration-heat-map classification based on VDI 3842 guideline for MP007.

Vibrations of concerning levels have been noticed at locations MP001 and MP004 beside the obvious vibrations on location MP007. For these locations local stress measurements have been performed. The dynamic material stress at the most strained locations have been below a typically applied limit of 20 N/mm² peak-to-peak regarding the reference value for dynamic material stress based on the API 618 standard. No further action is necessary.

3.2 Root cause analysis

The root cause analysis on site is the next step for reducing the elevated vibration level at location MP007.

The pulsation level inside the interstage piping has also been checked within this commissioning support. As expected, nothing obvious has been found. The acoustical study of pulsations does usually have an accuracy that is generating a high confidence on having an overall acceptable pulsation level. In case of having unexpected vibrations during start up, it is most likely, that these issues are related to structural problems.

Therefore, the dynamic response characteristic for the obvious measurement location needs to be

by: Patrick Tetenborg, Christian Jansen – JANSEN + TETENBORG

The first one is quite simple and only a question of a smart and universal design. The DPS has got a more than 50% higher counterforce capacity related to other available tuned mass dampeners in the market. This is directly related to the high absorber mass, which is providing the counterforce on the critical piping section. This simple aspect allows us to address modal masses of critical piping sections up to approx. 500 kg with only one DPS. Thus, the sizing does even fit for small as well as for larger piping systems (up to DN300). The standard DPS is designed to be applicable to compressor pipe runs of all typical sizes. A tailored size can be provided for specialized equipment.

The main advantage of the DPS is its **unique tuning mechanism.** All other available tuned mass absorbers are configured in the manufacturers workshop before being shipped to site. The tuning mechanism allows us to adjust the stiffness as well as the damping ration on site during the start-up support. This makes every single DPS applicable on resonance issues in a frequency range of 15 Hz up to 80 Hz. **The tuning and final optimization can be performed while the plant is in operation and the DPS is already installed at the pipe.** This is done by adjusting the stiffness using a screwdriver and a torque wrench first. After confirmation of a perfect setup for the natural frequency of the absorber mass the damping will be adjusted by using an oil of high viscosity. For this tuning only four configuration plugs are necessary, see figure 11.



Figure 11: Dynamic pipe support installation on a random pipe run.

To provide an impression on the improvement potential a comparison of response characteristics is prepared in figure 12. The figure shows the nondimensional amplification factor for the harmonic response functions of piping sections with different modal damping ratios (1% at the top, 2 % in the middle and 4 % at the bottom) and modal masses. Common values for damping at piping sections are usually in a range of 0.5 % up to 2.0 %. In all three cases a more or less strong amplification for the resonance case (frequency ratio = 1.0) becomes obvious.

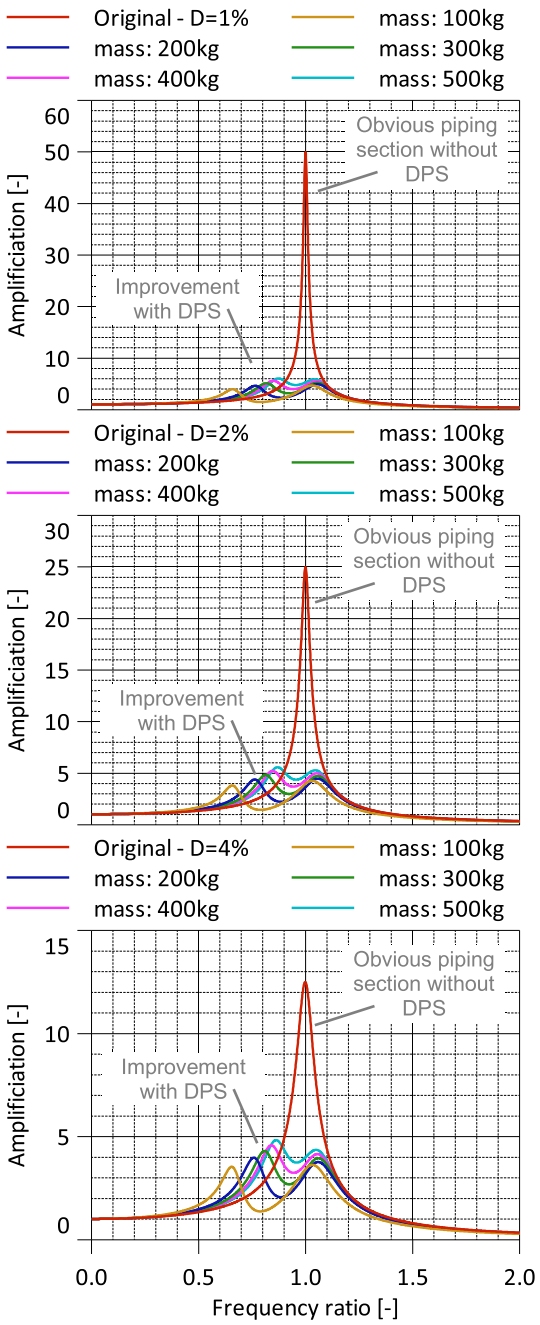

Figure 12: Dimensionless representation of the improved transfer functions by using the DPS at different damping ratios and masses of the critical eigenmode.

Additional response characteristics are presented for the different damping scenarios to describe the improvement with the on-site adjustable DPS. The

by: Patrick Tetenborg, Christian Jansen – JANSEN + TETENBORG

different response characteristics are representing the improvement in case of different modal masses of the critical piping system. The comparison shows, that the high counterforce capacity of the DPS works even better for smaller modal masses of the critical piping section. Nevertheless, also for vibration modes with modal masses up to 500 kg, the DPS achieves an total improvement on the highest amplification about a factor of 10 (for 1% modal damping) or even 5 (for 2% modal damping).

Thus, it will directly lead to a massive improvement of the vibration sensitivity for the addressed piping section. And this improvement will be finalized within the root-cause-analysis on site.

4.2 New optional frequency separation margins

In section 2.3 a simplified approach based on this new methodology and new tuned mass absorber has already been mentioned. A new classification for acceptable separation margins within the Design Approach 3 is applicable as an additional option for piping sections:

- Minimum mechanical natural frequency of any system element shall be designed to be greater than 2.4 times maximum running speed.
- *All predicted mechanical natural frequencies above 15 Hz (lowest working frequency of the DPS) and above the previous margin are acceptable. Dynamic Pipe Supports are available during commissioning and will be installed in case of resonance issues of the piping system.*

Fulfilling these separation margins might enable a reduced effort on numerical calculations regarding the necessity of the forced mechanical response analysis for piping sections. Having a set of multiple DPS available on-site will enable an immediate vibration mitigation for the involved parties during start-up.

Using this modified approach and separation margins leads to the following modified Campbell-diagram for this compressor intersection, figure 13.

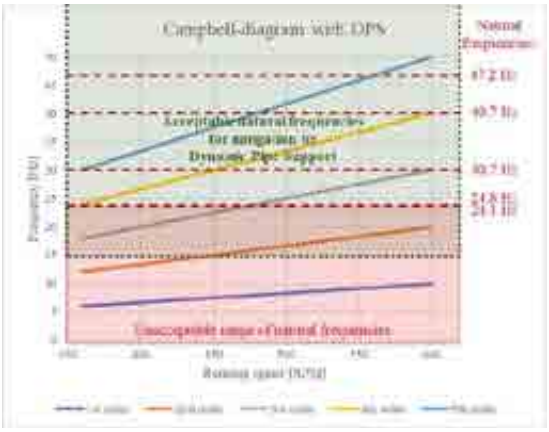

Figure 13: Modified Campbell-diagram for the compressor unit with acceptable frequency margins using the DPS technology for commissioning.

4.3 On-site improvement

To prove the performance of this approach, a comparison of the initial vibration situation and the reduced vibration level with installed DPS is shown in figure 14. The improved dynamic response characteristic highlights, that the DPS has directly improved the overall sensitivity for vibrations of that piping section.

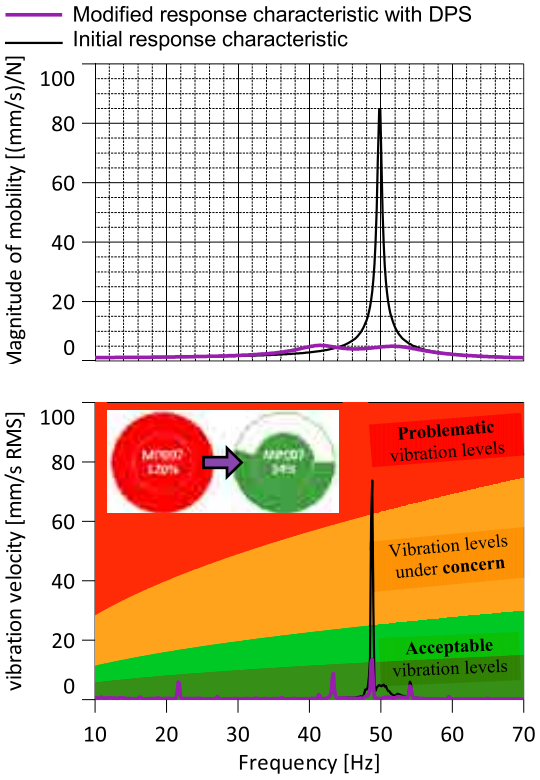

Figure 14: Comparison of the response characteristics and operational vibration situation for initial condition and situation with DPS.

by: Patrick Tetenborg, Christian Jansen – JANSEN + TETENBORG

The potential for a structural resonance is eliminated. Thus, the local spot of the vibration-heat-map has been improved from the “red zone” with 120% to the “green zone” with only 54%.

This local vibration optimization is only shown as an example. In general, a set of multiple DPS will be taken to site for the start-up support. Based on the local findings within the vibration-heat-map all spots of concern and problem will be analysed in detail. Finally, DPS units will be installed at every location, that needs to be improved and all vibration start-up issues for the piping structure are solved.

5 Conclusion

A numerical study of pulsations and vibrations is one of the most important design criteria for new reciprocating compressor plants. Modern software and accumulated experience of the design engineers have led to a high predictive accuracy in these studies. However, it is not uncommon to face increased vibrations during start-up. This may be due to inadequate construction work or slightly different boundary conditions between reality and assumptions within the calculations.

Thus, a methodology with a new tuned mass absorber has been presented, that solves vibration issues during commissioning immediately. Therefore, a vibration-heat-map will point out local vibration hot spots during the first start-up of a new or modernized reciprocating compressor unit. Acoustical issues are usually solved in advance by adjusting the pulsation damper and additional orifices in the piping system.

Thus, structural resonances are most likely the reason for elevated piping vibrations. Accepting new frequency separation margins (section 4.2) ensures, that these remaining resonance problems can be solved by the usage of the standardized DPS. A set of multiple DPS will be taken to site for performing the start-up vibration support and solving all occurring vibration issues within this support engagement.

6 References

[1] API 618: Reciprocating Compressors for Petroleum, Chemical, and Gas Industry Services. 5th Edition. 2007.

[2] VDI 3842: Schwingungen in Rohrleitungs-systemen. 2004.

[3] ISO 20816-8: Mechanical vibration - Evaluation of machine vibration by measurements on nonrotating parts - Part 8: Reciprocating compressor systems. 2018.

[4] Den Hartog, J. P.: Mechanische Schwingungen. 2. Auflage. Springer Verlag. Berlin. 1952.

[5] Petersen, C.: Dynamik der Baukonstruktionen. Vieweg & Sohn Verlagsgesellschaft. Braunschweig / Wiesbaden. 1996.

[6] Tetenborg, P.; Lenz, J.: New adjustable vibration absorber – first applications on site. 11th EFRC Conference Proceedings. Madrid. 2018.

7 Lund, E.: White Paper: The paths to Momentum TMDs with excellent performance, www.momentum-technologies.no. 2021.

SEALING & EMISSIONS

A non-lube sealing system in a high-pressure fuel gas compressor – field experience
by: Felix Ragg – BURCKHARDT COMPRESSION *237*

Improved plant reliability due to acoustical and vibrational optimisation
by: Bernhard Fritz, Georg Meyer, John Ladd – HOERBIGER *245*

A simplified approach to the design of nitrogen purge systems to improve safety and reduce emissions
by: Guido Pratelli, Christian Prinz – HOERBIGER *253*

Overcoming reliability challenges of sealing highpressure hydrogen diaphragm compression stages
by: Marije Oosterlaak, Rens Hulstijn, Yann Ardouin – HOWDEN *262*



Burckhardt Compression

A non-lube sealing system in a high-pressure fuel gas compressor – field experience

by:

Felix Ragg
Research & Developement
Burckhardt Compression AG
Winterthur, CH-8404 Switzerland
Felix.Ragg@burckhardtcompression.com

13th EFRC CONFERENCE
September 19th – 21st 2023, Zagreb

Abstract:
During the energy transition phase, natural gas as an energy source plays an important role due to its lower CO_2, NO_X and SO_X emissions compared to oil or coal. The transport over large distances of liquefied natural gas (LNG) is managed by vessels seaborne which require a boil-off gas (BOG) management system. Boil-off gas as fuel complies with the IMO Tier III regulations, unlike marine diesel but requires a fuel gas handling system with high demands placed on the boil-off gas compressor. The standard technical solution implemented for the high-pressure stages of a fuel gas compressor was lubricated ring type cylinders. The operational mode of the compressor e.g., the recycle mode, can result in an oil accumulation at the reliquification unit and subsequently in the LNG tank. The most enduring solution to eliminate any oil contamination is the conversion of the fuel gas compressor into a non-lubricated machine with a dry-running friction system. The challenge of operating an oil free compressor for high discharge pressure is the lifetime of the sealing system of the high-pressure stages. In particular, the high dynamic and static pressure difference acting on the piston rod sealing can limit the mean time between overhaul (MTBO) of the compressor. Therefore, the design of the rod sealing system, the applied sealing ring design and the choice of the ring material is crucial. The dry-running sealing system of the fuel gas compressor of a large LNG carrier covered in the present paper, achieved more than 10’000 hours of operation. The packing ring design and material was carefully selected and optimized to meet these high demands. Monitoring data and the wear analyses of the friction rings indicated a stable operation and gives a promising outlook for an increase of the maintenance intervals.

by: Felix Ragg – BURCKHARDT COMPRESSION

1 Introduction

During the energy transition phase, natural gas as an energy source plays an important role due to its lower CO_2, NO_X and SO_X emissions compared to oil or coal. The shipping of liquefied natural gas (LNG) is worldwide the most important manner of transport due to the geographical characteristics of producer and consumer. The storage of liquefied natural gas onboard vessels produces boil-off gas (BOG) despite isolated tanks and thus requires a BOG handling system. The most economical way is to use the boil-off gas as fuel. Aside from the economic aspect, the use of LNG boil-off gas as a fuel is advantageous due to environmental regulations, especially in emission control areas since the IMO (International Maritime Organization) Tier III regulations are thus fulfilled contrary to marine diesel. A BOG handling system is complex however, with high demands placed on the fuel gas compressor as the discharge pressure can range up to 320 bar e.g., for a MAN ME-GI dual-fuel engine. The present paper discusses the challenges of a sealing system for a fuel gas compressor that has a mean time between overhaul (MTBO) of more than 10'000 hours.

2 Technology

2.1 Fuel gas and reliquefication system



Figure 1: Example of a LNG carrier.

Over large distances the transport of LNG is managed seaborne by means of large LNG-carrier (figure 1) with tanks sizes ranging from 174'000 to 200'000 cubic meter. These tanks are isolated to the atmosphere as the boiling temperature of natural gas is at -162°C. Despite the isolation a fraction of the LNG will vaporize as boil-off gas. The rate at which the gas vaporizes, called boil-off rate, depends on temperature, pressure and gas mixture. Boil-off rates for above mentioned tank sizes lie between 2 and 4 t/h. Since tanks of the membrane type are limited in pressure, the boil-off gas needs to be removed to keep the pressure inside the tank within the limits. Beside routing the gas into a gas combustions unit, which is a seaborne equivalent of a flare, three economical deployments are available. These are, the combustion inside generators for the production of electricity, the reliquification and recycling into the tank and at last the usage as fuel gas to propel the vessel. The last-mentioned application is the most efficient one as it also fulfils the requirements regarding the emission controls within the IMO Tier III regulations.[5] When providing the boil-off gas to the ship's engine, one commonly used method is the direct injection of gas at pressure of 300 bar into a two-stroke dual-fuel engine based on the diesel cycle. But nevertheless, depending on the boil-off rate, more gas is vaporized than consumed by the engine, hence reliquefying is still a requirement. There are different liquefactions processes known, the present paper covers the Partial Reliquefication System (PRS) underlying the Joule-Thomson cycle, as shown in figure 2. Basically, the process is an open cycle where boil-off gas is used as refrigerant to pre-cool the gas. A fraction of the gas is reliquefied depending on the cooling efficiency of the heat exchanger and the pressure of the gas. The core component of the PRS is the Joule-Thomson valve (JTV) where the gas is expanded and due to its positive Joule-Thomson coefficient cooled down. The pressure difference at the Joule-Thomson valve required to achieve the boiling temperature, depends, as mentioned, on the temperature of the boil-off gas upstream of the valve. After a separator, the liquid phase is routed back to the tanks, while the flash gas is brought back into the suction line of the compressor. The combination of direct gas injection into a two-stroke engine and a reliquefying system requires a multi-stage fuel gas compressor providing gas pressures above 300 bar for injecting into the engine and pressures above 150 bar for the reliquefying process.[1]

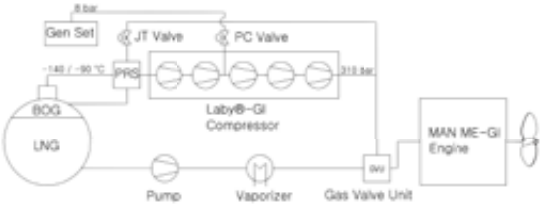

Figure 2: PI&D of the fuel gas and reliquefaction system.

2.2 Oil lubricated fuel gas compressor

The fuel gas compressor covered within this paper, is a 5-stage vertical compressor as shown in figure 3, that meets the requirements regarding the footprint for offshore applications. The maximum flow capacity of the compressor is in the range of 4'800 kg/h with a maximum discharge

by: Felix Ragg – BURCKHARDT COMPRESSION

pressure of 320 bar and an average piston velocity of 4.2 m/s. The compressor design takes varying suction temperatures (-160°C to 45°C) and pressures into account by having the first stages as labyrinth type seals implemented without the need of a boil-off gas pre-warming system. The last two stages on the other hand are equipped with a friction-based sealing system based on its superior sealing efficiency compared to its labyrinth counterpart. Depending on the operating case typical suction and discharge pressures of the head sided 4th stage are 42 bar and 104 bar respectively. Whereas the crank sided 5th stage then further compresses from 102 bar to 312 bar. The reason for allocating the stages as such, is the difference in compression volume as the piston rod occupies the 5th stage compression chamber which equals in less volume and hence a higher stage. As a result, the highest pressure difference needs to be sealed against the crank pressure with the piston rod sealing (packing). The friction-based sealing systems of the two high-pressure stages are by default lubricated (both, piston and piston rod sealing) to reduce frictional heat and wear of the sealing rings. The homogeneous piston rod sealing consists of 10 three-piece sealing rings with cover and support ring.



Figure 3: 5-stage fuel gas compressor with doubled 4th and 5th stage in the middle.

2.3 Oil-carry-over

Else than the lubrication oil inside the crank, the lubricant for the sealing system of the compressor is in direct contact to the compressed gas. Depending on the type of lubrication oil, e.g., PAG or mineral-oil based lubricants, the solubility of the oil in the gas is of crucial subject. During the compression, the gas temperature increases and oil vapour forms as well as aerosols. Common filtration systems upstream of the PRS of e.g., the coalescing filter type are able to remove aerosols from the gas stream but not oil vapour. This implies, the gas stream enters the PRS containing a certain amount of oil vapour which condensates inside the heat exchanger upstream of the JTV. The oil residue can not only foul the micro channels of the heat exchanger and reduce the flow but also decrease its efficiency. Accordingly, the fraction of reliquefication decreases since the gas stream could not be cooled down to the required temperature at given pressure. Moreover, oil particles can enter the LNG tank. The amount of oil vapour carry-over can be optimized by changing the type of oil, but without additional and by all means costly filtration systems like activated coal or cryogenic traps, the issue remains even if the oil entering the PRS is within the range of parts per million since it will accumulate over time.

2.4 Dry-running fuel gas compressor

2.4.1 Requirements and challenges

The most enduring solution to eliminate any oil contamination is the conversion of the fuel gas compressor into a non-lubricated machine with a dry-running friction system. However, the challenge with such a retrofit is, that the boundary conditions already are set as the compressor was originally designed for a lubricated service. A step piston design could not be applied which would have been mandatory with the present high pressure difference.[4] Especially the high pressure difference acting on the piston rod sealing can limit the MTBO of a dry-running compressor. Therefore, the design of the sealing system, the applied sealing ring design and the choice of the ring material is crucial.

2.4.2 Sealing system for dry-running compressor

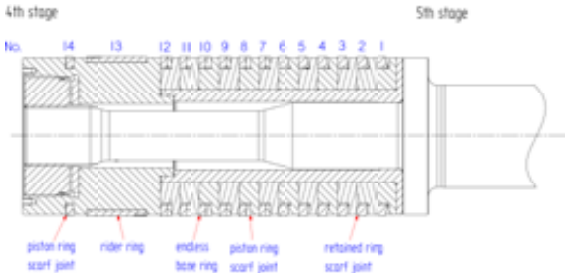

Figure 4: Composition of the 4th and 5th stage piston.

Piston and packing sealings of reciprocating compressors are exposed to a dynamic and a static pressure component. The dynamic pressure component is a characteristic feature of the compression process and is the difference between compression pressure and suction pressure.

by: Felix Ragg – BURCKHARDT COMPRESSION



Figure 5: Composition of the 5th stage piston rod sealing. The highlighted (P) denotes the location of the pressure measurement inside the packing.

It varies between the maximum or final pressure and suction pressure each crank rotation. The static pressure component is the difference between suction pressure and the pressure after the last sealing element, for example at the outlet of the packing. The static pressure component does not vary during the crank rotation. Each pressure component has a different effect on the operational behaviour of a sealing system.[3] The static pressure component effects mainly the leakage of a sealing system, whereas the dynamic pressure component effects wear, failure by fracture and/or plastic deformation of the sealing elements. This perception allows sealing systems to be optimized and requires sealing elements designed for the different effects of each pressure component.

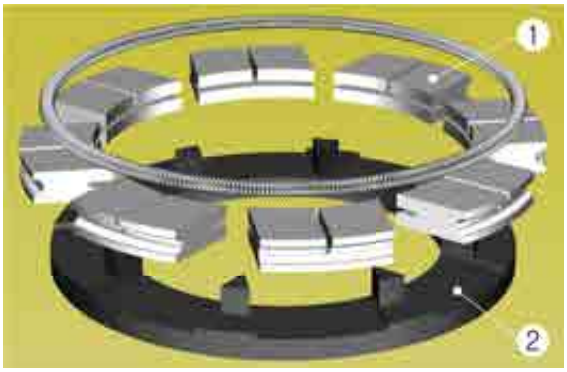

Figure 6: Sealing element with eight segments (1) and one endless guide ring (2).

To withstand the dynamic pressure load, a robust ring design which is not necessarily tight but allows for a pressure distribution across several sealing elements is convenient. On the other hand, gas tight sealing elements are required to reduce the leakage induced by the static pressure component. Applying the aforementioned design rules results in a heterogeneous sealing system made of robust pressure breakers and gas-tight sealing elements. Consequently, the 5th stage piston sealing system persists of six retained pressure breakers, designed to shelter the sealing rings from the dynamic pressure component, indicated in figure 4 by the numbers 1–6. The special design of these retained rings allows them to work as contactless rings after a running-in period. The six subsequent sealing rings (figure 4, rings no. 7–12) are one-piece rings with a scarf joint upon an endless support ring. Between 4th and 5th stage one rider ring is located (figure 4, ring no. 13). The 4th stage piston pressure difference allows a single sealing element (figure 4, ring no. 14). Especially the piston rod sealing exposed to high pressure load and high average piston speed is sensitive to friction heat dissipation. The reason is the indirect heat dissipation all piston rod sealings are submitted to. Since the ring material has a very low thermal conductivity the frictional heat is dissipated via convective heat transfer from the piston rod to the packing cups.



Figure 7: Pressure breaker with two endless rings (1) made of PEEK and (3) made of bronze. The actuator ring (2) presses both rings in the opposite direction. Two red arrows indicate the direction the rings are actuated.

The solution to this problem is the implementation of five optimized sealing rings,[2] each with eight individual movable segments as indicated in figure 6. Experience has shown that these rings generate a low frictional heat even operated at an average piston speed of 4.2 m/s. The material favourable for the high static pressure difference of up to 110 bar is modified PEEK containing solid lubricants and carbon fibres. Downstream, the sealing rings are supported by endless rings which have a sufficient strength. Figure 5 shows the composition of the packing with the sealing elements identified by numbers 9–13. To shelter the sealing rings from the high dynamic pressure of up to 210 bar, robust pressure breakers are essential. Each of the seven applied pressure breakers (figure 5, rings no. 2–8) are comprised of two endless rings which are pressed in opposite direction by an actuator ring,[2] as shown in figure 7 where the red arrows highlight the directions the rings are actuated. Thus, each ring

by: Felix Ragg – BURCKHARDT COMPRESSION

covers one half of the piston rod and throttling a fraction of the dynamic pressure difference. The materials of the two endless rings are modified PEEK and bronze filled with graphite. The first ring of the packing (figure 5, ring no. 1), serves as throttle ring but keeps mainly parts of the downstream rings from entering the cylinder.

3 Results

The above described non-lubricated sealing system was installed during a retrofit into a 5-stage fuel gas compressor located on an LNG carrier. After a short trial period of approximately 4'000 hours, the compressor started its new dry-running duty in April 2020 and was then in normal operation for 10'160 hours without shut-downs related to the sealing system. The on-board monitoring system and one additional pressure measurement inside the packing allowed the crew to observe the condition of the packing continuously. The piston and packing sealing system were exchanged during a planned maintenance of the compressor.

3.1 Condition of the piston rings

The piston of the 4th and 5th stage appeared in good state after dismantling. The piston rings showed no thermal damages such as melting and plastic deformation due to high temperatures. Additionally, no fractures or cracks were discovered at pressure breakers or sealing rings. Only three support rings (of rings no. 7, 8 and 12) of the 5th stage showed straight fractures. The running surfaces of the sealing rings and the rider ring indicated normal operation due to its smooth and shiny appearance. Finally, the piston cups which house the rings were flat and in good general condition. No abnormal wear condition was measured on the rings. The average wear of the sealing rings was found to be below 25% of its maximal allowable wear (which means the rings lost radially less than 25% of its allowable material). Such low wear coefficients indicate a favourable tribological conditions without negative influence due to gas contamination.

3.2 Condition of the packing rings

Since the packing was exposed to the highest load, its condition after the operating period was accordingly in a less good state as the piston rings but still functional. All pressure breakers showed fractures at the bronze rings (figure 8), and the first two rings (figure 5, rings no. 2–3) broke into small parts and vanished from the packing cup, most likely during the removal of the piston rod as some parts could be found inside the distance piece. Due to the fractures and hence created leak paths, some pressure breakers showed still severe erosion marks. The two sealing rings directly downstream of the pressure breakers (figure 5, rings no. 9 and 10) were found with several fractures at the segments; figure 9 shows the sealing ring number 9.



Figure 8: View of the fractured bronze ring of the last pressure breaker (ring no. 8).



Figure 9: Condition of the first sealing ring with broken segments (ring no. 9).



Figure 10: Condition of the last sealing ring (ring no. 13).

by: Felix Ragg – BURCKHARDT COMPRESSION

The reason is, that these rings were exposed to the full dynamic pressure after the upstream-located pressure breakers lost their functionality. All further sealing rings (numbers 11–13) were in good condition (see figure 10) without damage and only minor fretting marks at the segments. However, all support rings showed some extrusion. In terms of wear, the sealing rings showed a relative wear of below 30% on average. Relative wear means again the measured wear in relation to the maximum possible wear of the current ring design. The first sealing ring exposed to the full dynamic pressure load could not be measured due to its broken segments.

3.3 Packing pressure

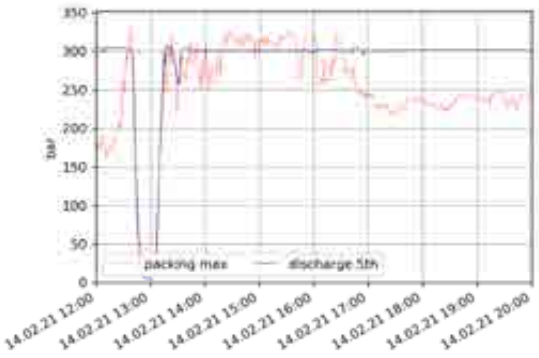

Figure 11: Extract of the packing pressure (packing max) and discharge pressure of the 5th stage (discharge 5th).

As mentioned, an additional pressure transmitter was installed to measure the pressure inside the packing. The transmitter, connected to the packing cup via a bore, was mounted outside the packing at the packing flange. Figure 5 shows the location of the pressure measurement schematically; between the pressure breaker number 8 and the first sealing element number 9. This pressure transmitter indicates indirectly the condition of the pressure breakers. Namely, with an increase of the measured pressure, the throttling efficiency of the pressure breakers decreases until a breakdown when the full dynamic pressure (in this case the 5th stage discharge pressure) reaches the gauge. Thereby the date of an overhaul can be predicted more precisely. As soon as the dynamic pressure reaches the sealing rings meant to seal the static pressure, one part of the heterogeneous packing will not be able to operate as designed. The sealing rings can handle the dynamic pressure due to their robust design, but these rings are not optimized for this pressure component and the wear rate will increase by an order of magnitude. Furthermore, failure by fracture can occur and decrease the overall lifetime of the packing drastically. Once such failures occur, the remaining service life of the sealing elements cannot be predicted any more, and an overhaul is recommended. The condition of the sealing rings can be approximated with average leakage values. The leakage of any non-lubricated friction-based sealing system varies over its service life and single peak events do not give a reasonable indication. But in case of extreme status of wear or severe failure by fracture, the leakage rate will increase drastically.

Figure 11 shows an excerpt of the packing pressure and discharge pressure data over 8 hours. During this period, the measured packing pressure exceeded for the first time the 5th stage discharge pressure (for approximately two hours). It can be assumed that at this point in time (14.02.2021) the pressure breakers were no longer capable of throttling the dynamic pressure reliable. Moreover, the periods in which the measured pressure inside the packing is higher than the discharge pressure are increasing from then on, as can be seen in figure 12 (top). Over the total service life of the packing, the constantly rising packing pressure is visible in figure 12 (top) until end of August 2021, when the packing pressure decreased again. A reason for the decreasing packing pressure could be, that due to wear previously generated gaps were closed although the endless pressure breaker rings were fractured.

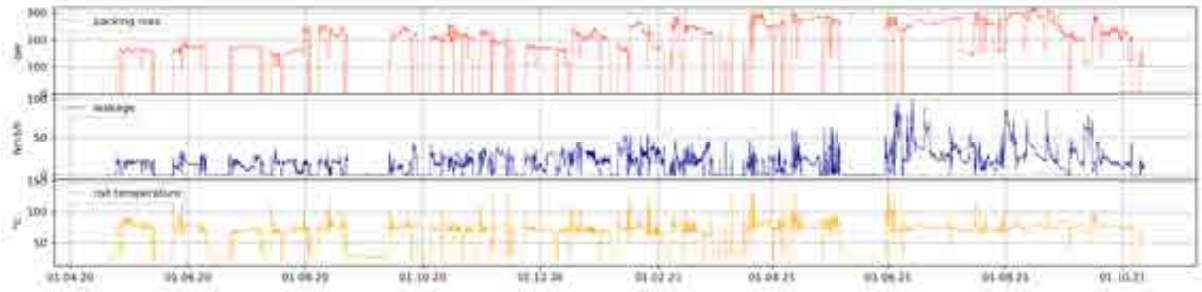

Figure 12: Packing pressure (top), packing leakage (centre) and piston rod temperature (bottom) over the entire service life of the packing.

by: Felix Ragg – BURCKHARDT COMPRESSION

The packing leakage data (figure 12 centre) show only a slight increase until May 2021 but more frequent peaks of up to 100 Nm3/h during the last quarter of the service period which, like the packing pressure reduced again at the end of the operating period. The piston rod temperature (figure 12 bottom) measured via infra-red thermometer gave little indication of the wear state of the packing rings (slight increase from March 2021 on and higher peaks). The condition of the packing in combination with the pressure data from inside the packing clearly show the importance of reliable pressure breakers throttling constantly over the service life of the packing. Since this premise was not fulfilled, as pressure data indicates, the static sealing elements handled the dynamic pressure and sheltered the down stream sealing rings such that these still could seal the static pressure difference satisfactory. The first sealing elements were exposed to the full discharge pressure for approximately one third of the operating period (February to September 2021) and still three out of five sealing rings were in good condition.

4 Conclusion

To prevent oil contamination of the PRS effectively, the originally lubricated fuel gas compressor was converted to non-lube service. A heterogeneous sealing system was implemented in the last two friction-based stages of the compressor. Despite the very unfavourable operating conditions for a dry-running sealing system (high differential pressure and high average piston speed), the compressor was in operation for more than 10'000 hours without any sealing system related shut-downs. Furthermore, monitoring data and wear analysis indicated a stable operation. The main challenge though was the highly loaded 5th stage piston rod sealing. The data analysis has shown that in particular the pressure breaker rings are the most critical part of this dry-running sealing system. Hence further development is focused on the improvement of the pressure breakers in terms of robustness and reliability. Nevertheless, the result gives a promising outlook for an increase of the maintenance intervals.

Abbreviations

PAG	Polyalkylene Glycole
PEEK	Polyetheretherketone

References

[1] J. Choi. Developement of partial liquefaction system for liquefied natural gas carrier application using exergy analysis. *International journal of naval architecture and ocean engineering*, 10:609–616, 2018.

[2] N. Feistel. Performance improvement of dry-running sealing systems by optimization of wear compensation. page 239 – 247, Vienna, Austria, 2014. 9th EFRC-Conference.

[3] N. Feistel. Heterogeneously designed sealing systems based on the redura principle. *COMPRESSORtech2*, pages 44 – 48, March 2015.

[4] T. Harder, N. Feistel, and F. Ragg. Oil-free compression of hydrogen – which role plays the crosshead compressor today and in future? page 207 – 213, Warsaw, Poland, 2021. 12th EFRC-Conference.

[5] C. Hwang, S. Oh, D. Kim, T. Gundersen, and Y. Lim. Energy, economic and environmental analysis of a BOG re-liquefaction process for an LNG carrier. *Energy Reports*, 8:2351–2362, 2022.


Enabling zero emissions.
For a better tomorrow.
Visit our booth!
Learn more by visiting
www.hoerbiger.com/emissions
today!
HOERBIGER

HOERBIGER

Optimization of pressure packing designs in consideration of rod temperatures

by:

Bernhard Fritz
bernhard.fritz@hoerbiger.com

Georg Meyer
georg.meyer@hoerbiger.com

John Ladd
john.ladd@hoerbiger.com

HOERBIGER Wien GmbH
Vienna, Austria

13th EFRC CONFERENCE
September 19th – 21st 2023, Zagreb

Abstract:
Typical engineering standards for compressor rod packings rely on rules of thumb and selection tables. While there is consensus that piston rod temperatures are one of the important design criteria for the lifetime of packing rings, they are generally unknown. With the Packing Performance Prediction Tool, an essential step towards developing a sophisticated design tool for pressure packings is underway. It allows detailed estimation of piston rod temperatures as a function of specific design parameters (number of rings, ring design, etc.). While the tool is still under development, first results are very auspicious. In this paper, a case study shows that the average lifetime of a compressor's rod packing could be greatly increased by upgrading to pressure-balanced rings. The tool is used retrospectively to estimate the rod temperatures for both ring types in the adopted solutions. Simulation results suggest that the mean rod temperature was indeed significantly lowered by the redesign. Based on the premise that lowering the rod temperature is one important aspect of increasing the packing lifetime, other possible future packing optimizations are discussed in theory.

by: Bernhard Fritz, Georg Meyer, John Ladd – HOERBIGER

1 Introduction

Most reciprocating compressors (recips) are of the double-acting type: the use of a crosshead between the piston road and the crankshaft allows the piston to compress at both the head-end (HE) and the crank-end (CE) side. For the HE side, leak-free sealing between the cylinder cover and the cylinder is easily realized via state-of-the-art gaskets. On the other hand, sealing between the reciprocating piston rod and the fixed distance piece is harder to do. This is the job of the rod seal, also known as the pressure packing, main packing or compressor packing.

The pressure packing is in fact the leakage-determining component of a reciprocating compressor. With increasing wear during operation, gaps open and gas leakage increases over time. Commonly, the leaking gas leaves the packing via the vent line tube, whose temperature can easily be monitored to detect high leakage rates. A study by Goebel [1] states that a significant percentage (11%) of unplanned compressor downtime is due to packing issues, making the pressure packing the third most vulnerable component of a reciprocating compressor — after issues related to compressor valves and the process itself. For non-lubricated piston rods the percentage is most likely even higher; the absence of oil leads to higher coefficients of friction, so more frictional heat is released. This increases the temperatures of the packing and the rod, which in turn increases the wear rates of the packing rings and makes the packing even more vulnerable compared to the other compressor components.

The vulnerability of packing rings emphasizes the relevance of improving packing know-how in order to engineer new packing designs that are more reliable and last longer. It is the consensus that piston rod temperatures are one of the important design criteria for the lifetime of packing rings. However, these temperatures are generally unknown. This paper focuses on the dependence of the piston rod temperature on design parameters; the newly developed, preliminary Packing Performance Prediction Tool (PPP-tool) is used to study the impact of packing length, number of rings, design of rings, etc. In particular, the commonly stated hypothesis that *"the packing length must not be greater than the compressor stroke to avoid a significant increase in piston rod temperature, leading to early packing failure"* needs to be checked. This is done using a case study, below.

The compressor that is the subject of the case study has suffered repeated unplanned shutdowns due to worn-out packing rings. In a first attempt to solve the problem, the average lifetime of the pressure packing was greatly increased by upgrading to pressure-balanced rings. Subsequently, both the number of rings and the length of the packing were increased to

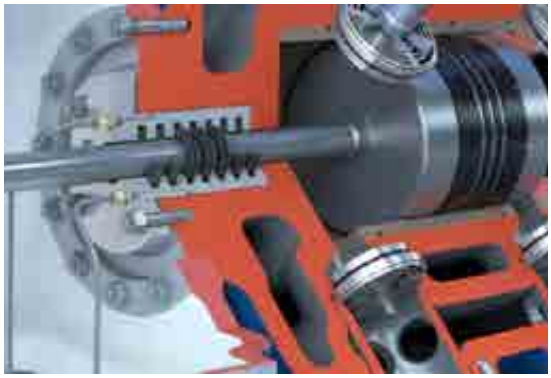

(a) Section view of a throw.

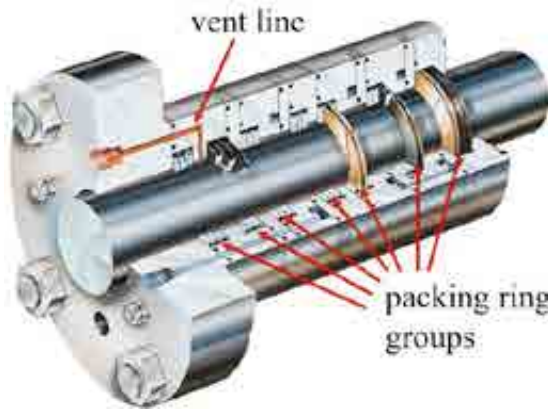

(b) Typical packing with seven ring groups.

Figure 1: Typical packing design.

give a further increase in lifetime. In retrospect, the PPP-tool is used to estimate rod temperatures for all the engineered solutions that were implemented, and sheds light on the likely impact of other possible packing modifications.

The tool is already sufficiently developed to represent the most important mechanisms – in terms of both compressor design and operation – that control the steady-state temperature of the piston rod. Its development is not yet complete, however, and it shows some limitations that are the current focus of development.

by: Bernhard Fritz, Georg Meyer, John Ladd – HOERBIGER

2 Basic function and design of pressure packings

This section gives a short overview of the basics of pressure packings, as needed to understand the modifications and results studied in this paper. More information is found in typical textbooks, e.g. [2].

Figure 1(a) shows one throw of a typical reciprocating compressor, including the piston rod assembly and the pressure packing. A pressure packing consists of several cups, each holding a packing ring group that can float freely within a groove Figure 1(b). Typically, a group consists of either a pair of rings with radial and tangential grooves ("R/T" rings, the conventional design) or a one-ring design (the modern design), which also consists of multiple segments and combines the principals of a radial ring and a tangential ring. Both designs are sketched in Figure 2. Each ring consists of multiple segments and is pre-stressed by a garter spring. The working principle is the same for both ring types: the ring segments are activated by the differential pressure, which pushes the ring against one side of the cup and against the piston rod (Figure 3). Unlike piston rings, packing rings do not incorporate a direct leak path. However, due to slight imperfections and misalignment, leakage cannot be prevented.

For applications at higher differential pressures, an additional backup ring is introduced to support the packing ring and prevent it from extruding into the clearance between housing and piston rod. The backup ring is simply a stiff ring placed between



Figure 2: (Top) The original R/T rings and (bottom) the modern, one-ring design; both images show a backup ring on the left side.

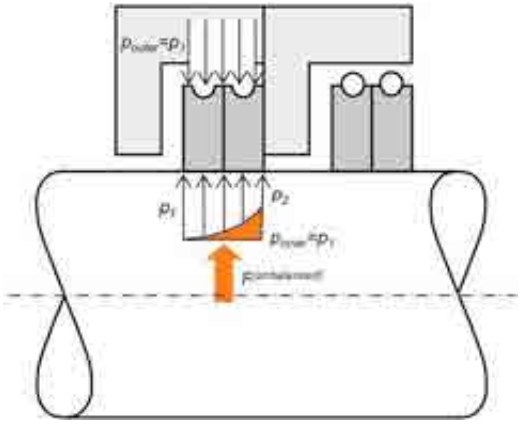

Figure 3: from [3]: pressure differential $p_1 - p_2$ across the ring pair gives rise to contact force $F^{(unbalanced)}$ between rod and ring pair.

sealing rings and cup, with a preferably small clearance to the piston rod.

According to Archard's equation of adhesive wear (1), the ring's wear rate $\dot{d}$ is proportional to the apparent pressure p times the relative velocity v between ring and piston rod, the hardness H of the surfaces being worn and the non-dimensional wear coefficient k. k is dependent on the materials in contact, the operation conditions and their cleanness [5] :

$$\dot{d} = \frac{kpv}{H}. \qquad (1)$$

In this specific case, the contact pressure p results from the unbalanced radial pressure components. p times the piston speed v is the so-called pv load.

In Figure 3, the orange annotations provide a graphical explanation of p. Friction not only causes ring wear, but is also a major source of heat generation. The contact pressure p changes with increasing ring wear and is a complicated function of the ring actuation, contact situation, ring stiffness and ring wear, amongst others.

The next section gives a short overview of the main assumptions and limitations of the PPP-tool, hopefully leading to a better assessment of results. The primary goal of the tool is not the prediction of packing lifetimes but the prediction of rod temperatures to be expected for completely new unworn rings giving the engineer a first indication of possible impacts of changes in the packing and ring design.

3 Assumptions and limitations of the Packing Performance Prediction Tool

The fundamentals and groundwork for a thermophysical model of cooled, dry-running pressure packings were presented in [3]. The model describes the thermal steady state, i.e.,

- the periodic mean temperature distribution along the rod in the periodic state of operation,

by: Bernhard Fritz, Georg Meyer, John Ladd – HOERBIGER

- the periodic mean packing ring temperatures, and
- the minimum/maximum temperatures at the ring-rod contact surface.

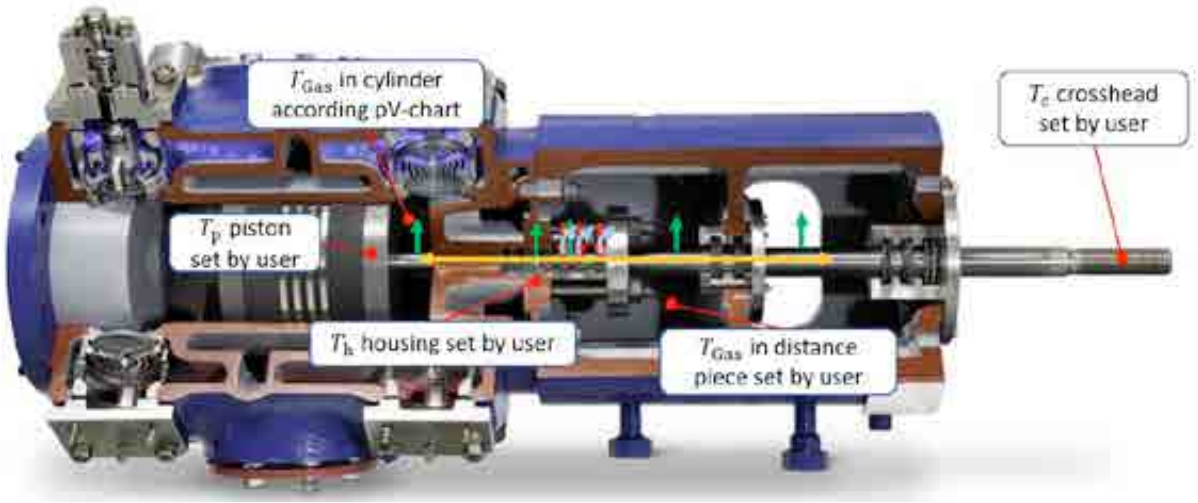

Figure 4: Scope and boundary conditions for the thermo-physical model of the PPP-tool. Yellow = heat conduction along rod. Green = convective heat transfer from rod to gas and gas to housing. Red = frictional heat generated at counter-face of packing rings. Blue = heat conduction through packing rings.

The original model was significantly extended and is currently available as a beta version as part of the packing wizard within ESM, HOERBIGER's component engineering tool. A thorough validation is currently underway with, on the one hand, a fully coupled transient computational fluid dynamic (CFD) simulation of a packing case and, on the other hand, test data from a newly installed and fully instrumented hydrogen research compressor. The tool and its validation will be the subject of a later publication.

In this section we will only summarize the basic details of the model and the main assumptions.

The simulation model was developed for cooled, dry-running pressure packings. A user must specify the temperature of the packing case as a boundary condition known from either actual measurements or experience. Additionally, the user must set boundary values (cf. Figure 4) for:

- the temperature of the piston T_p (if values other than the default value of $T_\mathrm{p} = T_\mathrm{s} + \frac{2}{3}(T_\mathrm{d} - T_\mathrm{s})$ are required, where T_s and T_d denote the suction and discharge temperature, respectively),
- the crosshead temperature, and
- the bulk temperature of the gas in the distance piece.

A value for the coefficient of sliding friction is required for the pairing of rod and packing ring material. Generally, it must be measured, for instance, on a dedicated tribo-rig. This friction coefficient will usually be the primary source of uncertainty, as the characterization of tribology is a challenging task in itself, and the coefficient of sliding friction will also depend on the gas, the temperature and other factors in a highly nonlinear way. This fact must be kept in mind when interpreting the model results. It can make sense to keep this value constant for different configurations in a comparative study.

Finally, a target mean leakage flow rate must be set before running the simulation. It can be achieved either by selecting predefined leakage classes, ranging from low (100 SCMH) to high (10,000 SCMH), or by assigning leakage areas to each ring individually. When a leakage class is selected, appropriate leakage areas are assigned automatically. The leakage areas are established in such a way that the last packing-ring (or the packing ring prior to a vent line) is sealing the static pressure, i.e., the pressure difference between suction and distance-piece pressure (or vent line pressure). The leakage areas of the upstream rings are defined to be larger by a factor of 10. The application engineer can overwrite and adjust this preselection manually if required.

The leakage area values set will affect the pressure cascade over the packing rings and the convective heat transfer from the rod to the gas and from the gas to the packing case in the cup region. Per default, the first packing ring facing the cylinder will take most of the dynamic pressure, and the last packing ring facing the distance piece will take most of the static pressure. This assumption is based on in-house measurements and on-site experience. It is supported by typical wear observations, which show the highest wear on the first and last rings of the packing. This issue is explained in more detail in [4].

The time-averaged periodic mean rod and packing ring temperatures are calculated from a time-averaged energy balance over the rod, cf. Figure 4, accounting for the frictional heat generated at the

by: Bernhard Fritz, Georg Meyer, John Ladd – HOERBIGER

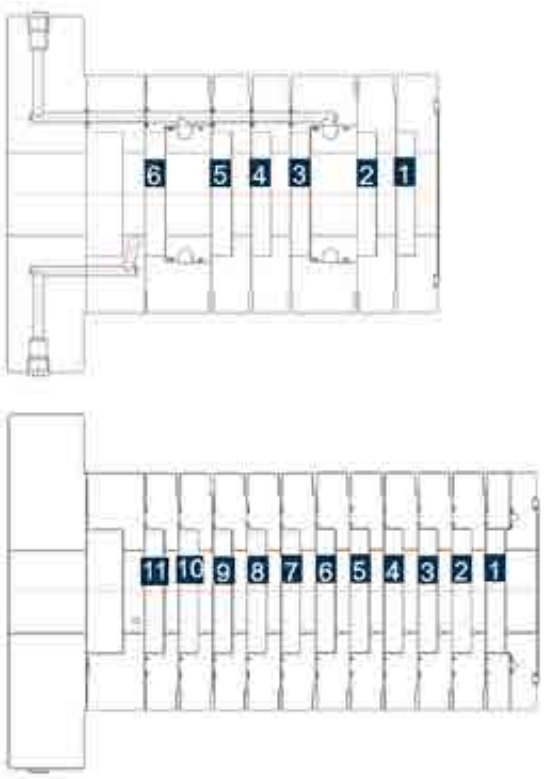

Figure 5: Section view of the original vented, non-lubricated packing case with six packing ring pairs (top), and the new, more compact but longer design (bottom).

contact surfaces between the rod and the packing rings, and the heat fluxes due to:

- conduction along the rod,
- conduction through the packing rings, and
- convective heat transfer in the:
  - cylinder,
  - cups, and
  - distance piece.

For details see [3]. Convective heat transfer in the three regions – cylinder, cups, and distance piece – is treated differently. New relations for the Nusselt numbers for each region have been constructed from many CFD simulations covering the majority of cylinder and packing line-ups expected.

Table 1: Basic geometry and parameters of the compressor.

Compressor parameters	
Speed	396 rpm
Bore	107.95 mm
Rod diameter	50.8 mm
Stroke	228.6 mm
Average piston speed	3 m/s
Suction pressure	64.7 bar
Discharge pressure	107 bar
Suction temperature	26.7 °C
Discharge temperature	72.9 °C
Isentropic exponent	1.4
Molar mass	2 kg/kmol

Recently, a detailed database has been established of material properties for the ring and rod materials, including specific heat capacity, thermal conductivity and density, and their temperature dependence.

To summarize, the underlying assumptions and current main limitations of the PPP-tool are:

- cooled packing case,
- dry Coulomb friction,
- thermal steady state, i.e., the transient start-up phase is not part of the analysis,
- constant thermophysical properties and ideal gas behaviour, and
- isotropic ring material.

4 Case study: new packings in practice

This case study concerns the packing of the second stage of a non-lube hydrogen compressor with a differential pressure of roughly 42 bar. The main compressor characteristics are given in Table 1.

The original packing (Figure 2, top) consists of six R/T-ring pairs, including backup rings, with an average lifetime of approximately 3000 hours. The corresponding packing case is shown in the top part of Figure 5, while Table 2 shows the basic design parameters of the original packings and the two modified versions.

For simplicity, in the first attempt to extend packing life only the ring design was changed, since this was the easiest measure for the operator. From the original R/T design (“V0”), all the rings were changed to the modern design (one-ring design). In addition, the new rings were pressure-balanced (“V1”): around the circumference of each ring are radial pressure balancing grooves that decrease the contact pressure, and this was effective in reducing both wear and temperature. The cup dimensions remained the same. These adaptions proved very successful in field: the lifetime of the packing increased by a factor of three, to approximately 12,000 hours.

Table 2: Basic design characteristics

	Original design V0	Design V1	Design V2
Ring type	R/T	Pressure-balanced	Pressure-balanced
Number of rings	6	6	11
Cup depth	15.6	15.6	14 mm
Package length	229 mm	229 mm	293 mm
Backup ring material	PEEK	Bronze	Bronze
Lifetime	3000 hrs	12,000 hrs	>2500 hrs

by: Bernhard Fritz, Georg Meyer, John Ladd – HOERBIGER

In the second step, the cup dimensions were modified ("V2"). The recess depth of each cup was slightly reduced, from 15.6 mm to 14 mm. More importantly, the cooling system was adapted to allow a more compact design and to increase the ratio of the number of rings to the length of the packing case. The width of each ring stayed the same, but the width of each backup ring was reduced. These measures would allow two extra rings to be added to the packing without increasing the overall packing length (Figure 5).

The packing length was increased to 293 mm, exceeding the stroke of the machine by 28% and resulting in a packing length/stroke ratio of 1.28. The increased length and more compact design allowed 11 pressure-balanced rings. The design changes follow the hypothesis that it is advantageous to use as many rings as possible as long as the max. piston rod temperature is not critical. Hence, the number of rings shall be seen as an optimization parameter, while the piston rod temperature is a limiting parameter, which needs to be checked case by case nevertheless.

This design has been realized recently in the field: it has been in operation for approximately 2500 hours and will hopefully outlive the previous designs.

The next section will show resulting thermal situation in terms of rod and packing ring temperatures given by the PPP-tool for the three designs, and the impact of some parameters.

5 Results

We apply the same assumptions for all simulations throughout this paper:

- pressure in distance piece equals ambient pressure;
- temperature in distance piece: 60°C;
- packing housing temperature maintained by the cooling system at 50°C
- crosshead temperature: 60°C
- coefficient of sliding friction: $\mu = 0.2$

A vital assumption to discuss is the coefficient of sliding friction. As mentioned before, this is not a constant that is suitable for all configurations: instead, it is highly dependent on the particular tribological system, e.g. gas, material, temperature, etc. However, $\mu = 0.2$ is a good approximation according to [2].

Let us start with the temperature predictions for the original design, V0. Figure 6 shows the temperature along the length of the piston rod, from the piston (0 mm) towards the crosshead, for both high (10,000 SCMH) and low (500 SCMH) leakage rates (SCMH is the abbreviation used for standard cubic meter per hour). The corresponding pressure curves in the cups are shown in Figure 7. Clearly, the differential pressure across each cup depends on the leakage area, and hence the leakage flow. At higher leakages, the differential pressures are more equally distributed along the rings.

Figure 6 shows that the maximum rod temperature (162°C) occurs at approximately 400 mm. This is a region of the piston rod that does not enter the compression chamber. The calculations show that

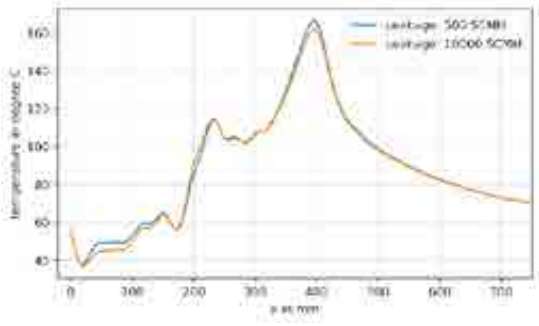

Figure 6: Temperature along the length of the piston rod, starting from the piston (x=0)

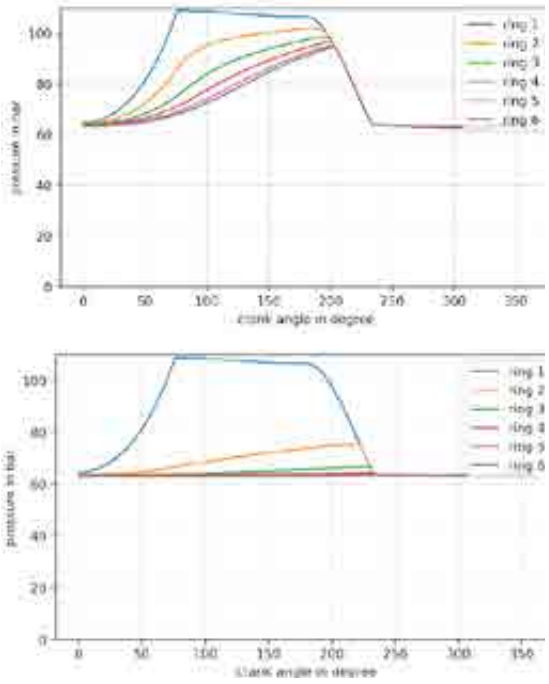

Figure 7: Cup pressures for (top) high leakage (10,000 SCMH) and (above) low leakage (500 SCMH).

heat transfer from the piston rod to the cylinder is very important: the cold gas flow coming through the suction valve provides significant cooling for the piston rod. It hence effectively removes frictional heat from the first cups. Figure 8 shows the piston rod temperature from the perspective of the cup numbers: the temperature increases with distance to the cylinder. There are two reasons for this: the last ring sees the highest differential pressure, but more importantly, it is furthest from the cylinder region with the highest heat transfer rates.

by: Bernhard Fritz, Georg Meyer, John Ladd – HOERBIGER

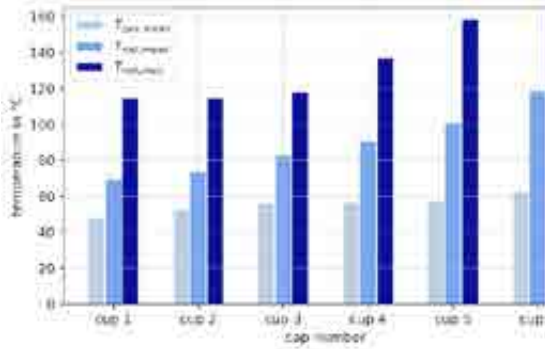

Figure 8: Time-averaged piston rod temperatures at the ring-rod contact surface (V0).

The impact of the leakage rate is not significant in this case: the maximum rod temperature changes only slightly, from 166°C at low leakage to 162°C at high leakage (Figure 6). Changing the backup ring material from PEEK to bronze additionally decreases the maximum temperature by 3 K (Figure 9).

Table 3: Simulation results

	No. of rings	Packing length	Max. temperature
V0	6 R/T	229 mm	161°C
V1	6 pressure-balanced rings	229 mm	123°C
–	6 pressure-balanced rings, compact design	204 mm	103°C
V2	11 pressure-balanced	293 mm	115°C

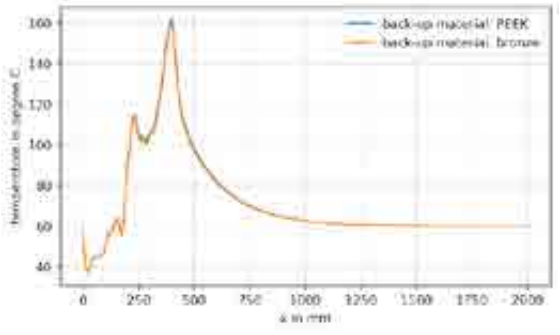

Figure 9: Impact of the material used for the backup rings: temperatures along the length of the piston rod, starting from the piston (x=0)

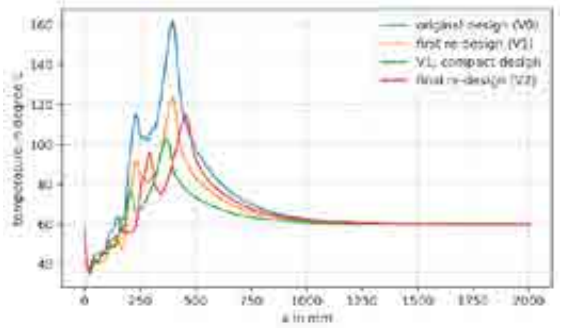

Figure 10: Temperatures along the length of the piston rod, starting from the piston (x=0) for the adapted designs.

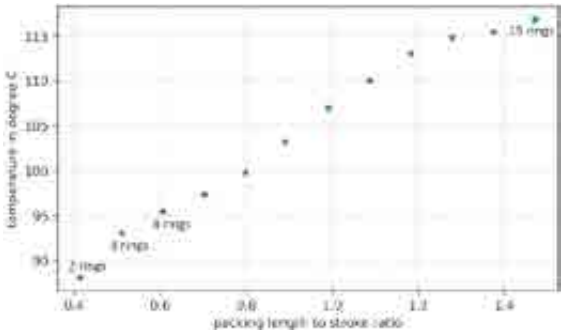

Figure 11: Maximum piston rod temperature vs. ratio of packing length to stroke.

The resulting temperatures for the original (V0) and the adapted designs (V1 and V2) are shown in Figure 10 and Table 3. The temperature is greatly reduced by switching to the pressure-balanced, one-ring design (from 162°C to 123°C), while keeping the cup dimensions constant. Additional changes to the cup design, reducing the packing length from 229 mm to 204 mm, would further reduce the temperature to 103°C. The final redesign (V2) yields a predicted maximum temperature of 115°C while increasing the packing length to 193 mm (packing length/stroke ratio = 1.28).

Finally, Figure 11 shows how the maximum piston rod temperature depends on the ratio of the packing length to the stroke. Starting with a two-ring design, adding cups increases both the number of rings and the total packing length. We see that the rate of temperature increase is high up to a packing length to stroke ratio of around 1.3, and decreases at higher values.

The numerical results agree well with feedback from the real compressor. Rod temperatures for the original design (V0) are quite high, though they do not suggest immediate overheating of the packing. The first redesigned package (V1) shows significantly lower temperatures (approximately 120°C), which do not indicate any likely problems. Most importantly, temperature estimates for the final redesign (V2) are below 120°C, again giving no indication of thermal problems and thus suggesting a

by: Bernhard Fritz, Georg Meyer, John Ladd – HOERBIGER

satisfactory lifetime, even though with 1.28, the ratio of packing to stroke length is far above 1.

6 Discussion and summary

This paper shows in detail, how the PPP-tool can be used to estimate the piston rod temperature as a function of the compressor design and operating conditions. A recent packing upgrade case study is shown, including the impact of design parameters on the piston rod temperature.

An accurate prediction of the piston rod temperature is important for the development of a sophisticated design tool for pressure packings. The PPP-tool is still in development, with ongoing validation both experimentally and numerically. However, keeping in mind its current major limitations (see Section 3), it is already a valuable tool for exploring the impact of design changes on the time-averaged piston rod temperature. This has been done for different design versions of a packing in a real compressor, trying to understand the impact of temperature on the life of the packings.

The numerical results look very reasonable and agree with observations on site. The results show a significant temperature drop induced by the change from classic R/T rings to a pressure-balanced one-ring design. On the real compressor, this change increased the lifetime of the packing by a factor of three.

The tool is also used to show the impact of increasing packing length on piston rod temperatures. Not surprisingly, it shows that increasing the packing length increases the rod temperature. However, and very interestingly, the predicted maximum temperature for a packing that is far longer than the machine's stroke (a packing-length-to-stroke ratio of 1.28) is only 115°C, which is low enough to avoid any likelihood of thermal problems. This suggests that the second redesign (V2), with 11 pressure-balanced rings, should have an even longer life, and challenges the hypothesis that the packing length must not be larger than the stroke.

This second redesign was implemented just a few months ago, so only 3,500 operating hours have been reported so far. However, at the time of writing the machine is still in operation and there are no indications of increased wear problems.

Current activities focus on further validation of the PPP tool: this involves on-site measurements of

- piston rod temperatures,
- crank angle resolved packing temperatures and pressures in the individual cups and
- leakage flows.

Especially measuring piston rod temperatures proves difficult, requiring visual contact if pyrometers are used.

Bibliography

[1] Goebel, Daniel. Reciprocating Compressor suction and discharge-valve monitoring, 2014-06, COMPRESSORtech2.

[2] Hanlon, Paul. Compressor Handbook, 2001, McGraw-Hill.

[3] Lindner-Silwester Tino, Hold Christian. The BCD packing ring – a new high performance design, 2010, 7th EFRC Conference.

[4] Ladd, J., Brandl A., Markey, K., 2019, Optimize Reciprocating Compressor Emissions Management Systems. Gas Machinery Conference, San Antonio 2019.

[5] R. Hahn and E. Holm, Electric contacts. New York: Springer, 1946.

HOERBIGER

A simplified approach to the design of nitrogen purge systems to improve safety and reduce emissions

by:

Guido Pratelli
Product Management
guido.pratelli@hoerbiger.com

Christian Prinz
Regional Unit Service Europe
christian.prinz@hoerbiger.com

HOERBIGER Wien GmbH
Vienna, Austria

13th EFRC CONFERENCE
September 19th – 21st 2023, Zagreb

Abstract:
Nitrogen purging of reciprocating compressor rod packings is common practice, but is often misunderstood and thus not used to best advantage. A thorough understanding of nitrogen purging in both theory and practice underpins the creation of purpose-designed nitrogen panels that make life easier for operators. Right from the detailed design phase of a project, through installation, commissioning and a lifetime of trouble-free operation, an optimized approach to nitrogen purging improves safety and environmental protection while cutting the cost of maintenance.
Modular design and standardisation of the panel design can greatly reduce the need for detailed engineering input at the design stage, without compromising on the flexibility needed to adapt to different compressors. Nitrogen panels should also ideally be used in combination with packing cases that incorporate purpose-designed vent sensing lines. The result is a purge system that is straightforward, easy to specify, reliable and cost-effective.

by: Guido Pratelli, Christian Prinz – HOERBIGER

1 Introduction

To support global efforts towards a net-zero-carbon future, reciprocating compressors were investigated with regards to their role as emission sources. Piston rod packing was identified as the primary culprit, posing a safety hazard, an environmental threat and a cost burden through the loss of compressed gas.

Modern ring designs perform well when properly selected, and so do the packing cases when properly maintained over time. However, there is no such thing as a "perfect" packing, and sealing rings and packing cases will always leak to some degree.

The difference between new and worn rings and packing cases can be staggering. Our own experience, supported by published data from sources such as OEM manuals, reports a 20-fold or greater increase in observed leak rates in worn conditions when compared to brand-new packing.

Contrary to conventional wisdom, keeping emissions under control is not just a matter of choosing the right packing rings and replacing them regularly. In fact, leakage paths from the rod packing include (Figure 1):



Figure 1: Leakage paths from rod packing.

1. Ring-to-ring leakage, via the gaps between ring segments and any scoring on the face of the ring or the machined faces of the packing cups; these leaks typically flow into the packing vent line.
2. Leakage along the surface of the piston rod in the event of scratching or wear of the last seal rings; these leakages accumulate in the distance piece.
3. Leakage between the metal-to-metal contact faces of the packing cups, especially if the packing case is not regularly and professionally repaired in machine shop. Leakage around the nose gasket can be due to incorrect case repair, misapplication of the gasket, stuffing box damage or installation errors. See Figures 2 and 3 as example of real-world instances of such issues. These leaks also accumulate in the distance piece.



Figure 2: Scoring on packing cup sealing surface



Figure 3: Damaged nose gasket.

It is specifically the leaks into the distance piece ("secondary leakage") that can flow uncontrolled into the compressor surroundings via the crankcase (Figure 4), where they may accumulate and form explosive atmospheres. In addition, the possible presence of highly toxic gases such as hydrogen sulphide can present an unacceptable hazard. Finally, corrosive process gases can also severely damage the running gear, via bearing attack and oil degradation, once they get into the crankcase.



Figure 4: Leakage path through the distance piece.

Even when the gas is non-toxic, leaks can be extremely harmful to the environment. Uncombusted methane, which is by far the largest component of natural gas and many refinery gases, is a much more potent greenhouse gas than CO_2. Since methane decays naturally in the atmosphere in about 12 years, its global warming potential (GWP), or CO_2 equivalence, varies greatly with the timescale considered: from a factor of 84 on a timescale of 20 years (GWP_{20}) to 28 on a timescale of 100 years (GWP_{100}).

by: Guido Pratelli, Christian Prinz – HOERBIGER

Some heavier hydrocarbons, when released in the atmosphere, will also influence climate by favouring the formation of ozone (O_3) and increasing the lifetime of CH_4. Reference [1] shows the calculated GWP_{100} of some non-methane hydrocarbons.

Many operators know these dangers and take steps to avoid them. A classic measure to control emissions is to purge the main packing, and sometimes the distance piece, with an inert gas such as nitrogen. This is done either via a quasi-static nitrogen barrier in the packing (as shown in Figure 5), or via a continuous nitrogen sweep that carries any process gas leakage away to a vent stack. Originally used purely for safety, purging is also an effective way to reduce the harm of fugitive emissions to the atmosphere, as long as the vented gas is properly disposed of.

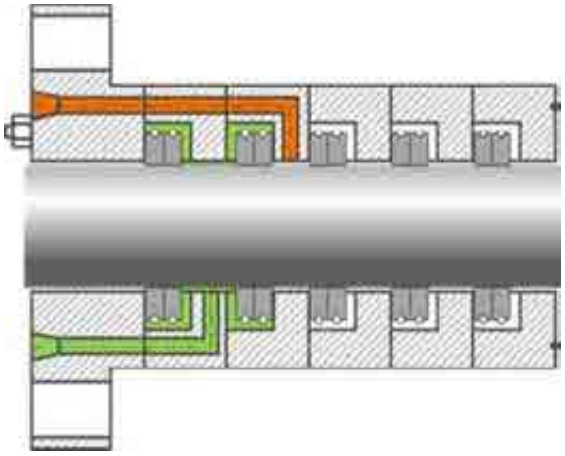

Figure 5: Schematic of a packing case showing nitrogen purge (green) and vent gas (orange).

Nitrogen purging is considered an effective way to reduce emissions from rod packings, but an intensive literature search yielded very few technical papers giving a comprehensive view of the topic (see Reference [2]). This lack was the motivation for the present paper.

2 Considerations with respect to API 618

API 618 (Reference [3]) is the reference standard for reciprocating compressor design in the process gas industry; its "*Annex I – Distance Piece Vent, Drain and Buffer Systems to Minimize Process Gas Leakage"* covers the topic of nitrogen purging systems. The fact that Annex I is indicated as "informative" should not be lost on the reader. API 618 stops short of defining precisely how a nitrogen purge system should be designed, instead simply describing a *"general philosophy"* for vent, drain and purging systems that is said to be *"not intended to cover all possible situations"* (see §I.1). To stress this point, the typical P&IDs of Figures I-1 and I-2 contain a clear note: *"This is a typical system and may require modifications based on specific user requirements".*

Having well warned the reader, the standard contains some good technical advice but stops short of defining once and for all how the nitrogen purging systems should be designed, leaving the topic to an *"agreement between purchaser and vendor".* It should therefore be no surprise that API 618 contains a certain number of inconsistencies or details that deserve clarification. For example: the schematic in Figure I-2 seems to advise the reader to pressurize the inboard distance piece **and** to purge the intermediate packing, while in fact these two options really are alternatives. Moreover, when a purged intermediate packing is used, the inboard distance piece should be vented, but this is not explained in the text. Another example is that the schematic does not explain how to regulate the purge pressure delivered to the intermediate packing or inboard distance piece.

In a nutshell, API 618 provides good guidance but ultimately leaves to the system designer and the compressor owner (or the EPC, in earlier project phases) the responsibility to design their own system based on their technical knowledge. This requires a technical alignment process, which takes time, costs money, and demands a certain degree of know-how that should not be taken for granted. This may ultimately represent a disincentive to invest in a nitrogen purging system, especially as a retrofit on an existing unit.

3 Standard purge systems and common pitfalls

The standard practice, as described in API 618 Annex I, is to supply nitrogen to each packing at a pressure of approximately 1 bar (15 psi) above the expected vent pressure. The nitrogen pressure can be regulated manually (a "constant-pressure" system) or controlled at a set differential above the stuffing box pressure by a suitable differential control valve (a "variable-pressure" system).

3.1 Constant-pressure systems

Constant-pressure systems require continuous monitoring and care; one reason is that the flare backpressure may not be constant, but the second and most important reason is that the pressure on the vent cup of the packing can rise sharply as the leakage rate increases, as an effect of the pressure drop in the vent line. Considering the high variability of the vent leakage rates (one or even two orders of magnitude with respect to a brand-new packing), this pressure rise can be significant.

by: Guido Pratelli, Christian Prinz – HOERBIGER

It has often been observed that if the purge pressure remains constant as the packing rings wear, the nitrogen pressure can become too low for the system to function. The performance of this commonly used purging arrangement may thus degrade over time.

3.2 Variable-pressure systems

A variable-pressure system provides better regulation in all conditions, though it adds some complexity. The differential regulator that sets the nitrogen pressure requires a reference pressure line that feeds back from the packing to the nitrogen panel. On lubricated compressors this line can become clogged with oil, so it is common to install an oil/gas separator between the compressor and the panel. The separator itself needs to be monitored and periodically drained, which is a source of hassle and additional costs. Also, it should be noted that the return line between the packing and the panel will generate a pressure drop, so not even a variable-pressure system is immune to performance degradation over time.

3.3 Double-compartment distance piece

While the generally accepted belief is that purging the main packing is sufficient to ensure safety, this is not the case. Purging the main packing case can effectively reduce two of the three sources of leakage (ring-to-ring and along the piston rod) but does nothing to prevent cup-to-cup or nose gasket leakage. It is therefore always recommended to provide a second barrier by purging either the intermediate packing (Figure 6) or the inboard compartment of the distance piece (Figure 7).

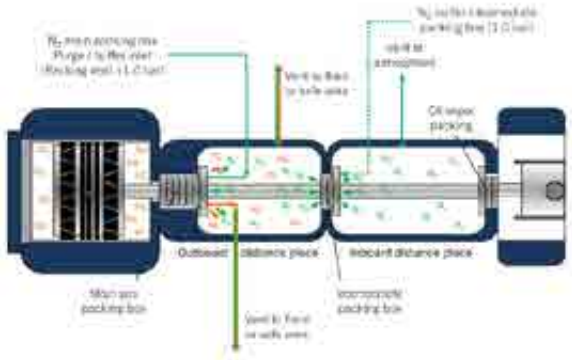

Figure 6: Purge arrangement for a double-compartment distance piece.

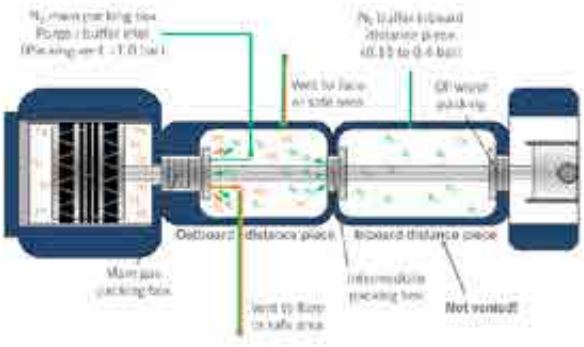

Figure 7: Alternative purge arrangement for a double-compartment distance piece.

3.4 Single-compartment distance piece

In the case of a single-compartment distance piece, the oil wiper packing may also be purged (Figure 8). This simple measure is, unfortunately, often neglected. A further issue is the fact that purged wiper packings tend to show less than optimal oil removal performance.

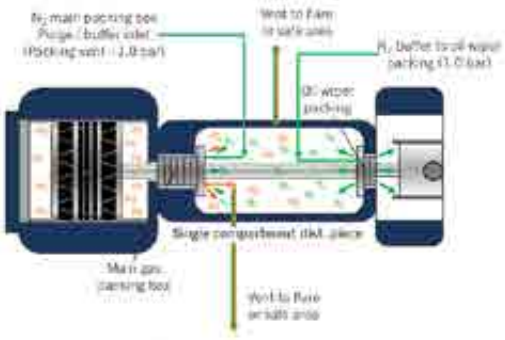

Figure 8: Purge arrangement for a single-compartment distance piece.

3.5 Nitrogen sweep systems

In some older designs, the distance pieces and even the crankcase may be swept with nitrogen; that means providing a constant flow of nitrogen, typically regulated by a needle valve, to dilute and carry away the possible process gas leaks. While the nitrogen flowrate required for purging is very low (so low, in fact, as to be unmeasurable in a perfectly functioning system), nitrogen sweeping requires a significant supply of nitrogen – up to 10 times the amount required by purging. This waste of nitrogen increases operating costs, and is not even an effective system compared to nitrogen purging.

When crankcases are swept with nitrogen, the fact that a large (sometimes very large) volume is filled with an inert gas of essentially the same density as air may pose an additional hazard to the operators.

by: Guido Pratelli, Christian Prinz – HOERBIGER

As a matter of fact, nitrogen will displace the oxygen in the air and may cause the operators to asphyxiate. Even though the effects of asphyxiation would probably be temporary, the fact that the operator may faint could cause him or her serious injuries. Operators are therefore required to wear supplied-air respirators (SCBA) when opening the crankcase covers at the start of any maintenance event (see API 618 §I.5 item n.).

All these extra costs and complications are hardly justified when considering that a properly designed purging system would prevent any process gas from reaching the crankcase in the first place.

3.6 Other common pitfalls

Other common pitfalls that we have seen in the field include:

- Directly connecting the vent lines of the main packing and the distance pieces at the compressor, as shown in the example of Figure 9. This means that in the event of a complete failure of the packing rings, there can be a backflow that pressurises the distance piece, most likely pushing process gas to the crankcase and from there to the atmosphere. Vent lines from the packing and distance pieces should ideally be routed to separate vent stacks; failing that, the merge point should be as far as possible from the compressor (see API 618 §I.5 item p).



Figure 9: Example of a compressor with packing and distance piece vent lines tied together – this should be avoided.

- Installing check valves on packing vent lines. While this may seem like a sensible measure to avoid backflows, a check valve can always become clogged, especially in the presence of oil or particles carried with the gas, and in the absence of a strong pressure-driven flow. Clogging of a vent line is a catastrophic hazard that needs to be avoided in all circumstances. Even when the risk of clogging is mitigated by some special design measure, a check valve always represents a restriction of the line, exacerbating the pressure-drop effect that degrades the performance of conventional purging systems. See API 618 §I.5 item h.
- Using a filter regulator to adjust the purge pressure. A filter regulator is an inexpensive way to manually regulate the nitrogen pressure ahead of the compressor, but in practice it acts like a needle valve by choking the flow. The pressure downstream of the regulator, therefore, would be constant only in the hypothetical case of constant upstream pressure and constant flow. But we know from experience that purge flows can vary greatly over time, thereby rendering a filter regulator completely useless for its intended purpose.
- Installing the nitrogen panels in places inaccessible to the operator (e.g. at floor level or at a height), making it difficult or impossible to perform regular monitoring and maintenance.
- Using glass-tube flowmeters to monitor the purge or vent flows. Glass tubes are susceptible to contaminants in the gas and can become clouded by sunlight, rendering the instruments unreadable over time. See an example in Figure 10.



Figure 10: Example of a glass tube flowmeter that has become unreadable over time.

4 Standardised nitrogen panels to enhance safety and lower TCO

Custom-designed nitrogen panels have been the norm for decades. Nevertheless, in our experience customers have rarely been completely satisfied with such product offerings. The most common negative comments were that the design process was cumbersome, with a lot of iterations in the requisition phase,

by: Guido Pratelli, Christian Prinz – HOERBIGER

and that even then, the end result was not 100% aligned to customer expectations.

With these criticisms in mind, we are proposing a different approach to the design of nitrogen panels. We believe we can simplify the requisition phase by grouping nitrogen panels into three "families", i.e. pre-engineered modular solutions that can adapt flexibly to each compressor configuration. The requisition phase is then reduced to the choice of one of the three available designs, each of which can be supplied in an open or a closed version. No other input is required besides the number of cylinders. This accelerates the decision-making process, making it easier and quicker for operators to upgrade their compressors.

One of the advantages of pre-engineering the panels is that it allows more time to be spent on the upfront design. It now becomes possible to perform a proper FMEA (failure mode and effect analysis), for instance, allowing all possible failure modes to be identified and mitigated through smart design choices. Standardisation allows maximum re-use of components, which in turn helps to keep costs down and reduces lead time.

Two of the three proposed designs essentially follow the constant-pressure and variable-pressure approaches of API 618 (Sections 3.1 and 3.2 respectively), with some small but meaningful improvement. The third design goes beyond API 618 requirements by controlling each packing individually.

4.1 Constant-pressure

The constant-pressure panel model (Figure 11) is the simplest solution; it guarantees compressor safety and basic monitoring functions at the lowest possible effort, without compromising the quality of the components or the panel's safety features. It regulates nitrogen pressure at a constant setpoint, which is differentiated for the main and intermediate packing or distance pieces. This is the perfect solution for compressors that are vented to atmosphere or to a flare system with near-constant pressure.

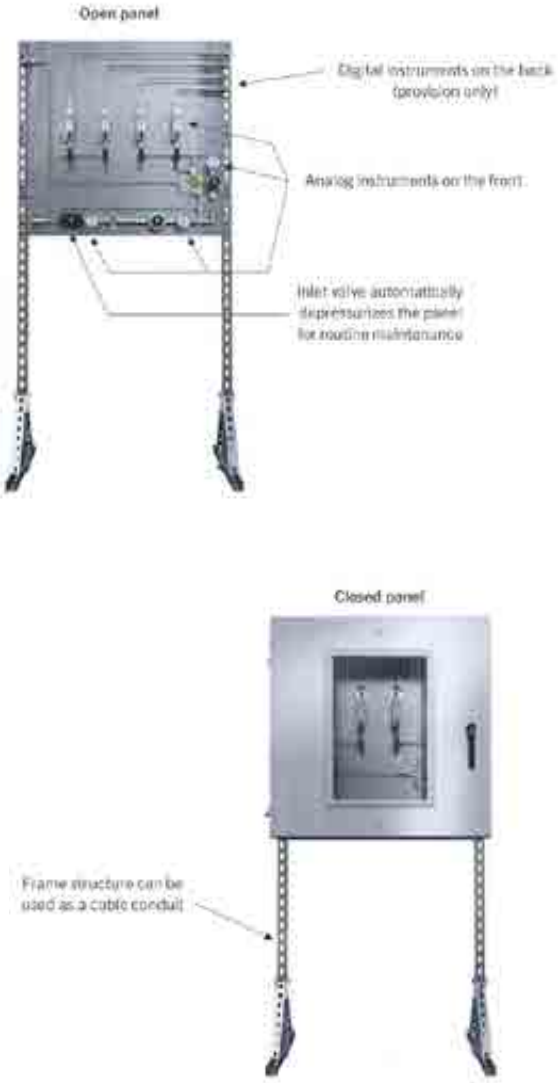

Figure 11: Constant-pressure panels.

4.2 Variable-pressure

The variable-pressure panel model (Figure 12) provides all the features of the previous class, with the additional advantage of dynamically regulating the nitrogen pressure to the main packing at 1 bar (15 psi) above the flare backpressure. This minimises nitrogen consumption and improves the system's ability to monitor the health of the compressor. The purge flowmeters are armoured, so they are more robust and do not become clouded over time. This is the ideal solution for most process gas units in refineries and petrochemical plants.

by: Guido Pratelli, Christian Prinz – HOERBIGER

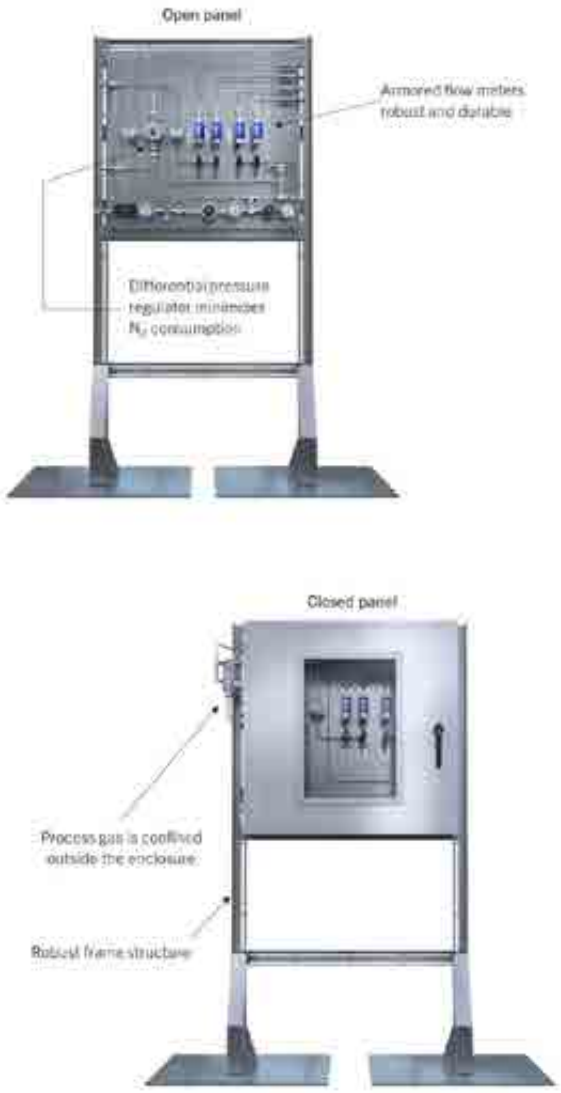

Figure 12: Variable-pressure panels.

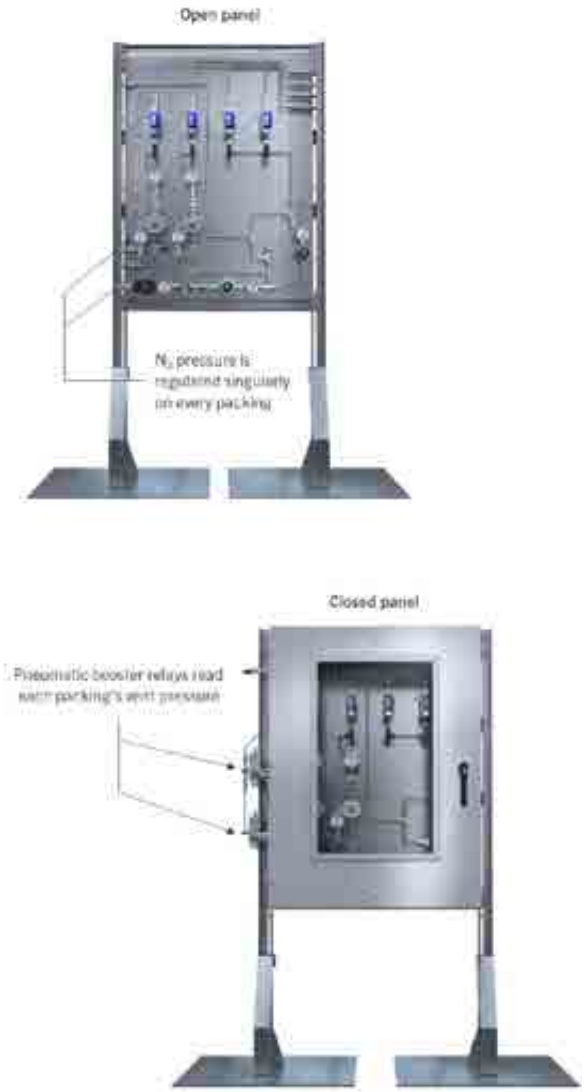

Figure 13: Individually regulated panels.

4.3 Individual packing regulation

The individually regulated panel model (Figure 13) provides the highest degree of regulation and advanced functionality. Nitrogen pressure is regulated individually on each cylinder, allowing the operator to monitor the health status of every single packing over time. If a packing fails, this panel will show which one, thus avoiding time-consuming inspections and minimising compressor downtime. This is the best solution for critical or un-spared process gas units in refineries and petrochemical plants.

5 Distinctive features of the new nitrogen panels

5.1 Open vs. closed panels

While open panels are made of stainless steel and therefore suitable for outdoor usage including marine environments, they might suffer from continued exposure to harsh weather conditions. A closed panel provides more protection for internal components, and discourages untrained personnel from tampering with the regulators or instruments. The panel enclosure is weatherproof but not airtight, so as to avoid pressurisation in case of any leakage, or accumulation of moisture. Finally, enclosures on the variable-pressure and individually regulated models are equipped with pneumatic booster relays to ensure that the process gas is always kept out of the enclosure, even if there is a malfunction – so leaks can never accumulate and create a hazard.

by: Guido Pratelli, Christian Prinz – HOERBIGER

5.2 Compatibility with sour gases

On constant-pressure panels, process gas never comes into contact with the panel, so there can be no problem with sour gas. On variable-pressure and individually regulated models, a vent sensing line from the packing is routed to the panel, so NACE compliance might be required, depending on the H_2S content of the gas.

It has been already explained that the closed versions of these two panels feature pneumatic booster relays that keep the process gas outside the panel. For the sake of standardization, these enclosed models are NACE compliant by default, without the need for the customer to specify this.

5.3 Ergonomics and maintainability

Nitrogen panels are not meant to be installed and then forgotten. Operators need to monitor them regularly, and maintenance activities such as cleaning the inlet filter, adjusting the regulators, and checking the tightness of tube fittings should always be performed according to a defined schedule. It is therefore important that panels are not installed casually, wherever there is available space, since this makes life difficult for operators.

All the new panels are designed according to human-centred design principles and supplied with a floor-mounted base. That means all components that need to be managed (e.g. pressure regulators) are at hand level, while all instruments that require regular monitoring (e.g. purge flowmeters) are at eye level. All the pneumatic fittings that need to be checked regularly and occasionally tightened are easily reachable.

The same is true for instruments that may require recalibration or replacement during their lifetimes. Finally, the tubing is in plain sight and includes visual aids such as flow arrows, helping technicians to intuitively understand the panel's functionality without having to check the manual.

5.4 Digitalisation and integration with the control room

Digitalisation can be a big obstacle to standardisation; there are many different options available for digital instruments, and virtually every customer has their own preferred vendors. Customers should therefore be able to install the digital instruments of their choice without jeopardising standardisation. Every analogue instrument on the front panel has a corresponding outlet on the back, so it can be paired with a corresponding digital instrument as its "digital twin".

This allows the panel to be connected to the plant's distributed control system (DCS) or programmable logic controller (PLC) – typically a lengthy process – whenever it is convenient, and not necessarily during a plant outage. The panel back frame and base act as cable conduits, with no need to attach an additional cable tray.

5.5 Protecting against overpressure

Component malfunction or incorrect regulation may lead to over-pressurisation of the nitrogen purge lines. This in turn represents a risk to machine integrity (see API 618 §I.5 item l.) API 618 Figure I-2 suggests installing a pressure relief valve (PRV) but does not consider that the main and intermediate packing and the distance piece compartment are not designed to handle the same pressures. For this reason, the new nitrogen panels feature two distinct PRVs with different setpoints. PRVs are factory-calibrated and certified (Figure 14).

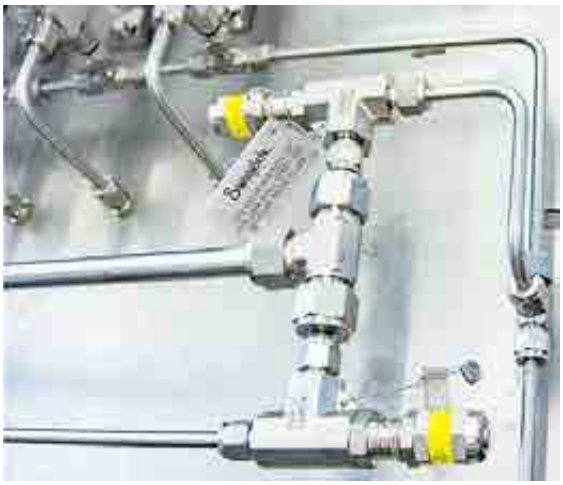

Figure 14: Detail of pressure relief valves on a nitrogen panel.

5.6 Safety during maintenance

On all conventional nitrogen panels there is an isolation valve on the N_2 inlet. This means that if the operator wants to perform routine maintenance (e.g. cleaning the filter mesh) and isolates the panel, the panel will remain pressurised and will pose a hazard when the operator tries to remove a component that is under pressure. The proposed design eliminates this hazard thanks to the use of an isolation valve with a downstream vent feature, which automatically depressurises the panel as soon as it is in the closed position. Even if the operation is performed when the compressor is running, there will be no backflow from the packing, because there are check valves at the N_2 outlets of the panel itself. This solution thus guarantees operator safety in all situations.

by: Guido Pratelli, Christian Prinz – HOERBIGER

6 Packing case design considerations

In many conventional purge systems, the vent line from the packing is routed through the panel itself in order to provide the pilot pressure for the differential pressure regulator. This creates several issues:

- On lubricated compressors, one or more liquid/gas separators need to be installed between the compressor and the panel. This adds cost and requires constant monitoring.
- As packing leakage increases over time, a pressure drop will develop along the vent line between the packing and the panel. This increasing pressure drop means that the panel will see a vent pressure that is too low, and as a result its performance will degrade over time.
- When retrofitting existing units, the existing packing vent line needs to be modified, causing extra work for the operator and requiring a typically lengthy Management of Change (MOC) process.

These issues can be solved by a packing case design with an additional vent sensing line to allow direct integration with the panel (Figure 15). The idea is as simple as it is effective. The packing case is equipped with two vent outlets: one on the bottom of the flange, connected to the vent and drain line, and a second on top of the flange, connected to the dome of the pressure regulator in the panel via a static sensing line. With no flow through the sensing line, there will be no pressure drop and therefore the panel will always read the correct pressure regardless of the packing leak rate. This arrangement eliminates the need to modify the existing vent line (no more MOC paperwork) and to install oil/gas separators: if there is no flow, there cannot be any oil carryover.

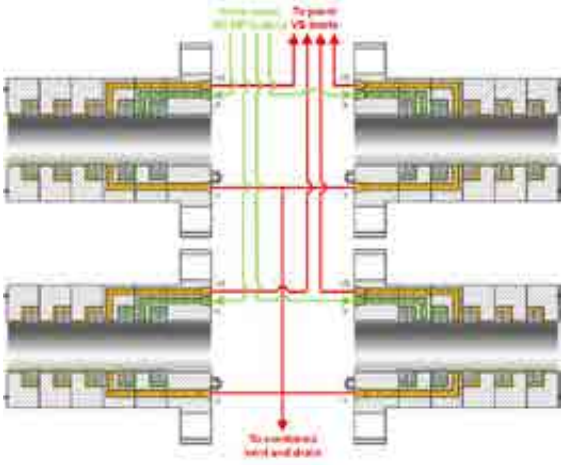

Figure 15: Routing of packings with a separate vent sensing (VS) connection to an individually regulated panel.

7 Conclusion

A simplified design philosophy for nitrogen panels is proposed, with three models that can replace individually engineered – and sometimes ad-hoc – nitrogen purge control systems. This approach improves the safety, reliability and effectiveness of purged packings while reducing the time spent on engineering. Resources previously taken up in creating custom systems can instead be channelled into making sure that standardised units combine high performance with reasonable costs, to the extent that they are also suitable for retrofits.

The three models are designed based on constant pressure, variable pressure, and individually regulated pressure for each packing in a multi-cylinder compressor, covering the full range of applications, from the straightforward to the most critical. High-quality components, carefully chosen layouts and attention to ergonomic factors all contribute to create nitrogen panels that are safe and effective from day one, and also easy to maintain throughout the lifetime of the plant.

Furthermore, treating the purge system as a component in its own right encourages proper understanding of the correct ways to install and maintain purge systems. The logical development is to combine a new variable-pressure or individually regulated panel with a packing case that has a separate vent sensing line. On one hand this eliminates the vent line pressure drop, which negatively affects the performance of the purging system over time. On the other hand it also eliminates oil clogging, which is often an issue with conventional designs and can be costly and time-consuming to overcome.

References

[1] Hodnebrog, Ø., Dalsøren, S. B., Myhr, G. (2018) Lifetimes, direct and indirect radiative forcing, and global warming potentials of ethane (C2H6), propane (C3H8), and butane (C4H10). *Atmospheric Science Letters*, **19**. https://doi.org/10.1002/asl.804

[2] Ladd, J., Brandl, A., Markey, K. (2019) Optimize reciprocating compressor emissions management. *Gas Compression Magazine*, March 2020.

[3] ANSI/API Standard 618-2008 (2010) Reciprocating Compressors for Petroleum, Chemical, and Gas Industry Services. Fifth Edition, December 2007.

Howden
A Chart Industries Company

Overcoming reliability challenges of sealing highpressure hydrogen diaphragm compression stages

by:

Marije Oosterlaak, Rens Hulstijn, Yann Ardouin
Research and Development
Howden Thomassen Compressors
Rheden, the Netherlands
marije.oosterlaak@howden.com, rens.hulstijn@howden.com,
yann.ardouin@howden.com

13th EFRC CONFERENCE
September 19th – 21st 2023, Zagreb

Abstract:
One of the challenges designers have to face when designing hydrogen diaphragm compressors operating above 500 bar is the reliability of the static sealing of the diaphragm heads. This sealing system is one of the key differentiating features of diaphragm compressors, preventing any leakage to atmosphere and is therefore essential to safe operation of these compressors.
In this paper, an in depth analysis of case studies is presented to illustrate the degree of complexity of a high pressure sealing system, showing amongst others that at such high pressures the assumption that the diaphragm head sealing system can be designed for static conditions is not always valid.
It explains how the conclusions of the analyses have been used to define a comprehensive sealing system design method for high pressures and how it differentiates from usual design practices for medium and low pressures. Factors of influence of the seal performance and reliability, design activities, validation steps and results are detailed.
Finally, an example of application and tests on a 1000 bar compression stage will be shown.

by: Marije Oosterlaak, Rens Hulstijn, Yann Ardouin – HOWDEN

1 Introduction

Hydrogen is considered an increasingly important part of the solution to reduce carbon dioxide emissions to eventually reach the European Net Zero Emissions target by 2050 and is considered strategically important for future energy security. For that reason, the hydrogen market increases rapidly, which is therefore also the case with the hydrogen compressor industry. There are various applications of hydrogen, such as capturing renewable energy in hydrogen, using it as a gaseous fuel in for example trucks and for the production of energy. It is expected that these applications will grow significantly over the coming years [1].

This paper focuses on the sealing system of the diaphragm compressor used for hydrogen fuelling stations. The critical aspects for fuelling stations are the high discharge pressure (the discharge fuelling pressures go above the pressure tank of 700 bar), the high purity level of the hydrogen and the number of starts and stops per day. These aspects make compressors used at fuelling stations a very challenging product. Since the diaphragm compressor has a hermetic sealing of the process gas from the lubricated parts, no losses of compressed gas can occur. It also has the ability to go up to a very high discharge pressure (above 2000 bar) and capacities up to about 100 kg/h. Current refuelling stations are usually designed with a lower capacity but this is expected to rise up to 170 kg/h with multiple compressors, making the diaphragm compressor very suitable for this type of application.

One of the challenges with high-pressure hydrogen diaphragm compressors is the sealing of the two diaphragm head plates. Obviously, the sealing is an important factor to guarantee the safety and reliability of the machine. One of the challenging aspects of the sealing design is that the sealing element is exposed to high-pressure and high temperature hydrogen. Discharge temperatures for hydrogen compressors can be as high as 250 °C. In addition, less obvious challenges were found during case studies.

This paper presents an in-depth analysis of case studies that show the degree of complexity of a high pressure sealing system. Design considerations are also described. In the second section, the basic construction of the diaphragm compressor and sealing system is explained and after that the challenges with high pressure hydrogen are discussed in more detail. section 4 provides information on other important and less obvious aspects of the sealing system, based on investigations that were performed after several observations during case studies. The resulting design considerations that should be taken into account for a sealing system are described in section 5. section 6 describes the tests and test results to validate the new design of the sealing system. The conclusions of this paper can be found in section 7.

2 Basic construction of diaphragm compressor and seal

To understand the challenges with the sealing design of the compressor, background information will be provided regarding the operating principle and design of the diaphragm compressor, in particular the design of the sealing system.

The diaphragm compressor is a positive displacement compressor, which increases the pressure of the supplied gas by mechanically reducing the volume in the compression chamber. It consists of two main assemblies: the mechanical frame and the diaphragm head (see Figure 1 and Figure 2). The main components of the diaphragm head are the gas plate and the oil plate, which are separated by multiple highly flexible diaphragm plates that separate the gas side from the hydraulic (oil) side. On the hydraulic side, a piston moves back and forth, the oil plate distributes the oil evenly under the diaphragm and the motion of the piston is transmitted to the diaphragm plates by the hydraulic fluid. The hydraulic fluid therefore drives the diaphragm plates up and down, increasing and decreasing the pressure of the gas within the compression chamber. The inlet and outlet valves ensure that the gas enters the compressor during the suction phase and that the gas is discharged under pressure to the system. The pressure-volume diagram of the diaphragm compressor is very similar to the one of a piston reciprocating compressor.

To ensure a full contact between the diaphragm and gas plate (to make sure that all of the gas is leaving the compression chamber during discharge), an excess of hydraulic fluid is injected in the oil volume below the diaphragm plates by a pump during each stroke. The excess of hydraulic fluid by this system is expelled through the pressure limiter (also known as overflow valve), to prevent an internal over pressure.



Figure 1: Diaphragm head assembly in yellow, assembled on a compressor frame

by: Marije Oosterlaak, Rens Hulstijn, Yann Ardouin – HOWDEN

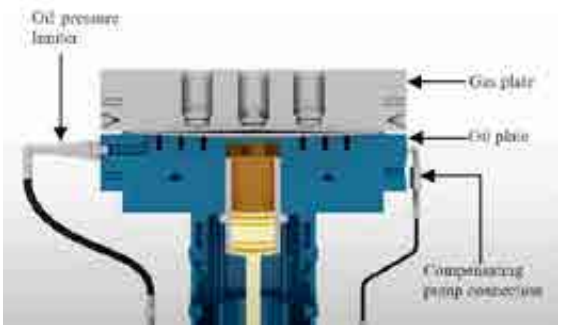

Figure 2: Diaphragm head cross section

To prevent any leakage to the environment, the gas and oil plate are firmly clamped and sealed by a triple arrangement of O-rings: one to prevent leakage from the gas compression chamber, one to prevent leakage from the hydraulic chamber and one behind the Head Integrity Detection System groove. In the event of leakage of gas or oil (for example due to a diaphragm failure or failure of the O-rings), this will be detected by our Head Integrity Detection System (HIDS). The gas or oil will be collected in a groove, which is connected to an external leak detection system.

Figure 3 and Figure 4 illustrate the location of the different O-rings and the contact zones between the oil and gas plate respectively. For this paper, the focus is on the sealing of the gas compression chamber because this is where most of the failures mode have been observed by the compressor OEM when compressing hydrogen above 500 bars.

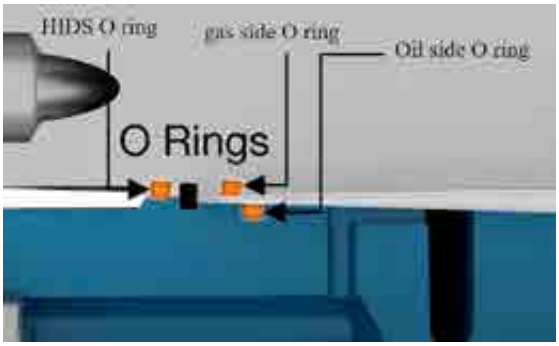

Figure 3: Location of the O-rings.



Figure 4: Contact zones around seal grooves

In the industry, both metallic seals and elastomeric seals are used.

Metallic seals are more resistant to the resulting high forces and can handle higher temperatures up to 700 °C while most of elastomers that can be used for this service have design temperatures below 200 °C.

Metallic rings are also used when required for compatibility with the process gas when no suitable elastomer is available; this is typically the case for some very corrosive gas mixtures or when the process gas would react with the elastomer material.

Finally metallic seals are not subject to damage by rapid gas decompression.

On the other hand, metallic seals are usually much more expensive that elastomer rings, and require specific groove design and assembly and replacement procedures.

Elastomer seals are much easier to replace at customer sites and can be installed in grooves manufactured with higher tolerances than for metallic seals. These seals do not require fatigue calculation.

3 Challenges with high pressure hydrogen

As explained in the previous chapter, the seal system consists of three grooves with a triple arrangement of O-rings which are clamped by the head bolts. For medium pressure cases (below 40 MPa) seals are available that are able to withstand the pressure and expected temperature and ensure good sealing of the diaphragm head. For these applications usually elastomer seals are used within the industry.

However, designing a reliable and safe sealing solution for high pressure hydrogen is more challenging, especially with regards to the gas side seal in direct contact with the high pressure hydrogen.

1) Due to the high pressure ratio's, up to 10, the gas temperature at discharge and inside the gas plate can be high compared to other positive displacement machines. Discharge temperatures up to about 250°C can be expected.

2) The gas side seal is exposed to high pressure hydrogen, this can cause extrusion of the seal due to the high pressure acting on the seal and forcing it out the groove if an extrusion gap is present. The high temperature increases this risk, because it reduces the mechanical properties of the seal material and therefore increases the risk of extrusion.

   Use of systems to prevent extrusion, such as back-up rings for example, is not preferred when it can be avoid in order to limit the number of parts to be used in the compressor head, for cost and maintainability reasons.

by: Marije Oosterlaak, Rens Hulstijn, Yann Ardouin – HOWDEN

3) Furthermore, permeability of the seal material to hydrogen leads the designer to consider possible presence of hydrogen in the seal. Combined with the rapid pressure fluctuations (between suction pressure and discharge pressure), this can cause rapid gas decompression inside the elastomer seal. The compressor offloading causes an even more stringent design case as the pressure decreases to atmospheric pressure instead of to suction pressure. Compressors operating in a refuelling station are likely to experience this often due to the high number of starts and stops per day. The high temperature increases the permeability of the seal material to hydrogen. This can be either an advantage or disadvantage (depending on how long the compressor has been pressurized), because the diffusion of hydrogen into the material increases and at the same time the speed at which the hydrogen can diffuse out of the material upon depressurisation also increases [2] [3].

4) The surface quality and roughness of the groove are also contributing to the efficiency of the sealing system; due to the small size of the hydrogen molecule and high pressure, a very small imperfection can cause a leak path for the gas.

In addition, when conducting an in depth investigation with seal manufacturers, almost no references were found in the industry for seals operating in similar cases, ie pressure cycles with pure hydrogen up to 1000 bar and temperatures above 150 °C. Some references were found at pressure lower than 1000 bars and above 500 bars.

Due to the challenges explained in points 1, 2 and 3 above, metallic sealing solutions are often preferred over non-metallic solutions.

4 Observations from case studies

Over the last 4 years, design and testing of high pressure compressors for Research and Development purposes or commercial use led to several case studies for improvement of the diaphragm head sealing system.

Except the ‘’obvious’’ challenges described above, several unexpected phenomena were discovered during these case studies. After performing extensive root cause analyses some additional failure modes of the sealing systems for high pressure hydrogen were identified. In depth analyses were performed to investigate and understand these failure modes; some examples will be explained in this chapter.

One of these unexpected failure modes was the relative movement of the oil and the gas plate. Observations first led to suspect such a movement, and a finite element analysis confirmed that due to the high pressure and the dimensions of the head, relative movement between the oil plate and the gas plate was likely to occur. The design limitations were therefore bending deformation of the plates instead of stress. This flexing also means relative movement between the seal groove and the counter surface, which adds an extra difficulty to the design as the sealing environment changed from static to semi-static. In the case study, several significant leakages were detected after a certain period of time. Figure 5 shows a picture of a seal which has been completely destroyed. Further investigations showed that this was due to fatigue in the seal caused by the combination of the relative vertical movement of the oil and gas plates and the fluctuating pressure load in the groove, which induces a cyclic loading at the frequency of the compressor speed (see

Figure 6).



Figure 5: Example of a destroyed metallic seal due to fatigue caused by relative vertical movement between oil plate and gas plate

During the design of the seal, it was not expected that the oil and gas plates (which were respectively 330mm and 470mm in height) would move due to the internal pressure. Also fatigue failures were never experienced by either the seal manufacturer or the compressor OEM in a such a seal before.

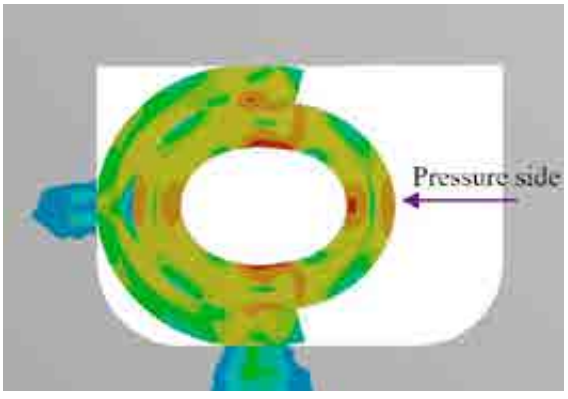

Figure 6: FEA of a seal similar to seal in figure 5 and 7 showing stresses to assess fatigue load. (red indicates the regions of high stress)

In a second case study, slight leakage to the Head Integrity Detection System was experienced over time. After disassembly and inspection, microscopic scratches were found on the seal that were initially not visible with the naked eye upon disassembly. The

by: Marije Oosterlaak, Rens Hulstijn, Yann Ardouin – HOWDEN

scratches were found to come from either relative movement between the gas plate and diaphragm plate, or from the seal moving in the groove due to the cyclic pressure. Figure 7 shows a picture of these scratches.

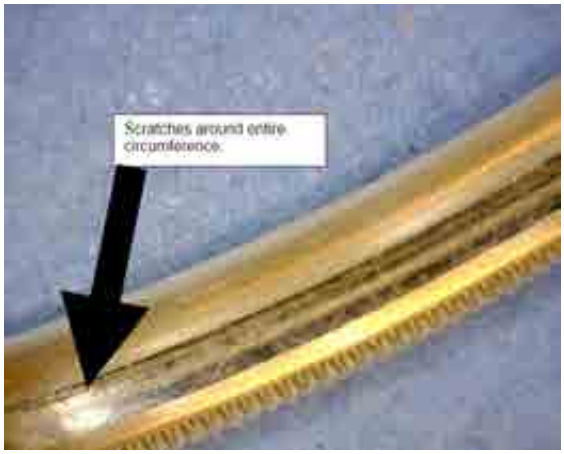

Figure 7: Example of a metallic seal with scratches around the entire circumference

Furthermore, it was found that reliability was an issue due to the nature of the small hydrogen molecule and the extremely high pressures. Even a slightest scratch or imperfection could result in a leakage of hydrogen. It was also found that the assumption of designing a seal for a static case was not sufficient for a reliable sealing solution. Either the flexibility and relative movement of the system needs to be prevented, or the seal should designed to be tolerant for this movement.

5 Design considerations about seal for high pressure hydrogen

One of the main new insights from the investigations on failure modes was that the relative movement or flexibility between the flanges caused leakage of the seal in case of high pressure hydrogen. It means that apart from designing a seal itself, a complete sealing system needs to be designed. Within this sealing system, either relative movement of the seal should be prevented or a solution should be designed in which the movement can be tolerated.

One of the solutions to assess the risk of relative movement around the sealing area is to check the contact pressure between the oil plate, the gas plate and the diaphragm stack. (See figure 4)If the contact pressure is sufficient, relative sliding can be prevented thanks to friction and separation of the flanges from the diaphragm stack is also prevented.

This guaranteed contact pressure between the flanges also gives the following advantages:

- If there is sufficient contact pressure in front of the seal (pressure side) this increases the sealing performance
- The seal will not see the highest pressure and temperature that occurs in the compression cycle, due to the metal-on-metal contact which causes a restriction of the passage area and dampens the pressure amplitude in the seal groove
- The high contact pressure will also prevent or greatly reduce the cyclic loading and therefore decreasing the fatigue loads and relative movement. (figure 5, 6 and 7)

Another possible solution is a design tolerant for movement of the flanges without compromising sealing performance and reliability. It is quite difficult to find a seal with enough spring back to compensate for the moving of the flanges whilst also not being vulnerable to the cyclic loading and movement of the seal in the groove. This is where the solution for a non-metallic seal could be investigated.

In addition to a proper seal selection and sealing system design, special attention should be given to part quality and procedures of handling the parts and mounting the seal because any defect or contamination could affect the sealing behaviour.

6 Validation & testing of the seal design

The purpose of these in-depth case studies and investigations on sealing system design alternatives was to release a reliable solution for high pressure hydrogen compression.

Design adjustments to the sealing system and seal itself were defined based on the design considerations described above. For validation, two different tests were performed: a small scale test in a laboratory and a full scale test in an actual operating compressor.

It should be noted that a seal will always be very slightly permeable, because a 100% leak tight seal is not achievable with high pressure hydrogen. This is taken into account in the design, that shall ensure there is no accidental leak of hydrogen to the atmosphere in order to not cause any safety risks or decreased reliability of the system.

The main purpose of the small scale test was to test the performance of different materials and designs of the seal itself. This small scale test was done in a laboratory, which allowed to have a good representation of the actual operating conditions and test for fatigue and rapid gas decompression.

During this test several seals have been tested in a cyclic hydrogen exposure test. Pressure was raised from atmospheric pressure to 1050 bar and back to atmospheric pressure within 5 seconds for a total of 5000 times, while the temperature of the test piece was equal to the maximum allowable temperature of the seals.

by: Marije Oosterlaak, Rens Hulstijn, Yann Ardouin – HOWDEN

This cyclic test was done several times with different samples of the same materials to validate repeatability of the results.

During the tests eventual leakage of gas through the seal, either due to damaged material or deformation caused by pressure, was monitored. Seals that were showing leakage above a pre-defined threshold were registered as not suitable for the application.

All the seals with leakage rate null or below the threshold have been inspected after the test. Some materials were not in acceptable conditions while one of the elastomer seals showed no signs of damage nor leakage and had a permeability well within the maximum allowable value.

After a successful small-scale test, a complete sealing system with elastomer seal was tested in an actual operating compressor at the most critical load case. For this test, a high pressure diaphragm head was designed including the new design rules for the sealing system based on the design considerations discussed previously. The purpose of the full-scale test was to validate the solution design at real scale or learn from unexpected failure modes.

The full-scale test consisted of a static and dynamic pressure tests.

During the static pressure test, the head was filled with helium at a pressure of 132 Mpa to test the strength of the components and was submerged in a water bath to test the leak tightness in a static case.

After this test was successfully completed, the diaphragm head was tested in an actual diaphragm compressor operating with a discharge pressure of 1000 bar and a pressure ratio of about 6.5. The test gas was helium. Several test rounds have been performed, with the first test round of 40 hours with many starts and stops in between. The other test rounds were shorter, as the purpose was to validate the repeatability and usually failures of previous designs after re-starts had been observed in the first running hours.

In between the test rounds the sealing system was inspected. During the test, the pressure in the Head Integrity Detection System was continuously measured to detect any leakage of the sealing system.

The results did not show any significant pressure increase in the Head Integrity Detection System and the seal was still in perfect condition after the first test round. Tests of repeatability after dismantling and replacing the seal showed stable repeatable results, which was the final step of validation of a new design for high pressure sealing in a diaphragm compressor.



Figure 8: User dashboard for monitoring of the diaphragm test compressor

7 Conclusion

When designing a sealing solution for a high pressure hydrogen diaphragm compressor, it is important to realize that a complete sealing system has to be designed for a semi-static case. Apart from more challenging conditions such as the high temperature, high pressure and corresponding risk of permeability of the seal to hydrogen, several in depth case studies showed that designing for a static case only is not sufficient.

This means that either movement of the seal should be avoided or the sealing solution should be designed to tolerate slight movement of the seal. One of the solutions to eliminate the relative movement around the sealing area is to increase the contact pressure between the oil and gas plate, so that sliding and vertical movement can be prevented. Another possible solution is to design a sealing system with a seal tolerant for movement of the flanges, for example by investigating solutions based on non-metallic seals.

To validate these design considerations, adjustments have been applied to the selected sealing design which was tested in a small-scale and full-scale test. Validation has been obtained by laboratory small scale tests with high pressure hydrogen and full-scale static and dynamic tests of a high pressure diaphragm head in a diaphragm compressor operating with helium at 1000 bars.

During both tests, the measured permeability was well within the maximum allowable value. After disassembly, the seal was still in perfect condition and repeatability has been proven after starts and stops sequences and simulated maintenance.

The next steps will be field test validation in hydrogen fuelling stations or another similar service.

by: Marije Oosterlaak, Rens Hulstijn, Yann Ardouin – HOWDEN

8 Bibliography

[1] L. van Lier, C. Tümer, M. Tedesco en L. Buijs, „Hydrogen compression boosting the hydrogen economy," pp. 7-9, 2022.

[2] IIT research institute, „Permeability data for aerospace applications," Chicago, Illinois, March 1968.

[3] Atomics international division, energy systems group, „Design Guide for Reactor Cover Gas Elastomer Seals," March 1975.

NOTES

NOTES

NOTES

NOTES

NOTES

NOTES

NOTES

Promoter
European Forum for Reciprocating Compressors e. V.
c/o Technische Universität Dresden
01062 Dresden, Germany
www.recip.org

Maja Schütz (Office Manager)
Telefon: +49 (351) 463-32815
E-Mail: contact@recip.org

EFRC Board
Gunther Machu (Chairman)
Erik Nennie (Secretary)
Franzisko Maywald (Cashier)

Editor
Herbert Steinrück, TU Wien

Conference Task Force
Christian Prinz, HOERBIGER
Sophie-Marie Amm, HOERBIGER
Gina Pinto, BURCKHARDT COMPRESSION
Said Kus, BURCKHARDT COMPRESSION
Leonard van Lier, TNO
Herbert Steinrück, TU WIEN

Programme Committee
Herbert Steinrück, TU WIEN (Head of Programme Committee)
Yann Ardouin, HOWDEN
Alessio Capanni, BAKER HUGHES
André Eijk, Independent Consultant
Konrad Klotsche, TU DRESDEN
Guido Kluth, SHELL
Marc Langela, STASSKOL
Massimo Maffeis, SIAD
Christian Prinz, HOERBIGER
Andrea Raggi, COZZANI
Cyril Wentzel, WENTZEL DYNAMICS

Advisory Board
Niek Albers, HOWDEN
Alessandro Baldussu, HOERBIGER
Albert Benoni, HOERBIGER
Klaus Hoff, NEUMAN & ESSER
Matthias Kornfeld, HOERBIGER
Leonard van Lier, TNO
Paul Modern, COOK
Maximilian Palir, HOERBIGER
Felix Ragg, BURCKHARDT
Matthias Richtig, HOERBIGER
Florian Schacherreiter, HOERBIGER
David Schroeder, HOWDEN
Klaus Stachel, HOERBIGER

Layout
Sanja Kaltenbrunner-Jelic, sanja.at e.U., 1160 Vienna, Austria

Coverphoto
eyeswashere on Unsplash

Druck
Druck.at, 2544 Leobersdorf, Austria

ISBN 978–3–200–09263–1
9 783200 092631

WWW.RECIP.ORG